Wind and Seismic Effects

Proceedings of the 22nd Joint Meeting

NIST SP 796

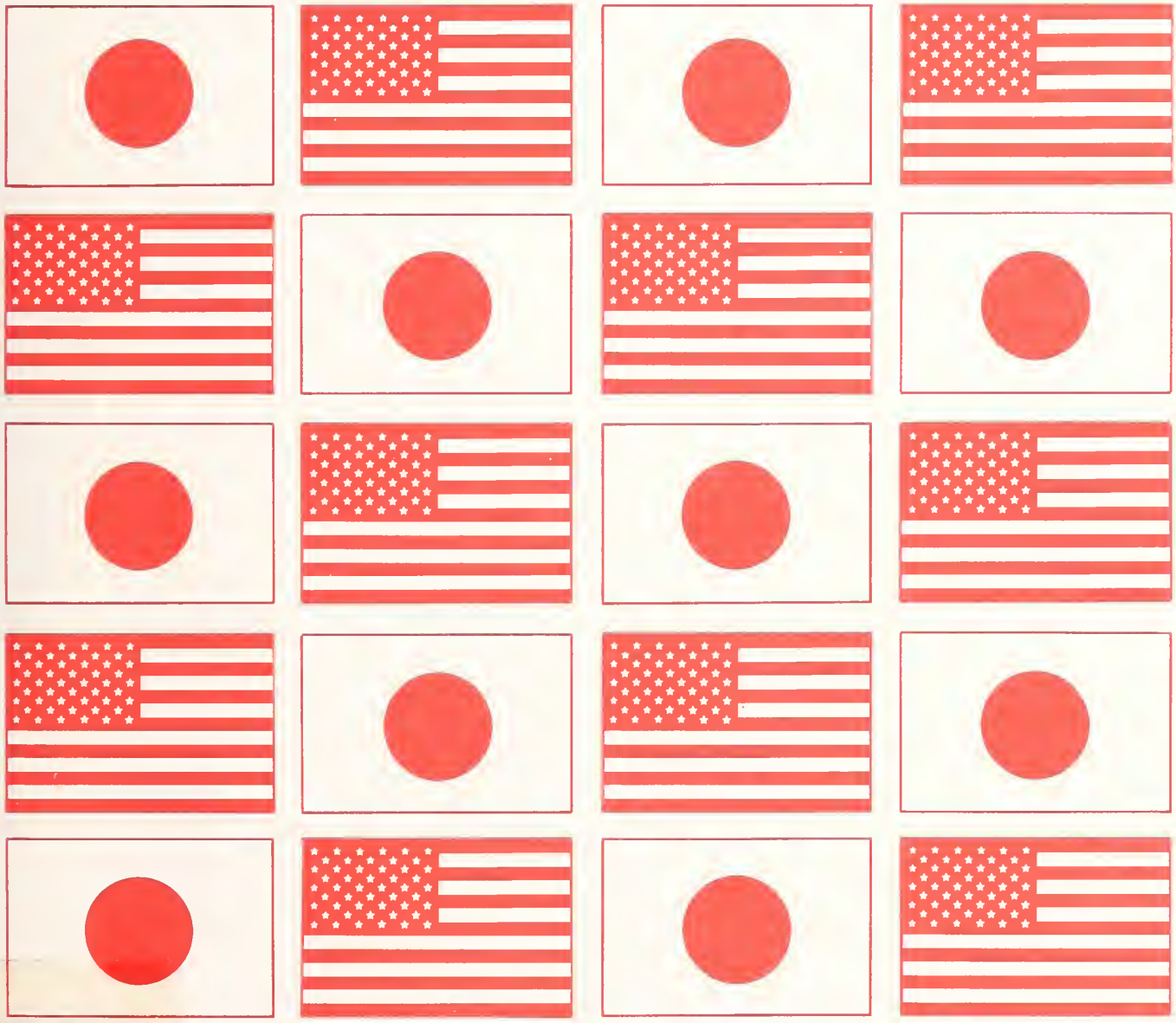

TMENT OF COMMERCE
itute of Standards and Technology

Wind and Seismic Effects

NIST SP 796

PROCEEDINGS OF
THE 22ND JOINT
MEETING OF
THE U.S.-JAPAN
COOPERATIVE PROGRAM
IN NATURAL RESOURCES
PANEL ON WIND AND
SEISMIC EFFECTS

Issued September 1990

Noel J. Raufaste,
EDITOR

Center for Building Technology
National Engineering Laboratory
National Institute of Standards and Technology
Gaithersburg, MD 20899

U.S. DEPARTMENT OF COMMERCE
Robert A. Mosbacher, Secretary

National Institute of Standards and Technology
John W. Lyons, Director

National Institute of Standards and Technology Special Publication 796
Natl. Inst. Stand. Technol. Spec. Publ. 796, 524 pages (Sept. 1990)
CODEN: NSPUE2

U.S. GOVERNMENT PRINTING OFFICE
WASHINGTON: 1990

For sale by the Superintendent of Documents, U.S. Government Printing Office, Washington, DC 20402-9325

PREFACE

Background

Responding to the need for improved engineering and scientific practices through exchange of technical data and information, research personnel, and research equipment, the United States and JAPAN in 1961 created the US-JAPAN Cooperative Science Program. Three collateral programs comprise the Cooperative Science Program. The US-JAPAN Natural Resources Development Program (UJNR), one of the three, was created in January 1964. The objective of UJNR is to exchange information on research results and exchange scientists and engineers in the area of natural resources for the benefit of both countries. UJNR is composed of 17 Panels each responsible for specific technical subjects.

The Panel on Wind and Seismic Effects was established in 1969. Seventeen U.S. and six Japanese agencies participate with representatives of private sector organizations, to develop and exchange technologies aimed at reducing damages from high winds, earthquakes, storm surge, and tsunamis. This work is produced through collaboration between U.S. and Japanese member researchers working in ten task committees. Each committee focuses on specific technical issues, e.g., earthquake strong motion data. The Panel provides the vehicle to exchange technical data and information on design and construction of civil engineering lifelines, buildings, and water front structures, and to exchange high wind and seismic measurement records. Annual meetings alternate between JAPAN and the U.S. (odd numbered years in JAPAN; even numbered years in the U.S.). These one-week technical meetings provide the forum to discuss on-going research and research results; one-week technical study tours follow the meetings.

The National Institute of Standards and Technology (NIST) provides the U.S.-side chairman and secretariat. The Public Works Research Institute (PWRI), JAPAN, provides the JAPAN-side chairman and secretariat.

The Panel has organized formal joint research programs. In 1981 cooperative research in Large-Scale Testing commenced under the auspices of the Panel. Also in 1981, joint research on Reinforced Concrete Structures was initiated. Full-scale testing was performed at the Building Research Institute (BRI), JAPAN, one of the six Japanese member organizations, with supporting tests in JAPAN and in the U.S. Two years later a joint research program on Steel Structures was initiated. Full-scale testing again was led by BRI with supporting tests in the U.S. and JAPAN. The US-JAPAN coordinated program for Masonry Building Research was started in 1985. A coordinated program for testing lifeline structures resulted in NIST's testing of full-scale bridge piers in its 50 Mn universal

testing facility to evaluate post-1972 seismic design criteria.

Task Committee meetings, exchanges of data and information through technical presentations at the annual Panel meetings, exchanges of guest researchers, visits to respective research laboratories and informal interactions between Panel meetings, joint workshops and seminars, and joint cooperative research programs have contributed to the development and effective delivery of knowledge that has influenced design and construction practices in both countries.

Direct communication between counterpart country organizations is the cornerstone of the Panel. Effective information exchanges and exchanges of personnel and equipment have strengthened domestic programs of both countries. There are opportunities for experts in various technical fields to get to know their foreign counterparts, conduct informal exchanges, bring their respective views to the frontiers of knowledge, and advance knowledge of their specialties.

The Panel's results have supported improvements in practices in both countries, they have for example:

1. created and exchanged digitized earthquake records for use as the basis of research for Japanese and U.S. geotechnics and structures;

2. produced data that advanced U.S. design and construction of bridge columns;

3. produced large-scale testing data that advanced seismic design standards for buildings;

4. created a database comparing Japanese and U.S. standard penetration tests to improve seismic design criteria for soil liquefaction;

5. created databases on storm surge and shore line interaction and on tsunamis and tsunami warning systems for use by designers to verify mathematical models of tsunamis and storm surge.

22nd Joint Panel Meeting

The 22nd annual U.S.-JAPAN Joint Panel meeting was held at NIST during 15-18 May 1990. Thirty-seven U.S. members from 17 Federal agencies, universities, and a trade association participated. JAPAN-side participation included twelve members from their six member Government agencies and one from academia. Thirty-nine papers were authored; 21 by U.S. members and 18 by Japanese. Thirty-two oral presentations centered on: Wind Engineering; Earthquake Engineering; Storm Surge and Tsunamis; US-Japan Cooperative Masonry

Research Program; Loma Prieta Earthquake of 17 October 1989; and reports from just completed Panel Task Committees Workshops on "Repair, Retrofit, and Performance of Structures" and the 6th Bridge Workshop on "Analysis, Design, Performance, and Strengthening of Bridges".

Some highlights of the meeting are listed below:

- eight of the Panel's ten Task Committees scheduled workshops within the coming 12 months;
- a tenth Task Committee was created on Passive, Active, and Hybrid Control Systems;
- a joint initiative was approved in support of the International Decade for National Disaster Reduction (IDNDR); work starts with an international workshop in JAPAN, May 1991; joint U.S.-JAPAN research will be identified for targeted countries;
- two Japanese reports on base isolation systems were translated into English for distribution to the U.S. engineering community.

Refer to Resolutions of the 22nd Joint Meeting in this section for additional Panel information; refer to Task Committee Reports, found at the end of these Proceedings, for specific Panel accomplishments.

During the following week, 19-26 May, Panel members visited construction projects, disaster areas, and laboratories including:

Sunshine Skyway Cable Stayed Bridge, Tampa FL. A 1200 foot main span, 4.1 mile cast in place $250 million bridge replaced a twin truss bridge destroyed by a freighter in 1980. This is one of 12 completed cable-stayed bridges in the U.S. A set of three shock absorbers serve as effective damping devices for cable vibration.

Historic Charleston Foundation and The Citadel, Charleston, SC. A two day workshop focused on effects of Hurricane Hugo of 21 September 1989 and strengthening and rehabilitating contemporary and historic structures against multi-hazard environments. A tour of hurricane damages was made through historic Charleston and to two barrier islands -- Sullivan and Isle of Pine. Workshop concluded with a TV press conference.

Harbor (I-110) Transitway and Bridge Retrofit, Los Angeles CA. CALTRANS hosted visits to construction of I-110's 2.6 mile elevated bus/carpool HOV freeway section of the 19.6 mile ($435 million) at-grade highway linking San Pedro to Santa Monica. At the interchange of Routes 10/210 discussions focused on CALTRANS retrofit of the elevated bridge ramp to better resist earthquake loads.

Offshore Platform Conference, Long Beach, CA. Four presentations were made followed by visit to an offshore platform:

- Mineral Management Service, DOI is the regulatory agency for the offshore oil and gas industry. They lease sea plots (3 X 3 miles) between the 3 and 200 mile limit (some are between the 9 and 200 mile limit).

- Sandia National Laboratory described a new long-life seafloor earthquake measurement system (SEM) to collect earthquake data near offshore oil production fields. The SEM is battery-powered (8 yr. expected life) digital data acquisition system that telemeters data by a sonar link. SEM earthquake data indicates the seafloor's vertical acceleration is nearly an order of magnitude weaker than corresponding on-shore vertical motions. The data show that dryland shakes in vertical and horizontal directions while seafloors shake predominately in horizontal directions. These results aid in designing earthquake resistant offshore structures.

- Scripps Oceanographic Institute has a joint project with the Port and Harbour Research Institute, JAPAN; one of the six Japanese Government members participating in the Panel. The joint work involves developing numerical models for creating computer codes for seismic response analysis of offshore structures' pile foundations and model tests.

- Shell Oil Company leases sea plots off the east, south, and west U.S. coasts. Platforms in the southern California area are designed for strength of a 200 year return period and ductility for a 1000 year return period. Service-life of structures is 20 years.

The Panel members visited the offshore platform Eureka, located nine miles off-coast of Long Beach, CA. The structure is adjacent to the Palos Verde fault. Its discovery well was drilled in 1976; pumping commenced in 1980. Three platforms are operational in this area; 2-drilling (Eureka and Ellen) and 1-production (Elly). Ellen and Elly are in 265 feet of water (weight, 24K tons). Eureka is about one mile away and is in 700 feet of water. Its weight is 38K tons. Each drilling platform has capability to drill 80 wells; about 60 percent of well drilling capacity has been used. Production of Eureka is about 14K barrels per day.

UCSD Structural Engineering Laboratory, San Diego, CA. Discussions centered on research on developing a systems approach to seismic retrofits of bridge columns. Laboratory work is heavily supported by CALTRANS. Observed testing a retrofitted concrete column to earthquake loads. The procedure involves wrapping a column with prestressed wire.

Testing reveals this procedure to be effective against seismic loads. Also observed was a test specimen portion of a full-scale bridge deck which was retrofitted against earthquakes.

The Panel's efforts are exemplary of effective joint research and of technology delivery between researchers from JAPAN and the U.S. Since its conception 22-years ago, about 2000 papers have been presented, more than 40 joint workshops and conferences have been held, and over 100 guest researchers have been exchanged. Published proceedings document the Panel's work. The Panel provides important information about the U.S. and Japan's civil engineering thrusts which influence both countries' research and provide the basis for improvements in building codes and standards.

Lastly, this work was made possible by financial support from the: Bureau of Reclamation; Corps of Engineers; Department of State; Federal Emergency Management Agency; Federal Highway Administration; Minerals Management Service; National Science Foundation; Naval Facilities Engineering Command; and Nuclear Regulatory Commission.

Noel J. RAUFASTE, Secretary
U.S.-Side Panel on Wind and Seismic Effects

ABSTRACT

The 22nd Joint Meeting of the U.S.-Japan Panel on Wind and Seismic Effects was held at the National Institute of Standards and Technology during May 15-18, 1990. This publication, the proceedings of the Joint Meeting, includes the program, list of members, panel resolutions, task committee reports, and 39 technical papers.

The papers were presented under six themes: (I) - Wind Engineering, (II) - Storm Surge and Tsunamis, (III) - Joint Cooperative Research Program, (IV) - Earthquake Engineering, (V) - Loma Prieta Earthquake, and (VI) - Summaries of Task Committee Workshop Reports.

KEYWORDS: accelerograph; bridges; codes; concrete; design criteria; disaster; earthquakes; geotechnical engineering; ground failures; inelastic; lifelines; liquefaction; Loma Prieta; masonry; repair and retrofit; risk assessment; seismicity; soils; standards; storm surge; structural engineering; tsunami; and wind loads.

CONTENTS

CONTENTS

CONTENTS

CONTENTS

* Papers presented during site visit at Charleston, South Carolina on Monday, May 21, 1989.

AGENDA FOR 22nd JOINT UJNR MEETING

Tuesday 15 May

0930 Meet in Lobby of Holiday Inn for NIST Shuttle Bus to Administration Building

1000 **OPENING CEREMONIES** (Lecture Room B, Administration Building)

Call to order by Noel RAUFASTE, Secretary-General US Side, UJNR Panel
Opening remarks by John LYONS, Director, National Institute of Standards and Technology
Remarks by Takashi KISAKA, Counsellor for Science and Technology, Embassy of JAPAN
Remarks by Richard N. WRIGHT, Chairman US Side, UJNR Panel
Remarks by Toshio IWASAKI, Chairman JAPAN Side, UJNR Panel
Introduction of US Members by US Panel Chairman
Introduction of JAPAN Members by JAPAN Panel Chairman
Elect Joint Meeting Chairman
Adopt Agenda
Discuss Panel's contributions to IDNDR (Panel Chairmen to review international statements and respective JAPAN/US National Committee activities)
Adjourn

1130 Group Photograph

1200 **Lunch:** Hosted by John LYONS, Director NIST

THEME - WIND ENGINEERING

1300-1500 Technical Session - Wind Engineering
Chairman: Toshio IWASAKI

1300-1320 Meteorological Data from Hurricane Hugo, Joseph H. GOLDEN*, NOAA
1320-1340 Monitoring the Aerodynamic Performance of a Classic Suspension Bridge, Harold R. BOSCH*, FHWA
1340-1400 Cooperative Research Program on Wind Tunnel Testing in Turbulent Flow, Koichi YOKOYAMA*, Robert L. WARDLAW, Hiroshi SATO, Takaaki KUSAKABE, Michael G. SAVAGE
1400-1420 Wind on Offshore Platforms, Charles SMITH*, MMS
1420-1440 Discussions
1440-1500 Break

(* identifies oral presenters)

TASK COMMITTEE MEETINGS

1500-1700 T/C Meetings
T/C "A", Employees Lounge
T/C "C" & "D", Lecture Room B
T/C "F", CBT Conference Room, Bldg 226, Rm B221
T/C "I", Building Materials Conf. Room, Bldg 226, Rm. A368

1700 Conclusion of Day 1

1815 Meet at Lobby of Holiday Inn; travel by bus to BLACKIE'S HOUSE OF BEEF, 22nd and M Street N.W., Washington, DC
1930 US Members Hosted Dinner at BLACKIE'S HOUSE OF BEEF
2200 Return to Holiday Inn

Wednesday 16 May

0800 Meet in lobby of Holiday Inn for NIST Shuttle Bus to Administration Building

THEME - STORM SURGE AND TSUNAMIS

0830-1010 **Technical Session - Storm Surge and Tsunamis**
Chairman: Richard WRIGHT

0830-0850 Deep Ocean Recordings of Tsunamis, Frank I. GONZALEZ*, NOAA/PMEL
0850-0910 Measurement and Modeling of Coastal Storm Effects, William E. ROPER*, H. Lee BUTLER, Andrew GARCIA, CORPS
0910-0930 Storm Surge Modeling in the United States, Chester P. JELESNIANSKI*, Jye CHEN, Wilson A. SHAFFER, NOAA/NWS
0930-0950 Discussions
0950-1010 Break

THEME - JOINT COOPERATIVE RESEARCH

1010-1150 **Technical Session - Joint Cooperative Research**
Chairman: Richard WRIGHT

1010-1030 Precast Concrete Structure, Shin OKAMOTO; Shinsuke NAKATA*; Hisahiro HIRAISHI; Takashi KAMINOSONO; Hitoshi SHIOBARA; Mizuo INUKAI
1030-1050 U.S. Coordinated Program for Masonry Building Research Fifth Year Status, James L. NOLAND (Presented by H.S. LEW)
1050-1110 Design Guidelines of Medium Rise RM Buildings, Yutaka YAMAZAKI; Shin OKAMOTO*; Tsuneo OKADA; Akira MATSUMURA; Toshiyuki KUBOTA
1110-1130 U.S.-JAPAN Cooperative Research on Hybrid Control of Seismic Response of Bridge Structures, Jiro TAGUCHI; Toshio IWASAKI, Yoshio ADACHI; Yasushi SASAKI; Kazuhiko KAWASHIMA*
1130-1150 Discussions

1200-1300 **Lunch:** Hosted by Denis KWIATKOWSKI, Assistant Associate Director, Office of Natural and Technological Hazards Programs, FEMA

THEME - EARTHQUAKE ENGINEERING

1300-1440 **Technical Session - Earthquake Engineering-Part I**
Chairman: Richard WRIGHT

1300-1320 Lateral Resistance of a Pile, Michio OKAHARA; Shoji TAKAGI; Keiji TAGUCHI (Presented by Koichi YOKOYAMA)
1320-1340 Major Seismic Building Upgrades at the Lawrence Livermore National Laboratory, Frank J. TOKARZ, LLNL; Gary E. FREELAND*, LLNL; James R. HILL, DOE
1340-1400 Attenuation Characteristics of Ground Strains Induced During Earthquakes, Ken-ichi TOKIDA; Keiichi TAMURA*; Koh AIZAWA
1400-1420 Discussions
1420-1440 Break

TASK COMMITTEE MEETINGS

1440-1700 Task Committee Meetings
T/C "B" Employees Lounge
T/C "E" Lecture Room B
T/C "H" Conference Room B113
T/C "J" Conference Room B111

1700 Conclusion of day 2
1800 Individual US members hosted dinners

Thursday 17 May

THEME - EARTHQUAKE ENGINEERING

0830 Meet in Lobby of Holiday Inn for NIST Shuttle Bus to Administration Building

0900-1200 **Technical Session - Earthquake Engineering-Part II**
Chairman: Toshio IWASAKI

0900-0920 Dynamic Centrifugal Model Tests of Embankments on Liquefiable Grounds, Yasuyuki KOGA; Junichi KOSEKI (Presented by Keiichi TAMURA)
0920-0940 Seismic Resistance Requirements of Roller Compacted Dams, Alan T. RICHARDSON* and Louis H. ROEHM, BUREC
0940-1000 Damage of Soil Liquefaction Caused by Earthquakes and Use of Geomorphological Maps, Takekazu AKAGIRI*
1000-1020 Discussions
1020-1040 Break
1040-1100 Dynamic Deformation Characteristics of Compacted Rockfills by Cyclic Torsional Simple Shear Tests, Norihisa MATSUMOTO; Nario YASUDA; Masahiko OKUBO; Yasushi KINOSHITA (Presented by Kinji HASEGAWA)
1100-1120 Allowable Residual Displacement of Gravity Quaywall Given by Optimum Seismic Coefficient from Economical Viewpoint, Tatsuo UWABE*
1120-1140 The Relation Between the Building Damages and the Vibration Properties of Ground (in the case of Spitak Earthquake), Keiichi OHTANI*; Hiroyoshi KOBAYASHI
1140-1200 Discussions

1200-1300 **Lunch:** Hosted by Robert D. HANSON, Director, Biological and Critical Systems Division, NSF

1300-1440 **Technical Session - Earthquake Engineering Part III**
Chairman: Toshio IWASAKI

1300-1320 New Seismic Design Specifications of Highway Bridges in Japan, Toshio IWASAKI; Kazuhiko KAWASHIMA; Kinji HASEGAWA*
1320-1340 Scatter of Mechanical Properties of Structural Steels Recently Supplied in Japan, Hirofumi AOKI*; Hiroyuki YAMANOUCHI
1340-1400 Development on Effective Use of New Materials for Building Structures, Hiroyuki YAMANOUCHI; Tatsuo MUROTA (Presented by Hirofumi AOKI)
1400-1420 Discussions
1420-1440 Break

THEME - T/C WORKSHOP REPORTS

1440-1540 **Technical Session - Summary T/C Workshop Reports**
Chairman: Toshio IWASAKI

1440-1500 T/C "C&D" Workshop on Repair and Retrofit and Performance of Structures (Presented by Shin OKAMOTO)

1500-1520 T/C "J" Workshop on Bridges (Presented by James COOPER)

1520-1540 Discussions

1540 End of Technical Sessions

1540-1630 T/C Chairmen Meeting with Panel Secretaries to review T/C meetings, T/C reports, and IDNDR.

1630 Conclusion of Day 3

1730 Depart Holiday Inn for Potomac River Cruise on the Spirit of Washington, 6th and Water Streets S.W., Washington, DC

1830 Cruise on The Spirit of Washington

Friday 18 May

0800 Meet in Lobby of Holiday Inn for NIST Shuttle Bus to Administration Building

THEME - LOMA PRIETA EARTHQUAKE

0830-1200 **Technical Session - Loma Prieta Earthquake**
Chairman: Richard N. WRIGHT

0830-0845 Initial Overview of the San Francisco Bay and Santa Cruz Mountains Ground Motion, Gerald BRADY*, USGS
0845-0900 Site Response and Liquefaction, Ellis KRINITZSKY and Gus FRANKLIN*, WES/CORPS
0900-0915 Dam Performance During the Loma Prieta Earthquake of October 17, 1989, Robert B. MacDONALD*, BUREC
0915-0930 Performance of Wood-Framed Structures in the Loma Prieta Earthquake, John TISSELL*, American Plywood Association
0930-0950 Discussions
0950-1010 Break
1010-1025 Seismic Performance of Nonstructural Elements During the Loma Prieta Earthquake, T.T. SOONG*, NCEER and SUNY
1025-1040 Socioeconomic Impact of Lifeline Performance Related to the Loma Prieta Earthquake, Ronald EGUCHI* and M. PHIPPS, Dames and Moore
1040-1055 Lifelines Performance During the October 17, 1989 Loma Prieta Earthquake, M. KHATER and C. SCAWTHORN, EQE Engineering, Jerry ISENBERG, Weidlinger Associates, L. LUND, Consulting Engineer, T. LARSEN, EQE Engineering, and Masanobu SHINOZUKA*, Princeton University
1055-1115 Discussions
1115-1145 Summary Report on the Loma Prieta Earthquake of October 17, 1989, Toshio IWASAKI*, Kazuhiko KAWASHIMA
1145-1200 Discussions

1200-1300 **Lunch:** Hosted by Walter W. HAYS, Deputy Chief Research Applications, Office of Earthquakes, Volcanoes, and Engineering, USGS

TASK COMMITTEE REPORTS AND RESOLUTIONS

1300-1430 **Task Committee Reports**
Chairman: Richard N. WRIGHT

T/C A	Strong Motion Instrumentation Arrays and Data
T/C B	Large-scale Testing Program
T/C C	Repair and Retrofit of Existing Structures
T/C D	Evaluation of Performance of Structures
T/C E	Natural Hazard Assessment and Mitigation through Land-use Programs
T/C F	Disaster Prevention Methods for Lifeline Systems
T/C H	Soil Behavior and Stability During Earthquakes
T/C I	Storm Surge and Tsunamis
T/C J	Wind and Earthquake Engineering for Transportation Systems

1430-1445 Break

1445-1545 Adoption of Final Resolutions (including Panel actions on IDNDR)

1545-1555 Break

CLOSING CEREMONIES

1555 Call to Order by N.J. RAUFASTE, Secretary- General US Panel

Closing Remarks by Toshio IWASAKI, Chairman JAPAN Panel

Closing Remarks by R.N. WRIGHT, Chairman US Panel

1615 Conclusion of Technical Sessions

1800 JAPAN-side hosted dinner at the Japan Inn, 1715 Wisconsin Avenue, N.W. Washington, D.C.

LIST OF PANEL MEMBERS

UNITED STATES PANEL ON WIND AND SEISMIC EFFECTS
MEMBERSHIP LIST
1990

Dr. Richard N. Wright
Chairman
Director, Center for Building Technology
National Institute of Standards and Technology
U.S. Department of Commerce
Gaithersburg, MD 20899
301.975.5900 FTS 879.5900 FAX 301.975.4032

Mr. Noel J. Raufaste
Secretary-General
Head, Cooperative Research Programs
Center for Building Technology
National Institute of Standards and Technology
U.S. Department of Commerce
Gaithersburg, MD 20899
301.975.5904 FTS 879.5904 FAX 301.975.4032

Dr. S. T. Algermissen
Research Geophysicist
Office of Earthquake Studies
Branch of Earthquake Tectonics
Geological Survey
U.S. Department of the Interior
Denver, CO 80225
303.236.1611 FTS 776.1519 FAX 303.236.1519

Dr. Celso S. Barrientos
Supervisory Physical Scientist
INESDIS-E/RA28
Suitland Professional Center, Room 315
National Oceanic and Atmospheric Administration
U.S. Department of Commerce
5001 Silver Hill Road
Suitland, MD 20746
301.763.4178 FAX 301.420.1883

Dr. Eddie N. Bernard
Director, Pacific Marine Environmental Laboratory
National Oceanic and Atmospheric Administration
U.S. Department of Commerce
7600 Sand Point Way, NE
BIN C15700/Building 3
Seattle, WA 98115-0070
206.526.6239 FTS 392.6800 FAX 206.526.6815

Dr. Roger D. Borcherdt
Branch of Engineering Seismology and Geology
Geological Survey
U.S. Department of the Interior
345 Middlefield Road, MS 977
Menlo Park, CA 94025
415.329.5619 FTS 459.5619 FAX 415.329.5163

Dr. A. Gerald Brady
Physical Scientist
Branch of Engineering Seismology and Geology
Geological Survey
U.S. Department of the Interior
345 Middlefield Road, MS 977
Menlo Park, CA 94025
415.329.5664 FTS 459.5664 FAX 415.329.5163

Mr. H. Lee Butler
Chief, Research Division
Coastal Engineering Research Center
U.S. Army Engineer Waterways Experiment Station
Office CEWES-CR
P.O. Box 631
Vicksburg, MS 39180-0631
601.634.2405 FTS 542.2405 FAX 601.634.4314

Dr. Ken P. Chong
Program Director of Structures and Building Systems
Directorate of Engineering
National Science Foundation
1800 G Street, N.W., Room 1108
Washington, D.C. 20550
202.357.9542 FAX 202.357.7636

Mr. James D. Cooper
Deputy Chief, Structures Division, HNR-10
Federal Highway Administration
U.S. Department of Transportation
6300 Georgetown Pike
McLean, VA 22101
703.285.2447 FAX 703.285.2379

Dr. A. G. Franklin
Chief, Earthquake Engineering & Geophysics Division
CEWES-GH Geotechnical Laboratory
U.S. Army Engineer Waterways Experiment Station
3909 Halls Ferry Road
Vicksburg, MS 39180-3909
601.634.2658 FTS 542.2658 FAX 601.634.3139

Mr. G. Robert Fuller
Chief, Manufactured Housing Compliance Branch
Room 9156
U.S. Department of Housing and Urban Development
Washington, DC 20410-8000
202.708.1920 FAX 202.708.0299

Mr. James H. Gates
Caltrans - Structures
P. O. Box 942874
Sacramento, CA 94274
916.445.1439 FAX 916.445.0574

Mr. Peter E. Gurvin
Assistant Director for Buildings Design and Engineering
Office of Foreign Buildings Operations
A/FBO, SA-6, Room 327
P.O. Box 12248
U.S. Department of State
Rosslyn Station
Arlington, VA 22209
703.875.6117 FAX 703.875.6204

Dr. Robert D. Hanson
Division Director, Division of Biological & Critical Systems
National Science Foundation
1800 G Street, N.W.
Washington, DC 20550
202.357.9545 FAX 202.357.9803

Dr. Walter W. Hays
Deputy for Research Application
Office of Earthquake Survey
905 National Center
Geological Survey
U.S. Department of the Interior
Reston, VA 22092
703.648.6711 FAX 703.648.6717

Dr. William B. Joyner
Geophysicist
Branch of Ground Motion & Faulting
Geological Survey
U.S. Department of the Interior
345 Middlefield Road, MS 977
Menlo Park, CA 94025
415.329.5640 FTS 459.5640 FAX 415.329.5163

Mr. Roger M. Kenneally
Structural Engineer
Structural and Seismic Engineering Branch
Seismic Section
Office of Nuclear Regulatory Research
U.S. Nuclear Regulatory Commission
Washington, DC 20555
301.492.3893 FAX 301.443.7836

Mr. James P. Knight
Office of Nuclear Safety (EH-33)
U. S. Department of Energy
Washington, D.C. 20545
301.353.3548 FTS 233.3548 FAX 301.353.5285

Mr. Richard W. Kramer
Technical Review Staff, D-3210
Bureau of Reclamation
U. S. Department of the Interior
P.O. Box 25007
Denver, CO 80225
303.236.8539 FTS 776.8539 FAX 202.647.5269

Mr. Paul F. Krumpe
Physical Scientist
Office of U.S. Foreign Disaster Assistance
Agency for International Development
U.S. Department of State
Washington, DC 20523
202.647.9758 FAX 202.647.5269

Dr. H.S. Lew
Chief, Structures Division
Center for Building Technology
National Institute of Standards and Technology
U.S. Department of Commerce
Gaithersburg, MD 20899
301.975.6061 FTS 879.6061 FAX 301.975.4032

Mr. Tingley K. Lew
Research Structural Engineer
Structures Division, Code L51
Naval Civil Engineering Laboratory
Port Hueneme, CA 93043
805.982.1234 FAX 805.982.1418

Dr. Shih-Chi Liu
Program Director, Structural Systems
Division of Biological and Critical Systems
National Science Foundation
1800 G Street, N.W., Room 1132
Washington, DC 20550
202.357.9780 FAX 202.357.9803

Mr. Robert B. MacDonald
Manager, Geology Branch
Engineering and Research, Code D-3610 A
Bureau of Reclamation
U.S. Department of the Interior
Building 67, Denver Federal Center
Denver, CO 80225
303.236.6904 FTS 776.8643 FAX 303.236.6763

Dr. Richard D. Marshall
Structural Research Engineer
Structures Division
Center for Building Technology
National Institute of Standards and Technology
U.S. Department of Commerce
Gaithersburg, MD 20899
301.975.6071 FTS 879.6071 FAX 301.975.4032

Dr. Wayne N. Marchant
Chief, Research and Laboratory Services Division
P. O. Box 25007
Code D-3700
Bureau of Reclamation
U.S. Department of the Interior
Denver, CO 80225
303.236.5983 FTS 776.5983 FAX 303.236.7664

Dr. Francis G. McLean
Chief, Geotechnical Engineering and Embankment
Dams Branch
P.O. Box 25007
Bureau of Reclamation
U.S. Department of the Interior
Denver, CO 80225
303.236.3854 FTS 776.3854 FAX 303.236.6763

Mr. Herbert Meyers
Chief, Earth Geophysics
National Geophysical Data Center
National Oceanic and Atmospheric Administration
U.S. Department of Commerce
325 Broadway
Boulder, CO 80303-3328
303.497.6521 FTS 320.6521 FAX 303.497.6513

Dr. William E. Roper
Assistant Director
Research and Development (Civil Works)
US Army Corps of Engineers
20 Massachusetts Avenue, N.W
Washington, DC 20314-1000
202.272.0257 FAX 202.272.0907

Dr. Erwin L. Schaffer
Assistant Director, Wood Products Research
Forest Products Laboratory
Forest Service
U.S. Department of Agriculture
One Gifford Pinchot Drive
Madison, WI 53705-2398
608.264.5672 FTS 364.5672 FAX 608.231.9592

Mr. Charles E. Smith
Research Program Manager
Offshore Minerals Management
Technology Assessment and Research Branch
Minerals Management Service
U.S. Department of the Interior
381 Elden Street
Herndon, VA 22070-4817
703.787.1559 FAX 703.787.1010

Dr. T. T. Soong
Samuel P. Capen Professor
Department of Civil Engineering
National Center for Earthquake Engineering Research
State University of New York at Buffalo
212 Ketter Hall
Buffalo, NY 14260
716.636.2469 FAX 716.636.3733

Mr. Kenneth F. Sullivan
Lifelines Project Manager
Earthquakes and Natural Hazards Division
Federal Emergency Management Agency
Washington, DC 20472
202.646.2889 FAX 202.646.3104

Mr. Edward F. Younger
Director, Structural Engineering Service
Code 088C1
Office of Facilities
Department of Veterans Affairs
810 Vermont Avenue, N.W.
Washington, DC 20420
202.233.2864 FTS 373.2864 FAX 202.233.7854

ALTERNATE MEMBERS

Dr. Clifford J. Astill
Program Director
Division of Fundamental Research for Critical
Engineering Systems
National Science Foundation
1800 G Street, N.W.
Washington, DC 20550
202.357.9500 FAX 202.357.9803

Dr. Mehmet K. Celebi
Research Civil Engineer
Branch of Engineering Seismology and Geology
Geological Survey
U.S. Department of the Interior
345 Middlefield Road, MS 977
Menlo Park, CA 94025
415.329.5623 FTS 459.5623 FAX 415.329.5163

Mr. Michael Changery
Chief, Applied Climatology Branch
National Climatic Center
National Oceanic and Atmospheric Administration
U. S. Department of Commerce
Federal Building
Asheville, NC 28801
704.259.0765 FTS 672.0765 FAX 704.259.0246

Mr. Vincent P. Chiarito
Research Structural Engineer
Structural Mechanics Division
Structures Laboratory
U.S. Army Engineer Waterways Experiment Station
3909 Halls Ferry Road
Vicksburg, MS 39108-6199
601.634.2714 FAX 601.634.2309

Dr. James F. Costello
Senior Structural Engineer
Structural and Seismic Engineering Branch
Structural Section
Office of Nuclear Regulatory Research
U.S. Nuclear Regulatory Commission
Mail Stop 007NL
Washington, DC 20555
301.492.3818 FAX 301.443.7836

Mr. Lucian G. Guthrie
Structural Engineer
Office of Chief of Engineers
HQUSACE (CEEC-ED)
U.S. Department of the Army
20 Massachusetts Avenue, N.W.
Washington, DC 20314-1000
202.272.8673 FAX 202.272.1485

Mr. James R. Hill
Manager, Natural Hazards Mitigation Programs
Office of Safety, Health and Quality Assurance
U.S. Department of Energy
Washington, DC 20545
301.353.4508 FAX 301.353.5285

Dr. James R. Houston
Chief, Coastal Engineering Research Center
US Army Engineer Waterways Experiment Station
P.O. Box 631
Vicksburg, MS 39180-0631
601.634.2000 FAX 601.634.2655

Mr. Robert R. Ledzian
Senior Staff Assistant for Research
Office of Liaison - Engineering Research, Code 3020
Bureau of Reclamation
U.S. Department of the Interior
18th & C Streets, N.W.
Washington, DC 20240
202.343.2013 FAX 343.2252

Mr. Ronald J. Morony
Director, Innovative Technology and Special
  Projects Division
Office of Policy Development and Research
U.S. Department of Housing and Urban Development
Washington, DC 20410-6000
202.755.0640 FAX 202.755.0299

Dr. J. Eleonora Sabadell
Director, Natural and Manmade Hazards Mitigation
Program
Directorate of Engineering
National Science Foundation
1800 G Street, N.W.
Washington, DC 20550
202.357.9780 FAX 202.357.9803

Dr. John B. Scalzi
Program Director for Structures and Building Systems
National Science Foundation
1800 G Street, N.W.
Washington, DC 20550
202.357.9542 FAX 202.357.7636

JAPAN PANEL ON WIND AND SEISMIC EFFECTS
MEMBERSHIP LIST
1990

Dr. Toshio Iwasaki
Chairman
Director-General
Public Works Research Institute
Ministry of Construction
1, Asahi, Tsukuba-shi,
Ibaraki-ken 305
Tel. 0298-64-2211

Dr. Yoshio Adachi
Secretary-General
Director, Planning and Research Administration Department
Public Works Research Institute
Ministry of Construction
1, Asahi, Tsukuba-shi,
Ibaraki-ken 305
Tel. 0298-64-2211

Mr. Tadao Dohi
Head, Geographic Department
Geographical Survey Institute
Ministry of Construction
1, Kitazato, Tsukuba-shi
Ibaraki-ken 305
Tel. 0298-64-1111

Mr. Tokunosuke Fujitani
Chief, The Second Research Laboratory
Applied Meteorology Research Division
Meteorological Research Institute
Japan Meteorological Agency
1-1 Nagamine, Tsukuba-shi,
Ibaraki-ken 305
Tel. 0298-51-7111

Mr. Minoru Fujiwara
Head, Bridge Division
Structure and Bridge Department
Public Works Research Institute
Ministry of Construction
1, Asahi, Tsukuba-shi,
Ibaraki-ken 305
Tel. 0298-64-2211

Dr. Masaya Hirosawa
Deputy Director General
Building Research Institute
Ministry of Construction
1, Tatehara, Tsukuba-shi,
Ibaraki-ken 305
Tel. 0298-64-2151

Dr. Kazuhiko Kawashima *
Head, Earthquake Engineering Division
Earthquake Disaster Prevention Department
Public Works Research Institute
Ministry of Construction
1, Asahi, Tsukuba-shi,
Ibaraki-ken 305
Tel. 0298-64-2211

Dr. Yoshikazu Kitagawa
Director
Testing and Evaluation Department
Building Research Institute
1, Tatehara, Tsukuba-shi,
Ibaraki-ken 305
Tel. 0298-64-2151

Mr. Yasuyuki Koga
Head, Soil Dynamics Division
Construction Method and Equipment Department
Public Works Research Institute
Ministry of Construction
1, Asahi, Tsukuba-shi,
Ibaraki-ken 305
Tel. 0298-64-2211

Dr. Norihisa Matsumoto
Head, Fill Type Dam Division
Dam Department
Public Works Research Institute
Ministry of Construction
1, Asahi, Tsukuba-shi,
Ibaraki-ken 305
Tel. 0298-64-2211

Mr. Tatsuo Murota
Director, Structural Engineering Department
Building Research Institute
Ministry of Construction
1, Tatehara, Tsukuba-shi,
Ibaraki-ken 305
Tel. 0298-64-2151

Dr. Shinsuke Nakata
Head, Structural Division
International Institute of Seismology and Earthquake Engineering
Building Research Institute
Ministry of Construction
1, Tatehara, Tsukuba-shi,
Ibaraki-ken 305
Tel. 0298-64-2151

Dr. Setsuo Noda
Director, Structural Engineering Division
Port and Harbour Research Institute
Ministry of Transport
3-1-1, Nagase, Yokosuka,
Kanagawa-ken 239
Tel. 0468-41-5410

Mr. Keiichi Ohtani
Head, Earthquake Disaster Prevention Laboratory
National Research Center for Disaster Prevention
Science and Technology Agency
3-1, Tennodai, Tsukuba-shi,
Ibaraki-ken 305
Tel. 0298-51-1611

Mr. Shin Ohtsuka
Head, Typhoon Research Division
Meteorological Research Institute
Japan Meteorological Agency
1-1, Nagamine, Tsukuba-shi
Ibaraki-ken 305
Tel. 0298-51-7111

Mr. Michio Okahara
Head, Foundation Engineering Division
Structure and Bridge Department
Public Works Research Institute
Ministry of Construction
1, Asahi, Tsukuba-shi
Ibaraki-ken 305
Tel. 0298-64-2211

Dr. Shin Okamoto
Director, International Institute of Seismology and Earthquake Engineering
Building Research Institute
Ministry of Construction
1, Tatehata, Tsukuba-shi,
Ibaraki-ken 305
Tel. 0298-64-2151

Dr. Norio Oyagi
Director, Third Research Division
National Research Center for Disaster Prevention
Science and Technology Agency
3-1, Tennodai, Tukuba-shi,
Ibaraki-ken 305
Tel. 0298-51-1611

Dr. Yasushi Sasaki
Director, Earthquake Disaster Prevention Department
Public Works Research Institute
Ministry of Construction
1, Asahi, Tsukuba-shi,
Ibaraki-ken 305
Tel. 0298-64-2211

Dr. Masaaki Seino
Head, Seismology and Volcanology Research Division
Meteorological Research Institute
Japan Meteorological Agency
1-1, Nagamine, Tsukuba-shi
Ibaraki-ken 305
Tel. 0298-51-7111

Mr. Yukitake Shioi
Director, Structure and Bridge Department
Public Works Research Institute
Ministry of Construction
1, Asahi, Tsukuba-shi,
Ibaraki-ken 305
Tel. 0298-64-2211

Dr. Katsutoshi Tanimoto
Director, Hydraulic Engineering Division
Port and Harbour Research Institute
Ministry of Transport
3-1-1, Nagase, Yokosuka,
Kanagawa-ken 239
Tel. 0468-41-5410

Mr. Ken-ichi Tokida
Head, Ground Vibration Division
Earthquake Disaster Prevention Department
Public Works Research Institute
Ministry of Construction
1, Asahi, Tsukuba-shi,
Ibaraki-ken 305
Tel. 0298-64-2211

Dr. Takaaki Uda
Head, Coastal Engineering Division
River Department
Public Works Research Institute
Ministry of Construction
1, Asahi, Tsukuba-shi,
Ibaraki-ken 305
Tel. 0298-64-2211

Dr. Tatsuo Uwabe
Chief, Disaster Prevention Laboratory
Structural Engineering Division
Port and Harbour Research Institute
Ministry of Transport
3-1-1, Nagase, Yokosuka-shi
Kanagawa-ken 239
Tel. 0468-44-5030

Dr. Hiroyuki Yamanouchi
Head, Structural Dynamics Division
Structural Engineering Department
Building Research Institute
Ministry of Construction
1, Tatehara, Tsukuba-shi,
Ibaraki-ken 305
Tel. 0298-64-2151

Dr. Yutaka Yamazaki
Head, Large-scale Structure Testing Division
Production Department
Building Research Institute
Ministry of Construction
1, Tatehara, Tsukuba-shi,
Ibaraki-ken 305
Tel. 0298-64-2151

Mr. Koichi Yokoyama *
Head, Structure Division
Structure and Bridge Department
Public Works Research Institute
Ministry of Construction
1, Asahi, Tsukuba-shi,
Ibaraki-ken 305
Tel. 0298-64-2211

* Secretary

LIST OF TASK COMMITTEE MEMBERS

Task Committee	US Side	Japanese Side
A. Strong-Motion Instrumentation Arrays and Data	*A.G. Brady M.K. Celebi A.F. Franklin W.B. Joyner R.B. MacDonald F.G. McLean H. Meyers	*S. Noda S. Hattori M. Ichikawa Y. Ishiyama K. Ohtani Y. Sasaki H. Yamanouchi
B. Large-Scale Testing Programs	*H.S. Lew C.E. Smith	*K. Ohtani Y. Koga S. Noda S. Okamoto K. Yokoyama H. Yamanouchi
C. Repair and Retrofit of Existing Structures	*K.P. Chong P.E. Gurvin H.S. Lew R.J. Morony J.B. Scalzi	*M. Hirosawa T. Iwasaki S. Okamoto H. Shinohara
D. Evaluation of Structural Performance	*G.R. Fuller M.K. Celebi R.D. Marshall J.B. Scalzi	*S. Okamoto T. Hanafusa** K. Masamura** T. Murota** M. Okahara H. Shinohara H. Yamanouchi K. Yokoyama**
E. Natural Hazard Assessment and Mitigation Through Land Use Programs	*S.T. Algermissen C.S. Barrientos A.G. Brady G.R. Fuller R.D. Marshall	*K. Kawashima S. Hattori T. Iwasaki M. Nagaoka Y. Sugimura T. Uwabe

Task Committee-continued	US Side	Japanese Side
F. Disaster Prevention Methods for Lifeline Systems	*S.C. Liu M.K. Celebi J.D. Cooper T. Liu J.B. Scalzi J.S. Spencer K.F. Sullivan S. Wu	*Y. Sasaki K. Kawashima T. Murota S. Noda K. Ohtani M. Shinozuka T. Uwabe
H. Soil Behavior and Stability During Earthquakes	*A.G. Franklin F.G. McLean C.E. Smith	*K. Tokuda Y. Koga N. Matsumoto M. Okahara Y. Sugimura H. Tsuchida
I. Storm Surge and Tsunamis	*H. Meyers C.S. Barrientos E.N. Bernard L. Butler	*T. Uda M. Ichikawa K. Kurashige K. Masamura M. Okada N. Oyagi H. Takahashi K. Tanimoto
J. Wind and Earthquake Engineering for Transportation Systems	*J.D. Cooper A.G. Franklin J.H. Gates J.B. Scalzi	*S. Saeki M. Fujiwara T. Iwasaki K. Kawashima M. Okahara Y. Sasaki K. Yokoyama

*Chairman

February 1990

RESOLUTIONS OF THE TWENTY-SECOND JOINT MEETING U.S.-JAPAN PANEL ON WIND AND SEISMIC EFFECTS (UJNR)

National Institute of Standards and Technology
Gaithersburg, MD 20899

May 15-18, 1990

The following resolutions are hereby adopted:

1. The Twenty-Second Joint Panel Meeting provided an opportunity to exchange valuable technical information which was beneficial to both countries. In view of the importance of cooperative programs on the subject of wind and seismic effects, the continuation of Joint Panel Meetings is considered essential.

2. The following activities have been conducted since the Twenty-First Joint Meeting:

   a. Guest researchers from both countries performed joint research that advanced the state of wind and earthquake engineering.

   b. Technical documents, research reports and proceedings of workshops were exchanged.

   c. The Japanese MOC documents, on base isolation systems for buildings were translated into English. They will be reviewed by both sides for corrections and approval, published, and disseminated to appropriate US and Japanese engineering community members. The National Technical Information Service of DoC will hold a press briefing to promote the availability of these reports.

   d. Workshops and a special Panel Theme were held:

      a) Joint Workshop on Repair, Retrofit and Evaluation of Structures, Task Committees (C) and (D), at Gaithersburg, MD, May 12-14, 1990.

      b) Sixth Bridge Workshop, Task Committee (J), at Lake Tahoe, Nevada, May 7-12, 1990.

      c) Held a special Panel Theme on "Loma Prieta Earthquake of October 17, 1989" to summarize the investigations performed by both sides.

3. Experiences from the post-Hurricane Hugo U.S. fact finding team visits to the affected U.S. East Coast and to the Virgin Islands on September 1989 were reported. Experiences from the UJNR Coordinated Post-earthquake fact finding team's

visits to the sites of damaged structures from the October 17, 1989, Loma Prieta Earthquake were reported. The Panel recognizes the importance of using these findings and experiences and encourages similar exchanges of information from future post-disaster investigations. Information transfer will include reports,
seminars, and special Panel sessions as used at the Twenty-Second Joint Meeting.

4. The Panel will continue to seek methods to contribute to the International Decade of Natural Disaster Reduction (IDNDR) such as exchanging Proceedings of Task Committees and Panel Meetings with their respective Country's National Committees of IDNDR, compiling bibliographies of research findings on wind and seismic effects, and holding workshops and seminars. This work will be performed by the U.S. and Japan Sides' Secretaries.

5. The Panel approves the redefinitions of the scope of T/C "E" which redirects its emphasis to ground motion, microzonation, and seismic design forces. The Panel also approves its name change to Task Committee (E) on "Ground Motion and Seismic Design Forces".

6. The Panel recognizes the importance of research being carried out both in the U.S. and Japan on passive, active, and hybrid control systems. At the recommendation of Task Committees (B), (F) and (J), the Panel approves the establishment of a new Task Committee (T/C "G") on Passive, Active, and Hybrid Control Systems.

7. The Panel recognizes the importance of the work by both sides in the US-Japan Joint Research Program on Precast Seismic Structural Systems (PRESSS). Information about the program will continue to be exchanged during the coming year.

8. The Panel accepts each Task Committee's report developed during the Twenty-Second Joint Meeting. Each report presents objectives, current and proposed scope of work, and past and expected accomplishments.

9. The Panel endorses the following proposed Task Committee workshops:

   a. Task Committee (A) is planning its 3rd Workshop on Processing Strong Motion Records, with concentration on array data. The workshop is targeted for May or June 1991.

b. Task Committee (C) is planning a workshop on the Design Approaches and Construction Methods for Repair and Retrofit of Buildings and Structures; May, 1991, in Japan.

c. Task Committee (D) proposes holding a workshop on "Structural Performance Evaluation Methodologies" prior to the 23rd Joint Panel Meeting in Tsukuba.

d. Task Committee (E) proposes holding a workshop on Ground Motion and Seismic Design Forces in Japan in 1991.

e. Task Committee (F) proposes holding a workshop on Disaster Prevention for Lifeline Systems, tentatively scheduled in the U.S. in 1991.

f. Task Committee (H) proposes holding its second workshop on Remedial Treatment of Potentially Liquefiable Soils, in Japan, between October 1990 and March 1991.

g. Task Committee (I) will hold its workshop on Tsunamis, in Honolulu in November 1990.

h. Task Committee (J) will hold its Seventh Bridge Workshop, scheduled in Japan just prior to the 23rd UJNR Joint Meeting.

Scheduling for these workshops shall be performed by the US and Japan chairmen of the respective Task Committees with concurrence of the Joint Panel chairmen. Results of each activity shall be presented at the 23rd Joint Panel Meeting.

10. The Panel recognizes the importance of continued exchange of personnel, technical information, research results, and recorded data that lead to mitigating losses from earthquakes and strong winds. The Panel also recognizes the importance of using available large-scale testing facilities in both countries. Thus, these activities should continue to be strengthened and expanded and, as appropriate, share Task Committee activities at other meetings that have technical interests in the Task Committee activities. To facilitate these exchanges, the Panel will provide official endorsement.

11. The Twenty-Third Joint Meeting of the UJNR Panel on Wind and Seismic Effects will be held at PWRI, Tsukuba, Japan, May 1991. Specific dates, program, and itinerary will be proposed by the Japan Panel with concurrence of the U.S. Panel.

Theme I

Wind Engineering

Meteorological Data From Hurricane Hugo

by

Joseph H. Golden[1]

ABSTRACT

We shall describe and examine critically the meteorology of Hurricane HUGO as it passed through the Eastern Caribbean on maximum surface winds and central pressure place it as a Category 4 hurricane on the Saffir/Simpson scale. While it was approaching the Leeward Islands, reconnaissance aircraft measured a record-tying 165 kts. Selected data from surface sites, NOAA aircraft and satellites have been gathered and will be used to synthesize HUGO's evolving dynamic structure as it ravaged the U.S. Virgin Islands and Eastern Puerto Rico. Peak winds and rainfall amounts were within the envelope of extrema produced by three previous intense hurricanes which have impacted the region this century. However, we shall demonstrate that Hurricane HUGO underwent some unusual mesoscale oscillations in its track through the Eastern Caribbean. Contrary to widespread rumors in the news-media, we could find no evidence from an extensive aerial damage survey of any tornadoes; however, eyewitness accounts and damage assessments both point to the periodic production of destructive microbursts beneath the major rainbands and eyewall of HUGO. Flooding and landslides were minimal except for serious urban flooding in San Juan, and rainfall amounts up to 13-15 inches were found in orographically favorable areas of the islands. Finally, we shall summarize overall forecasting performance for HUGO in the Caribbean, and conclude that, overall, official track forecasts and warning lead-times were better than 10-year averages for previous tropical cyclones affecting this area. We conclude by pointing out the degraded state of the surface and upper-air observing network in the region and suggest follow-up research and needed improvements in the network for both forecasters and researchers.

KEYWORDS: Meteorology; forecasting; warning; hurricane; wind; pressure; reconnaissance.

---

[1]Office of the Chief Scientist, NOAA
Washington, D.C. 20235

1. INTRODUCTION

Hurricane HUGO had its origins in a strong tropical disturbance which moved off the African coast on September 9, 1989. The disturbance was accompanied by an area of intense thunderstorms which was visible on satellite imagery. The official National Hurricane Center (NHC) track for HUGO begins on the 10th, when a tropical depression formed to the southeast of the Cape Verde Islands (see Fig.1). HUGO moved westward at a fast clip, 18 knots, across the Eastern Atlantic, intensifying to tropical storm stage on the 11th and full hurricane on the 13th (Fig. 2 satellite photo, when HUGO was about 1100 n mi east of the Leeward Islands).

Hurricane HUGO therefore belongs to a class of major hurricanes which has been termed "Cape Verde" storms. These storms usually originate from strong African wave disturbances which intensify as they move off the West African Coast and produce a tropical depression (in rare cases, tropical storm) as they pass close to the Cape Verde Islands. This early intensification and vortex development climatologically favors further intensification, as the storm traverses a long stretch of very warm tropical Atlantic waters at low latitudes (thus reducing chances of weakening or early recurvature, due to interactions with mid latitude westerly flow aloft). Other notable Cape Verde hurricanes of this century which have affected Puerto Rico and the Virgin Islands include the famous West Indian hurricane of September 10-20, 1928; the "San Ciprian storm" of 1932; the "Santa Clara storm" of 1956; Frederic and David, 1979; and Donna, 1960. The 1928 "San Felipe" hurricane traversed the island of Puerto Rico from the eastsoutheast and produce 30-year record rainfalls (up to 25-30 inches), a lowest barometer reading of 27.50" at Guayama, and recorded windspeeds gusting to 160 mph (probable peak gust). Additional details on the San Felipe Hurricane are given by Fassig (1928). That same hurricane reintensified after moving off the northwest coast of Puerto Rico and struck the Southeast Florida Coast as a category 4 storm on the Saffir-Simpson scale (Hebert et al, 1984). According to Hebert and Taylor (1988), the September, 1928 hurricane was also the second deadliest hurricane to affect the U.S. during this century, killing 1836 people in the Lake Okeechobee, Florida area (Table 1). Goodman (1989) did a statistical analysis of these and other tropical storms that affected Puerto Rico during 1886-1988. He concluded (well before HUGO) that there was at least a 50% probability of a tropical cyclone "hit" or "near miss" in Puerto Rico during the 1989 season. Other

interesting meteorological aspects of Hurricane HUGO, in the context of the 1989 Atlantic hurricane season as a whole, are discussed by Case (1990).

During the night of September 14, 1989, Hurricane HUGO began to slow its forward speed and turn more towards the westnorthwest. This was in response to a weakening of the high pressure ridge to the north of the storm. As sometimes noted by hurricane forecasters when a hurricane slows its forward motion in a favorable tropical air/ocean environment, HUGO appeared to strengthen appreciably on the 14th and 15th. A visible NOAA-GOES satellite photo of HUGO on the 14th is shown in Fig.3 (note the well-developed eye).

2. AIRCRAFT RECONNAISSANCE

When the first NOAA reconnaissance aircraft was able to reach HUGO at mid-day on the 15th, the central pressure in the eye was 918 mb, and one-minute sustained windspeeds of 165 kts were measured at 1500 ft altitude. These data indicated that HUGO had intensified to a rare category 5 status on the Saffir-Simpson scale (Hebert et al, 1984). Fig. 4 shows an enlarged visible GOES satellite image of HUGO near the time of the NOAA aircraft penetration. It should be noted that the minimum pressure found at this time ties the Atlantic record (with Hurricane GLORIA, 1985, when it was north of Puerto Rico). Fig.5a, 5b shows the radar PPI reflectivity pattern measured by the NOAA WP3D aircraft with its 5 cm fuselage radar, and a NW-SE radar cross-section through the hurricane's eye obtained with the 3 cm tail radar, respectively (see Dodge et. al, 1990). These remarkable photographs show that the eyewall sloped outward slightly with height, and had higher reflectivities reaching greater heights (14 km) in the northwestern sector than in the southeastern portion of the wall-cloud. Most unusual was the location of the highest reflectivities (in excess of 50 dBz) in the southwest quadrant of the eyewall. Close to the time of Fig. 5a,b, one of the NOAA WP3D aircraft penetrated the eyewall at 1500 ft (unfortunately, near the reflectivity maximum in the southwestern quadrant of the wall-cloud in Fig. 5a). The aircraft-measured radial plots of one-minute average tangential winds and surface pressure are shown in Fig. 6. Note that the pressure drops most rapidly inward through the inner rainbands and especially the wall-cloud of HUGO, to a minimum of 918 mb in the eye itself. Correspondingly, the extreme pressure gradients in the same core region are associated with windspeed maxima, at flight altitude, of about 73 and 80 m/s (through the SW and NE portions of the wallcloud, respectively). During this flight penetration, the NOAA aircraft experienced extreme turbulence and/or windshear, lost one of its four engines (which caught fire), and dropped from 1500 down to 800 ft before recovering flight control and circling inside HUGO's eye. Fortunately, the aircraft was able to return safely to land at the nearest airport on Barbados. Subsequent inspection revealed no structural damage, and F. Marks and others at NOAA/HRD/AOML in Miami are researching the data taken during this and other flights into HUGO; these data include Doppler wind measurements made in the rainbands of HUGO with the aforementioned NOAA P-3 tail radar (see also Marks and Houze, 1984, for Doppler analyses made on Hurricane Debby).

3. MESOSCALE VARIATIONS IN STORM AND STRUCTURE

The well-developed eye of HUGO approached the Lesser Antilles during the afternoon of the 16th. A remarkable striated structure in the cirrus outflow clouds emanating from the hurricane's northern portion is illustrated in the visible satellite photo of Fig.7. A time-series plot of aircraft-measured surface central pressures and eye diameters estimated from aircraft radars is shown in Fig.8. Note that the time-history of surface pressure in the eye begins near the time of the record-equalling measurements on the afternoon of the 15th--core pressures rose appreciably during the following 24 hour period. An unusual feature is that the peak aircraft winds during the same period remained nearly constant at about 140 mph. Some of the problems in relating aircraft reconnaissance winds, usually measured at 10,000 ft, to surface winds measured by anemometers in hurricane have been addressed by Powell (1980), Black et al (1988) and Powell and Black (1990). Eye diameters fluctuated during this same period until mid-day on the 16th, when Air Force reconnaissance aircraft reported a double, concentric eyewall structure (the significance of the double eyewall structure for intense hurricanes was noted by Willoughby et al, 1984 for a class of hurricanes and Golden in the NAS/NRC Report on Hurricane ALICIA, 1983 - see Savage et al, 1984). The outer eyewall diameter of HUGO was about 30 km, and the inner one was about 18 km across. An unusual feature of the hurricane, as it passed through the Lesser Antilles and Virgin Islands from mid-day on the 16th through the morning of the 19th (when it was northwest of Puerto Rico) was the large fluctuations of the eye's diameter (from 15 to 35 km across, see Fig.8).

4. IMPACTS ON THE ISLANDS

During the late night hours of Saturday, September 16, the eye of Hurricane HUGO passed over the island of Guadeloupe (see Fig.1, near 16.4°N, 61.8°W). The capital city, Pointe-A-Pitre, reported a final weather observation of heavy showers and thunderstorms with NNW winds of 29 kts, gusting to 84 kts. At the same time the island of St. Maarten reported NE winds 13-15 kts, and St. Kitts, north winds 21 kts gusting to 33 kts. Reports after HUGO's passage over Guadeloupe revealed that about half the capital was destroyed, including the airport and there were 11 fatalities (Table 2). HUGO continued moving westnorthwestward into the Caribbean Sea as a category 4 hurricane with peak sustained winds of 140 mph (as measured by reconnaissance aircraft). Besides Guadeloupe, the smaller island of Montserrat to the northwest suffered severe damages and 10 people were killed.

The storm slowed its forward motion to 8 kts during the day of the 17th and deepened about 15 mb (flight-level maximum winds from reconnaissance aircraft fluctuated from 95-145 kts during the same period). By the evening of the 17th, both satellite and aircraft eye fixes indicated that HUGO was turning more towards the northwest, thus increasing the threat to the U.S. and British Virgin Islands, especially St. Croix and St. Thomas, as well as the northeast coast of Puerto Rico. A basemap of key islands and city locations cited in the text is given in Fig.9. A GOES satellite view of HUGO on the afternoon of Sept. 17 is given in Fig.10.

St. Croix clearly experienced an unusually prolonged battering of hurricane force (and much greater) winds from late evening on the 17th into the next morning. It was noted in the 9:00 p.m. AST advisory from the National Hurricane Center that St. Croix reported sustained winds of 85 mph and gusts to 97 mph, with St. Thomas reporting gusts to 90 mph during the preceding hour. Both islands further reported wind gusts of 100 mph during the following hour. Fig.11 shows a mesoscale analysis of HUGO's track through the U.S. Virgin Islands and Eastern Puerto Rico, derived from San Juan's NWS radar film and NHC's official fixes. Note that by early afternoon on the 17th, in response to subtle, poorly-observed large scale changes in HUGO's environment (noted above), the storm took a turn toward a more northwesterly course at 12 mph. The impacts of the hurricane's environment on its present and future motion and the density of observations on that scale were considered by Chan et al (1980) and Peak et al (1986). The eye slowed and executed a trochoidal loop near Frederiksted, St. Croix at around 0200 AST Sunday, September 18 (Fig.11), before slowly curving westnorthwestward (also noted by Lawrence and Mayfield, 1977 for another hurricane). The eye also underwent some interesting structural changes as it approached St. Croix. These are documented in Fig.12, a sequence of photos from the NWS 10 cm radar at San Juan. Note the contractions and expansions of the eye and the position of the northern eyewall over St. Croix for several hours late on the 17th into the 18th. Storm, damaging winds resumed over St. Croix after eye passage around 0400 AST on September 18. A composite analysis derived from airborne 5 cm radar data and flight-level (700 mb) winds on the NOAA P-3 aircraft, as HUGO was approaching St. Croix on the afternoon of the 17th, is shown in Fig.13.a. Note the well-defined circular wall cloud with strongest reflectivities in the NW and SE quadrants, and a swath of 135 kt maximum windspeeds around the NE and E quadrants in Fig.13. All surface observations from St. Croix and St. Thomas airports ceased before mid-afternoon on Sunday due to extensive wind damage and communication outages. Our overall assessment of structural damages and probable surface windspeeds is given by Marshall (1990) in a companion paper. We can now understand the extensive nature and severity of the damage on St. Croix from examination of Figs.11 and 12.

After pummeling the U.S. Virgin Islands for several hours, Hurricane HUGO slowly looped into Vieques Sound during the predawn hours of September 18, between the islands of Culebra and Vieques (Figs.9,11). Note especially the 2 well-defined trochoidal loops in HUGO's track on Fig.11. Similar hurricane track motions were documented for hurricane ALICIA, 1983, prior to its destructive landfall on Galveston Island, Texas (Savage et. al. 1984) and for Hurricane Carla, 1961. The most severe surface damage found by our study team from HUGO was on the islands of Culebra and St. Croix, both of which were just to the right of the cusp-points in Hugo's track (see Fig.11).

The damage on Vieques, to the left of the track, was not quite as extensive in scale but was almost as severe. After brushing the eastern portion of Vieques at around 0730 AST on the 18th, HUGO's eye looped slowly westward over the northeastern portion of Puerto Rico between 0800 and 0900 AST. Satellite data and San Juan radar (Fig.12) indicate that the eyewall on the west side of the eye moved over land near the towns of Ceiba (Roosevelt Roads NAS), Fajardo and Luquillo (see Figs.9,11), while the east side of the eye remained over water. It was during the last few hours of HUGO's approach to Puerto Rico that Culebra probably experienced the

worst wind effects, with the southeasterly flow (associated with the most dangerous northeast quadrant of HUGO's eyewall, Fig.12) channeled through the hills on both sides of the Ensenada Honda Harbor (Fig.9). HUGO's ill-defined eye appeared to bounce NNW off the northeast coast of Puerto Rico (Fig.11) and by noon on Monday, September 18, the eye was over water north of San Juan with maximum sustained winds of 125 mph and minimum sea-level pressure of 957 mb. The storm's radar structure, as documented by the 5 cm belly radar from the NOAA WP3D aircraft is shown in Fig.13.b. Note that the southeastern half of the storm is nearly devoid of rainbands!

An analysis of the storm-total precipitation from HUGO over Puerto Rico is shown in Fig.14. Note that maximum rainfall amounts of 10-14 inches are found in the mountainous terrain (3,000 ft maximum heights), near the center of the island. These maxima occurred in orographically-favorable locations (compare with Figs.11 and 12) which experienced primarily strong upslope flow during HUGO's passage. These rainfall amounts agree will with those forecasted in the official NHC advisories and bulletins on Hurricane HUGO as it was approaching.

5. SOME UNIQUE DATA

A storm chaser, Jim Leonard, was able to position himself in a multi-story condominium in Luquillo, and produced a remarkable videotape of the approach and passage of HUGO's eye directly over him. The videotape documents damaging wind and rain effects on nearby structures during major rainband and eyewall passages in HUGO, as well as chaotic state of the adjacent sea surface. He used a digital barometer to measure a lowest pressure. San Juan, which remained outside the eye, recorded a minimum pressure of 970.3 mb. The radar sequence in Fig.11 supports the pressure data indications that HUGO was filling as it crossed the northeast coast of Puerto Rico. However, we must emphasize that the western eyewall passed just to the east of the metropolitan San Juan, probably affecting Loisa and Pinones (see Figs.9 and 11); moreover, this geometry is entirely consistent with the large gradations of damage and surge effects (especially overwash) documented by the team from Catano eastward. Our assessment of the damage to homes and commercial buildings and probable associated windspeed maxima is given in Marshall (1990).

A very unique aspect of Hurricane HUGO occurred on the afternoon of the 18th, when the storm was north of San Juan (Fig. 13). During our interview with the meteorologist-in-charge of the San Juan WSFO, Israel Matos, he made the point of recalling that he and some of his staff had felt an earthquake on Puerto Rico on Monday afternoon. We have since confirmed that a magnitude 4.8 (Richter scale) earthquake occurred at 1447 AST and it was centered in the U.S. Virgin Islands. This was certainly a significant earthquake event in a seismically-active area, and perhaps further research is warranted on the possible linkages to HUGO, if any.

6. OBSERVATIONAL GAPS

The team found an appalling lack of recorded meteorological surface data, especially winds, over Puerto Rico and the U.S. Virgin Islands in HUGO's path. As noted in other recent NAS/NRC hurricane study-team reports (e.g. Savage et al, 1984 on Hurricane ALICIA), many anemometers were in place, but most were either damaged or destroyed by HUGO's winds, or lacked recording equipment and/or back-up power. Only two wind records have been obtained so far: one from the National Weather Service (NWS) Forecast office at San Juan Munoz Airport and the other at Roosevelt Roads NAS both sites on Puerto Rico (Figs.9,14). A time history of peak wind gusts for these sites is shown in Fig.15 a,b, resp. Recall that San Juan Airport probably experienced the fringes of HUGO's western eyewall between (1300-1400 GMT, while Roosevelt Roads NAS experienced the eye itself about 1 1/2-2 hours earlier).

The NWS Forecast Office at San Juan recorded peak gusts of 92 mph between 1350 and 1415 GMT, and the maximum sustained wind speed was 77 mph. Adjustment for the 6.1 meter height of the F420 C anemometer would increase the plotted windspeed in Fig.15a by about 7 percent. The fastest mile speeds for standard conditions were derived from the measured 10-minute mean speeds using the procedure described by Marshall (1984), and the maximum value of 88 mph occurred at 1350 GMT. Similarly, the anemometer site at Roosevelt Roads is well-exposed, and height of the propeller/vane anemometer is 7 meters. The time history of recorded peak gusts, unadjusted for anemometer height in Fig. 15b shows peak gusts of 120 mph occurred between 1150 and 1220 GMT. This site experienced a brief passage of the hurricane's eye at 1250 GMT (dip in windspeeds). Maximum sustained windspeeds were about 98 mph. Fastest-mile speeds were derived using the procedure used for the San Juan Airport (NWS) data, and for Roosevelt Roads the maximum value of 110 mph occurred at 1320 GMT.

We have had to reconstruct probable one-minute sustained windspeeds and peak gusts for the other nearby islands, using our aerial damage survey and reduction of reconnaissance aircraft-measured winds at

10,000 ft. down to the surface, using new research results of Powell and Black (1989). These surface windspeed estimates for Hurricane HUGO are summarized in tabular form by Marshall (1990). There was an unofficial estimate of winds gusting to 150 kts in the harbor at Culebra (by a mariner, Mr. Herbert, who rode out the storm in his sailboat and videotaped his anemometer). Therefore, overall, we believe that the highest winds occurred on Culebra and St. Croix (estimated peak gusts to 67 and 70 m/s, respectively. Another unique data set has recently come to light: a mini-network of six anemometers installed by the FAA at San Juan Airport survived HUGO's passage. This system, called the Low-level Wind Shear Alert (LLWAS) system, has been installed at a number of airports across the U.S. and its territories to warn pilots of dangerous wind shear and downburst events in the airport terminal area. An LLWAS anemometer system was in place at Houston's Hobby Airport during the passage of Hurricane ALICIA, 1983 but the NAS/NRC team report noted the failure of the system to provide any wind data during ALICIA due to a lack of recording equipment and back-up power by FAA program managers. Fortunately, the team's recommendations were heeded, and we understand that wind data were recorded during most of HUGO, from 4 of 6 LLWAS sensors on San Juan Airport. One of the sensors measured a peak gust of 43 kts. These data, combined with a more complete record from NWS San Juan airport, should provide a unique microscale (few km domain) analysis of surface wind distribution near the western eye-wall passage of hurricane HUGO during its temporary filling stage.

FORECAST PERFORMANCE

The team found that, overall, the accuracy and timeliness of most of the official bulletins and advisories issued by NHC and Hurricane Local Statements by NWS San Juan during Hurricane HUGO's approach and passage through the Eastern Caribbean were state-of-the-art. This is especially so considering the paucity of hourly surface and twice-daily upper air reporting stations in the area (there are fewer regularly-reporting upper sites on the Eastern Caribbean islands today than 20 years ago). The warning lead times for the various islands are shown in Fig.16, and clearly indicate that most places had at least 1-2 days warning of HUGO's approach. These lead times were significantly better than is often possible for hurricanes approaching landfall along the U.S. mainland coast.

The hurricane forecasters at NOAA's National Hurricane Center in Miami produce an official forecast track, updated at six-hourly invervals, throughout the hurricane's life-cycle. Fig.17 shows the final smoothed verifying track for Hurricane Hugo (derived from all NOAA and U.S. Air Force reconnaissance aircraft fixes and satellite eye positions-bold line) and the official forecasted tracks. The official forecast track is produced by the hurricane forecaster after he subjectively assesses the outputs from a dozen or so numerical models and guidance products. Ward (1990) has assessed the performance of the models run on HUGO by the NWS' National Meteorological Center. Our Table 3 shows the mean errors for 6 of the models routinely used by NHC--with only a few exceptions the recently-revised statistical/dynamical model (NHC83) developed by Neumann and his colleagues at NHC consistently outperformed all the other models, even the more sophisticated dynamical ones such as SANBAR (barotropic), BAM (beta-advection model), and the QLM (quasi-Lagrangian model). The interested reader is referred to Ward's (1990) article for more details on the models. This outcome may, we believe, have more to do with the state of the observational database in the Caribbean and techniques used to initialize the models than with any inherent scientific deficiencies in the models themselves.

Note that as HUGO approached the Leeward Islands and entered the Eastern Caribbean, there was a persistent left bias in the official NHC forecasts for the hurricane's future track in that region. This led to initial forecasts for HUGO's landfall on the south coast of Puerto Rico which were not corrected until Sunday night, September 17. Nevertheless, both Mr. Matos, the MIC at the San Juan NWS forecast Office and the forecasters at NHC were aware of this bias, so that the people living in the U.S. Virgin Islands had plenty of time to make all necessary preparations; most importantly, there was also an early decision, based on updated NHC advisories with rising hurricane strike probabilities, to evacuate people in San Juan to shelters. We must emphasize that current hurricane track forecasting models and techniques available to NHC cannot forecast mesoscale changes or oscillations in hurricane tracks as depicted for HUGO in Fig.11 earlier. Moreover, there are currently no forecast models for predicting the intensity changes for HUGO implied by the eye-pressure changes shown in Fig.6.

We have found several locations in our aerial damage survey over the U.S. Virgin Islands where the debris patterns strongly suggest the production of destructive "microbursts" (Fujita, 1985). Fig.18a,b show good examples of mircoburst damage, as seen from our low-flying aircraft, over St. Croix and Vieques. The most distinctive features of microburst events

are the narrow confines and divergent nature of the debris trails from destroyed structures. Fujita (1978) found that much of the severe damage to structures he found in Corpus Christi, Texas from Hurricane CELIA, 1971 was due to the formation of intense microbursts (surprisingly), in the western eyewall and a few major rainbands, as the storm made landfall. We have found no evidence of any tornadoes from either the aerial or the ground damage surveys we performed on Puerto Rico and the U.S. Virgin Islands. In any case, it is likely that the general wind damage caused by the hurricane itself, and those more concentrated damage areas from microbursts, both would tend to mask any separate tornado damage tracks from subsequent identification.

7. CONCLUSIONS AND RECOMMENDATIONS

One of the major issues in HUGO's aftermath in the Caribbean has been the appalling lack of recorded surface windspeeds and other meteorological data (especially pressure and rainfall). Without these critical measurements in the future, there can be no resolution to the question of correlation of the observed damage of structures with the actual wind loads generated by hurricanes. In addition, there is a continuing need for operational and research aircraft reconnaissance into hurricanes, but there is also an urgent need for more rugged, reliable surface instrumentation to properly calibrate and reduce the aircraft data gathered on hurricanes approaching landfall to appropriate surface values. Moreover, surface recording stations are too sparse in the Caribbean to measure the actual surface wind maxima at the point of hurricane landfall. This situation is compounded by the fact that some of the most important surface observing sites have been closed by the Caribbean nations involved because of high manpower and maintenance costs.

RECOMMENDATION 1. Develop and deploy high quality, automated surface observing instruments which are rugged enough to withstand hurricane wind speeds, and of affordable cost. The Australians have developed a relatively inexpensive device for measuring maximum windspeeds (and wind directions), called the "Maxometer", which they have deployed along sections of their hurricane-prone coastlines. We further recommend that responsibility to deploy and maintain instruments during local hurricanes be given to selected universities in the coastal States and on islands in the Caribbean with engineering or meteorology programs.

We have also found that, even though the official forecasts and warnings for HUGO in the Caribbean were entirely adequate and state-of-art, there is a need for improvements in our hurricane forecasting capability. However, such efforts will have limited potential for breakthroughs because there is a lack of upper-level wind observations of the hurricane's environment. Complete vertical wind profiles are available only twice per day from a shrinking number of upper air rawindsonde sites in the Eastern Caribbean. These are supplemented by cloud motion derived estimates of layer-mean winds aloft from satellite cloud tracking (only from cloudy to partly cloudy regions).

RECOMMENDATION 2. We need to install more conventional rawinsonde stations, perhaps in a cost-sharing arrangement with the Caribbean countries involved. A better long-term solution, and one with minimal manpower requirements, will be to install wind PROFILERS on selected islands. These instruments are rugged, operate in all weather continuously, and have been installed on a few South Pacific island sites as part of the TOGA climate program. Finally, there needs to be research to better define and exploit the NEXRAD Doppler radar capabilities for estimating surface windspeeds in hurricanes (we note that a NEXRAD installation is planned for San Juan, PR).

RECOMMENDATION 3. There needs to be a systematic approach and sustained, long-term effort at developing improved hurricane prediction models which give consistent results for future track and/or intensity changes in different regions. The current situation is one where the hurricane forecaster must subjectively pick the hurricane model of the day, based on recent performance for the particular hurricane in a particular area (there are now at least 10-12 different hurricane prediction models and techniques in operation or quasi-operational (test) use by NHC and the National Meteorological Center).

Finally, we have found that lifelines were particularly susceptible to total loss or prolonged disruption from HUGO's course through Puerto Rico and the Virgin Islands. Power and telephone lines were downed everywhere, mainly from toppled trees and flying debris. Future mitigation efforts should stress the importance of putting utilities underground whenever possible (already done on the island of Tortola). There also needs to be a careful reexamination, after HUGO, of the probability of windspeeds in excess of current codes in the Caribbean to determine if code revisions are needed.

There continues to be great pressure for shoreline development (commercial as well as residential) on hurricane and other storm prove shorelines in Puerto Rico and the Virgin Islands. There will be a continuous threat of beach erosion and overwash, and other storm surge and wave impacts on these exposed coastal properties. Indeed, our team found that HUGO's surge and wave impacts on the developed coastal areas of northeastern Puerto Rico have made that region even more susceptible to future damage from winter storms in the Atlantic.

RECOMMENDATION 4. Fund impact studies on offshore mining of sand for beach replacement and determine the cost-to-benefit ratios. In addition, fund programs to evaluate and improve, when necessary, codes and enforcement for beach-use management. Finally, support and fund programs for unified, long-range planning for public/private/government use of existing beach resources.

8. ACKNOWLEDGEMENTS

All of the material in this paper is derived from my work as Team Leader of a quick-response study team organized by the National Research Council's Committee on Natural Disasters and dispatched to Puerto Rico and the Virgin Islands within 3 days of HUGO's onslaught there. The other team members who have contributed greatly to the overall effort and much of this paper are: R.D. Marshall, NIST; J. L. Vogel, NWS/NOAA, Ben Aguirre, Texas A&M University, and David Bush, Duke University. I am grateful to my colleagues Peter Black, Frank Marks, Mark Powell and Hugh Willoughby, HRD/AOML/NOAA for sharing some of their excellent data sets and preliminary analyses with me; likewise, additional lagniappes go to Miles Lawerence and Bob Case of NHC/NWS/NOAA for many of the operational data sets on HUGO, and to Jack Parrish, AOC/NOAA for some of the NOAA P-3 figures. Satellite data were kindly provided on loan by Dane Clark, NESDIS/NOAA. The manuscript was ably typed by Donna Robertson, NOAA/CS.

9. REFERENCES

1. Baynton, H.W. (1978). "Radar Design for Determining the Strength of Tropical Cyclones in the Bay of Bengal 1976." Monthly Weather Review, 105 (11), 1458-1461.
2. Black, P.G., R. L. Elsberry, L. K. Shay, R. P. Partridge, and J. D. Hawkins (1988). "Atmospheric Boundary Layer and Oceanic Mixed Layer Observations in Hurricane Josephine Obtained from Air-Deployed Drifting Buoys and Research Aircraft." J. Atmos. Oceanic Tech., 5(6), 683-695.
3. Carbone, R. E. and F. D. Marks, Jr. (1989). "Velocity Track Display (VTD): A Real-Time Application for Airborne Doppler Radar Data Hurricane." AMS Conference on Hurricanes and Tropical Meteorology, San Diego, CA, pp. 11-12.
4. Case, R (1990). "Hurricane-Strong Storms Out of Africa." Weatherwise, 43(1) February, 1990, 23-29.
5. Chan, J. C. L., W. M. Gray, and S. Q. Kidder (1980). "Forecasting Tropical Cyclone Turning Motion from Surrounding Wind and Temperature Fields." Mon, Wea. Rev., 108, 778-792.
6. Dodge, P. P., J. S. Griffin, F. D. Marks, Jr., and R. W. Burpee (1990). "Interactive Analysis of NOAA P-3 Aircraft Data Support of Operational Hurricane Forecasting." Preprints, Sixth International Conf. on Interactive Info. and Proc. Systems for Meteor., Oceano., and Hydrology, Amer. Meteor. Soc., Boston, MA, 3 pp.
7. Fassig (1928). "San Felipe-the Hurricane of September 13, 1928, at San Juan, P.R. "Mon. Wea. Rev., 56(9), 350-352.
8. Fujita, T.T. (1978). "Manual of Downburst Identification for Project NIMROD." SMRP Research Paper 156. Dept. of Geophys. Sci., U. of Chicago, 104 pp.
9. _____, (1985). The Downburst, Microburst, and Macroburst. The Univ. of Chicago, 122 pp.
10. Goodman, R.R. (1989). "An Historical Look at Tropical Cyclone Paths in Relation to Puerto Rico and the Virgin Islands." Technical Note, National Weather Service Southern Region Headquarters, Ft. Worth, TX, 6 pp.
11. Hebert, P. J., and G. Taylor (1988). "The Deadliest, Costliest, Most Intense U.S. Hurricanes of this Century (and other Frequently Requested Hurricane Facts)." NOAA Technical Memorandum NWS NHC 18, Nat'l Hurricane Center, Miami, FL, 28 pp.
12. _____, _____, and R.A. Case (1984). "Hurricane Experience Levels of Coastal County Populations - Texas to Maine." NOAA Tech. Memo. NWS NHC 24, Nat'l Hurricane Center, Miami, FL, 127 pp.
13. Jarvinen, B. R., and M. B. Lawrence (1985). "An Evaluation of the SLOSH Storm-Surge Model." Bull. Amer. Meteor. Soc., 66(11), 1408-1411.
14. Lawrence, M. B., and B. M. Mayfield (1977)." Satellite Observations of Trochoidal Motion During Hurricane Belle 1976." Monthly Weather Review, 105(11), 1458-1461.

15. Marks, F. D., Jr. and R. A. Houze, Jr. (1984). "Airborne Doppler Radar Observations in Hurricane Debby." Bull. Amer. Meteor. Soc., 65(6), 569-582.
16. Marshall, R.D. (1984). "Fastest-Mile Wind Speeds in Hurricane Alicia. "NBS Technical Note, No. 1197, NBS, Gaithersburg, MD
17. _____, R.D. (1990). "Performance of Structures in Hurricane HUGO." Paper presented at 22nd Joint Meeting, UJNR, Panel on Wind and Seismic Effects, Gaithersburg, MD.
18. Peak, J. E., W. E. Wilson, R. L. Elsberry, and J. C.-L. Chan (1986). "Forecasting Tropical Cyclone Motion Using Empirical Orthogonal Function Representations of the Environmental Wind Fields." Mon. Wea. Rev., 114, 2466-
19. Powell, M.D. (1980). "Evaluations of Diagnostic Marine Boundary-Layer Models Applied to Hurricanes." Mon. Wea. Rev., 108, 757-765.
20. _____, and P. G. Black (1990). "The Relationship of Hurricane Reconnaissance Flight-Level Wind Measurements to Winds Measured by NOAA's Oceanic Platforms." Submitted to J. Wind Engr., 12 pp.
21. Ward, J. H. (1990). "A Review of NMC Numerical Forecast Guidance for Hurricane HUGO." Submitted to Weather and Forecasting, Amer. Meteor. Soc, Boston, MA.
22. Willoughby, H. E., F. D. Marks, Jr., and R. J. Feinberg (1984). "Stationary and Moving Convective Bands in Hurricanes." J. Atmos. Sci., 41(232), 3189-3226.

Table 1. The most intense United States hurricanes of this century (at time of landfall). After Hebert and Taylor(1988).

MOST INTENSE HURRICANES, UNITED STATES 1900-1982
(At time of landfall)

	HURRICANE	YEAR	CATEGORY	MILLIBARS	INCHES
1.	Florida (Keys)	1935	5	892	26.35
2.	CAMILLE (La./Miss.)	1969	5	909	26.84
3.	Florida (Keys)/South Tex.	1919	4	927	27.37
4.	Florida (Lake Okeechobee)	1928	4	929	27.43
5.	DONNA (Fla./Eastern U.S.)	1960	4	930	27.46
6.	Texas (Galveston)	1900	4	931	27.49
7.	Louisiana (Grand Isle)	1909	4	931	27.49
8.	Louisiana (New Orleans)	1915	4	931	27.49
9.	CARLA (Texas)	1961	4	931	27.49
10.	Florida (Miami)	1926	4	935	27.61
11.	HAZEL (S.C./N.C.)	1954	4*	938	27.70
12.	Southeast Fla./La.-Miss.	1947	4	940	27.76
13.	North Texas	1932	4	941	27.79
14.	AUDREY (La./Tex.)	1957	4#	945	27.91
15.	Texas (Galveston)	1915	4#	945	27.91
16.	CELIA (S. Texas)	1970	3	945	27.91
17.	ALLEN (S. Texas)	1980	3@	945	27.91
18.	New England	1938	3*	946	27.94
19.	FREDERIC (Ala./Miss.)	1979	3	946	27.94
20.	Northeast U.S.	1944	3*	947	27.97
21.	S. Carolina/N. Carolina	1906	3	947	27.97
22.	BETSY (Fla./La.)	1965	3	948	27.99
23.	Southeast and Northwest Fla.	1929	3	948	27.99
24.	Southeast Florida	1933	3	948	27.99
25.	South Texas	1916	3	948	27.99
26.	Miss./Ala.	1916	3	948	27.99
27.	South Texas	1933	3	949	28.02
28.	BEULAH (S. Texas)	1967	3	950	28.05
29.	HILDA (Louisiana)	1964	3	950	28.05
30.	GRACIE (S. Carolina)	1959	3	950	28.05
31.	Texas (Central)	1942	3	950	28.05
32.	Southeast Florida	1945	3	951	28.08
33.	Florida (Tampa Bay)	1921	3	952	28.11
34.	CARMEN (Louisiana)	1974	3	952	28.11
35.	EDNA (New England)	1954	3*	954	28.17
36.	Southeast Florida	1949	3	954	28.17
37.	ELOISE (Northwest Fla.)	1975	3	955	28.20
38.	KING (Southeast Fla.)	1950	3	955	28.20

* Moving more than 30 miles per hour.
\# Classified category 4 because of extreme tides.
@ Reached Cat. 5 intensity three times along its path through the Caribbean and Gulf of Mexico. The lowest pressure reported was 899 mb (26.55 in.) at 1742Z 8-7-80 off the northeastern tip of Yucatan Peninsula.

Table 2. Estimated number of deaths associated with Hugo.

South Carolina	13	Antigua and Barbuda	1
North Carolina	1	Guadeloupe	11
Virginia	6	Montserrat	10
New York	1	St. Kitts and Nevis	1
Puerto Rico	2	TOTAL	49
U.S. Virgin Islands	3		

Table 3.

HURRICANE HUGO
TRACK ERRORS
(Errors in n.m.)

	12 HRS	24 HRS	36 HRS	48 HRS	72 HRS
Official (NHC)	33	65	98	122	154
(No. of Cases)	(43)	(41)	(39)	(37)	(33)
CLIPER	37	73	119	161	216
	(43)	(41)	(39)	(37)	(33)
SANBAR	28	55	92	141	302
	(15)	(15)	(14)	(13)	(11)
QLM	81	90	119	172	268
	(19)	(18)	(17)	(16)	(14)
NHC83	38	61	88	106	178
	(42)	(40)	(38)	(36)	(32)
BAM	50	84	123	154	268
	(17)	(16)	(15)	(14)	(13)
NHC83 Revised	50	61	91	119	149
	(39)	(37)	(35)	(33)	(29)

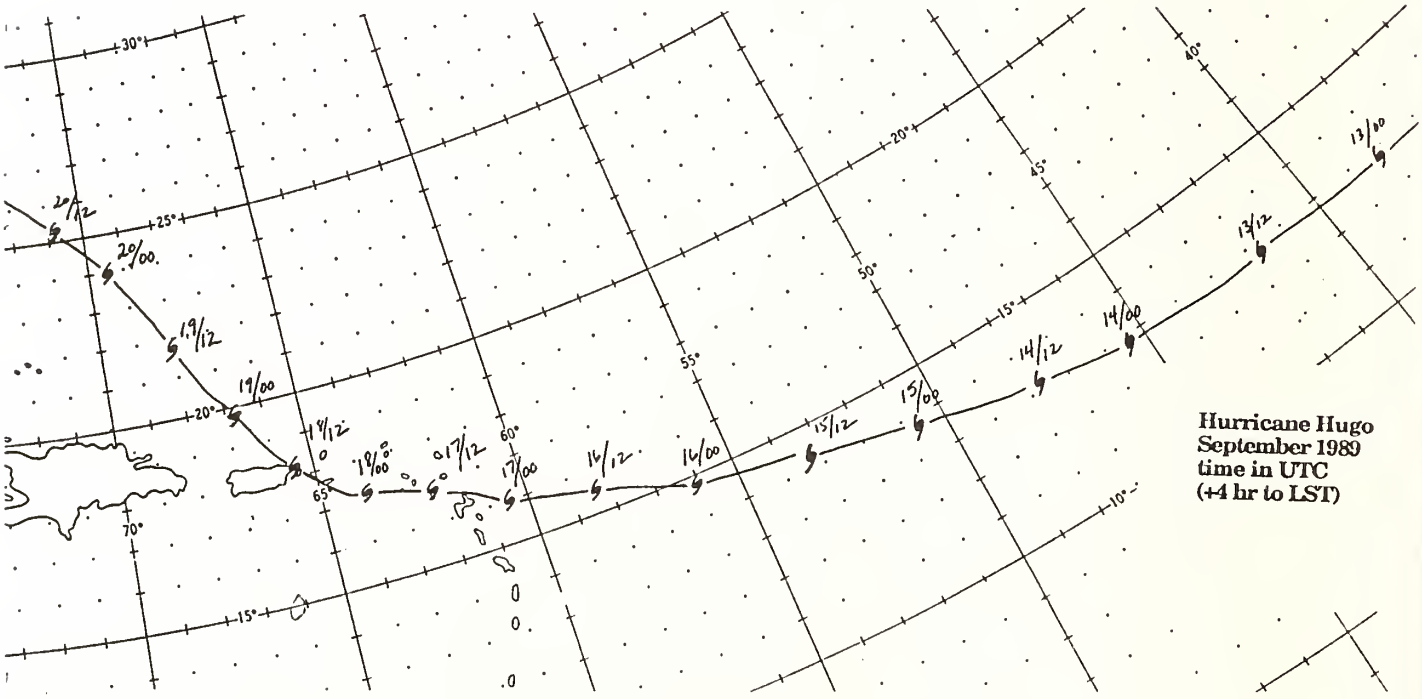

Figure 1. "Best-fit" smoothed track of successive eye positions for Hurricane HUGO at 12-hourly intervals, based on aircraft and satellite fixes (begins when HUGO had already attained full hurricane status on 9/13/89).

Figure 2. NOAA visible GOES satellite view of HUGO shortly after it became full hurricane at 16 GMT, 9/13/89. South America coast in lower left, north is toward the top.

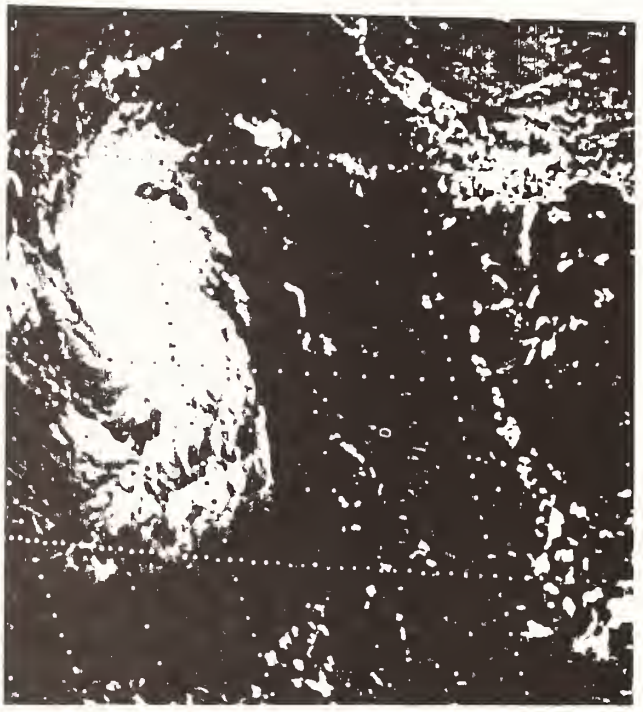

Figure 3. Same as Fig. 2 except HUGO had intensified further, photo at 1630 GMT, 9/13/89.

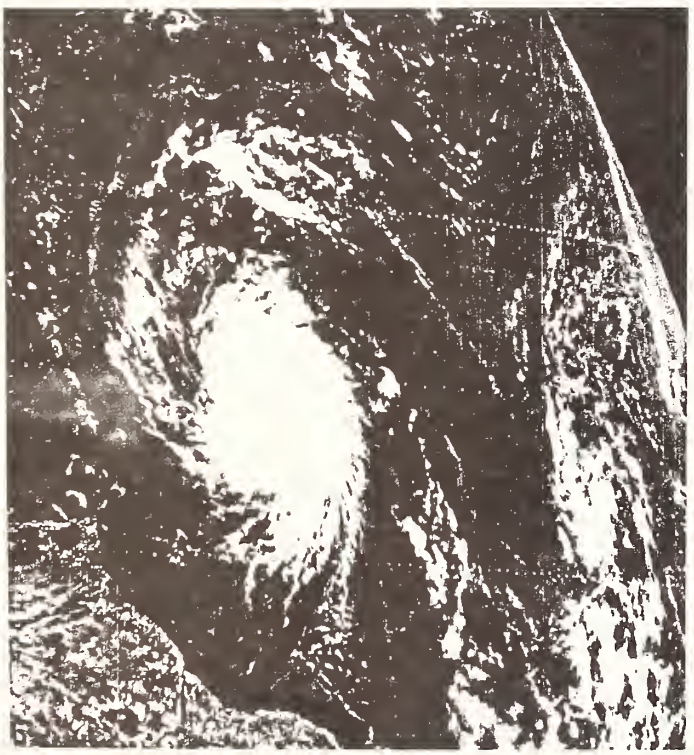

Figure 4. Same as Fig. 3 except near time of NOAA aircraft's first penetration into HUGO at time of maximum strength, 1600 GMT on 9/15/89.

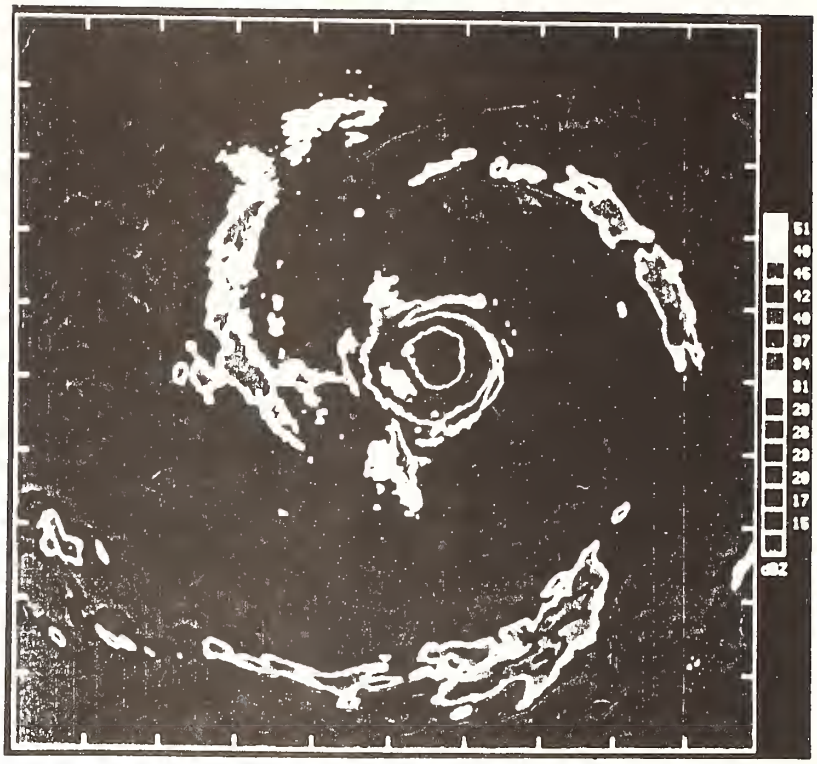

Figure 5a. Composite radar reflectivity PPI analysis from NOAA P-3 aircraft flight into Hurricane HUGO centered on 1727 GMT, 9/15/89. Highest reflectivities (proportional to rainfall rates) are in southwestern eyewall and a few-major rainbands. Total spatial domain = 240 x 240 km. Courtesy Frank Marks, HRD/AOML/NOAA.

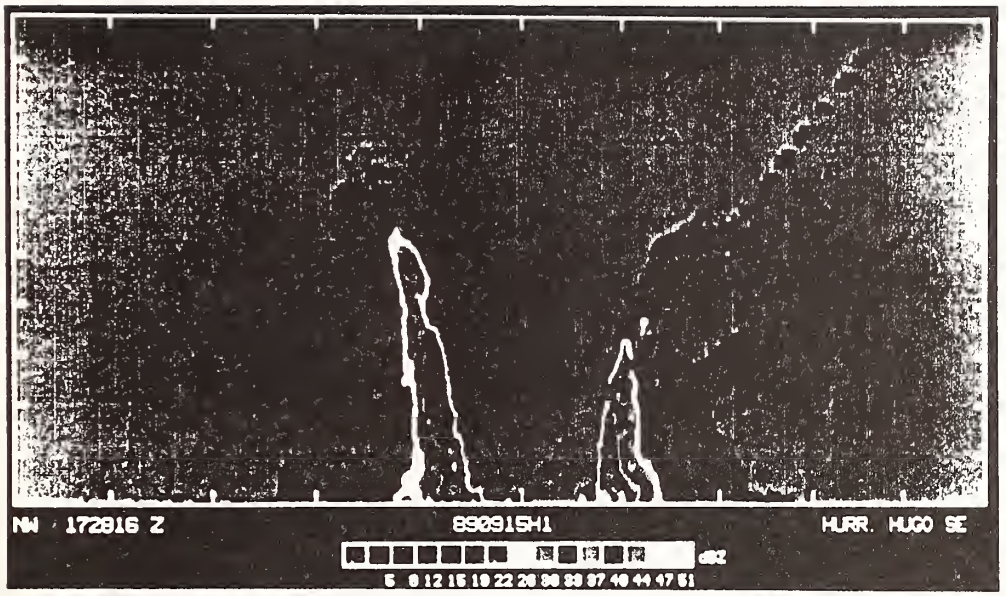

Figure 5b. Radar-cross section of reflectivities through eye of Hurricane HUGO (NW-SE section in Fig. 5a) at 1728 GMT, 9/15/89 derived from NOAA P-3 aircraft's 3 cm tail radar. Courtesy Frank Marks, HRD/AOML/NOAA. Height scale in increments of 2 km.

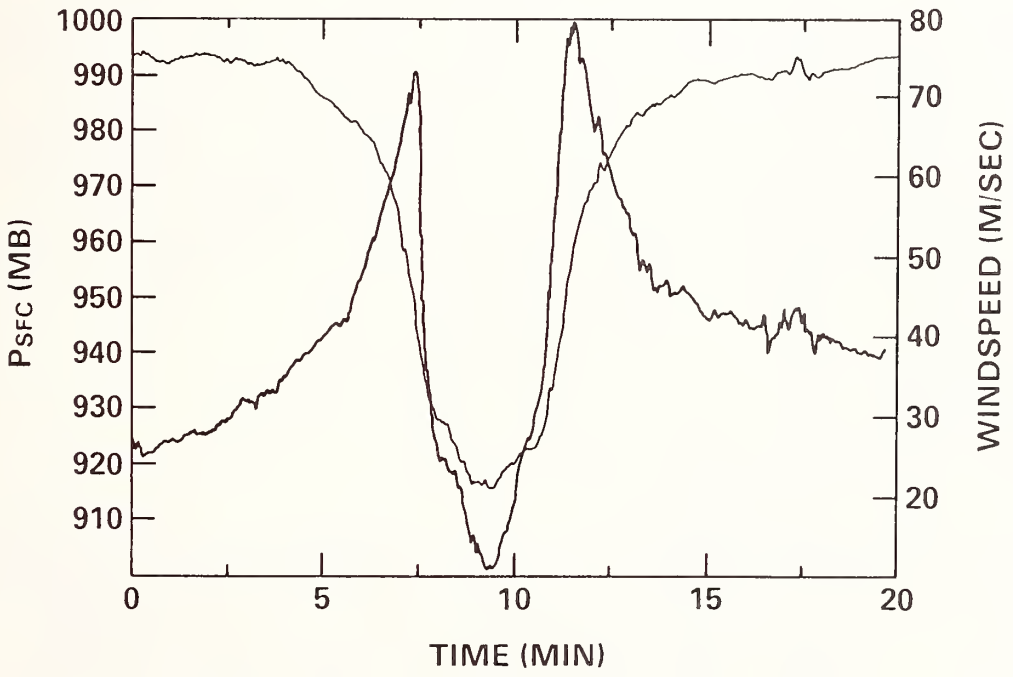

Figure 6. Radial plots of one minute sustained winds at 1500 ft flight-level and derived surface pressure (thin line) through Hurricane HUGO, from NOAA P-3 aircraft flight on 9/15/89. Courtesy Frank Marks, HRD/AOML/NOAA.

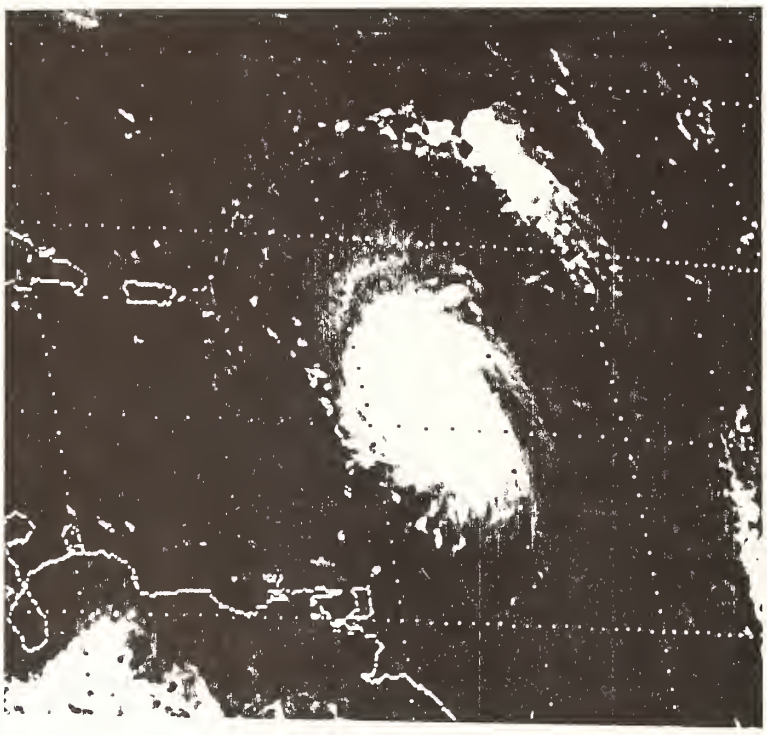

Figure 7. Same as Fig. 4 except visible satellite photo at 1330 GMT, 9/16/89 as Hurricane HUGO was approaching Leeward Islands.

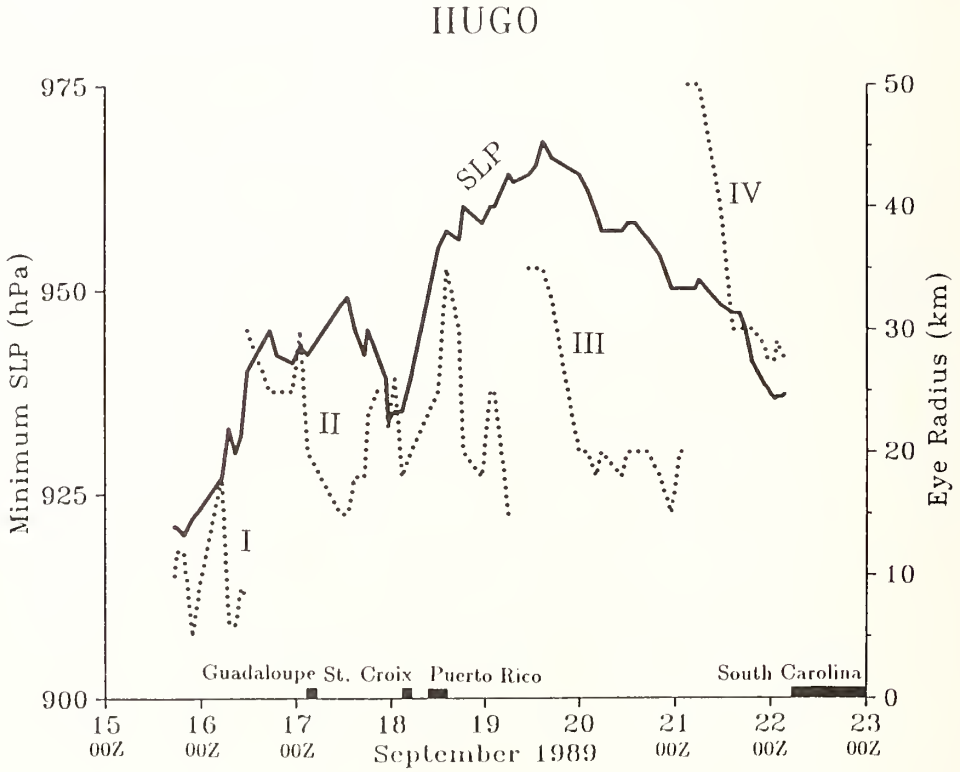

Figure 8. Composite time-series plots of measured minimum sea-level pressures (bold-line) in Hurricane HUGO vs. eye radii (dotted curve) determined from USAF and NOAA reconnaissance aircraft and surface radar data, from 9/15-23/89. Courtesy Hugh Willoughby, HRD/AOML/NOAA. Four major cyclical eye stages are identified, and occasionally when eye curve appears to jump upward, there was a double-concentric eyewall structure for a short time.

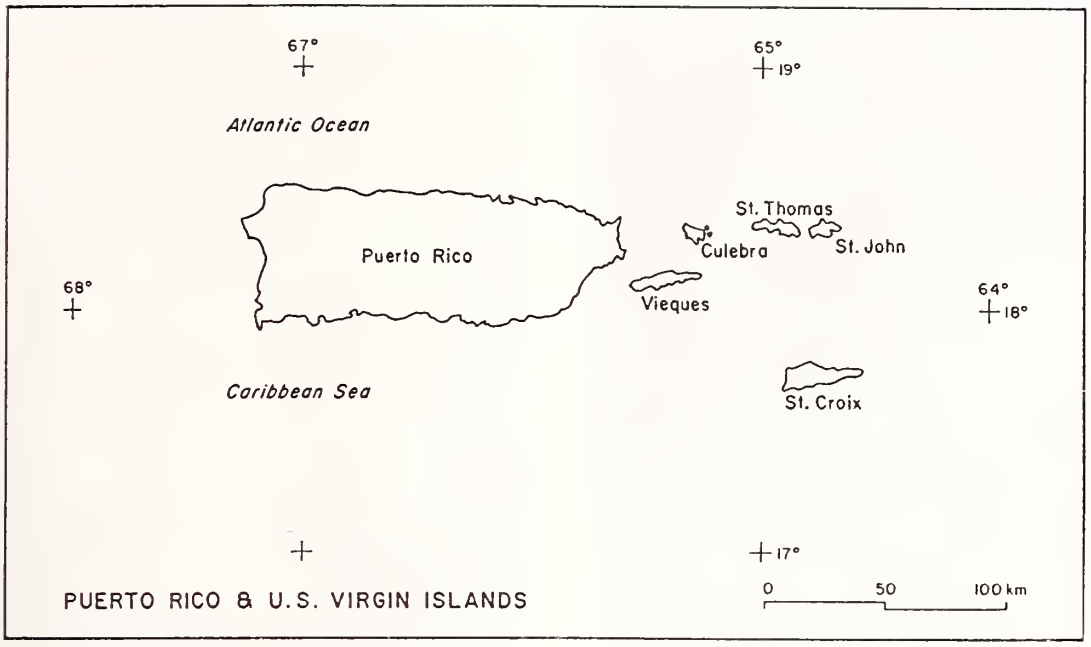

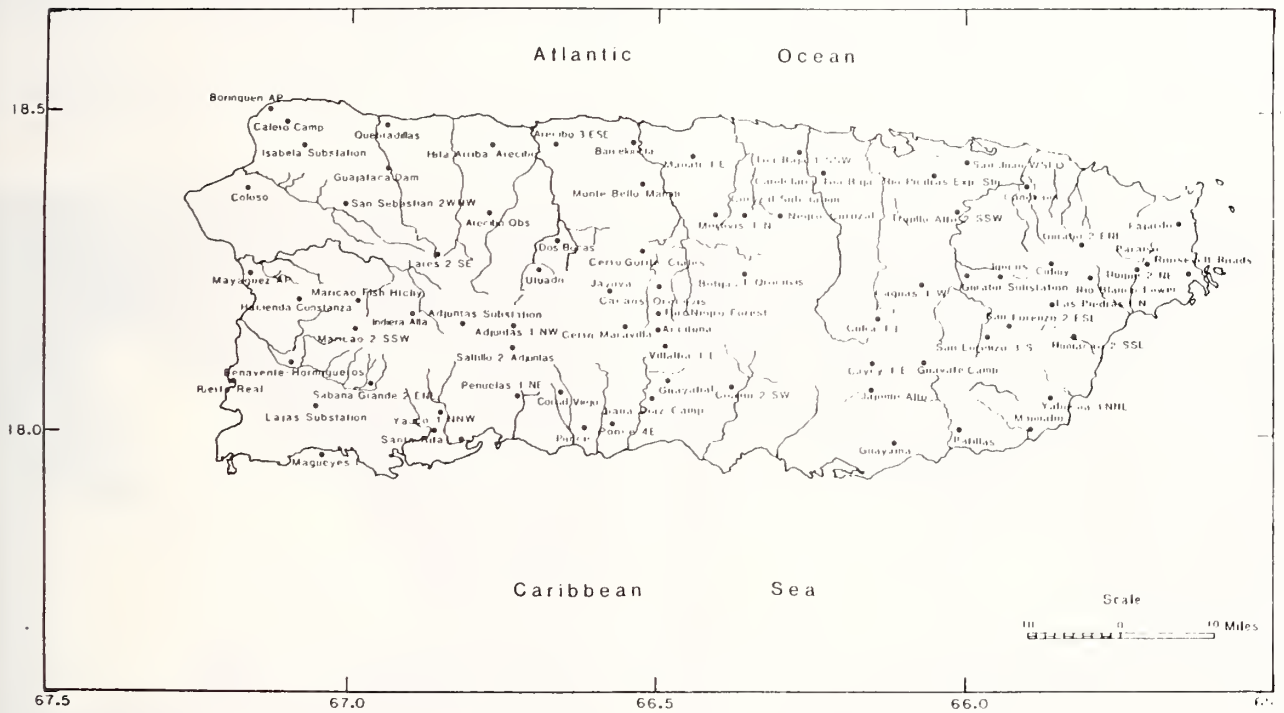

Figure 9. Upper map shows Puerto Rico and adjacent-owned islands of Culebra and Vieques, as well as U.S. Virgin Islands principally impacted by HUGO. Lower map is enlarged for details of rivers and towns in Puerto Rico mentioned in text.

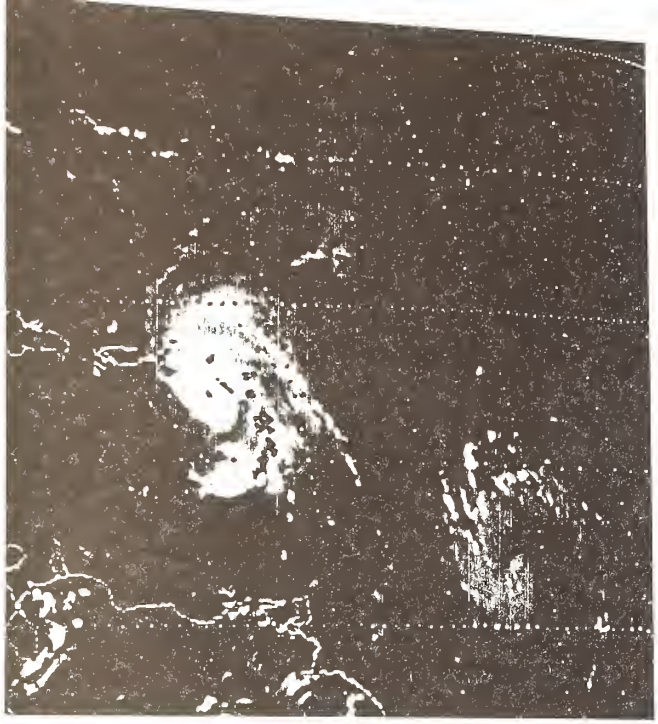

Figure 10. Same as Fig. 7, except satellite view at 1930 GMT, 9/17/89. Note Tropical Storm "Iris" to SE of Hurricane HUGO.

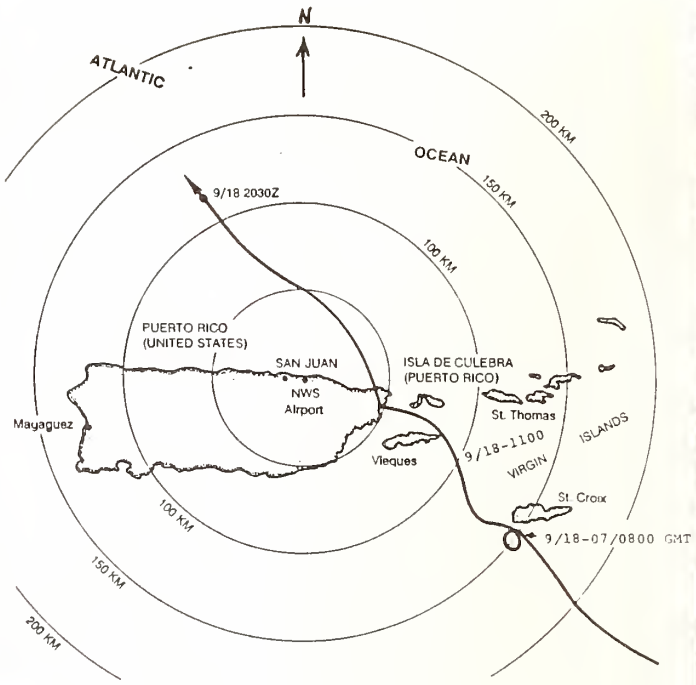

Figure 11. Mesoscale analysis of Hurricane HUGO's eye positions, derived from tracking of San Juan NWS radar as storm approached within range (250 km) during late afternoon on 9/17/89.

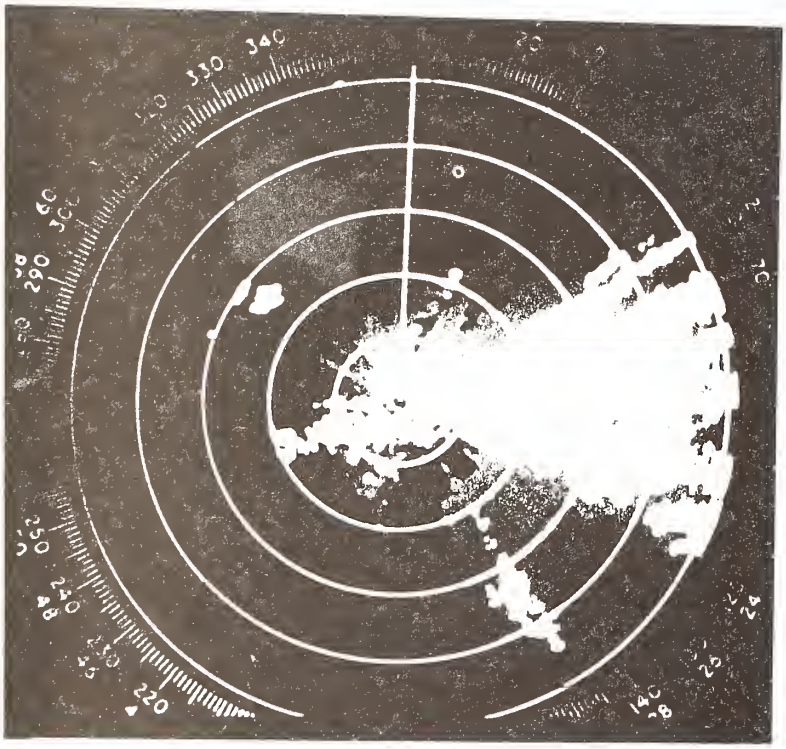

9/18-0359 GMT

9/18-0705 GMT

Figures 12a,b. Sequence of photos at times indicated on 9/18/89 from 10 cm NWS radar at San Juan airport, showing Hurricane HUGO's rainbands and eye, as it approached along track shown in Fig. 11. Range-circles are shown every 50 km and St. Croix is located at 122° azimuth/150 km range from San Juan.

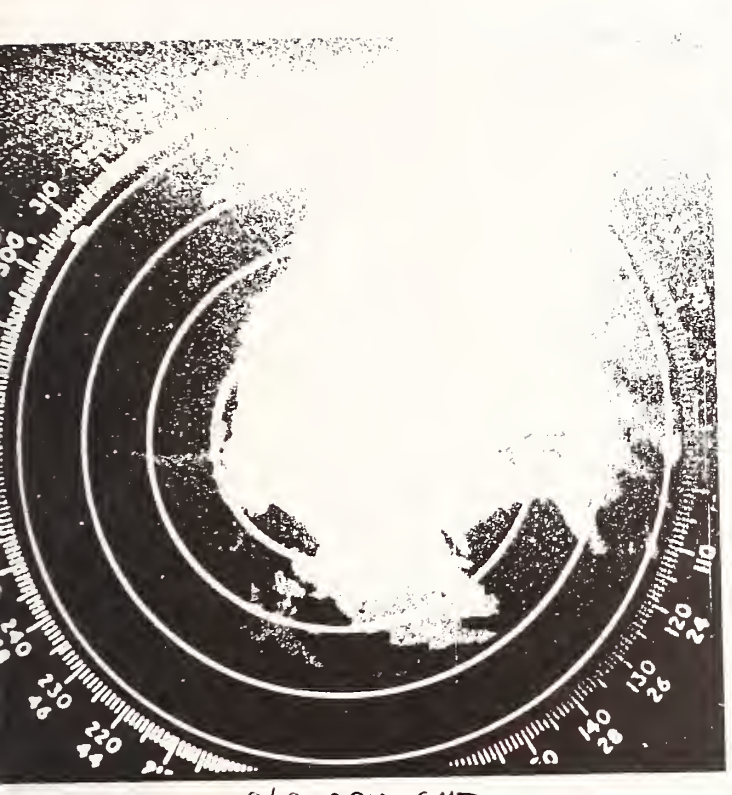

9/18-0910 GMT

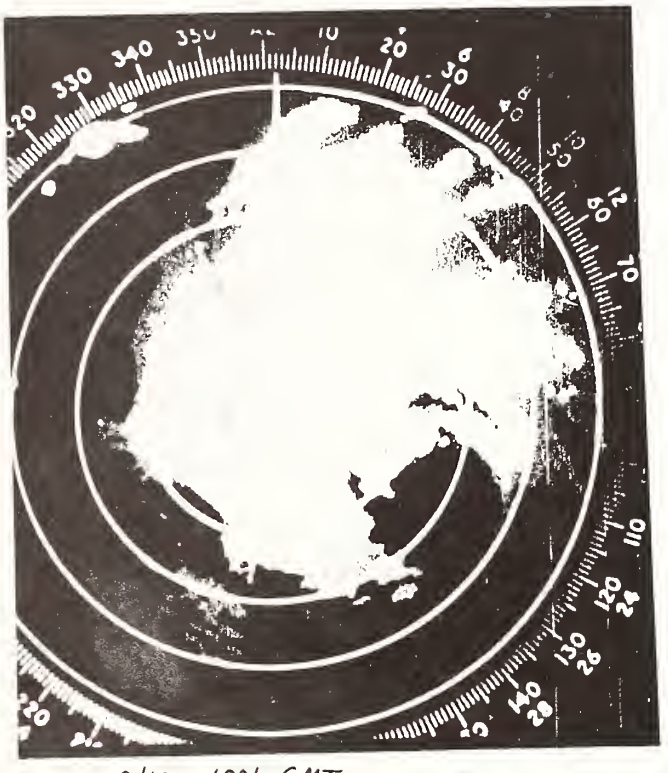

9/18- 1001 GMT

Figures 12c,d. Sequence of photos at times indicated on 9/18/89 from 10 cm NWS radar at San Juan airport, showing Hurricane HUGO's rainbands and eye, as it approached along track shown in Fig. 11. Range-circles are shown every 50 km and St. Croix is located at 122° azimuth/150 km range from San Juan.

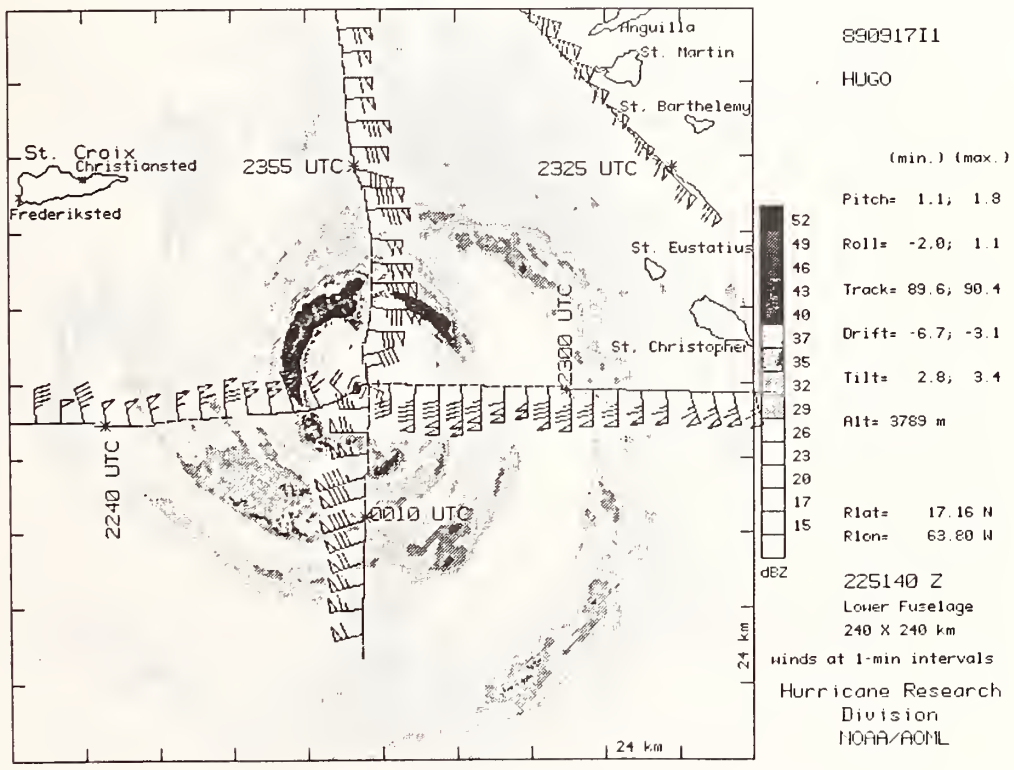

Figure 13a. Composite analysis of radar reflectivities flight track and one-minute sustained winds at 10,000 ft flight altitude of NOAA P-3 aircraft, centered around time 2251 GMT, 9/17/89 as HUGO was nearing St. Croix (upper left). Wind symbol convention is triangle=50kts and long barb=10kts, short barb=5kts. **Courtesy Marks and Powell,HRD.**

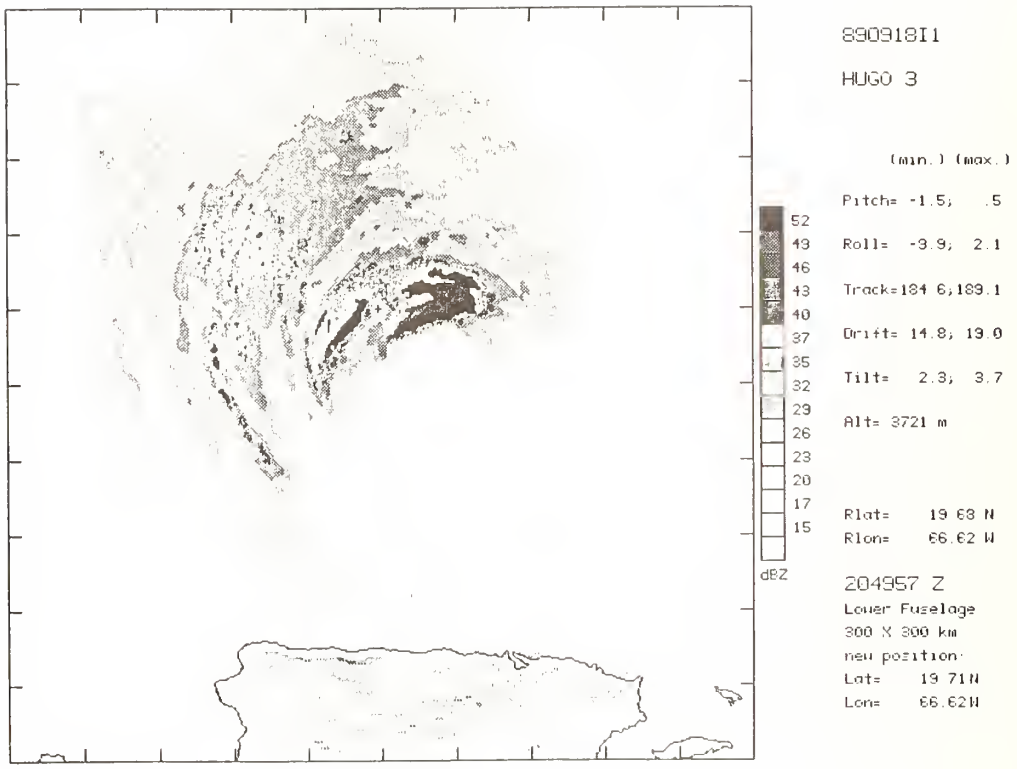

Figure 13b. Similar to 13a, except composite radar analysis (without aircraft winds) when HUGO had weakened somewhat north of Puerto Rico, centered on time 2050 GMT, 9/18/89.

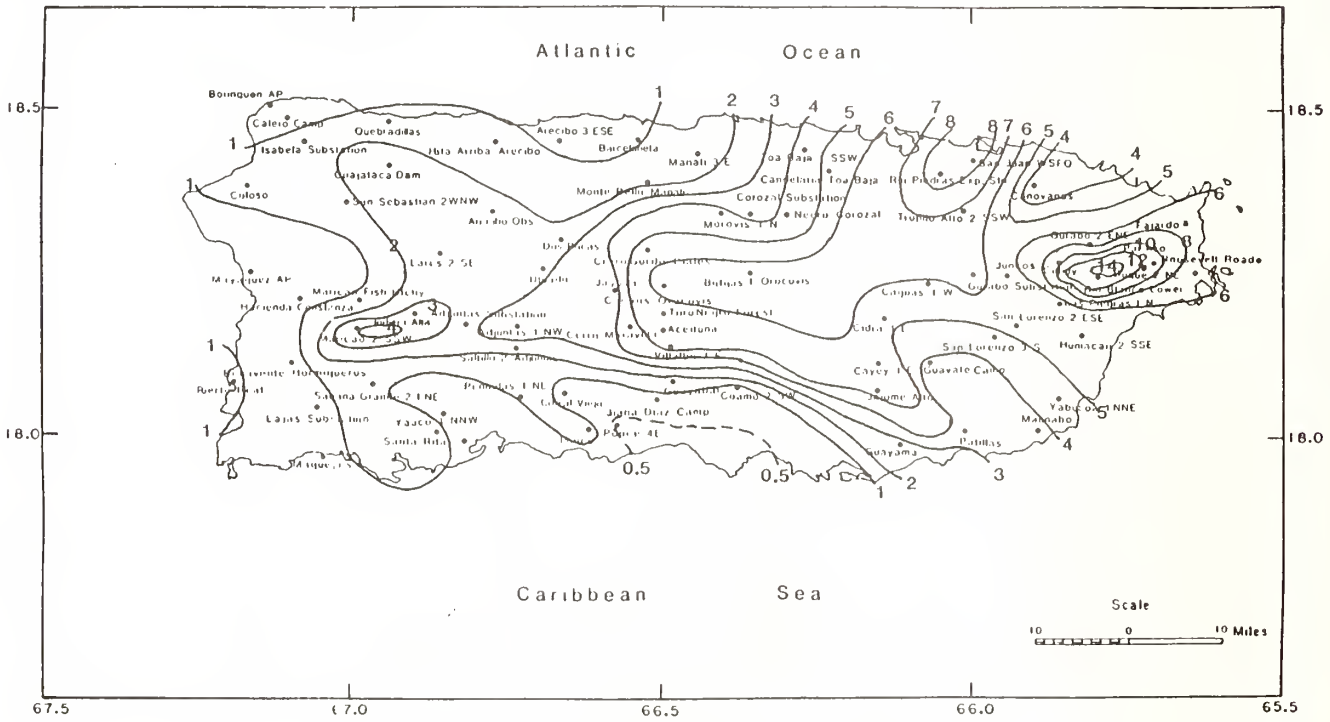

Hurricane HUGO Rainfall (Inches)

7 a.m. 9/17 to 7a.m. 9/19/89

Figure 14. Analysis of storm total rainfall over Puerto Rico from Hurricane HUGO, isohyets in inches. Compare with rivers shown in Fig. 9.

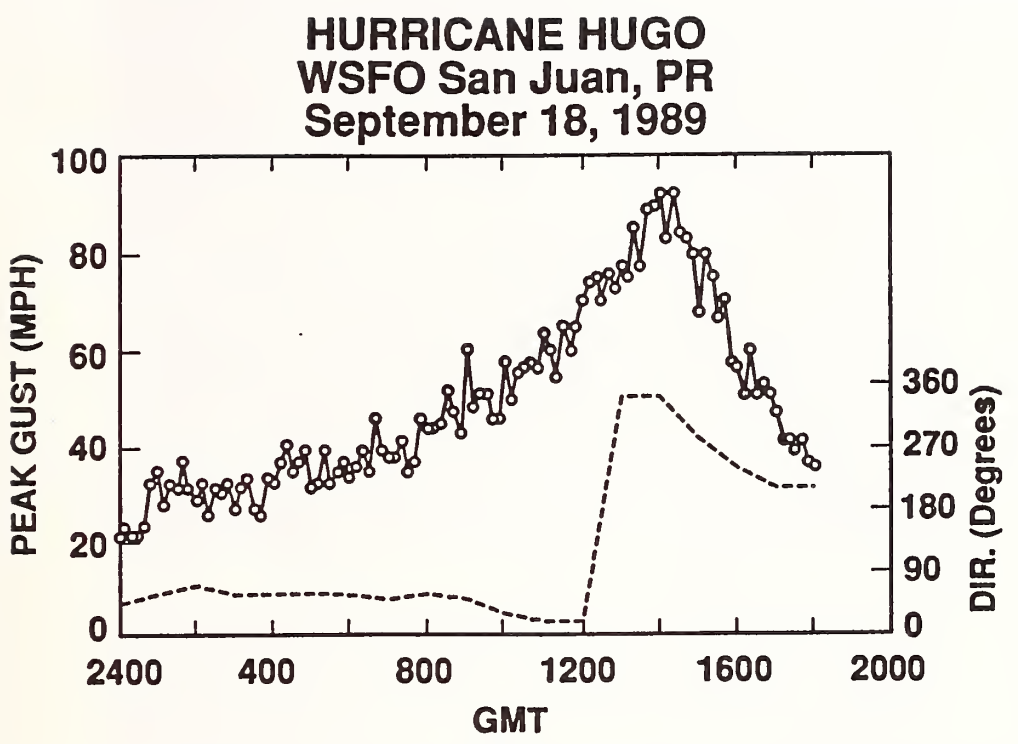

Figure 15a. Time-plot of measured peak gust windspeeds during Hurricane HUGO's strongest period at NWS San Juan, P.R. See text for details. Courtesy of R.D. Marshall.

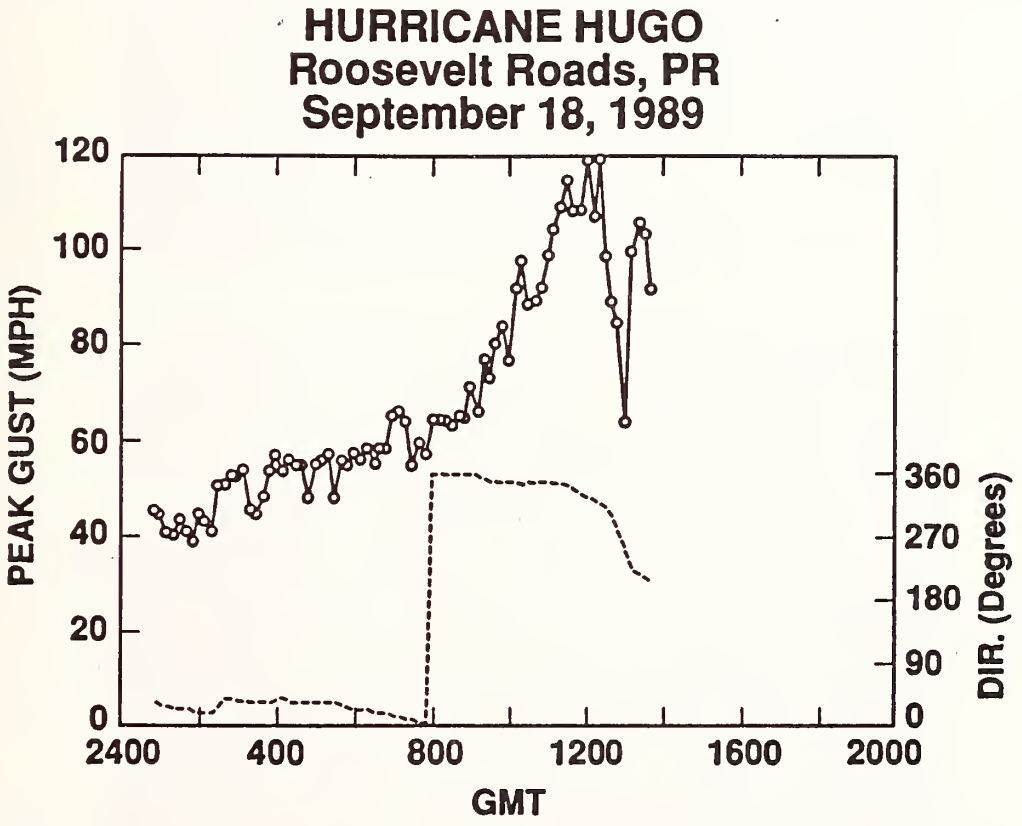

Figure 15b. Same as 15a, except for Roosevelt Roads NAS, P.R.

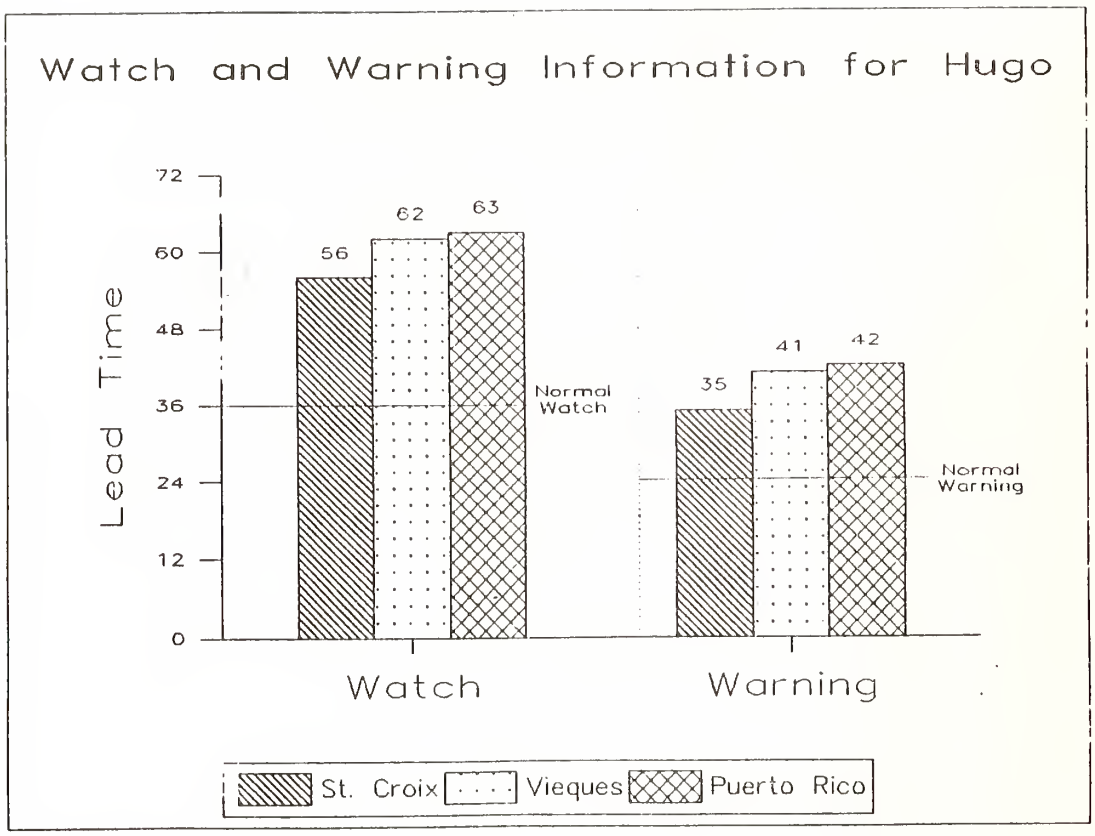

Figure 16. Histogram of warning-lead times from official NWS advisories for Hurricane HUGO in Puerto Rico and U.S. Virgin Islands. Courtesy D. Wernly, NWS/OM.

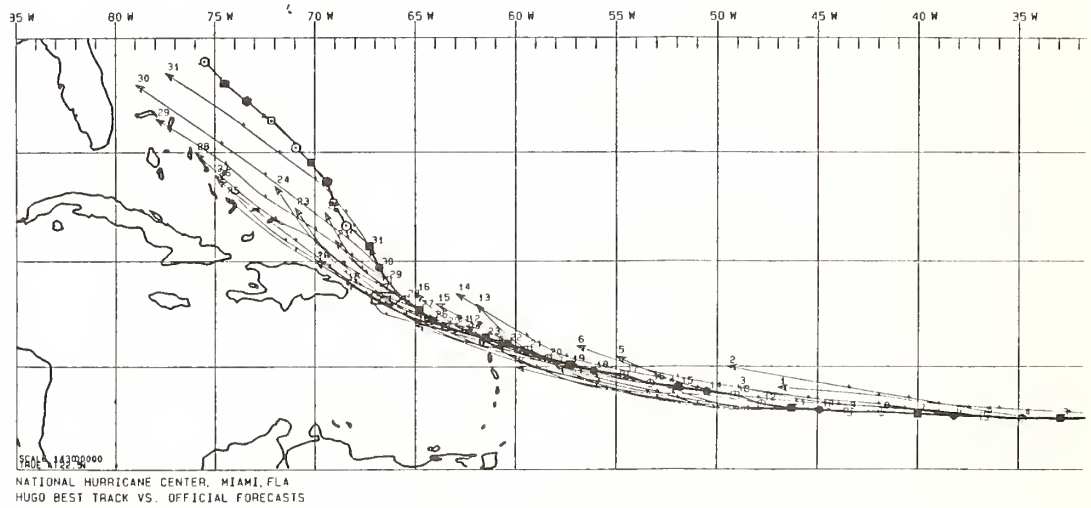

Figure 17. Comparison of final, smoothed track for Hurricane HUGO (bold-line) with official forecasts of future track issued at 12-hourly intervals by NHC, Miami. Courtesy of M.B. Lawrence and R. Case, NHC/NWS.

Figure 18a. Apparent microburst damage in 2 residential areas of St. Croix (aerial photos).

Figure 18b. Close-up aerial photo of microburst damage near north coast, Vieques.

Monitoring the Aerodynamic Performance of a Classic Suspension Bridge

by

Harold R. Bosch[1]

ABSTRACT

More than 50 years ago, a classic girder-stiffened suspension bridge was constructed near the small town of Sedgwick on the Atlantic coast of Maine. Spanning Eggemoggin Reach near Penobscot Bay, the Deer Isle-Sedgwick Suspension Bridge is similar in design and appearance to the ill-fated original Tacoma Narrows Bridge. The inherent flexibility of the design and the selection of a relatively poor aerodynamic cross section have resulted in a bridge which has behaved quite dynamically throughout its many years of service. Despite periodic structural modifications aimed at increasing the structure's stiffness and controlling the wind-induced motions, the bridge continues to exhibit some sensitivity to the forces of wind. In 1981, the Federal Highway Administration and Maine Department of Transportation jointly installed an instrumentation system on the Deer Isle Bridge to monitor and evaluate its aerodynamic performance. This paper will provide details on the instrumentation, describe the process of data reduction, present some preliminary findings, and discuss future plans for this ongoing research study.

KEYWORDS: Aerodynamics; bridge; dynamics; long-span; measurements; suspension; wind.

1. INTRODUCTION

Full scale measurements at bridge sites are an important part of the Federal Highway Administration's (FHWA's) wind research program. The wind data obtained provides detailed information regarding prevailing conditions (speeds, direction, angle-of-attack) and turbulence properties (intensity, spectrum, scale) which is often not available from other sources. The structural response data provides information on the structure's dynamic properties (frequencies, mode shapes, damping) which can be compared with computed values. Wind and structural measurements are often used in the design of wind tunnel experiments and to evaluate the effectiveness of aerodynamic retrofits. They can also provide a means for determining the adequacy of experimental and analytical techniques.

In 1970, the FHWA installed its first field wind instrumentation system on the Newport, Rhode Island Suspension Bridge in cooperation with the Rhode Island Turnpike and Toll Bridge Authority. Since that time, wind and response measurements have been taken on the Sitka Harbor Cable-Stayed Bridge (Alaska), Perrine Memorial Bridge (Idaho), and Pasco-Kennewick Intercity Bridge (Washington). New and improved instrumentation systems are currently in place on the Luling Cable-Stayed Bridge (Louisiana) and Deer Isle-Sedgwick Bridge (Maine). Through a cooperative arrangement with the Maine Department of Transportation (MEDOT), FHWA is monitoring the aerodynamic performance of the Deer Isle Bridge in order to provide recommendations regarding bridge rehabilitation. This study is well underway and will be described in more detail in what follows.

2. DEER ISLE-SEDGWICK BRIDGE

The Deer Isle-Sedgwick Bridge, illustrated in Figure 1, is a conventional suspension structure located near Penobscot Bay on the coast of Maine. Built in 1938, the bridge spans Eggemoggen Reach and consists of a girder-stiffened deck similar in cross section to the original Tacoma Narrows Bridge. The main span is 1080 ft (329m) in length with side spans of 484 ft (148m) and approach spans of 100 ft (40m) for a total bridge length of 2308 ft (704m). The structure is symmetrical with two towers and the roadway has a 6.5% grade to provide vertical navigational clearance of 85 ft (26m) at midspan. The 2-lane deck consists of a 4.5 in (11cm) concrete slab having a width of 20 ft (6m). Stiffening girders are 6.5 ft (2m) deep and spaced 23.5 ft (7m) apart.

3. BRIDGE SITE

The bridge site is situated in Hancock County approximately 55 miles (88km) east of Augusta and 35 miles (56km) south of Bangor. The bridge carries State Route 15 over Eggemoggen Reach and connects Sedgwick on the mainland with Deer Isle and Stonington on the Islands. The longitudinal axis of the structure lies on a NE-SW orientation with the mainland being at the north end of the bridge and Little Deer Isle at the south end. The countryside to the north consists of heavily forested, rolling hills varying in elevation to a few hundred feet. To the south and east are many forested, low-lying islands, Deer Isle being the largest, with the Atlantic Ocean beyond. To the west there is Penobscot Bay with a small mountain range beyond.

---

[1]Research Structural Engineer
Federal Highway Administration
McLean, Virginia 22101-2296 U.S.A.

4. INSTRUMENTATION

4.1 Sensors

A large array of instruments has been installed on the Deer Isle Bridge to monitor the wind environment and structural response to wind loadings. The positions of sensors on the bridge are indicated in Figure 2. Mean wind speed and direction are measured by two skyvane sensors mounted on the top and bottom of the north bridge tower. The upper skyvane is 18 ft (5.5m) above the tower top while the lower one is located approximately 33 ft (10m) above the water. Air temperature is measured by three thermistor probes installed at the top and bottom of the same tower and at the instrument house north of the bridge. Six tri-axis anemometers are used to monitor wind turbulence quantities (speed, direction, intensity, scale) at the elevation of the bridge span. These anemometers are mounted on 12 ft (3m) outriggers cantilevered from the east side of the superstructure and spaced in a logarithmic array. Each anemometer set is aligned with the bridge so that the "U" component is normal to the longitudinal bridge axis (facing southeast), "V" component is parallel to the bridge axis (facing northeast), and "W" component points upward. The tri-axis anemometers employed are dynamic instruments which are capable of tracking velocity fluctuations in the frequency range of interest.

Bridge deck response is monitored by six pairs of single-axis, servo accelerometers installed along the north side span and main span. Accelerometer stations on the side span are located at midspan and the quarter point nearest the north tower. For the main span, stations are located at midspan, both quarter points, and the eighth point nearest the north tower. At each station, an accelerometer mounted inside a weathertight enclosure is clamped to the bottom flange of each stiffening girder. The axis of each accelerometer is oriented to point upward to measure vertical motion. The pair of accelerometers at each station define the vertical displacement and rotation of the span at that point. The whole array of stations are used to determine mode shape and frequency for the structure.

To define tower motion, three accelerometers are used at the top cross girder of the north tower. Two of these are mounted at the top of each tower leg with their axes oriented to point northeast. This defines bending and twisting of the tower top. The third is pointed southeast to indicate tower sway.

4.2 Recorder

Data recording equipment as well as lab test equipment, parts, and supplies are housed in a small instrument house located just off the north end of the bridge. This building is outfitted with heat, air conditioning, telephone, security system, and motor-generator (for conditioning incoming power). Analog signals from all sensors located on the bridge are routed to this instrument house via multi-conductor, shielded cable installed on the west side of the bridge. Approximately 20,000 ft (6096m) of cable was required to instrument the Deer Isle Bridge. To insulate the instrumentation from lightning strikes, protection devices were installed in each accelerometer enclosure and at the input panel in the instrunent house.

The analog signals from the bridge sensors are passed through signal conditioning and amplified to provide maximum resolution in the recording system. Anemometer gains were adjusted to accommodate wind velocities up to 100 mph (161km/h) and accelerometer gains adjusted to handle .25g. Amplified signals from the deck anemometers and all accelerometers are low-pass filtered at 10 Hz to avoid aliasing of the data. All signals are then routed to the recorder.

The recorder is an automated data acquisition system (DAS) equipped with three 11-track cartridge tape drives providing enough capacity for 24 hours of recording. Figure 3 illustrates the data path and control logic employed by the data acquisition system. The DAS continuously scans up to 64 channels of analog input at a rate of 20 Hz. Data recording does not begin until either wind velocities or bridge accelerations exceed preset levels for a selected period of time. Once initiated, recording continues until signals drop below these threshold values. This mode enables unattended operation and optimizes use of available data storage capacity. While recording, the system continuously scans all channels, converts the analog signals to digital data, and stores this data on magnetic tape for later processing. When one tape fills, the recorder automatically switches to another drive and continues without loss of data. Wind speed and direction measured by the two tower anemometers are also recorded on strip-chart recorders. This recording is continuous and documents the day-to-day wind conditions at the site regardless of whether or not the DAS is active.

5. DATA REDUCTION

After wind and bridge response data has been recorded on digital tape, the tapes are forwarded to Turner-Fairbank Highway Research Center (TFHRC) for preprocessing and evaluation. This data reduction is accomplished by FHWA staff using various microcomputers. Data tapes are first scanned for errors. Raw data is converted to engineering units using sensor calibrations obtained in the field and channel statistics such as minimum, maximum, mean, and standard deviation are compiled for 10/20-minute blocks of data. This information is used to evaluate system performance and to identify events which warrant detailed study. Mean wind

speed and direction obtained from the skyvane sensors on the tower are displayed in polar form and evaluated to detect any trends in the recorded data. Figure 4 is a polar plot of wind activity at the top of the north bridge tower. This graph is updated each time new information is obtained. Hourly means are obtained from the continuous chart recordings and plotted in time-history fashion for each month. As demonstrated in Figure 5, this technique is a useful means of compressing large volumes of data and enables identification of significant storm events.

As events of interest are identified during the preprocessing, copies of the data are made for more detailed analysis using mainframes. The data processing sequence is illustrated in Figure 6. This analysis is accomplished in three stages. In the initial stage, raw data is converted to engineering units and summarized using program TAPSUM much the same as was done during preprocessing. The intermediate stage prepares anemometer data from selected events for detailed analysis by applying response corrections and rotating the data into the desired coordinate system. This is accomplished using program MASTER. The final stage of data processing involves spectral analysis of the time series data. In ANAL2, time series data is first prepared for analysis by point averaging, detrending, and tapering. Next, fast Fourier transform techniques are employed to process data from 1, 2, or 3 channels simultaneously. This analysis provides statistics on all the data as well as power spectral densities and auto correlations for the individual series. In addition, co-spectral and quadrature spectral densities, coherence, squared coherence, phase difference, and lagged cross-correlations are available for each pair of series.

To determine bridge displacements, the "conditioned" acceleration time histories are processed through program COMBIN. Here, the signals from the accelerometer pair at each bridge station are averaged to extract the bending component of motion. Next, the signals are differenced to extract the twist component. The acceleration time histories for each sensor as well as those for bending and twist at each station are then processed through MDIASM, a sophisticated double integration routine, to obtain the associated displacements. Finally, these results are input to BRPLOT, containing various 2-D and 3-D plotting routines, for evaluation of mode shapes and animation of bridge motion.

6. RESULTS

Wind spectra have been obtained for selected wind events and compared with three empirical functions--one proposed by Panofsky and Dutton, another by Simiu and Scanlan, and a third by Ramsdell. Typical spectra are presented in Figure 7 for the U-components of four deck level anemometers. The wind was from the southeast with a mean wind speed of 44 mph (20.5m/s) and a turbulence intensity of about 10%. The measured spectra compare quite well with the Ramsdell and "P/D" models.

To study the influence of the structure's bluff cross section on the turbulence characteristics as the wind passes around the bridge, anemometer 3a was moved to the west side of the deck opposite anemometer 4 and redesignated 3b. Figure 8 illustrates typical results obtained from undisturbed and disturbed air flows measured by sensors 4 and 3b respectively. For this event, wind was from the southeast with a mean speed of 40 mph (19m/s). The spectra from anemometer 3b, located in the wake of the structure, demonstrate a marked increase in energy at the higher frequencies.

The along-span coherency of the wind was computed using the logarithmic spacing of the 6 deck anemometers. These spacings range from 105 to 1050 ft (32 to 320m). Coherency results for a 43 mph (20m/s) quartering wind from the south are presented in Figure 9. These plots exhibit the characteristic decay with increasing separation distance between sensors. Approximate exponential functions are included for comparison. Similar results are presented in Figure 10 for a 44 mph (20.5m/s) perpendicular wind from the southeast. The coherence appears to decay more rapidly for this case.

A summary of wind measurements at deck level based upon data from 7 tapes is presented in Figure 11. The polar plot illustrates the distribution of mean wind speeds and directions relative to the bridge span. The maximum wind speed included in this data is 40 mph (19m/s). Above the wind distribution plot is a graphical representation of the associated peak accelerations measured at all deck stations. Although not all possible directions and speeds are represented, this figure clearly demonstrates the pronounced bridge sensitivity to perpendicular winds. The maximum acceleration observed in this dataset was 0.1g.

The affect of wind speed on bridge motion is illustrated in Figure 12. These results are based upon measurements at accelerometer 5 and anemometer 5. On the first graph, peak accelerations are plotted versus the U component of wind. For the second and third, RMS accelerations are plotted versus the W and V components, respectively. A strong relationship between bridge accelerations and wind speed is clearly evident. The significance of wind angle on bridge response in presented in the last graph. Here, it is apparent that the average level of bridge motion increases as the wind becomes more perpendicular to the structure. Figure 13 is an example of a measured acceleration record and the computed displacement time history for accelerometer 9. The maximum displacement computed from the dataset was about 4 in (10cm).

7. CONCLUSIONS

All data collected to date has been preprocessed and summarized; however, only a small portion has received detailed analysis and evaluation. Therefore, the results presented above must be considered preliminary. Wind and bridge response measurements at the site are still underway and "production" processing of the extensive database has just begun. With this in mind, the following observations may be made:

- spectral functions computed from wind data look reasonable,
- computed spectral functions compare well with the Ramsdell model,
- the structure's shape generates strong "local" turbulence with increased energy at higher frequencies,
- bridge motion is more likely to occur when winds are perpendicular to the span, and
- bridge activity tends to increase steadily as wind speed increases.

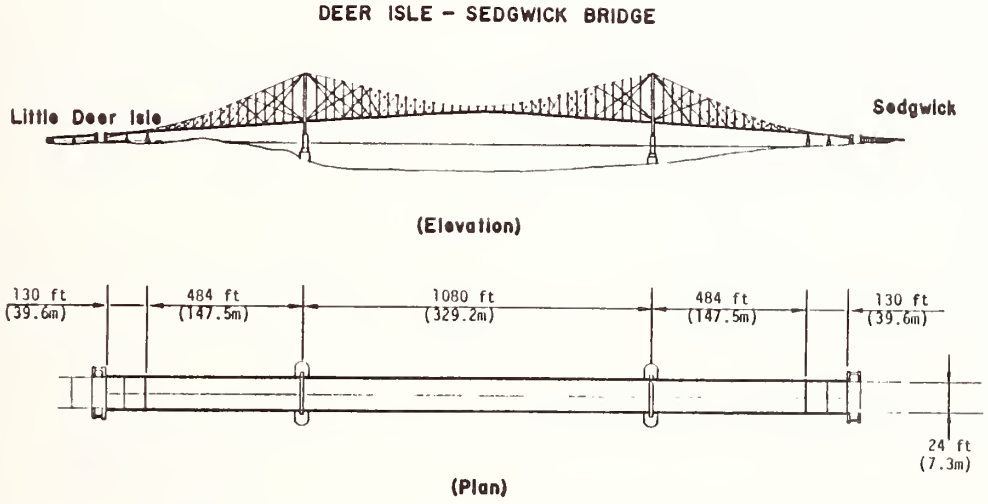

Figure 1. Bridge Plan And Elevation Views.

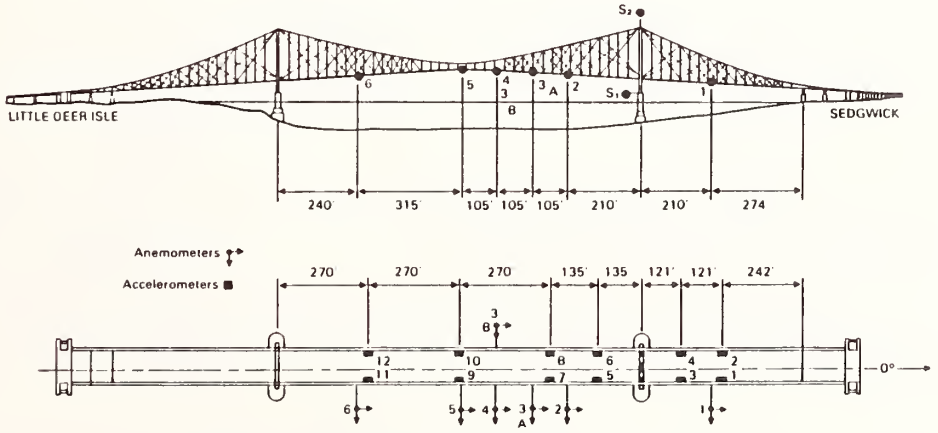

Figure 2. FHWA Instrumentation Layout.

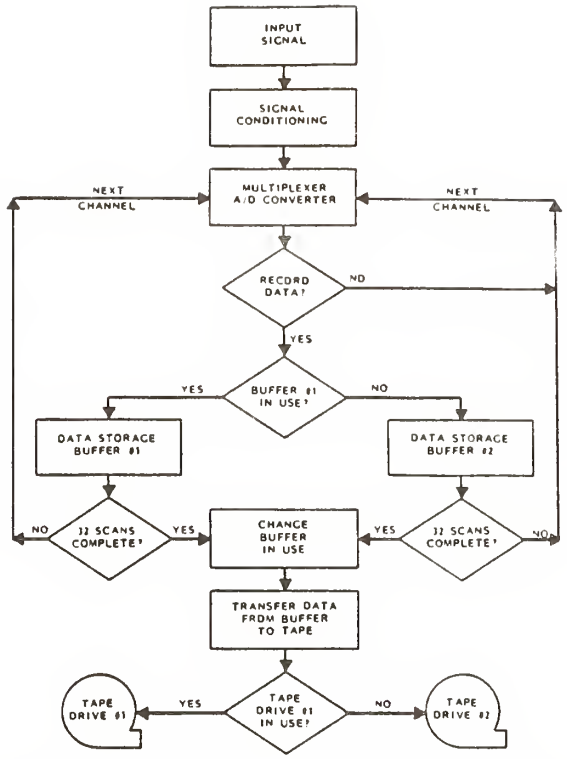

Figure 3. Data Acquisition System Schematic.

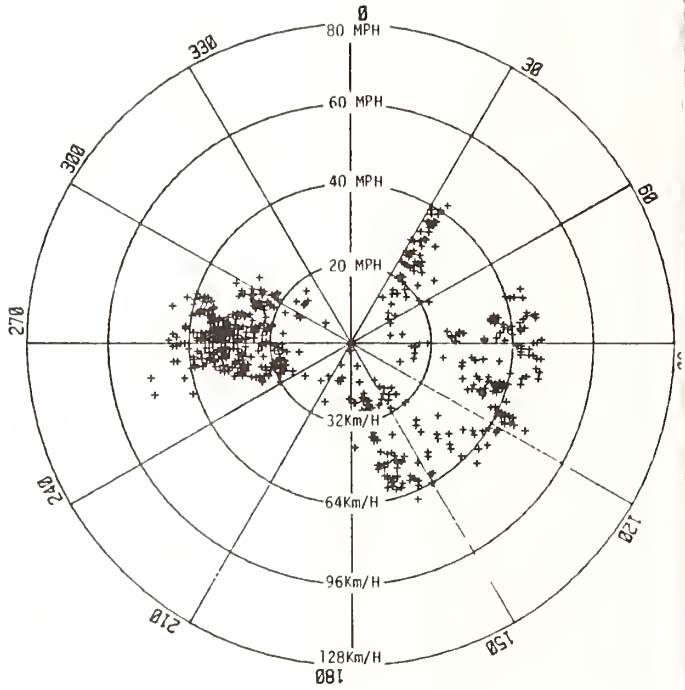

WIND ANGLE VS. RESULTANT WIND VELOCITY

TOP OF NORTH TOWER

Figure 4. Polar Plot Of Recorded Wind Events.

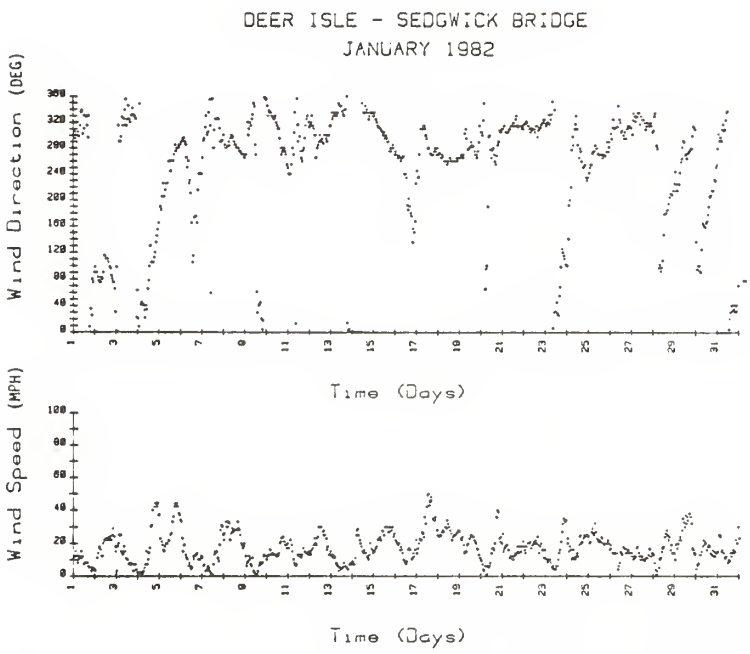

Figure 5. Monthly Summary Of Wind Activity.

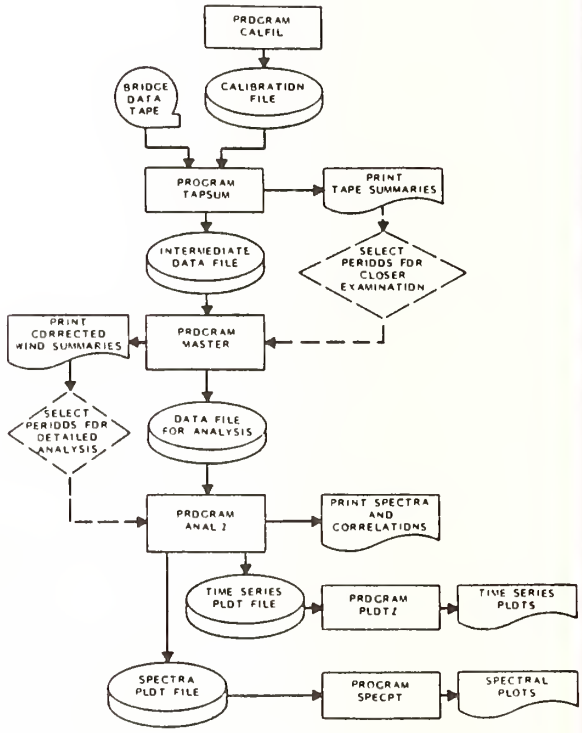

Figure 6. Data Processing Sequence.

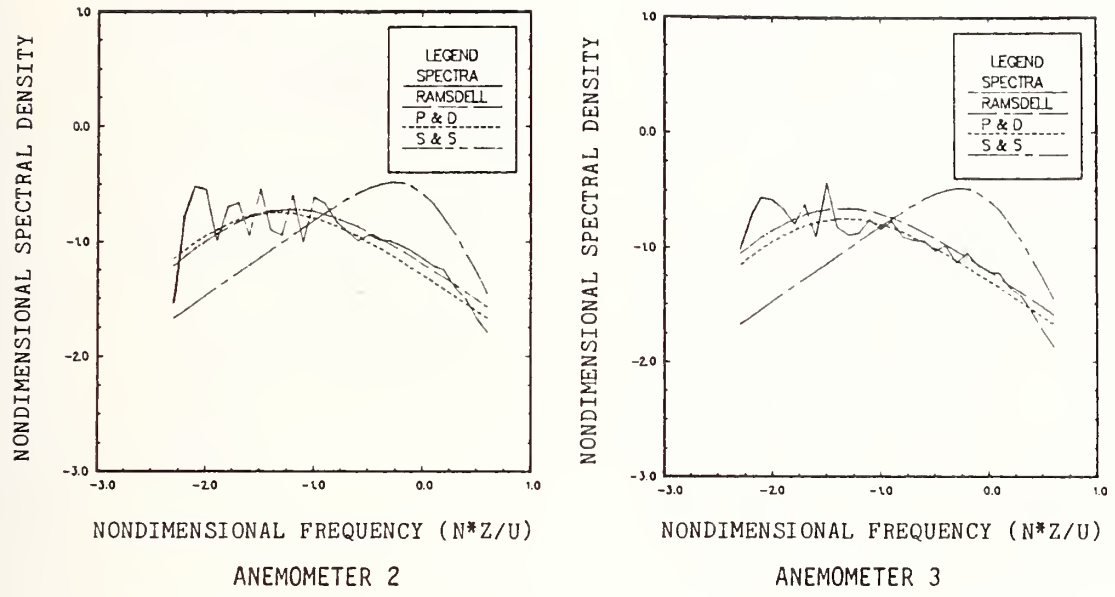

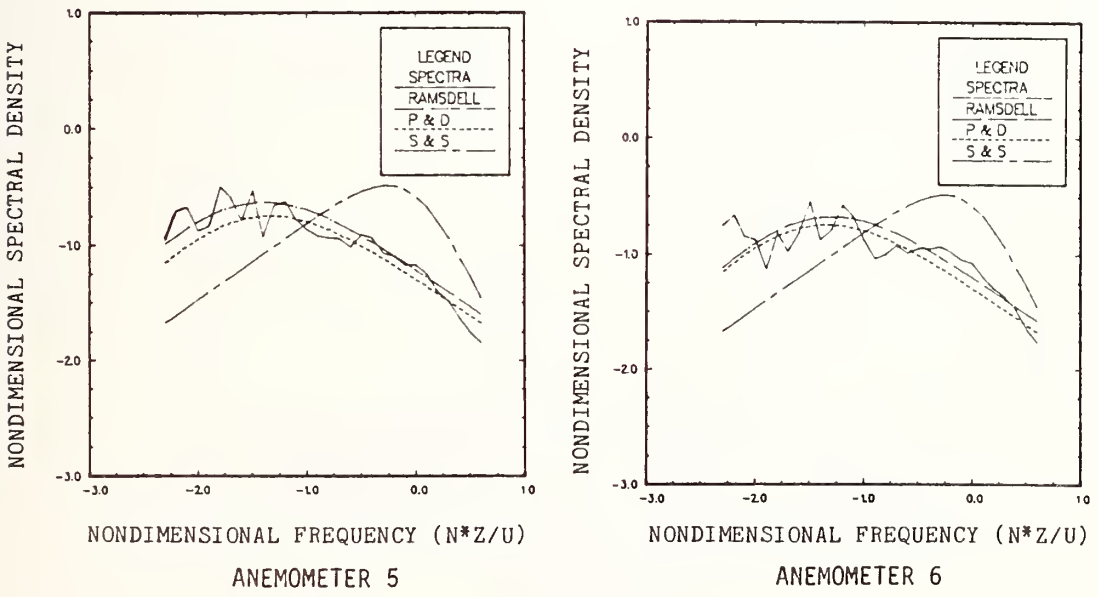

Mean Speed: 44 m/h (20.5 m/s); Direction 80°

Figure 7. Wind Spectral Density For Four Anemometers - U Components.

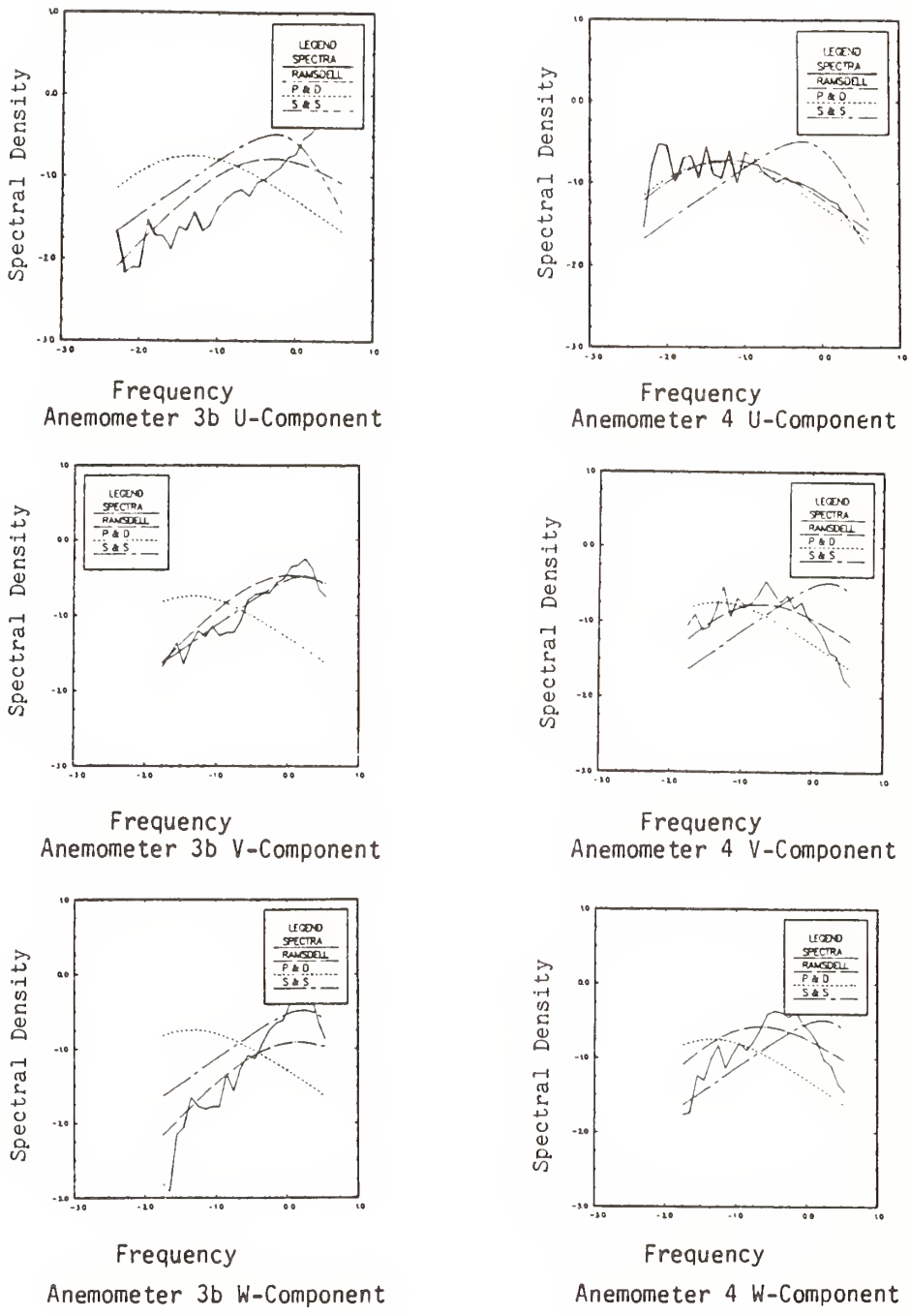

Mean Wind Speed: 40 m/h (19 m/s); Direction 90°

Figure 8. Wind Spectral Density For Upwind And Downwind Anemometers.

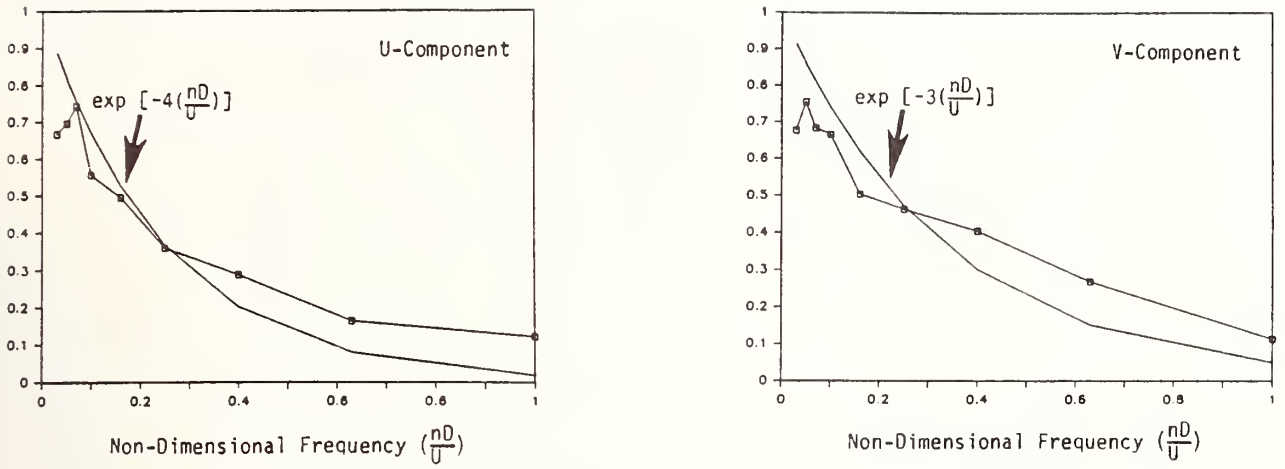

Figure 9. Along-Span Coherency For A 43 mph (20m/s) Quartering Wind (133°).

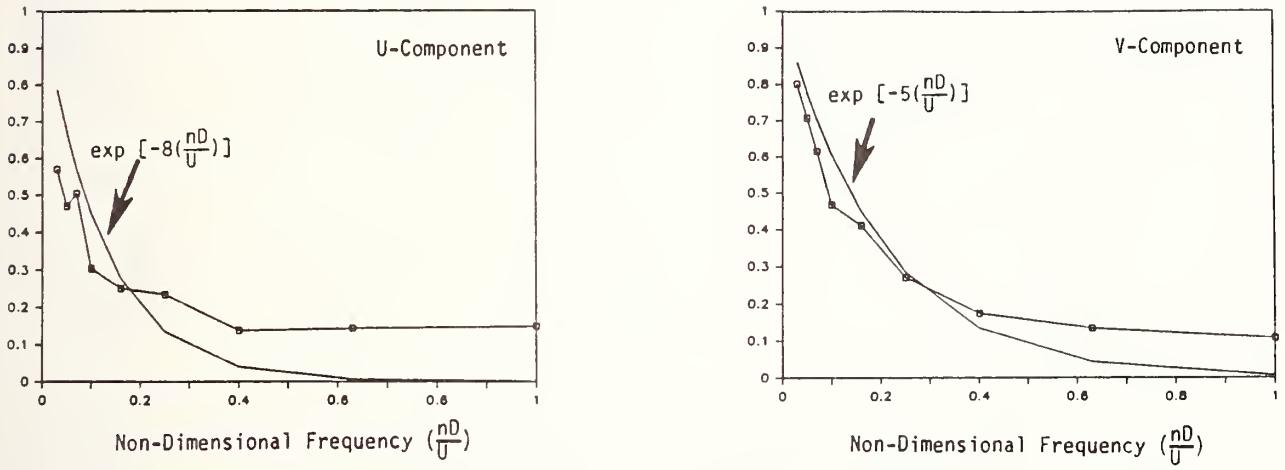

Figure 10. Along-Span Coherency For A 44 mph (20m/s) Perpendicular Wind (80°).

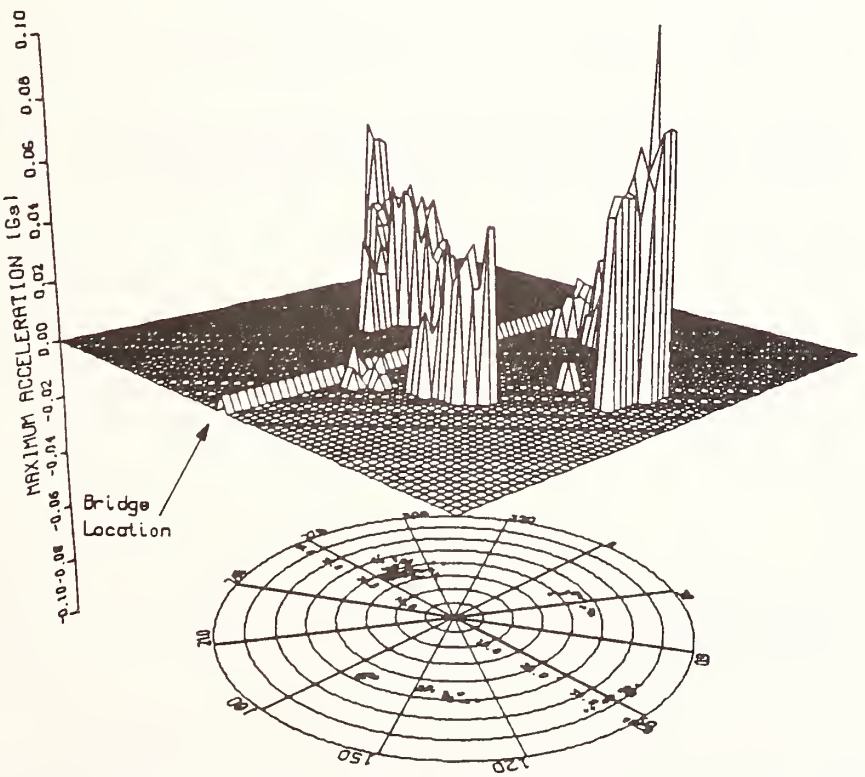

Figure 11. Summary Plot Of Wind Speeds And Maximum Bridge Accelerations.

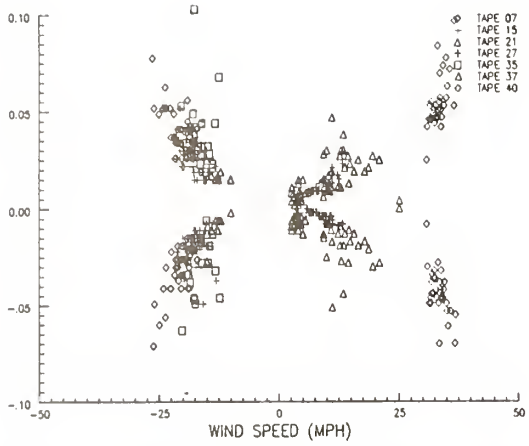

a. MAXIMUM AND MINIMUM ACCELERATIONS DUE TO U-COMPONENTS

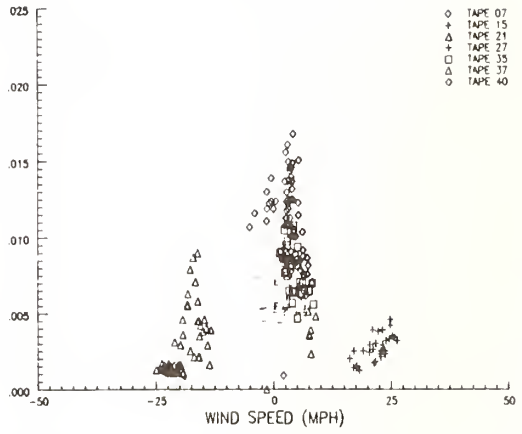

c. STANDARD DEVIATION OF ACCELERATION DUE TO V-COMPONENTS

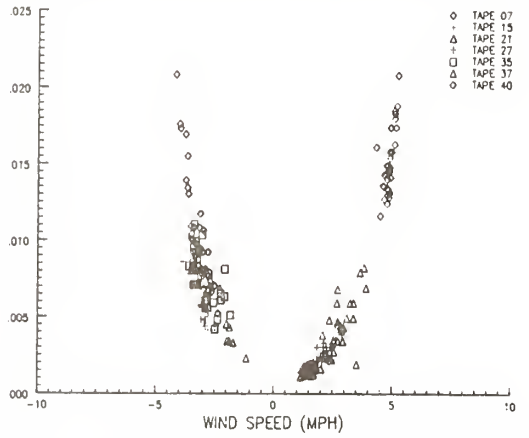

b. STANDARD DEVIATION OF ACCELERATION DUE TO W-COMPONENTS

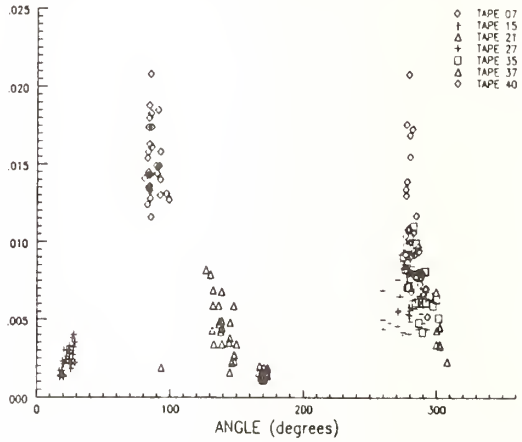

d. STANDARD DEVIATION OF ACCELERATION DUE TO WIND ANGLES

Figure 12. Bridge Acceleration Versus Wind Speed And Angle - Accelerometer 5.

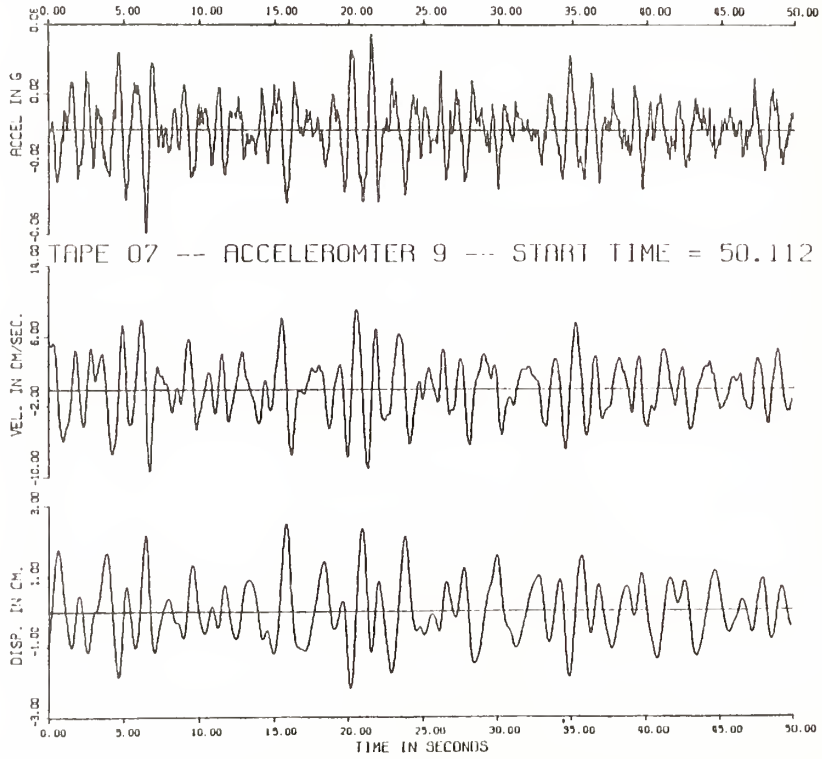

Figure 13. Bridge Acceleration, Velocity, Displacement - Accelerometer 9.

Cooperative Research Program on Wind Tunnel Testing in Turbulent Flow

BY

Koichi Yokoyama*1, Robert L. Wardlaw*2, Hiroshi Sato*3,

Takaaki Kusakabe*4, and Michael G. Savage*5

ABSTRACT

National Research Council Canada and Public Works Research Institute, Japan are carrying out a cooperative research on the wind tunnel testing method in turbulent flow. This project includes spring mounted rigid model test, taut strip model test, and 2 phases full model wind tunnel tests using heavy and light models.

In this report, the outline of this research is explained at first. And summary of wind tunnel tests are introduced.

KEYWORDS

Wind tunnel, Turbulent Flow, Cable stayed bridge, full model test, Cooperative research

1. INTRODUCTION

The design of long span bridges requires the consideration of the effects of strong wind. Therefore, wind tunnel test is usually performed to determine the wind-induced response of the bridge at design stage.

Many long span bridges are planned and constructed and the wind effects on structures are eagerly studied in North America, Europe, Japan and other countries. However, the wind tunnel testing method has been developed in each country and the standard testing method and assessment of the results have not been established.

The Governments of Canada and Japan have the technical cooperation program on wind and seismic effects on structures. National Research Council Canada (NRCC) and Public Works Research Institute (PWRI) are the counterpart organizations.

Recently, both laboratories have started a cooperative research project and have jointly undertaken a series of winds tunnel tests on wind-induced oscillations of cable-stayed bridge in smooth flow and in turbulent flow. Included in the project are a study on comparison of results of wind tunnel tests performed in different wind tunnel facilities and proposal on the standard wind tunnel testing method of cable-stayed bridges.

In this report, described are the outlines of the cooperative research work between Canada and Japan and results of wind tunnel tests consisting of spring mounted rigid model test, taut strip model test, and full model test.

2. OUTLINE OF THE PROJECT

2.1 Purpose of the project

The purpose of this project is to establish procedures and guidelines for wind tunnel tests of full bridge models in smooth flow and boundary layer turbulent flow. This will be performed by making the influence derived from difference of method clear, through comparing wind tunnel tests between Canada and Japan.

The methods of wind tunnel tests have been developed in each country. There have been exchanges of information on techniques of wind tunnel testing, however there are many differences among countries. So it seems significant to make the influence derived from differences of method clear , through comparing wind tunnel tests between Canada and Japan.

2.2 Program of the project

This project began in 1987 and will be over in 1990. This research consists of spring mounted rigid model test, taut strip model test and 2 phases full model tests as shown in Figure 1.

(1) Spring mounted rigid model test

The spring mounted rigid model test in smooth flow is carried out to study fundamental characteristics of the bridge deck. Results of this test are compared with results of full model test. This test is performed only in PWRI.

(2)Taut strip model test

The taut strip model test in smooth flow and in turbulent flow is carried out to study fundamental 3-dimensional effects and effects of turbulence on bridge

---

*1 Head Structure Div. Public Works Research Institute, Ministry of Construction, 1, Asahi, Tukuba-Shi, Ibaraki-Ken, 305, Japan

*2 Head, Low Speed Aerodynamics Laboratory, National Research Council Canada, Montreal Road, Ottawa, Ontario, Canada, K1A, 0R6

*3 Dr. Eng., Head, planning Div.,PWRI

*4 Research Engineer, Structure Div., PWRI

*5 Research Officer, Low Speed Aerodynamics Lab., NRCC

deck. Results of this test are also compared with results of full model test. This test is performed only in PWRI.

(3)Full model tests.

These tests are the core of this cooperative research. Similar full model tests were performed in both NRCC and PWRI, and they are compared. The final result of this cooperative research is drawn out from these test. There are two phases of full model tests. Namely, heavy models are used in the 1st phase and light models are used in the 2nd phase. Japanese research engineers joined both phases of full model tests carried out in Canada and Canadian research officer joined on the 1st phase test in Japan.

At present, all wind tunnel tests mentioned above have been completed. Through discussing on these results, it will become possible to establish manual or guideline on wind tunnel testing method.

3. DESIGN OF EXPERIMENT

3.1 Bridge model for wind tunnel test

3.1.1 Deck Section

The shape was not intended to resemble any particular bridge but rather it was considered representative of modern plate and girder construction. Figure 2 shows the shape used in the full model tests. In NRCC, there is full model of the Quincy Bridge. The Quincy Bridge model was built with a length scale of 1:75 so that the overall length of 7220 mm would fit between the concrete fillets of 9 m wide NRCC low speed wind tunnel. It seems that using this model is efficient and economical. So in the 1st phase of full model test, the Quincy Bridge is referenced to decide characteristics of deck. Table 1 summarizes the deck sectional characteristics.

The full model of PWRI has half geometrical scale. This scale was decided in consideration of the boundary layer wind tunnel in PWRI which is 6 m wide and 3 m high. All characteristics of the full model in PWRI are derived from the full model of NRCC.

3.1.2 Cable and Tower Assembly

The deck was divided into three spans, in NRCC, a center span of 3658 mm and two side spans of 1781 mm, and was supported by 56 cables attached to two towers. Figure 3 is elevation views of the installations and shows the structural supports for the models. In NRCC the towers and end points of the bridge were supported on an isolated corner foundation to minimize the interference created by the vibrations of the wind tunnel shell, but in PWRI the model was only set on the floor of the wind tunnel.

The cables for the model were made from small diameter stainless steel piano wire except the light model at PWRI in the 2nd phase. In PWRI, the geometrical scale is half of NRCC's model, and diameter of cables were reduced in the 2nd phase of full model test. So it becomes impossible to get a piano wire that is small enough. Coil springs were used to adjust the elongation stiffness of cables in the 2nd phase at PWRI. The stiffness of the different cables were not constant and were based on the requirements of the Quincy Bridge model. The properties of the cables are detailed in Figure 4. The cables were anchored directly to the stiffening spines of the deck to minimize the mechanical damping of the bridge model.

3.1.3 Models for Spring mounted rigid model test and taut strip model test.

Spring mounted rigid model test and taut strip model test are performed before full model tests to predict the fundamental characteristics of response, which are determined by shape of cross section, in wind. Table-2 shows the condition of tests.

The shape used in these tests did not have the stiffening spines required for the full model tests. Since the spines were set in the corners, it was expected that their presence would not significantly alter the flow field around the deck. The major difference between the deck sections of these tests and full bridge model tests was the higher reduced mass and inertia of the full bridge.

3.2 Flow properties

In regards to the full model test, the bridge was tested in three different flow conditions, smooth flow, and with moderate and heavy turbulence. The summery of the flow properties is given in Table 3. The moderate turbulence was created with triangular spires equally spaced across the inlet to the test section. The heavy turbulence was created by mounting a flow trip across the test section floor downstream of the spires. The smooth flow condition has residual turbulence level. Figure 5 shows the arrangement of these turbulent generators at PWRI for example.

The length scales for the vertical and streamwise turbulence were based on visual best fits with the Von Karman spectra.

The properties for full model test were not decided when the taut strip model test was performed, so that the flow properties on taut strip model test were different from full model test. Three kinds of turbulent flow were used for the taut strip model test.

3.3 Instrumentation of wind response

The motion of the bridge was monitored by the displacement transducers. Displacement transducers are different between NRCC and PWRI. In NRCC, transducers are such types that are applied to an eddy current. In PWRI they are such types that are applied to the photoelectric effect. So in NRCC, targets are aluminum plates attached to the bottom of girder of model and pickups of transducers are put close to the targets. On the other hand in PWRI, targets are small light bulbs and pickups of transducers are put out of wind tunnel. Vertical and torsional displacements are measured at center and quarter of main span, and center of side span.

The wind velocity and turbulence were monitored by two ways. The turbulence of the wind simulation was monitored with a two channel hot film or wire probe. The mean velocity was measured with a pitot tube.

4. RESULTS OF TEST

Analysis of results of wind tunnel test is almost completed on spring mounted test, taut strip model test, and the 1st phase full model tests using heavy model. These results are introduced here.

4.1 Spring mounted rigid model test.

The results of the test can be expressed clearly in Figure 6 that shows relation between wind velocity and amplitude of vibration of a model. There are two wind velocities which the amplitude of vertical vortex-induced vibration become the peak value. The lower reduced wind velocity is about 1 and the higher is about 2. Here, wind velocity is reduced or non-dimensional wind velocity that is amount of wind velocity divided by the frequency of model and width of deck. In regards to torsional vibration, vortex-induced vibration is caused at about 1.2 and flutter is caused at above 2.5 of reduced wind velocity.

4.2 Taut strip model test

Relations between wind velocity and response of model in smooth flow and in turbulent flow are shown in Figure 7 and Figure 8 respectively. Where the intensity of streamwise turbulence I_u is 5.3%. Results are summarized as written below.

(1) Buffeting

As comparing Figure 8 with Figure 7, buffeting is caused by turbulence.

(2) Vortex-induced vibration

In smooth flow, there are two peaks of wind velocity on vertical bending vibration and there is one peak on the torsional vibration. On vertical vibration, the 1st peak (observed at the low wind velocity) was the 1st bending mode, and the 2nd peak (observed at the higher wind velocity) was a high frequency bending mode. The reduced velocity was about 1.0 on the 1st peak. On torsional vibration, that was 1.2. There is good agreement between spring mounted rigid model test and taut strip model test except on the 2nd peak of bending vibration.

In turbulent flow, each of vortex-induced vibrations vanished or was reduced without changing of wind velocity.

(3)Flutter

The maximum torsional amplitude becomes one degree at reduced velocity 2.5. This was not changed in turbulent flow so much as shown in Figure 8.

4.3 Full model tests in the 1st phase

4.3.1 The full model test in NRCC (1988)

(1) Buffeting Response

The displacement recorded by the three transducers at each station were resolved into vertical, lateral, and torsional motion. The mean, peak, and standard deviation of the responses for each of these degrees of freedom were calculated for the three valid stations for deck sections for all three flow conditions. The peak values are the magnitude of the maximum deviation in either positive or negative direction from the mean position of the bridge. Figure 9 shows the standard deviation and peak values as a function of the reduced wind velocity for the torsional and vertical motions. For these figures the velocity was reduced by the appropriate deck section width and the corresponding natural frequency in the first torsional or vertical bending mode.

A frequency analysis of the center span motion for the vertical and torsional motion was carried out in both the moderate and highly turbulent flow. The dominant modes were the lowest modes on each vertical and torsional vibration.

(2) Vortex-induced vibration

Vortex-induced vibration was not observed.

(3)Flutter

The test In smooth flow shows torsional instability at reduced wind velocity of 3.2. The RMS amplitude becomes 0.5 degree at reduced velocity of 3.6.

4.3.2 The full model test in PWRI (1988)

(1) Buffeting Response

There is no important difference on instrumentation and analysis at PWRI from that of NRCC. Figure 10 shows the standard deviation as a function of the reduced wind

velocity for the torsional and vertical motions.

According to frequency analysis, the dominant modes were the lowest modes on each vertical and torsional vibration.

(2) Vortex-induced vibration

Vortex-induced vibration was not observed.

(3)Flutter

The RMS amplitude becomes 0.5 degree at reduced velocity of 5.7.

5. DISCUSSION

Flutter and buffeting were observed in every type of test. In regards to vortex-induced vibration, it was observed in the spring mounted rigid model test and the taut strip model test, however it was not observed in the 1st phase full model test. The reason is a heavy mass of the full model. The reduced mass of the full model is 3.6 and 4.4 times heavier than that of the spring mounted rigid model and the taut strip model respectively. Taking account of these results, mass and mass moment of inertia were reduced to compare vortex-induced vibration in the 2nd phase full model test. Also full models of the 1st phase were too heavy to compare buffeting and flutter between full model test and spring mounted rigid model test or taut strip model test. Due to such reasons, discussion is limited to comparison of the 1st phase full model tests performed in NRCC and PWRI. Further discussion will be performed after completion of the analysis on the 2nd phase of the full model tests.

5.1 Similarity of test condition

It is very difficult to make exactly similar flows and models. As a matter of fact, any wind tunnel tests have error and restriction of facilities, and the influence they cause must be estimated. Due to this reason, similarity of the test is compared below.

Flow properties are summarized in Table 3. On high turbulent flow, intensity measured in PWRI was a little smaller than in NRCC. On length scale, there are considerable and unexpected differences between NRCC and PWRI. As intensity of turbulence affects the amplitude of buffeting, making a correction will be needed. On length scale, it is not clear how it influences. But the unexpected difference itself must be further discussed.

In regards to characteristics of models, Table 4 summarizes differences. Only structural damping becomes problem and others were well adjusted. The difference of damping affects behavior of flutter developing and onset wind velocity of flutter.

5.2 Flutter

Torsional responses in smooth flow are compared in Figure 11. In NRCC, flutter was caused at lower wind velocity than in PWRI. When amplitude is small, one reason is supposed difference of damping. Figure 12 shows the influence of structural damping and inertia obtained from spring mounted rigid model tests in PWRI. As shown In Figure 12, onset velocity of flutter increases with damping and inertia increasing. The products of structural damping and dimensionless inertia become 0.10 and 0.64 in NRCC and PWRI respectively. These data suggest that it is not a strange difference on small amplitude vibration. On the other hand, there is a small difference of structural damping where amplitude is large. But there is also not a small difference on large amplitude of flutter. There is no idea of the reason that explains this difference yet.

5.3 Buffeting

Amplitude of buffeting is compared in Figure 13. These data are measured at a station of center of the mair span in the flow with high turbulence. It is clear that amplitude observed In NRCC is almost 2 times larger than in PWRI at every wind velocity. The amplitude of buffeting is changed by intensity of turbulence. However it seems there is not enough difference of intensity that causes such a difference of amplitude between by NRCC and by PWRI.

6. Concluding Remarks

In this report, outline of the project is explained and results of tests performed In the first 2 years are introduced. Further discussion is needed to get final results. There is no comparison on vortex-induced vibration. On this problem, the 2nd phase full model tests using lighter models have been already completed In NRCC and PWRI, and analysis is being performed.

There are no small differences between the results of NRCC and PWRI. Of course, some differences should be Inevitable. But by analysing components and the reason of differences, many problems will become clearer on the precision of the wind tunnel test, methods of results correction, and reasonable procedure for wind tunnel test. To get these fruits, not only advanced discussion but also additional test will be needed.

ACKNOWLEDGEMENT

Authors wish to express appreciation to the Japanese Science And Technology Agency for financial aid to this cooperative research.

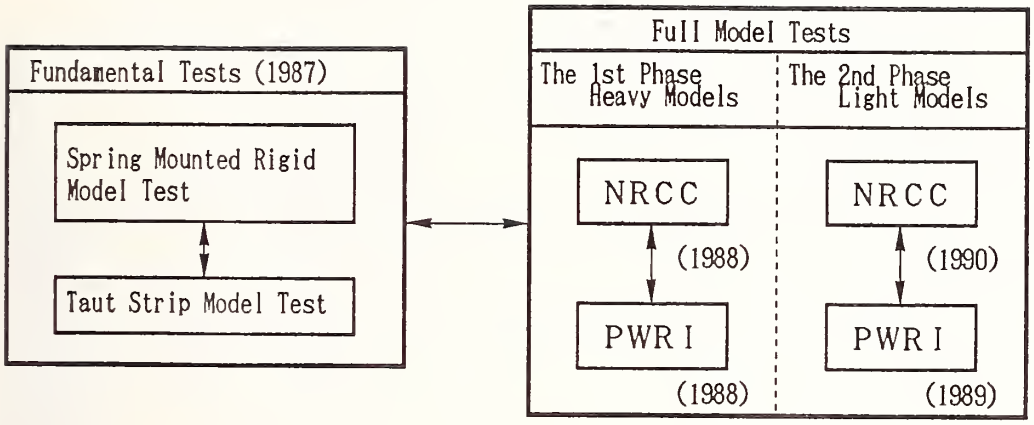

Figure-1 PROGRAM OF COOPERATIVE WIND TUNNEL TEST

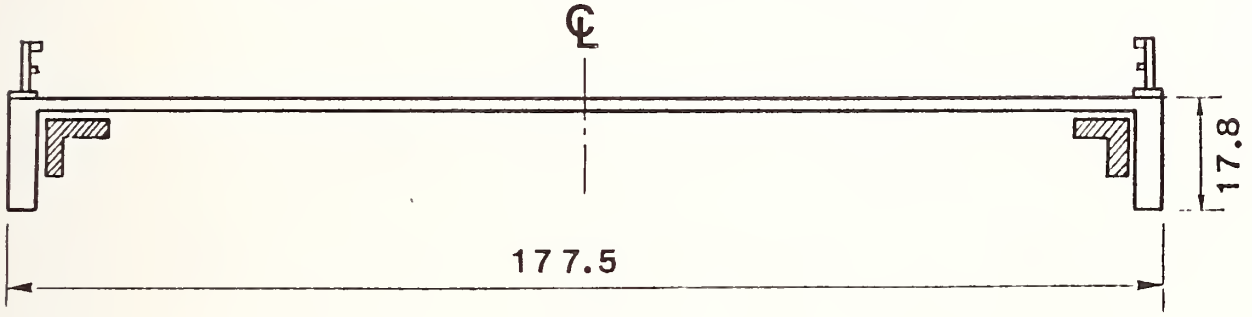

(1)NRCC

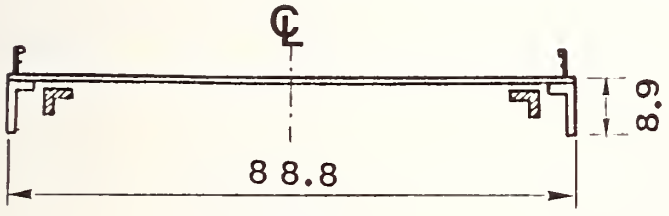

(2)PWRI

:STIFFENING SPINES

Figure-2 CROSS-SECTION OF BRIDGE DECK

Table-1 Deck Sectional Properties

Width (m)	0.177
Depth (m)	0.0177
Mass/Unit Length(Kg/m)	3.31
Reduced Mass($m/\rho B^2$)	87
Mass Moment of Inertia(Kg • m)	0.0174
Reduced Inertia($I/\rho B^4$)	14.5

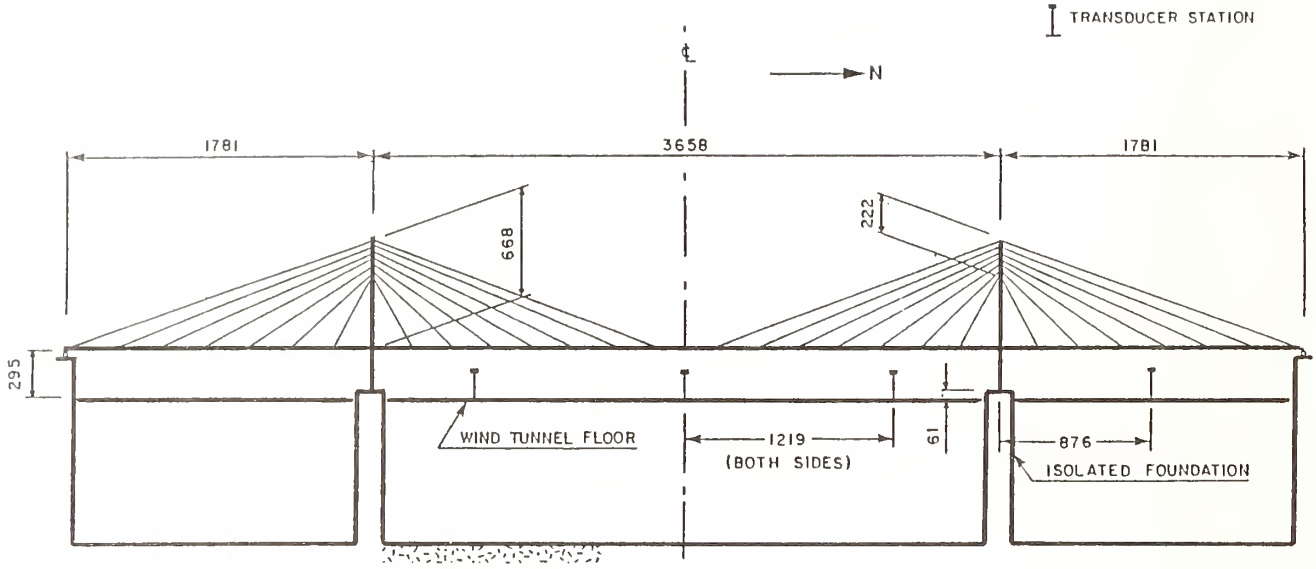

(1)NRCC

(UNIT:mm)

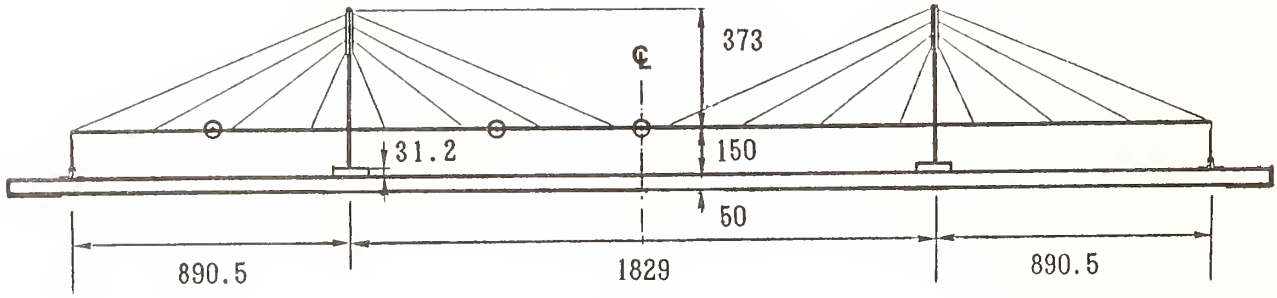

(2)PWRI

Figure-3 ELEVATION VIEW OF MODEL

CABLE NO.	EA(10^3N)	CABLE TENSION(N)
①	12.9	7.93
②	12.9	9.73
③	10.6	7.77
④	10.6	6.91
⑤	5.2	5.80
⑥	5.2	4.75
⑦	5.2	3.88

CABLE NO.	EA(10^3N)	CABLE TENSION(N)
⑧	5.2	3.81
⑨	5.2	4.63
⑩	5.2	5.52
⑪	8.6	6.78
⑫	8.8	8.22
⑬	8.8	8.74
⑭	10.8	9.12

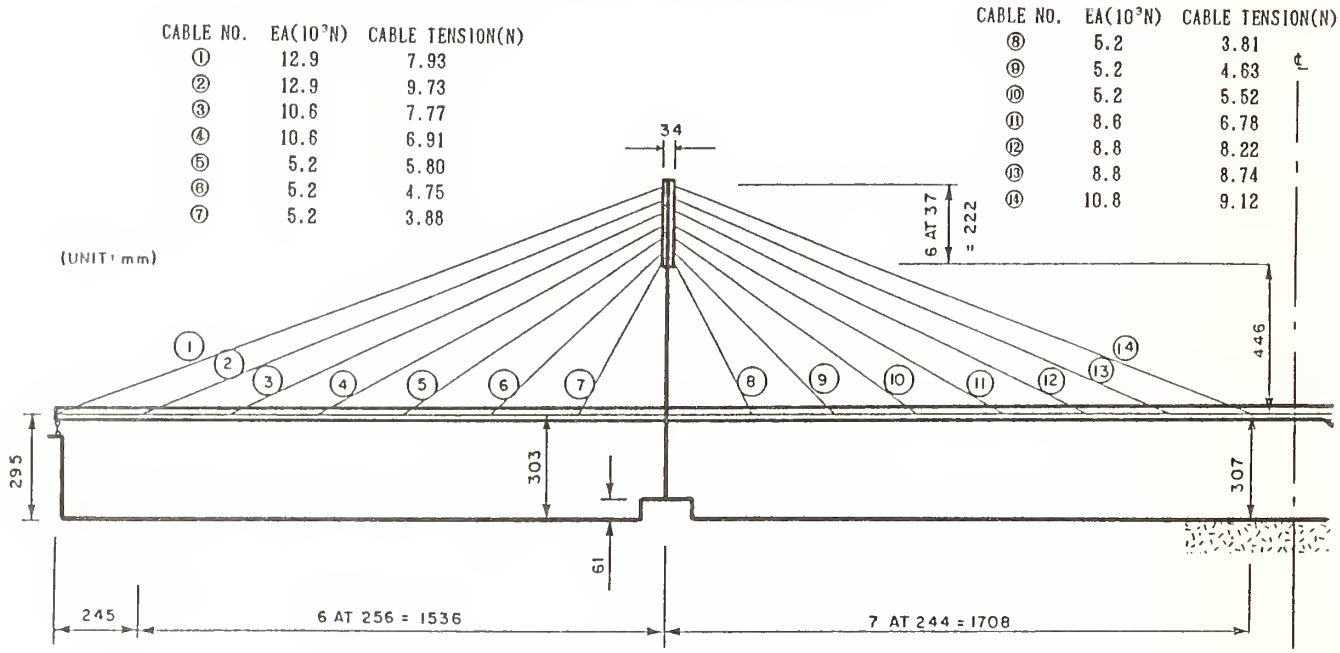

Figure-4 CABLE ARRANGEMENT (NRCC)

Table-2 CONDITION OF TEST
(SPRING MOUNTED TEST AND TAUT STRIP MODEL TEST)

Condition	Spring Mounted Rigid Model Test	Taut Strip Model Test
Width B (m)	0.40	0.10
Depth D (m)	0.04	0.01
Length of Model (m)	0.97	1.20
Mass/Unit Length m(kg/m)	4.70	0.233
Reduced Mass ($m/\rho B^2$)	24.0	19.8
Mass Moment of Inertia (kg • m)	0.117	1.57×10^{-4}
Reduced Inertia ($m/\rho B^4$)	3.61	1.34
Natural Frequency (Hz)		
Vertical Bending Mode	1.97	7.61
Torsional Mode	3.86	13.9
Stractural Damping (Log Decrement)		
Vertical Bending Mode	0.020	0.025
Torsional Mode	0.017	0.041

Table-3 Characteristics of Turbulent Flow

Caracteristics / name of Flow		Intensity		Scale	
		I_u	I_w	L_u^x/B	L_w^x/B
NRC(1988)	Flow A	0.099	0.067	1.9	1.2
	Flow B	0.207	0.148	3.0	0.9
PWRI (1988)	Flow I	0.092	0.052	6.0	0.7
	Flow II	0.163	0.104	4.0	1.1

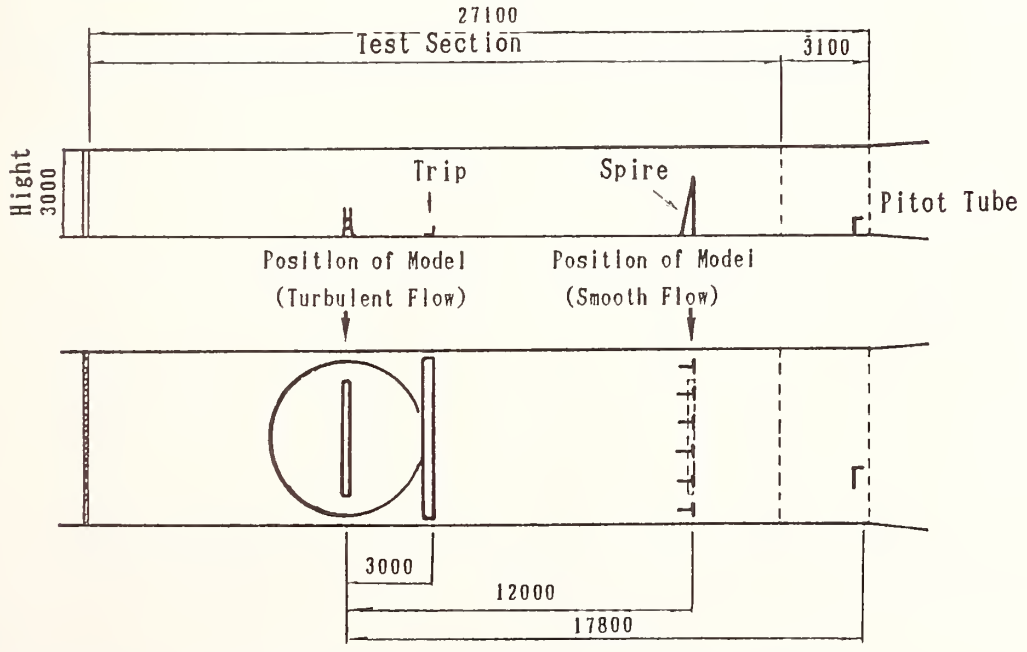

Figure-5 ARRANGEMENT OF TURBULENCE GENERATER (PWRI)

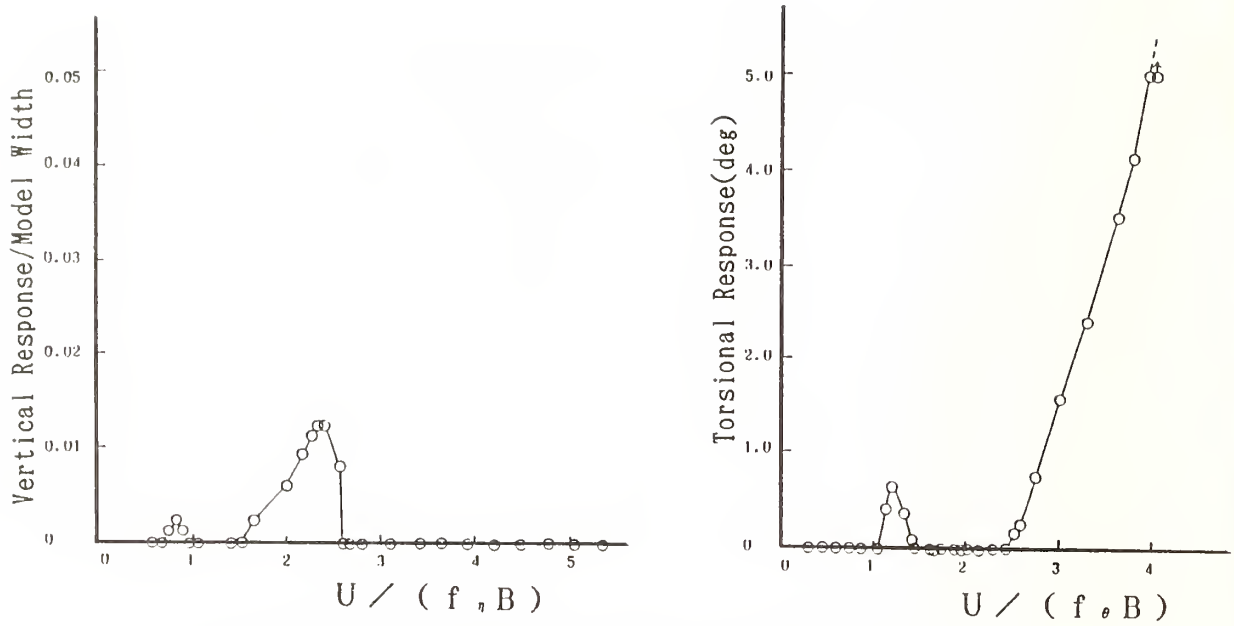

Figure-6 RESULTS OF SPRING MOUNTED TEST

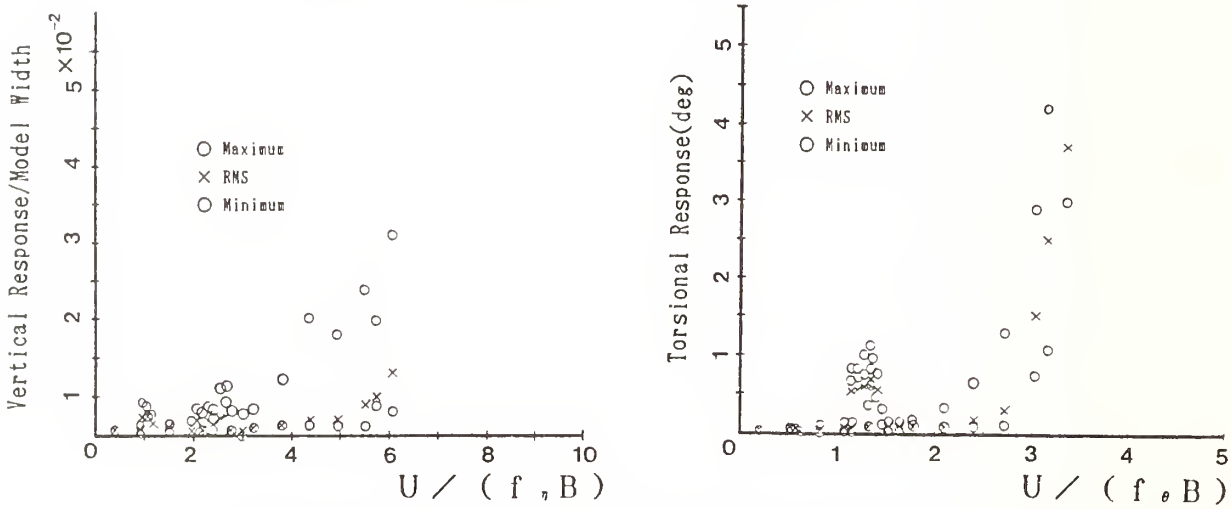

Figure-7 RESULTS OF TAUT STRIP MODEL TEST (SMOOTH FLOW)

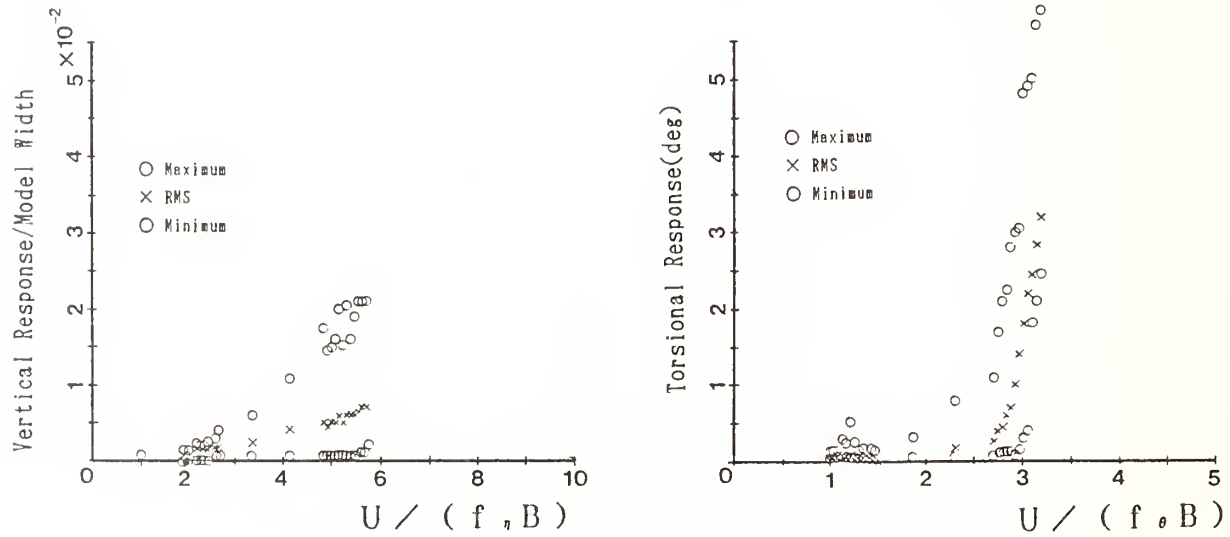

Figure-8 RESULTS OF TAUT STRIP MODEL TEST (LOW TURBULENCE)

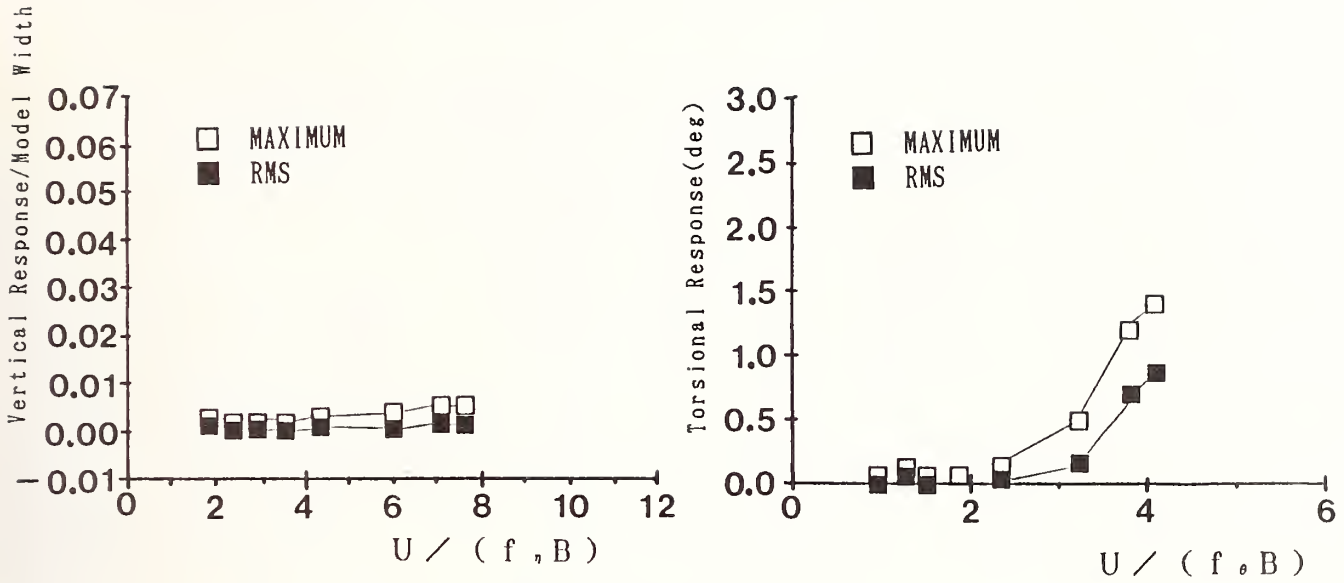

(1) In Smooth Flow

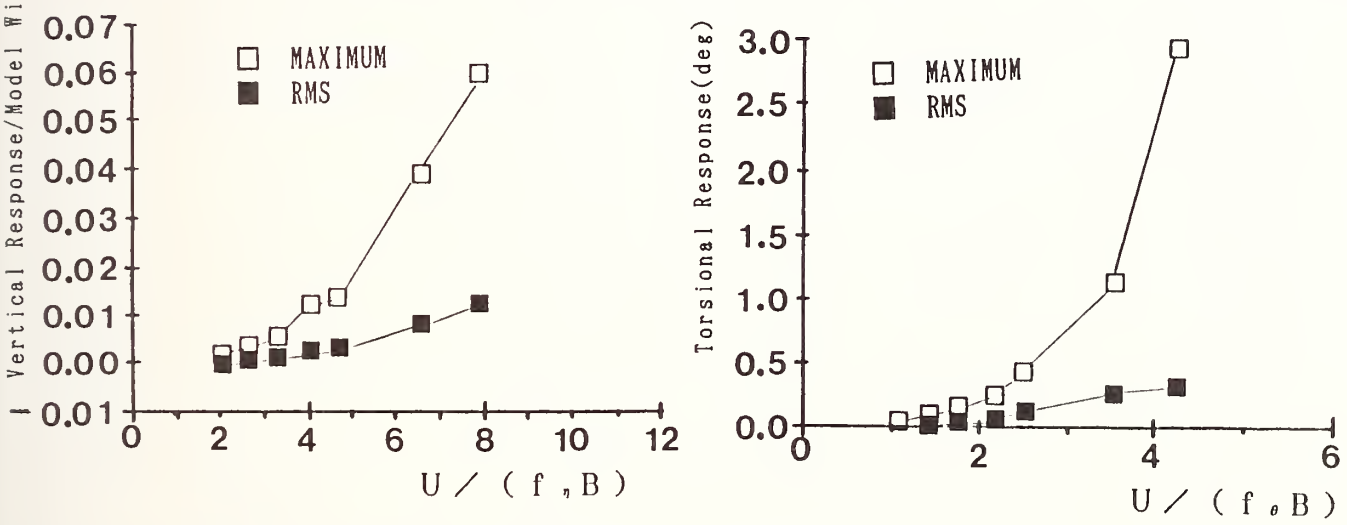

(2)In Heavy Turbulent Flow

Figure-9 RESULTS OF FULL MODEL TEST (NRCC)

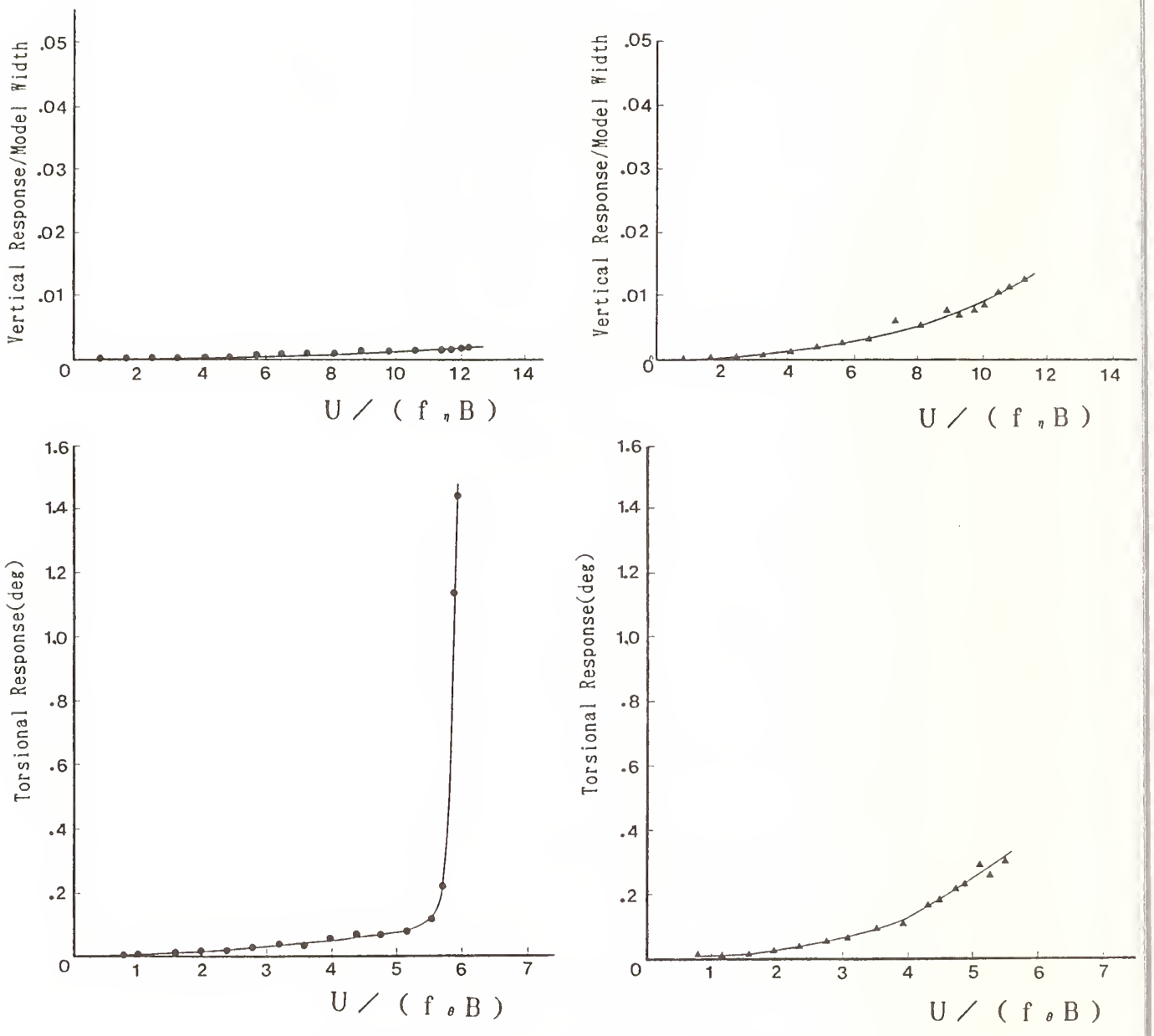

(1) In Smooth Flow

(2) In Heavy Turbulent Flow

Figure-10 RESULTS OF FULL MODEL TEST (PWRI)

Table-4 COMPARISON OF MODELS BETWEEN NRCC AND PWRI

Condition	NRCC	PWRI
Width B (m)	0.1775	0.0888
Depth D (m)	0.0178	0.0089
Length of Model L (m)	7.22	3.61
Reduced Mass ($m/\rho B^2$)	89.3	86.3
Reduced Inertia ($m/\rho B^4$)	14.9	11.7
Natural Frequency (Hz)		
Vertical Bending Mode	4.54	6.96
Torsional Mode	8.59	14.4
Stractural Damping (Log Decrement)		
Vertical Bending Mode		
Measured at amplitude of B/200	0.018	0.024
Torsional Mode		
Measured at amplitude of 0.5°	0.055	0.041
Measured at amplitude of 0.1°	0.007	0.055

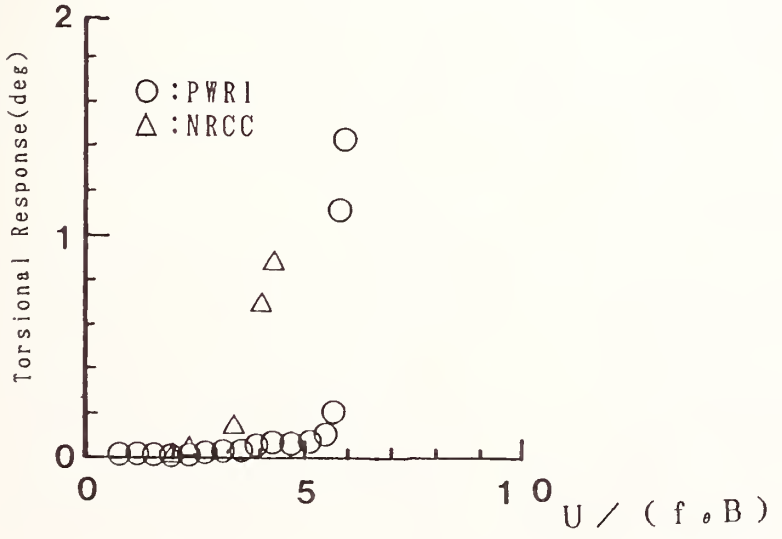

Figure-11 COMPARISON OF FLUTTER

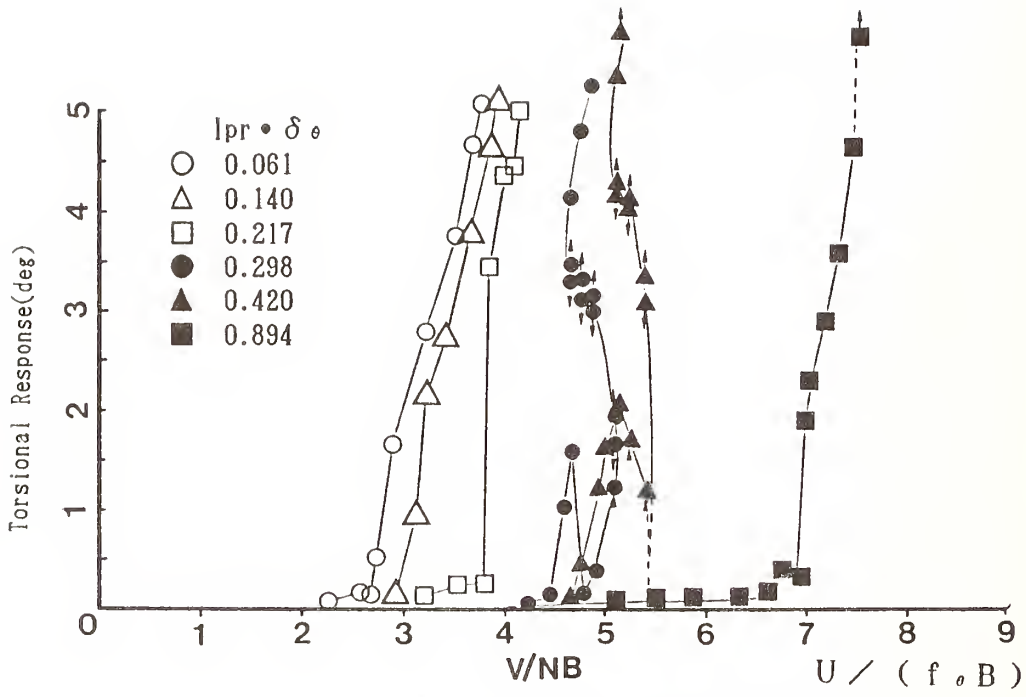

Figure-12 EFFECTS OF DAMPING

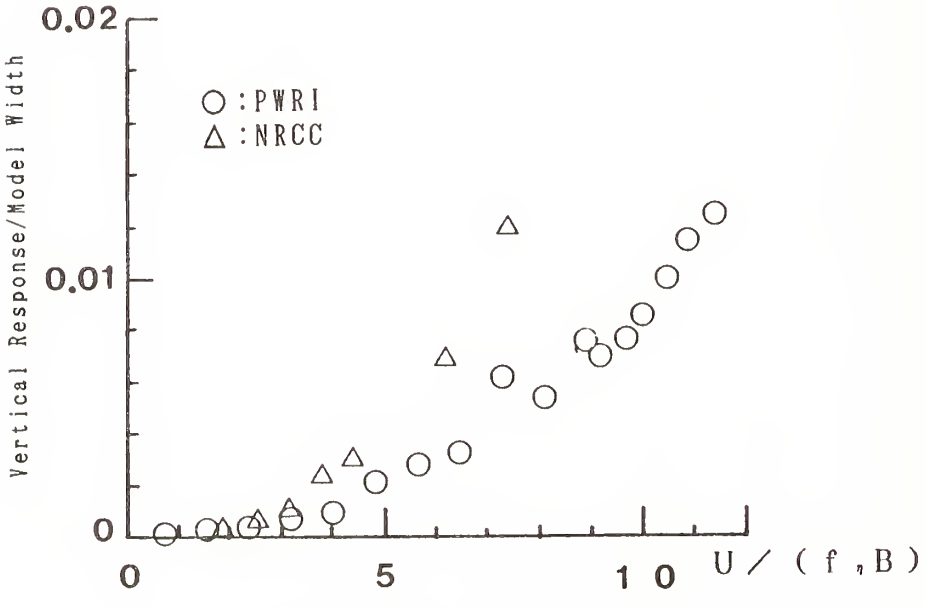

Figure-13 COMPARISON OF BUFFETING

Wind on Offshore Platforms

by

Charles E. Smith*

ABSTRACT

Increasing political and economic demands for more energy have focused a need to develop technologies to explore and produce oil and gas resources offshore. These technologies include methods to analyze and describe data on natural events like wind, waves, currents, ice, and earthquakes, and to compute the loads such events produce on offshore facilities. This paper reviews the currently accepted procedure for determining wind forces on offshore platforms on the U.S. Outer Continental Shelf (OCS). It also includes a brief overview of the relationship between wind and other environmental events that exert loads on offshore structures.

KEYWORDS: Offshore platforms; oil and gas operations; wind criteria; wind loads.

1. INTRODUCTION

The fundamental and practical aspects of modern wind engineering practice as it relates to design of offshore facilities have evolved from methods developed for land-based structures. This evolution is the result of a more directed awareness of wind-related problems, the trend for higher and more flexible buildings, and the increasing use of cladding systems for which wind loading is the primary design consideration.[1]

Wind loads are not unique for offshore structures, however, over water-winds tend to be more severe because of the lack of sheltering effects of terrain, and the fact that storm systems gain more energy over water. What is unique for offshore structures is that maximum or near-maximum wind load may occur simultaneously with maximum wave and current loads and higher than normal water levels. The major mass and resulting wind force area of an offshore facility is located at the uppermost elevation of the structure so that the wind loads are applied at levels that produce maximum overturning moments.

2. EFFECTS OF WIND

What is wind? This may be a trivial question to some, but a brief description may provide a better perspective of its relation to offshore structures. In essence, wind is the horizontal movement of air in response to differences in atmospheric pressures. The earth is traversed by major surface wind systems known as trade winds which interact with the water of the oceans to produce major current systems. Within the major wind systems, short-term disturbances occur, and are responsible for the extreme winds of interest to the structural engineer when he designs offshore facilities.

The disturbances that are of primary importance to the design of offshore structures in the United States are those associated with tropical hurricanes. Understanding the basic mechanics of these storms, and the way they relate to the development of other loads on the structure is very important. The effect of wind may manifest itself in several ways; wind loads that act directly on structures, wind generator waves, wind generator currents, and wind generator surge conditions (fig. 1).

For offshore facilities, wind forces act upon the portion of structures exposed above the water level. This includes any equipment, deck houses, and derricks which are located on the platform as shown in figure 2. The major parameters used for design purposes are as follows:[2,3]

1. the frequency of occurrence of sustained wind speed from various directions,

2. the spatial variations of the basic wind speed, in particular, the variation with altitude, and

3. the temporal variations in the basic wind velocity manifested as gusts.

For design, the wind speed may be classified as gusts, which are wind velocities that are averaged over less than 1 minute, and sustained winds which

---

*Research Program Manager
Technology Assessment and Research Branch
Minerals Management Service
Herndon, Virginia 22070-4817

are velocities that are averaged over 1 minute or longer. Most engineers recommend that wind data be adjusted to a standard elevation, such as 33 feet (10 meters) above mean water level, using a specified averaging time such as 1 hour. Wind data can be adjusted to any specified averaging time or elevation using standard profiles and gust factors as is shown in a later section of this paper.[2]

Building codes have traditionally specified the wind pressures to be used in the design of buildings and other land-based structures. However, since offshore structures are more susceptible to extreme winds than land-based structures, it is much more important that design criteria accurately assess maximum loading events than those specified by building codes. Reference 2 provides guidelines for extreme wind speeds for several areas in U.S. waters. To supplement this information, hindcasting is considered the most appropriate technique for developing the necessary environmental exposures (fig. 3).[4]

The Minerals Management Service (MMS) requires that offshore structures be designed to withstand loading events, both wind and wave, with return periods of 100 years unless the owners can demonstrate, through appropriate analyses, that less severe design events are appropriate.[5] For operations elsewhere, particularly in more harsh environments where new platform concepts are proposed, different design criteria may be required. For example, in the deep-water regions of the Gulf of Mexico, some companies use a 200-year return period.

3. OTHER WIND EFFECTS

As opposed to land-based structures, winds offshore are primary contributors to other environmental events which exert loads on offshore structures. Wind-driven waves, produced by the friction that exists between the wind and the ocean surface have the single greatest effect on offshore operations. Wind-driven waves develop and grow when a certain wind prevails from the same direction for a period of time. The length of the unrestricted path of wave development is called the fetch as shown in figure 4. The fetch can also be defined as the distance over which the wind blows to generate observed waves at a given position (fig. 5). Four factors, wind speed, duration, fetch, and water depth determine wave height (fig. 6). For example, if a 30-knot wind blew over an average of water of unlimited fetch for 5 hours, 7 1/2-foot waves would develop. If the same 30-knot wind blew over the same area of water for 30 hours, the waves would reach 16 feet.[6]

In addition to wind-driven waves, tides, and wind-driven currents are also important considerations in platform design. In determining the maximum water level for platform design, the storm-tide elevation is the datum upon which storm waves are superimposed. Wind-generated currents are combined in a vector sum with tidal currents (associated with astronomical tides) and circulational currents (associated with oceanic-scale circulation patterns). Wind-driven currents can add substantially to the loads on offshore structures because the loading function (Morrison equation) is based on the square of the water particle velocity.

4. General Design Criteria

General requirements for determining wind loads on offshore oil and gas facilities on the U.S. OCS are contained in the American Petroleum Institute Recommended Practice 2A (API-RP2A). This document recommends that sustained wind velocities be used in the computation of overall platform wind loads and that gust velocities be used for the design of individual structural elements (fig. 7).

The variation of wind velocity with respect to time is shown in figure 8 and the variation with height is given by the relationship as shown in figure 9. The referenced wind velocity height is taken at 33 feet (10 meters) above the referenced water depth. The exponent used in the velocity relationship is usually assumed to be between 1/7 and 1/13 depending upon the sea state, relative distance from land, and the duration of the design wind velocity. For most designs in the open ocean, the exponent is approximately equal to 1/13 for gusts and 1/8 for sustained winds. Typical velocity coefficients for various wind durations and heights are given in figure 10. The API-RP2A document states that the wind force on a structural member should be calculated by using the following wind velocity/force relationship:

$$F = 0.00256\ (V)^2\ CA$$

Where:

F = Wind force (lbs)
V = Wind velocity (mph)
C = Shape coefficient
A = Projected area (ft^2)

As in most onshore designs, local wind effects such as pressure concentrations and internal pressures must be considered. For these situations, it is recommended that the same analytical guidelines be used as set forth in Section 6 of the ANSI A58.1-82 Standard, "Building Code Requirements for Minimum Design Loads in Buildings and Other Structures." In general, for all wind approach angles to the structure, forces on vertical surfaces are assumed to act normal to the surface and in the direction of the wind. For surfaces not in a vertical attitude with respect to wind direction, appropriate relationships should be used to take into account the direction of the wind in relation to the attitude of individual members (fig. 11).

In the absence of more refined data, API-RP2A recommends the following shape coefficients (C) for objects perpendicular to wind flow:

Beams	1.5
Sides of Buildings	1.5
Cylindrical Sections	0.5

Overall Projected Area of
the Structure.....1.0

The question of shielding is left to the judgment of the designer. No specific guidelines are set forth; however, if the second object is considered to be located close enough behind the first to warrant the use of a shielding coefficient to limit the load on that object, then it can be used. Typical shielding values for structural members are given in reference 7.

Certain requirements are stated for so-called wind-sensitive structural components. These components are defined as equipment or objects located on the platform that are exposed to wind and whose height exceeds five times their horizontal dimension, or whose dynamic properties make them very responsive to the action of the wind. For these objects, detailed analyses are required where the time-varying aspects of the wind loads acting on the object must be considered. It is recommended that the analytical procedure, as set forth in Appendix A6 of the ANSI A58.1-82 Standard, be used as a guide in determining gust loadings on wind-sensitive appendages on a platform.

5. Other Wind/Force Criteria

In addition to the API recommended method, the American Bureau of Shipping (ABS) and Det norske Veritas (DnV) have also established formulas to calculate wind forces on offshore structures. Of the three, the DnV formula provides the most conservative values, whereas the ABS formula yields values slightly less than those obtained using the API method. Reference 8 contains a useful comparison between the methods with a detailed explanation of the coefficients and their variability with height above water level and wind speed.

6. Compliant Structures

Compliant structures are more susceptible to the dynamic effects of wind than are conventional fixed leg platforms. The presence of waves, wind, and currents causes these platforms. Because of their compliance to have mean and fluctuating offsets in the direction of the applied loads. Compliant structures can have natural periods that are much longer than those of conventional platforms.

It is well known that significant fluctuation of wind velocity occurs at periods up to hundreds of seconds. Figure 12 shows typical wind and wave spectra with typical platform periods noted for comparison purposes. From this figure, it is easily seen that the wind can provide large energy inputs for certain degrees-of-freedom of a tension leg platform.

Many models of wind spectra have been proposed in design codes and the scientific literature. Unfortunately, they disagree in the low frequency range which is of most interest for the design of compliant structures. Much of the data upon which these model spectra are based were obtained over land, and measurements in strong winds, particularly hurricanes, are scarce.[9]

Wind-tunnel tests have proved useful for estimating the fluctuating wind loads acting on platforms. The extent to which these fluctuating loads can cause resonant-type conditions in compliant structures is very difficult to ascertain. Reliable information on full-scale hydrodynamic damping, which controls the magnitude of the resonant amplifications, is not available. Reference 10 presents various aspects of wind-tunnel testing of compliant structures. The reference discusses various methodologies for obtaining and using wind-tunnel data and techniques for measuring wind and wave effects simultaneously.

7. Conclusions

This paper was written to provide the reader with an understanding of the key considerations in determining the response and performance of offshore facilities to wind-induced loads. As compared to onshore structures, wind loads on offshore structures act in combination with other loads produced by waves and currents. Wind loads are not unique for offshore structures, but because of their significant effects in combination with the other environmental loads, they must be carefully considered in the design process. This is absolutely vital in the design of compliant platforms. The references cited should be consulted to acquire a more rigorous overview and appreciation of the aspects of winds acting on offshore facilities.

8. References

1. Wind Loading and Wind-Induced Structural Response, A State-of-the Art Report, Prepared by the Committee on Wind Effects, American Society of Civil Engineers, New York, New York, 1987.

2. Recommended Practice for Planning, Designing, and Constructing Fixed Offshore Platforms, API Recommended Practice 2A (RP 2A), Eighteenth Edition, American Petroleum Institute, Washington, D.C., April 1, 1989.

3. Gaythwaite, J., The Marine Environment and Structural Design, Van Nostrand Reinhold Company, New York, New York, 1981.

4. Environmental Exposure and Design Criteria for Offshore Oil and Gas Structures, Marine Board, National Academy of Sciences, Washington, D.C., May 1980.

5. U.S. Code of Federal Regulations, 30 CFR, Part 250--Oil and Gas and Sulphur Operations in the Outer Continental Shelf, Subpart I--Platforms and Structures.

6. Wind, Waves, and Weather, Unit V, Lession 1, Rotary Drilling, Petroleum Extension Service, University of Texas, Austin, Texas 1984.

7. Wind Loading and Wind-Induced Structural Response, A State-of-the-Art Report, Committee on Dynamic Effects of the Structural Division, American Society of Civil Engineers, New York, New York, 1987.

8. Hsu, T. H., Applied Offshore Structural Engineering, Gulf Publishing Company, Houston, Texas, 1984.

9. Forristall, G. Z., Wind Spectra and Gust Factors Over Water, OTC 5735, Offshore Technology Conference, Houston, Texas 1988.

10. Wind Effects on Compliant Offshore Structures, Proceeding, Structural Congress '86, American Society of Civil Engineers, New Orleans, Louisiana, September 15-18, 1986.

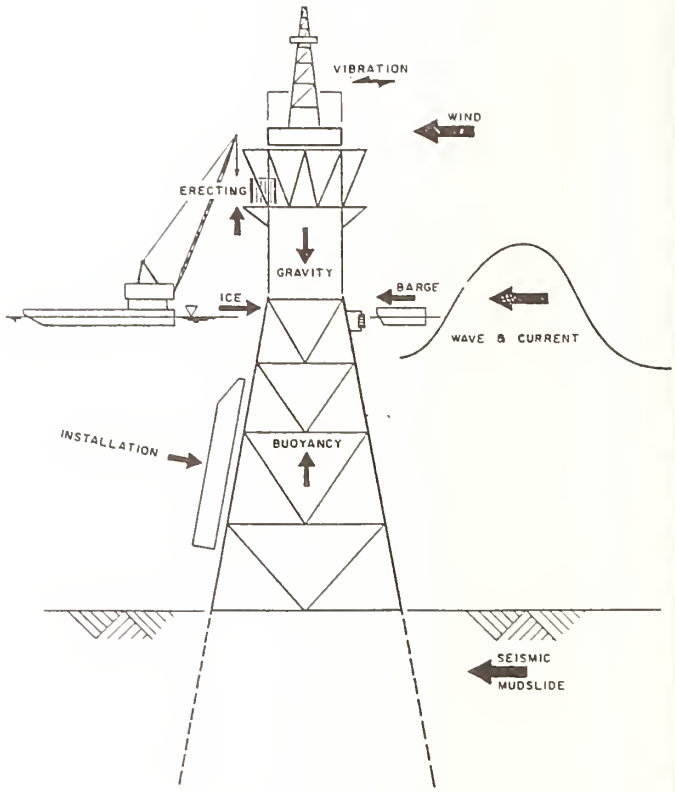

Figure 2 Model offshore platform illustratin typical load sources.

IMPORTANCE OF WINDS

WIND LOADS
WAVE GENERATION
SURGE GENERATION
CURRENT GENERATION

Figure 1 Examples of important wind contribution to loads on offshore structures.

WIND DATA SOURCES

VISUAL OBSERVATIONS
COMPUTATIONS FROM PRESSURE MEASUREMENTS

Figure 3 Typical means for determining win speeds offshore.

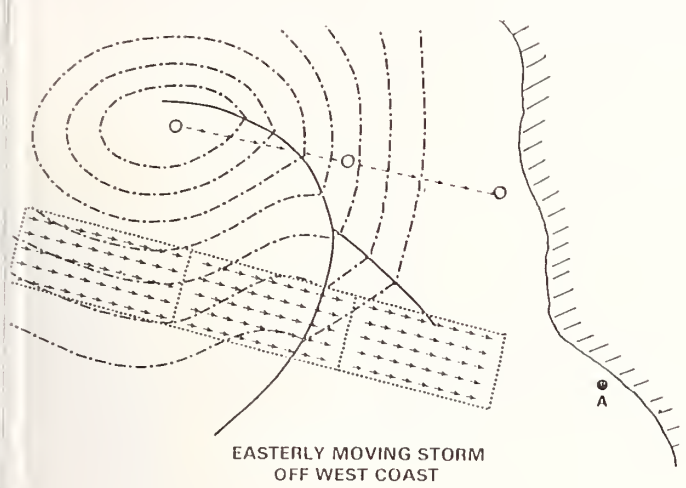

Figure 4 Moving wind field illustrating wave growth path towards a structure at a fixed location.

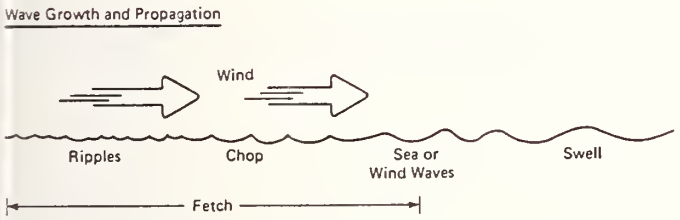

Figure 5 View of a wave generating area, showing development of smaller, generally steeper and short-crested waves in the early stages.

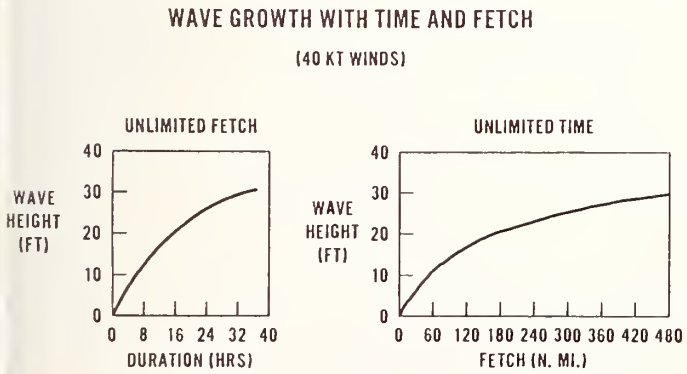

Figure 6 Collation of wave height, wind duration, and fetch.

1.3.2 Winds

2.3.1c Dynamic Wave Analysis

4. Winds

2.3.2 Wind

2.3.2a General

2.3.2b Wind Velocity Profiles and Gust Factors

2.3.2c Wind Velocity and Force Relationship

2.3.2d Local Wind Force Considerations

2.3.2e Shape Coefficients

2.3.2f Shielding Coefficients

2.3.2g Wind Sensitive Structures

2.3.2h Wind Tunnel Data

Table 2.3.4-2 Guideline Extreme Wind Speeds for Twenty Areas in the United States Waters

Figure 7 Section of API-RP2A which applies to wind aspects of platform design.

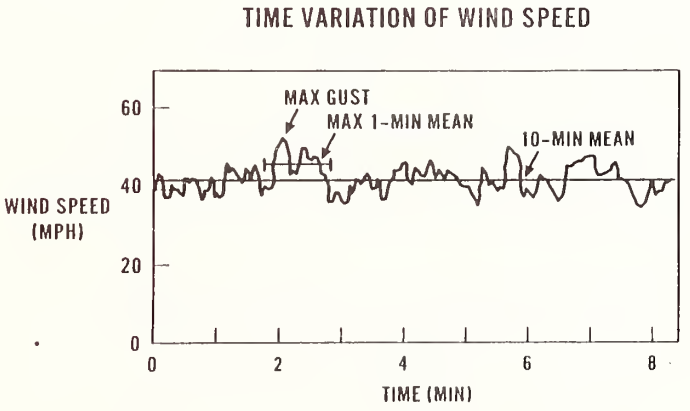

Figure 8 Variation of wind speed at a fixed elevation showing typical averaging time intervals.

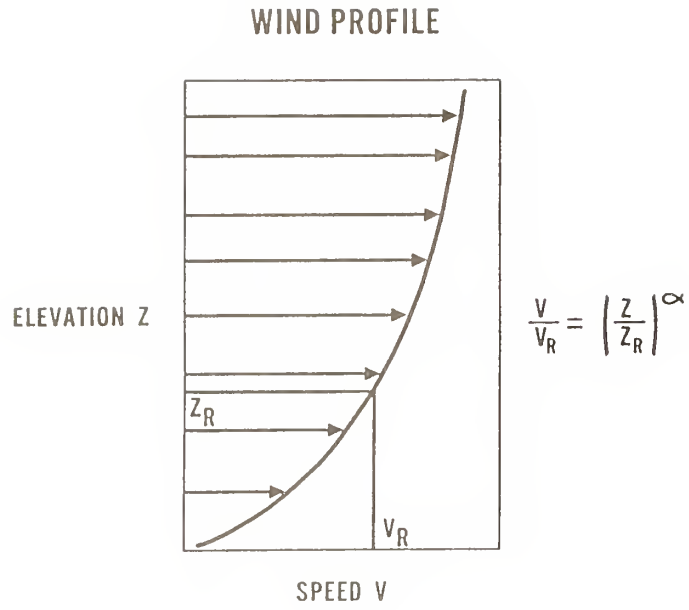

Figure 9 General wind profile recommended by API-RP2A in designing offshore platforms.

HEIGHT ABOVE SWL (M)	(FT)	AVERAGING TIME INTERVAL 1 HR A	10 MIN B	1 MIN C	15 SEC D	5 SEC E	3 SEC F
10	32.8	1.00	1.06	1.22	1.32	1.40	1.43
20	65.6	1.10	1.17	1.34	1.42	1.50	1.53
30	98.4	1.16	1.24	1.41	1.48	1.56	1.59
40	131.2	1.20	1.29	1.46	1.52	1.60	1.64
50	164.0	1.24	1.32	1.50	1.56	1.64	1.67
60	196.8	1.27	1.35	1.53	1.58	1.66	1.69
80	262.4	1.31	1.40	1.57	1.63	1.71	1.74
100	328.0	1.34	1.43	1.62	1.66	1.74	1.77
120	393.6	1.37	1.46	1.65	1.69	1.77	1.80
140	459.2	1.39	1.48	1.67	1.71	1.79	1.82
150	492.0	1.40	1.50	1.69	1.72	1.80	1.83

A,B TYPICAL AVERAGING TIME INTERVALS USED FOR ANALYZING AND REPORTING DATA

C THE EXPOSED SUPERSTRUCTURE, REGARDLESS OF DIMENSIONS, TO BE USED WHEN DETERMINING THE WIND FORCES ASSOCIATED WITH A MAXIMUM WAVE OR CURRENT FORCE, WHICHEVER PREDOMINATES

D PARTS OR THE WHOLE OF THE SUPERSTRUCTURE ABOVE THE LOWEST STILL WATER LEVEL WHOSE GREATEST DIMENSION, HORIZONTALLY OR VERTICALLY, EXCEEDS 50 METERS (164 FT), FOR WHICH A FIFTEEN SECOND MEAN SPEED APPLIES

E PARTS OR THE WHOLE OF THE SUPERSTRUCTURE ABOVE THE LOWEST STILL WATER LEVEL WHOSE GREATEST DIMENSION, HORIZONTALLY OR VERTICALLY, DOES NOT EXCEED 50 METERS (164 FT), FOR WHICH A FIVE SECOND MEAN SPEED APPLIES

F INDIVIDUAL MEMBERS, AND EQUIPMENT SECURED TO THEM ON OPEN DECKS FOR WHICH THE THREE SECOND MEAN GUST SPEED APPLIES

Figure 10 Wind velocity factors for differing average time intervals.

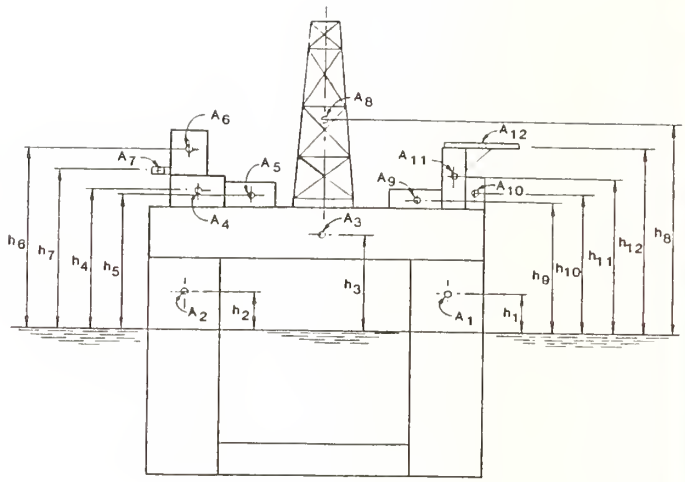

Figure 11 Wind-exposed areas on a model of a floating offshore drilling rig.

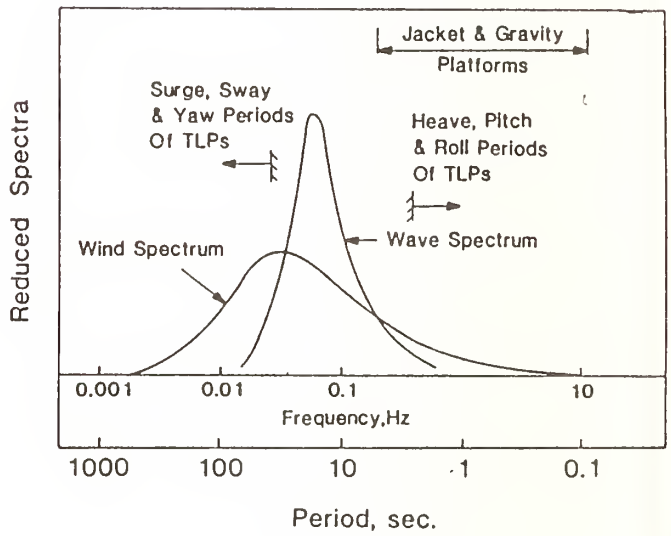

Figure 12 Excitation and frequency ranges of offshore platforms.

Theme II

Storm Surge and Tsunamis

Deep Ocean Recordings of Tsunamis

by

Frank I. Gonzalez[1]

ABSTRACT

Excellent deep ocean tsunami measurements were recently acquired in the Gulf of Alaska, using bottom pressure recorders developed over the last decade at NOAA's Pacific Marine Environmental Laboratory. The observations were made as part of the Pacific Tsunami Observation Program, which has maintained a deep ocean network since 1986. Successful acquisition of these data demonstrates the feasibility of long-term tsunami monitoring in the deep sea with self-contained instrumentation on the ocean bottom.

KEYWORDS: Tsunami; pressure; measurements; PacTOP.

1. INTRODUCTION

Along the U.S. and Hawaiian coast, six major tsunamis have inflicted about 350 casualties and half a billion dollars in property damage over the last 44 years (Bernard and Goulet, 1981). Along the entire Pacific rim, an average of one destructive tsunami a year has occurred over the last 100 years, and more than five tsunamis are generated each year of sufficient amplitude to be observed (Lockridge, 1987). High quality measurements of even these smaller tsunamis would be extremely valuable to tsunami research. Indeed, such data are now essential to further improvements in our understanding of tsunami generation and propagation, since theoretical developments and huge increases in computational power over the last two decades have far outstripped the usefulness of our existing observational data base.

This is because most tsunami measurements in the data base have been made by coastal tide gauges, which are inadequate for a number of reasons. Small tsunami amplitudes and periods are typically an order of magnitude smaller than the tidal signals for which a tide gauge is designed; as a result, time and height scales of a tide gauge are generally inadequate. The gauges are frequently characterized by a nonlinear response and are invariably located in protected inlets and harbors which may themselves have complex responses to an incident tsunami. Local atmospheric forcing can increase the background noise level in the tsunami frequency band and severely decrease the signal-to-noise ratio (SNR), so that tsunami arrival is unambiguous only when it is serendipitously preceded by a sea level record which is quiet compared to the incident tsunami energy. But the arrival of the tsunami itself can then excite local resonant modes of oscillation.

Any of these factors can seriously distort the signal of interest and render the records useless for research into the fundamental physics of tsunami evolution: generation, deep ocean propagation, shoaling, and coastal inundation. These investigations require accurate tsunami measurements in the deep ocean and at coastal sites fully exposed to the open ocean.

2. PacTOP

To acquire the necessary data, the National Oceanic and Atmospheric Administration (NOAA) and the U.S. Army Corps of Engineers (USACE) have entered into a collaborative effort known as the Pacific Tsunami Observational Program (PacTOP), which has developed and maintains a long-term tsunami monitoring network. NOAA is responsible for the continued occupation and maintenance of five deep ocean stations, utilizing bottom pressure recorders and moorings such as those shown in Figure 1; the USACE provides coastal tsunami measurement

[1] NOAA/Pacific Marine Environmental Laboratory, 7600 Sand Point Way NE, Seattle, WA 98115

capabilities at six primary pressure gauge sites in shallow water exposed to the open ocean, and three secondary sites situated in coastal inlets (Gonzalez, et al., 1987).

The deep ocean BPR network is designed to monitor critical portions of the seismically active Aleutian-Alaskan Seismic Zone. This region generated three of the six most recent tsunamis that attacked the U.S. and Hawaiian coast; furthermore, these three tsunamis accounted for more than 82% of the casualties and 85% of the property damage (Bernard and Goulet, 1981). Future tsunami threats to Alaska, the U.S. west coast and the Hawaiian Islands are concentrated in sub-regions of the Aleutian-Alaskan Seismic Zone known as the Fox, Unimak and Shumagin Seismic Gaps; these have been identified with significant potential for large tsunamigenic earthquakes (Nishenko and Jacob, 1990).

One source station is located in the Shumagin Gap itself, on the landward slope of the Aleutian Trench, three directional array stations form a triangle centered about 250 km southeast of the source, and one far-field station is located 2200 km distant from the source, near the great-circle route from the Shumagin Gap to Crescent City, California. Four of these five station locations are shown in Figure 2; the fifth station is located at the southern apex of the equilateral triangle formed with stations AK7 and AK8, and is not shown because the BPR was not recovered at this site during the 1987-88 field season.

3. INSTRUMENTATION

Two types of BPR units and their associated moorings are presently in use (Figure 1). Each BPR utilizes a Paroscientific Digiquartz Model 410K (0-10,000 psia) transducer and records a 56.25-second average pressure every 56.25 seconds (64 samples per hour), with a resolution better than 1 mm equivalent sea water head for signals of period of a few minutes or longer. (A new generation of BPRs currently under development will be capable of acquiring 15 s samples with the same resolution.) The units are entirely self-contained and store data internally, with a capacity corresponding to about 14 months of operation; this allows for early summer deployment and late summer recovery, if necessary. Eble et al (1989) discuss instrument characteristics and BPR data processing procedures in some detail.

Schematics of the two mooring designs are presented in Figure 1. Important ancillary components shown include an acoustic release that disengages an anchor, sufficient buoyancy in the form of glass spheres or or syntactic foam to raise the anchor-less unit to the surface, and a marker buoy with a number of recovery aids (VHF transmitter, strobe light, radar reflector, marker flag).

Two or more oceanographic cruises are conducted each year to recover and re-deploy BPRs at each of the deep ocean PacTOP stations; as a practical matter, Gulf of Alaska weather patterns restrict these cruises to the summer months. Out of seventeen deployment/recovery cycles to date, one instrument has been lost, another has flooded, and some data loss has occurred in the records obtained; equipment and data recovery rates for the project are currently 88% and 82%, respectively.

4. TSUNAMI RECORDINGS

Three large intraplate earthquakes recently occurred in the Alaskan Bight, with magnitudes 6.9 M_S on 17 November 1987, 7.6 M_S on 30 November 1987, and 7.6 M_S on 6 March 1988 (Lahr et al., 1988). The epicenters were somewhat south of the subduction zone associated with the Yakataga Seismic Gap, a region similar to the Shumagin Seismic Gap in that it is also associated with a high probability of experiencing an eventual great tsunamigenic earthquake (Savage and Lisowski, 1986; Nishenko and Jacob, 1990).

The transformation of seismic energy to tsunami energy during all three earthquakes was relatively inefficient, since the apparent faulting mechanism in all three cases was primarily strike-slip, and most of the crustal motion was therefore horizontal. Nonetheless, each earthquake did generate a small tsunami which was

detected both on the coast and in the deep ocean. Gonzalez et al.(1990a) provide a discussion of all of the PacTOP and coastal tide gauge observations of these events, and Gonzalez et al. (1990b) have compared the deep ocean BPR observations with numerical simulations using a nonlinear shallow water tsunami model.

Figure 2 is a summary map for the earthquake and tsunami of 6 March 1988. Contours of a quadrupole feature are displayed southwest of Yakutat which represent estimates computed using Okada's (1985) expressions for the ratio of vertical seafloor displacement to total seismic slip; units are cm/m, the contour interval is 1, outermost contours have the values ±1, solid lines indicate uplift, and dashed lines indicate subsidence. Computed extrema and rms values were ±12 cm/m and 3.8 cm/m, respectively. Lisowski and Savage (1989) estimated total right-lateral slip due to both the 30 November and 6 March earthquakes to be 2.9 ± 1.2 m using geodetic means, and 4.5 m using the seismic moment. The average of these two estimates is 3.7 m, and if half of this slip occurred on 6 March, then the model computations suggest extrema and rms vertical displacements of ±22 cm and 7 cm, respectively.

Tsunami records obtained at the PacTOP deep ocean stations and Alaskan coastal tide gauge stations are also displayed in Figure 2. BPR data are 60-min high-pass filtered, and tide gauge data are 3-60 minute band-pass filtered. Tsunami estimated time of arrival (ETA), as computed by NOAA's Pacific Tsunami Warning Center, is indicated by a vertical arrow on each record. The maximum recorded coastal wave height was 21 cm at Yakutat, while the maxima recorded at BPR stations were 2.8 cm at WC9, 2.4 cm at AK7 and 1.6 cm at AK8.

At AK10 on the slope of the Aleutian Trench, at least one cycle of a coherent, relatively low frequency wave of amplitude 0.4 cm is seen to arrive at about the tsunami ETA. The observed period of 5.2 minutes is also long compared to that of the background energy but consistent with tsunami periods measured at the other three stations. Tsunami detection at this station is therefore possible, but nonetheless uncertain, since the observed amplitude of 0.4 cm is of the same order as the background noise level.

The records at AK7, AK8 and WC9 display tsunami wave systems which are classically dispersive and amplitude-modulated to form distinct wave packets, as predicted by theory (see, e.g., Kajiura, 1963, or Mei, 1983). Tsunami first motion is negative at AK7 and AK8, and this is consistent with subsidence in the southwest quadrant of the computed seafloor displacement pattern. The SNR at WC9 is too low to be certain of tsunami first motion, but it does appear to be negative; interpreting this observation in terms of the model seafloor displacement is difficult in this case, since the source/station geometry is such that refraction effects may be important.

Finally, it is also of considerable interest to note the apparent detection of seismic surface wave energy in the BPR records, a few minutes after the earthquake main shock (Figure 2). Wave velocities estimated from the time of arrival at stations AK7 and AK8 were 3-4 km/s, in good agreement with speeds which might be expected for Rayleigh (R1) waves and/or vertical shear (SV1) waves in oceanic crust (Brune, 1979). The data are clearly aliased, but deployment of the new generation of BPRs characterized by a 15 s sampling interval promises to provide improved resolution of these low-frequency seismic phenomena.

5. CONCLUSIONS

Theoretical and numerical capabilities in tsunami research have outgrown the existing observational data base, which is composed primarily of coastal tide gauge records that suffer from nonlinear distortions, inappropriate time and height scales, the frequent presence of energetic local resonance phenomena, and low SNR for small amplitude tsunamis. High quality tsunami measurements are now needed in the deep ocean and at exposed coastal locations if our understanding of tsunami generation, propagation and inundation are to be improved. Small tsunamis are statistically common in the Pacific basin, and their accurate measurement would be extremely valuable

to the tsunami research effort. PacTOP has successfully acquired excellent deep ocean tsunami records characterized by maximum amplitudes of only a few centimeters, clearly demonstrating the feasibility of long-term deep ocean tsunami monitoring with self-contained bottom pressure recorder units.

6. ACKNOWLEDGEMENTS

U.S. coastal tide gauge records were provided by L. Hickman and S. Gill of NOAA's National Ocean Service Tidal Analysis Section, and the Langara tide gauge record was provided by F. Stephenson of the Tides and Currents Section, Canadian Hydrographic Service. Tsunami travel time estimates were provided by W. Mass and R. Silcox of NOAA's Pacific Tsunami Warning Center. This work is contribution No. 1195 of the Pacific Marine Environmental Laboratory's Tsunami Project.

7. REFERENCES

1. Bernard, E.N. and R. Goulet, 1981: Tsunami Research Opportunities. National Science Foundation, Washington, D.C., 50 pp.
2. Brune, J.N., 1979, Surface waves and crustal structure, *Geophys. Monogr.*, No. 13, *The Earth's Crust and Upper Mantle*, P.J. Hart (Ed.), Amer. Geophys. Union., pp. 230-242.
3. Eble, M.C., F.I. Gonzalez, D.M. Mattens and H.B. Milburn, 1989, Instrumentation, field operations, and data processing for PMEL deep ocean bottom pressure measurements, *NOAA Tech. Memo ERL PMEL-89*, 71 pp.
4. Gonzalez, F.I., E.N. Bernard, H.B. Milburn, D. Castel, J. Thomas, J.M. Hemsley, 1987, The Pacific Tsunami Observation Program (PacTOP), *Proc. 1987 Inter. Tsunami Symp., IUGG* , pp. 3-19.
5. Gonzalez, F.I., M.C. Eble, E.N. Bernard, H.B. Milburn and D.M. Mattens, 1990a, Deep Ocean and Coastal Tsunami Observations: The 1987-88 Alaskan Bight Earthquakes, submitted to *J. Geophys. Res.*
6. Gonzalez, F.I., C.L. Mader, M.C. Eble and E.N. Bernard, 1990b, The 1987-88 Alaskan Bight Tsunamis: Deep Ocean Data and Model Comparisons, submitted to *J. Natural Hazards.*
7. Kajiura, K., 1963, The leading wave of a tsunami, *Bull. Earthquake Res. Inst.*, University of Tokyo, *41*, pp. 525-571.
8. Lahr, J.C., R.A. Page, C.D. Stephens and D.H. Christensen, 1988, Unusual earthquakes in the Gulf of Alaska and fragmentation of the Pacific plate, *Geophys. Res. Lett., 15*, pp. 1483-1486.
9. Lisowski, M. and J.C. Savage, 1989, Deformation in the Yakataga Seismic Gap, Southern Alaska, associated with the Gulf of Alaska Earthquakes of November 1987 and March 1988, (Abstract) *EOS Transactions*, 44, 1439.
10. Lockridge, P.A., 1987: Historical Tsunamis in the Pacific Basin. In Natural and Man-Made Hazards : Proceedings of the International Symposium held at Rimouski and Quebec City, Canada, 3-9 August, 1986. M.I. El-Sabh and T.S. Murty (eds.), D. Reidel Publishing Co., pp. 171-181.
11. Mei, C.C., 1983, *The Applied Dynamics of Ocean Surface Waves*, Chapter 2, John Wiley and Sons, New York, .740 pp.
12. Nishenko, S.P. and K.H. Jacob, 1990, Seismic potential of the Queen Charlotte-Alaska-Aleutian Seismic Zone, *J. Geophys. Res.*, 95, pp. 2511-2532.
13. Okada, Y., 1985, Surface deformation due to shear and tensile faults in a half-space, *Bull. Seism. Soc. Am.*, *75*, pp. 1135-1154.
14. Savage, J.C. and M. Lisowski, 1986, Strain accumulation in the Yakataga seismic gap, southern Alaska, *J. Geophys. Res.*, *91*, pp. 9495-9506.

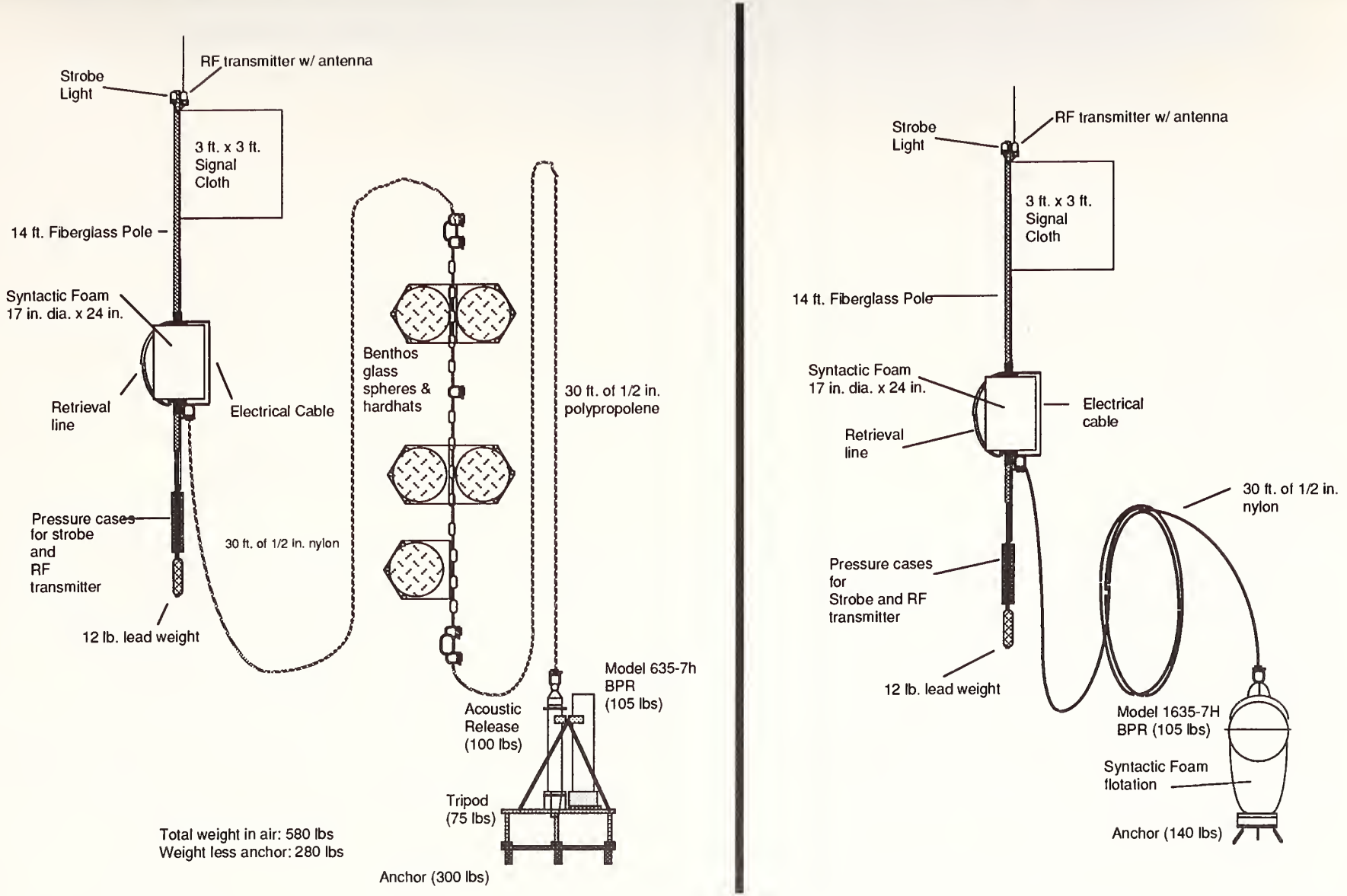

Figure 1. Bottom pressure recorder moorings. Most PacTOP moorings are of the earlier design shown on the left.

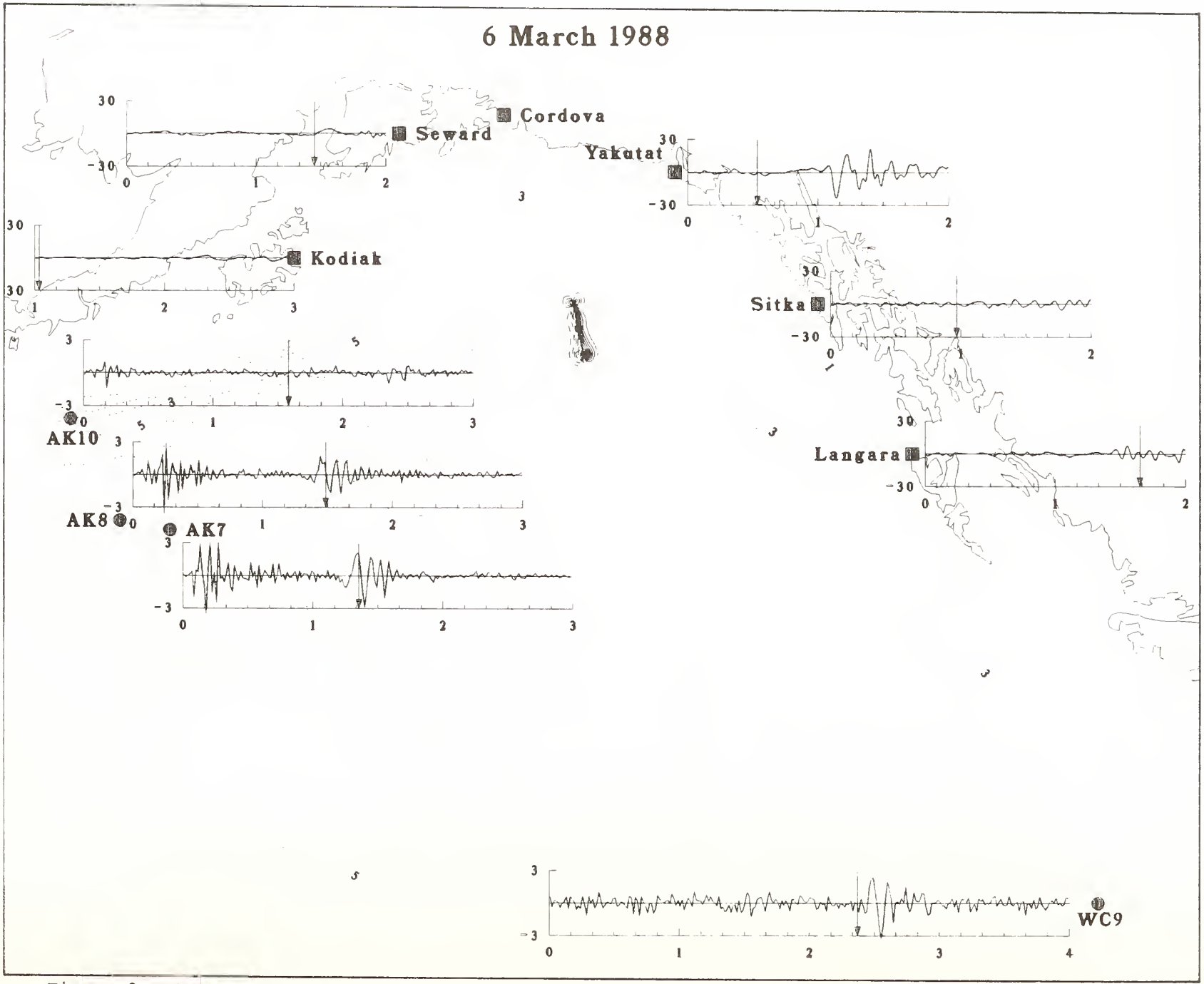

Figure 2. Summary map for 6 March 88. BPR and coastal tide gauge data are plotted near each station. Vertical axes are in cm, horizontal axes are in hours after earthquake main shock. Bathymetric contours are in kilometers. Vertical arrows indicate tsunami estimated time of arrival (ETA), and quadrupole feature southwest of Yakutat represents seafloor displacement estimates (see text).

Measurement and Modeling of Coastal Storm Effects

BY

William E. Roper[1], H. Lee Butler[2], and Andrew Garcia[3]

ABSTRACT

This paper describes techniques used by the Coastal Engineering Research Center (CERC), U.S. Army Engineer Waterways Experiment Station, for measurement and modeling of coastal storm effects. Use of time-dependent numerical models for simulating water levels and flows in open coastal waters, estuaries, bays, or lakes has become a standard practice. This practice has been extended to modeling wave conditions generated by the storm and beach response to storm attack. Historical CERC research on model development and measurement advances is discussed by relating these advances to practical investigations performed for various Corps Districts and Divisions. In addition, the paper presents a synopsis of the recent storm, Hurricane Hugo, which devastated the coastline and infrastructure of South Carolina. Research teams were dispatched to the scene to obtain high quality measurements of high watermarks, beach profiles, and structural damage.

KEYWORDS: Storm Surge; Waves; Hurricane; Numerical Modeling; Beach Response; Erosion; Measurement Techniques; Hugo.

1.0 INTRODUCTION

The U.S. Army Corps of Engineers, as the U.S. Government agency responsible for protection of the coasts of the nation, must be able to accurately predict coastal flooding from storms in order to make sound engineering decisions regarding the design, operation, and maintenance of various coastal projects. This mission requires the acquisition of high quality field data for the validation of predictive numerical models of surge, waves, and beach erosion.

Efficiency in design of coastal protection is becoming more and more important. Development of coastal regions, costs of damages from storm-induced water levels, and costs of protection from these waters are all increasing. Adequate protection for coastal regions is desired; however, due to monetary constraints, the amount of water level protection that can be considered adequate becomes a question for which there is no easy answer. Therefore, inherent in any coastal protection project (new or rehabilitation effort), there is a need to develop the best possible estimate of stage- and erosion-frequency relationships for the project area, as well as an estimate of the error in these relationships. Research and development in the area of water level and beach erosion prediction is directly linked to the needs of the Corps District user who has the responsibility of providing economical and practical designs for each coastal project.

This paper briefly presents the type of models and approach used by the Corps in simulating storm events and their effects as well as on the advances being made in instrumentation development and field data

[1]Assistant Director, Directorate of Research and Development, Civil Works Program, Headquarters, U.S. Army Corps of Engineers, Washington, D.C.

[2]Chief, Research Division, Coastal Engineering Research Center, U.S. Army Engineer Waterways Experiment Station, Vicksburg, MS.

[3]Research Oceanographer, Prototype Measurement and Analysis Branch, Engineering Development Division, Coastal Engineering Research Center, U.S. Army Engineer Waterways Experiment Station, Vicksburg, MS.

collection methods which permit acquisition of quality data sets for use in model validation. In addition, a discussion of the recent storm, Hurricane Hugo, which devastated the coastline of South Carolina at the end of the summer of 1989, and its impacts is presented. Also presented are descriptions of field data collection and modeling efforts associated with the event.

2.0 FIELD MEASUREMENTS

Recognizing that development and improvement of storm surge and nearshore wave hindcast numerical models are crucially dependent upon appropriate atmospheric and hydrodynamic data, efforts within CERC are focused on acquiring the needed data. Because these required data are typically perishable, that is, of limited or little value if not acquired during or shortly after a storm, instrumentation and the logistics necessary to conduct post-storm surveys have to be in place prior to the time of storm landfall.

During the last decade, CERC has maintained a nucleus of personnel experienced in conducting post-storm surveys. Because the local infrastructure is typically disrupted after passage of a storm, experience in conducting post-storm surveys includes the ability to communicate, travel, and sustain operations unassisted in the area for at least several days. Moreover, the team must make efficient use of the limited time available to complete as many meaningful measurements as possible. This involves rapidly identifying and selecting accessible areas that have experienced significant storm effects.

In addition to post-storm high water mark and beach profile surveys, valuable data acquired during an event include wind, tide, and wave data. Acquisition of wind data is officially the responsibility of the National Weather Service (NWS). However, anemometers used primarily for providing environmental data for other purposes, such as tracking exhaust plumes from industrial and public utility plants, often provide valuable supplementary information.

For the purpose of verification of storm surge models, tide gage data acquired along open coasts have broader application as the data are less affected by site specific characteristics. To acquire these data, the Corps is cooperating with the National Ocean Service to establish a coastal tide gage network designed to withstand hurricane effects. There are presently ten sites within this network with new sites being established at the rate of one or two annually.

Acquisition of wave data during storm events relies primarily upon having instruments in place prior to passage of a storm. The Corps presently acquires wave data at approximately 50 nearshore sites along the oceanic coasts of the continental United States and within the Great Lakes. Data acquired by NOAA buoys located farther offshore supplement those acquired by the Corps. The remote sensing of surface waves, such as performed by satellites, may at some future time complement the existing wave data acquisition network. There also is the possibility of developing a wave buoy which may be deployed in the path of an approaching storm from an aircraft.

3.0 NUMERICAL MODELING

In coastal regions, storm surge analysis is essential to proper planning and design of engineering works and in assessing the extent and levels of flooding. The theoretical approach to estimating the frequency and levels of flooding in coastal waters has been to apply numerical models for simulating the storm-induced water motions. Earlier studies involved investigating project impacts for a Standard Project Hurricane (SPH). Such a storm is usually defined as a hurricane having a severe combination of values of meteorological

parameters (such as the storm radius, forward speed, pressure deficit, and track) which give high sustained wind speeds considered reasonable for a given location. Later studies have shifted to using the joint probability method (JPM) to establish the frequency of flood level occurrence.

The typical storm surge model solves the vertically integrated, time-dependent, shallow water wave equations of fluid motion. Such models as the WES Implicit Flooding Model (WIFM) developed by Butler (1) have been employed in several Corps studies in the past two decades. These studies included investigations in support of a hurricane barrier protection plan for Lake Pontchartrain, a northern boundary for the city of New Orleans, Louisiana (2).

In the early 1980's, a study was conducted to investigate the frequency of storm plus tide flood levels along the coast and within the bays of southern Long Island, New York (3). The study involved the development of two WIFM models, collection of field data for tidal calibration, computation of coastal and back-bay stage frequencies, and analysis of alternative barrier (dune) and inlet gate configurations. The JPM approach was used to determine stage frequencies for hurricanes, extra-tropical storms (northeasters), and tide events along the south shore of Long Island. New statistical procedures were used to minimize the computational effort while providing accurate error estimates (4,5).

Following the Long Island study, a request to apply similar technology to an area just north of Boston, Massachusetts, was made by the New England Division of the Corps. The purpose of the study (5,6) was to determine flood levels in the back-bay reaches of the Saugus-Pines River system as well as develop the frequency of water volumes caused by storm waves overtopping seawalls protecting a residential area called Roughans Point. Flooding caused by wave overtopping is an annual occurrence. In order to determine the economic viability of possible protective measures, it was necessary to establish the frequency of the flood levels caused by wave overtopping for both the existing conditions and the proposed protective measures.

Wave overtopping is a complex phenomenon which is governed by a number of sometimes interdependent variables such as tide, storm surge, wave height and period, and structure height and slope. To study this problem five models were used in conjunction. The WIFM model was used to calculate the still-water level, and a spectral wave model estimated the characteristics of waves which would attack the structures at the water levels predicted by the surge model. A physical model produced an analytical relationship for determining overtopping rates given water level, wave height and period, and structure characteristics. A flood routing model calculated the maximum stage in the interior of Roughans Point caused by each simulated event. A probability model chose events to simulate, assigned probabilities to those events and constructed the stage-frequency curves. These investigations resulted in defining the most economical seawall, berm/revetment plan which would provide sufficient protection for events with a given frequency of occurrence.

Recent model studies have included investigations for portions of the coastlines of New Jersey (7) and California (8) to assist the evaluation and implementation of comprehensive shore protection plans for these coastlines. These studies included four broad areas: (1) deepwater wave climate analysis and nearshore wave refraction, (2) numerical modeling of long-term shoreline change, (3) numerical modeling of storm-induced beach erosion, and (4) development of stage-frequency relations for the

back-bay and open coast and related frequency of erosion. These studies represent an integrated attempt to quantitatively evaluate long-and short-term coastal processes on a regional scale for use in engineering design.

The numerical modeling system currently used by the Corps for simulating storm processes and related effects is the Coastal Modeling System or CMS (9). The CMS was developed by CERC and comprises a number of numerical models used in coastal studies. The system provides a means to organize existing and new CERC modeling software into consistent, standardized versions, using established implementation procedures and data formats. This in turn permits easier Corps-wide access to the technology. Resident in system (or planned) are codes for modeling long wave hydrodynamics (such as tides, storm surge, seiches, and tsunamis), tropical (hurricane) and extra-tropical windfields, spectral wave models, wave transformation models, and sediment transport models (longshore transport, dune erosion, beach morphology, and basic sediment transport).

Current research and development is aimed at improving wind estimation models and treating the combined effect of wind generated waves and surge in a more rigorous manner. Research in several programs as well as knowledge gained in specific mission support studies are contributing to the advancement of storm surge modeling and related effects. This research includes a major thrust using both a morphological approach and the use of a system of deterministic models for tide, waves, wave-induced currents, and sediment transport. Recent advancements in three-dimensional model development will provide a means of simulating the vertical structure of the storm flow field and consequently a better estimate of associated sediment transport.

4.0 HURRICANE HUGO

4.1 Synopsis

Hurricane Hugo is the costliest hurricane in U.S. history. The American Insurance Association reports $3.0 billion dollars as a preliminary estimate of insured property damage for the U.S. mainland and $1.9 billion dollars for Puerto Rico and the U.S. Virgin Islands. Both figures are subject to upward revision. Hurricane damage estimates for past storms often have been two to three times the insured property damage, thus the damage total due to Hugo may exceed $10 billion dollars (10).

The first aircraft reconnaissance of Hugo was made on 15 September 1989 when the storm was located several hundred kilometers east of the Leeward Islands. The aircraft reported a maximum wind speed of 165 knots, the highest winds observed during the duration of the storm. Hugo moved on a westerly course that took the eye across the Islands of Guadeloupe, St. Croix, and Vieques, Puerto Rico. After leaving Puerto Rico, the storm took a more northerly track toward the U.S. mainland. At the same time the forward speed of the storm increased significantly. Because the track at this time was nearly parallel to the South Atlantic coastline of the United States, small changes in the storm's direction resulted in large changes in the predicted landfall site.

Thirty-six hours before landfall in South Carolina, NWS predictions had the storm coming ashore near the northern border of the State of Florida. Just 12 hours prior to landfall, the eye of Hugo was expected to cross the coastline near the city of Savannah, Georgia, and evacuation was undertaken. Late on the evening of 21 September, Hugo came ashore at Charleston, South Carolina, tracked across the state and turned northward and moved through the western edge of Virginia.

Hugo came across the barrier islands

fronting the mainland, causing devastation from just south of Charleston (Folly Island) to the North Carolina border, a distance of about 200 km. In addition to the coastal damage, Hugo caused substantial tree blowdown across large areas in both South and North Carolina. The storm generated numerous small tornadoes which touched down and cut off trees at a 3 m height across the two states. Infrastructure damage behind the beach was severe. Homes located on the barrier islands were moved from their foundations and boats were transported across inland bays and lagoons to the mainland.

Federal and State agencies were mobilized for victim assistance and damage assessment. In addition, there was concern for new flooding from high lunar tides (exceeding 1 m above normal) expected in mid-October. The dune line had been destroyed over 95 km of coastline. A combination of the Federal Emergency Management Agency decision, resource and tasking, and a request for state assistance, led to building emergency berms along the seafront for a total distance of 65 km to protect the infrastructure from more significant damage caused by the high lunar tide. The mission proved a great success, saving millions of dollars of additional damage at a cost of about $2.8 million.

4.2 Field Measurements

For the purpose of delineating structural and beach damage as well as documenting the impacts of Hugo to assist future research efforts, CERC sent three teams of engineers, scientists, and technicians to survey high watermarks, beach profiles, and structural damage. These data will eventually be very helpful for validation of Corps storm surge model methodology and beach response models. It is necessary for surge height calculations to be very accurate because an extra 30 cm of height for a seawall can be a very large cost. Mindful of the need to acquire accurate data on the storm's impact, a team was positioned in a North Carolina mainland town to move in at first light and begin making high water mark measurements. Due to the severe infrastructure damage, logistics were near impossible but a great number of measurements were completed.

A second team was dispatched to Myrtle Beach, South Carolina, to undertake measurement of beach profiles. The State had collected over 75 profile measurements within 3 months prior to the storm. Profiles change little during the summer in this area, so a field effort directly after the storm would result in a high quality data set depicting the effect Hugo had on the beach and its dune system. Again, hurricane impacts on beaches and dune systems are important to the Corps because project justification is based on flood and/or storm damage protection. There is a need to know how high a dune needs to be, or how wide a beach, in order to survive a given storm surge and waves. In recent years, CERC has developed numerical models to investigate dune erosion, but there are very little data to verify the models. Some survey monuments were lost in the storm but profile measurements were completed for those which survived. Additional data were obtained from both infrared and visual aerial photography along the beach and as far as 10 km inland.

A third team surveyed structural projects and beach damage along the entire affected area. Included were inspections of seawalls and associated beach elevation, revetments, barrier island overwash and breaching, jetties and bulkheads, dune systems and breaching, and other structure integrity. Findings can be summarized as follows. Where the large dunes held, there was less upland damage and conversely, substantial upland structural damage occurred where dunes were destroyed. The beaches eroded along the entire

study area, and in some cases the old marsh surface was exposed. Some sand went offshore, and most of it back onto the island. Coastal structures had varying degrees of damage. Most large ones survived, providing some degree of protection. Most of the smaller protective shore front structures were completely destroyed with heavy damage to houses behind them. There was little or no apparent damage to the landward portion of navigation structures, such as the jetties at Murrells Inlet, South Carolina.

4.3 Model Analysis

Hugo weakened as it crossed Puerto Rico and appearances seemed it might not be much of a storm when it made landfall on the east coast of the United States. Then it began moving erratically and strengthening. Hugo changed direction several times, and appeared to be heading for landfall about 45 km south of Charleston, until another direction change at the last moment brought the eye ashore at Charleston.

Because of the counterclockwise wind motion in a hurricane, the maximum winds and largest surge and waves are on the right side of the eye as it moves forward toward the shoreline. The maximum winds for Hugo (shortly before landfall) were about 45 km north of the eye of the storm. If the eye of the storm had made landfall 45 km south of Charleston, instead of passing directly over the city, the surge at Charleston would have been much higher.

CERC performed computer simulations of Hugo using both a wind model and surge model (NOAA's SLOSH model (11)). These simulations produced results which can be graphically visualized to show the hurricane leaving Puerto Rico and weakening, the path meandering, then strengthening, and finally collapsing after making landfall. The models were used to investigate what would have happened if the eye of the storm made landfall 45 km south of Charleston instead of directly over the city. Hugo actually produced maximum surge levels north of Charleston in a relatively unpopulated area. High water mark measurements gave a maximum surge of over 6 m above mean sea level. Simulating the same event, but with a landfall 45 km south of Charleston, the entire city would have been under water. The actual measured surge at Charleston was 3.2 m above mean sea level. The simulated surge for a hurricane landfall south of Charleston gives a surge height greater than 6 m. There would have been hurricane force winds and waves on top of that surge.

Charleston is a relatively small, low-lying city, with a population of about 70,000. A 6-7 m surge would have been more disastrous for a larger city like Jacksonville, Florida, which has a population of about 500,000. The last 20 years have been a relatively quiet period for hurricanes, and people tend to forget past hurricanes. There is real potential for major disaster from these storms. This potential inspires continued research efforts to improve model and measurement technology for assisting project design to achieve successful results when the project is constructed.

Additional studies will be performed using the data acquired for Hugo. This event has provided a unique opportunity to investigate the accuracy and dependability of models for simulating wind, surge, wave, and beach erosion phenomena. Continuing studies will include modeling the hurricane windfield for input to a detailed surge model. The surge model will simulate combined tide and storm effects by using tidal constituent data by Schwiderski (12) plus an elevation due to the inverted barometer effect for open ocean boundary conditions. A spectral wave model will be used to simulate wave conditions generated by Hugo. Combining these computations with the surge plus tide simulation, an estimate of the total water level produced by the

storm can be made. These data will be archived in a database for later forcing a storm erosion model which will be applied at the sites where profile data were taken. All of the model simulations will be made as a "blind" test of model accuracy and dependability.

5.0 ACKNOWLEDGEMENTS

The research presented in this paper, unless otherwise noted, was sponsored by the Office of the Chief of Engineers, U.S. Army, and is published by its permission.

6.0 REFERENCES

(1) Butler, H.L., "Evolution of a Numerical Model for Simulating Long-Period Wave Behavior in Ocean-Estuarine Systems," Estuarine and Wetland Processes with Emphasis on Modeling, Marine Science Series, Vol. 11, Plenum Press, New York, NY, 1980.

(2) Butler, H.L., "Finite Difference Numerical Model for Long-Period Wave Behavior: With Emphasis on Storm Surge Modeling," Proceedings of the 1st National U.S. Army Corps of Engineers-Sponsored Seminar on Two-Dimensional Flow Modeling, The Hydrologic Engineering Center, Davis, CA, 7-9 Jul 1981.

(3) Butler, H.L. and Prater, M.D., "Innovative Determination of Near-shore Flood Frequency," Proceedings of the 20th International Conference on Coastal Engineering, ASCE, Taipei, Taiwan, 9-14 Nov 1986.

(4) Prater, Mark D., Hardy, Thomas A., Butler, H. Lee, and Borgman, Leon E., "Estimating Error of Coastal Stage Frequency Curves," Proceedings of the 19th International Conference on Coastal Engineering, ASCE, Houston, TX, 3-7 Sep 1984.

(5) Butler, H. Lee and Hardy, Thomas A., "Practical Approach for Determining Stage Frequency," Proceedings of the 18th Joint Meeting, Panel on Wind and Seismic Effects, UJNR, Gaithersburg, MD, 12-15 May 1986.

(6) Hardy, T.A. and Crawford, P.L., "Frequency of Coastal Flooding at Roughans Point, Broad Sound, Lynn Harbor, and the Saugus-Pines River System," Technical Report CERC-86-8, U.S. Army Engineer Waterways Experiment Station, Vicksburg, MS, 1986.

(7) Kraus, Nicholas C., Scheffner, Norman W., Hanson, Hans, Chou, Lucia W., Cialone, Mary A., Smith, Jane M., and Hardy, Thomas A., "Coastal Processes at Sea Bright to Ocean Township, New Jersey," Misc. Paper CERC-88-12, U.S. Army Engineer Waterways Experiment Station, Vicksburg, MS, 1988.

(8) _____, "Coast of California Storm and Tidal Wave Study, State of the Coast Report, San Diego Region," in publication, U.S. Army Engineer District, Los Angeles, Los Angeles, CA.

(9) Cialone, Mary A., "Coastal Modeling System, Theory and Documentation," Instructional Notebook in publication, U.S. Army Engineer Waterways Experiment Station, Vicksburg, MS.

(10) Lawrence, Miles, "Preliminary Report Hurricane Hugo 10-22 September 1989," National Hurricane Center, NOAA.

(11) Jelesnianski, C.P., Chen J., Shaffer, W.A., and Gilad, A.J., "SLOSH-A Hurricane Storm Surge Forcasting Model," Oceans '84, Inst. of Electrical & Electronic Engineers, New York, NY, 1984.

(12) Schwiderski, E.W. and Szeto, L.T., "The NSWC Global Ocean Tide Data Tape (GOTD), Its Features and Application, Random-Point Tide Program," Technical Report NSWC TR 81-254, Naval Surface Weapons Center, Dahlgren, VA, 1981.

Storm Surge Modeling in the United States

by

Chester P. Jelesnianski, Jye Chen and Wilson A. Shaffer
Techniques Development Laboratory
Office of Systems Development
National Weather Service, NOAA
Silver Spring, MD 20910

ABSTRACT

The National Weather Service of the U. S. has developed the Sea, Lake, and Overland Surges from Hurricanes, (SLOSH), model to forecast storm surges whenever a tropical storm threatens. The model is applied to 33 basins, Fig 1, along the Gulf of Mexico and the Atlantic Coasts of the United States. It is being applied to sections of the People's Republic of China, India and the islands of the Bahamas. The model is also used as a tool for storm evacuation planners to delineate areas of potential flooding.

1. INTRODUCTION

SLOSH--is a numerical-dynamical computer model designed to compute tropical storm surges. The model was designed in the National Weather Service's Techniques Development Laboratory for "real-time" forecasting. The storm surge--a significant increase in water level accompanying a storm--has long been known as the major threat to life. In one incident alone, storm surge from the 1900 Galveston hurricane resulted in 5000 to 6000 deaths.

Tide gage observations taken during a storm's passage show that the storm surge lasts, typically, about 6 hours and affects about 100 miles of coastline. Very large, slow-moving storms can produce significant surges for a much longer period and affect a longer stretch of coastline. To emphasize the threat posed by the surge, consider the surge from Hurricane Camille in 1969 which reached 24 feet, or the surge from Hurricane Hugo in 1989 which reached 20 feet.

2. THE SLOSH MODEL

The SLOSH model is two-dimensional, covering a segment of the continental shelf, inland water bodies and terrain. The equations of fluid motion are solved numerically, incorporating finite amplitude effects but not the advective terms from the equations of motion. SLOSH uses a time-history bottom stress (Platzman, 1963; Jelesnianski, 1967), corrected for finite amplitude effects. At any given point, the computed surge is designed to reproduce the time-history of a long-period gravity wave as shown on a tide gage hydrograph or stage record. Short period phenomena, such as wind waves and their associated "run-up", are ignored.

Most SLOSH basins use a polar grid, such as the one shown for the Lake Pontchartrain/New Orleans basin Fig. 2a. This polar grid allows a fine mesh in the primary area of interest. One advantage of this grid is that boundary conditions are imposed far from the area of interest. Other basins use an elliptical/hyperbolic grid which have special properties that can be used advantageously, Figs 3(a,b).

On every grid "square" of the model, a value of terrain height or water depth is supplied, thus tailoring the model to a specific basin area. Literally hundreds of maps (USGS quadrangle or topographic maps, NOS bathymetric charts, and various types of plats) are used to specify these values. The model incorporates barriers which impede the flow of water and allows for the overtopping of these barriers. Such barriers, include dunes, levees, spoil areas, natural ridges, reefs, and various man-made structures. The model also treats sub-grid size flow through cuts between barriers, channel flow, and width variations along rivers.

As the computations proceed in time and if water overtops barriers, water spills into areas behind the barriers and is acted on by storm driving forces. Model computations are turned on for newly wetted grid squares. Likewise, as water recedes, computations are turned off on dried grid squares. Water penetrates inland until impeded by other barriers or naturally rising terrain. It is possible for a storm to produce massive inundation across low lying terrain, extending many miles inland.

Imbedded within SLOSH is a tropical storm wind model. For a computational run of SLOSH for a given storm event, the user must supply simple, time-dependent meteorological parameters.

These are: position (latitude and longitude) of the hurricane, central pressure, and storm size (distance from storm center to the maximum wind).

These inputs are entered at 6-hour intervals, beginning 48 hours before landfall and ending 24 hours after landfall. In the event the storm does not make landfall, the time of the storm nearest to a basin's defined origin is used instead of landfall time. Note that wind is not an input parameter. The SLOSH storm model produces a vector wind field throughout the basin by balancing forces according to the meteorological input parameters. Fig. 4. depicts a computed surge envelope of highest waters generated by hurricane Betsy, 1965, for the Lake Pointchartrain basin. The surge contours were drawn from output surge data by a line printer on the image or computational plane, Fig. 2b. This is a typical result when computing with historical storms for any of the basins of Fig. 1.

3. MODEL ACCURACY

We attempt to simulate inland flooding with historical storms in order to verify the SLOSH model. Surge data consists of tide gage observations, staff gage records and high water marks. High water marks inside buildings or structures are the least accurate due to contamination by wave action and inadequate damping or overdamping of the water levels by the structure. Often high water marks vary by 20% for two nearby locations.

Before a SLOSH simulation, the hurricane's track is determined as precisely as the data allow. In addition to the track, we estimate, the storm's radius of maximum wind and its central pressure.

In Fig. 5, we show the combined results of simulations for several basins. The error is generally within $\pm$ 20% for the significant surges, with a few observations falling outside that range. A total of 572 surge observations were used to develop this figure. These observations were taken throughout the area affected by the surge--around the maximum surge, on inland terrain, at the storm's periphery, and along inland water bodies. Note that the tide gage data are limited to the lower observed heights; tide gages frequently fail during major surge events.

The SLOSH model is not "tuned" for a particular geographic location, but uses "universal" specifications for constants such as the model's drag coefficient, bottom stress, etc. This allows us to adapt SLOSH to any geographical location, whether or not it has ever experienced a storm, and have confidence in the model's computations.

4. EVACUATION PLANNING WITH SLOSH

Although SLOSH originated as a forecast model, it is also used as a tool to delineate areas of potential storm flooding. With this information, an evacuation planner can identify areas for evacuation, determine which highways can be used for evacuation routes, and site shelters in safe areas.

To find a region's potential for storm surge flooding, a large number of hypothetical storms are simulated to impact the area, with the flooding due to each one archived. These storms are varied in intensity, size, and landfall point along climatologically likely tracks. Typically, several hundred storms are simulated in a basin. This number is sufficient to highlight critical storm paths that may pose excessive flooding in an area.

A spinoff of the simulations is an "atlas" of flooding within a basin. This atlas comprises displays of flooding for each storm run for the coast, a forecaster can turn to the atlas, match his forecast storm (path, size, and intensity) to one already in the atlas, and get an approximation of the flooding due to that storm.

The atlas also contains composites of flooding. For example, areas flooded by a storm coming from a given direction, regardless of its landfall point, and having a given intensity, may be combined. This composite aids the forecaster by pointing out critical regions where flooding may be extreme.

The immense data base for storm evacuation planning are stored in Micro PC's for instant recall in colorized, graphical output. This is a continuing development in the National Weather Service of the United States.

4. REFERENCES

1. Jelesnianski, C. P., 1967: Numerical computations of storms surges with bottom stress. Mon. Wea. Rev., 95, 740-756.

2. Platzman, George W., 1963: The dynamical prediction of wind tides on Lake Erie. Meteorological Monographs, Amer. Met. Soc., 4, 44 pp.

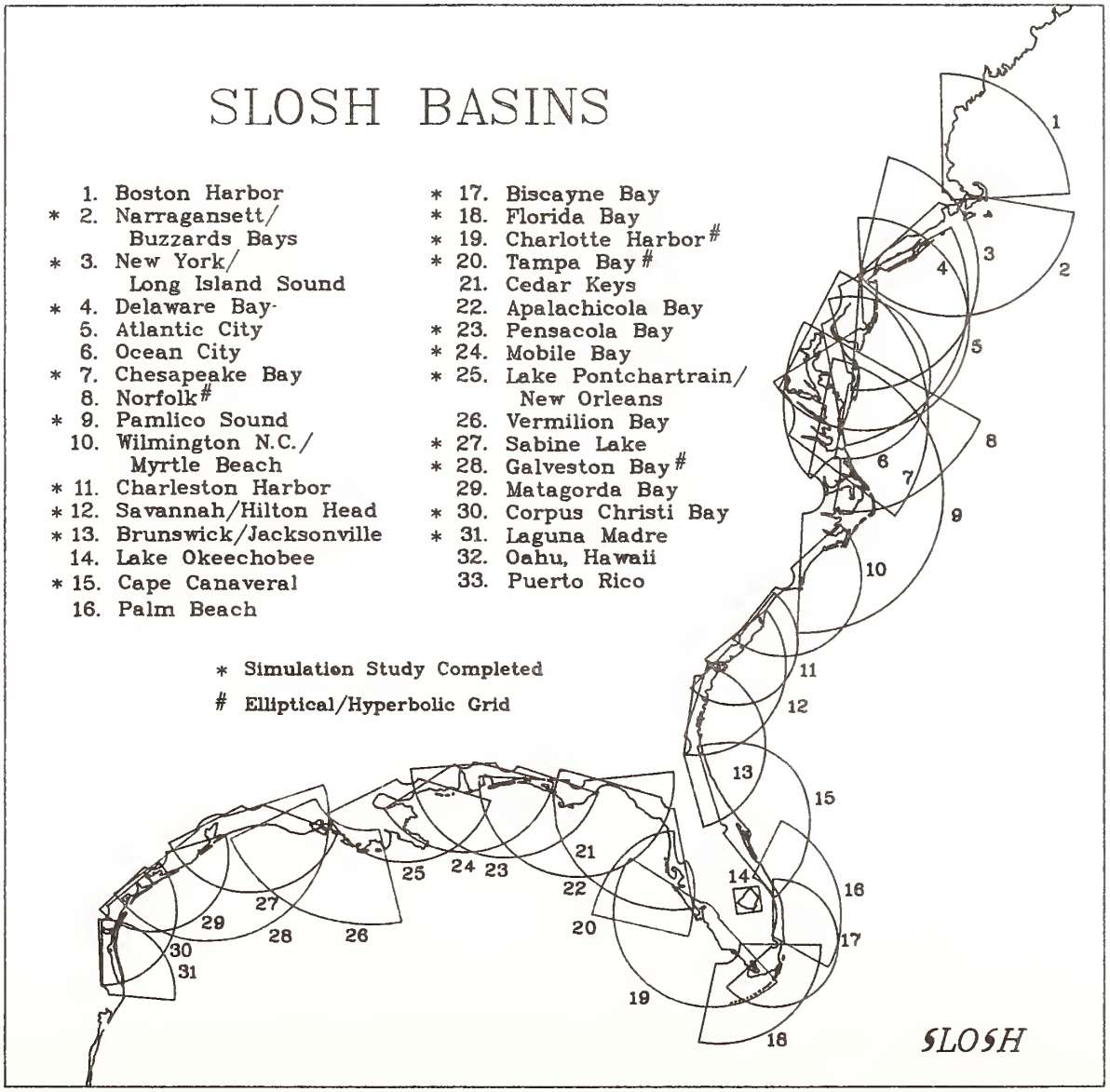

Figure 1. Slosh basins along the Gulf of Mexico and the Atlantic Coasts of the U.S.

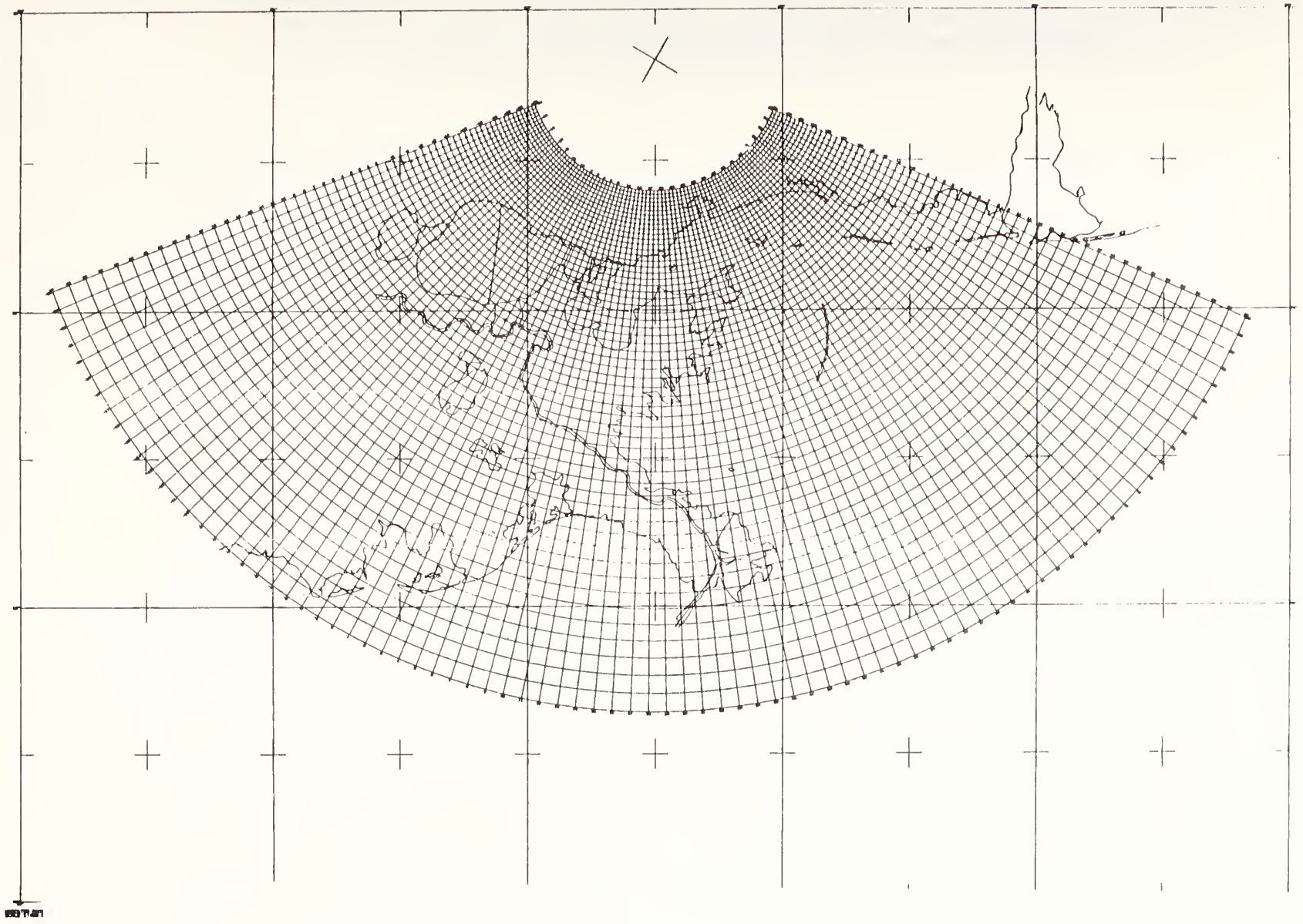

Figure 2a. A plane, polar coordinate system projected on a Mercator chart, tangent to the earth at New Orleans, Louisiana.

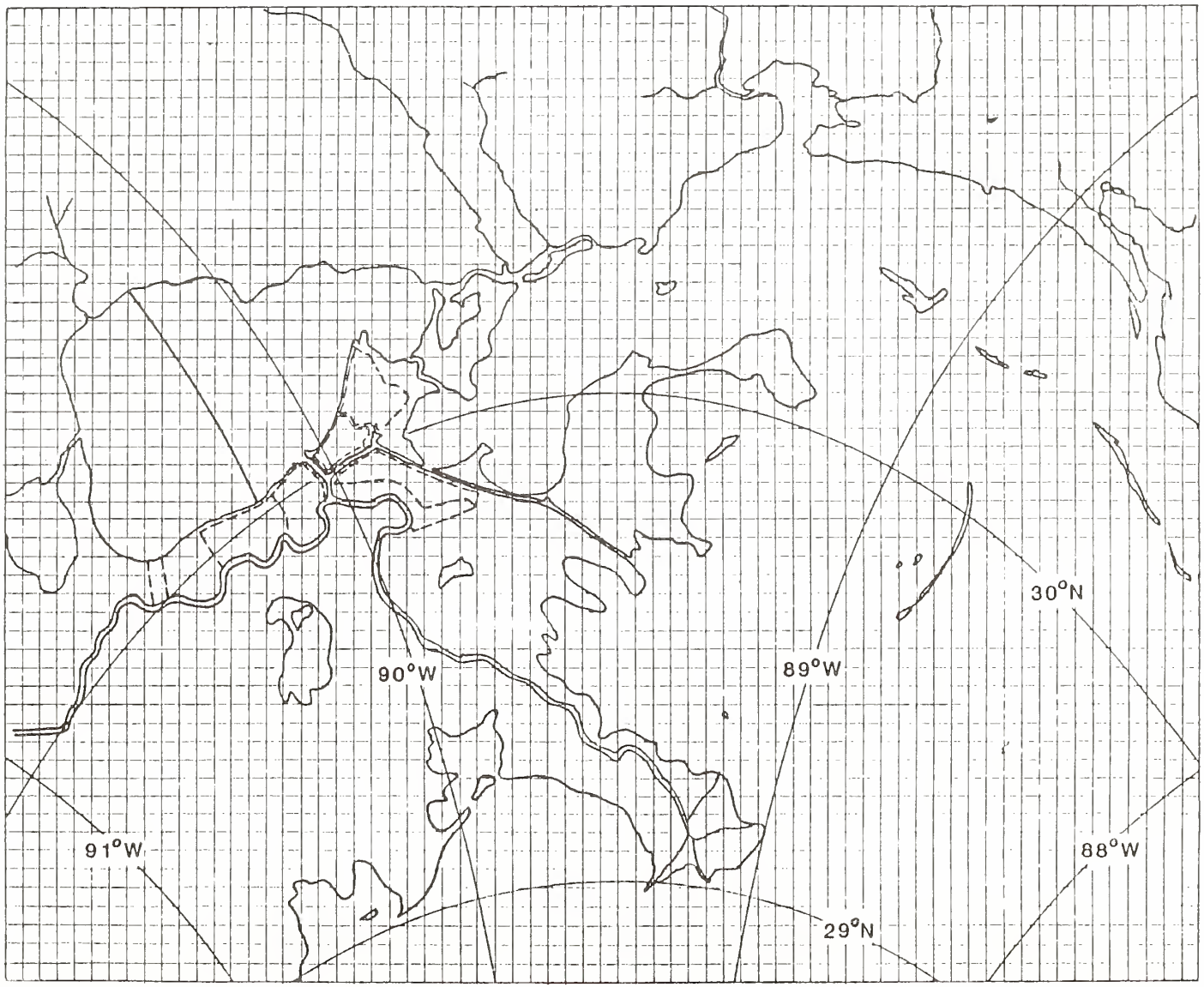

Figure 2b. A transformation of Fig. 2a. onto an image plane. The grid lines intersect as squares. Equally spaced surge values can be printed with a line printer. The projected latitude-Longitude lines are distorted accordingly.

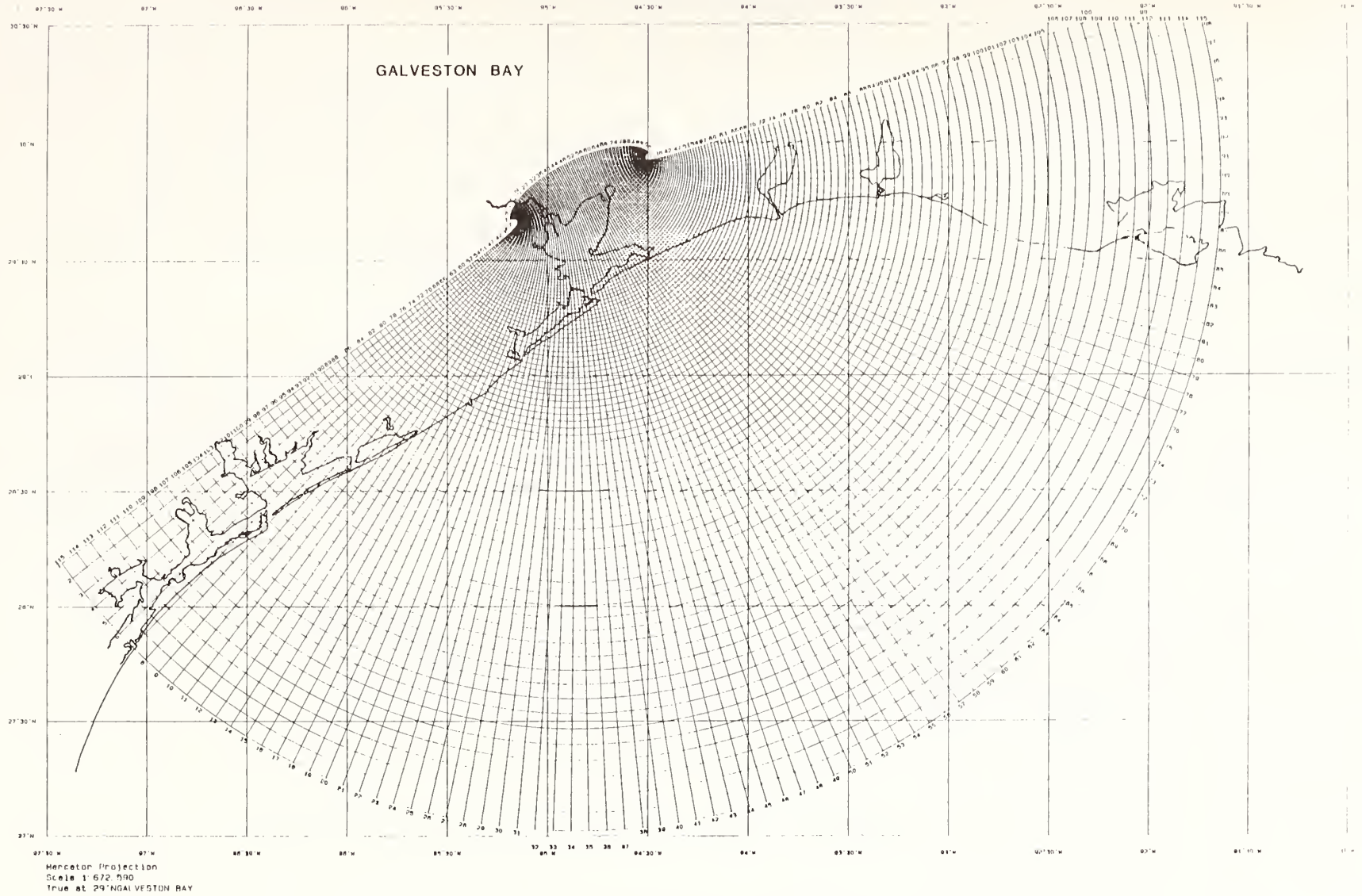

Figure 3a. An elliptical-hyperbolic grid for a bay or estuary.

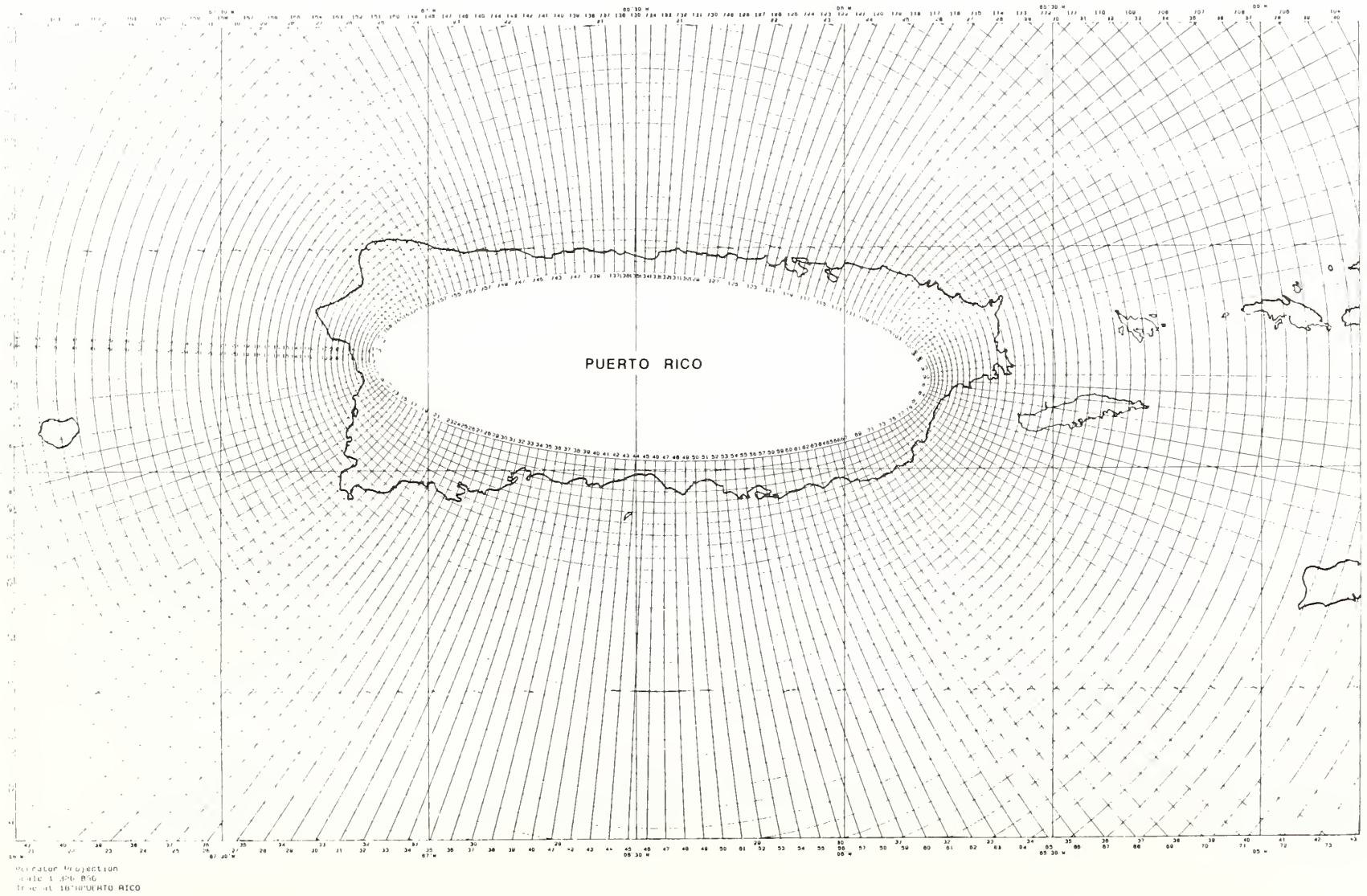

Figure 3b. An elliptical-hyperbolic grid for an island.

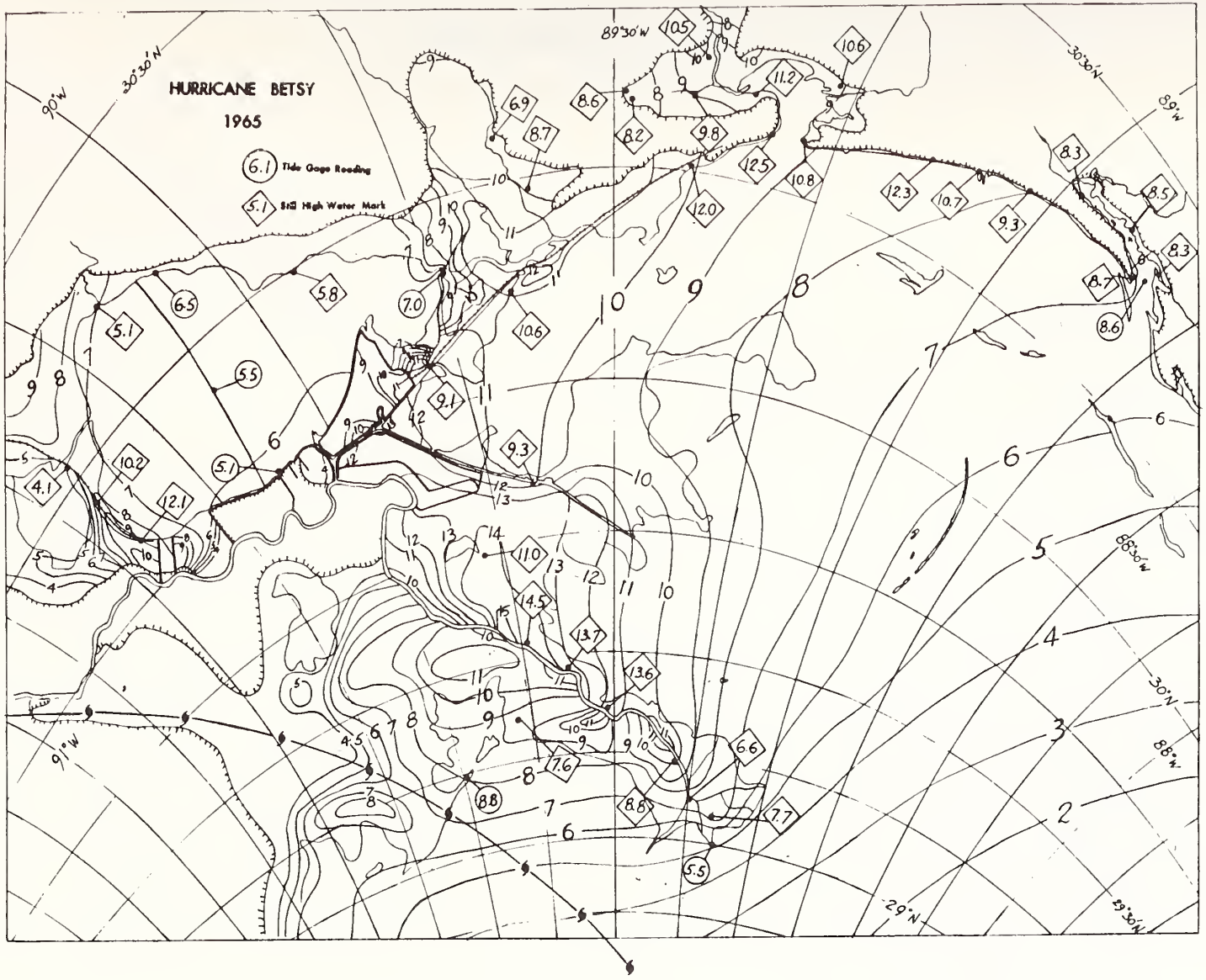

Figure 4. Contoured surface envelop of highest computed surge for Hurricane Betsy, 1965, and extent of inland inundation. The contours were hand drawn from a computed output on the grid of Fig. 2b.

Figure 5. Observed surge heights versus surge forecasts by the SLOSH model for nine storms in nine basins. A total of 572 tide gage, staff gage and high water mark observations are shown. Generally, the model is within ± 20% for significant surge heights.

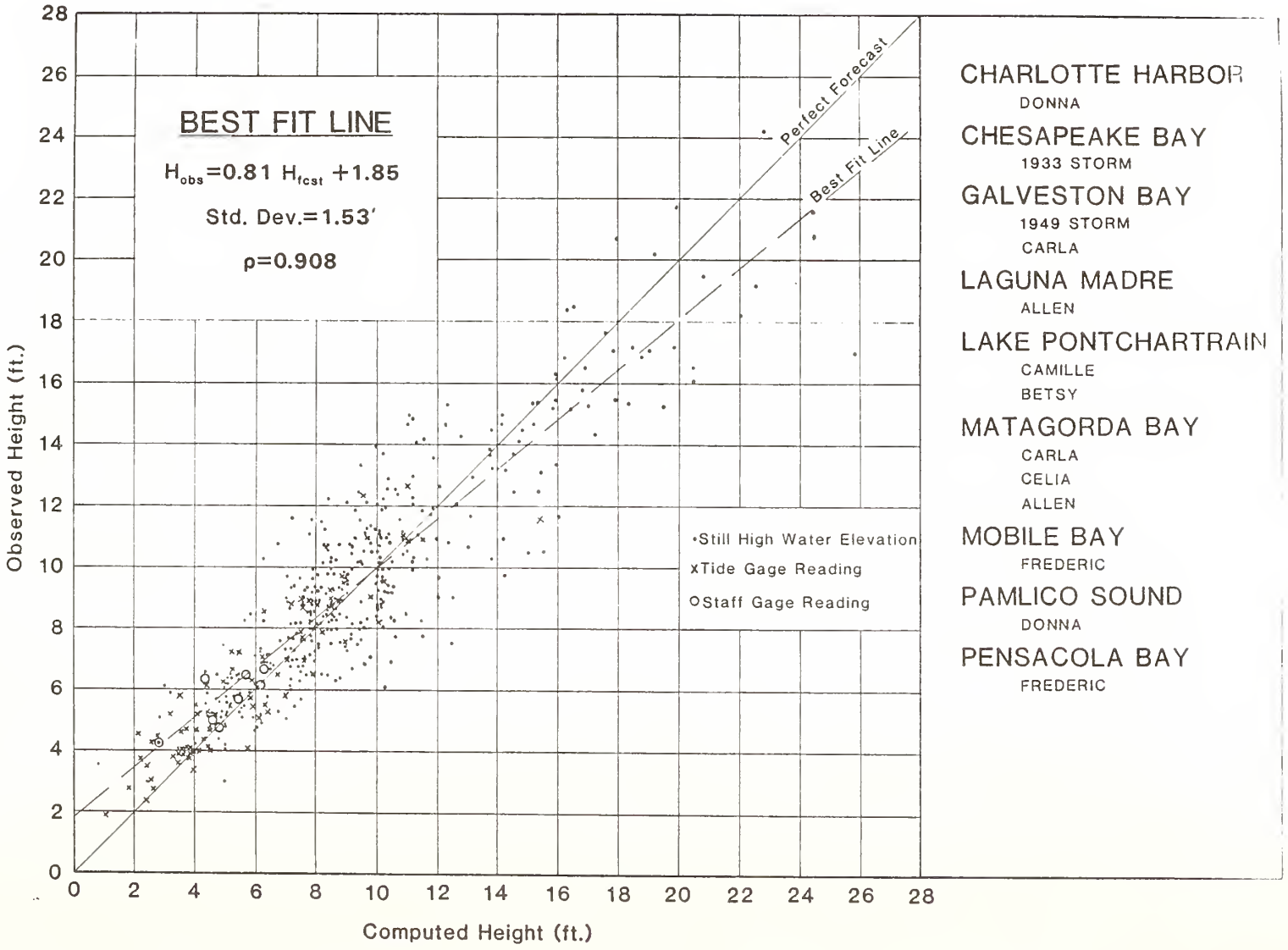

Theme III

Joint Cooperative Research Program

The Japan Research Plan on Precast Concrete Seismic Structural System (PRESSS Japan)

by
Shin OKAMOTO*
Shinsuke NAKATA*
Hisahiro HIRAISHI*
Takashi KAMINOSONO*
Hitoshi SHIOHARA*

* : PRESSS Project Team
Building Research Institute
Ministry of Construction

ABSTRACT

This report is the research project plan from Japanese side on Precast Concrete Seismic Structural System (PRESSS) for U.S. - Japan Cooperative Research Program which started since 1981 . This PRESSS program is the fourth phase item under the auspice of the UJNRwhich will continue for four years from this fiscal year .Our Japanese side program include not only the academic research development but also the establishment of design guideline and the design manual for precast concrete joints . Through this project , a feasibility study on "hinge-device system" is also discussed.

1. Background & Objectives

Precast concrete buildings have been widely constructed since 1960's in Japan. In 1965, Architectural Institute of Japan published a design recommendation for wall-panel precast concrete building. Since then, the number of precast wall panel concrete building increased responding to the increasing demand of urban housing supply. In 1974, the Japan Building Center established "Guideline for High-rise Precast Wall Panel Reinforced Concrete Structures", the scope of which is extended up to 8 storied building and it is based on ultimate strength concept. Most recently, aiming at the savings of shore and reduce construction period, half-precast construction systems, which use prefabricated beam and slab and made monolithic by topping concrete at the construction site, has been developed and widely used now.

In addition to that, the problem of shortage in numbers of construction labors is urgent in Japan. Construction companies try to rationalize and reduce the need of number of labor at construction site. Prefabrication is one of the solution of the problem. Some construction companies have already developed precast frame building system. However the systems are different each other. Thus, construction plan using the precast building systems require special screening by the Japan Building Center at present. It cause a delay of construction schedule and prevent construction of precast building from extensive usage. Further more, lack of detailed design recommendation is an another problem.

Taking into consideration of these Japanese conditions, the development of commonly used design method of precast concrete frame building is indispensable. U.S.-Japan Coordinated Research Program on Precast Concrete Building will cover new guidelines for design and construction. The coordination between United States and Japan will make it possible to develop new guideline for precast concrete buildings more earlier and more effectively.

2. Scope of Research

The scope of this research project is as follows:

(1) Type of Structural System

Moment resistant frame system and Moment resistant frame with shear wall system will be investigated

(2) Limitation of Building Height

Building with less than 15 stories (less than 45 meters)

(3) Material Strength

Concrete Design Strength $f_c < 500$ kgf/cm^2

Longitudinal Reinforcement Yield Strength ft 3000 - 5000 kgf/cm^2

Lateral Reinforcement ft 3000 - 13000 kgf/cm^2

(4) Details of Connection of Precast Member

In Japan so many types of connection are used in practice varied that it is impossible to test all of existing connection systems within the project. Therefore, all of connection systems are not necessary included in the scope of this project. The selection of connection systems will be done according to mechanical characteristics of each connection systems.

(5) Nonstructural walls

Nonstructural walls or cladding of buildings are dealt with only from the viewpoint that they should not have an unfavorable influence to the structural members.

3. Target of Research Development

The objective of this project is to develop a methodology of earthquake resisting design and a methodology for quality control of precast concrete building during production and construction.

The target for development is moment resisting frame building made of precast concrete which have high flexibility for planning design, as much as monolithically constructed reinforced concrete buildings.

The Philosophy of seismic design will be based on design philosophy of ductile moment resisting frame. Design philosophy may be followed from recently revised draft code named "Design Guideline for Earthquake resisting Reinforced Concrete Building Based on Ultimate Strength Concept," published from Architectural Institute of Japan in 1988.

For precast concrete buildings, several different design philosophy exists which include :

(1) CAST-IN-PLACE EQUIVALENT DESIGN

(2) SLIP ALLOWING DESIGN

(3) HINGE DEVICE DESIGN

"CAST-IN-PLACE EQUIVALENT DESIGN " is design concept which make possible to design building replaceable by precast construction without significant change of design. "SLIP ALLOWING DESIGN" is design concept which allows occurring slip behavior in hysteretic loop due to connection characteristics by compensation of increased strength. Intensive study of non-linear dynamic response analysis considering slip type hysteresis will

needed. "HINGE DEVICE DESIGN" is design concept which expect and utilize hysteretic energy absorption at specially designed connector.

In this project, design concept of "CAST-IN-PLACE EQUIVALENT DESIGN" will be focused on and practical guideline based on this philosophy is planed to be developed. Design (2) and (3) are planed to be studied in future in accordance with mutural coordination between U.S. and Japan PRESS.

4. Research Products

As a result of research in this project, several design recommendation and manuals are planed to developed, especially concerning with "CAST-IN-PLACE EQUIVALENT DESIGN". These design recommendation and manuals should cover not only existing joint construction systems, but also new types of devices flexibly, which will be developed in the future. Research products are as follows;

(1) Development of design recommendation for precast concrete building

This design recommendation covers moment resisting frame with or without shear wall to fifteen storied buildings. The guideline is utilized in practice by structural designers and buildings superintendent in specific governmental offices where check and evaluate design procedure before construction of buildings. This recommendation should describes required seismic performance and the rules for calculation procedure. The contents will be as following;

1) Scope
2) Structural planning
3) Stiffness evaluation
4) Design loads for members with joint region
5) Required strength and ductility for members and joint regions

(2) Development of Design Manual for Precast Member Connections

Design manual for Precast Member Connection is planed to be developed in order to show design procedure, by which designer will able to design connection with satisfactory performance with respect to strength and ductility.

This design manual should be practically used among structural designer, makers of precast , constructors, constructing managers, and inspectors in governmental office.

This manual should describe required performance of joints, design procedure of detail , and the technical background data useful for joint design as an appendix.

The contents of will be as following;

1) Scope
2) Design loads and design required ductility for joints
3) Fundamental rules of design for members with joints
4) Insurance of joint strength
5) Insurance of joint ductility
6) Design ensuring durability
7) Production and transportation
8) Site construction

Appendix A: design example of members and joints

Appendix B: Joint data

Appendix C: Evaluation Standard of joint performance

(3) Establishment of guideline for site construction and erection

The guideline for production and erection contains the items which make us of precast concrete members and site constructors should follow so that constructed precast concrete buildings can keep required quality in the process of their production and erection.

This guideline does not contain the items of a qualification check for makers and constructors on quality insurance.

5. Research Plan

5.1 Development of Design Recommendation for precast concrete building

(1) Making Frame Work of Design Recommendation

For the first stage, it is necessary to develop the frame work. Frame work means a logical structure of design recommendation. By the examination of the frame work, the scope of research work will be clearly defined and understood. A compilation of existing design philosophy which is used by precast engineer will be also necessary in this preliminary stage.

Thus the item which is needed to investigate at first stage will include:

- How to modify current three earthquake resisting design procedure; so called route 1, route 2 and route 3, i.e.

route 1: one of alternate design method of route 3, route 1 does not require the check of lateral strength capacity, which is a kind of strength oriented design. The scope of route 1 is limited to low-rise building which have enough amount of lateral resisting member, and minimum ductility is required.

route 2: another alternate design method which does not require the check of lateral strength capacity, which rely on ductility to some extent.

route 3: all-mighty procedure but which require the check of lateral strength capacity.

- How to handle buildings which have both monolithic members and precast members. This problem will arise because the scope of route 1, route 2 and route 3 are defined separately corresponding to different structural system, i.e. reinforced concrete, steel and so on.
- Examination of existing design philosophy of precast wall panel construction design, which is currently used by Japanese design engineers

(2) Making Draft of Design Recommendation

Then the details of design recommendation should be made based on analytical and experimental research. The problem which should be solved will include:

- The scope and limitation of structural system
- The scope and limitation of number of story, eccentricity, distribution of story stiffness in height direction
- Lateral strength demand for precast structural system
- Strength and ductility demand to joint which connects between precast members including two types of connection as follows;
  i) connections used in building designed by capacity design concept
  ii) connections used in building designed by traditional design concept
- The design philosophy of imperfectly integrated precast floor diaphragm transferring in-plane force induced by earthquake action
- The design philosophy of serviceability

(3) Experimental Studies on Effectiveness of Design Recommendation

Tests of full scale three-story three-frame specimens representing the bottom three stories of fifteen-story precast frame structure are planned to be designed. The objects of this experimental research program is summarized as follows;

- Correlation study between analytical model and experimental result

- Check of construction manual for quality control , which is planed to be developed as the fruit of cooperative research program between BRI and member from precast industry.
- The check of the design manual for precast member connection which is also planed to be developed in this project.
- Total Verification of Precast structural system.

5.2 Development of Design Manual for Precast Member Connections

In Japan, no design manuals for precast member connection exists, which describes the philosophy as well as appropriate example of many kind of connection details. So we need such manual which can be helpful for precast concrete engineer.

The manual will describe a design methodology of connection which transfer stresses safely and have enough ductility to cyclic loadings under the combination of design load.

Experimental and analytical research will be done for the purpose of obtaining basic data for documentary of design manual for precast member connection. The experimental research will be divided into three categories as follows;

(1) Tests of Sub-element Consisting Precast Connection

Joint materials and interfaces are defined here as sub-element of precast connection. The stress condition of sub-element are rather simple than that of whole connections. Thus the data about the sub-element can be basic in design of connections.

The sub-element should be identified and classified. Then the sub-element will be tested under monotonically increasing load. Temporally idea for tests of the sub-element will varied as follow;

Sub-element in Beam and column connections:

- concrete interface test considering the stress at the connection of beam to column or beam to beam subjected to shear as well as bending moment axial load, (variables: roughness of concrete interface, amount of dowel bars, inclination of compressive strut which cross the discontinuous interface, thickness of leveling mortar, axial load level, strength of leveling mortar, etc.)
- bond test of longitudinal reinforcement in beam which lay along the interface between precast concrete and topping concrete.(variables: the shape of cap tie, diameter of longitudinal bars, amount of cap tie, etc.)
- mechanical integrity of T-shape section beam consisted of precast beam and in-situ topping concrete (variables; amount of reinforcement across concrete interface)

Sub-element in Shear Wall:

- interface between wall panel and boundary element (variables: inclination of compressive strut to interface, amount of shear reinforcement, roughness of concrete interface, shape of shear cotter, etc.)

(2) Test of Precast Member Subassembledges

Based on the test data of connection materials and interface, analytical model will be developed which predict strength of connections. In order to assure the correlation between prediction of model and test, test of subassembledges of precast member is needed. For these subassebledge tests, cyclically loading which simulate earthquake will be used in order to evaluate ductility of connection.

Through these tests, the concept of connection design will be proposed and verified. Subassembledge tests will include:

- column:
  the effect of axial load, shape of cotter, dowels to ductility will be examined
- beam:
  concrete interface at beam end
  the method of consideration of dowel effect
  concrete interface between precast concrete and topping concrete
  shape of cap tie, amount of cap tie
- shear wall
  vertical joint
  horizontal joint
  joint wall panel and beam
- beam-column-joint subassembledge:
  anchorage method of beam longitudinal reinforcement
- floor system
  connection of slab panel
- connection of beam to girder
  beam end reinforcement in stress discontinuous zone

(3) Test of Superassmbledge

One-bay one-story frame specimens will be tested, The object of this test is as follows:

- Experimental verification of design of collapse mechanism
- Evaluation of story stiffness
- Correlation study between Model and experiment

5.3 Development of Construction Manual for Quality Control

This manual will be developed as the fruit of Cooperative research program between BRI and member from Precast industry.

5.4 Conceptual Flow of Research

Figure 1 shows the Time schedule and conceptual flow chart of research concerning development of 1) design recommendation and 2) design manual of precast member connection.

6. Research Budget and Executive Structure

Building Research Institute, Ministry of Construction of Japanese Government will spend about 120 Million Yen as a national project in total from 1989 to 1993(in fiscal year).

Parallel to this project, JTCC-PRESSS have been negotiating with Japanese constructors and precast concrete industry to carry a cooperative research. If it is possible, they will expense necessary for additional research and which will be able to support this project separately.

Figure 2 shows tentative research executive structure of Japanese side. It has two main committee, the functions of which is as follows;

(1) Advisory Panel Promoting Cooperative Research

a. approval of cooperative research executive structure
b. approval of cooperative research plan
c. approval of policy of compilation of research result
d. approval of policy concerning publishing of research result and treatment of patent.
e. promoting and utilization of the accomplished results of Project

(2) Joint Technical Consulting Committee (JTCC-PRESSS)

a. coordination of research and development targets with U.S.-PRESS committee
b. coordination of research plan of Japan side
c. coordination of utilization policy of research result with U.S-PRESS committee
d. advice researches on carrying out of research works
e. critical review of research result

7. Research Schedule

The Project of BRI financially supported by Ministry of Construction will last for four years, Thus it will continue since April 1989 until March in 1993. Although Project U.S. is supposed to become a six-year project starting in 1990. So JTCC-PRESSS should be extended for more two years. As a counter part of U.S.-PRESSS Committee.

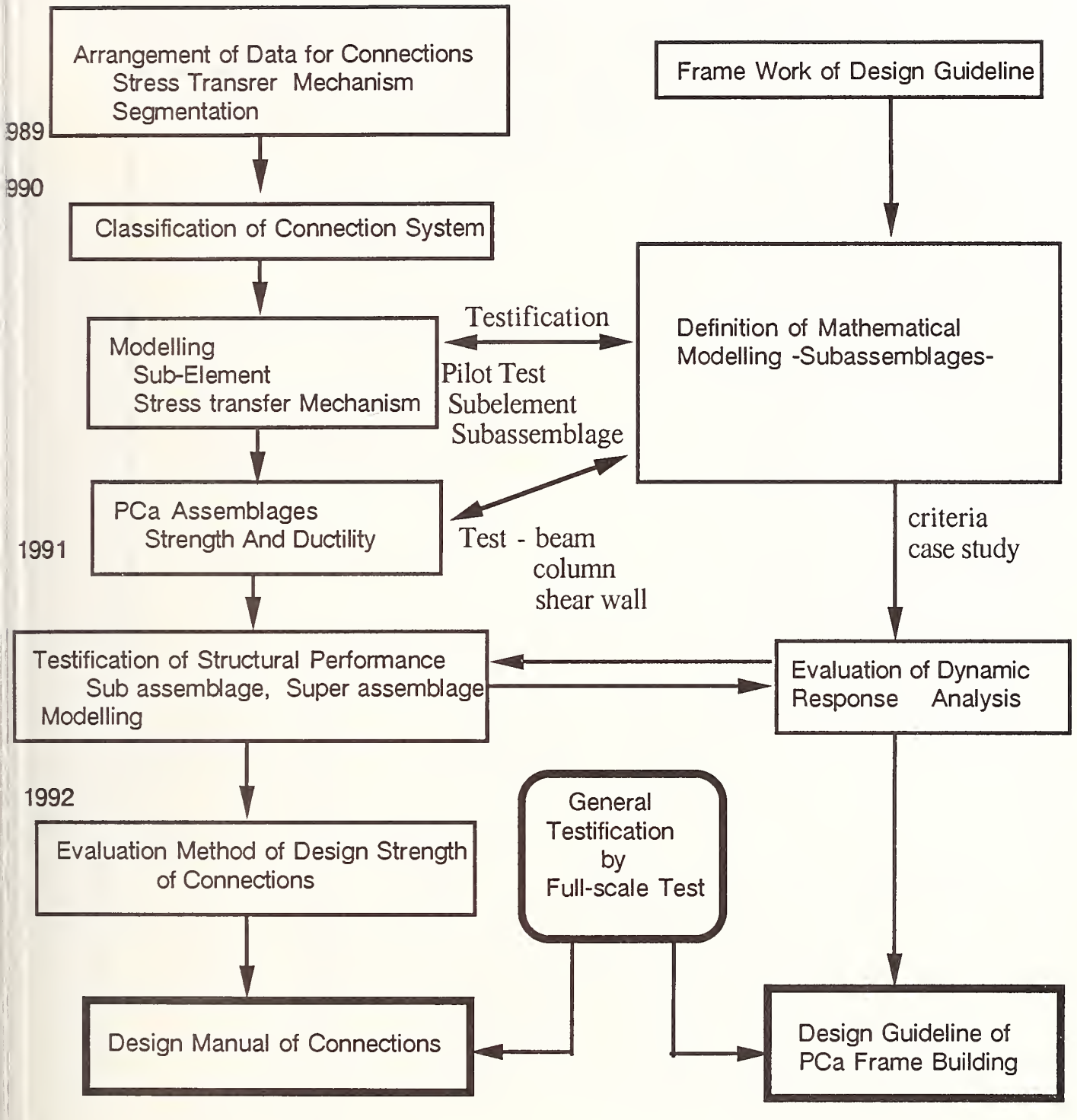

Fig. 1 Conceptual Flow of Research

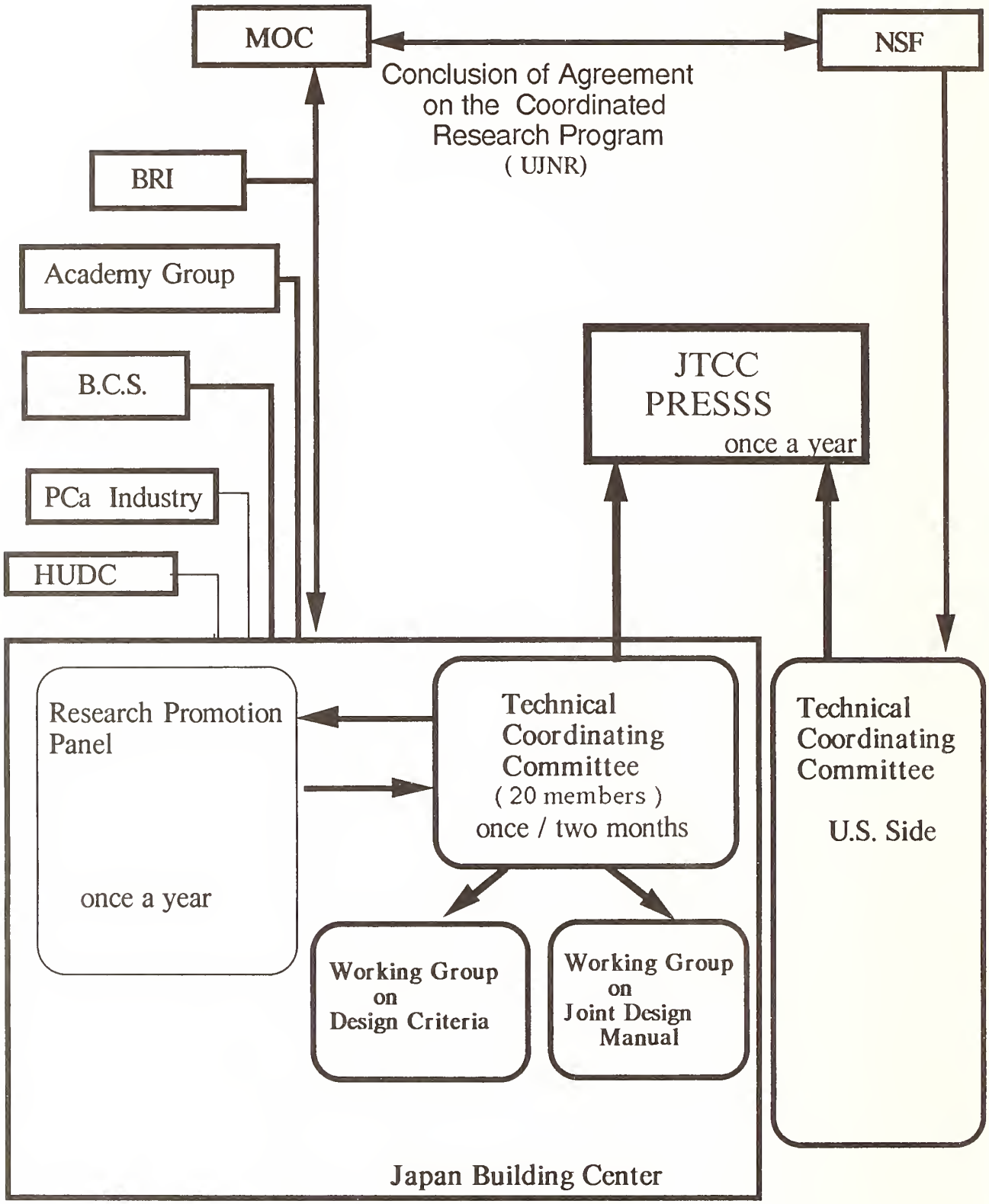

Fig. 2 PRESSS Executive Structure

U.S. Coordinated Program for Masonry Building Research
Fifth Year Status

by

James L. Noland[1]

ABSTRACT

The U.S. program, which consists of twenty-eight specific research tasks, is coordinated with a parallel program in Japan. Both are conducted under the auspices of the UJNR Panel on Wind and Seismic Effects. The primary purpose of the U.S. program is to support the development of a limit state design procedure for masonry as well as provide experimental data, analytical methods, etc. Several technical accomplishments have been made in both modeling and experimental areas. The technology transfer plan includes dissemination of research reports, topical reports and a summary report on the specific research areas as well as by presentations and papers. Design and criteria recommendations will be an extremely important mode of technology transfer and are expected to support design standard development.

KEYWORDS: Masonry; structures; standards; experiment; reports.

1. INTRODUCTION

The U.S. Coordinated Program for Masonry Building research is an integrated set of 28 specific research tasks being conducted by the U.S. Technical Coordinating Committee for Masonry Research (TCCMAR/US). The U.S. program is coordinated with a parallel program in Japan to exchange information and concepts for the mutual benefit of both countries. Both programs are conducted under the auspices of the UJNR Panel on Wind and Seismic Effects. The U.S. program is funded by the National Science Foundation.

2. PROGRAM OBJECTIVES

Primary program objectives are:

a. Development of design and criteria recommendations for limit state design of reinforced masonry buildings and components.

b. Development of a consistent experimental database on the behavior of masonry materials, components and systems.

c. Development of analytical non-linear models for research and design office use for detailed analysis, system analysis, and dynamic loads determination.

d. Improved material and subassemblage experimental procedures for obtaining masonry properties.

e. Improved masonry fabrication procedures and standards.

f. Developing an increased awareness among engineers, architects, code bodies and the public of the capabilities of reinforced masonry in all seismic zones.

g. Interfacing with standards development groups to support development of a consensus limit state standard for masonry.

3. APPROACH

With NSF support, the Technical Coordinating Committee for Masonry Research/U.S. (TCCMAR/U.S.) was formed in February 1984. TCCMAR/U.S. was and is comprised of researchers from academic and industrial organizations who have strong backgrounds in research into the properties and characteristics of reinforced masonry materials, structural components and systems, analytical techniques, structural dynamics, building codes, and earthquake engineering. TCCMAR was not intended to be a closed group; researchers may be and have been added as needs develop. Current TCCMAR researchers are listed in Table 1.

The initial TCCMAR purposes were 1) to specifically define the research topics, both experimental and analytical, necessary to develop a

---

1. Atkinson-Noland & Associates, Boulder, Colorado

consistent masonry structural technology for the U.S. and 2) to establish communication with its Japanese counterpart to enable Japanese and U.S. programs to be coordinated for the benefit of both.

Program evaluation and research needs assessment are continuing activities of TCCMAR. The original plan is not a static entity but rather one which can and has been modified as work has progressed and needs either revised or added.

The U.S. research plan is a phased step-by-step program of separate, but coordinated research tasks. Emphasis is being placed upon intra-task information exchange and consultations so the experimental and analytical efforts are mutually supportive.

The program includes both experimental and analytical research tasks. The experimental and analytical efforts are conducted in parallel with each becoming more complex and sophisticated as knowledge and experience accumulate. The U.S. plan is thus a "building block" approach.

The U.S. program is being conducted on a project basis to provide the task and schedule coordination required for efficient and orderly conduct of the program.

4. SCHEDULE

The schedule herein (Figure 1) contains a list of the specific research tasks which comprise the U.S. program and their starting and ending dates. Primarily because of funding difficulties the schedule has been revised. The program has been extended until January 1994, i.e., one year after the completion of the full-scale test project.

5. TECHNICAL ACCOMPLISHMENTS

The U.S. program is proceeding generally according to expectations. At this point in time, which is about the 60 percent point, technical accomplishments have become apparent. It must be recognized, however, that the major technical results are yet to come.

Because the primary objective of the U.S. program is to provide a basis for limit state design and an associated generic modeling capability, the following seem significant among the results achieved to date:

a. A finite element model (FEM) has been formulated and implemented capable of reproducing some aspects of post-peak strength response of reinforced shear walls. The material models have the capability to represent the reduction in peak compressive strength due to tensile cracking and allow reorientation of initial cracks to a final crack state. The model is capable of reproducing fully cyclic load-deformation histories and is operable on 286 and 386-based PCs.

b. Structural component models (SCM) have been developed and calibrated using the results of the one-story wall tests. The models will soon be extended to more complex stress states, and will be combined for use in analyzing pierced walls. The models will be extended to be able to handle cases involving unloading and reloading.

c. A non-linear lumped parameter model (LPM) has been developed to do time-history analyses of masonry structures. New non-linear "spring" elements have been introduced to represent masonry shear walls in building system models. The LPM will include rotational degree of freedom, and will be tested against experimental results.

d. Approximately 30 reinforced shear walls have been tested. A database has been developed for the cyclic behavior of single-story reinforced masonry shear walls with different in-plane compressive loads and reinforcement rates. Limit states have been identified for application in the design recommendations to be made.

e. Three different two-story coupled reinforced masonry shear wall specimens have been tested resulting in a database for the fully-reversed cyclic behavior of such specimens with different degrees of coupling.

Stable hysteretic behavior was observed at overall story drifts of at least one percent. Limit states have been identified for application in design recommendations. Simple models predicted collapse loads within ten percent and complex models satisfactorily predicted collapse and deflections.

f. Force-deflection characteristics of prestressed precast concrete plank floor diaphragms have been established experimentally both parallel and perpendicular to plank direction. Limit states have been identified and corroborated by observations of plank behavior in the two-story coupled shear wall tests.

g. Data describing the behavior of other diaphragm systems, e.g., timber, steel deck and steel deck-concrete, has been collected. A comprehensive final report presents the data to define hysteretic models for the diaphragms and other design conditions.

h. Reinforced concrete and clay masonry walls responded elastically when subjected to out-of-plane dynamic motions typical of design ground motion in soil type 1 in the highest U.S. seismic zones. Limit states for application in design recommendations have been identified.

i. Tests of grouted hollow clay and concrete unit prisms in concentric compression indicated that masonry is a generic material, i.e., that no unusual behavioral traits are present to separate grouted hollow-unit clay and concrete masonry. The compressive tests established stress-strain curves including the post-peak descending branch and limit state values. Tests of prisms loaded in eccentric compression established strain gradient effects and necessary to define equivalent rectangular stress values for use in flexural design.

j. Tests have been conducted on reinforcement bond-slip and lap splice behavior using grouted, reinforced hollow clay and concrete specimens. Both push-pull and pull-pull loads were applied. Results have been used to formulate models and identify limit states for application in design recommendations.

k. A design criteria was developed for shear walls that was adopted in the 1988 Uniform Building Code, Section 2413.

l. A proposed design criteria was developed for Masonry Frames for the 1991 UBC. The criteria is now under review.

m. A new proposed design equation was developed for masonry shear walls. This equation was submitted for inclusion in the 1991 UBC and is now under review.

6. TECHNOLOGY TRANSFER

The technology developed, data, and other findings which result from the research must be made available to the public for study and use in an active manner in order to have the greatest utilization possible. For a program such as this which extends over a substantial period of time, it is appropriate that the technology developed, etc., be documented and released as an on-going activity as well as the documentation and dissemination which will occur at the completion of the work.

The Technology Transfer component which has been defined for the program consists of the following:

a. Task Reports - One or more reports have been and will be prepared for each research task comprising the coordinated program. Task reports are complete technical research reports. Each task report is a "stand-alone" document and fully describes the subject of the report. In the case of reports on experimental research, all pertinent data is included in a clear and understandable form. Copies of task reports are distributed initially to about 75 concerned individuals. Arrangements have been made to furnish the

Earthquake Engineering Research Library at UC-Berkeley with copies of all Task Reports which have been and will be released. Completed task reports are listed in Table 2.

b. Papers - Papers published in technical journals and conference proceedings are an important part of technical transfer because they focus on individual issues and are more widely read than larger documents. TCCMAR researchers have and will continue to prepare such papers.

Arrangements have been made to provided complete copies of the proceedings of all the meetings of the Joint U.S.-Japan Technical Coordinating Committee on Masonry Research to the Earthquake Engineering Research Library at UC-Berkeley.

c. Presentations - Presentations on various aspects of the Coordinated program to professional, code, industry, and other concerned groups are encouraged and many have and will continue to be, made. Typically, no papers are associated with presentations, but some material may be distributed.

d. Seminars & Workshops - Participation in seminars and workshops is another form of Technology Transfer which is encouraged because of the more in-depth communication which can occur. Some participation has occurred and more is anticipated.

e. Topical Reports - Reports will be prepared on each basic topic addressed in the Program and will be a treatise on the subject. Anticipated topical reports are listed in Table 3.

f. Technical Summary Report - The technical summary report is to be prepared late in the program will present basic technical findings and conclusions and sufficient supporting data and information to substantiate them. Topical Reports will be the primary references, but task reports will be listed if additional detail is required.

g. Design and Criteria Recommendations - Recommendations for reinforced masonry building design and criteria will be formulated documented in a manner suitable for review and adoption by code bodies. Recommendations will also be made for standard tests which provide masonry material properties.

7. STANDARDS/CODES

A critical issue in the U.S. is, and has been the transfer of technol ,y developed by research into practice. In the U.S. an important factor in implementing research into practice is the incorporation or provision for new technology by the design standards.

In the U.S., design standards are developed by non-governmental professional groups using various forms of consensus processes. Hence, the NSF-supported U.S. Coordinated Program for Masonry Building Research cannot develop standards, but will develop recommendations (Task 10).

Discussions and negotiations over the last year have served to establish mechanisms and processes for transfer of technology (i.e. research data and recommendations) to a consensus design standards development committee sponsored by The Masonry Society, the American Concrete Institute and the American Society of Civil Engineers. A one-year pre-standardization effort to collect and document background information pertinent to limit state structural design and to develop a draft limit state design standard for masonry was organized and funded by industry. The pre-standardization work along with the technology developed by the coordinated masonry research program will be utilized by the national masonry standards committee to produce a limit state design standard for masonry. The basics of the process are illustrated by the figure 2.

The first meeting of the Joint Committee was on December 11 & 12, 1989 in Denver. A task group was

organized to formulate a single set of operating procedures. In addition to developing a limit state design standard, the Joint Committee will maintain the recently completed working stress standard, and address other issues pertinent to masonry structures design and construction.

The second meeting of the Joint Committee was held in Toronto in March 1990. James Colville of the Department of Civil Engineering, University of Maryland was inducted as the chairman of the Joint Committee.

TABLE 1

TCCMAR RESEARCHERS

Daniel Abrams University of Illinois Urbana, IL	Samy Adham Agbabian Associates El Segundo, CA
Richard Atkinson Atkinson-Noland & Associates Boulder, CO	Russell Brown Clemson University Clemson, SC
Robert Englekirk Englekirk & Hart Los Angeles, CA	Robert Ewing Ewing & Associates Rancho Palos Verdes, CA
Ahmad Hamid Drexel University Philadelphia, PA	Gary Hart Englekirk & Hart/UCLA Los Angeles, CA
Gilbert Hegemier Univ. of CA-San Diego La Jolla, CA	John Kariotis Kariotis & Associates South Pasadena, CA
Richard Klingner Univ. of Texas-Austin Austin, TX	Ronald Mayes Computech Engin. Services Berkeley, CA
James L. Noland Atkinson-Noland & Associates Boulder, CO	Max Porter Iowa State University Ames, Iowa
M.J.N. Priestley Univ. of CA-San Diego La Jolla, CA	Frieder Seible Univ. of CA-San Diego La Jolla, CA
P.B. Shing University of Colorado Boulder, CO	Leonard Tulin University of Colorado Boulder, CO

TABLE 2 - TASK REPORTS[1]

Task No.	Author/s - Title
1.1-1:	Atkinson and Kingsley, Comparison of the Behavior of Clay and Concrete Masonry in Compression, September 1985.
1.2(a)-1:	Hamid, A., Assis, G., Harris, H., Material Models for Grouted Block Masonry
1.2(b)-1:	Young, J.M., Brown, R.H., Compressive Stress Distribution of Grouted Hollow Clay Masonry Under Strain Gradient, May 1988.
2.1-1:	Hart, G. and Basharkhah, M., Slender Wall Structural Engineering Analysis Computer Program, (Shwall, Version 1.01), September 1987.
2.1-2:	Hart, G. and Basharkhah, M., Shear Wall Structural Engineering Analysis Computer Program (Shwall, Version 1.01), September 1987.
2.1-3:	Nakaki, D. & Hart, G., Uplifting Response of Structures Subjected to Earthquake Motions, August 1987.
2.1-4:	Hart, G., Sajjad, N., and Basharkhah, Inelastic Column Analysis Computer Program (INCAP, Version 1.01), March 1988.
2.1-5:	Hong, W.K., Hart, G.C., Englekirk, R.E., Force-Deflection Evaluation and Models for University of Colorado Flexural Walls, December 1989.
2.1-6:	Hart, G.C. Jaw, J.W., Low, Y.K., SCM Model for University of Colorado Flexural Walls, December 1989.
2.3-1:	Ewing, R., Kariotis, J., El-Mustapha, A., LPM/I, A Computer Program for the Nonlinear, Dynamic Analysis of Lumped Parameter Models, August, 1987.
2.3-2:	Ewing, R., El-Mustapha, A., Kariotis, J., Influence of Foundation Model on the Uplifting of Structures, July 1988.
3.1(a)-1:	Scrivener, J., Summary of Findings of Cyclic Tests on Masonry Piers, June 1986.
3.1(b)-1:	Seible, F. and LaRovere, H., Summary of Pseudo Dynamic Testing, February 1987.
3.1(c)-1:	Merryman, K., Leiva, G., Antrobus, N., Klingner, R., In-Plane Seismic Resistance of Two-Story Concrete Masonry Coupled Shear Walls, September 1989.

1. TASK REPORTS ARE AVAILABLE THROUGH THE EARTHQUAKE ENGINEERING RESEARCH LIBRARY, BERKELEY, CA.

3.2(a):	Hamid, A., Abboud, B., Farah, M., Hatem, K., Harris, H., Response of Reinforced Block Masonry Walls to Out-of-Plane Static Loads, September 1989.
3.2(b)-1:	Agbabian, M., Adham, S., Masri, S., Avanessian, V. Traina, Out-of-Plane Dynamic Testing of Concrete Masonry Walls, Volumes 1 and 2, July 1989.
4.1-1:	Limin, H., Priestley, N., Seismic Behavior of Flanged Masonry Shear Walls, May 1988.
4.2-1:	Hegemier, G. Murakami, H., On the Behavior of Floor-to-Wall Intersections in Concrete Masonry Construction: Part I: Experimental
4.2-2:	Hegemier, G., Murakami, H., On the Behavior of Floor-to-Wall Intersections in Concrete Masonry Construction: Part II: Theoretical
6.2-1:	Scrivener, J., Bond of Reinforcement in Grouted Hollow-Unit Masonry: A State-of-the-Art, June 1986.
6.2-2:	Soric, Z. and Tulin, L., Bond Splices in Reinforced Masonry, August 1987.
8.1-1:	Hart, G., A Limit State Design Method for Reinforced Masonry.
9.1-1:	Kariotis, J.C., Johnson, A.W., Design of Reinforced Masonry Research Building, September 1987.
9.2.2:	Seible, F., Design and Construction of the Charles Lee Powell Structural Systems Laboratory, November 1986.
9.2.3:	Seible, F., The Japanese Five-Story Full Scale Reinforced Masonry Building Test, January 1988.
11.1-1:	TCCMAR, Summary Report: U.S. Coordinated Program for Masonry Research, September 1985 to August 1986.
11.1-2:	Status Report: U.S. Coordinated Program for Masonry Building Research, November 1988.

TABLE 3

TOPICAL REPORTS PLANNED

No.	Topic	Pertinent Tasks
TR1	Material Properties & Tests	1.1, 1.2, 1.3
TR2	Reinforced Masonry Walls: In-Plane Shear and Combined In-Plane Shear and Vertical Compression	2.1, 2.2, 3.1(a), 3.1(b) 3.1(c), 4.1, 9.4
TR3	Reinforced Masonry Walls: Out-of-Plane Forces Combined with Vertical Compression	2.4(a), 2.4(b), 3.2(a) 3.2(b1), 3.2(b2)
TR4	Diaphragms	2.3, 2.4(a), 2.4(b), Category 5 Tasks, 9.4
TR5	Bond and Splicing of Reinforcement in Masonry	Category 3 Tasks, 4.1, 6.2
TR6	Limit State Design Concepts for Reinforced Masonry	Categories 1-9
TR7	Modeling of Masonry Components and Building Systems	Category 2 Tasks, 3.1(b), 7.1, 9.4
TR8	Large Scale Testing of Masonry Building Systems	3.1(b), 3.1(c), Category 9 Tasks
TR9	Determination of Earthquake Induced Forces on Masonry Buildings	2.1, 2.3, 2.4(a), 2.4(b), 7.1, 8.1, 8.2, 9.4

U.S.-JAPAN COORDINATED PROGRAM FOR MASONRY BUILDING RESEARCH

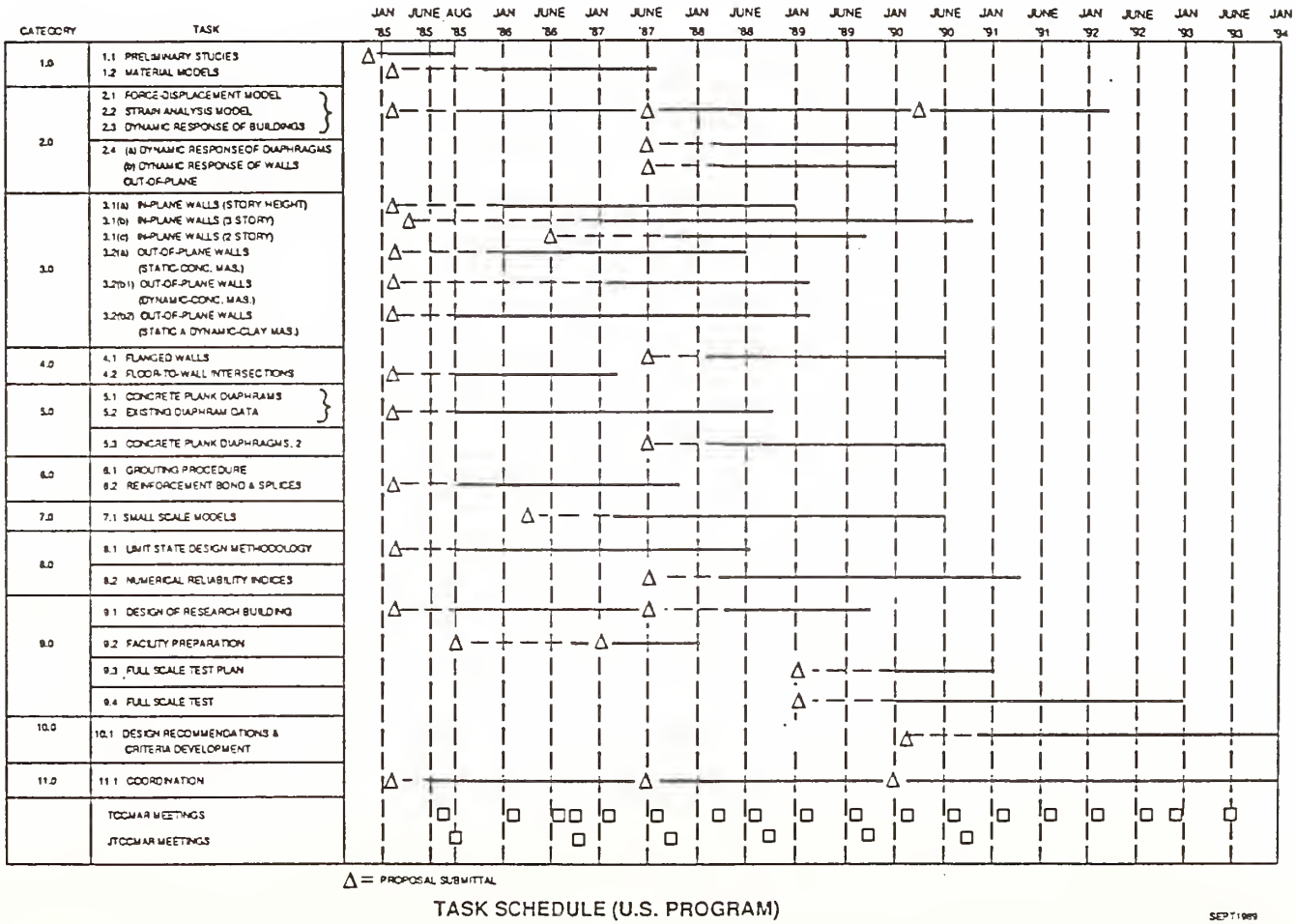

TASK SCHEDULE (U.S. PROGRAM)

Figure 1

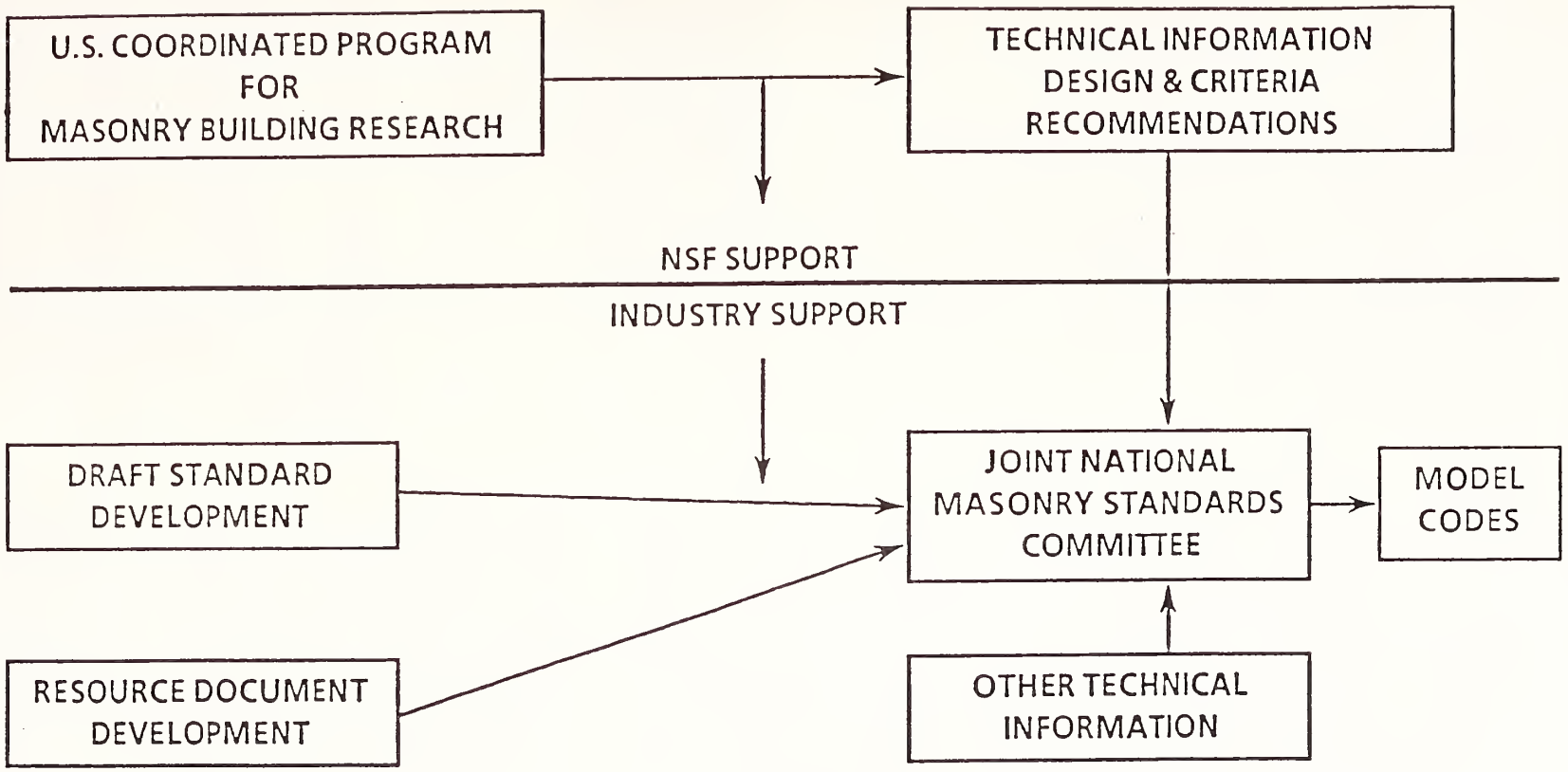

FIGURE 2 : INTEGRATION OF RESEARCH INTO DESIGN STANDARDS

Design Guidelines of Medium Rise RM Buildings

by

Yutaka YAMAZAKI*1, Shin OKAMOTO*2

Tsuneo OKADA*3, Akira MATSUMURA*4 and Toshiyuki KUBOTA*5

SUMMARY

Design guidelines of medium rise RM buildings were made by TECCMAR/Japan and were released March 1989. The design guidelines consist of eleven chapters. They are: 1. General, 2. Quality of Material, 3. Material Strength and Allowable Stress, 4. Constants of Materials, 5. Structural Planning, 6. Structural Calculation, 7. Allowable Stress Design, 8. Total Flexural Resisting Moment, 9. Lateral Load Carrying Capacity, 10. Foundation, and 11. Joint and Anchorage of Reinforcement, Covering Concrete Thickness and Arrangement of Reinforcement.

In this paper, outline of these design guidelines is presented.

KEY WORDS

RM Building, Design Guidelines of RM Buildings, Seismic Design of Masonry Buildings

INTRODUCTION

The final goal of the U.S.-Japan coordinated research on masonry buildings in Japan is to realize a medium rise reinforced masonry (RM) building with less wall width ratio than the one required for present masonry structures. Design guidelines for a medium rise RM building were made by TECCMAR/Japan based upon the synthetic experimental and analytical research which had been carried out since 1984.

In the existing design codes for masonry buildings in Japan, the number of stories is limited up to three and a large amount of walls (high wall width ratio) is required. In order to realize the earthquake resistant masonry buildings which have larger story number but less wall width ratio than the one required by the existing design codes, a ductility design concept as well as a strength design concept was employed in the design guidelines.

The contents of the RM design guidelines are presented in APPENDIX II.

RM STRUCTURES AND THEIR REQUIRED SEISMIC PERFORMANCE

RM Structures (Sections 1.1 and 1.4)

The RM structures which are dealt with in the design guidelines are reinforced masonry structures which are consist of reinforced masonry (RM) bearing walls and wall girders, and reinforced concrete (RC) slabs, foundations and foundation beams.

The RM bearing walls and wall girders are to be fully grouted reinforced masonry systems which are made by stacking open-end type concrete or clay RM units, as shown in Figs. 1a and 1b, with using joint mortar in parallel with arranging reinforcements into unit cells vertically and horizontally, as shown in Fig. 2.

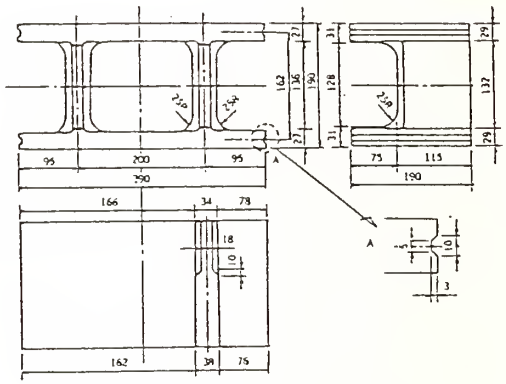

Fig. 1a Concrete RM Unit

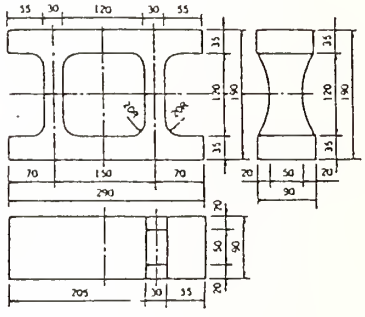

Fig. 1b Clay RM Unit

A RM building is basically to be an apartment house type structure in which sufficient amount of walls is expected to be provided in the transverse direction.

*1 Head, Large Scale Structure Testing Division, Production Department, Building Research Institute, Ministry of Construction, 1-Tatehara, Tsukuba-shi, Ibaraki Prefecture, #305 Japan

*2 Director, International Institute of Seismology and Earthquake Engineering, BRI

*3 Professor, Institute of Industrial Science, University of Tokyo, Roppongi, 7-22-1, Minatoku, Tokyo, #106 Japan

*4 Professor, Dept. of Architecture, Kanagawa University, Rokkakubashi, Kanagawa-ku, Yokohama, #221 Japan

*5 Professor, Dept. of Architecture, Kinki University, 3-4-1, Kowakae, Higashiosaka-shi, Osaka, #577 Japan

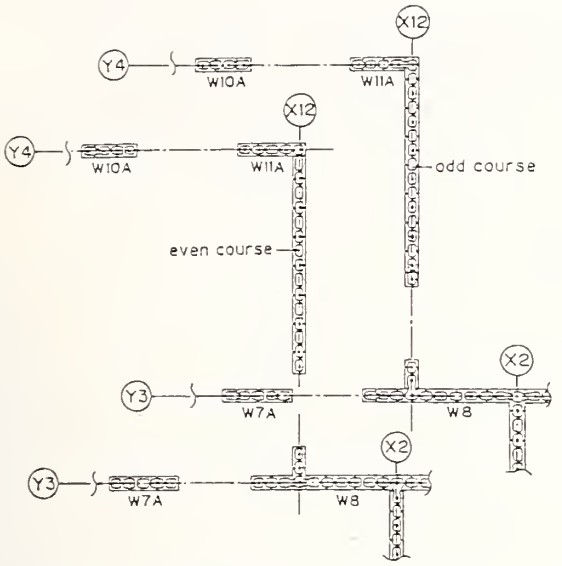

Fig. 2 Typical Bonding and Reinforcing Patterns in the 5 story Full Scale RM Test Building

The RM structures shall be designed by either "Design Method A" or "Design Method B" and should satisfy the specifications listed in Table 1 for each design method. In Table 1, the rigidity and eccentricity factors are related to both vertical and horizontal stiffness distribution limitations in a structure and are defined in the Building Standard Law [See Ref. 1]. The story drift angle in Table 1 is defined as the one produced in each story of a structure when subjected to design lateral seismic shear forces which also are specified in the Building Standard Law. The value of the limitation, 1/2,000, for the story drift angle was determined not to produce large story drift angle, such as 1/200, against severe earthquakes, say 300-400gals ground motion level [Ref. 2]. Specifications on "shear stress of wall" and "wall width ratio" are mentioned in the following.

Table 1 Specifications for Design Methods A and B

		for Design Method A	for Design Method B
Shear Stress of Wall (kg/cm^2)		$\tau \leq \sqrt{F_m}/2$ (3.1)	$\bar{\tau} \leq 4 \cdot \sqrt{F_m/180}$ (5.5)
Rigidity Factor (6.4)		≥ 0.3	≥ 0.6
Eccentricity Factor (6.4)		≤ 0.3	≤ 0.15
Story Drift Angle (rad) (6.3)		$\leq 1/2,000$	
Standard Wall Length Ratio (for 1st Story) (5.5)	5 stories	$15cm/m^2$	
	3 stories	$12cm/m^2$	
Minimum Wall Length Ratio (for 1st Story) (5.5)	5 stories	$10cm/m^2$	$12cm/m^2$
	3 stories	$7cm/m^2$	$9cm/m^2$
Story Height (1.1)		$\leq 4.0m$	$\leq 3.5m$
Building Height (1.1)		$\leq 16m$	$\leq 16m$

τ: shear stress of each wall (kg/cm^2)
$\bar{\tau}$: nominal shear stress of walls in each story (kg/cm^2)
F_m: specified compressive strength of RM assembrage
Rigidity and Eccentricity Factors: defined in Japan Building Standard Law
Story Drift Angle: story drift angle when subjected to design seismic force
Wall Width Ratio: defined in each loading direction

Required Seismic Performance (Section 1.3)

1.3 Required Seismic Performance
(1) A RM building shall be a structure which does not cause any trouble on serviceability against moderate earthquakes and does not collapse in the event of severe earthquakes.
(2) A failure mechanism of a RM building basically shall be governed by flexural yielding at the base of walls at the first story and wall girder ends.
(3) A RM building shall be a structure which possesses the ultimate lateral strength and deformability corresponding to a structural performance coefficient (symbolized as D_S hereafter) of 0.5 or more.

Application:
(1) Though a failure mechanism of a RM building basically shall be governed by flexural yielding at the base of walls at the first story and wall girders, flexural yielding at the top of walls located at top story and a foundation beam to which a wide wall is connected may be permitted.
(2) Narrow walls may lead flexural yielding or shear failure prior to flexural yielding of wall girders to which the nallow walls are connected. In this case, it is needed to confirm that the yielding or the failure of those walls does not affect seriously on seismic performance of the overall structure and also that local collapse in the structure does not occur. Similarly, if there is possibility of shear failure in some wall girders, it is needed also to confirm that the failure of those wall girders does not lead local collapse in the structure.

The items (1) and (2) in main body in Section 1.3 will concretely signify that:
(i) shear cracking does not occur in most structural components against design lateral seismic shear forces corresponding to the moderate earthquakes, and
(ii) a failure mechanism of a RM structure shall be governed by flexural yielding which certifies that almost no strength degradation occurs up to a story drift angle of 1/200 and that no major strength deterioration does up to that of 1/100, as well as possessing sufficient lateral strength against design lateral seismic shear forces corresponding to the severe earthquakes.

DESIGN CRITERION

1.4 Design Criterion
A RM building shall be designed both by a working stress design method specified in Chapters 6 and 7, and by an ultimate

lateral strength design method specified in Chapter 9 as well as satisfying structural specifications described in the following Chapters except Chapter 8 (Design Method A). However, a RM building which satisfies the special structural specifications described in the following chapters shall be designed without carrying out the ultimate lateral strength design (Design Method B).

The RM structures can be designed either by Design Method A or by Design Method B. In case of Design Method A, seismic performance corresponding to the value of 0.5 in the structural performance coefficient D_s or larger is to be certified through ultimate lateral strength design of an entire structure and ductility design of structural components, whereas, in case of Design Method B, seismic performance corresponding to the value of 0.55 * in the converted base shear coefficient $\tilde{C}_B$ * or largeris to be certified through calculating total flexural resisting moment of an entire structure.

Limitation on the values representing characteristics of a structure when applying Design Method B is stricter than the one for Design Method A as listed in Table 1, because in Design Method B necessary amount of wall width and reinforcement is determined based upon calculation of flexural resisting moment without appropriately assuming yielding mode of the structure, instead of carrying out the ultimate lateral strength design.

The outline of Design Methods A and B is represented in Table 2.

Table 2 Summary of Design Method

			Design Method A	Design Method B
Elastic Design	Long Term	Beam	$\tau_L \leq \alpha \cdot f_s$	$\tau_L \leq \alpha \cdot f_s$
		Wall	$(\tau_L \leq f_s)$	$(\tau_L \leq f_s)$
	Short Term	Beam	$_DQ_S = Q_L + \min(n \cdot Q_E, \Sigma M_y/l_o)$ where $n \geq 1.5$ $_DQ_S \leq {}_AQ$	$_DQ_S = Q_L + \min(n \cdot Q_E, \Sigma M_u/l_o)$ where $n \geq 3.0$ $_DQ_S \leq Q_{su}$
		Wall	$_DQ_S = Q_L + Q_E$ $_DQ_S \leq {}_AQ$	$_DQ_S = Q_L + \min(n \cdot Q_E, \Sigma M_u/l_o)$ where $n \geq 3.0$ $_DQ_S \leq Q_{su}$
		Story Drift	Scory drift Angle $\leq 1/2,000$ against Q_E	
Strength and Ductility Design	Flexure	Structure	Ultimate strength and Ductility Design $D_S \geq 0.5$	Total Flexural Resisting Moment Design $\tilde{C}_B \geq 0.55$
	Shear	Wall and Beam	$Q_{su} \geq Q_L + (1.0 \sim 1.3)\, Q_{mu}$	—

τ_L: shear stress due to long term design load
α: coefficient decermined according to shear-span ratio, $1 \leq \alpha \leq 2$
f_s: allowable shear stress for long term design load
$_DQ_L$: shear force acting on a member due to long term design load
$_DQ_E$: shear force acting on a member due to seismic design load
ΣM_y: sum of yield flexural moments on both ends of a member
l_o: face-to-face span length of a member
n: coefficient to increase shear force
$_DQ_S$: shear force due to short term design load
$_AQ$: allowable shear strength
ΣM_u: sum of flexural strength on both ends of a members
Q_{su}: ultimate shear strength
Q_{mu}: shear force acting on a member at mechanism
D_s: coefficient of structural performance
$\tilde{C}_B$: converted base shear coefficient

5.5 Wall Width Ratio

(1) In each direction at each story, the wall width ratio L_w in cm/m^2 which is defined as the total width of bearing walls in cm in each direction divided by the floor area of the story considered shall satisfy Equation 5.5.1.

$$L_w \geq \alpha \cdot \beta \cdot Z \cdot L_{wo} \quad \text{and} \quad L_w \geq Z \cdot L_{wn} \qquad (5.5.1)$$

where,

L_{wo}: standard wall width ratio in cm/m^2 indicated in Table 5.5.1 when the thickness of walls t in cm is the smallest thickness t_o which is defined in Section 5.3(2)

α: reduction factor calculated by Equation 5.5.2 when the thickness of walls t is greater than the smallest thickness t_o which is defined in Section 5.3(2)

$$\alpha = \frac{\Sigma\ (t_o \times \text{length of each wall})}{\Sigma\ (t \times \text{length of each wall})}$$

$$\alpha \geq 1 - 3/L_{wo} \qquad (5.5.2)$$

β: reduction factor calculated by Equation 5.5.3 related to the specified compressive strength of RM assemblage used

$$\beta = \sqrt{180/F_m} \qquad (5.5.3)$$

F_m: specified compressive strength of RM assemblage in kg/cm^2

Z: seismic hazard zoning coefficient defined in the Building Standard Law

L_{wm}: minimum wall width ratio in cm/m^2 indicated in Table 5.5.1

Table 5.5.1 Limitation of Wall Width Ratio

Story from the Top (ground story)	Standard Wall Width Ratio $L_{wo}(cm/m^2)$	Minimum Wall Width Ratio $L_{wm}(cm/m^2)$	
		Design Method A	Design Method B
1-3	12	7	9
4 and 5	15	10	12

(2) The nominal shear stress when applying Design Method B shall satisfy Equation 5.5.4.

$$\bar{\tau} \leq 4.0 \sqrt{F_m/180} \qquad (5.5.4)$$

where

* $\tilde{C}_B = Q_u/(Z \cdot R_t \cdot F_{es} \cdot W)$
where
Q_u: ultimate lateral strength of a structure
Z: seismic hazard zoning coefficient (= 0.7 - 1.0)
R_t: design spectral coefficient
F_{es}: shape factor = $F_e \cdot F_s$ (F_e = 1.0 - 1.5, F_s = 1.0 - 1.5)
W: structure weight

$\bar{\tau}$: nominal shear stress in kg/cm^2 produced in the walls in each direction at each story when subjected to the short term design load corresponding to $C_o \geq 0.2$

$$\bar{\tau} = Q / \Sigma A_w$$

Q: seismic shear force in kg at each story

A_W: sum of wall area in cm^2 in each direction at each story

F_m: specified compressive strength of RM assemblage in kg/cm^2

(3) The calculation of the wall width ratio shall be based on the following items (i) through (iii).

(i) The bearing walls with the width more than 59cm can be taken into account.

(ii) The bearing walls supported only by wall girders can not be taken into account.

(iii) Full width of the bearing walls with the small openings specified in Section 5.4 can be taken into account.

The shear stress produced in a 5 story RM building against the short term design load is estimated as an example.

Assume:

wall width ratio: $15cm/m^2$

shear stress due to the long term design load: 0

wall thickness: 19cm

story weight: $1,200kg/m^2$

seismic hazard zoning coefficient: 1.0

Then, nominal shear stress is calculated as

$$\bar{\tau} = \frac{0.2 \times 1200 \times 5}{15 \times 19} = 4.21 \text{ kg/cm}^2$$

Taking shear stress concentration coefficient η into account, shear stress produced in a critical (wide) wall in the story becomes;

$$\tau = \eta \cdot \bar{\tau} = 6.32 \text{ kg/cm}^2 \quad (\eta = 1.5)$$
$$6.74 \text{ kg/cm}^2 \quad (\eta = 1.6)$$

The allowable shear stress f_s for the short term design load in case of $F_m = 180kg/cm^2$ is obtained based on the equation, $f_s = \sqrt{F_m}/2$, specified in Section 3.1 as;

$$f_s = 6.71 \text{ kg/cm}^2$$

This example shows that shear stress produced in most walls is smaller than the allowable shear stress level and that no shear cracking is expected to be produced in most walls in RM buildings having standard weight against the short term design load corresponding to $C_o = 0.2$.

QUALITY OF MATERIALS

RM Units (Section 2.1)

Masonry units for RM buildings shall conform to the "Standard of Quality of Masonry Units for Medium Rise RM Buildings". In the Standard, units are classified into two kinds according to their materials made from, namely, concrete and burned clay (or ceramics). Concerning dimensions of units, these are also assorted into two types, such as "12" type and "23" type. The "12" type has its sizes with the ratio of thickness to length as 1 : 2. The "23" type has the ratio of 2 : 3. Combinations of dimensions have variation in some range, as listed in Table 3.

Table 3 Dimensions* of RM Units

Type	Thickness(mm)	Length(mm)	Height(mm)
12	200	400	100, 150, 200 225, 250, 300
	225	450	
	250	500	
	300	600	
23	200	300	100, 150 200, 225, 300
	266.7	400	
	300	450	

* Dimensions are expressed in nominal sizes, i.e., distances from center to center of the thickness of morter joints.

The Standard also classifies the quality of units into three grades according to their compressive strength and water absorption. Table 4 denotes its classification. Difference in strength values between units of concrete and clay in the same grade comes mainly from their conformity of water absorption values in each grade.

Table 4 Strength and Water Absorption

Material	Grade	Compressive Strength, min. kg/cm^2 Net Area	Water Absorption Ratio, max. % vol.
Concrete	1	400	10
	2	300	15
	3	200	20
Clay	1	600	10
	2	500	15
	3	400	20

Specified Compressive Strength (Sections 2.2, 2.3 and 2.5)

Specified compressive strength of grout concrete and mortar shall be more than $180kg/cm^2$. Compressive strength of joint mortar shall be high enough to obtain the specified strength of RM assemblage. Specified compressive strength of concrete which is used in R/C portion shall be ranged between $180kg/cm^2$ and $270kg/cm^2$.

Specified compressive strength of RM assemblage shall be ranged between $180kg/cm^2$ and $270kg/cm^2$.

Materials of RM Assemblage (Section 2.4)

Specified conpressive strength of RM assemblage shall be verified by prism testing as a rule.
Instead of applying prism testing, specified compressive strength of RM assemblage may be verified by using Equation A 2.4.1.

$$F_m = e_s \{ (1-\beta')F_u + \beta' F_g \} \quad (A\ 2.4.1)$$

where

F_m = specified compressive strength of RM Assemblage (kg/cm^2)
F_u = specified unit strength (kg/cm^2)
F_g = specified grout strength (kg/cm^2)
β' = cavity ratio of unit
e_s = masonry reduction factor, which value is 0.75 as a rule. However when strength of joint mortar is less than F_u, it shall be ratio of the former to the latter, and not larger than 0.75.

Specified compressive strength of grout shall be more than that of RM assemblage as a rule.

Allowable Stresses of RM Assemblage (Section 3.1)

Allowable stress of RM assemblage shall be in accordance with the values in Table 5.

Table 5 Allowable Stress of RM Assemblage

Description	Allowable Stresses (kg/cm^2)	
	For Stresses due to Long Term Design Load	For Stresses due to Short Term Design Load
Compression	$F_m/6$	$F_m/3$
Shear	$\sqrt{F_m}/3$	$\sqrt{F_m}/2$

Modulus of Elasticity of RM Assemblage (Section 4.1)

Young's modulus of elasticity shall be obtained by compression prism test as a rule.
It may also be estimated by Equations A4.1.2a and A4.1.2b, rather conservatively (Fig. 3a).

Young's modulus of elasticity:
for concrete masonry;

$$E_m = 1.68 \times 10^5 \sqrt{F_m/180} \quad (kg/cm^2) \qquad (A4.1.2a)$$

for clay masonry;

$$E_m = 1.31 \times 10^5 \sqrt{F_m/180} \quad (kg/cm^2) \qquad (A4.1.2b)$$

If moduli of elasticity of constituent materials are known, Young's modulus of elasticity of masonry may be estimated by using Equation A4.1.3 (Fig. 3b).

$$E_m = (1-\beta')\ E_u + \beta' E_g \quad (kg/cm^2) \qquad (A.4.1.3)$$

Where E_m = Young's modulus of elasticity of masonry
E_u = Young's modulus of RM unit
E_g = Young's modulus of grout
β' = cavity ratio of unit

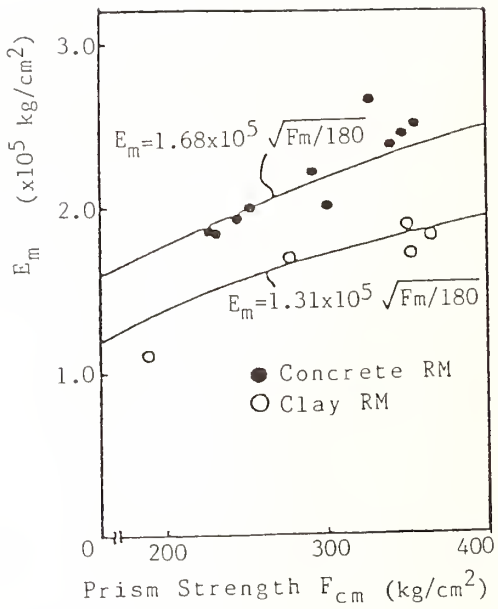

Fig. 3a Young's Modulus of Elasticity vs. Prism Strength

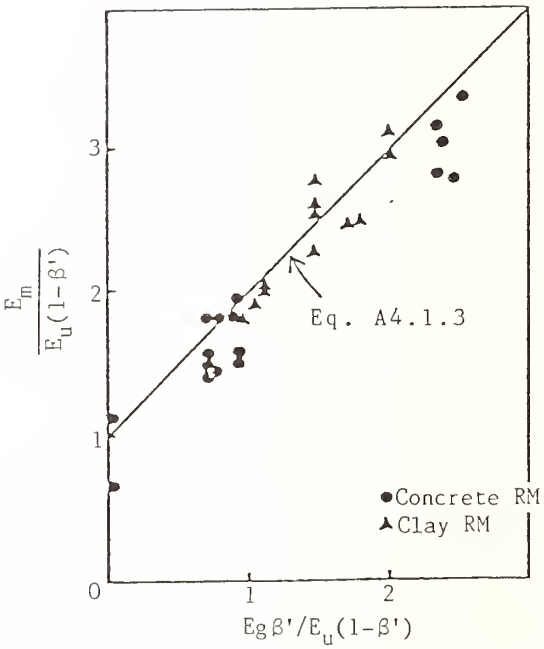

Fig. 3b Eq. A4.1.3 and Test Results

Shear modulus of elasticity is able to be estimated by Equation A4.1.1 using a value of Poisson's ratio measured in compression prism test.

$$G_m = \frac{E_m}{2(1+\nu m)} \qquad (A4.1.1)$$

where G_m = shear modulus of elasticity of masonry
ν_m = Poisson's ratio of masonry:

STRUCTURAL SPECIFICATIONS FOR RM COMPONENTS

Bearing Walls

5.3 Bearing Walls

(1) The bearing walls shall be greater than 59cm in width.

(2) The minimum thickness of bearing walls shall be greater than 19cm and 1/20 of the vertical distance between main lateral supports.

(3) The bearing walls of the upper story shall be located above those of the adjacent lower story as a rule.

(4) The bearing walls shall have no openings as a rule. However, the small openings regulated in Chapter 5.4 may be provided.

(5) The vertical and horizontal shear reinforcements conforming to Section 7.2, Chapters 9 and 11 (Section 7.2, Chapters 8 and 11 for Design Method B) shall be provided in the bearing walls.

7.2.4 Arrangement of Reinforcements in the Bearing Walls

(1) Vertical and shear reinforcements shall be arranged with those more than the required amount of reinforcements determined from the allowable stress design and specified amount of reinforcementsin Table 7.2.1.

Table 7.2.1 Reinforcements in Bearing Walls

Story from the Top	End Flexural Reinforcement	Intermediate Vertical Reinforcement	Vertical Reinforcement Ratio	Shear Reinforcement
from 1 to 2	≧1-D16 and ≦2-D25	Space ≦Length of Unit or ≦40cm	≧0.2%	Ratio ≧0.2% (0.25%) Space ≦Height of Unit or ≦20cm
from 3 to 5				Ratio ≧0.25% (0.3%) Space ≦Height of Unit or ≦20cm
Size of Reinforcement	D16-D25	D10-D16		D10-D16
Note: Values in parentheses denote those for Design Method B.				

(2) Surroundings of the small openings specified in Section 5.4 shall be properly reinforced by arranging 1-D10 reinforcement or larger ones.

(3) Number of reinforcements which could be arranged in a unit hole shall be less than 2. However, the number of reinforcements shall be less than 4, if the thickness of RM units is thick enough to arrange the reinforcements in two lines.

Wall Girders

5.6 Wall Girders

(1) Wall girders shall be provided to effectively connect bearing walls each other at every story.

(2) The end of wall girders shall be supported by a bearing wall (including an intersecting bearing wall).

(3) Wall girders shall have sufficient capacity against both vertical and horizontal design load, and shall satisfy the following items (i) through (v).

(i) Width of wall girders shall be more than the thickness of a bearing wall connected to them.

(ii) Depth of wall girders shall be more than 45cm.

(iii) The ratio of clear span l_o in cm to depth D in cm of wall girders, l_o/D, shall be more than 1.5.

(iv) The lateral and shear reinforcements conforming to Section 7.3, Chapters 9 and 11 (Section 7.3, Chapters 8 and 11 for Design Method B) shall be provided in the wall girders.

7.3.4 Arrangement of Reinforcements in Wall Girders

(1) Lateral and shear reinforcements shall be arranged with those more than the required amount of reinforcements determined from the allowable stress design and specified amount of reinforcements in Table 7.3.1.

Table 7.3.1 Reinforcements in Wall Girders

	End Flexural Reinforcement	Intermediate Lateral Reinforcement	Lateral Reinforcement Ratio	Shear Reinforcement
Amount of Reinforcements	≧1-D16 and ≦2-D25 (≧1-D19 and ≦2-D25)		≧0.25%	≧0.25% (≧0.3%)
Space		≦40cm		≦20cm
Size of Reinforcement	D16-D25	D10-D25		D10-D16
Note: Values in parentheses denote those for Design Method B.				

(2) In case of short beams, the end flexural reinforcements shall be more than 1-D16 reinforcement and the shear reinforcement ratio shall be more than 0.3%.

(3) Number of reinforcements which could be arranged in a unit hole shall be less than 2.

Floor Slabs

5.8 Floor Slabs

(1) Floor slabs as a main structural component shall be constructed by reinforced concrete and have sufficient capacity against vertical load. They shall also have sufficient strength and rigidity to transfer the stress caused by lateral force to bearing walls and wall girders (or to foundation beams at the lowest story).

(2) Thickness of the floor slabs shall be more than 13cm.

Foundations and Foundation Beams

5.10 Foundations and Foundation Beams

(1) Foundation beams shall be effectively and continuously provided beneath the bearing walls at lowest story.

(2) Foundations and foundation beams shall have sufficient strength and rigidity against vertical and lateral load, and satisfy the following items (i) though (v).

(i) Foundations and foundation beams shall be cast-in-place reinforced concrete.

(ii) Width of foundation beams shall be more than the thickness of bearing walls connected to.

(iii) Foundation beams shall be reinforced at four corners in their section against flexural moment. The flexural reinforcements shall be restrained by shear reinforcements.

(iv) Foundations shall be properly arranged beneath the bearing walls as a rule.

(v) Foundations and foundation beams shall have sufficient resistance against torsional stress produced due to eccentric arrangement of foundations and/or piles.

7.7 Foundation Beams

(1) Design stress for foundation beams shall be calculated based on Section 7.1.

(2) Design of foundation beams shall be carried out in accordance with AIJ R/C Standards.

(3) Foundation beams shall satisfy the following items (i) through (iii).

(i) The amount of both upper and lower flexural reinforcements shall be more than 2-D16 as a rule.

(ii) The spacing of shear and intermediate lateral reinforcements shall be less than a half of the depth of foundation beams and shall be less than 30cm.

(iii) Shear reinforcement ratio shall be more than 0.2%.

Bearing Wall-Wall Girder Joints

5.11 Bearing Wall-Wall Girder Joints

(1) The thickness of bearing wall-wall girder joints shall be more than the one of adjacent bearing walls and wall girders.

(2) Small openings shall be permitted to be provided for the joints to which a bearing wall having the width l more than 159cm is connected.

(3) Small openings in the joints shall satisfy the following items (i) through (iv).

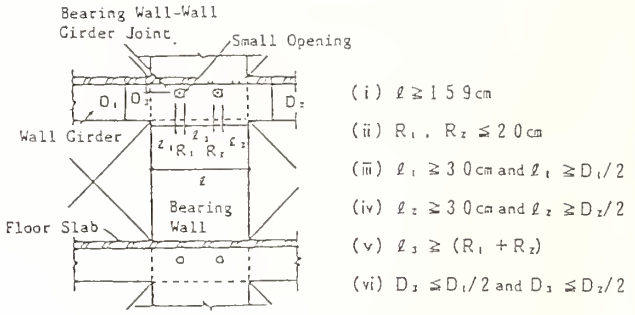

Fig. 5.11.1 Small Openings in Bearing Wall-Wall Girder Joint

(i) Clear length R (to be the diameter for round shape and the longer side for rectangular shape) shall be less than 20cm.

(ii) The distance l_1 and l_2 between the side of bearing walls and the edge of small openings shall be more than 30cm and a half of the depth D_1 and D_2 of wall girders connected to.

(iii) The plural small openings in the joint shall be arranged side by side, and the distance between the edges of two small openings l_3 shall not be less than the sum of clear length R_1 and R_2 of those small openings as a rule.

(iv) The small openings shall not be located at a lower half portion of the joints.

7.8 Bearing Wall-Wall Girder Joints

(1) The long and short term allowable stress design of the bearing wall-wall girder joints shall be abbreviated to be carried out. However the examination specified in Section 9.5.4 shall be needed for the joints which satisfy the following items in the whole, whether Design Methods A or B is applied.

(i) The width of bearing walls to which the joint is connected is smaller than 98cm.

(ii) The joints to which the wall girders are connected in the both side

(iii) The amount of tension side flexural reinforcements in the wall girders stated in the above item (ii) is more than $13cm^2$.

(2) The surroundings of small openings in the joints which are specified in Section 5.11 shall be reinforced in accordance with the specifications in Section 11.4.3.

Seismic Slit Joints and Shear Keys

5.12 Others

(1) Seismic slit joints shall be provided between bearing walls/wall girders and secondary walls in order not to have bad influence on strength and deformation capacity of those bearing walls/wall girders.

(2) Shear keys shall be provided as a rule, in order to fully transfer the shear forces, on upper surface of foundation beams and floor slabs on which the bearing walls are arranged.

STRESS ANALYSIS

6.2 Stress Analysis

(1) Stress and deformation of RM buildings shall be evaluated using elastic stiffness of structural components as a rule, in which;

(i) Stress under the vertical design load can be obtained applying abbreviated methods which are practically applied under actual circumstances.

(ii) The long term axial stress acting on the bearing walls can be evaluated against the vertical design load subjected to the floor area surrounded by bisectional lines which devide corner angles at bearing wall intersections, clear distance between two parallel bearing walls, and clear length of wall girders.

(2) The effective width of orthogonal walls and floor slabs shall be appropriately taken into account to evaluate stiffness of T-shape structural components.

(3) The effect of torsion shall be taken into account if the center of gravity and the center of rigidity at each story do not coincide with each other.

Application:

(1) Stress and deformation of RM buildings can be evaluated using a frame analysis method in which flexural and shear deformation and rigid zone at bearing wall-wall girder joints are taken into account. Axial deformation also shall be taken into account for those bearing walls in which large axial deformation is expected. The rigid zone area taken into account is determined based on the AIJ R/C Standards.

(2) The stiffness of foundation beams shall be taken into account. Deformation of the ground and piles can be appropriately evaluated as well.

(3) Young's modulus and elastic shear modulus of RM structural components shall be those for the RM assemblage specified in Section 4.1. The effect of existence of reinforcements may be taken into account as well.

(4) The plural bearing walls which surround openings having the value of an equivalent opening ratio of 0.4 or less can be considered as an equivalent non-opening single bearing wall. The shear stiffnesses in this case shall be evaluated in accordance with the shear stiffness reduction factor specified in the AIJ R/C standards (Eq. A 6.2.1).

Shear stiffness reduction factor γ

$$\gamma = 1 - 1.25\sqrt{\frac{h_o\, l_o}{hl}} \qquad \text{(A 6.2.1)}$$

where

$$\sqrt{\frac{h_o\, l_o}{hl}} \leq 0.4$$

and

h: vertical distance between main lateral supports of bearing walls

l: width of bearing walls

h_o, l_o: clear height and width of the opening, respectively

(5) The reduction of shear stiffness may be neglected for the small openings specified in Section 5.4.

(6) The flexural stiffness of wall girders in which clear length is comparatively short (designated as "short beams") may be reduced up to 50% of their elastic stiffnesses.

TOTAL FLEXURAL RESISTING MOMENT IN DESIGN METHOD B

8.1 Check of the Total Flexural Resisting Moment

The following Equation 8.1.1 shall be satisfied in the case that design method B is used.

$$(\Sigma Mbu + \Sigma_1 Mwu) \geq 0.55 \cdot Z \cdot Rt \cdot \sum_{i=1}^{n} (Ai \cdot Wi \cdot hi) \qquad (8.1.1)$$

where,

ΣMbu: total summation of moment capacity of wall girders at nodal points (kg cm)

$\Sigma_1 Mwu$: total summation of moment capacity of walls at the bottom of 1st story (kg cm)

Z : seismic hazard zoning coefficient

Rt : design spectral coefficient

Ai : lateral shear distribution factor at i-th story

Wi : weight of the building above the i-th story (kg)

hi : height of the i-th story (cm)

n : number of story

For the buildings to which design method B is adopted, the structural regulations such as wall width ratio, profile of plan and elevation, etc. are required strictly. However, the state at ultimate stage of the structure is not clear because only allowable stress design method is used.

In this section the simplified check of the lateral load carrying capacity is obligated. The mechanism as shown in Fig. 4 is assumed whithout checkinig the yielding mechanism in the calculation.

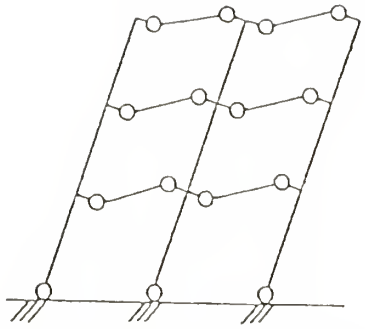

Fig. 4 Yielding Mechanism assumed in the Design Method B

LATERAL LOAD CARRYING CAPACITY

Fundamental Concept (section 9.1)

9.1 Fundamental Concept

(1) The lateral load carrying capacity of RM buildings shall be greater than the required lateral load carrying capacity expressed by Eq. 9.1.1.

$$Qun = Ds \cdot Fes \cdot Qud \qquad (9.1.1)$$

where,

Qun : required lateral load carrying capacity at each story

Ds : structural performance coefficient specified in Section 9.2

Fes : shape factor which is determined based on the eccentricity and variation of lateral stiffness along the building height

Qud : lateral seismic shear force at each story

(2) Failure mode of members shall be flexural yielding mode as a rule.

(3) Failure mode of a building shall be total failure mode in which flexural yielding occurs at the bottom of the 1st story walls and at the ends of wall girders as a rule.

(4) Walls, wall girders, foundation beams and surroundings of small openings shall be reinforced according to the requirements specified in Section 9.5.

The procedure of the check is as follows;

(i) to calculate ultimate strength of each component,

(ii) to calculate lateral load carrying capacity in every direction and to decide the stress and yield type for each component under yielding mechanism of a building,

(iii) to decide the structural performance coefficient "Ds" at the direction considered using the "component type" for wall girders and bearing walls stipulated in Section 9.2,

(iv) to calculate the required lateral load carrying capacity at each story and compare with the lateral load carrying capacity obtained from item (ii),

(v) to do the ductility design for bearing walls, wall girders, foundation beams and surroundings of small openings according to the requirements specified in Section 9.5.

Structural Performance Coefficient (Section 9.2)

9.2 Structural Performance Coefficient D_S

(1) The structural performance coefficient, D_S, shall be the maximum value which is defined in Table 9.2.1 for walls according to the component types.

Table 9.2.1 Structural Performance Coefficient

	in the case that only F_1 component is considered for the calculation of lateral load carrying capacity	in the case that F_1 and F_2 components are considered for the calculation of lateral load carrying capacity	in the case that F_1, F_2 and F_3 compomponents are considered for the calculation of lateral load carrying capacity
Ds	0.5	0.55	0.6

(2) The judgment whether F1, F2 or F3 is selected may be performed according to the conditions in Table 9.2.2 a) and b) in which the conditions are stipulated for walls, wall girders and foundation beams.

Table 9.2.2 a) Component Types of Bearing Walls

Conditions \ Component Type	F1	F2	F3
Failure Mode	Flexural Failure*		other conditions
Upper Limit of $\bar{\tau}u/Fm$	0.07	0.10	
Upper Limit of $\bar{\sigma}oe/Fm$	0.2	0.25	

Table 9.2.2 b) Component Types of Wall Girders and Foundation Beams

Components	Conditions \ Component Type	F1	F2	F3
Wall Girders	Failure Mode	Flexural Failure*		other conditions
	Upper Limit of $\bar{\tau}u/Fm$	0.07	--	
Foundation Beams	Failure Mode	Flexural Failure*		other conditions
	Upper Limit of $\tau u/Fm$	0.15	0.20	

* The flexural failure implies that the ratio of the shear capacity to the shear at mechanism is greater than 1.1 for walls and 1.0 for wall girders and foundation beams, respectively. Furthermore, the ratio of the shear capacity to the shear at mechanism should satisfy the requirements of Section 9.5.

$\bar{\tau}u$: average shear stress at mechanism (kg/cm^2)

$$\bar{\tau}u = Qmu / Ae \qquad (9.2.1)$$

where,

Qmu : shear at mechanism (kg)

Ae : sectional area of wall or wall girder in which the sectional area of slab and transverse wall within the effective range specified in Section 9.4 may be included. (cm^2)

$\bar{\sigma}oe$: average axial stress of bearing wall at mechanism (kg/cm^2)

$$\bar{\sigma}oe = (Nm + Nw) / Ae \quad (9.2.2)$$

where,

Nm : axial force at mechanism (kg)

Nw : axial force from transverse wall which affects the strength of the bearing wall and is same as the value of Section 9.4.1

Ae : sectional area of bearing wall in which the sectional area of transverse wall within the effective range may be included

Fm : specified compressive strength of RM assemblage

τu : shear stress of foundation beam at mechanism (kg/cm^2)

$$\tau u = Qmu / (b \cdot j) \quad (9.2.3)$$

where,

Qmu : shear of foundation beam at mechanism (kg)

b : width of the foundation (cm)

j : distance between the centroids of compressive and tensile force at the section (cm)

(3) In the case that yield hinges occur at wall girders which are connected to a bearing wall at top and bottom, the lowest level of component type among the component types of wall girders shall be selected for the bearing wall.

(1) Structural Performance Coefficient

From the response analysis of the building designed by these guidelines, the response of story drift angle was less than 1/200 under the 50 kine input of Hachinohe 1968NS, Taft 1952EW and El Centro 1940NS. Furthermore, the component test indicates that the bearing wall with medium amount of shear reinforcement and low level axial index ($\bar{\sigma}o/Fcm$) has deformability of more than 1/130 story drift angle (Fig. 5). In case of wall girder it was more than 1/100 (Fig. 6). Therefore, the coefficient of structural performance is decided to be 0.5 for the structure with ductile members, 0.6 for the structure including brittle members and 0.55 for the middle. The reason that the simple summation is allowed for the structure with various component types is such that the yielding deformation at maximum load was almost 1/400 for most of the tested members.

(2) Component Type

The component type may be classified by the factors: the deformability such as failure mode, axial force index ($\bar{\sigma}oe/Fm$), shear-span-ratio (M/QD), level of shear stress, amount of shear reinforcement, etc., which affect the deformability. For the classification of component type, the factor of failire mode is stressed first, because the earthquake response of this kind of structure is rather small and the structure has the deformability of 1/200 to 1/100 in story drift angle if the failure mode is flexural. However, it seems to be difficult to give enough deformability to the structure under high axial and/or shear stress. Hence the limitation for them was provided.

For the bearing walls the relation between the limit of deformation angle, which is defined when the load is decreased 20% after maximum load, and shear stress index ($\bar{\tau}u/Fm$) is shown in Fig. 7. The deformation angle more than 7.5×10^{-3} rad. is expected when the $\bar{\tau}_u/Fm$ is less than 0.07. For the wall girdirs the relation is shown in Fig. 8. The deformation angle more than 10×10^{-3} rad. is expected when $\bar{\tau}_u/Fm$ is also less than 0.07.

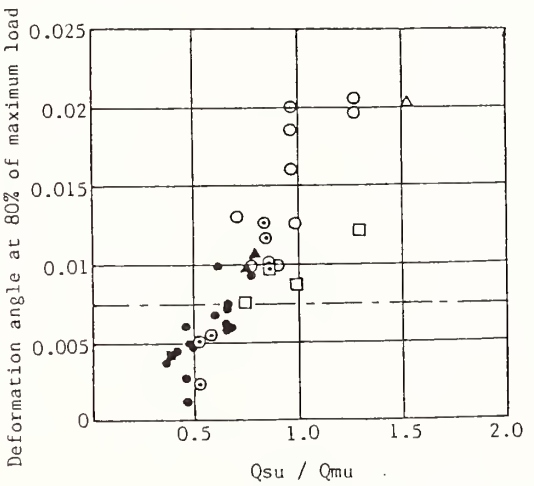

Fig. 5 Deformabiliy of Bearing Wall

Symbols:
- ○ flexural failure, concrete unit
- ⊙ shear failure after flexural yield, concrete unit
- ● shear failure, concrete unit
- □ flexural failure, clay unit
- ⊡ shear failure after flexural failure, clay unit
- ■ shear failure, clay unit
- △ flexural failure, with transverse component
- ▲ shear failure after flexural failure, with transverse component
- ▲ shear failure, with transverse component

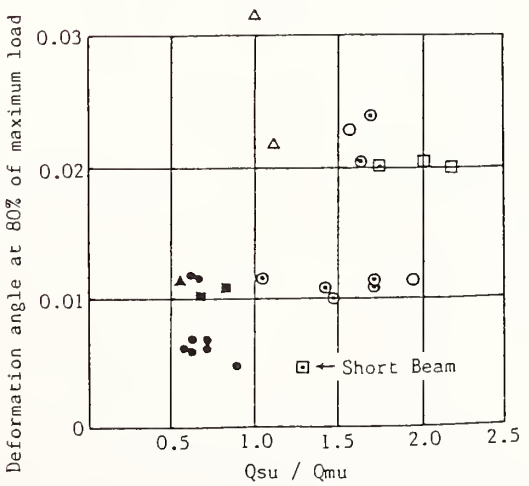

Fig. 6 Deformability of Wall Girder

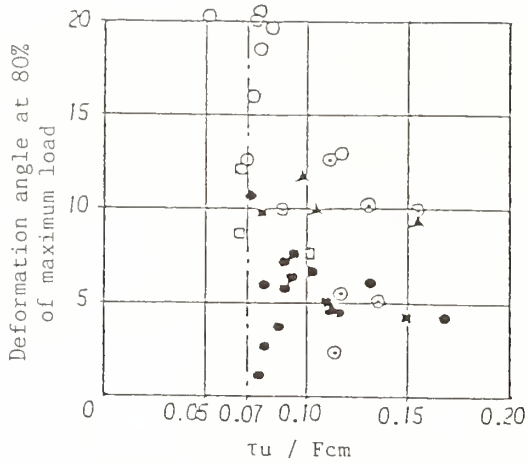

Fig. 7 Shear Stress and Deformability of Bearing Wall

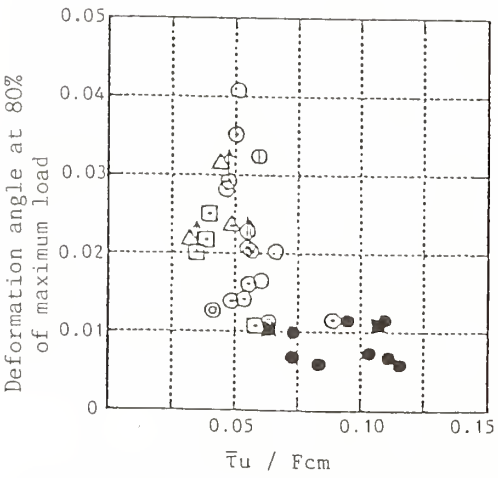

Fig. 8 Shear Stress and Deformability of Wall Girder

Calculation Method for Lateral Load Carrying Capacity (Section 9.3)

9.3 Calculation Method for Lateral Load Carrying Capacity

(1) Accurate calculation method such as incremental load applying analysis or simplified method based on virtual work principal shall be used for the calculation of lateral load carrying capacity.

Though the incremental load applying analysis or the limit analysis is desired for the calculation of the lateral load carrying capacity, the simplified method based on virtual work principal assuming the yielding at the ends of wall girders may be used because adequate accuracy may be obtained for the structures in which the strengths of walls are bigger than those of wall girders. The moment distribution method is not suitable for this kind of structures.

The moment and shear force for each component calculated by the above mentioned method may be used as the moment and shear at mechanism. However, for wide walls the forces calculated by the simplified method are sometimes different from those by the accurate method. The increase of design shear forces for the wide walls is reccommended if the simplified method is used for the calculation.

Ultimate Strength of Components (Section 9.4)

9.4.1 Bearing Wall

(1) The Eq. 9.4.1 shall be used for the flexural strength of bearing walls.

$$Mu = \Sigma(at \cdot \sigma y)\, lw + 0.5\,\Sigma(aw \cdot \sigma wy)\, lw + 0.5 \cdot Nm \cdot lw + Nw \cdot e \quad (kg \cdot cm) \quad (9.4.1)$$

where, Mu = 0 when it is negative,

at : sectional area of flexural reinforcement in which the vertical reinforcement sectional area of transverse wall within the effective range may be included (cm^2)

σy : material strength of flexural reinforcement specified in Section 3.3 (kg/cm^2)

lw : 0.9 times the total length of the bearing wall (cm)

aw : sectional area of vertical reinforcements at the center part of the bearing wall in which the reinforcement sectional area of transverse wall within the effective range may be included (cm^2)

σwy : material strength of the above mentioned reinforcement specified in Section 3.3 (kg/cm^2)

Nm : axial force of the bearing wall at mechanism (kg)

Nw : axial force from the transverse wall which affects the strength of bearing wall

In the case of the wall as shown in Fig. 9.4.1 the calculation shall be as follows.

i) $Nw = 0.25\, N_1$ for the bearing wall W1

ii) $Nw = 0.25(N_1 + N_2)$ for the bearing wall W2

iii) $Nw = 0.25\, N_2$ for the bearing wall W3

N1 and N2 are the long term load (kg) of the transverse walls.

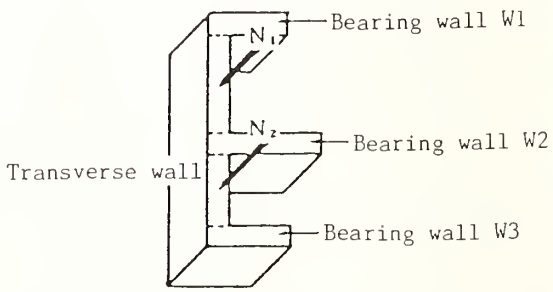

Fig. 9.4.1 Axial Force of Transverse Wall

e : the distance (cm) between the compression extreme fiber of the bearing wall and the center line of the transverse wall (Fig. 9.4.2)

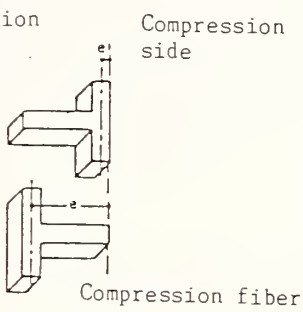

Fig. 9.4.2 Distance Between Compression Extreme Fiber and Centroid of Transverse Wall

(2) The Eq. 9.4.2 shall be used for the shear strength of bearing walls.

$$Qsu = \left\{ \frac{0.053 pte^{0.23} (Fm + 180)}{M/(Q \cdot l) + 0.12} + 2.7\sqrt{pwe \cdot \sigma wy} + 0.1\,\bar{\sigma}oe \right\} te \cdot j \cdot r \quad (kg) \quad (9.4.2)$$

where,

te : equivalent thickness when total sectional area Aw including the the sectional area of transverse wall within effective range is replaced by the rectangular section with the total length l (cm)
This shall be less than 1.5 times the thinkness of the bearing wall.

pte : equivalent flexural reinforcement ratio (=100 Σ at / (te · lw)) (%)

at : sectional area of flexural reinforcement in which the sectional area of transverse walls within the effective range may be included (cm^2)

Fm : specified compressive strength of RM assemblage (kg/cm^2)

l : total length of the bearing wall (cm)

lw : 0.9 times the total length of the bearing wall (cm)

pwe: equivalent shear reinforcement ratio (= a_w/(te · s))
The "a_w" is sectional area of one pair of shear reinforcement and the "s" is the space of it. When this value is more than 0.012t/te it shall be 0.012t/te.

σwy: material strength of shear reinforcement of bearing wall (≦3000 kg/cm^2)

j : (8/7) lw (cm)

r : reduction factor of shear capacity due to small openings, which value shall be the smaller value of

$$1-lo/l \text{ and } 1-\sqrt{\frac{ho\ lo}{h\ l}}$$

h : vertical distance between the main lateral supports in the bearing wall (cm)

ho : height of small opening (cm)

lo : width of small opening (cm)

σoe : ΣN/ ΣAw
ΣN= Nm +Nw

Nm : same value to that in Eq. 9.4.1

Nw : same value to that in Eq. 9.4.1

Aw : total sectional area of bearing walls including transverse walls within the effective range (cm)

M/(Q·ℓ): shear span ratio at mechanism which shall be 1 and 3 when it is less than 1 and more than 3, respectively
M and Q are the bending moment and shear force of the section at mechanism.

(1) Formulae for flexural strength

Figure 9 shows the relationship between the experimentally obtained shear stress at maximum load, ${}_t\tau max = Qmax/t \cdot l$, and shear stress calculated by Eq. 9.4.1, ${}_c\bar{\tau}mu = \Sigma cMu/t \cdot l$, whose data were obtained from 12 specimens, which were failed in flexure, among 57 specimens in total. The test data are almost same as the calculated value by the equation. In this case the results of material test were used for the yield strength of reinforcement. In these guidelines the equation by which the average strength can be calculated is adopted, because the design of each component against shear failure becomes critical if the equation which gives lowest value is used.

(2) Effect of transverse wall on flexural strength

The test results of bearing walls with transeverse walls show that all vertical reinforcement in transverse walls yielded when the deformation angle was 1/200 to 1/100. The full-scale five story test showed that total sectional area was effective at final stage. Since the target of the deformation angle in these guidelines, however, is a little smaller, 1/400 to 1/300, than 1/200 to 1/100, the effective range is limitted in the requirement.

(3) Shear strength

Figure 10 shows the relationship between the experimentally obtained shear stress at maximum load, ${}_t\tau max = Qmax/t \cdot l$, and shear stress calculated by Eq. 9.4.2, ${}_c\bar{\tau}su = cQu/t \cdot l$, whose data were obtained from 45 specimens, which were failed in shear or failed in shear after flexural yield, among 57 specimens in total. All data are plotted above the diagonal line. The equation seems to give the lowest limit. The material test results are used for the calculation above.

(4) Effect of transverse wall on shear strength

There are 3 specimens with transverse walls. The wall with transverse walls at the center failed in shear after flexural yield and the wall

with transverse walls at the ends failed in shear. The ratio of the strength of the wall with transverse walls to that without transverse walls is 1.43 in average and the ratio of the strength with transverse walls to that without transverse walls calculated by Eq. 9.4.2, in which te is assumed to be 1.5, is 1.36 in average.

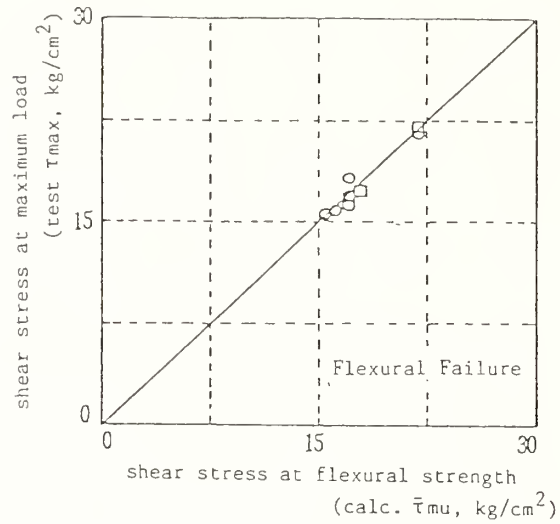

Fig. 9 Shear Stress at Maximum Load versus Shear Stress at Flexural Strength

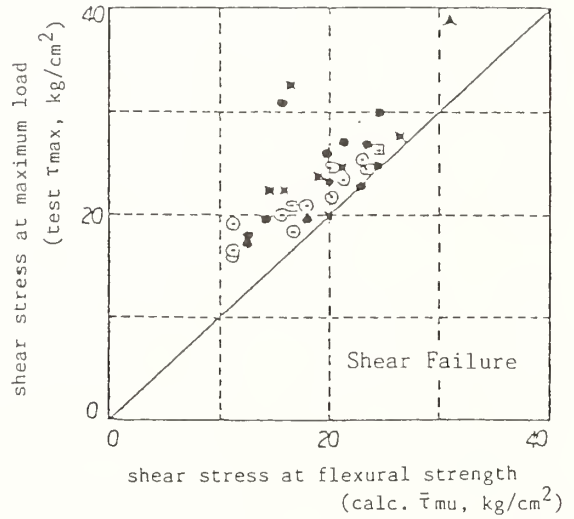

Fig. 10 Shear Stress at Maximum Load versus Shear Stress at Shear Strength

9.4.2 Wall Girders and Foundation Beams

(1) The Eq. 9.4.1 shall be used for the flexural capacity of wall girders.

$$Mu = 0.9 \cdot \Sigma(at \cdot \sigma y \cdot d) \quad (kg \cdot cm) \quad (9.4.3)$$

where,

at : sectional area of flexural reinforcement in which the sectional area of the slabs within the effective range shall be included (cm^2)

σy : material strength of the flexural reinforcement specified in Section 3.3 (kg/cm^2)

d : effective depth of the wall girder (refer to Section 7.3.2) (cm)

(2) The Eq. 9.4.4 shall be used for the shear strength of the wall girders.

$$Qsu = 0.9\left\{\frac{0.053\, pte^{0.23}\,(Fm+180)}{M/(Q \cdot d) + 0.12} + 2.7\sqrt{pwe \cdot \sigma wy}\right\} be \cdot j \quad (kg) \quad (9.4.4)$$

where,

be : equivalent width of the wall girder when total sectional area of the wall girder including the sectinal area of the slab within the effective range ΣAg is replaced to the rectangular section with depth D (cm) This value shall be less than 1.5 times the width b of the wall gider.

$$be = \Sigma Ag / D, \quad be \leqq 1.5\, b$$

pte : equivalent flexural reinforcement ratio
$(= 100\Sigma at / (be \cdot d))$ (%)

at : sectional area of flexural reinforcement in which the sectional area of slab reinforcement within the effective range may be included (cm^2)

Fm : specified compressive strength of RM assemblage (kg/cm^2)

D : depth of the wall girder (cm)

pwe : equivalent shear reinforcement ratio $(= a_w/(be \cdot s))$
The "a_w" is the sectional area of a pair of shear reinforcement and the "s" is the space of it. When this value is more than 0.012 b/be, it shall be 0.012 b/be.

σwy : yield point of shear reinforcement of the wall girder ($\leqq$ 3,000 kg/cm^2)

M/(Q·d): shear span ratio at mechanism which shall be 1 and 3 when the value is less than 1 and more than 3, respectively
M and Q are bending moment and shear force of the section at mechanism.

j : (7/8)d may be used.

(3) The flexural strength of the foundation beam may be calculated by Eq. 9.4.3. The shear strength of the foundation beam may be calculated by Eq. 9.4.4 in which the reduction factor 0.9 in the equation may be changed to 1.0.

(1) Flexural strength and shear strength of wall girder

Equations 9.4.3 and 9.4.4 were examined using the test results of 33 specimens in total.

The comparison of the test results and the calculated values by Eq. 9.4.3 is shown in Fig. 11. The specimens, plotted under the diagonal

line which shows the ratio of test results to calculated value is 1.0, were failed in shear. For the specimens failed in flexurure, the ratio is 1.2 to 1.5.

The comparison of the test results and the calculated values by Eq. 9.4.4 is shown in Fig. 12. The specimens, plotted under the diagonal line were failed in flexurure. For the specimens failed in shear, the ratio is 1.1 to 1.5. Equation 9.4.4 seems to be coservative. The failure modes are clearly divided by the diagonal line as shown in Fig. 13.

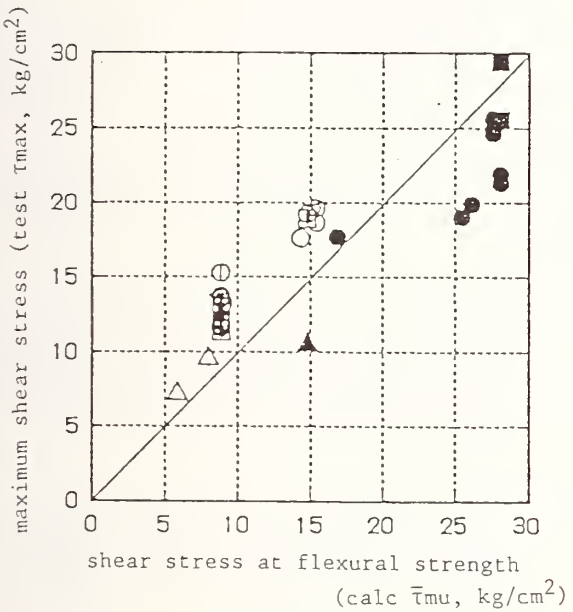

Fig. 11 Maximum Strength versus Flexural Strength of Wall Girder

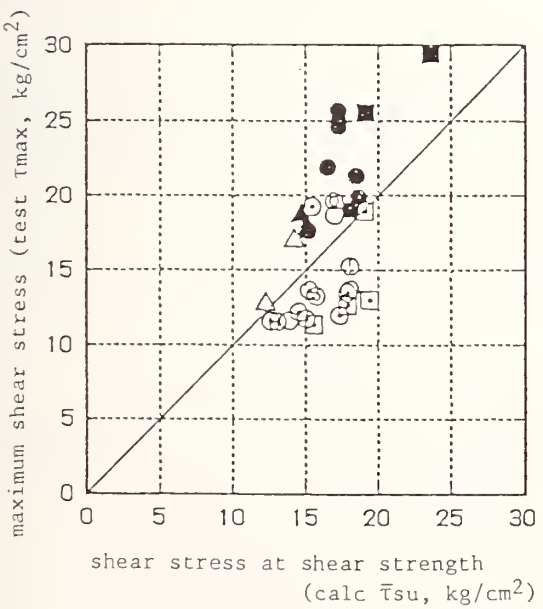

Fig. 12 Maximum Strength versus Shear Strength of Wall Girder

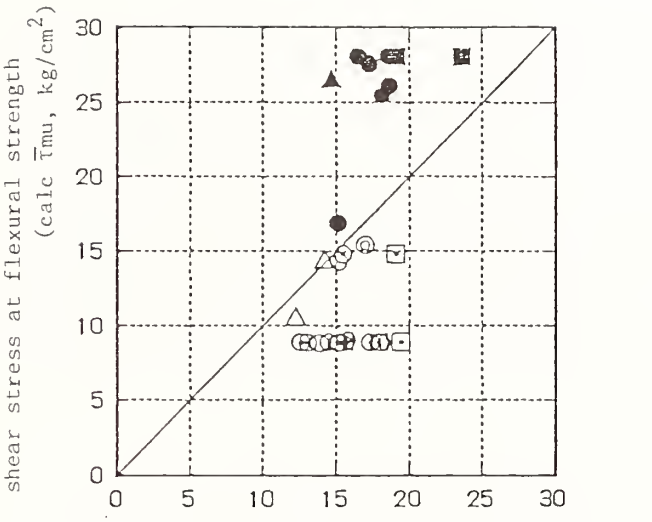

Fig. 13 Flexural Strength versus Shear Strength of Wall Girder

Ductility Design of Components (Section 9.5)

9.5.1 Walls

(1) For the component type F1 and F2 of bearing walls, the ratio of the shear strength and the shear force at mechanism shall be larger than the value in Table 9.5.1.

Table 9.5.1 Lowest Limit of Qsu/Qmu for Bearing Walls

$\bar{\sigma}oe$ / Fm	F1	F2
≤ 0.10	1.20	1.10
0.10<, ≦0.15	1.25	1.10
0.15<, ≦0.20	1.30	1.15
0.20<, ≦0.25	--	1.20

(2) Adequate confining reinforcement which resists the crash of concrete shall be provided at both ends of the bearing wall where yield hinge is expected at mechanism. However, the bearing wall of which $\bar{\sigma}oe/Fm$ is less than 0.1 and wall width is less than 2.5m, or the bearing wall with transverse walls is exepted.

(1) The ratio Qsu/Qmu required for bearing walls

In order to assure the flexural yield failure, the shear strength Qsu is neccesarily greater than the shear force at mechanism. The flexural strength does not decrease so much under repeating load, but this shear strength decreases under repeating load in plastic range especially under high axial force. If the value σ_{oe}/F_m is greater than 0.25 in Table 9.5.1, this bearing wall may be the component of F3 in which the ductility is not expected. For the bearing wall with transverse walls, the ductility may be

expected and the values in Table 9.5.1 may be decreased by 0.1, because the strength of the wall with transverse walls is a little greater than the calculated one and the decrease of shear strength is small under repeating load when the transverse walls exist at both ends of the bearing wall.

(2) Reinforcing at the ends of the bearing wall against crash in compression

High ductility is required at the bottom of the first story bearing wall. Since the ductility of flexure largely depends on the limit of compressive strain of concrete, confinement is needed in order to protect crash after maximum stress.

9.5.2 Wall Girders and Foundation Beams

(1) The shear strength of the wall girders and foundation beams of which component type is F1 shall satisfy Eq.9.5.1.

$$Qsu \geq QL + n \cdot Qmu \qquad (9.5.1)$$

where,

Qsu: shear strength of the wall girder and foundation beam specified in Section 9.4.2 (kg),

QL : shear force under long term load (kg),

Qmu : shear force at mechanism (kg)

n : coefficient multiplied to shear force to ensure the ductility, which shall be larger than 1.1.

9.5.3 Reinforcement of Small Openings of Bearing Walls

(1) In case that a small opening regulated in the term (2) of Section 5.2 exists in the bearing wall, additional diagonal reinforcement and ridge reinforcement required by Eq. 9.5.2 shall be provided around the small opening.

(i) sectional area of additional diagonal reinforcement at corners of the small opening (cm^2)

$$a_{td} = \frac{ho + lo}{2\sqrt{2} \cdot l} \cdot \frac{Qmu}{\sigma y} \qquad (9.5.2\ a)$$

(ii) sectional area of additional vertical ridge reinforcement at corners of the opening (cm^2)

$$a_{tv} = \frac{ho}{2(l-lo)} \cdot \frac{Qmu}{\sigma y} \qquad (9.5.2\ b)$$

(iii) sectional area of the additinal horizontal ridge reinforcement at the corners of the opening (cm^2)

$$a_{th} = \frac{lo}{2(h-ho)} \cdot \frac{h}{l} \cdot \frac{Qmu}{\sigma y} \qquad (9.5.2\ c)$$

where,

l : width of the bearing wall with small opening (cm)

h : vertical distance between main lateral supports of the bearing wall with small opening (cm)

lo : clear width of the small opening (cm)

ho : clear height of the small opening (cm)

Qmu: shear force of the bearing wall at mechanism to which the value specified in Table 9.5.1 shall be multiplied for the component type F1 and F2 members (kg)

σy : material strength of the additional diagonal and ridge reinforcement (kg/cm^2)

The Equation 9.5.2 is same as used in the AIJ R/C Code.

Around the very small openings, about 10cm diameter, no special reinforcement is needed in principle.

9.5.4 Bearing Wall-Wall Girder Joints

(1) The bearing wall-wall girder joints which come under terms (1)-(i) through (iii) of Section 7.8 shall de designed against the shear force applied to the joints at mechanism.

Application

(1) The shear force Qp in the bearing wall-wall girder joints at mechanism can be smaller one calculated by equations below;

$$Qp = Tb1+Tb2 - \frac{Q_{w1}+Q_{w2}}{2} \qquad (A\ 9.5.1)$$

$$Qp = \left(Tw1+Tw2 - \frac{Q_{b1}+Q_{b2}}{2}\right) \cdot \frac{lp}{Dp} \qquad (A\ 9.5.2)$$

where,

T_{bi} : yield force of tensile reinforcement at i-end of the wall girder($\Sigma at \cdot \sigma y$)

T_{wi} : yield force of tensile reinforcement at i-end of the bearing wall ($\Sigma at \cdot \sigma y$)

Q_{bi} : shear force at i-end of the wall girder

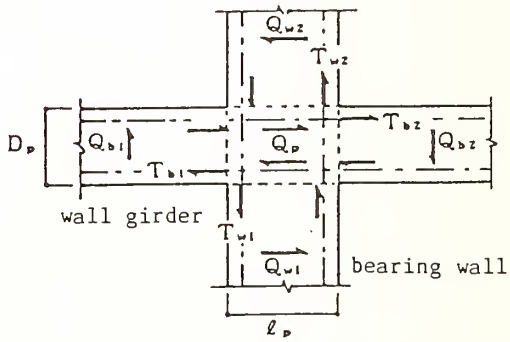

Fig. A 9.5.1 Stress at Bearing Wall-Wall Girder Joint

Q_{wi} : shear force at i-end of the bearing wall
lp : length of the bearing wall-wall girder joint
Dp : height of the bearing wall-wall girder joint
σy : material strength of flexural reinforcement

(2) The shear force used for the equations above may be obtained from the following way;
(i) the shear force at mechanism stipulated in Section 9.3,
(ii) the shear force of wall girders or bearing walls obtained in Chapter 6,
(iii)

$$\frac{Q_{w1}+Q_{w2}}{2} = 2\left(\frac{l_1}{l_{o1}} \cdot M_{b1} + \frac{l_2}{l_{o2}} \cdot M_{b2}\right) / (h_1+h_2) \qquad (A\ 9.5.3)$$

(iv)

$$\frac{Q_{b1}+Q_{b2}}{2} = 2\left(\frac{h_1}{h_{o1}} \cdot M_{w1} + \frac{h_2}{h_{o2}} \cdot M_{w2}\right) / (l_1+l_2) \qquad (A\ 9.5.4)$$

where,
M_{bi} : flexural strength at i-end of the wall girder at i-end
M_{wi} : flexural strength at i-end of the bearing wall, which may be $\Sigma(aw \cdot \sigma y)\, \ell w$
l_i : span length at the left and right
l_{oi} : clear span length at the left and right
h_i : height of the bearing wall
ho_i : clear height of the bearing wall

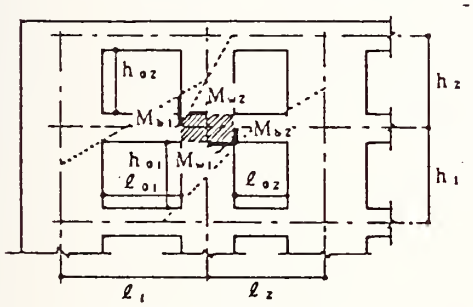

Fig. A 9.5.2 Notation for Design of Bearing Wall-Wall Girder Joint

(3) The strength of bearing wall-wall girder joints may be calculated by the following equation.

$$uQp = 0.15 \cdot Fm \cdot lp \cdot t \qquad (A\ 9.5.5)$$

where,
Fm : specified strength of the RM assemblage
lp : length of the bearing wall-wall girder joint
t : thickness of the bearing wall-wall girder joint

From the test result the average shear stress divided by prism strength $u\tau p = uQp/(l \cdot t)$ of bearing wall-wall girder joint at maximum load was 0.18 Fcm and 0.15 Fcm kg/cm.

CONCLUDING REMARKS

These design guidelines for medium rise RM buildings were completed March 1989 by TECCMAR/Japan based upon the composite experimental and analytical research which had been carried out since 1984.

These design guidelines are ready to be slightly revised this year. The major points to be revised are the specification on the wall width ratio and the minimum amount of reinforcement required in design method B. In a revised edition, the wall width ratio is expected not to be specified in main body of the design guidelines.

APPENDIX I - REFERENCES

[1] H. Hiraishi, T. Okada, S. Okamoto and Y. Yamazaki, "OUTLINE OF SEISMIC DESIGN GUIDELINES OF NEWLY DEVELOPED REINFORCED MASONRY BUILDINGS", The 2nd JTCCMAR, Keystone, 1986

[2] T. Okada, Y. Yamazaki, T. kaminosono and M. Teshigawara, "PHILOSOPHY OF STRUCTURAL DESIGN GUIDELINES FOR MEDIUM RISE RM BUILDINGS", The 4th JTCCMAR, San Diego, 1988

[3] Y. Yamazaki, T. Okada and S. Okamoto, "DESIGN GUIDELINES OF MEDIUM RISE RM BUILDINGS (1)", 5th JTCCMAR, Tsukuba, 1989

[4] T. Kubata and M. Teshigawara, "DESIGN GUIDELINES OF MEDIUM RISE RM BUILDINGS (2)" 5th JTCCMAR, Tsukuba, 1989

[5] A. Matsumura, "DESIGN GUIDELINES OF MEDIUM RISE RM BUILDINGS (3), 5th JTCCMAR, Tsukuba, 1989

APPENDIX II - CONTENTS OF DESIGN GUIDELINES OF MEDIUM RISE RM BUILDINGS

5.9 Cantilevered Members
5.10 Foundations and Foundation Beams
5.11 Bearing Wall-Wall Girder Joints
5.12 Others

6. Structural Calculation
 6.1 Design Loads and Their Combination
 6.2 Stress Analysis
 6.3 Story Drift Angle
 6.4 Stiffness Distribution
 6.5 Uplift of Foundation

7. Allowable Stress Design
 7.1 Moment and Shear Force for Design
 7.2 Bearing Walls
  7.2.1 Design Method
  7.2.2 Allowable Flexural Strength
  7.2.3 Allowable Shear Strength
  7.2.4 Arrangement of Reinforcement
 7.3 Wall Girders
  7.3.1 Design Method
  7.3.2 Allowable Flexural Strength
  7.3.3 Allowable Shear Strength
  7.3.4 Arrangement of Reinforcement
 7.4 Sub Beam
 7.5 Floor Slab
 7.6 Cantilevered Members
 7.7 Foundation Beams
 7.8 Bearing Wall-Wall Girder Joints
 7.9 Projection from Roof Slab

8. Total Flexural Resisting Moment

9. Lateral Load Carrying Capacity
 9.1 Fundamental Concept
 9.2 Structural Performance Coefficient D_s
 9.3 Calculation of Lateral Load Carrying Capacity
 9.4 Ultimate Strength of Components
  9.4.1 Bearing Walls
  9.4.2 Wall Girders and Foundation Beams
 9.5 Ductility Design of Components
  9.5.1 Bearing Walls
  9.5.2 Wall Girders and Foundation Beams
  9.5.3 Reinforcement of Small Openings of Bearing Walls
  9.5.4 Bearing Wall-Wall Girder Joints

10. Foundation

11. Joint and Anchorage of Reinforcement, Covering Concrete Thickness and Arrangement of Reinforcement
 11.1 Joint of Reinforcement
 11.2 Anchorage of Reinforcement
 11.3 Covering Concrete Thickness
 11.4 Arrangement of Reinforcemt
  11.4.1 Bearing Walls
  11.4.2 Wall Girders
  11.4.3 Bearing Wall-Wall Girder Joints
  11.4.4 Joint Reinforcements

U.S.-Japan Cooperative Research Program on Hybrid Control of Seismic Response of Bridge Structures

by

Jiro TAGUCHI[1], Toshio IWASAKI[2], Yoshio ADACHI[3], Yasushi SASAKI[4] and Kazuhiko KAWASHIMA[5]

ABSTRACT

This paper presents current research activities on passive and active control for application to bridge structures conducted at the Public Works Research Institute. Japanese -side research program for U.S.-Japan Cooperative Research on Hybrid Control, which is defined as a combined approach of passive and active control of seismic response, of bridge structures is also presented.

1. INTRODUCTION

Base isolation is now being increasingly used in bridges in Japan for reducing the structural response. Base isolated bridge, which is supported by isolators and energy dissipators, causes less amount of structural response during an earthquake, and with use of base isolation it is expected to increase seismic safety of the bridge even during a significant earthquake.

On the other hand, active control which can control the structural response more effectively than the passive control is now being considered for application to seismic design of structures. It is expected to bring a significant improvement of seismic performance of structures including highway bridges. The main obstacle of the active control is the large amount of energy required to supply to the structure. Because of such obstacle, the active control is now being tried to apply for controlling the structural response against wind.

Combination of active and passive control, which is defined here as hybrid control, seems attractive for solving this obstacle. Appreciable amount of decrease of structural response by means of passive control will make the energy supply significantly small in the active control to achieve the control of structural response within a satisfactory level during a significant earthquake. Increase of lateral displacement of the deck induced by introducing the passive control may be improved by the active control.

This paper presents the current research activities conducted at the Public Works Research Institute, Ministry of Construction, on development of design method for base-isolated highway bridges and a fundamental study on the application of active control for reducing the seismic response of a highway bridge[1)2)3)4)]. Japanese-side program of the cooperative research program on hybrid control, which is now being initiated since April 1990 at the Public Works Research Institute, Ministry of Construction, is also presented.

2. CURRENT RESEARCH DEVELOPMENT FOR BASE ISOLATED HIGHWAY BRIDGES

2.1 Guideline for Design of Base-Isolated Highway Bridges (Draft)

For studying an application of base isolation to seismic design of highway bridges, a committee chaired by Professor Tsuneo KATAYAMA, University of Tokyo, was formulated through 1986 to 1989 at the Technology Research Center for National Land Development. Three programs were studied in the committee, i.e., 1) survey for isolators and energy dissipators which can be used for highway bridge, 2) study on key points in design of base-isolated highway bridges, and 3) design of base-isolated highway bridges. As a final outcome of the study at the committee, "Guideline for Design of Base-Isolated Highway Bridges (draft) " was published in March 1989[5)].

The draft guideline includes the following contents:

---

1) Former Director General
2) Director General
3) Director,Planning and Research Administration Department
4) Director, Earthquake Disaster Prevention Department
5) Head, Earthquake Engineering Division, Earthquake Disaster Prevention Department, Public Works Research Institute, Ministry of Construction

4.2.4 Evaluation of Sectional Force and Displacement due to Inertia Force
4.3 Check of Bearing Capacity for Lateral Force
4.3.1 General
4.3.2 Seismic Coefficient Used for Check of Bearing Capacity for Lateral Force
4.3.3 Evaluation of Natural Period
4.3.4 Evaluation of Damping Ratio
4.3.5 Evaluation of Sectional Force and Displacement due to Inertia Force
4.3.6 Equivalent Seismic Coefficient Used for Check of Bearing Capacity for Lateral Force
4.3.7 Bearing Capacity for Lateral Force
Chapter 5 Dynamic Response Analysis
5.1 Method of Dynamic Response Analysis
5.2 Modelling of Base-Isolated Bridge for Dynamic Response Analysis
5.3 Input Motion for Dynamic Response Analysis
5.3.1 Input Motion for Check of Design by Means of Seismic Coefficient Method
5.3.2 Input Motion for Check of Bearing Capacity for Lateral Force
5.4 Investigation of Safety
Chapter 6 General Provision for Design of Structural Details
6.1 General
6.2 Distance between Structures
6.3 Design Gap of Expansion Joint
6.4 Devices for Preventing Falling-off of Superstructure from Substructure
6.5 General Provision for Design Details of Base Isolation Device
Appendix
I Design of Base-Isolated Highway Bridges
II Design Method of Base Isolation Device
III Example of Design Calculation of Base-Isolated Highway Bridge (in the Case of Ground Condition of Group I)
IV Example of Design Calculation of Base-Isolated Highway Bridge (in the Case of Ground Condition of Group II)
V Example of Structural Details
VI Example of Various Base-Isolation Device

2.2 Joint Research between PWRI and Private Firms on Development of Base Isolation System for Highway Bridge

Based on the study made for proposing "Guideline for Design of Base-Isolated Highway Bridges", for aiming to develop a further practical design method of base-isolated highway bridges superior from both seismic safety and construction cost point of view, a joint research program between PWRI and 29 private firms on "Development of Base-Isolation Systems for Highway Bridges" was initiated since 1989. The research is scheduled to continue for three years until 1992.

Scopes of the joint research contain the following research/development programs :

1) Development of isolator and energy dissipator suitable for highway bridge with utilizing new materials and technologies
2) Development of expansion joint and falling-off prevention device suitable for base-isolated bridge
3) Development of design method for base-isolated bridge
4) Application of base-isolation for highway bridge

In the project 1), it is aimed to develop less expensive isolator and energy dissipator which are superior for long-term use as well as function. In the project 4), application of base isolation for super-long multiple-continuous highway bridge with total length over 1 km and for seismic retrofitting of vulnerable existing highway bridges is being investigated.

The 29 private firms joined in the joint research program consist of material makers such as rubber and automobile tire makers, bearing supports fabricators, consulting engineering firms, steel superstructure fabricating companies, and general constructors.

Table-1 shows the research subjects and contributions.

2.3 Construction of Base-Isolated Highway Bridges

Seven base-isolated highway bridges as shown in Table-2 are currently being constructed by the support of the Ministry of Construction for the purpose of incorporating the base isolation design into the practical use. After completion of the construction, a series of tests including a push-pull test, forced excitation test with use of an eccentric-mass shaker and strong motion observation is scheduled to be made for studying the dynamic characteristics of the bridges.

Among the seven bridges presented in the Table-2, the design has been already completed for Nagaki-gawa Bridge, Maruki Bridge, Karasuyama No.1 Bridge and Miyakawa Bridge, and construction of the substructures is now under way.

3. A FUNDAMENTAL RESEARCH ON APPLICATION OF ACTIVE CONTROL TO HIGHWAY BRIDGE

3.1 Seismic Response Control by Means of Active Mass System

To study an application of active control for reducing seismic response of bridge, a simple analysis idealizing the bridge by a one degree of freedom system incorporating an active mass on the deck was made[6]. Fig.1 shows an analytical model with an active mass.

Equations of motion of the bridge with the active mass system can be written as

$$\begin{bmatrix} m_s & 0 \\ 0 & m_d \end{bmatrix} \begin{Bmatrix} \ddot{x}_s \\ \ddot{x}_d \end{Bmatrix} + \begin{bmatrix} c_s & 0 \\ 0 & 0 \end{bmatrix} \begin{Bmatrix} \dot{x}_s \\ \dot{x}_d \end{Bmatrix} + \begin{bmatrix} k_s + k_d & -k_d \\ -k_d & k_d \end{bmatrix} \begin{Bmatrix} x_s \\ x_d \end{Bmatrix} = \begin{Bmatrix} f_s \\ f_d \end{Bmatrix} + \begin{Bmatrix} -u \\ u \end{Bmatrix} \quad (1)$$

where,

m_s, c_s, k_s : mass, damping coefficient and stiffness of the bridge

x_s, $\dot{x}_s$, $\ddot{x}_s$: relative displacement, velocity and acceleration of the bridge

f_s : external force applied to the bridge

m_d, k_d : mass and stiffness of the active mass system

x_d, $\dot{x}_d$, $\ddot{x}_d$: displacement, velocity and acceleration of active mass relative to the bridge

f_d : external force applied to the active mass

u : control force of active mass system

The control force is assumed to be determined by a linear combination of displacement and velocity of the bridge and the active mass as

$$u = \{G_s^{\circ} \; G_d^{\circ}\} \begin{Bmatrix} \dot{x}_s \\ \dot{x}_d \end{Bmatrix} + \{G_s^{K} \; G_d^{K}\} \begin{Bmatrix} x_s \\ x_d \end{Bmatrix} \quad (2)$$

in which, G_s° and G_d° represent control gain vector of velocity and displacement of the bridge, respectively, and G_s^{K} and G_d^{K} represent control gain vector of those of the active mass, respectively. Substituting Eq.(2) into Eq.(1), one can obtain the equations of motion of the total system as

$$\dot{\underline{X}} = \underline{A}\,\underline{X} + \underline{B}\,u + \underline{D} \quad (3)$$

where

$$\underline{X} = \{x_s \; x_d \; \dot{x}_s \; \dot{x}_d\}^T$$

$$\underline{A} = \begin{bmatrix} -\underline{M}^{-1}\underline{C} & -\underline{M}^{-1}\underline{K} \\ \underline{I} & \underline{O} \end{bmatrix}$$

$$\underline{B} = \{-m_s^{-1} \quad m_d^{-1} \quad 0 \quad 0\}^T$$

$$\underline{D} = \{-m_s^{-1} f_s \quad m_d^{-1} f_d \quad 0 \quad 0\}^T$$

$$\underline{M} = \begin{bmatrix} m_s & 0 \\ 0 & m_d \end{bmatrix}$$

$$\underline{C} = \begin{bmatrix} C_s & 0 \\ 0 & 0 \end{bmatrix}$$

$$\underline{K} = \begin{bmatrix} k_s + k_d & -k_d \\ -k_d & k_d \end{bmatrix}$$

I : unit matrix

Introducing state variables X, the control force by Eq. (2) can be rewritten as

$$u = \underline{G}\,\underline{X} \quad (4)$$

in which

$$\underline{G} = \{G_s^{\circ}, \; G_d^{\circ}, \; G_s^{K}, \; G_d^{K}\}$$

It is an important role to determine appropriate control gain vector G in order to adequately control structural response using active mass system. Various methods to determine control gains has been studied and proposed in the literature. In this study, the following two control methods are considered.

1) Optimal Feedback Control Method

In the optimal feedback control method, control gains have to be determined so that the objective function J be minimized base on an optimal control theory.

$$J = \frac{1}{2} \int_0^{\infty} (\underline{X}^T \underline{Q}\,\underline{X} + R\,u^2)\, dt \quad (5)$$

in which matrix Q and R denote weighting factors on state variables and control force, respectively.

Control gain vector G can be obtained by matrix P which satisfies Algebraic Riccati Equation as

$$\underline{A}^T\underline{P} + \underline{P}\,\underline{A} + \underline{P}\,\underline{B}\,R^{-1}\underline{B}^T\underline{P} - \underline{Q} = \underline{0} \quad (6)$$

$$\underline{G} = R^{-1}\underline{B}^T\underline{P} \quad (7)$$

2) Modal Control Method

Modal control method gives a control force as a linear combination of modal responses, which are generally called as generalized coordinate. The control force can be obtained as

$$u = \sum_{j=1} \underline{k}_j \, \underline{r}_j \quad (8)$$

in which K_j and r_j represent control constants and j-th generalized coordinate, respectively.

Control constants are determined using a method developed by Porter et.al as

$$k_j = \frac{\prod_{i=1}^{m} (\rho_i - \lambda_j)}{\phi_j \prod_{i \neq j}^{m} (\lambda_i - \lambda_j)} \quad (9)$$

in which

λ_j : complex eigenvalue of j-th mode of uncontrolled system

ρ_j : complex eigenvalue to be assigned of j-th mode of controlled system

Ψ_j : j-th element of a vector obtained from complex modal vector, and matrices A and B

3.2 Bridge Analyzed and Analytical Conditions

Fig. 2 shows a bridge analyzed which is of three span continuous girder bridge with deck length of 90 m. Response in longitudinal direction is considered for the analysis. Fundamental natural frequency is evaluated as 0.99 Hz. Damping ratio inherent of the bridge is assumed as 0 for aiming to isolate the effect of

the active mass system.

Since the selection of the proper mass is one of the important design parameters in the active mass system, 3 cases with a mass ratio, which is defined as a ratio of the active mass to the mass of the superstructure (1,035 tf), of 1/10, 1/100 and 1/1000 are considered in the analysis. Spring coefficient k_d of the active mass system is assumed so that the natural frequency of the active mass system becomes 1/4 of the fundamental natural frequency of the bridge (0.99Hz).

Control gain vector is determined in the following ways:

1) Optimal Feedback Control Method

Weighting matrix Q is assumed to be as

$$\underline{Q} = \begin{bmatrix} Q_s^{v} & 0 & 0 & 0 \\ 0 & Q_d^{v} & 0 & 0 \\ 0 & 0 & Q_s^{d} & 0 \\ 0 & 0 & 0 & Q_d^{d} \end{bmatrix} \qquad (10)$$

in which, Q_s^{v} and Q_s^{d} denote weighting factors for relative displacement and velocity of the bridge, respectively, and Q_d^{v} and Q_d^{d} represent those of active mass. Because bending moment developed at the pier which is the most important parameter for seismic design of substructure is generally proportional to relative displacement of the bridge, the control force is assumed to be determined only by Qsd (i.e., $Q_s^{v}=Q_d^{v}=Q_d^{d}=0$) in this study. The weighting factor of control force R is fixed as 1.0, and three cases with Q_s^{d} of 10^{6}, 10^{8} and 10^{10} are considered. Table-3(a) shows the control gain vectors thus determined.

2) Modal Control Method

Control gain vector is determined so that damping ratio of the total system becomes 0.1, 0.2 and 0.3 without changing natural frequency of the bridge. Natural frequency of the bridge was not changed so that effect of the input ground motion on seismic response be the same with the analysis assuming the optimal feedback control. Table-3(b) shows the control gain vectors thus determined.

Two ground motion acceleration records obtained at ground surface near the Kaihoku Bridge during the Miyagi-ken-oki Earthquake (M 7.4) in 1978 (referred as Kaihoku Record) and on the Hatiro-Gata during the Nihonkai-chubu Earthquake (M 7.7) in 1983 (referred as Hachiro-gata Record) are used for the input motion. Peak acceleration of the two records was assumed as the same with the ones actually measured.

3.3 Effect of Active Mass System Assuming Optimal Feedback Control Method

Figs. 3 and 4 show the response displacement and acceleration of the bridge assuming the optimal feedback control method when subjected to the Kaihoku Record. The mass ratio m_d/m_s of 1/100, and weighting factor Q_s^{d} of 10^{6} and 10^{10} are assumed. According to these results, when Q_s^{d} is assumed as 10^{6}, sinusoidal response is seen in both displacement and acceleration, which implies that an apparent damping ratio of the system is quite small. Predominant frequency (0.99Hz) of the response corresponds to the natural frequency of the system consisted of the bridge and the active mass. Peak response displacement of the deck is 6.8cm.

On the other hand, when Q_s^{d} is taken as 10^{10} both displacement and acceleration responses become quite small as compared with the case assuming Q_s^{d} as 10^{6}. Acceleration response has a similar shape with the input ground acceleration. This implies that apparent damping ratio seems very large.

Effect of active control system is studied in terms of peak response. Fig.5 shows how peak response displacement and acceleration of the bridge vary in accordance with the weighting factor Q_s^{d} and the mass ratio m_d/m_s. Peak response displacement decreases monotonously in accordance with increase of Q_s^{d} for both Kaihoku and Hachiro-gata Records. However, peak response acceleration does not decrease monotonously, and has its peak at $Q_s^{d} = 10^{8}$ for the Kaihoku Record. It should be noted that in some cases the response acceleration does not decrease monotonously even if control gain vector increases. This is attributed to the stroke of the active mass, as will be discussed later.

Fig. 6 shows stroke of the active mass. For the Kaihoku Record with the control of $Q_s^{d} = 10^{10}$, peak control force becomes 199 tf which corresponds to 19% of the dead weight of the superstructure (1,035tf). The stroke of the active mass to get the peak control force of 199 tf significantly depends on the mass ratio m_d/m_s. When r_m = 1/1000 the peak stroke of the active mass becomes extremely large, i.e., 37.4 m. It is impossible to ensure such large stroke of $\pm$ 37.4 m in the bridge with the span length of 30m. On the other hand, when r_m = 1/10 the peak stroke of the active mass becomes 0.42 m, which may be in the range of a practical use. However, although the stroke of the active mass is within a tolerable range, the mass with 10% of the dead weight of the superstructure is excessive for a practical use. Therefore, it is quite important to design the system so that the mass and the stroke are in the tolerable range.

3.4 Effect of Active Mass Assuming Modal Control Method

Fig.7 shows peak response displacement and acceleration computed assuming the modal control method. Peak responses of the bridge decrease monotonously in accordance with increase of the damping ratio of the system h_s. This is quite natural because damping ratio of the system is assumed to increase by means of

the active mass system. Fig.8 shows the control force and the stroke of the active mass. As was the case of the optimal feedback control, the control force is not affected by the mass ratio, because it is compensated by the stroke of the active mass.

4. U.S.-JAPAN COOPERATIVE RESEARCH PROGRAM ON HYBRID CONTROL OF STRUCTURAL RESPONSE

Although the active control is an attractive approach, energy required to supply for controlling the seismic response of bridge structures within a desirable level is excessive. This obstacle seems quite difficult to solve with use of the the currently existing technology, in particular in Japan where occurrence of an earthquake with magnitude over 8 has to be taken into account in seismic design. Hence, it is considered difficult to apply active control system for controlling seismic response of bridges in near future.

Therefore, at this stage a combined approach of passive and active control, which is defined here as hybrid control, seems more superior for controlling seismic response of bridges.

The advantages of the hybrid control can be expected as

1) By introducing active control to a base-isolated bridge, deck response displacement, which sometimes becomes excessive for avoiding to use expansion joint with large gap, can be reduced. Thus, the hybrid control extends the applications of base isolation.

2) Control energy can be significantly reduced as compared with the energy required in active control.

3) Dependence on active control can be decreased, which, in turn, decreases inconvenience caused by miss-working or malfunction of the control system.

Base on such considerations, the hybrid control seems more superior than the active control for aiming to reduce structural response of bridges during a significant earthquake. Therefore, a 5-year research program on hybrid control of seismic response was initiated in the Public Works Research Institute from April 1990. The objectives of this research program are to study an application of the hybrid control for bridge structures (reter to Fig.9) as

1) Control of super long-span continuous bridges
2) Control of bridges on relatively soft ground
3) Improvement of seismic performance of bridges on the important urban route

For such targets, the following research items are considered for study :

1) Development of passive control element suitable for hybrid control system
   - Development of variable damper
   - Development of damper with fail-safe function
2) Development of active control system suitable for hybrid control
3) Development of optimal hybrid control system by combining 1) and 2)

This research program is to be executed as a U.S.-Japan cooperative research program through the activities of the Panel on Wind and Seismic Effects of UJNR.

REFERENCES

1) Kawashima, K. : Development and Future Scope of Seismic Isolation of Structures - A Review -, Proc. of Japan Society of Civil Engineering, Structural Eng./Earthquake Eng., Vol.398/I-10, 1988

2) Kawashima, K. : Research Needs for Development of Seismic Design, Seismic Isolation and Active Control Technology, Proc. JSCE, Special Issue for Disaster Prevention, 1989

3) Kawashima, K. et al. : Shaking Table Test on Dynamic Response of Base-Isolated Bridges, Civil Engineering Journal, Vol. 30-10, 1988

4) Japan-New Zealand Workshop on Base Isolation of Highway Bridges, Head Office of Ministry of Works and Development, Wellington, New Zealand, 1987

5) Guideline for Design of Base-Isolated Highway Bridges, Final Report of A Committee for Study of Application of Base Isolation to Seismic Design of Highway Bridges (Chairman : Professor T. Katayama), Technology Research Center for National Land Development, March 1989

6) Kawashima, K., Hasegawa, K. and Yoshida, T. : Active Control of Seismic Response of Structure by Means of Mass Damper, Civil Engineering Journal, Vol. 31-5, 1989

Table 1 Research Theme and Organizations

Research Theme	P	Ka	Si	Ob	Ku	Tn	H	Ni	Su	M	G	Or	Ti	I	Nk	Ko	Ns	Ol	Y	To	Bs	Bb	Se	Sh	Pc	J	N	Chief	Sub-Chief
1. Development of Device for Isolation																												
1.1 High Energy Absorbing Rubber Bearing								○											○	○	○			○				
1.2 Friction Damper													○									○	○					
1.3 Steel Damper								○							○												Ol	Bs
1.4 Link Bearing Develop of																	○											
1.5 Viscous Damper																		○										
1.6 Test Method	○							○							○		○	◎	○	○	○	○	○	○				
2. Development of Expansion Joint and Falling-off Prevention Device for Isolated Bridge																												
2.1 Expansion Joint				○									○														Tc	—
2.2 Falling-off Prevention Device	○												○					○										
3. Development of Design Method for Isolated Bridge																												
3.1 Design Philosophy	○	○	○	○		○						○	◎					○							○	○	○	
3.2 Dynamic Responce Analysis Method	○		○		○	◎		○			○			○													Ka	Pc
3.3 Design Method of Device for Isolation	○						○	○				◎	○		○		○	○	○	○	○	○	○	○				
3.4 Simplified Design Method	○	○	◎		○	○					○	○																
3.5 Design Method of Expansion Joint and Falling-off Prevention Device	○			○			○								○			○							◎			
4. Application of Base Isolation to Bridge																												
4.1 Application to Prestressed Concrete Bridge	○	◎							○	○			○													○		
4.2 Application to Steel Bridge	○													○	○	○										◎	Ob	J
4.3 Application to Multiple Super-long Bridge	○			◎					○							○									○	○		
4.4 Application to Seismic Retrofit	○									○				○				○								◎		

P: Public Works Research Institute, Ka: Kajima, Si: Shimizu, Ob: Ohbayashi, Ku: Kumagai, Tn: Takenaka Doboku + Takenaka, H: Hazama, Ni: Nishimatsu, Su: Sumitomo, M: Mitsui, G: Goyoh, Ok: Okumura, Ti: Taisei + Tokyo Fablic + Nippon Chuzo, I: Ishikawajima Harima, Nk: NKK + Nippon Chuzo, Ko: Kobe Steel, Ns: Nippon Seiko, Oe: Oiles, Y: Yokohama Rubber, To: Toyo Rubber, Bs: Bridgestone, Bb: BBM, Se: Seibu Polymer, Sh: Showa Densen, Pc: Pacific Consultants, J: Japan Engineering Consultant, N: New Structural Engineering Consultants.

Table 2 Construction Project of Base-Isolated Highway Bridge

Owner	Bridge Name	Type of Superstructure	Length (m)
Hokkaido Developing Bureau	Onnetoh Bridge	Steel Girder	456
Tohoku-Regional Bureau, MOC	Nagaki-gawa Bridge	〃	97
Kantoh-Regional Bureau, MOC	Not Yet Selected	Not Yet Decided	Not yet Determined
Chubu-Regional Bureau, MOC	〃	〃	〃
Iwate-ken	Maruki Bridge	Prestressed Concrete	92
Tochigi-ken	Karasuyama Bridge	〃	250
Shizuoka-ken	Miyagawa Bridge	Steel Girder	110

Table 3 Control Gain

(a) Optimal Feedback Control

Case		Gain			
m_d/m_s	Q_s^d	G_g^c [N·s/m]	G_d^c [N·s/m]	G_s^k [N/m]	G_d^k [N/m]
$\frac{1}{10}$	10^6	160	-5.34	22	-26
	10^8	1,560	-52.2	2,100	-2,560
	10^{10}	9,630	-322	79,800	-97,300
$\frac{1}{100}$	10^6	160	-0.54	22	4
	10^8	1,570	-5.24	2,120	378
	10^{10}	9,640	-36.2	79,900	14,300
$\frac{1}{1000}$	10^6	161	-0.05	22	-1
	10^8	1,570	-0.53	2,120	-66
	10^{10}	9,640	-3.22	80,000	-2,480

(b) Modal Control

Case		Gain			
m_d/m_s	h_s	G_g^c [N·s/m]	G_d^c [N·s/m]	G_s^k [N/m]	G_d^k [N/m]
$\frac{1}{10}$	0.1	1,210	-40.5	402	763
	0.2	2,420	-48.5	804	750
	0.3	3,640	-56.6	1,210	653
$\frac{1}{100}$	0.1	1,210	-4.05	402	139
	0.2	2,420	-4.85	804	133
	0.3	3,630	-5.66	1,210	127
$\frac{1}{1000}$	0.1	1,210	-0.40	402	13.9
	0.2	2,420	-0.49	804	13.2
	0.3	3,620	-0.57	1,210	12.5

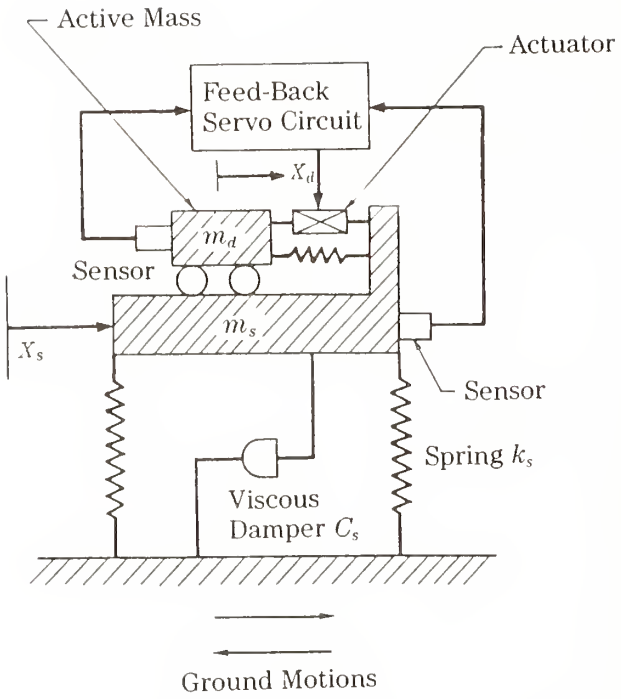

Fig.1 Analytical Model of One-Degree-of-Freedom System with Active Mass Damper

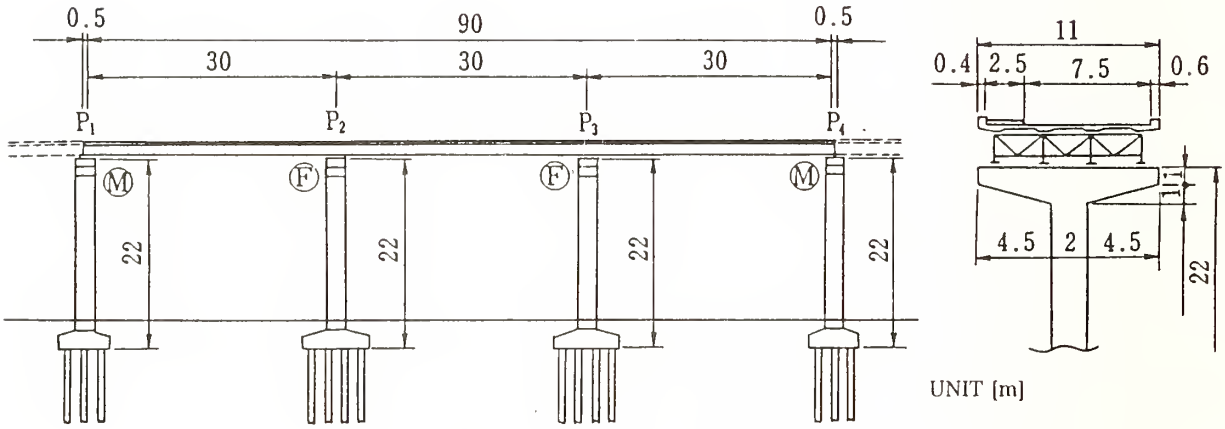

Fig.2 Highway Bridge Analyzed

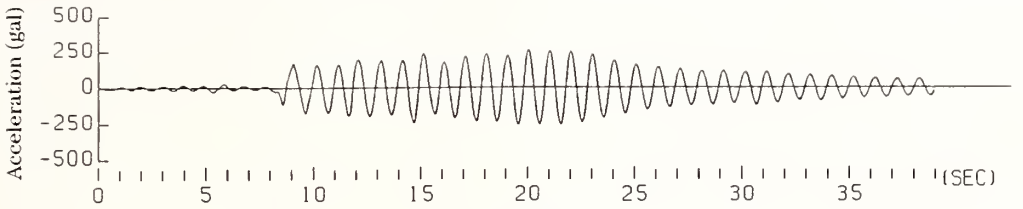

(a) Acceleration

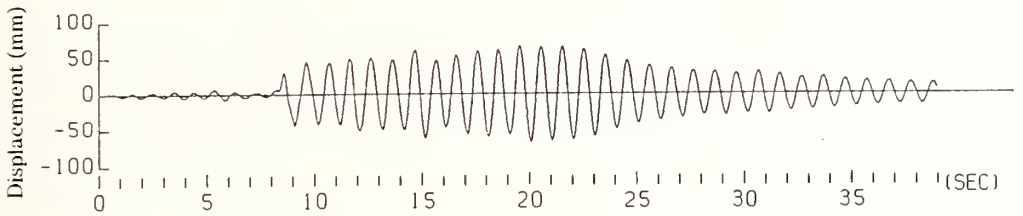

(b) Displacement

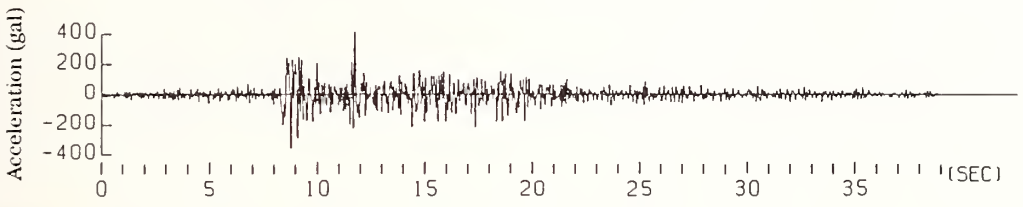

(c) Input Acceleration

Fig.3 Computed Response by Optimal Feedback Control with $Q_a{}^d = 10^5$ ($m_d/m_a = 1/100$)

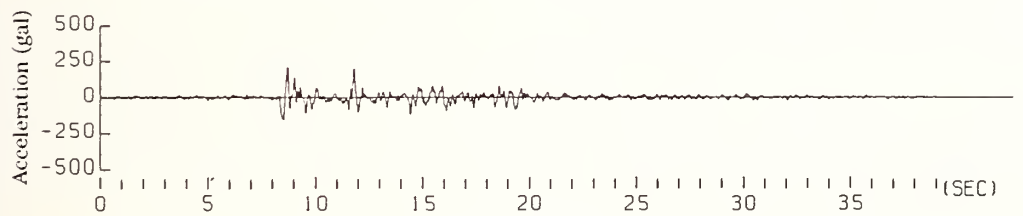

(a) Acceleration

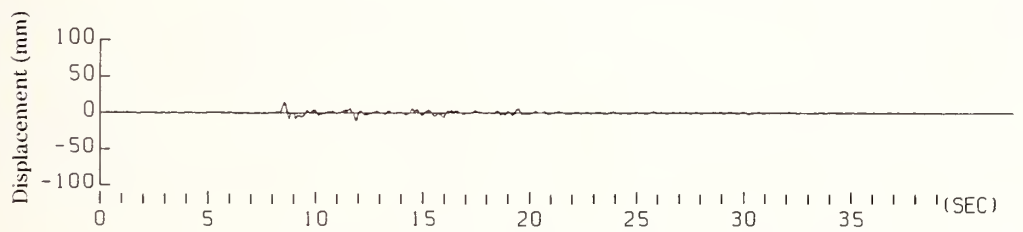

(b) Displacement

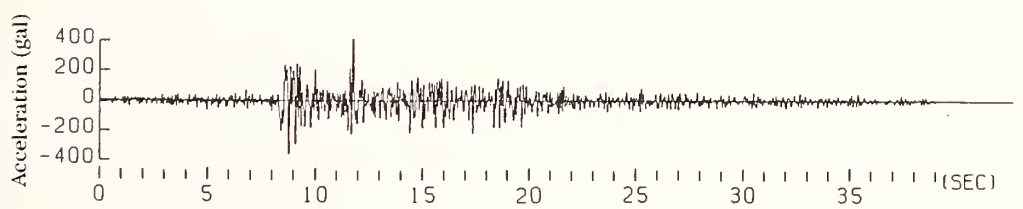

(c) Input Acceleration

Fig.4 Computed Response by Optimal Feedback Control with $Q_a{}^d = 10^{10}$ ($m_d/m_a = 1/100$)

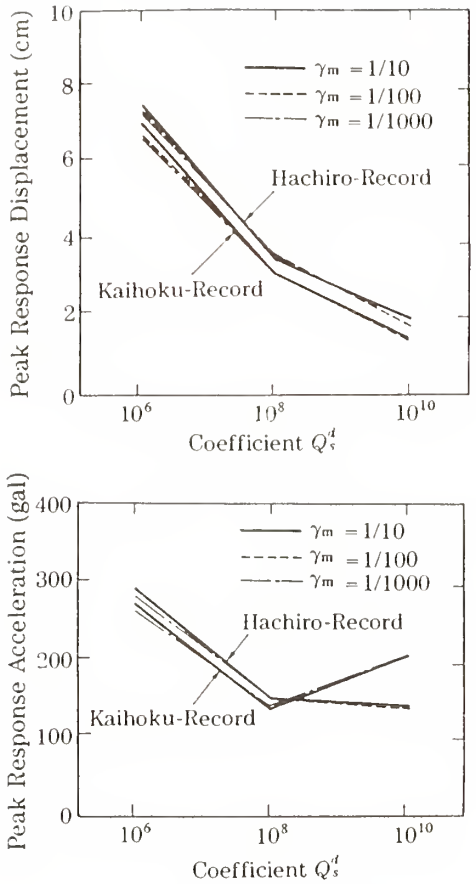

Fig.5 Control of Response by Means of Optimal Feedback Control

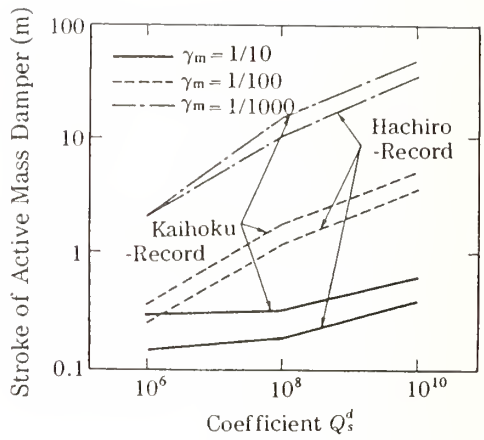

Fig.6 Stroke Required by Optimal Feedback Control

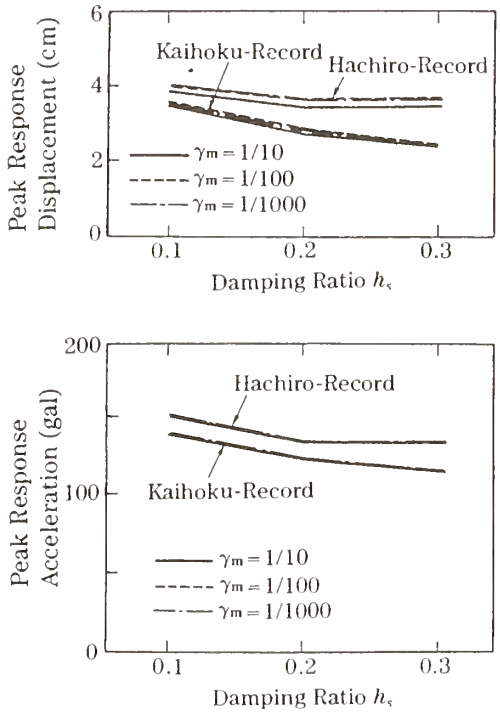

Fig.7 Control of Response by Means of Modal Control Method

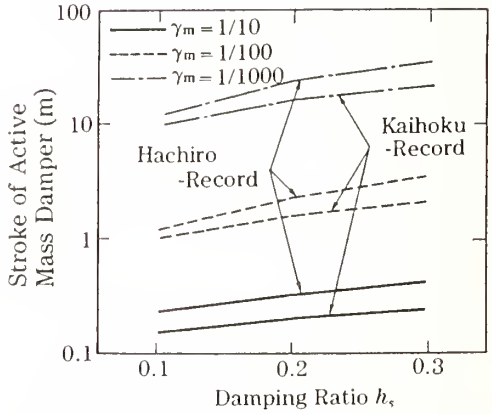

Fig.8 Stroke Required by Modal Control Method

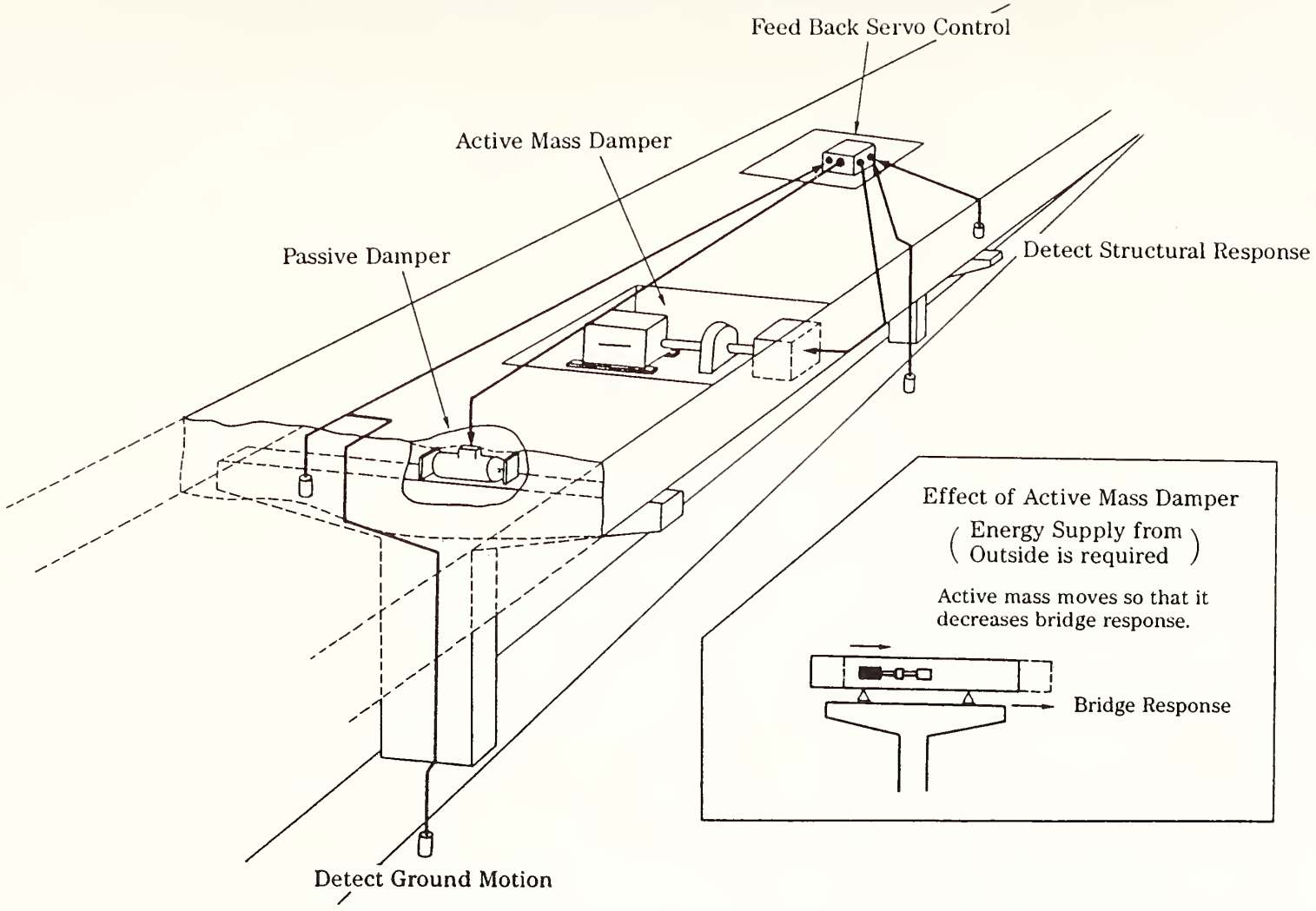

Fig.9 Hybrid Control of Bridge Structures

Theme IV

Earthquake Engineering

Lateral Resistance of a Pile

BY
Michio Okahara[1], Shoji Takagi[2] and Keiji Taguchi[3]

ABSTRACT

In order to investigate static horizontal resistance of piles, numerous horizontal loading tests were performed and the results analyzed using statistical techniques. Through analysis of these horizontal loading tests, we examined factors influencing amounts of yield displacement and evaluated both amounts of allowable displacement and coefficients of ground reaction in a horizontal direction, assuming that yield displacement is defined as the amount of displacement at the point where residual displacement rapidly increases with respect to horizontal displacement.

KEY WORDS: Pile, horizontal loading test data, yield displacement, allowable displacement, horizontal ground reaction coefficient

1. INTRODUCTION

It has for many years been necessary to establish a method of predicting pile behavior under conditions where horizontal force and moment act on a pile. In the case of static behavior alone, this subject is complicated by the dependency of pile behavior on various factors each such as non-uniformity and non-linear characteristics of the ground, the type of pile, and the method of pile construction.

Approaches to predicting horizontal behavior of a pile can be generally classified mainly into the following three categories regarding the concept of horizontal ground reaction:

1) The ultimate ground reaction method
2) The (linear or non-linear) elastic ground reaction method
3) The elastic-plastic ground reaction method

In Secifications of Substructures in "Specification for Highway Bridges" Part Ⅳ (hereafter referred to as Guide), the linear elastic ground reaction method is adopted, which assumes that the ground reaction is proportional to pile displacement and which sets coefficients of ground reaction in a horizontal direction and allowable amounts of horizontal displacement for piles of relatively small diameters. However, since both the size of pile foundations and varieties have been increasing with bridge scale, a more rational approach must be established when designing bridges. In this report, we have investigated horizontal resistance properties of piles by analyzing data obtained from loading tests by means of statistical methods.

2. SUMMARY OF HORIZONTAL PILE LOADING TEST DATA

Horizontal loading test data were collected for the 415 cases to be analyzed. The primary data (Table 1) available for the following statistical analyis were selected from among these data, which were important to our investigation. Figures 1 and 2 show the frequency distributions of pile diameter and length, respectively.

In the following sections: "3. Studies of elastic limitation on the horizontal behavior" and "4. Studies of the coefficient of horizontal ground reaction", statistical methods were applied to the secondary data groups selected

[1]Engineer Head, Foundation Engineering Division, Structure and Bridge Department, Public Works Reseach Institute, Ministry of Construction
[2]Senior Research Engineer, Foundation Engineering Division, Ditto
[3]Research Engineer, Foundation Engineering Division, Ditto

so that validity was retained for respective purposes and methods (Table 2 and 3).

3. INVESTIGATION ON LIMIT OF HORIZONTAL ELASTIC BEHAVIOR

3.1 Yield displacement and its definition

When the horizontal force and moment act on the pile foundation, its behavior in a horizontal direction is usually non-linear. This means that soils are not perfectly elastic and a region where plastic deformation occurs gradually grows larger with increasing loads. In the Guide, the non-linear behavior of pile foundation is treated as the "apparent" linear behavior, utilizing the coefficent of horizontal subgrade reaction (K_H) obtained in a linear condition. This is because elastic design within a region of allowable horizontal displacement should enable soil resistance to an immense and repetitive load, such as seismic force. We have here, from a similar point of view, investigated with respect to the displacement necessary to attain not only mechanical stability of a pile, but also to withstand an increase of harmful residual displacement.

Figure 3 shows the relationship between residual displacement of a pile head after removing the load and its strain (which is defined as the ratio of the amount of pile head displacement to the pile head diameter before removing the load). From the figure, which is a typical example, one can see that residual displacement rapidly increases beyond a certain amount of pile head strain. It is thus suggested that large plastic deformation of soils could not only be prevented but also its stability as a foundation could be preserved if the pile head displacement were designed to be below the point of inflection where the amount of residual displacement begins to increase rapidly. The following investigations were carried out by defining the amount of pile head displacement corresponding to that of the inflection point for residual displacement, to be the yield displacement.

3.2 Results Of Yield Displacement Analysis

The amount of yield displacement of a pile derived from data is affected by various factors such as pile size, type, method of construction, and hardness or softness of the soil. Yield displacement was evaluated for respective data, and correlations examined between the following indices: yield displacement (Sy), ratio of the yield displacement to the pile diameter (Sy/D), type of pile and modulus of the ground deformation (E_{50}).

Figures 4 and 5 present relationships between Sy vs. E_{50} and Sy/D vs. E_{50}. Here, the modulus of the ground deformation E_{50} was N up to depth $1/\beta$.

($\beta = \sqrt[4]{(K_H D)/(4EI)}$)

Since the results show great variation, there does not seem to be any index governing variation of yield displacement as seen in the figures. Therefore, relative frequency of Sy/D, and the average values and coefficient of variation were obtained based on statistics. By assuming that the frequency distribution of Sy/D is a normal logarithmic distribution, probability of non-excess for three cases (10%, 15,9% and 30%) were checked.

Results of such statistical treatments presented in Figure 6 and Table 4 are summarized as follows:

(1) The coefficients of variation for respective types of piles obtained from Figure 4 fall in the region of 76%-105%, showing a wide distribution. This observation may be due to unknown characteristics of soils and artificial causes at the time of pile construction and loading tests.

(2) Statistical values obtained for cast in-situ piles seem to be different from those for other types of piles. This is because the quality of cast in-situ piles varies greatly with the quality of construction, and because soils around a pile are likely to soften excavation works, while distortion and cracking of a pile

resulting from loading tests change its section rigidity and a pseudo-yield point is therefore likely to be formed.

(3) The average value of Sy/D is evaluated as 3.8% for the total distribution of all piles, and those for three probabilities of non-excess are in the range of 0.9 to 1.7%. Considering the probability of non-excess of 10 to 15.9%, a figure approximately 1% of the pile diameter is a reasonable index, including the amount of yield displacement.

3.3 Displacement Allowable In Designing Pile Foundation

Since a foundation is an underground structure, it is necessary to set an appropriate model of calculation, critical terms and allowable values with respect to its design. In pile design for highway bridges in Japan, ground with non-linear physical characteristics is treated as having linear characteristics while, horizontal behavior of a pile has been checked by using the linear method of elastic ground reaction, and horizontal stability of a pile foundation has been examined by measuring amounts of horizontal displacement at the design ground level. The concept of yield displacement described in the previous section is derived from the concept that the amount of displacement corresponds to the limit of horizontal elastic behavior of piles and soils. As long as the amount of displacement is below that of yield displacement, the assumption that soils are elastic is reasonable and no significant errors should occur when designing.

Therefore, the yield displacement defined above can be used as the allowable displacement, which prevents formation of harmful residual displacement and restrains horizontal behavior of a pile, keeping it within its elastic regime. These results suggest that the horizontal displacement allowable in designing should be rationally estimated by a certain ratio, approximately 1%, of the pile diameter.

4. INVESTIGATION OF COEFFICIENTS OF HORIZONTAL GROUND REACTION

4.1 Subjects

The ground reaction coefficient has complicated characteristics: strain dependability, dependability on load width, dependability on load time. Since calculated values of the ground reaction coefficient vary with strain level, strain level must be evaluated when designing. The fact that since the piles foundation is elastic, the depth of foundation able to resist loads is well known to change with pile diameter and rigidity, and with softness or hardness of the ground must also be considered. Moreover, since types of foundation vary according to purpose, the interation between the pile and the soil must be investigated. We have investigated these points using data obtained by horizontal loading tests of piles as follows.

4.2 Methods and Results

The strain level due to loads acting on the pile head was assumed to be 1% of the pile diameter in order to investigate an equation for estimating ground reaction coefficients in a horizontal direction. This is the standard amount of displacement so that the horizontal reaction coefficient is calculated within the region of elasticity in the behavior of pile and soil. In order to examine possible tumbling of the pile and characteristics of the ground, the loading area of pile(A_H) is given by Eq. 4. Eq.1 is the equation used to estimate the ground reaction coefficient:

$$K_H = K_{HO} (B_H / 30)^{-3/4} \quad (1)$$

Here, K_H: the coefficient of horizontal ground reaction ($Kg\ f/cm^3$)

K_{HO}: the coefficent of gruond reaction in a horizontal direction (Kg/cm^3) equivalent to the value

determined from a flat plate loading test conducted by means of a rigid disk of 30cm diameter and obtained by the equation:

$$K_{H0} = E_0/30 \quad (2)$$

B_H: the equivalent loading width of a pile (cm) perpendicular to the direction of loading and obtained by the equation:

$$B_H = \sqrt{A_H} \quad (3)$$

A_H: the loading area of a pile (cm^2) perpendicular to the direction of loading and obtained by the equation:

$$A_H = D \times 1/\beta \quad (4)$$

D: the diameter of pile (cm)

$1/\beta$: the depth of foundation related to horizontal resistance (cm)

β: the property value of a pile $\sqrt[4]{K_H D/(4EI)}$ (cm^{-1})

EI: the bending rigidity of a pile ($Kg\ cm^2$)

Using the secondary data group shown in Table 3, reverse-calculated values of K_H were obtained for the 1% level of pile head strain from individual loading tests. These values were then compared with those estimated using Eq.1 from results of the basic survey carried out at the same positions. Here, the reverse-calculated values of K_H were obtained from amounts of displacement at the ground surface of pile using the Hayashi-Chang Equation.

Fig.7 compares the reverse-calculated values of K_H with those of K_H calculated by Eq.1. The broken lines denote turning lines related to the least-square method, and the solid lines show the regions of 1:1, 2:1, and 1:2, respectively. Fig.8 shows the normalized probability distribution form ratios of the reverse-calculated K_H to the K_H calculated by Eq.1, assuming a normal logarithmic distribution.

The following observations were obtained from these results:

(1) A good correlation does not appear to exist between the reverse-calculated K_H and the estimated K_H, revealing considerably scattered data.

(2) Estimated K_H tends to be slightly larger than the reverse-calculated K_H.

(3) The method, in which 1-% of the pile diameter is adopted as the standard displacement for calculation of the horizontal ground reacion coefficient, shows applicability to various types of piles, while the use of Eq.1 was found to be generally suitable for estimating the ground reaction coefficient in a horizontal direction.

5. CONCLUSION

In this study we have examined resistance characteristics of piles in a horizontal direction by using the elastic ground reaction method in the pile design. Results suggest that yield displacements in loading tests of piles are approximately 1% of the pile diameter, and that the yield displacement seems to correspond with the diameter of the pile. Moreover, from these results, we have proposed an equation able to estimate both allowable displacement and coefficients of ground reaction in a horizontal direction on the design ground level; error widths of data obtained were relatively large because loading tests were carried out for soils whose mechanical properties are not well known.

Although this paper has dealt with static loading tests, it is also important to study resistance characteristics of dynamic loads due to actual seismic force. It will be necessary to carry out further investigations regarding such subjects, including characteristics of dynamic pile resistance in a horizontal direction.

REFERENCE

1) Japan Road Association; Specifications of Substructures in the "Specifications for Highway Bridges" part Ⅳ, May 1980, February 1990.

2) Uto, Maeda, Gose; "An Investigation

of the Standard Displacement of a Pile in a Horizontal Direction", Bridge and Foundation, Sept. 1987.

3) Okahara, Takagi, Nakatani, Taguchi, Sakamoto; "Survey of Horizontal Resistance Properties of Piles by Loading Test Data", Public Works Research Institute Data, 2721, Jan.

4) Okahara, Takagi, Nakatani, Taguchi, Sakamoto; An Investigation of the Standard Displacement of Pile by Data from Horizontal Loading Tests", No.1 and 2, Proceedings of the 24th Conference on Soil Mechanics, 1989.

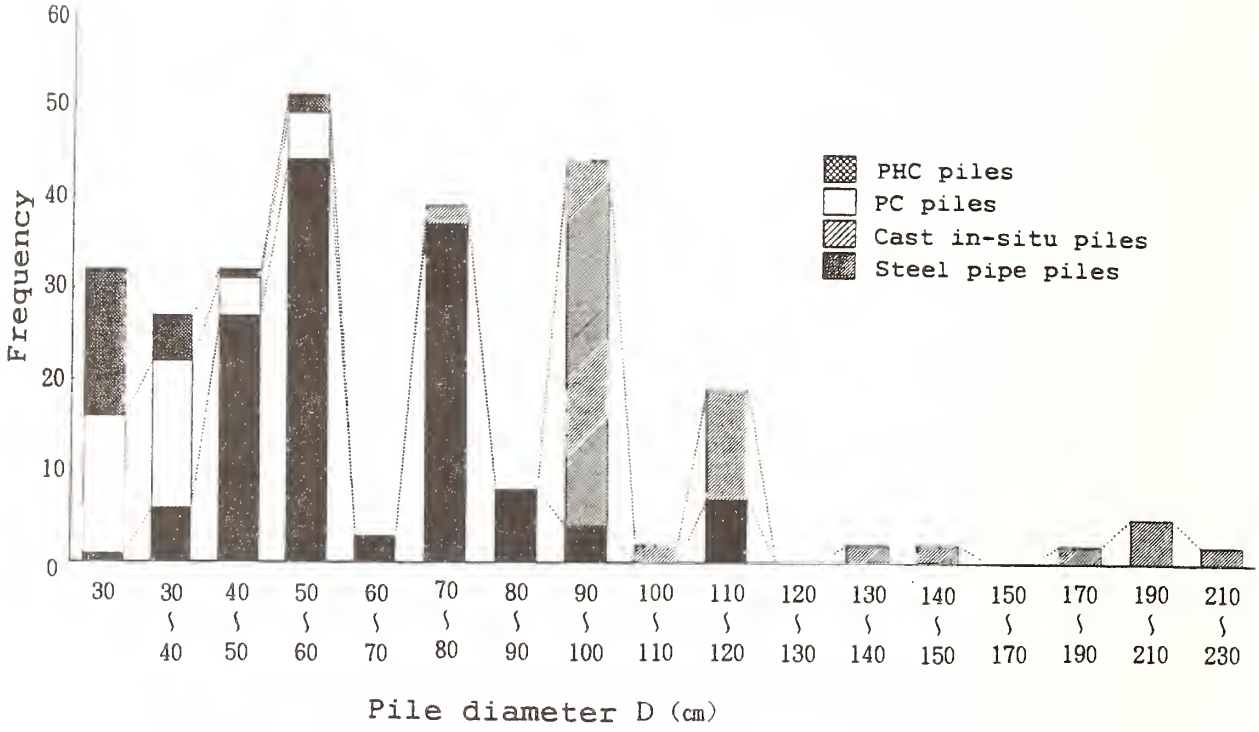

Figure 1. Frequency distribution of pile diameter

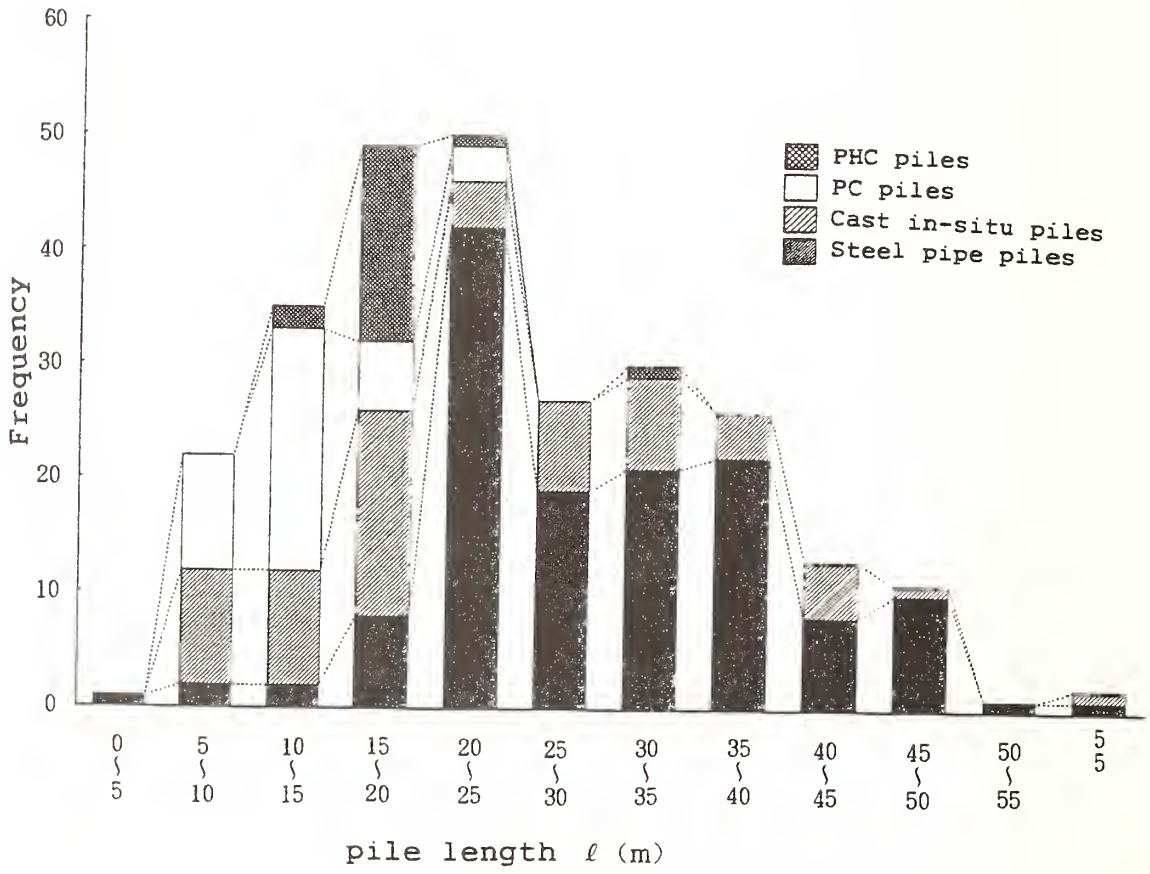

Figure 2. Frequency distribution of pile length

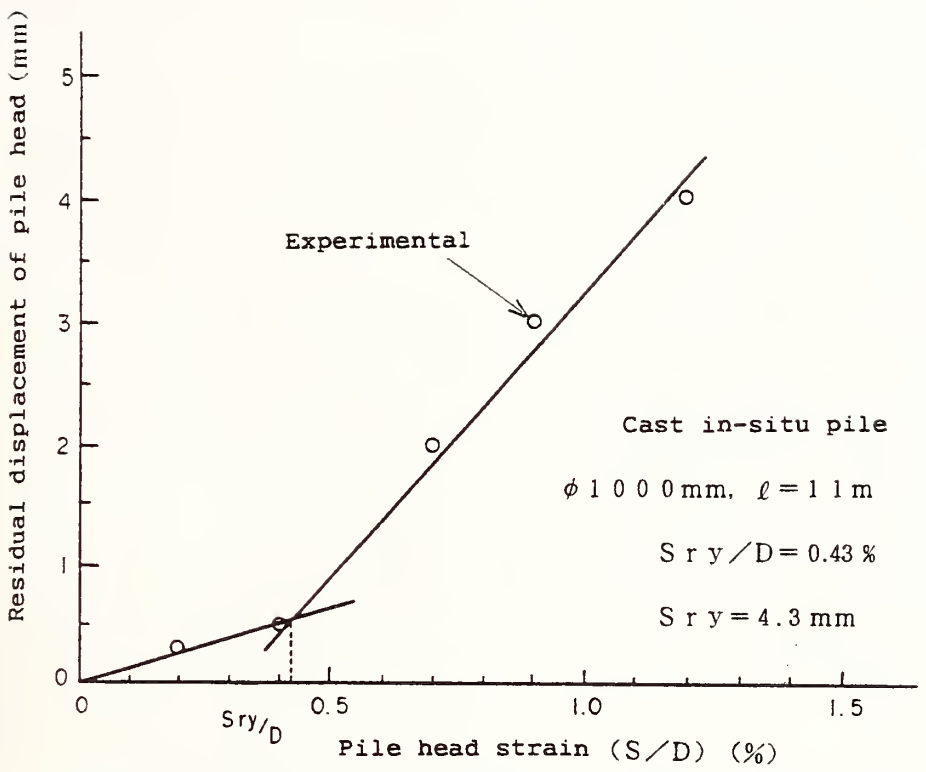

Figure 3. An example showing a sudden increase point of residual displacement obtained from loading test data

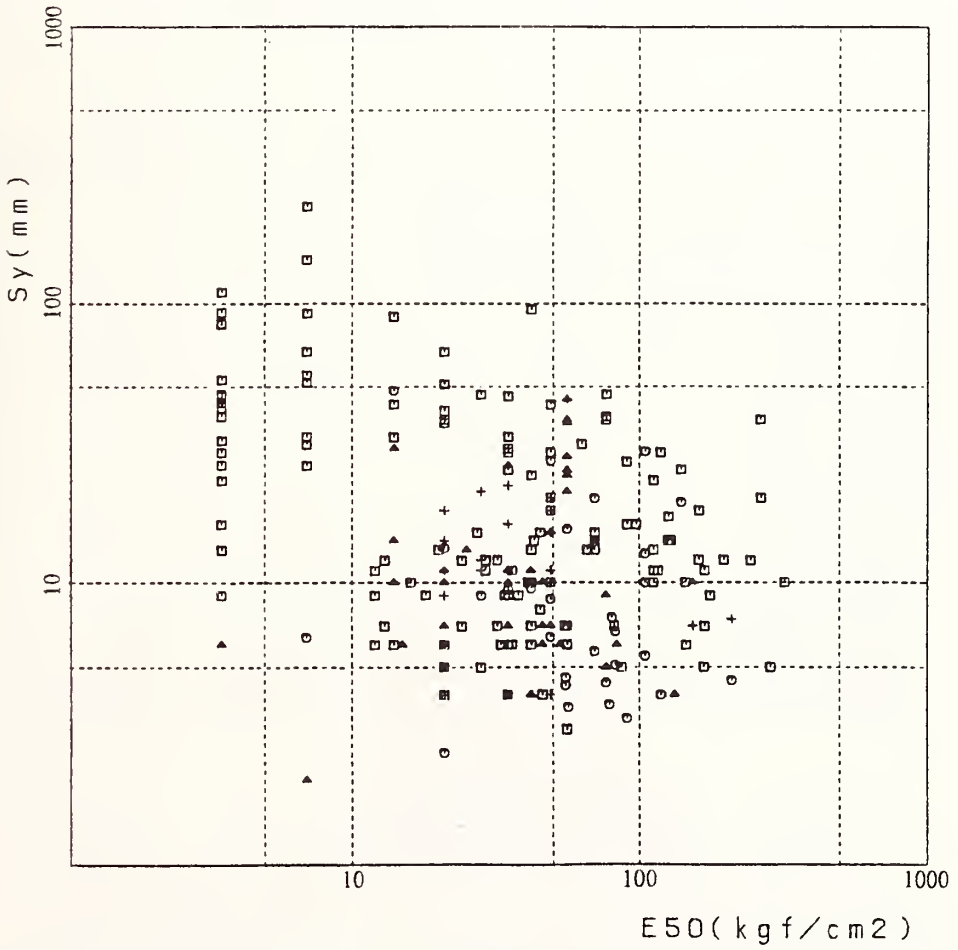

Figure 4. Relation of Sy ~ E_{50} for all piles

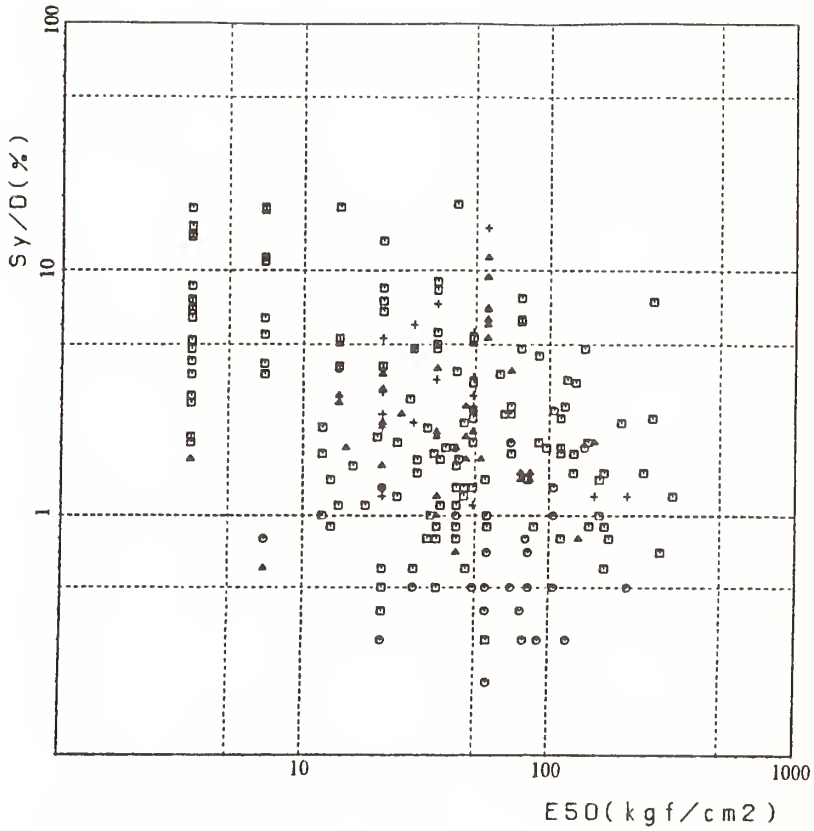

Figure 5. Relation of Sy/D~ E_{50} for all piles

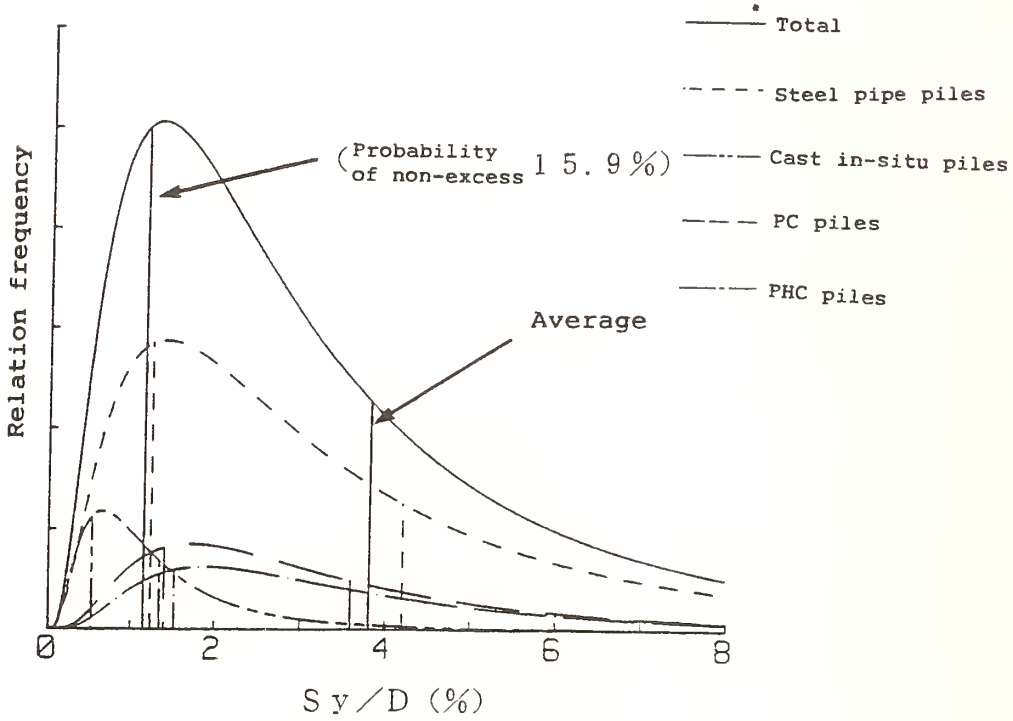

Figure 6. Frequency distribution of Sy/D

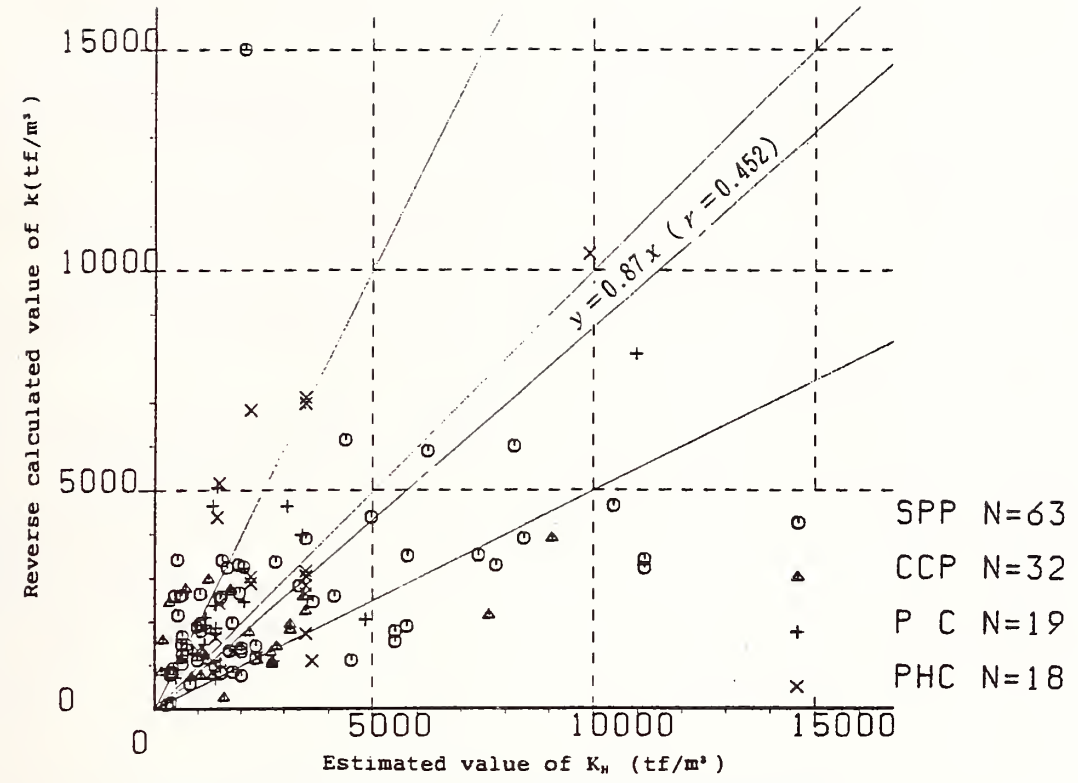

Figure 7. Comparison of the reverse calculation K_H with the estimated K_H

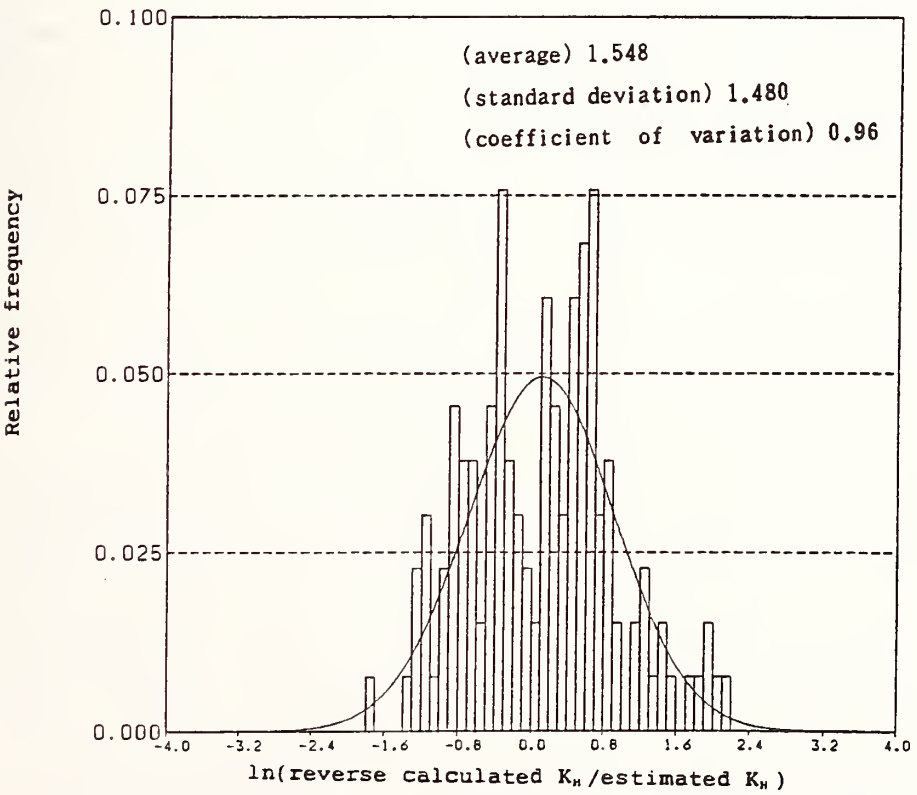

Figure 8. Relative distribution of ln(reverse calculated K_H /estimated K_H)

Table 1. The number of data collected from loading tests and the number in the primary data group

	Collected data	Primary data	First selection terms
Steel piles	237	137	① Those whose standard penetration test data was insufficient
Cast in-situ piles	100	30	② Those consisting of unknown piles components
PC piles	48	40	③ Those use special types of pile and construction method.
PHC piles	30	24	④ Those whose curve of Weibull distribution is larger than the Pmax obtaind from loading tests: Py>Pmax
Total	415	231	⑤ Those whose data of load~displacement do not follow the Weibull distribution curve.

Pmax : Maximum loading load Py : Yield load estimated

Table 2. The number in the secondary data group and selection terms(Allowable)

	Primary data	Secondary data	Second selection terms
Steel piles	137	117	① Those whose height of loading load from the ground surface is larger than the pile diameter H>D ② Those whose Smax obtained from loading tests does not reach 1% of the pile diameter Smax<0.01D ③ Those whose circle number of measurement for load~displacement under the loading test is less than 2 ④ Those in which 80% of the Pu shown as a Weibull distribution curve is larger than the Pmax obtained from loading tests 0.80Pu>Pmax
Cast in-situ piles	30	16	
PC piles	40	31	
PHC piles	24	24	
Total	231	188	

Smax : Maximum horizontal displacement Pu : Ultimate load estimated
Pmax : Maximum loading load

Table 3. The secondary data and its selection terms (K_H)

		Primary data	Secondary data	Second section terms
1 %	Steel piles	137	117	①Those whose estimated yield load is larger than the Pmax obtained from loading tests and whose Smax is less than 1% of the pile diameter. ②Pile groups, those whose pile head is fixed and whose heights are not known.
	Cast in-situ piles	30	16	
	PC piles	40	31	
	PHC piles	24	24	
	Total	231	188	

Smax : Maximum horizontal displacement Pmax : Maximum loading load

Table 4. Results obtained from statistical treatments of Sy/D

			Steel pipe piles	Cast in-situ piles	PC piles	PHC piles	total
Sy/D	Range(%)		0.3 ～22.4	0.3 ～4.0	0.7～11.3	1.1～14.9	0.3～22.4
	Average(%)		4.2	1.3	3.6	3.8	3.8
	Standard deviation(%)		4.4	1.1	2.8	2.9	3.9
	Variational coefficient(%)		105	85	78	76	103
	Probability of non-excess	10.0%	1.0	0.4	1.1	1.3	0.9
		15.9%	1.2	0.5	1.4	1.5	1.2
		30%	1.9	0.7	2.0	2.1	1.7

Major Seismic Building Upgrades at the Lawrence Livermore National Laboratory

by

F.J. Tokarz[1], G.E. Freeland[2], and J.R. Hill[3]

ABSTRACT

The Lawrence Livermore National Laboratory is a U.S. Department of Energy research complex located near San Francisco and Oakland, California. The Laboratory, established in 1952, is located in a highly seismic region which is surrounded by both major (San Andreas) and local fault systems. In fact, in 1980 the Livermore Earthquake (M-5.8) caused considerable damage at the Laboratory. As a result, the Laboratory has spent some $25 million (1990 U.S. dollars) in a seismic upgrade program to enhance life safety of each employee, and to minimize potential damage against future earthquakes. This paper focuses on the major seismic upgrades (retrofits) of three buildings: (1) a two-story physics office building, (2) a five-story computer office building and (3) a seven-story administration building. Also, included herein are brief descriptions of the Laboratory, seismic setting, impact of the 1980 Livermore Earthquake on Laboratory facilities, and a discussion of the seismic design criteria employed over the years, with particular emphasis on criteria used since the 1980 Livermore Earthquake.

1. INTRODUCTION

1.1 Description of Laboratory

Lawrence Livermore National Laboratory (LLNL) was established in 1952. The Laboratory is operated by the University of California for the U.S. Department of Energy (DOE).

The Laboratory site is approximately one square mile (640 acres) [2.59 km^2] in size and contains municipal services similar to those normally found in any small city; police and fire department, a medical department, and water/sewer/electrical/natural gas distribution systems. Presently, personnel at the site number around 11,000. There are approximately 200 permanent buildings that enclose about 3.9 million sq. ft. [3.62x10^5 m^2] (gross) of floor space, and over

[1] Division Leader, Plant Engineering Department, Lawrence Livermore National Laboratory, POB 808 L-654, Livermore, CA 94550

[2] Civil and Structural Section Leader, Plant Engineering, Lawrence Livermore National Laboratory POB 808 L-654, Livermore, CA 94550

[3] Manager, Natural Hazards Mitigation Program, U.S, Department of Energy, 19901 Germantown Road, Germantown, MD 20874

1,000 trailers on site (single, stand alone units or joined together to form one or two story complexes). The Laboratory's annual budget is approximately $1 billion [U.S. dollars]; it's facilities (excluding utilities and the contents of buildings) are estimated as being worth $810 million [U.S. dollars].

1.2 Seismic Setting of Laboratory

LLNL is located in the Livermore valley about 40 miles [64.4 km] east of San Francisco and Oakland, California. This site is in the coastal region of Central California, one of the most seismically active regions in the United States. Figure 1 indicate the major fault systems which pose a seismic hazard to Laboratory facilities. To the west (60 kilometers) lies the major San Andreas fault zone which extends the entire state of California. Closer in, but still to the west, are branches of the San Andreas; the Hayward and Calaveras fault zones. These latter faults are approximately 25 and 17 kilometers from the Laboratory, respectively. And finally, several local active faults surround the Laboratory within the Livermore Valley.

The Laboratory has spent some $5M [U.S. dollars] to characterize the seismic hazard it faces.[1,2] This study, started in 1979 and completed in 1984, included literature reviews, geological mapping, drilling bore holes, excavation, interpretation of aerial photography, soil dating, seismological studies and geophysical surveys. The Laboratory's work was reviewed by a consulting firm and a three-member panel of academic experts.

Major conclusive findings indicate: (1) no evidence of active earthquake faults underneath the Laboratory; (2) land slide and soil liquefaction at the Laboratory are improbable; and (3) the major threat to the Laboratory is that of strong ground motion. Further, the greatest seismic threat to the Laboratory is from a moderate-size (M=5.5 to 6.5) earthquake on local faults in the Livermore Valley. Major earthquakes on the San Andreas, Hayward and Calaveras faults are less of a threat than local faults due to their distance from the Laboratory.

Figures 2a and 2b characterizes the seismic hazard to the Laboratory as the result of the $5 million [U.S. dollars] study. Figure 2a shows the expected peak free field ground acceleration verses the mean number of events per year. Figure 2b gives a response spectra normalized to 1g. These Figures represent the most current information available, and are used for the design of new Laboratory facilities.

1.3 Impact of 1980 Livermore Earthquake[3,4]

On January 24, 1980, LLNL experienced an earthquake with a Richter magnitude of 5.8, followed within three minutes by three relatively large after shocks with magnitudes of 5.1, 4.0, and 4.2. On January 26th, another earthquake with a Richter magnitude of 5.4 occurred. The epicenter of the January 24th event was about 13 miles [20.9 km] northwest of the Laboratory; the epicenter of the January 26th event was about 4 miles [6.4 km] northwest of the Lab. The peak ground accelerations at LLNL were estimated to be in the range from 0.2g to 0.3g.

Although no one was seriously injured, the 5.8 earthquake caused considerable damage and disruption at the Laboratory[3]. This is the only earthquake that caused

significant damage to DOE facilities during the past 46 years[5]. Building walls of concrete and masonry were cracked and broken. Extensive cracking occurred in concrete structures throughout the Laboratory. Most of this cracking was not a threat to the structural integrity of the buildings or structures. However, Building 311, a two-story physics concrete-frame office building suffered considerable column damage at the juncture of the second floor and roof lines, equipment shifted from mounting pads, and staircases cracked. Building 113, the Laboratory's five-story computer office building, suffered extensive cracking to its central lateral-force resisting concrete core. Building 111, a seven story administrative building, suffered damage to an exterior seven story, free-standing stair tower. Extensive cracking was observed in the central core concrete walls, a second floor soft-story, and at column to beam connections.

In other Laboratory buildings, some connections between tilt-up concrete walls and their supporting structural-steel frames had failed. A few structural steel welds failed, several loose or stretched bolts were noted, and damage to the connections of structural members was found throughout the site. A few structural steel framing members buckled in some of the buildings. Many elevators could not be used because counterweights had been knocked loose from their mounting brackets, bending the guide rails. Surprisingly, the Laboratory had very little window glass breakage. However, concrete anchors used to fasten down various types of equipment and tanks were twisted or torn and, in some cases, were completely pulled out of the concrete. Trailer support stands moved and toppled. Many trailers shifted, causing their outside doors to jam or be blocked, so that they could not be immediately opened.

The Laboratory spent approximately $10 million (in 1982 U.S. dollars) in earthquake restoration, repair, and upgrades from 1981-1985. Approximately $7 million [U.S. dollars] of this was directed toward seismic tie-down of: office equipment and library shelving; mechanical and electrical equipment; trailers; ceiling and light fixtures; acoustical tile and lay-in panel ceilings; mechanical restraints to cranes;and the replacement of rigid with flexible connections to propane tanks.

Approximately $3 million of the $10 million [U.S. dollars] was spent on major building upgrades of Building 311 and Building 113. Another $6.5 million (in 1990 U.S. dollars) is currently being spent to upgrade Building 111. All three of these major upgrades are discussed in detail later.

2. MAJOR BUILDING UPGRADES

2.1 Seismic Criteria for New Buildings

In general, the seismic design criteria used for Laboratory facilities has the following major safety goals: (1) no loss of life; (2) no building collapses, and (3) no compromise of containment in hazardous facilities.

The seismic criteria used at the Laboratory reflect four eras: (1) pre-1971; (2) 1971-1980; (3) 1980-1989, and (4) present (U.S. DOE 6430.1a[6]/UCRL-15910.[7]).

Pre-1971 Before 1971 all facilities were constructed to meet the latest edition of the Uniform Building Code (UBC) in effect at the time of construction.

1971 to 1980 The 1971 San Fernando earthquake, (magnitude 6.3), caused far more damage than expected by earthquake engineers. As a result, the Laboratory expended a considerable effort to review its earthquake design criteria and its facilities. The result was an upgrade to our hazardous facilities criteria such that the upgraded criteria exceeded UBC criteria. No changes were implemented for conventional facilities.

1980 to May 1989 All Laboratory buildings, structures, systems, and components were categorized into one of four safety classifications: High Hazard, Moderate Hazard, Low Hazard, and No Hazard (Conventional Building). Each safety classification had its own design basis earthquake criteria. Table 1 summarizes Laboratory seismic criteria used post-1980 Livermore through May 1989 for new facilities.

High Hazard structures, systems, and components (Seismic Category I items) went through a two-step design process. Seismic Category I structures, systems, and components are those items whose continued integrity and/or operability are essential to assure the capability to shut down and maintain a safe shutdown condition, and to prevent or mitigate the consequences of accidents which could result in potential off-site exposures. The first process consisted of evaluation and design in the elastic range of response. It was done using a dynamic response spectrum analysis (Figure 3) with a corresponding horizontal Design Basis Earthquake (DBE) peak ground acceleration (PGA) of 0.50g applied simultaneously with a vertical PGA of ± 0.33g. Engineering evaluations and design were done by using UBC Strength Allowables. Connection evaluation and design included an additional load factor of 1.5. That is, the connection design/evaluation used forces which were 1.5 times those seismically calculated,. The second part of the design process allowed for inelastic response Seismic Category I items were checked against forces due to a DBE with a horizontal PGA of 0.80g applied simultaneously with a vertical PGA of ±0.53g. For this check, the item was to remain functional during and after the earthquake.

Moderate Hazard structures, systems, and components (Seismic Category I items) also went through a two-step design process. The first process consisted of evaluation and design in the elastic range of response. It was done using a dynamic response spectrum analysis (Figure 3) with a corresponding horizontal peak ground acceleration (PGA) of 0.25g DBE applied simultaneously with a vertical PGA of ± 0.17g. Engineering evaluations and design were done using UBC analysis methods along with UBC Strength Allowables. Connection evaluation and design again accounted for an additional load factor of 1.5. The second part of the design process allowed inelastic response and checked the integrity of the Moderate Hazard Seismic Category I items against forces due to a DBE with a horizontal PGA of 0.50g applied simultaneously with a vertical PGA of ± 0.33. For this check, the item was to remain functional during and after the earthquake.

Non-Seismic Category I items were designed using LLNL's No Hazard, Standard Facility Criteria. An item in a lower Safety Classification must not cause failure of an item in a higher Safety Classification.

Low and No-Hazard conventional structures, systems, and components were designed to the following guidelines:

1. One and Two-Story Buildings and Structures Used current UBC requirements with a more conservative seismic base shear coefficient of 0.25 (static). Connection evaluation and design, due to seismic forces, accounted for an additional load factor of 1.5. To assure that the building's structural elements could reach their maximum potential for ductility.

Analysis procedures, design procedures, and material strength allowables met the requirements of the latest edition of the UBC and DOE Facilities General Design Criteria.

2. Buildings and Structures Greater Than Two Stories As a minimum, buildings and structures over two stories in height were designed to meet the seismic design requirements for 1) above.

Buildings and structures over two stories in height were also evaluated and designed using a response spectra (Figure 3) with a corresponding horizontal peak ground acceleration (PGA) of 0.5g applied simultaneously with a vertical PGA of ±0.33g.

Engineering evaluations and design was accomplished by the use of inelastic analysis methods combined with inelastic stress allowables. Primary concern was to ensure prevention of building collapse, thereby allowing the building occupants to egress safely following an earthquake having major intensity at the site. Major damage to the structure (perhaps even non-repairable) following this level of design motion was permissible.

3. All Buildings and Structures with Significant Cross Axes Coupling and/or Torsional Response The design of buildings and structures placed within this category met the requirements of 2) above.

2.2 Seismic Criteria for Building Upgrades

The engineering design approach used for the seismic upgrade of existing LLNL facilities was somewhat different than the previously defined criteria required for "new" LLNL facilities. For the seismic upgrade on No-Hazard (Conventional) and Low-Hazard structures, the basic premise of the LLNL seismic upgrade criteria was to ensure "life safety" in the event of a major earthquake. That is, the building could endure major structural and non-structural damage, but no collapse. The occupants should be able to exit the building without incurring loss of life. In the case of Moderate/High Hazard structures, systems, and components the basic premise of the LLNL seismic upgrade criteria was to ensure both life safety and functionality of the Seismic Category I items. Seismic Category I items must be able to perform their required mission. Applicable codes and standards were consulted at the time of the upgrade.

The specific seismic upgrade criteria used on the three major building upgrades are discussed in the following sections.

2.3 Major Upgrade of Building 311

Building 311 was originally designed under the requirements of the 1961 Uniform Building Code (UBC) and constructed during 1964 as a two-story, cast-in-place reinforced concrete structure with 37,000 ft.^{2} [3,437 m^2] of gross floor space (see Figure 4). It is 95ft. [29m] by 190

ft. [57.9m] in plan and consists of two levels plus a penthouse for mechanical equipment located on the roof. The typical bay size is 23 ft. 9 in. [7.239m] by 23 ft. 9 in. [7.239m].

Building 311's primary lateral force resisting system was a "non-ductile moment resisting frame" founded on drilled piers. The first floor is a slab-on-grade, and the second floor and roof are framed with concrete beams, girders, and infilled with concrete pan joists. Building columns are of reinforced concrete. There are no column ties within the Building columns other than in the immediate vicinity of the ground, second floor, and roof slabs. The non-ductile frames were designed using a uniform lateral force distribution (1961 UBC) and a base shear coefficient of 0.067. This type of framing system has a history of partial or total collapse in moderate to strong earthquake shocks. A significant difference exists between today's current seismic building codes for new construction and the 1961 Uniform Building Code. The 1979 and 1982 editions of the UBC would require Building 311 to resist a non-uniformly applied static earthquake force with a base shear coefficient of 0.094. The 1988 UBC and DOE Order 6430.1a would require a base shear coefficient of 0.22 and 0.235, respectively.

Building 311 suffered considerable structural damage during the 1980 Livermore earthquake. This included vertical column splitting, concrete cracking, and cracking at the beam/column joints. Within hours following the earthquake, LLNL structural investigation teams were assembled and in the field. Engineering consulting firms were hired to review Building 311, (as well as Building 113, and Building 111). A sign was posted at all entrances and exits of Building 311 informing both visitors and building occupants as to the inherent structural deficiencies (weaknesses) with respect to the ability of the building to safely resist earthquake forces. With the installation of temporary wood column shoring, Building 311 was considered safe for habitation while the Laboratory proceeded with haste to complete building repairs. Laboratory personnel were allowed to re-occupy the building during the remedial crack repairs. Concrete cracks were repaired by injecting high-strength epoxy grout into the cracks, a procedure that can effectively restore earthquake damaged concrete structures to nearly their full design strength.

After the earthquake, the Laboratory decided to upgrade the seismic performance of Building 311 with respect to both damage control and life safety concerns. The seismic upgrade criteria required; (1) the use of 1979 UBC design allowables, (2) a UBC base shear coefficient of .25, (3) a connection static force design multiplier (all connections) of 1.5, and (4) no building collapse at 0.50g peak ground acceleration with design response spectra shown in Figure 3.

The structural upgrade solution was to construct and attach to the existing building a series of external two-story-high concrete shear walls (buttresses) on three of the four sides of Building 311, two on the west end, two on the east end, four on the south side, and none on the north side, (see Figure 5). The concrete buttresses are anchored to the ground using 3-ft. [.914m] diameter by 40-ft. [12.192m] long drilled concrete piers, four piers per buttress. The buttresses are attached to the second-floor level of the building by rebar welded to steel-channel drag struts. These struts are, in turn, attached to the underside of the second-floor concrete beams by specially designed steel bolts (see Figure 6). The second-floor connectors use a straight pattern of ten (10) custom-

made bolts spaced approximately 9 inches [22.86 cm] apart on center at each buttress. These bolts have a length of 16 inches [40.64 cm] with an overall diameter of 3-3/4 inches [9.53 cm] for that portion of the bolt passing through the concrete beam. The bolts are necked down at each end to a 1-1/4 inch [3.18 cm] diameter threaded portion for bolting to the steel drag struts. Buttresses are also attached to the concrete roof slab by the use of rebar embedded in the buttress and welded to a steel plate drag strut, which is, in turn, attached to the top of the respective concrete roof beam by 13 specially-made shear connectors spaced approximately seven inches on center (see Figure 7).

A modification to the above design provided high load capacity drag strut connections commensurate with the non-uniform load distribution across the second floor drag strut bolts and the roof shear connectors. This was done since the first drag strut connecting anchor, adjacent to a buttress, must resist seismic forces several times larger than the last anchor furthest from a buttress. Load distributions to the anchors were determined by a series of computer models of typical buttress/drag strut configurations. Design variables considered during this process included: connector strength at elastic and inelastic levels, connector stiffness, concrete bearing, tensile, shear, and compressive stress levels, and overall total connector system stiffness (tension stiffness vs. compression stiffness).

The structural upgrade costs of Building 311 were approximately $1.5 million (in 1982 U.S. dollars). Replacing the building would have cost approximately $4.6 million (in 1982 U.S. dollars). The construction time for the structural upgrade took about 10 months.

2.4 Major Upgrade of Building 113

Building 113 is a five-story reinforced concrete structure, approximately 90 ft. [27.43 m] square in plan dimensions (3 bays by 3 bays), containing about 42,000 $ft.^2$ [3,902 m^2] of office space (see Figure 8). The building has a partial basement and a 14-ft. [4.27 m] high steel-frame penthouse for mechanical equipment located on the roof. Each of the five stories is 13-ft. [3.96 m] high, and the basement floor is 17-ft. [5.18 m] below the first floor level. The basement forms a passageway to the adjoining computer center building.

The five-story structure is founded on 24-in. [61 cm] diameter cast-in-place reinforced concrete piles. The building has reinforced concrete waffle slabs supported on reinforced concrete columns, spaced on 30-ft. [9.14 m] centers each way, and a core of reinforced concrete shear walls located in the west half of the structure. The shear walls enclose two stair wells and elevator shafts, and are arranged so that the center of their rigidity falls close to the geometric center of the building. The center core of shear walls were originally designed to carry about 80% of the lateral forces acting on the building, with the remaining 20% being resisted by the perimeter reinforced concrete "non-ductile moment resisting frames."

Building 113 was designed in 1964 to meet the requirements of the 1961 Uniform Building Code (UBC). The original building design provided for a lateral force base shear coefficient of 0.057. The 1982 edition of the UBC would have required Building 113 to resist a statically applied lateral earthquake force with a base shear coefficient of 0.14. The 1988 UBC and DOE Order 6430.1a would require a base shear coefficient of 0.183 and 0.196 respectively.

The January 1980 earthquake caused no damage to the building's columns and moment frames, structural damage was confined to the central-core concrete shear walls. The walls developed extensive diagonal tension cracking and sliding shear cracking along horizontal construction joints, which also showed signs of grinding or spalling. Cracking occurred throughout the building, but more extensively in the lower stories.

Immediately following the 1980 earthquake, Building 113 was vacated for approximately 3 days while a structural evaluation of the building was performed. It was found to be safe to house it's occupants. As the ground acceleration of the January 1980 earthquake was estimated to be about 0.25g at the Laboratory site, therefore, Buildings 113, 111, and 311 were subjected to earthquake forces at least four times greater than that provided for in the original design. High-strength epoxy grout was injected into the central-core shear wall cracks, repairing them in the same manner as was done for Building 311.

By February of 1981, the Laboratory had begun the engineering effort to structurally upgrade Building 113 and to increase it's earthquake resistance with respect to life safety. The Building 113 seismic upgrade performance requirements were as follows:

1. The building shall be capable of resisting, with no collapse, a 0.5g horizontal peak ground acceleration with LLNL's design response spectra (Figure 3);

2. Extensive damage at this earthquake level (0.5g) is acceptable provided that people can safely exit the building; and

3. The new structural elements required for preventing the collapse of the building at 0.5g shall meet the design requirements of the current UBC. In addition, major connections shall include an additional safety factor of 1.5.

Many different schemes for upgrading the building's structure were investigated. In the end, by considering such factors as cost, aesthetics, and disruption as being equal, it was decided that the best approach was to keep the majority of the new construction on the outside of the building. This would allow the building to remain occupied during reconstruction. The existing foundation pile system was considered to adequately meet the life safety seismic criteria for the upgrade. Therefore, the upgrade scheme that was finally decided upon used steel "K" braced frames attached, both to the outside face of the building perimeter, and to the existing foundation system (see Figure 9).

The "K" brace frame design was based on the premise that the reinforced concrete, center core shear walls will absorb a lot of energy while degrading during the specified 0.5g no collapse earthquake. A damping value of 10% was used in the dynamic evaluation for the building's integrated, composite "K" brace frame computer model. A conservative amount of building period shift was allowed in the dynamic solution to account for softening of the structure with a corresponding decrease in intensity of seismic inertia forces. Consideration was given for secondary effects such as P-Delta contributions. An upper bound of 4 was used for the global ductility of the steel frame with special considerations for each structural element using Newmark-Hall type procedures. The American Institute of Steel Construction (AISC) design procedures for plastic design of steel members, along with considerations for member instability, were used in the design process. The UBC static design

procedures, required for all new structural elements, included a braced frame load factor of 1.25 with no 1/3 increase allowed in material allowables. The 0.5g life safety design criteria controlled over the UBC static design criteria for the design of the structural elements.

The "K" brace frames are made of high-strength steel (F_y=50,000 psi [3.515x10^9kg/cm^2]) rectangular tubular welded sections, with 3/4-inch [1.91 cm] diameter Nelson stud anchors welded to their backs (see Figure 10). The outside edges of the building's concrete floor and roof slabs were chipped back to expose the reinforcing bars, and the "K" frames were installed along the outside perimeter of the building by attaching the Nelson studs to the building-slab edges with high-strength concrete grout. The "K" frames were attached to each other with welded steel plates, and to the existing foundation system by constructing new concrete grade beams. "K" frames were placed in all of the first and second story outside building bays, but only in the outside middle bays of the third, fourth, and fifth stories, thus forming an inverted "T" configuration at each building face.

The new building frames were designed to safely resist all of the seismic forces acting on Building 113 as a result of a major earthquake. Cost of the structural upgrade was approximately $1.1 million (in 1982 U.S. dollars). It is estimated that replacing the building would have cost about $5.9 million (in 1982 U.S. dollars). The construction time needed for doing the structural portion of the upgrade was about nine months.

2.5 Major Upgrade of Building 111

Building 111 was designed in 1966, constructed in the late 1960(s), in accordance with the provisions of the 1964 Uniform Building Code (UBC). Building 111 is primarily used as an office building. The structure was constructed entirely of reinforced concrete (RC) and built in a cross-shape plan with three seven-story wings, one five-story wing, and a central core area containing elevators, stairs, air conditioning duct shafts, and utility conduits (see Figure 11). There are two staircases in addition to the ones located at the building core. The first of these is an integral part of the south end of the north-south wing. The other was originally designed to behave as an independent, free-standing, reinforced concrete (cantilever beam) seven-story high stair tower, immediately to the south of the east-west wing. The story heights (floor to floor) are 18 ft. 0 in. [5.49 m] for the first story and 13 ft. 6 in. [4.11 m] for the upper stories. The north-south wing is 212 ft. 6 in. [64.77 m] long and 82 ft. 6 in. [25.15 m] wide at the first floor level. The east-west wing is 120 ft. [36.58 m] long and 42 ft. [12.80 m] wide. The junction of the two wings is approximately 1/3 the distance from the north end of the north-south wing. The width of the north-south wing reduces to 42 ft. [12.80 m] at the second floor and remains so at the upper floor levels. The north end of the building, beyond the east-west wing, has only five floors. The building is founded on cast-in-place reinforced concrete piles 20 inches [50.8 cm] in diameter embedded 44 ft. [13.41 m] into the ground, and contains 102,000 $ft.^2$ [9,476 m^2] of gross floor space with a current population of 323 occupants.

The "vertical load carrying system" of the building is comprised of 4-1/2 inch [11.43 cm] thick RC roof and floor slabs supported using 14

in. [35.56 cm] by 24 in. [60.96 cm] deep RC beams spanning 40 ft. [12.19 m] between 14 in. [35.56 cm] by 24 in. [60.96 cm]. RC columns spaced at 10 ft. [3.05 m] on center along the outside perimeter of the building wings. The exterior edges of the floor and roof slabs are supported by 3 ft. 1 in. [.940 m] deep by 10 in. [25.4 cm] thick pre-cast concrete spandrel beams topped by 14 in. [35.56 cm] deep by 17 in. [43.18 cm] wide RC beams cast in place with the floor slabs. These RC beams are connected to the pre-cast spandrels by vertical steel dowels. The portions of the floor and roof slabs in the building's center core area, adjacent to the interior stairs and elevator shaft, are supported by the RC walls enclosing the shafts.

The "lateral force resisting system" as originally designed is comprised of (1) vertical RC shear walls at the exterior ends of the south, east, and west wings; (2) RC walls enclosing the elevator, stair, and duct shafts; (3) RC walls enclosing portions of the five-story wing; and (4) the transverse beam/column frames spaced at 10 ft. [3.05 m] on center along each wing (see "vertical load carrying system").

The original building design (1964 UBC) provided for a lateral force, base shear coefficient of 0.057. The 1982 edition of the UBC would have required Building 111 to resist a statically applied lateral earthquake force with a base shear coefficient of 0.14. The 1988 UBC and DOE Order 6430.1a would require a base shear coefficient of 0.183 and 0.196, respectively.

As a result of the January 1980 earthquake, Building 111 suffered diagonal tension cracking to the central-cores' (RC) shear walls. Cracking occurred to the RC floor and roof slabs (diaphragms) in the vicinity of the buildings' center-core and end-wing, shear walls. The transverse beam/column frames suffered damage at the beam/column joints, and the free-standing seven-story high stair tower was found to have swayed approximately 3 inches [7.62 cm] in the north-south direction, striking the building, and causing minor damage. The condition of Building 111 was investigated with respect to continued habitation, found safe to house its occupants, and crack repairs commenced using epoxy grout injection techniques. The outside seven-story stair tower was closed-off until a structural upgrade could be implemented.

By the Spring of 1981, engineering studies identified the seismic deficiencies found within Building 111. The list of major structural deficiencies, based on the original design of Building 111, include the following:

1. The foundation of the east wing was not connected to the south wing.

2. The ends of the west wings have solid multi-story concrete walls terminating at a lower level on a concrete frame and thus creating "soft stories".

3. The seven-story cantilevered stair tower is unsafe and should be structurally upgraded.

4. The concrete shear wall at the end of the east wing has an offset in it's vertical plane at the second floor.

5. The steel reinforcement at the beam/column joints is not laterally confined and the anchorage and laps of bars are inadequate. These frames will only provide nominal seismic resistance.

6. The building lacks adequate shear wall strength capacity.

7. The roof and floor slab diaphragm cord members lack adequate reinforcement.

8. The connection of the diaphragm collectors, cords, and tie elements (south, east, and west wings) to the building's center core is inadequate.

9. The reinforcement anchorages for the present spandrel beams is not adequate.

The first three structural seismic deficiencies of the above list have been corrected. The stair tower is now laterally supported at each floor level and at the roof by structural-steel tube connections to Building 111. High-strength steel bolts were used to connect the tubes to the stair tower. Cinch anchors and grouted steel bolts connect the tubes to Building 111's peripheral beams and columns (see Figure 12). The second story window openings in the concrete walls at the west end of the west wing and the northeast and northwest corners of the five-story wing were filled with reinforced concrete to provide additional seismic resistance and the elimination of the "soft stories". Concrete grade beams have been added at the first floor breezeway (now enclosed) at the end of the east wing adjacent to the building core.

LLNL is presently in the process of retrofitting the remaining Building 111 structural seismic deficiencies at an approximate cost of $6.5 million (in 1990 U.S. dollars). It is estimated that replacing the building would have cost about $32 million [U.S. dollars]. The construction time required for the building upgrade is 12 months. Construction is currently scheduled to be complete by January, 1991.

The Building 111 seismic upgrade performance requirements, are as follows:

1. The building shall be capable of resisting, with no collapse, a 0.5g horizontal peak ground acceleration with the acceleration response spectrum shown in Figure 13. (Note, this response spectrum was based on the 1988 UBC spectrum shape.)

2. Extensive damage at the earthquake ground motion level defined in (1) is acceptable provided that people can safely exit the building.

3. All new structural elements required for preventing the collapse shall meet the design requirements of the current UBC. In addition, brittle-type connections shall include an additional safety factor of 1.5.

4. Minimize disruption to the building occupants during the construction phase of the strengthening process.

5. Maximize aesthetics for the resulting construction while minimizing total project cost.

A minimum of six solutions were developed and considered in detail with respect to the seismic upgrade of Building 111. Considerations for minimum disruption and project costs, with the safety of building occupants being equal for all proposed solutions, again drove the upgrade scheme to the outside of the building, thus, allowing the building to remain occupied during the implementation of the upgrade solution.

Figure 14 in an artist rendering, illustrating the Building 111 current upgrade. Two large reinforced concrete (RC) towers will be located at the exterior of the building. One tower is located adjacent to the east wing on the south side, and the other tower is located adjacent to the south wing of the east side. The two towers rise from a 6 ft. 8 in. [2.03 m] thick reinforced concrete mat supported on thirty nine 36 inch [91.44 cm] diameter drilled RC piers

extending 50 ft. [15.24 m] to 66 ft. [20.12 m] (depending on location) below the new foundation mat.

Each RC tower is connected to the adjacent building wing with channel shaped steel collector members installed on each side of three floor beams starting on the third floor to the roof. Each collector member extends full width of the office wings, is securely anchored into the concrete tower, and is bolted and bonded with epoxy grout to the concrete floor or roof beam. Construction of the collector members will be accomplished by removing the precast concrete panels at four bays in each wing to permit access. Plywood sheets will be laid on top of the existing ceilings for construction contractor personnel to drill holes in the existing concrete and install the collector members. This means of construction will permit uncleared construction personnel to perform the work without penetrating secured building areas. Epoxy grout is injected between the steel collector member and the existing concrete beam along with having a steel plate anchor at the exterior end. The horizontal collector tie beams are constructed to transmit the collector member forces into the concrete towers. A few additional RC walls will be constructed internal to the building to help in distributing shear forces.

3. CONCLUSIONS

The Lawrence Livermore National Laboratory experienced considerable damage as the result of the 1980 Livermore Earthquake. Subsequently, a major study was undertaken and completed in 1985 to quantify the seismic hazard the Laboratory faces. The design criteria used for new facilities and upgrades (retrofits) of existing facilities are consistent with the results of this study. Based on post-1980 inspection of Laboratory facilities, by both independent consultants and Laboratory staff, all buildings requiring upgrade to assure "life safety" have been identified. Three major structural building upgrades were involved: Building 311, Building 113, and Building 111. Upon completion of the Building 111 upgrade, currently under construction, no further upgrades are required or planned.

4. REFERENCES

1. "Final Report, Lawrence Livermore National Laboratory Seismic Exposure Comparison Report and Spectra Report," prepared for LLNL by Geomatrix Consultants, Inc. (1985).

2. J. F. Scheimer, "Lawrence Livermore National Laboratory Site Seismic Safety Program—Summary of Findings," UCRL-53674 (1985).

3. G. E. Freeland, Lawrence Livermore National Laboratory Earthquake Safety Program: UCAR 10129 (1984).

4. R. C. Becker, et al, the LLNL Earthquake Impact Analysis Committee report on the Livermore, California earthquakes of January 24 and 26, 1980: UCRL-52956, (1980).

5. J. R. Hill, Injury and Property Damage Experience from National Hazards 1943 to 1989, Second DOE National Phenomena Hazards Mitigation Conference, Knoxsville, Tennessee (1989).

6. U.S. Department of Energy, "General Design Criteria", DOE Order 6430.1a, April 6, 1989.

7. R. P. Kennedy, et al, "Design and Evaluation Guidelines for Department of Energy Facilities Subjected to Natural Phenomena Hazards": UCRL-15910 Draft (1988).

8. G.E. Freeland, "Earthquake Safety Program at Lawrence Livermore National Laboratory," DOE Natural Phenomena Hazard Mitigation Conference - 1985.

9. G. E. Freeland and Manohar Sethi, Seismic Upgrade of Building 311, 8th World Conference on Earthquake Engineering, San Francisco, CA (1984).

L.L.N.L. SEISMIC DESIGN CRITERIA
NEW FACILITIES, 1980 TO MAY 1989

FACILITY USE SAFETY CLASSIFICATION

LOW HAZARD AND NO HAZARD (CONVENTIONAL)	MODERATE HAZARD	HIGH HAZARD
(1) 1 & 2 STORIES V= 0.25 W UBC ALLOWABLES 1.5 CONNECTION FACTOR	**(1) CATEGORY I** a) 0.25g RESPONSE SPECTRA UBC ALLOWABLES 1.5 CONNECTION FACTOR b) 0.8g RESPONSE SPECTRA REMAIN FUNCTIONAL	**(1) CATEGORY I** a) 0.5g RESPONSE UBC ALLOWABLES 1.5 CONNECTION FACTOR b) 0.8g RESPONSE SPECTRA REMAIN FUNCTIONAL
(2) 2 STORIES OR IRREGULAR a) SAME AS (1) b) 0.5g RESPONSE SPECTRA NO COLLAPSE EVALUATION	**(2) NON-CATEGORY I** CASE-BY-CASE (GO TO NO HAZARD CRITERIA)	**(2) NON-CATEGORY I** CASE-BY-CASE (GO TO NO HAZARD CRITERIA)

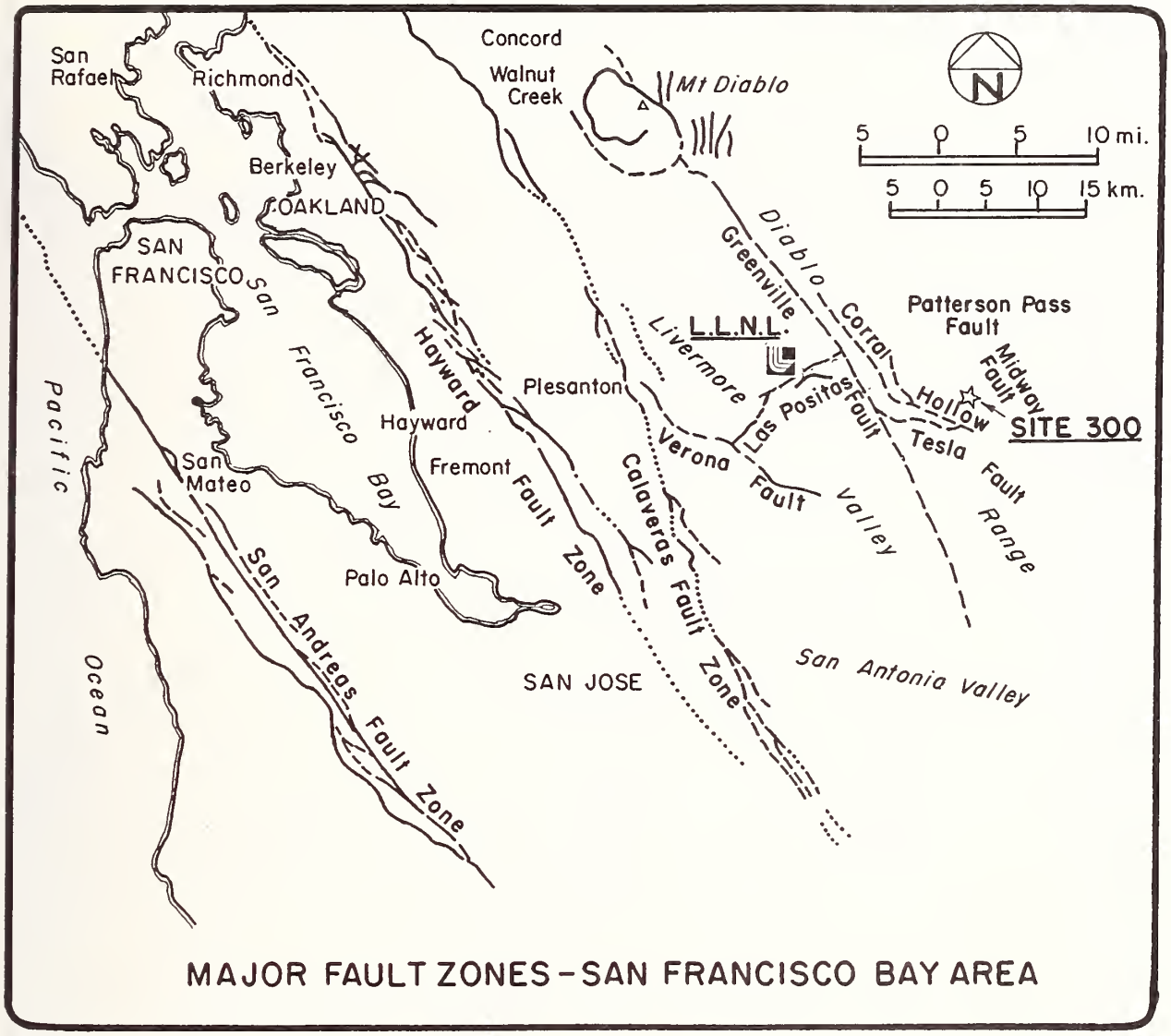

MAJOR FAULT ZONES - SAN FRANCISCO BAY AREA

Figure 1 Major earthquake fault zones which pose a seismic hazard to LLNL.

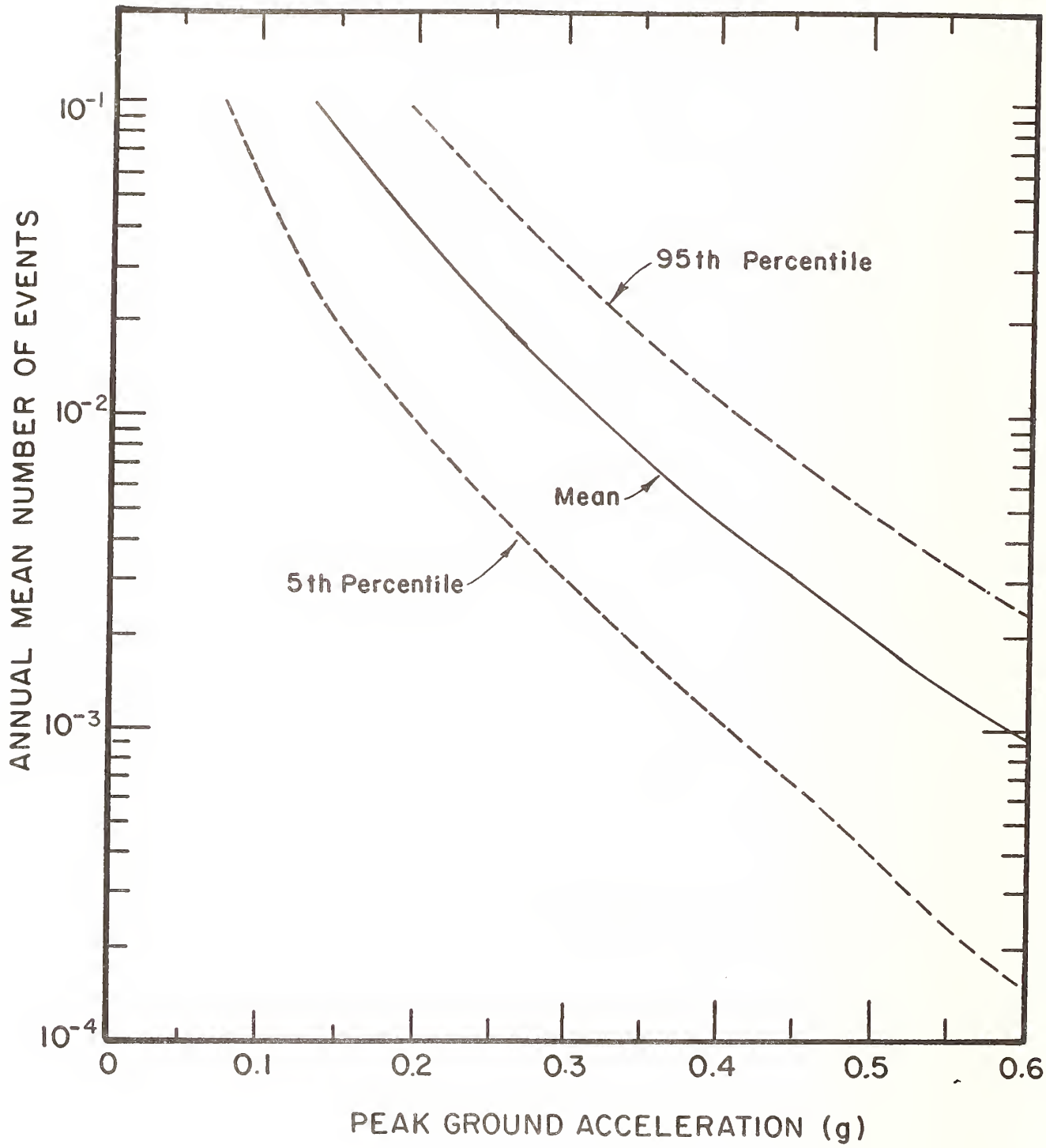

Figure 2a Seismic Hazard Curves for all LLNL site: Peak Ground Acceleration (g).

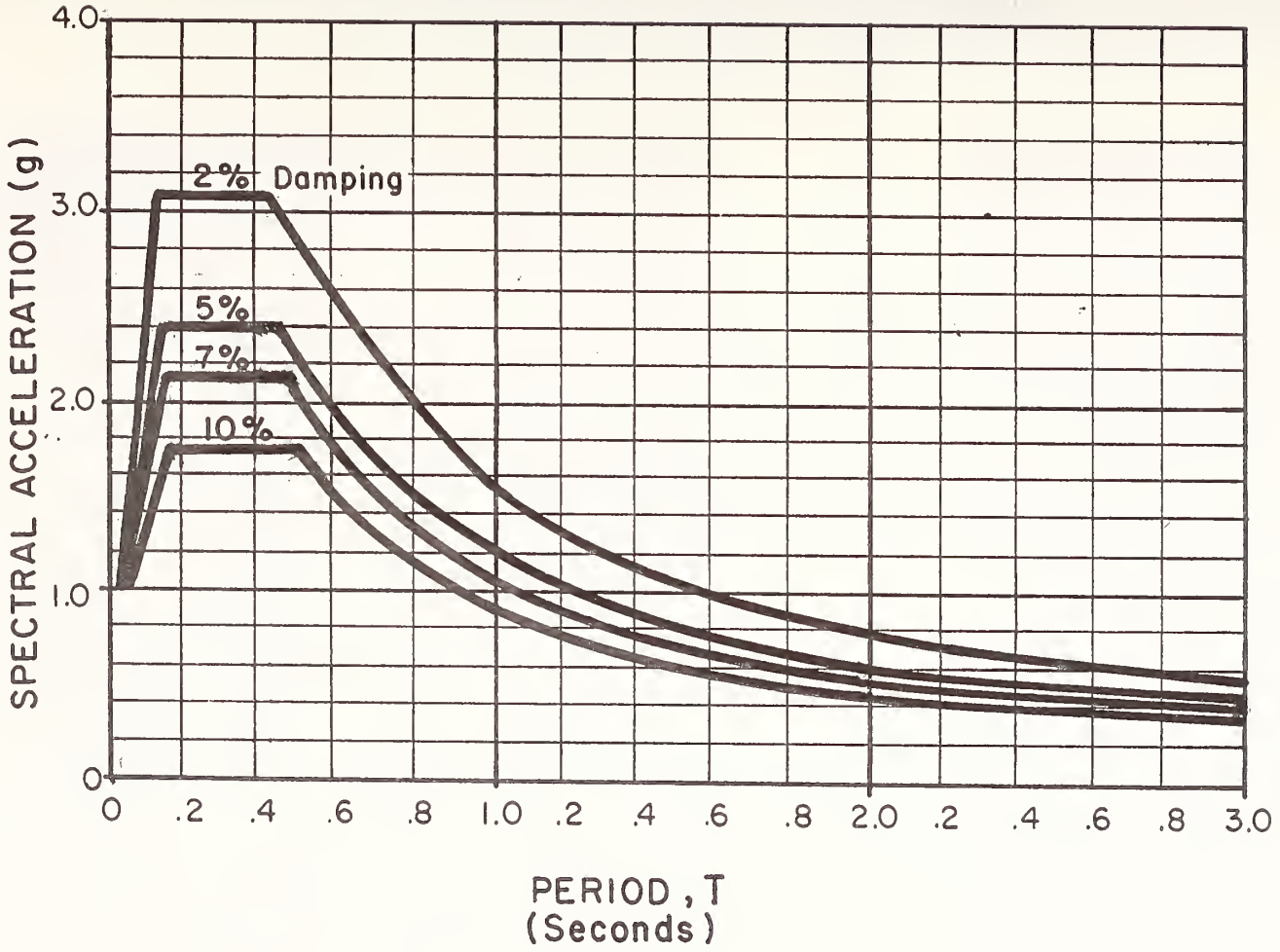

Figure 2b LLNL Seismic Design Acceleration Response Spectra normalized to 1g, currently used for new facilities.

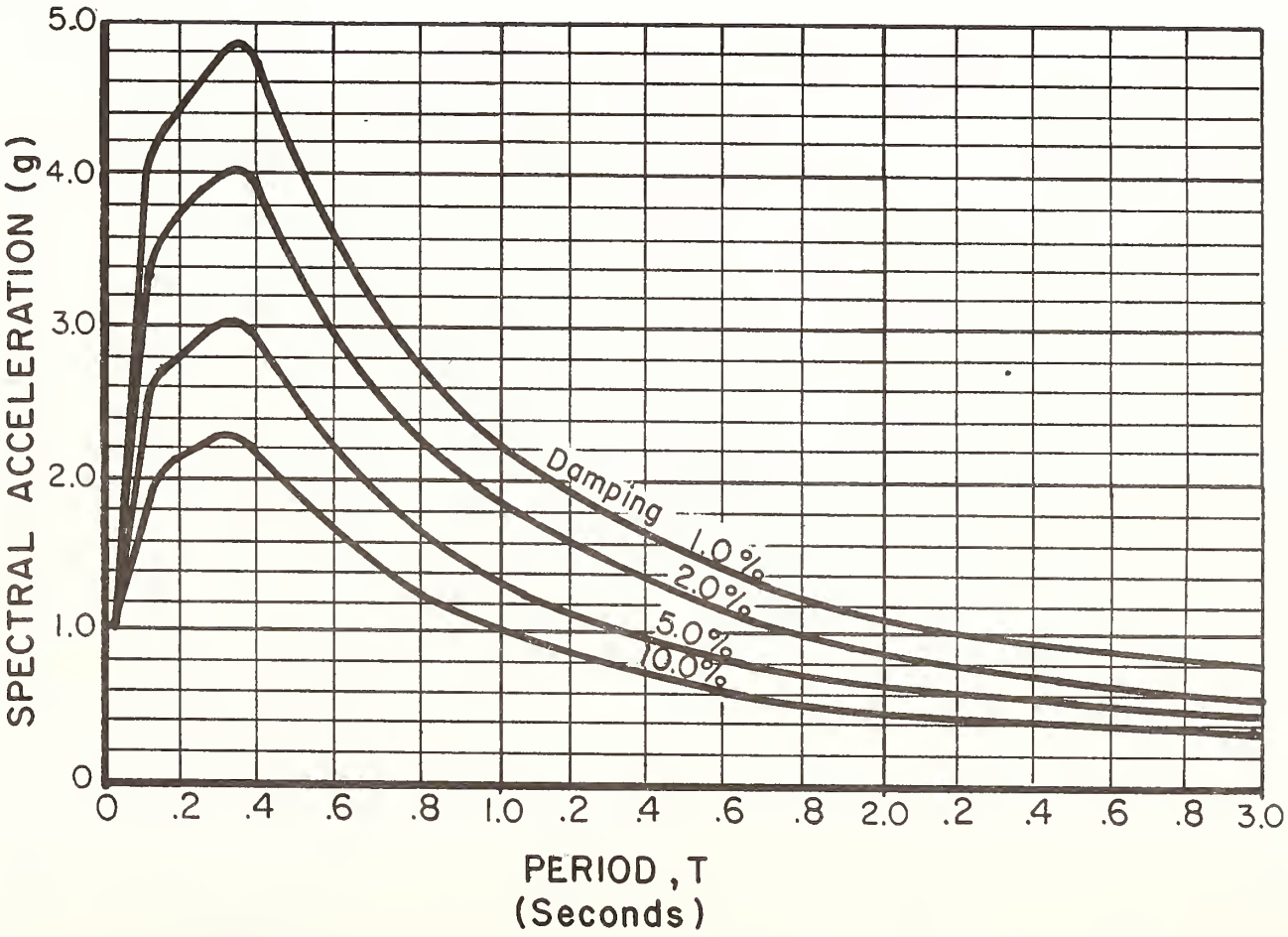

Figure 3 LLNL Design Acceleration Response Spectra normalized to 1g, used 1971 to May 1989.

Figure 4 Building 311, as originally designed and constructed.

Figure 5 Building 311, after major seismic upgrade showing external buttresses.

Figure 6 Building 311, Second floor drag-struct anchor bolts.

Figure 7 Building 311, Roof level drag-struct shear anchors.

Figure 8 Building 113, as originally designed and constructed.

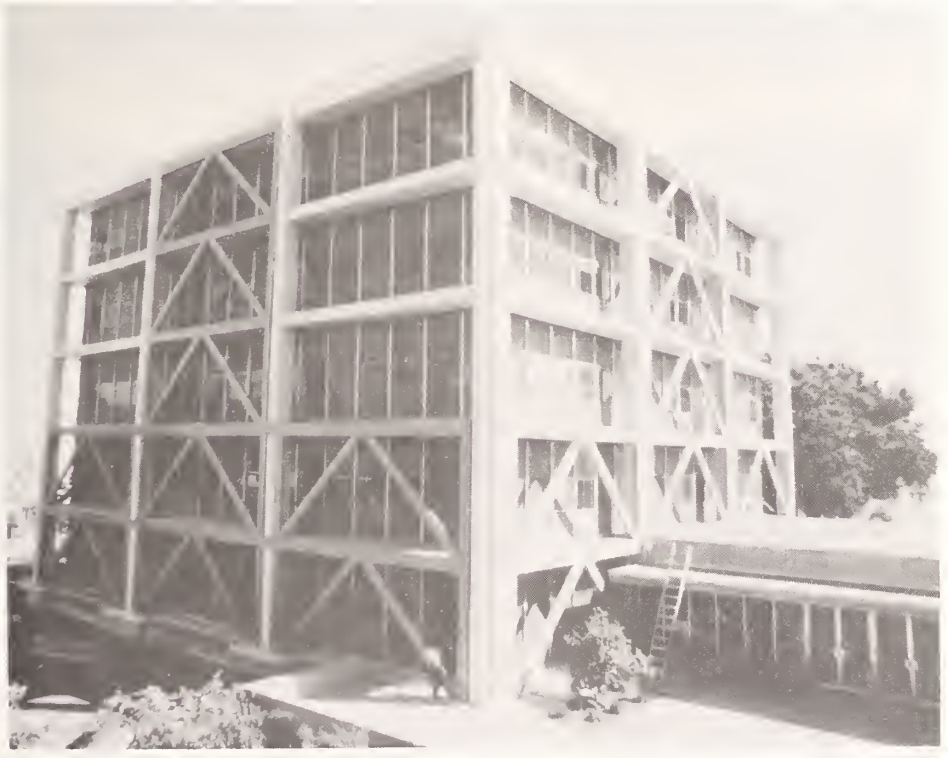

Figure 9 Building 113, after major seismic upgrade showing "K" brace frames.

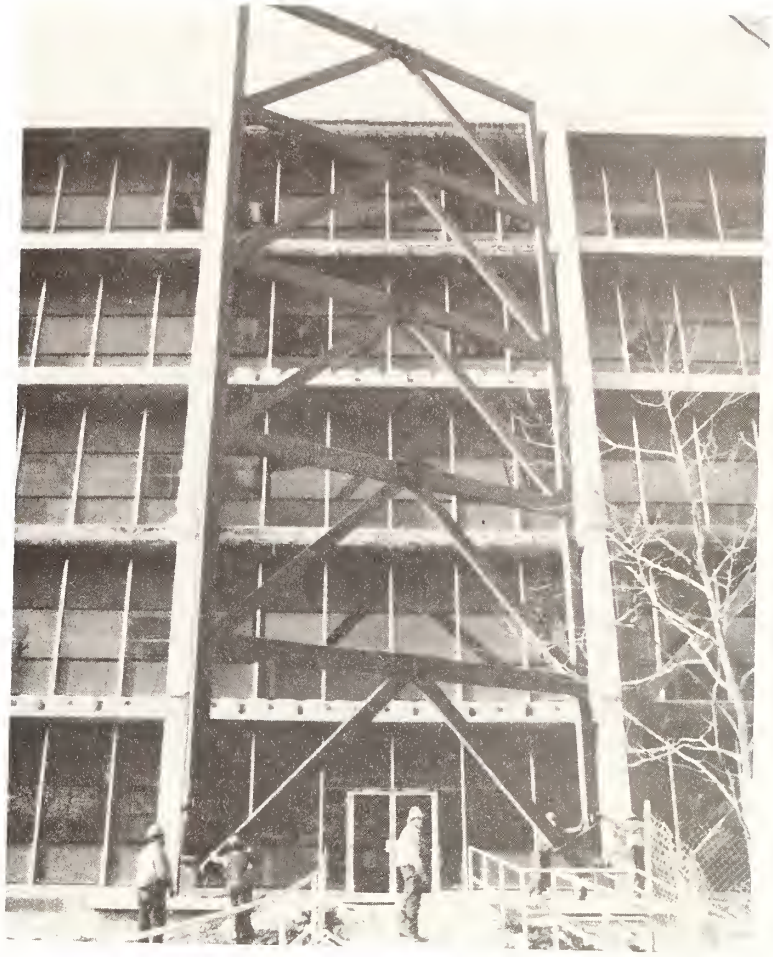

Figure 10 Building 113, "K" brace frames being lifted into place.

Figure 11 Building 111, as originally designed and constructed.

Figure 12 Building 111, stair tower upgrade, lateral supports are attached to each building floor level.

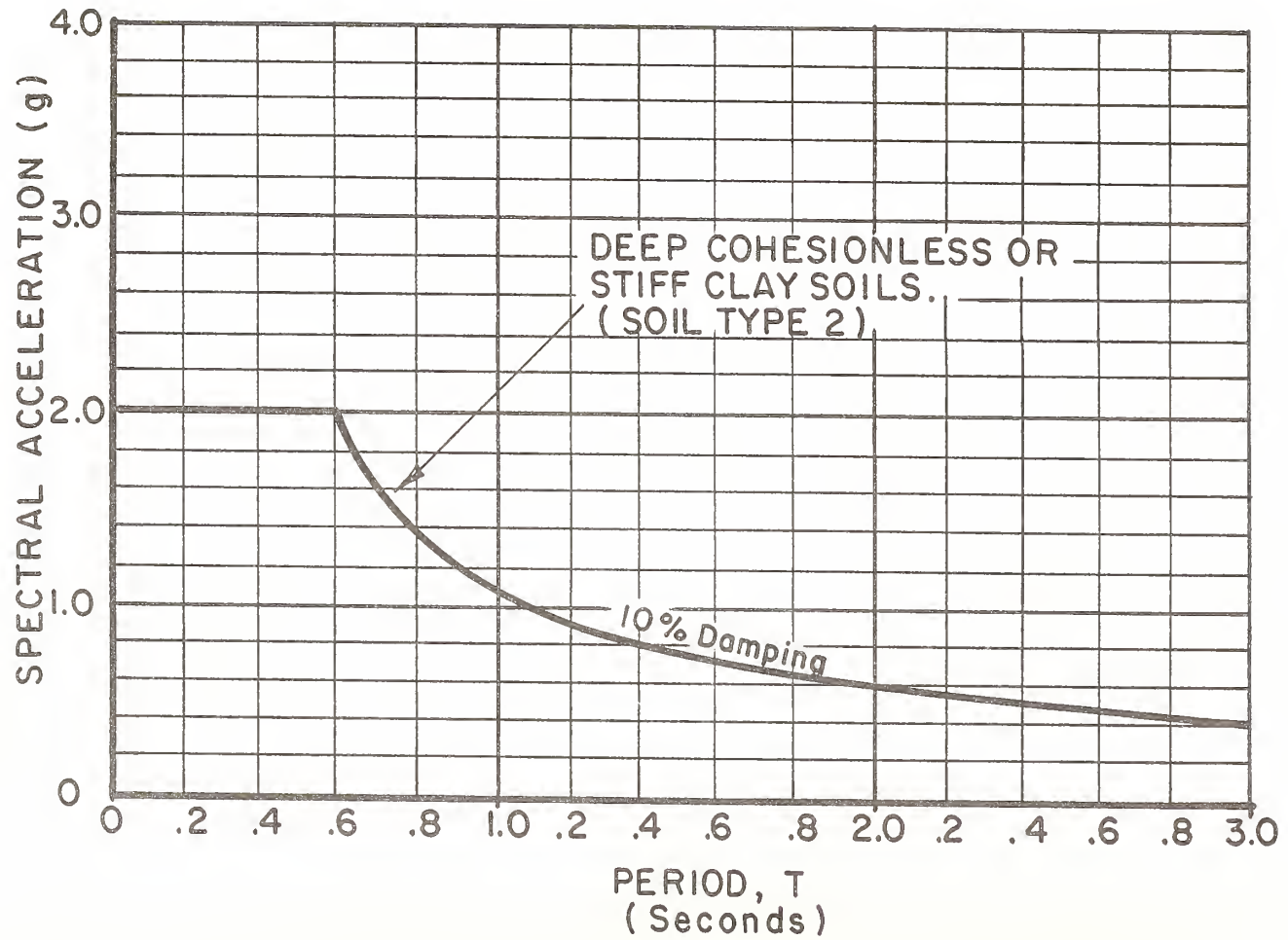

Figure 13 LLNL Seismic Design Acceleration Response Spectra (10% Damping) normalized to 1g, based on the 1988 Uniform Building Code spectrum shape, used for B-111 upgrade.

Figure 14 Building 111, artist rendering of the completed seismic upgrade (currently under construction) showing the new external towers (buttresses).

Attenuation Characteristics of Ground Strains Induced During Earthquake

by

Ken-ichi TOKIDA*1, Keiichi TAMURA*2 and Koh AIZAWA*3

SUMMARY

The appropriate estimation of ground strains induced during earthquake is indispensable for the seismic design of buried lifeline facilities such as pipeline systems.

The ground strains induced during earthquake are estimated with use of the dense instrument array data obtained at the Public Works Research Institute during past 78 earthquakes, and the empirical formulae of attenuation of maximum ground strains in terms of earthquake magnitude and epicentral distance are proposed.

KEY WORDS : Array Observation System, Ground Strain, Attenuation Characteristics

1. INTRODUCTION

It is well recognized that dynamic behavior of lifeline facilities such as tubular piping systems embedded in ground essentially depends on the dynamic response of subsurface grounds. The seismic deformation method, which considers ground strains induced during earthquakes as seismic effects instead of inertia forces, was developed and is now in practical use for seismic design of extended structures embedded in ground [1]. Although investigations on actual ground strains induced during earthquake are essential to assess appropriate seismic effects to be considered in the seismic deformation method, few studies have been conducted, mostly due to the lack of measured data [2].

This paper presents analysis on the ground strains with use of the dense instrument array data obtained at the Public Works Research Institute (PWRI) during past 78 earthquakes. The empirical formulae of attenuation of maximum ground strains in terms of earthquake magnitude and epicentral distance are proposed by multiple regression analysis.

2. ARRAY INSTRUMENTATION AT PWRI SITE [3]

Theare are tow local laboratory arrays called Field-A and Field-B in PWRI campus, as shown in Fig.1. Subsurface geological condition around the PWRI is almost uniform, i.e. diluvial sandy and silty deposits with approximate thickness of 50 m rest on gravel formations. Shear wave velocity of the upper and lower diluvial deposits is approximately 250 m/s and 400 m/s, respectively.

Fig.2 shows the instrumentation at Field-A and Field-B. 13 three-components accelerometers are installed at Field-A, that is 3 on the ground surface, 5 at the depth of 2 m and 5 at the depth of about 50 m, along a cross shaped configuration with each length of 100 m. 6 three-components accelerometers are installed at Field-B, that is, 1 at the depth of 2 m, 4 at the depth of 50 m and 1 at the depth 96 m, along a L shaped configuration with the length of 100 m and 50 m. The direction of the cross configuration as well as the direction of the sensors is oriented along north-south and east-west directions.

Signals from 19 accelerometers at both Field-A and Field-B are simultaneously transmitted by cable to the central processing room, where the signals are digitized with a time interval of 1/100 second by 12 bits AD converters. The observation was started in July, 1979.

3. CALCULATION METHOD OF GROUND STRAINS

A tetrahedron consisting of 4 obsevation points(i, j, m and p) as shown in Fig.3 is considered to calculate ground strains. According to a standard three dimensional finite element analysis procedure [4], the ground displacement u(t), v(t) and w(t) in x(East-West), y(North-South) and z(Up-Down) directions, respectively, in the tetrahedron are assumed to be linear as

$$\begin{aligned} u(t) &= \alpha_1 + \alpha_2 X + \alpha_3 y + \alpha_4 Z \\ v(t) &= \alpha_5 + \alpha_6 X + \alpha_7 y + \alpha_8 Z \\ w(t) &= \alpha_9 + \alpha_{10} X + \alpha_{11} y + \alpha_{12} Z \end{aligned} \qquad (1)$$

*1 Head, Ground Vibration Division, Earthquake Disaster Prevention Department, Public Works Research Institute, Ministry of Construction.
*2 Senior Research Engineer, ditto.
*3 Research Engineer, ditto.

in which $\alpha_i (i=1 \sim 12)$ represent constants. Determining α_i by prescribing coordinates of the four observation points i, j, m and p, Eq.(1) can be written in the form

$$\begin{Bmatrix} u(t) \\ v(t) \\ w(t) \end{Bmatrix} = \frac{1}{6V} \begin{bmatrix} u_i(t) & u_j(t) & u_m(t) & u_p(t) \\ v_i(t) & v_j(t) & v_m(t) & v_p(t) \\ w_i(t) & w_j(t) & w_m(t) & w_p(t) \end{bmatrix} \cdot H \tag{2}$$

$$H = \begin{Bmatrix} a_i+b_ix+c_iy+d_iz \\ a_j+b_jx+c_jy+d_jz \\ a_m+b_mx+c_my+d_mz \\ a_p+b_px+c_py+d_pz \end{Bmatrix}$$

where

x_k, y_k, z_k (k=i, j, m, p): coordinates of k-th observation point

$u_k(t)$, $v_k(t)$, $w_k(t)$ (k=i, j, m, p): ground displacement at k-th observation point

$$a_i = \begin{vmatrix} x_j & y_j & z_j \\ x_m & y_m & z_m \\ x_p & y_p & z_p \end{vmatrix} \qquad b_i = -\begin{vmatrix} 1 & y_j & z_j \\ 1 & y_m & z_m \\ 1 & y_p & z_p \end{vmatrix}$$

$$c_i = -\begin{vmatrix} x_j & 1 & z_j \\ x_m & 1 & z_m \\ x_p & 1 & z_p \end{vmatrix} \qquad d_i = -\begin{vmatrix} x_j & y_j & 1 \\ x_m & y_m & 1 \\ x_p & y_p & 1 \end{vmatrix} \tag{3}$$

Other constants a_k, b_k, c_k, and d_k (k=j, m, p) can be obtained bychanging the subscript in the order of j, m and p.

$$6V = \begin{vmatrix} 1 & x_i & y_i & z_i \\ 1 & x_j & y_j & z_j \\ 1 & x_m & y_m & z_m \\ 1 & x_p & y_p & z_p \end{vmatrix} \tag{4}$$

Representing ground strains as,

$$\{\varepsilon\} = \begin{Bmatrix} \varepsilon_x \\ \varepsilon_y \\ \varepsilon_z \\ \gamma_{xy} \\ \gamma_{yz} \\ \gamma_{zx} \end{Bmatrix} = \begin{Bmatrix} \partial u/\partial x \\ \partial v/\partial y \\ \partial w/\partial z \\ \partial u/\partial y + \partial v/\partial x \\ \partial v/\partial z + \partial w/\partial y \\ \partial w/\partial x + \partial u/\partial z \end{Bmatrix} \tag{5}$$

substitution of Eq.(2) into Eq.(5) gives

$$\{\varepsilon\} = \frac{1}{6V}[B]\{\delta\}$$

$$= \frac{1}{6V}[B_i, B_j, B_m, B_p]\{\delta\} \tag{6}$$

where

$$[B_k] = \begin{bmatrix} b_k & 0 & 0 \\ 0 & c_k & 0 \\ 0 & 0 & d_k \\ c_k & b_k & 0 \\ 0 & d_k & c_k \\ d_k & 0 & b_k \end{bmatrix} \qquad (k=i, j, m, p) \tag{7}$$

$$\{\delta\} = \begin{Bmatrix} \delta_i \\ \delta_j \\ \delta_m \\ \delta_p \end{Bmatrix} \tag{8}$$

$$\{\delta_k\} = \begin{Bmatrix} u_k \\ v_k \\ w_k \end{Bmatrix} \qquad (k=i, j, m, p) \tag{9}$$

It should be noted here that the ground strains $\{\varepsilon\}$ estimated by Eq.(5) represent the average ground strains in a tetrahedron.

4. CALCULATION OF GROUND STRAINS DURING EARTHQUAKE

The array data have been obtained at PWR1 site during past 100 earthquakes between 1979 and 1989 as shown in Table 1. Among those data, the data obtained during 78 earthquakes with the Japan Meteorological Agency (JMA) magnitude of 4.0 or greater are used for this analysis.

Fig.4 shows acceleration time histories recorded at A2C0(GL-2m) and A46C0(GL=-46m) during the earthquake of February 27, 1983 (EQ-28), with a JMA magnitude of 6.0 and an epicentral distance to the site of 22km. The amplification ratio of maximum acceleration A2C0/A46C0 is 2.0 and 2.6 for N-S component and E-W component, respectively.

Fig. 5 shows displacement time histories of the ground for EQ-28, which are calculated by the double integration of acceleration records. Acceleration records are integrated frequency domain with the lower and higher cut-off frequency of 0.2 Hz and 20 Hz. The amplification ratio of maximum displacement A2C0/A46C0 is 1.4 and 2.0 for N-S and E-W component, respectively.

8 tetrahedrons are formulated to calculate ground strains at Field-A as shown in Fig. 6(a) and 6(b), that is 4 upper-side tetrahedrons for calculating upper level ground strains and 4 lower-side ones for lower level ground strains. 2 tetrahedrons are

considered to calculate lower level ground strains at Field-B as shown in Fig. 6(c).

Fig. 7(a) and (b) show time histories of the upper and lower level ground strains at Field-A calculated for EQ-28, respectively. As seen from Fig. 7, the maximum value of upper level normal ground strains (ε_x, ε_y) is $(100 \sim 200) \times 10^{-6}$ and is larger than that of the lower level normal ground strains, which is about 50×10^{-6}. The maximum value of upper level shear ground strain (γ_{xy}) is about 100×10^{-6} and is lager than that of lower level shear ground strain, which is about 50×10^{-6}.

5. ATTENUATION CHARACTERISTICS OF GROUND STRAINS

It is very important to estimate seismic effect properly in the practical design of structures. Up to the present, not a few attenuation equations of peak ground motions (acceleration, velocity and displacment) have been proposed and they are applied to the seismic design of structures.

In the past analyses on attenuation characteristics of maximum ground motions and absolute acceleration response spectra, based on accelerograph records, the following empirical formula is often used as a practical formula [5].

$$X = a \times 10^{bM} \times (\Delta + \Delta_0)^c \qquad (10)$$

where

X : Maximum acceleration, velocity and displacement / absolute acceleration response spectral amplitude
M : Magnitude of earthquake
Δ : Epicentral distance [km]
Δ_0: Constant to adjust X for small epicental distance
a, b, c : Coefficients

The attenuation characteristics of ground strains on the horizontal plane ε_x, ε_y and γ_{xy}, which are important to be considered in the seismic design of underground structures, are discussed in this analysis. Since the peak values of the ground strains are different among the tetrahedrons, the average of the peak ground strains over the 4 (Field-A) or 2 (Field-B) tetrahedrons is defined as the maximum ground strains. Furthermore, larger value of ε_x and ε_y is defined as the maximum normal strain ε.

The same expression with Eq.(10) is assumed to represent the attenuation characteristics of maximum ground strains. Δ_0 in Eq.(10) is assumed to be 30 km. The empirical formulae of maximum ground strains are written as

$$\left.\begin{matrix}\varepsilon \\ \gamma\end{matrix}\right\} = a \times 10^{bM} \times (\Delta + 30)^c \qquad (11)$$

where

ε : Maximum normal strain
γ : Maximum shear strain

Table 2 shows the coefficients a, b and c obtained by multiple regression analysis. From Table 2, the attenuation formulae of the maximum ground strains are obtained as

Upper Level ground strains at Field-A:

$$\varepsilon = 1.237 \times 10^{0.493M} \times (\Delta + 30)^{-0.741} \times 10^{-6}$$
$$\gamma = 0.894 \times 10^{0.548M} \times (\Delta + 30)^{-0.774} \times 10^{-6}$$

Lower Level ground strains at Field-A:

$$\varepsilon = 1.285 \times 10^{0.309M} \times (\Delta + 30)^{-0.370} \times 10^{-6}$$
$$\gamma = 1.549 \times 10^{0.293M} \times (\Delta + 30)^{-0.319} \times 10^{-6}$$

Lower Level ground strains at Field-B:

$$\varepsilon = 1.506 \times 10^{0.358M} \times (\Delta + 30)^{-0.569} \times 10^{-6}$$
$$\gamma = 4.860 \times 10^{0.312M} \times (\Delta + 30)^{-0.596} \times 10^{-6} \qquad (12)$$

Fig.8 shows the attenuation of maximum ground strains ε and γ calculated by Eq.(5) for each event, comparing with predicted value by Eq.(12). The followings are pointed out from Fig.8.

1) The maximum normal upper level ground strains and lower level ground strains at Field-A are distributed in the range from 5×10^{-6} to 200×10^{-6} and from 4×10^{-6} to 60×10^{-6}, respectively. The maximum shear strains are distributed in the range from 5×10^{-6} to 350×10^{-6} and from 4×10^{-6} to 100×10^{-6} for the upper level ground strains and lower level ground strains, respectively. The maximum normal and shear lower level ground strains at Field-B are distributed in the range from 3×10^{-6} to 70×10^{-6} and from 6×10^{-6} to 100×10^{-6}, respectively.
   The maximum shear ground strain is larger than the maximum normal ground strain calculated from the array data and the upper level ground strain is larger than the lower level ground strain.
2) According to the empirical attenuation equations of ground strain at Field-A, the coefficient b, which represents the effect

of earthquake magnitude on the maximum ground strains, of the upper level ground strains is larger than that of the lower level ground strains. The coefficient c, which represents the effect of epicentral distance on the maximum ground strains, of the upper level ground strains is smaller than that of the lower level ground stains. Those facts indicate that the upper level ground strains are more sensitive to earthquake magnitude and attenuation rate of the upper level ground strains with epicentral distance is larger, as compared with the lower level ground strains.

3) Comparing the empirical formulae of attenuation of the lower level ground strains for Field-A with that for Field-B, the coefficient b is almost same, and the coefficient c for Field-A is a little lager than that for Field-B.
4) Compared with the coefficient c of the attenuation equations of maximum ground accelerations based on SMAC accelerograms, which is -1.2 to -1.3 [5], the coefficient c for maximum ground strains is larger. This means that attenuation of maximum ground strains with epicentral distance is smaller than that of maximum ground accelerations.

6. CONCLUSION

The ground strains induced during earthquakes were evaluated by a finite element method, with use of the dense instrument array data obtained at the Public Works Research Institute. The empirical formulae of attenuation equation of maximum ground strains (Eq.(12)) were presented by multiple regression analysis based on the array data of 78 earthquakes.

The result of this study might be regarded as basic information for assessing the ground strains during earthquakes, however, it should be noted that those results were derived from the data recorded by relatively small ground motions. The accumulation of strong motion records and further investigations should be encouraged.

ACKNOWLEDGEMENTS

This research was motivated based on the array data which has been collected for years under the direction by Dr. T. Iwasaki, Dr. Y. Sasaki, T. Arakawa and Dr. K. Kawashima. The autors would like to express their sincere gratitude to them.

REFERENCES

[1]Public Works Research Institute, "A Proposal for Earthquake Resistant Design Method", Technical Memorandum of PWRI, No.1185, March, 1977(in Japanese)

[2]Arakawa T., Kawashima K. and Tamura K., "Finite Ground Strains Induced during Earthquake for Application to Seismic Design of Underground Structures", Fifth International Conference on Numerical Methods in Geomechanics, April, 1985

[3]Ohkubo T., Iwasaki T. and Kawashima K., "Dense Instrument Array Program of the Public Works Research Institute and Preliminary Analysis of the Records", Proc. of 13th Joint Meeting U.S.-Japan on Wind and Seismic Effects, U.J.N.R., May, 1981

[4]Zienkiewicz, O. C. "The Finite Element Method in Engineering Science", McGraw-Hill, 1971

[5]Kawashima K., Aizawa K. and Takahashi K., "Attenuation of Peak Ground Motion and Absolute Acceleration Response Spectra", Proc. of Eighth World Conference on Earthquake Engineering, July, 1984

[6]Tokida K., Tamura K. and Aizawa K., "Analysis on Strong Ground Motions during Earthquakes Observed by Dense Array at PWRI – Attenuation Characteristics of Ground Strains Induced During Earthquake – ", Technical Memorandum of PWRI, No.2798, August,1989(in Japanese)

[7]Sasaki Y., Tamura K. and Aizawa K., "Analysis on the Finite Ground Strains Induced During Earthquakes", Proc. of Third U.S.-Japan Workshop on Earthquake Disaster Prevention for Lifeline System, U.J.N.R., May, 1989

Table 1 Earthquakes Observed at PWRI

	NO.	DATE TIME	EPICENTER REGION	LON.	LAT.	DEPTH(KM)	JMA MAG.	EPICEN. DIST(KM)
	1	1979.10.09 14:18:49	SW IBARAKI PREF	139° 50' 0"	36° 9' 0"	50	4.1	22
	2	1979.11.25 19:15:23	OFF IBARAKI PREF	141° 0' 0"	36° 41' 0"	90	5.4	104
	3	1979.12.15 12:27:21	CENTRAL CHIBA PREF	140° 22' 0"	35° 31' 0"	80	4.2	72
	4	1979.12.17 08:23:49	COAST OF IBARAKI PREF	140° 35' 0"	36° 28' 0"	60	4.3	60
	5	1980.02.02 18:57:16	NORTHERN KANTO	139° 51' 0"	36° 6' 0"	50	4.2	20
	6	1980.04.22 14:34:16	S OFF CHUBU	137° 55' 0"	32° 9' 0"	400	6.6	484
	7	1980.05.07 03:07:36	NORTHERN KANTO	139° 57' 0"	36° 4' 0"	50	4.0	13
	8	1980.05.12 01:01:03	NORTHERN KANTO	140° 4' 0"	36° 12' 0"	60	4.4	9
	9	1980.06.18 16:25:08	TOKYO BAY REGION	140° 1' 0"	35° 38' 0"	80	4.6	55
	10	1980.06.29 16:20:08	IZU PEN REGION	139° 14' 0"	34° 55' 0"	10	6.7	154
	11	1980.09.24 04:10:23	SOUTHERN KANTO	139° 48' 0"	35° 58' 0"	80	5.4	30
×	12	1980.09.25 02:54:23	SE COAST OF KANTO	140° 13' 0"	35° 31' 0"	80	6.1	69
	13	1980.09.25 02:54:23	SE COAST OF KANTO	140° 13' 0"	35° 31' 0"	80	6.1	69
	14	1981.01.28 12:47:44	NORTHERN KANTO	139° 51' 0"	36° 10' 0"	60	5.0	21
	15	1981.03.12 04:16:41	SOUTHERN KANTO	140° 16' 0"	35° 54' 0"	60	4.7	30
	16	1981.03.02 18:24:44	E OFF KANTO	141° 8' 0"	35° 48' 0"	40	5.8	102
×	17	1981.03.03 21:52:12	NORTHERN KANTO	139° 48' 0"	36° 10' 0"	60	3.5	25
	18	1981.09.14 05:24:08	NORTHERN KANTO	140° 7' 0"	36° 12' 0"	70	4.8	10
×	19	1981.10.14 06:35:41	NORTHERN KANTO	139° 56' 0"	36° 3' 0"	50	3.5	15
	20	1981.11.30 09:27:00	NORTHERN KANTO	139° 54' 0"	36° 4' 0"	50	4.4	17
	21	1982.03.07 08:14:36	E COAST OF KANTO	140° 39' 0"	36° 28' 0"	60	5.5	64
	22	1982.07.23 23:23:51	E OFF KANTO	141° 57' 0"	36° 11' 0"	30	7.0	169
	23	1982.10.25 00:50:01	E COAST OF KANTO	140° 31' 0"	35° 54' 0"	40	4.2	47
	24	1982.12.08 06:45:47	NORTHERN KANTO	139° 53' 0"	36° 6' 0"	50	4.2	17
×	25	1982.12.16 08:55:53	NORTHERN KANTO	139° 55' 0"	36° 2' 0"	50	3.9	17
	26	1982.12.29 19:31:03	NORTHERN KANTO	139° 59' 0"	36° 12' 0"	50	4.0	12
	27	1983.01.08 03:18:59	NORTHERN KANTO	139° 54' 6"	36° 5'12"	52	4.9	16
	28	1983.02.27 21:14:21	SOUTHERN KANTO	140° 9'18"	35° 56'12"	72	6.0	22
	29	1983.04.24 20:21:55	NORTHERN KANTO	139° 56'24"	36° 1'54"	55	4.4	16
	30	1983.05.04 10:05:47	NORTHERN KANTO	139° 53'30"	36° 4'36"	55	4.3	17
	31	1983.07.02 07:03:42	E COAST OF S TOHOKU	141° 11'30"	36° 54'18"	54	5.8	132
	32	1983.09.02 12:05:47	E OFF KANTO	141° 1' 6"	36° 40' 0"	49	5.2	104
	33	1983.10.15 11:58:08	NORTHERN KANTO	139° 53'24"	36° 5'18"	56	4.7	17
	34	1983.10.28 10:50:32	NORTHERN KANTO	140° 1'24"	36° 12'12"	60	5.1	10
×	35	1983.10.28 12:41:14	NORTHERN KANTO	139° 59'48"	36° 13' 0"	56	3.8	13
	36	1983.12.11 04:53:28	NORTHERN KANTO	140° 7'36"	36° 15' 6"	56	4.3	15
×	37	1983.12.12 18:18:08	NORTHERN KANTO	140° 1' 0"	36° 13' 0"	52	3.6	12
	38	1983.12.30 11:30:40	E COAST OF KANTO	140° 45' 0"	35° 40'30"	52	5.3	79
	39	1984.01.01 18:03:41	S OFF KINKI	136° 50'30"	33° 37'12"	388	7.3	405
	40	1984.01.02 18:22:27	NORTHERN KANTO	139° 54' 0"	36° 5'18"	52	4.1	16
×	41	1984.01.09 19:23:56	NORTHERN KANTO	140° 1'48"	36° 12'18"	59	3.6	11
	42	1984.01.17 20:13:41	E OFF KANTO	141° 14'48"	36° 26'54"	43	5.6	111
	43	1984.01.18 00:31:56	E OFF KANTO	141° 16' 0"	36° 26'42"	43	5.9	113
	44	1984.02.21 20:51:52	NORTHERN KANTO	140° 7'42"	36° 8' 0"	79	5.0	6
	45	1984.03.06 11:17:20	NEAR TORISHIMA	139° 12'18"	29° 20'24"	452	7.9	758
×	46	1984.03.25 07:25:12	NORTHERN KANTO	140° 2'54"	36° 5' 0"	55	3.5	6
	47	1984.05.23 07:38:12	NORTHERN KANTO	139° 51'12"	36° 8'54"	61	4.6	20
	48	1984.05.30 09:49:37	NORTHERN KANTO	139° 56'36"	36° 1'54"	54	4.2	16
	49	1984.06.30 02:45:26	NORTHERN KANTO	139° 51'42"	36° 8'42"	61	5.0	19
	50	1984.06.30 07:09:57	NORTHERN KANTO	139° 49'30"	36° 9'30"	60	4.3	23
	51	1984.07.26 13:52:19	NORTHERN KANTO	140° 3'18"	36° 11' 0"	61	4.8	7
	52	1984.11.11 21:33:18	NORTHERN KANTO	140° 4'36"	36° 11'36"	56	4.0	8
×	53	1984.12.01 22:16:56	NORTHERN KANTO	139° 52'54"	36° 4'12"	51	3.7	19
×	54	1985.02.03 18:20:21	SW IBARAKI PREF	139° 50'24"	36° 10'24"	58	3.8	22
	55	1985.03.20 14:53:50	SW IBARAKI PREF	139° 53'18"	36° 4'24"	54	4.6	18
	56	1985.05.22 16:16:43	SW IBARAKI PREF	139° 56'36"	36° 1'42"	56	4.3	16
	57	1985.07.11 23:58:19	SOUTHERN IBARAKI PREF	140° 17'30"	35° 56'42"	46	4.2	28
×	58	1985.08.10 13:13:47	UNKNOWN					
	59	1985.08.13 19:58:02	SW IBARAKI PREF	139° 54'30"	36° 9' 6"	56	4.0	15
	60	1985.09.12 09:33:07	SW IBARAKI PREF	139° 54'30"	36° 4'24"	50	4.1	16
	61	1985.10.04 21:25:52	SOUTHERN IBARAKI PREF	140° 9'30"	35° 52' 6"	78	6.1	29
	62	1985.11.22 13:17:01	SW IBARAKI PREF	139° 58'36"	36° 1'54"	52	4.9	14
	63	1986.02.12 11:59:32	E OFF IBARAKI PREF	141° 5' 0"	36° 25' 0"	44	6.1	96
	64	1986.06.15 08:53:23	SW IBARAKI PREF	139° 52'18"	36° 9' 6"	57	4.0	19
	65	1986.06.24 11:53:10	SE OFF BOSO PENINSULA	140° 43'12"	34° 49'24"	73	6.5	156
	66	1986.09.20 12:04:58	NORTHERN IBARAKI PREF	140° 39'36"	36° 28'24"	56	5.0	65
	67	1986.11.15 15:06:44	E OFF IBARAKI PREF	140° 55'42"	36° 23'42"	43	5.0	82
	68	1986.11.29 07:29:35	E OFF IBARAKI PREF	141° 10'48"	36° 23'30"	42	5.8	104
	69	1987.02.06 22:16:15	E OFF FUKUSHIMA PREF	141° 53'48"	36° 57'42"	35	6.7	188
×	70	1987.02.12 04:52:04	UNKNOWN					
	71	1987.02.22 05:39:02	SW IBARAKI PREF	139° 46'54"	36° 1'30"	90	4.4	29
×	72	1987.02.23 08:05:03	SW IBARAKI PREF	140° 8' 6"	36° 12'30"	52	3.9	11
	73	1987.03.10 09:37:45	NORTHERN IBARAKI PREF	140° 43'24"	36° 28'54"	66	4.8	71
×	74	1987.03.25 18:32:00	SW IBARAKI PREF	140° 3'12"	36° 11'54"	59	3.6	9
	75	1987.04.07 09:40:43	E OFF FUKUSHIMA PREF	141° 52' 0"	37° 18' 0"	44	6.6	207
	76	1987.04.10 19:59:40	SW IBARAKI PREF	139° 52'30"	36° 7'12"	61	4.9	18
	77	1987.04.23 05:13:23	E OFF FUKUSHIMA PREF	141° 37'36"	37° 5'18"	47	6.5	175
×	78	1987.05.28 00:31:17	SW IBARAKI PREF	139° 50'36"	36° 10' 0"	59	3.7	21
	79	1987.06.11 16:00:32	SW IBARAKI PREF	140° 2'54"	36° 10'48"	55	3.9	8
	80	1987.06.30 18:17:08	SW IBARAKI PREF	140° 5'18"	36° 11' 0"	57	4.9	7

NOTE : LOCATION OF PWRI IS AS FOLLOWS. 140° 4.5'E, 36° 7.4'N

Table 1 Earthquakes Observed at PWRI (continued)

	NO.	DATE TIME	EPICENTER REGION	LON.	LAT.	DEPTH(KM)	JMA MAG.	EPICEN. DIS(KM)
×	81	1987.07.05 16:58:08	SW IBARAKI PREF	140° 4'42"	36°12'12"	56	3.6	9
	82	1987.07.12 13:31:30	SW IBARAKI PREF	140° 3'36"	36° 8'42"	57	4.6	3
	83	1987.07.27 16:06:47	SW IBARAKI PREF	140° 4' 6"	36°10'12"	56	4.1	5
×	84	1987.08.24 15:23:41	SW IBARAKI PREF	139°55'30"	36° 4'18"	51	3.7	15
	85	1987.09.24 13:55:21	E OFF IBARAKI PREF	141°19' 6"	36°37'36"	41	5.8	125
×	86	1987.11.23 17:40:08	SW IBARAKI PREF	140° 3'18"	36°12' 0"	54	3.5	9
	87	1987.12.10 18:32:45	SW IBARAKI PREF	140° 0'42"	36°12'42"	59	4.0	12
	88	1987.12.17 11:09:17	KUJUKURI COAST BOSO PEN	140°29'48"	35°22'18"	58	6.7	92
×	89	1988.02.07 16:59:25	SW IBARAKI PREF	140° 0'54"	36° 6'48"	53	3.5	5
	90	1988.03.18 05:34:29	TOKYO PREF	139°38'48"	35°39'42"	96	6.0	64
	91	1988.07.15 09:51	SW IBARAKI PREF	140° 6' 0"	36°14' 0"	62	4.5	13
	92	1988.09.16 03:19	SW IBARAKI PREF	140° 5' 0"	36°12' 0"	59	4.4	9
×	93	1988.10.31 01:25	SW IBARAKI PREF	140° 7' 0"	36°11' 0"	56	3.8	8
	94	1988.12.28 18:02	SW IBARAKI PREF	139°56' 0"	36° 4' 0"	53	4.3	14
	95	1989.02.19 21:27	SW IBARAKI PREF	139°55' 0"	36° 0' 0"	54	5.6	20
	96	1989.03.06 23:39	NORTHERN CHIBA PREF	140°44' 0"	35°42' 0"	61	5.9	76
	97	1989.03.11 16:12	SOUTHERN IBARAKI PREF	140°35' 0"	35°55' 0"	42	4.9	51
×	98	1989.03.17 20:52	SW IBARAKI PREF	139°56' 0"	36° 6' 0"	58	3.9	13
	99	1989.04.12 04:41	SW IBARAKI PREF	139°54' 0"	36° 5' 0"	58	4.2	16
	100	1989.04.26 02:18	NORTHERN CHIBA PREF	140°29' 0"	35°54' 0"	65	5.3	44

NOTE : LOCATION OF PWRI IS AS FOLLOWS. 140° 4.5'E, 36° 7.4'N

x : unused in this analysis

Table 2 Coefficients of Attenuation Equation

Field	Strain		Coefficient a	Coefficient b	Coefficient c	Correlation Coefficient	Standard Error	Number of Data
A	Upper Level Ground Strain	ε	1.237	0.493	-0.741	0.829	0.206	65
		γ	0.894	0.548	-0.774	0.856	0.210	65
	Lower Level Ground Strain	ε	1.285	0.309	-0.370	0.708	0.213	74
		γ	1.549	0.293	-0.319	0.699	0.212	76
B	Lower Level Ground Strain	ε	1.506	0.358	-0.569	0.736	0.197	66
		γ	4.860	0.312	-0.596	0.690	0.190	53

Attenuation Equation : $\left.\begin{matrix}\varepsilon\\ \gamma\end{matrix}\right\} = a \times 10^{bM} \times (\Delta + 30)^{c} \times 10^{-\sigma}$

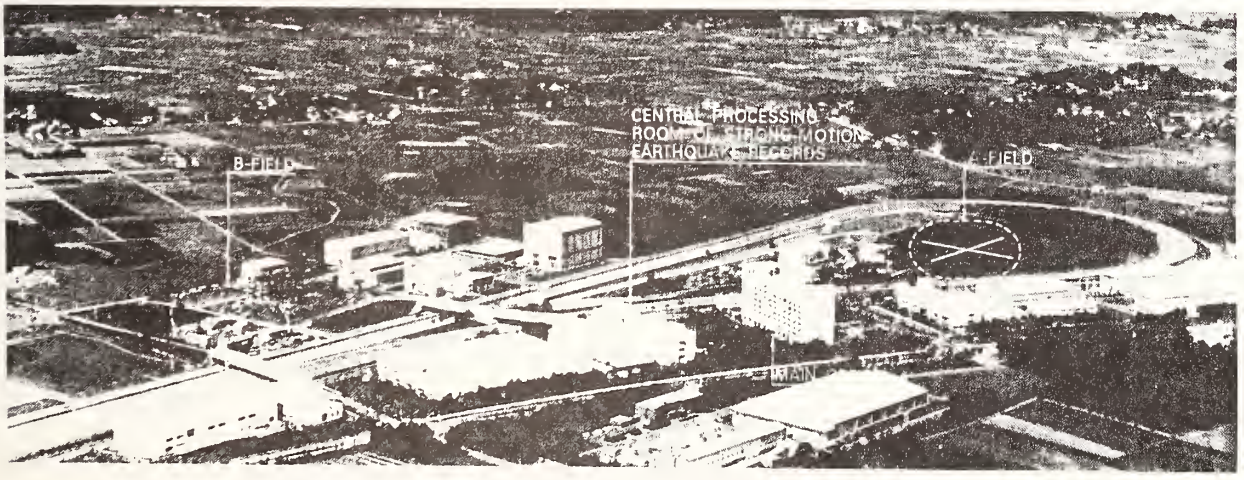

Figure 1 Local Laboratory Array at PWRI

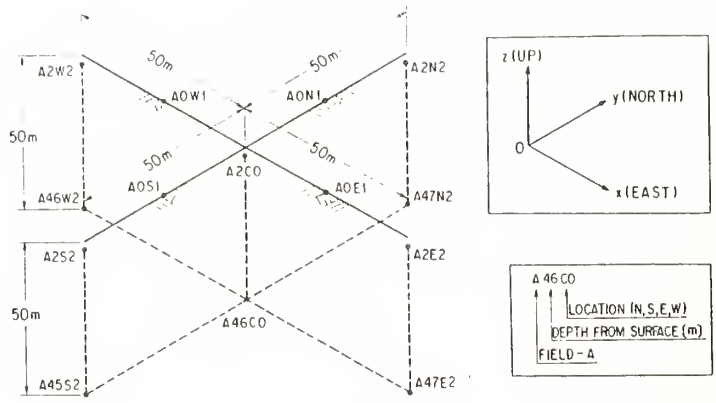

(a) Field-A

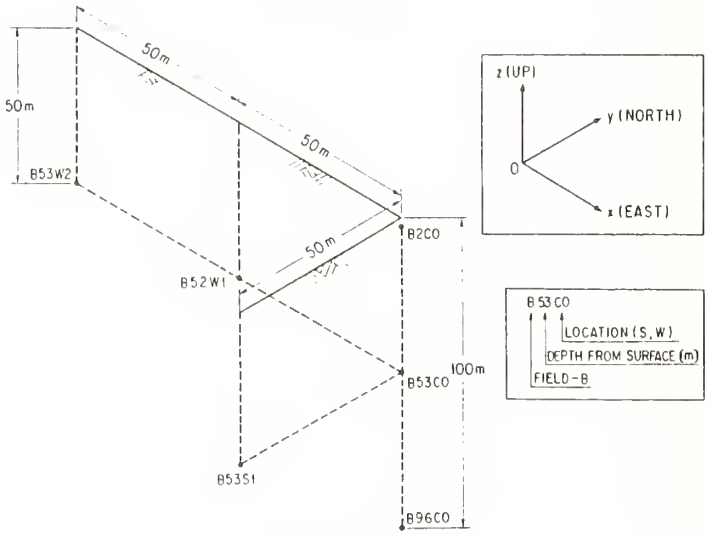

(b) Field-B

Figure 2 Array Configuration at PWRI

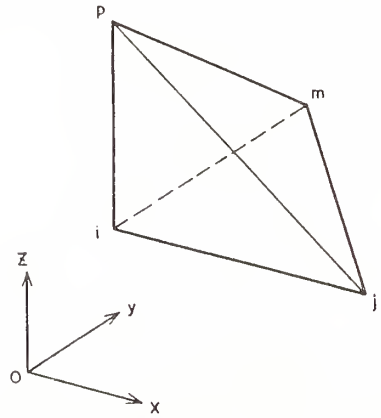

Figure 3 Tetrahedron for Calculation of Ground Strains

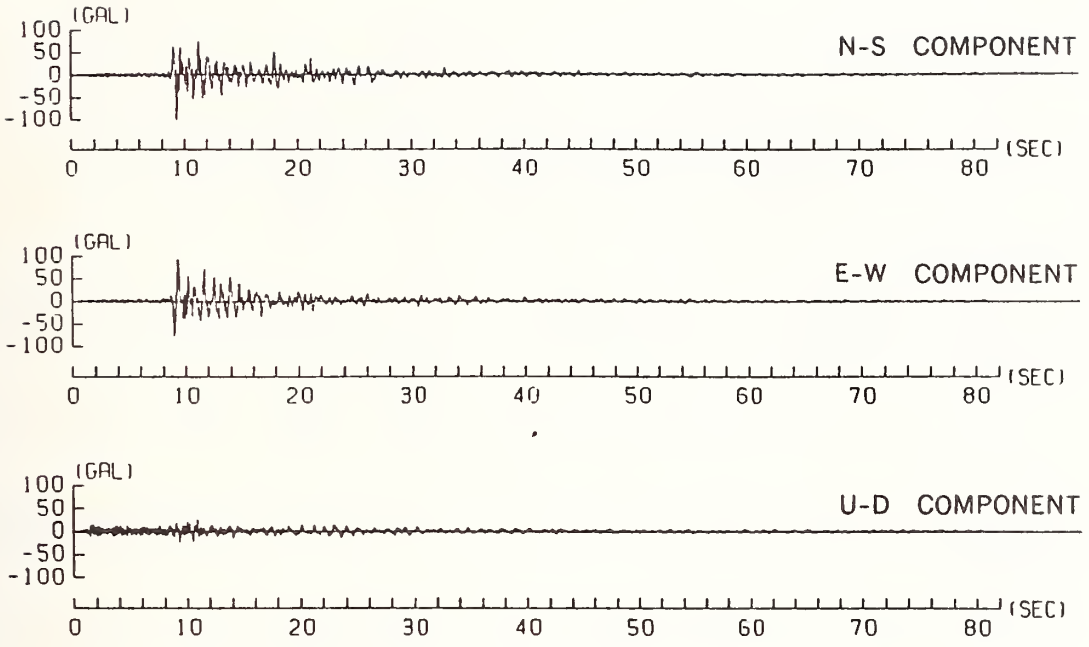

(a) A2C0

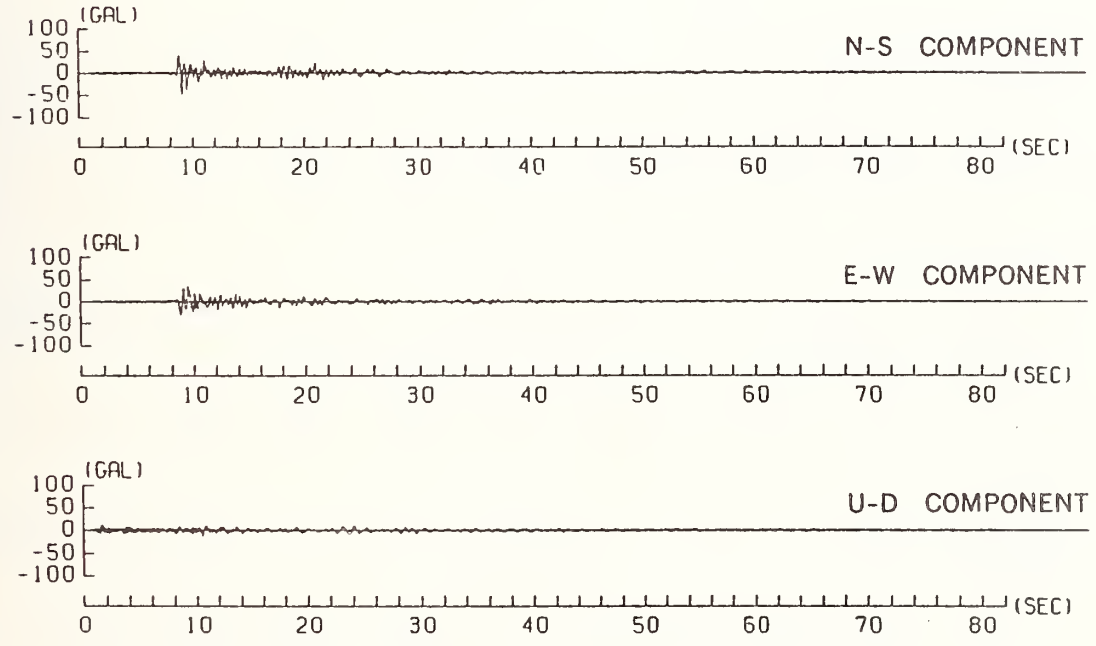

(b) A46C0

Figure 4 Time History of the Obseved Acceleration (A2C0 and A46C0, EQ-28)

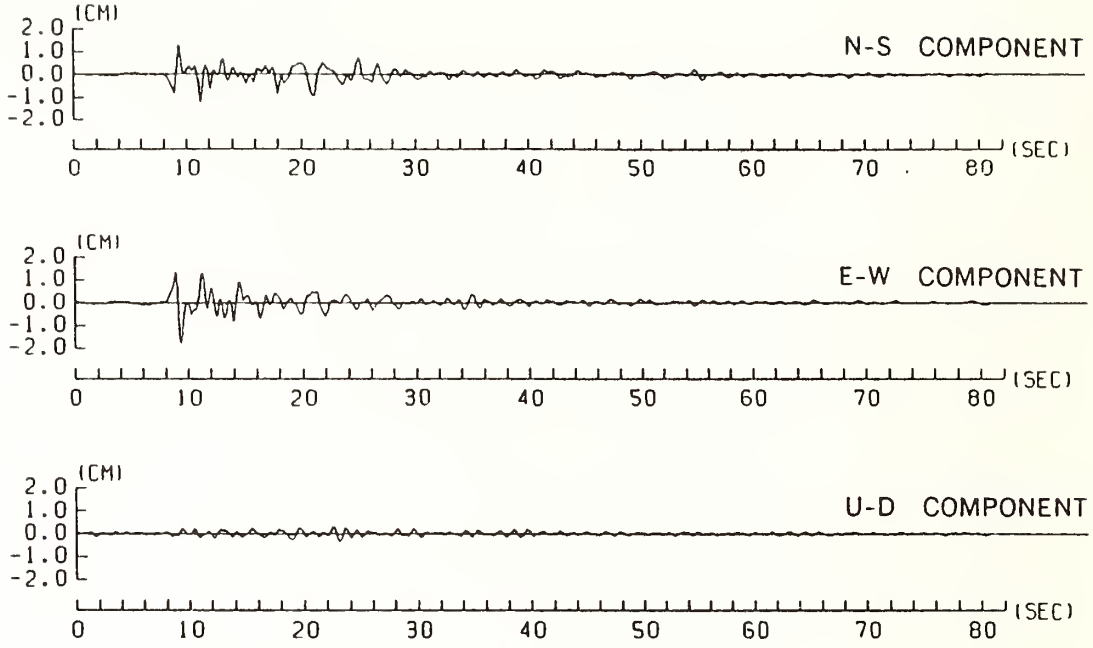

(a) A2C0

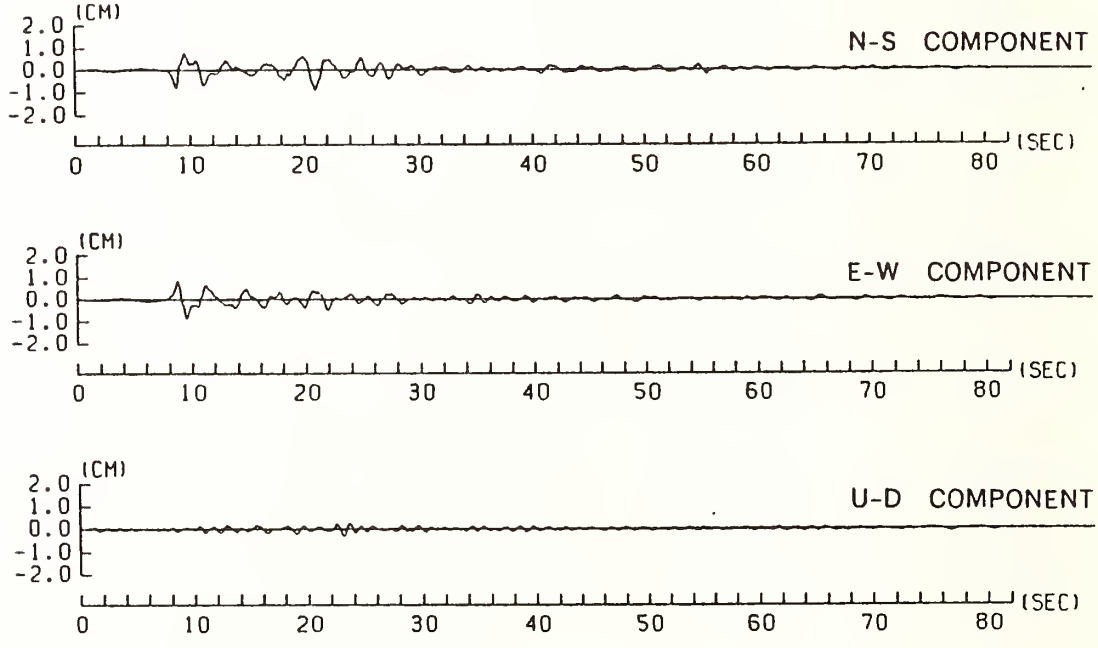

(b) A46C0

Figure 5 Time History of the Calculated Displacement (A2C0 and A46C0, EQ-28)

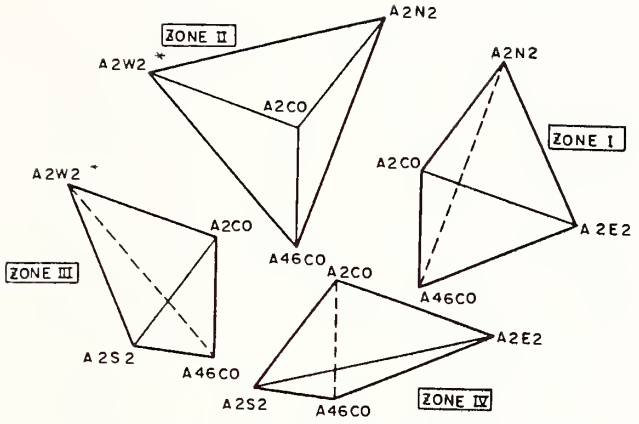

(a) Upper Level Ground Strains at Field-A

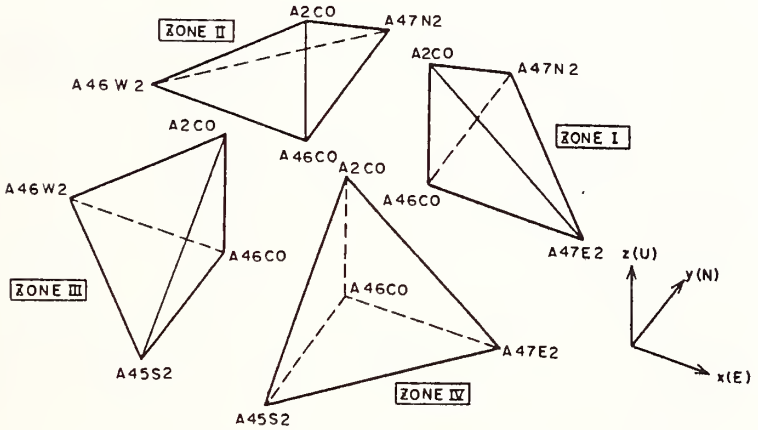

(b) Lower Level Ground Strains at Field-A

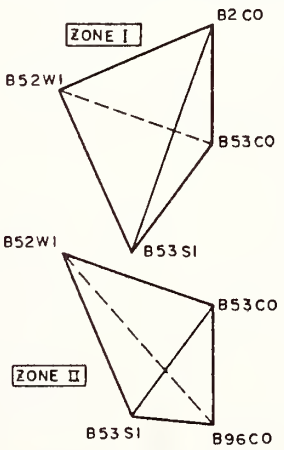

(c) Lower Level Ground Strains at Field-B

Figure 6 Tetrahedrons Formulated to Calculate Ground Strains

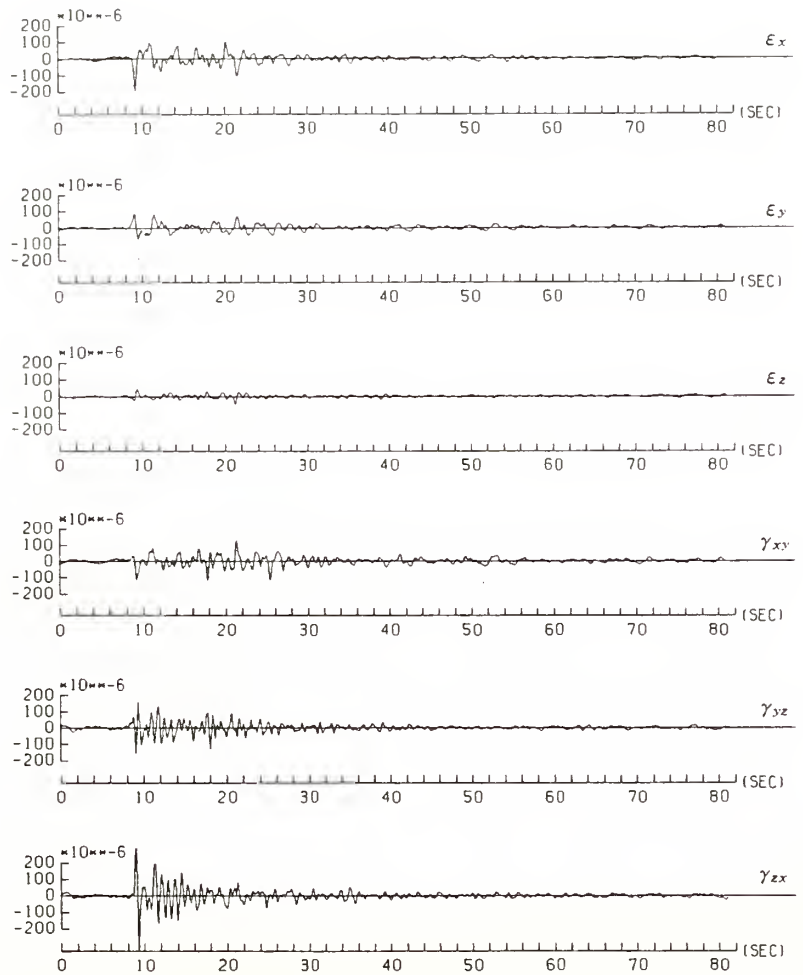

(a) Upper Level Ground Strains at Field-A

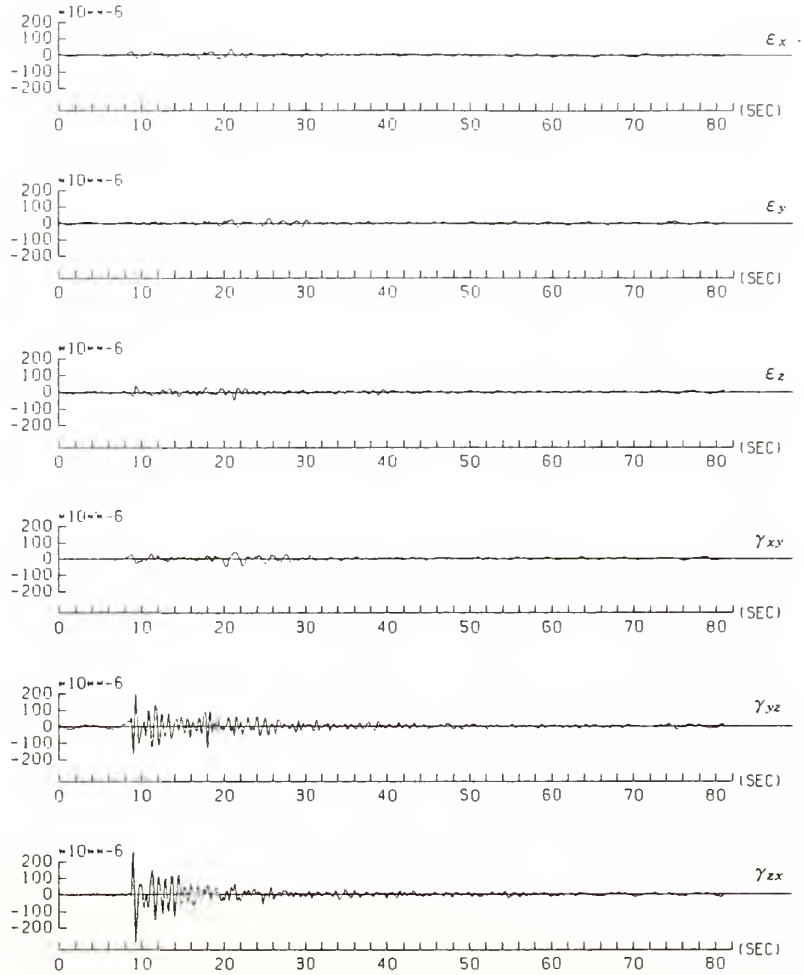

(b) Lower Level Ground Strains at Field-A

Figure 7 Time History of the Calculated Ground Strains(Zone I, EQ-28)

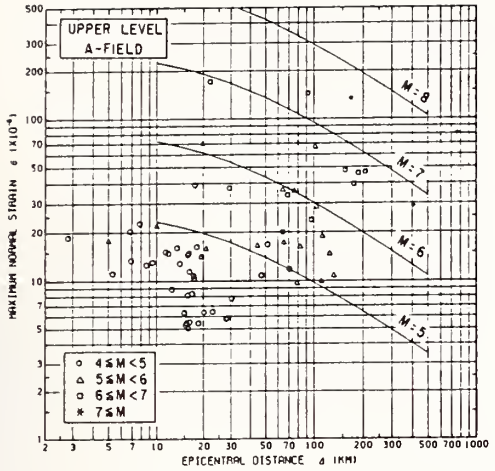

(1) Maximum Normal Strain ε

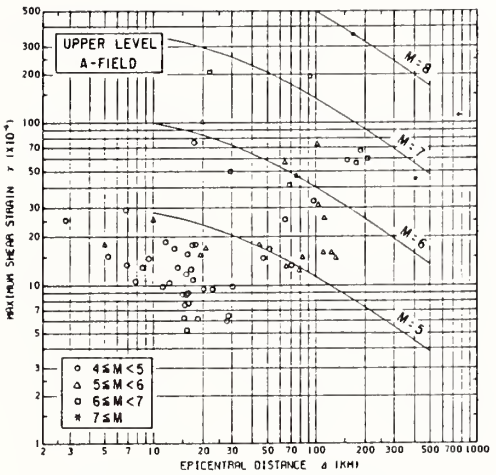

(2) Maximum Shear Strain γ

(a) Upper Level Ground Strains at Field A

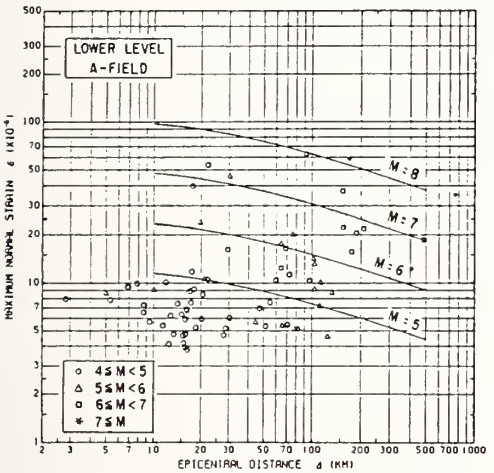

(1) Maximum Normal Strain ε

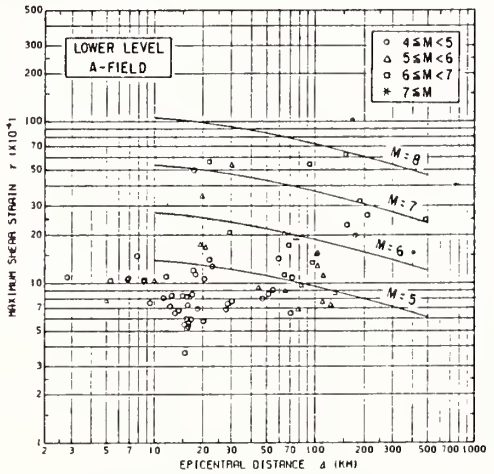

(2) Maximum Shear Strain γ

(b) Lower Level Ground Strains at Field A

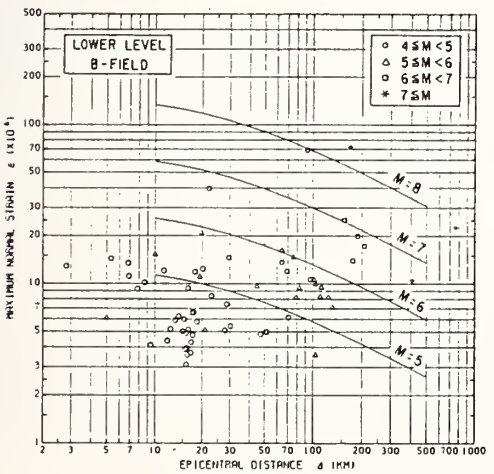

(1) Maximum Normal Strain ε

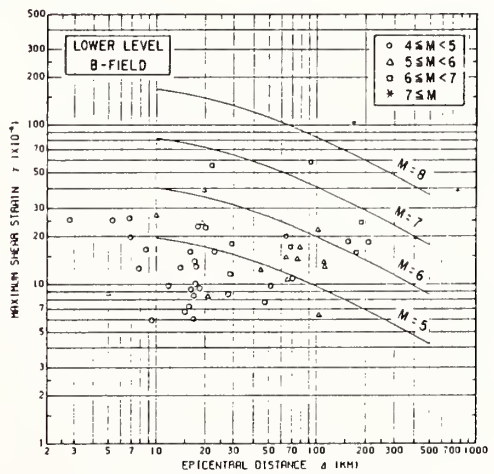

(2) Maximum Shear Strain γ

(c) Lower Level Ground Strains at Field B

Figure 8 Attenuation Characteristics of Maximum Ground Strains

Dynamic Centrifugal Model Tests of Embankments on Liquefiable Grounds

BY

Yasuyuki Koga[1] and Jun-ichi Koseki[2]

ABSTRACT

Model tests using a geotechnical dynamic centrifuge were performed to study a seismic behavior of embankments on liquefiable grounds. Effects of a scale factor and a seismic history were investigated. Tests on a shape of the embankment or a thickness of the ground were also conducted.

KEY WORDS: Embankment, Geotechnical Centrifuge, Liquefaction

1. INTRODUCTION

Liquefaction of a sandy ground causes a settlement of an embankment founded on the ground. A lot of model tests have been executed to reveal the seismic behavior of the embankment, but few of them have been done under a high confining stress.

A centrifugal model test is a test method which can simulate the same stress condition in a scaled model ground as in an actual ground. It has been applied to a dynamic problem using an earthquake simulator[1)2)3)].

This paper deals with dynamic centrifugal model tests of a horizontal sand layer and an embankment on the layer.

2. TEST PROCEDURE

Fig.1 shows a cross section of test models. They are classified into horizontal layer models and embankment models. An effect of a scale factor was investigated using 30*g* models and 50*g* models. The model dimensions were determined for both models so that a prototype size in a 1*g* field may almost coincide with each other. A shape of the embankment and a thickness of the sand layer were changed in models 1-1 and 1-2.

A sand layer was prepared by pouring Toyoura sand through air in a rigid soil container. The surface of the layer was rounded in accordance with a rotational radius. In the embankment models a colored sand mesh was drawn to observe the deformation of the sand layer through a transparent front glass of the container.

After setting the container in a vacuum box the sand layer was saturated with silicone oil which is 30 times as viscous as water for the 30*g* models and 50 times for the 50*g* models. An embankment was made of a mixture of Toyoura sand and a clay-sand which has a ratio of 4:1 in weight and a water content of 15%. Fig.2 shows a location of transducers.

A sinusoidal shaking was conducted after applying a centrifugal acceleration. It was repeated several times increasing an amplitude. A summary of the test cases and the test conditions are shown in Table 1. A prototype wave frequency in the 1*g* field was 2*Hz* for both the 30*g* models and the 50*g* models. An effect of a seismic history was investigated by comparing the results obtained in the first shaking steps with those obtained after them.

3. EFFECT OF SCALE FACTOR

3.1 Comparison of Time Histories

Fig.3 shows measured data of the horizontal layer models, and Fig.4 shows those of the embankment models. Time axes in the figures are controlled to have the same prototype length in the 1*g* field for the 30*g* model and the 50*g* model. In Fig.5 and Fig.6 the time axes are shortened to show changes after the shaking.

There were qualitative agreements between the result of the 30*g* models and that of the 50*g* models as follows:

(1) An increase of an excess pore pressure proceeded faster in a shallow part of the horizontal sand layer than in a deep part, and a rapid change of a responce acceleration occured earlier in the shallow part. There was almost no acceleration responce after the liquefaction. The excess pore pressure dissipated faster in the deep part.

(2) A change of an excess pore pressure beneath the embankment (P4 in the embankment model) was small during the shaking, but it increased after the shaking. An excess pore pressure dissipated faster below the embankment (P6) than in the side layer (P3) of the same depth.

(3) The rapid change of a responce acceleration did not occur in or below the embankment (A4 and A6) while it occured in the side layer (A2).

(4) A crest settlement of the embankment started as the excess pore pressure increased. It proceeded at a nearly constant rate during the shaking, but it stopped after the shaking.

The dissipation of the excess pore pressure finished in about 5*second* in the 30*g* models, and it did in about 3*second* in the 50*g* models. The duration for both models was equivalent to 150*second* in the 1*g* field. It increased as the excess pore pressure generated fast.

---

[1]Head, Soil Dynamics Division, Construction Equipment and Method Department, Public Works Research Institute, Ministry of Construction, Japan. [2]Researcher, ditto.

In this test the viscosity of the silicone oil used as a pore fluid of a sand was determined assuming that it is in inverse proportion to an apparent permeability of the sand although Inatomi et al.[2] showed experimentally that it is not so. Within the limits of this test it may well be adequate to use the simple assumption, because the duration of the dissipation was almost equivalent.

3.2 Resistance against Liquefaction

Fig.7 shows the relationship between the input acceleration and the number of cycles until the rapid change of the response acceleration (A4 to A6) due to the liquefaction in the first shaking steps of the horizontal layer models. Fig.8 shows one between the input acceleration and the number of cycles until the excess pore pressure reaches a limiting value which is maintained during the liquefaction. The input acceleration is converted into a prototype value in the 1*g* field to compare the result of the 30*g* models with that of the 50*g* models.

It is seen from the figures that the resistance of the sand layer against a liquefaction was lower in the 50*g* models than in the 30*g* models. Although the reason is not known yet, it is possible that a change of a frictional resistance at a contact point of the sand particles may have reduced the resistance of the sand in an undrained condition as the viscosity of the silicone oil increased.

3.3 Crest Settlement

Fig.9 shows the relationship between the input acceleration and the induced crest settlement of the embankment in the first shaking steps of the embankment models. Both values are converted into prototype ones in the 1*g* field. The prototype settlement was larger in the 50*g* models than in the 30*g* models if the prototype input acceleration was the same. It is estimated that the difference is caused by the change of the resistance against the liquefaction, so the effect is investigated as follows:

(1) Fig.10 shows the relationship between the prototype input acceleration and the number of cycles until the responce acceleration in the side layer (A2) changes rapidly due to the liquefaction. The 50*g* models had a lower resistance against the liquefaction than the 30g models as is seen in the Fig.7.

(2) Fig.11 shows the relationship between the prototype crest settlement and the number of cycles used in the Fig.10. There was almost no difference between the 30*g* models and the 50*g* models. This number of cycles can be assumed to represent the resistance of the whole layer against the liquefaction, then it is estimated that the prototype crest settlement in the 50*g* models may be almost the same as in the 30*g* models if they have the same resistance against the liquefaction.

(3) A prototype crest settlement in several shaking steps with a seismic history is compared between the 30*g* models and the 50*g* models in Fig.12, and the number of cycles defined as in the Fig.10 is compared in Fig.13. Both the induced settlement and the accumulated settlement were larger in the 50*g* models than in the 30*g* models, and the 50g models had a lower resistance against the liquefaction. The results agree with those obtained in the first shaking steps.

4. EFFECT OF SEISMIC HISTORY

The effect of a seismic history was investigated on the result obtained in the six cases of model 63-1. The shaking amplitude was changed in the first step of each case, and it was increased gradually in the following steps.

4.1 Crest Settlement

Fig.14 shows the relationship between an input acceleration and an induced or accumulated crest settlement. The induced settlement in the first step of each case without the seismic history was larger than the one in the following steps of cases 63-1-2 and 63-1-3 with the seismic history, and it was smaller than the accumulated settlement of the pre-shaken cases.

The difference in the accumulated settelement was small between these cases, therefore the case 63-1-2 is used as a representative case with the seismic history in the following comparisons.

4.2 Excess Pore Pressure

Fig.15 shows the relationship between the input acceleration and a maximum excess pore pressure ratio at a depth of 10cm (P2 and P5). An initial effective vertical stress is calculated one-dimensionally using a measured unit weight of the sand layer and the embankment.

With or without the seismic history the ratio in the side layer (P2) was nearly 1.0 when the input acceleration was about 4*g*, but the ratio was higher with the seismic history when the input acceleration was more than 7*g*. Below the embankment (P5) the ratio was higher with the seismic history than without it over a whole range of the input acceleration.

It is considered that with the seismic history a densification of the sand layer due to a reconsolidation after the liquefaction reduces the generation of the excess pore pressure, and the rate of the densification seems to be larger below the embankment than in the side layer.

4.3 Response Acceleration

Fig.16 shows a relationship between the input acceleration and a ratio of a maximum response acceleration to the input one. With or without the seimic history the ratio was almost the same in the side layer (A2). Below the embankment (A6)

it was higher with the seismic history when the input acceleration was more than 7*g*. In the embankment (A4) the ratio increased as the input acceleration increased with the seismic history, and it decreased without the seismic history.

These results agree with the consideration that the effect of the densification due to the seimic history is higher below the embankment than in the side layer. The difference in the induced crest settlement between the virgin cases and the pre-shaken cases may be caused by both the disification and the residual deformation of the pre-shaken cases.

5 EFFECT OF EMBANKMENT SHAPE AND SAND LAYER THICKNESS

5.1 Crest Settlement

A crest settlement induced in the first steps is compared between models 63-1, 1-1 and 1-2 in Fig.17. There was not a distinct difference, but the settlement was larger in models 1-1 and 1-2 than in model 63-1 when the input acceleration was about 5*g*.

Generally it is estimated that the thinner sand layer in model 1-1 may result in the smaller settlement than in model 63-1, and that the larger embankment in model 1-2 may result in the larger settlement than in model 63-1. Altouogh the reason for the disagreement of the test results with the estimation is not known yet, it is possible that a small change in the model preparation may have caused variations in the characteristics of the models such as the density and the saturation degree of the sand layer which affected the test results. Further investigations are needed to evaluate the effect of these variations, and a careful preparation of the model with a high repeatability is necessary.

5.2 Deformation of Sand Layer

Fig.18 shows an observed deformation of models 63-1, 1-1 and 1-2. A settlement of the embankment accompanied with a lateral deformation of the sand layer and a settlement of the layer below the embankment. The lateral deformation was larger in a shallow part of the layer, and it was restrained by a bottom plate of the container. The settlement of the layer may have been caused by both the lateral deformation and the reconsolidation after the liquefaction. There could not be seen a distinct difference among the three models.

6 CONCLUSIONS

The result of dynamic centrifugal tests performed using horizontal layer models and embankment models with a centrifugal acceleration of 30*g* or 50*g* is summarized as follows:

(1) A comparison of the measured data of the 30*g* models and the 50*g* models showed that there were several qualitative agreements between them on a dynamic response characteristics. A lower resistance against a liquefaction in the 50*g* models resulted in a larger prototype crest settlement, and it may have been caused by the change of a viscosity of a silicone oil used as a pore fluid. It is estimated that the prototype crest settlement in the 50*g* models may be almost the same as in the 30*g* models if they have the same resistance against the liquefaction.

(2) To investigate the effect of a seismic history a comparison was made between the results obtained in the first shaking steps of the embankment models and those obtained in the following steps. The effect on the excess pore pressure and the response acceleration was larger in or below the embankment than in the side layer. It is considered that the rate of a densification of the sand layer due to a reconsolidation after the liquefaction is larger below the embankment than in the side layer. A smaller induced crest settlement with the seismic history was obtained, and it may have been caused by both the densification and the residual deformation.

(3) The test result did not clarify the effect of a shape of an embankment and a thickness of a sand layer on the crest settlement. The settlement of the embankment accompanied with a lateral deformation of the sand layer and a settlement of the layer below the embankment irrespective of the shape or the thickness.

REFERENCES

1) Koga, Y., Taniguchi, E., Koseki, J. and Morishita, T : Sand Liquefaction Tests Using a Geotechnical Dynsamic Centrifuge, Proc. of the 20th Joint Meeting of U.S.-JAPAN Panel on Wind and Seismic Effects, US/JAPAN Natural Resources Conference, 1988.

2) Inatomi, T., Kazama, K., Noda, S. and Tsuchida, H. : Centrifuge Dynamic Model Tests in PHRI, Proc. of the 21th Joint Meeting of U.S.-JAPAN Panel on Wind and Seismic Effects, US/JAPAN Natural Resources Conference, 1989.

3) Ledbetter, R. H. : Modelling of Earthquake Induced Pore Pressure Behavior, Proc. of the 21th Joint Meeting of U.S.-JAPAN Panel on Wind and Seismic Effects, US/JAPAN Natural Resources Conference, 1989.

Table 1 Test Cases and Conditions

Model	Case	Centrifugal Acc. (g)	Input Sinusoidal Wave	Input Acc. (g) 1st	2nd	3rd	4th	5th	6th	Dr of Sand Layer (%)
63-1	63-1-1	30	60Hz,20cycle	1.2						*
	63-1-2			2.5	4.1	5.2	7.3	8.7	12.7	*
	63-1-3			3.7	5.6	7.1	8.3	12.5		*
	63-1-4			5.5						*
	63-1-5			7.3						*
	63-1-6			9.0						*
1-1	1-1-1	30	60Hz,20cycle	3.4	4.9	6.3	8.0			61
	1-1-2			4.9	6.3	8.0				62
1-2	1-2-1	30	60Hz,20cycle	3.3	5.3	7.0	8.8			64
	1-2-2			5.0	6.7	8.5				70
1-3	1-3-1	30	60Hz,50cycle	2.3	3.3	4.5	5.6			64
	1-3-2			3.4	4.3	5.2				61
	1-3-3			4.5	5.6					59
1-4	1-4-1	50	100Hz,50cycle	4.0	5.3	7.0	8.4			64
	1-4-2			4.8	6.4	7.8				61
	1-4-3			2.6	3.8					64
1-5	1-5-3	50	100Hz,20cycle	7.0	10.8	14.0	16.1			52
	1-5-4			5.8	9.2	11.7	13.9			60

* The relative density of the sand layer for model 63-1 is not known due to mismeasurement. It is assumed to be almost the same as others, because the sand layer was prepared in the same way.

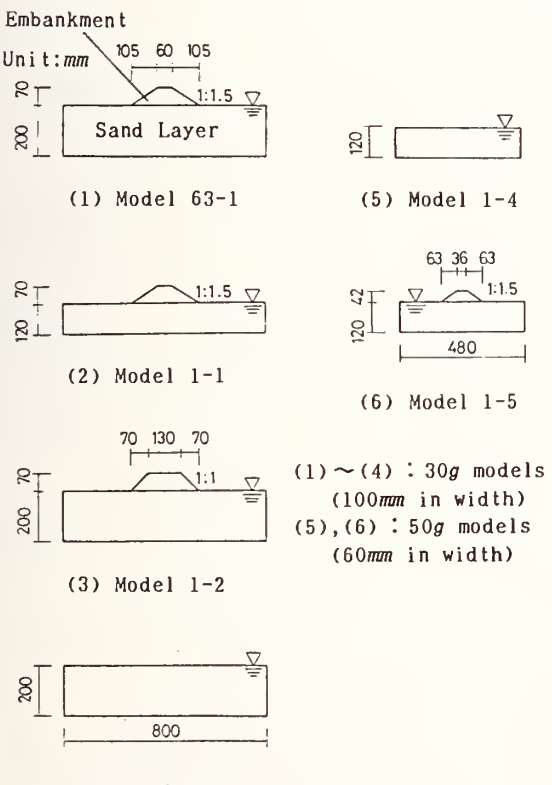

Fig.1 Test Models

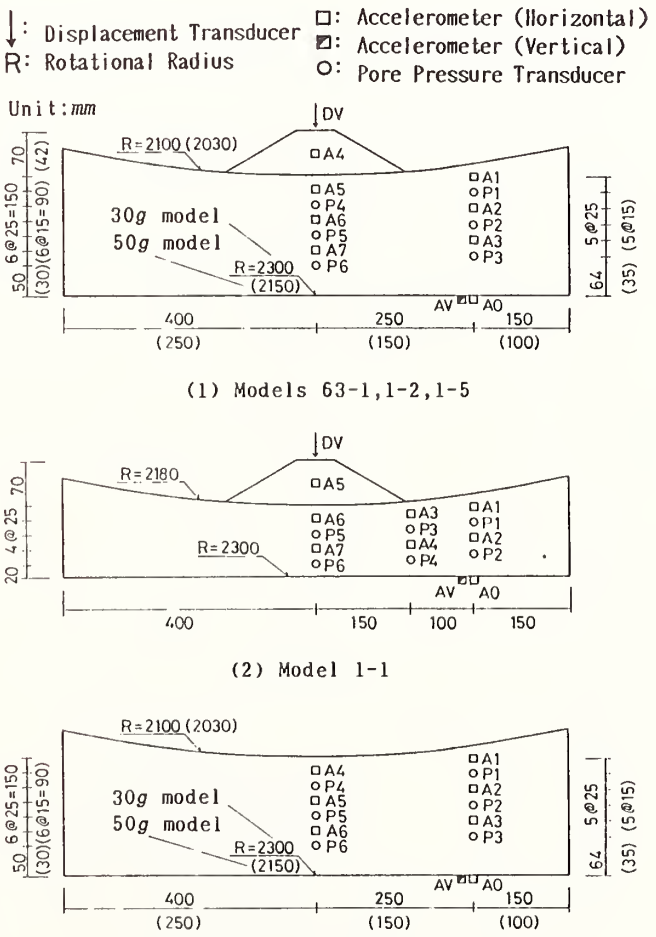

Fig.2 Location of Transducers

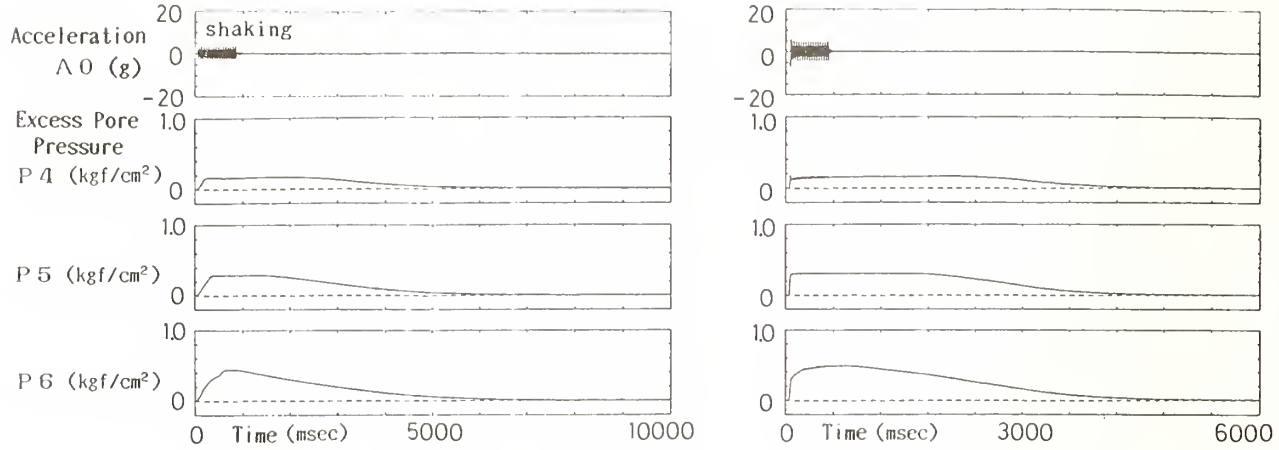

(1) Case 1-3-2 (30g) in the 1st shaking

(2) Case 1-4-2 (50g) in the 1st shaking

Fig.5 Measured Data of Horizontal Layer Models (Changes after the shaking)

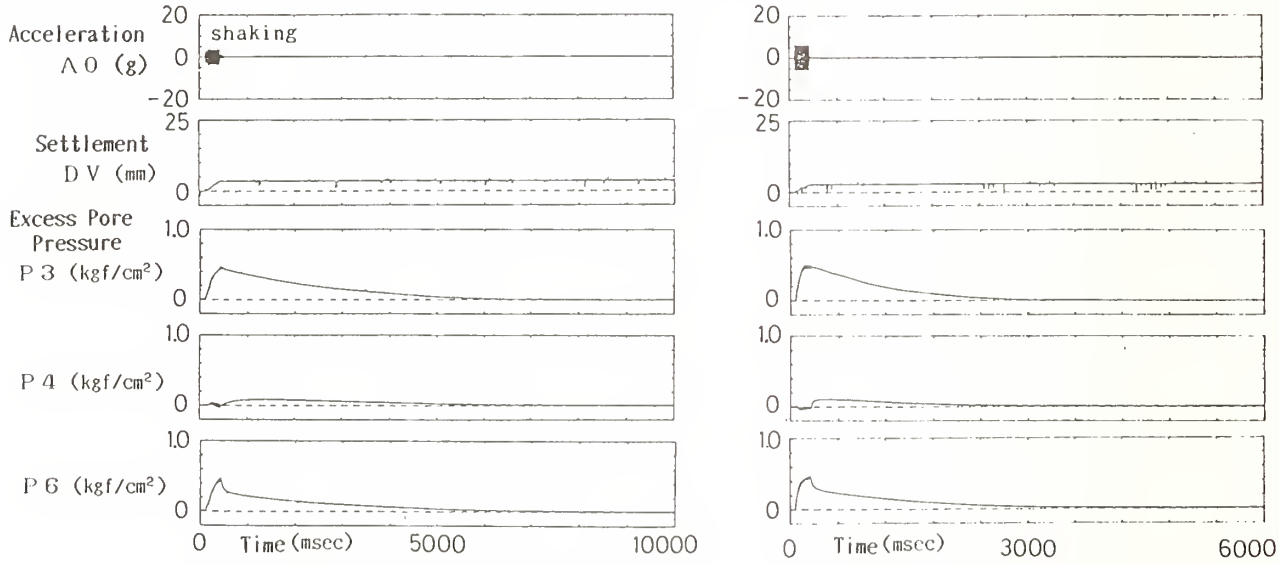

(1) Case 63-1-3 (30g) in the 1st shaking

(2) Case 1-5-4 (50g) in the 1st shaking

Fig.6 Measured Data of Embankment Models (Changes after the shaking)

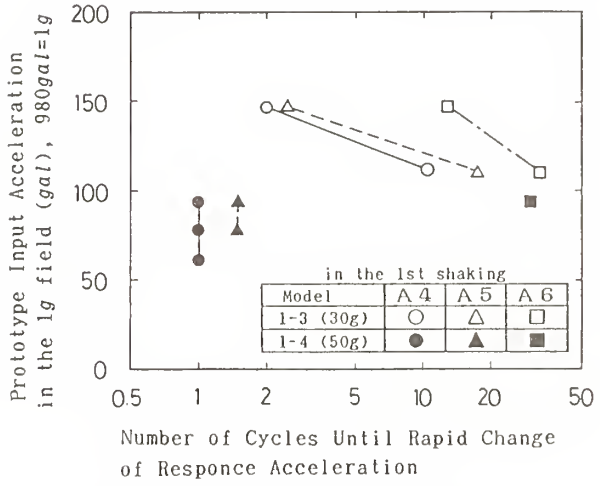

Fig.7 Input Acc. vs. Number of Cycles Until Rapid Change of Responce Acc. (Horizontal layer model)

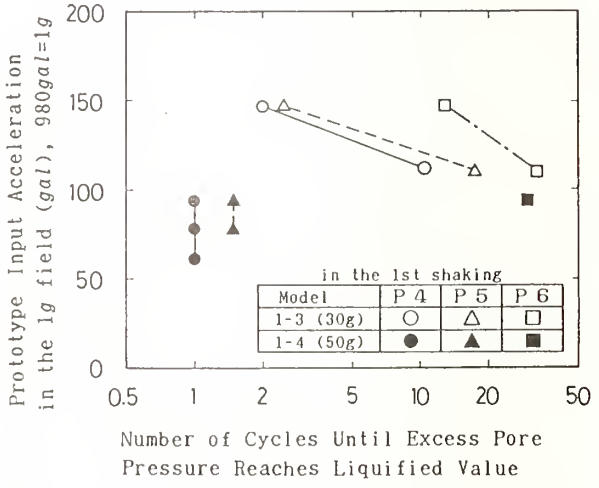

Fig.8 Input Acc. vs. Number of Cycles Until Excess Pore Pressure Reaches Liquified Value (Horizontal layer model)

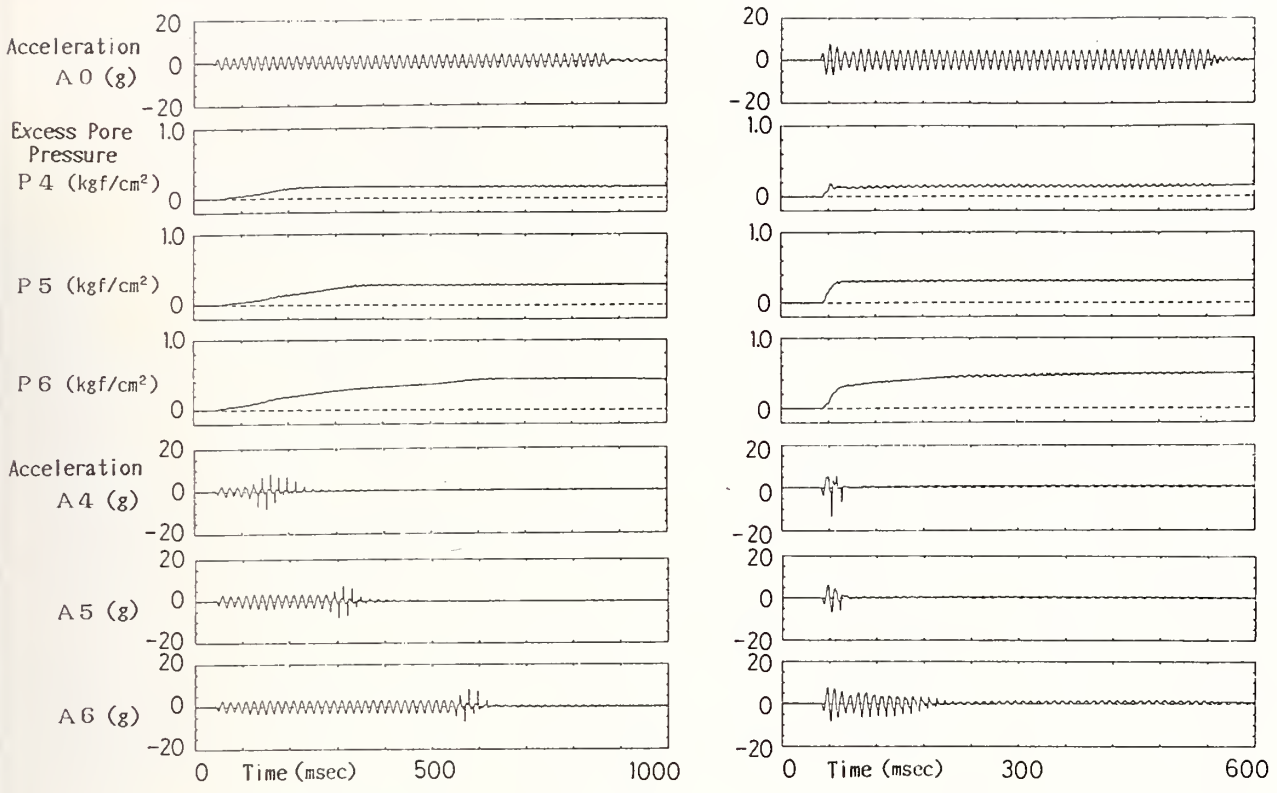

(1) Case 1-3-2 (30g) in the 1st shaking (2) Case 1-4-2 (50g) in the 1st shaking

Fig.3 Measured Data of Horizontal Layer Models

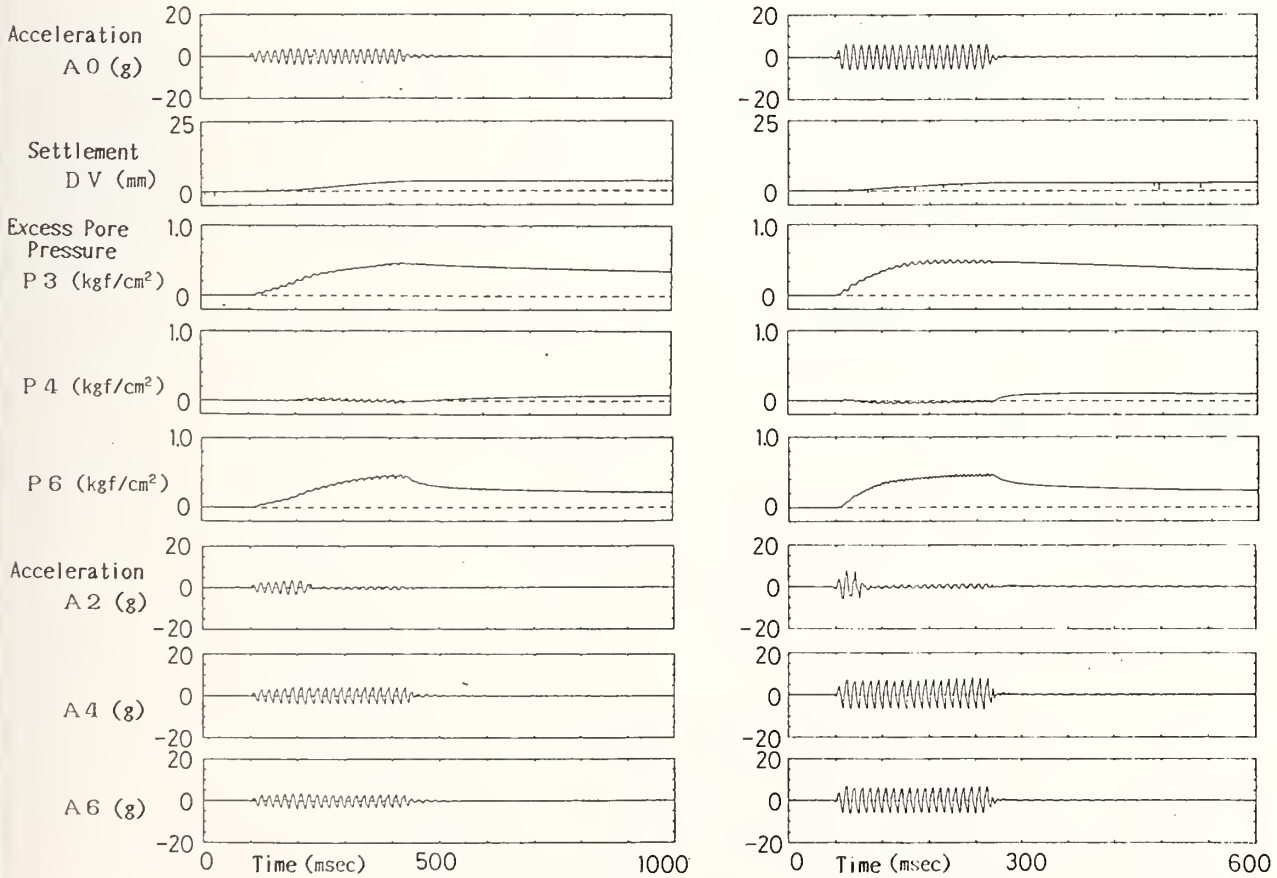

(1) Case 63-1-3 (30g) in the 1st shaking (2) Case 1-5-4 (50g) in the 1st shaking

Fig.4 Measured Data of Embankment Models

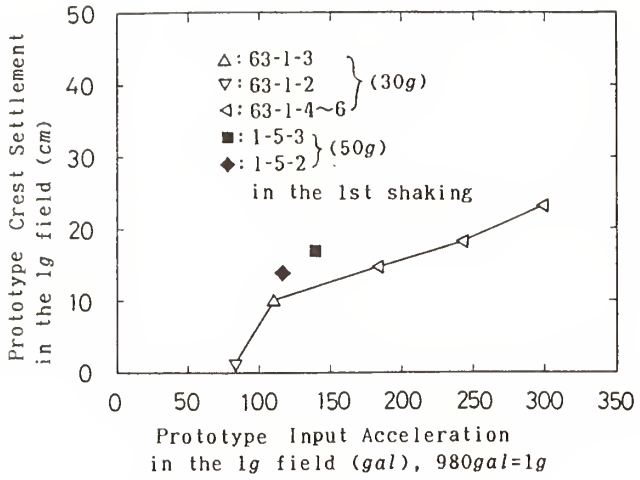

Fig.9 Input Acc. vs. Crest Settlement

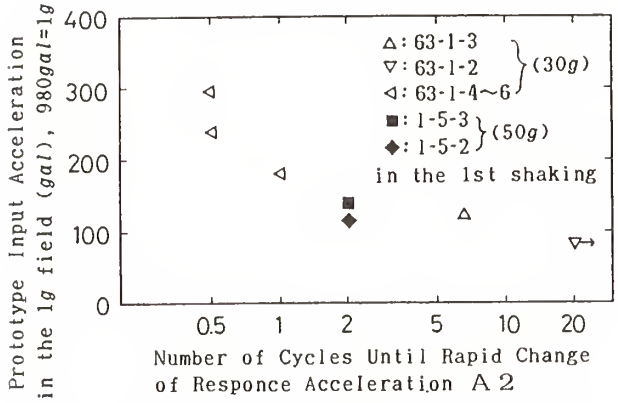

Fig.10 Input Acc. vs. Number of Cycles Until Rapid Change of Responce Acc. A 2

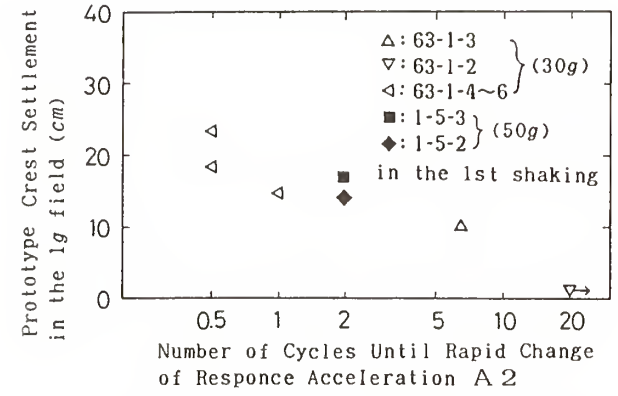

Fig.11 Crest Settlement vs. Number of Cycles Until Rapid Change of Responce Acc. A 2

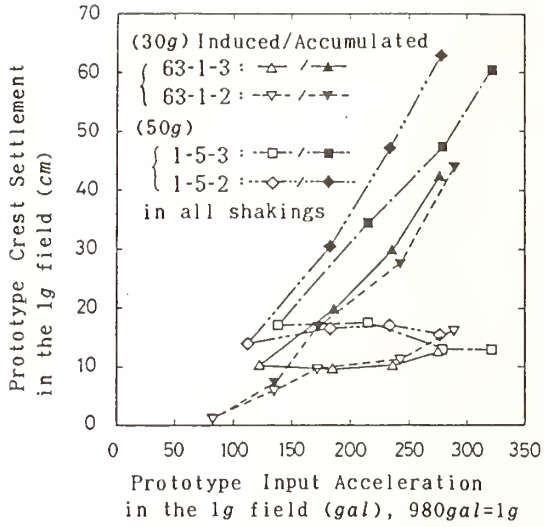

Fig.12 Input Acc. vs. Crest Settlement (with seismic history)

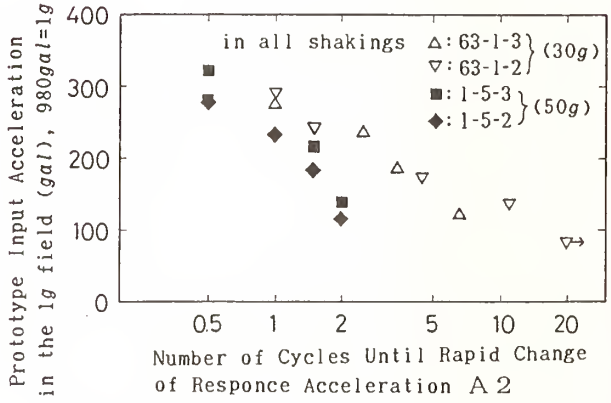

Fig.13 Input Acc. vs. Number of Cycles Until Rapid Change of Responce Acc. A 2 (with seismic history)

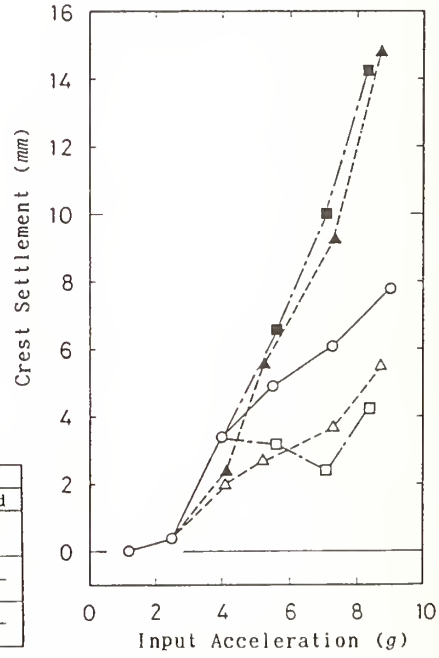

Notation for Fig.14

Seismic History (Case)	Type of Settlement	
	Induced	Accumulated
Virgin (63-1-1~6)	—○—	
Pre-shaked (63-1-2)	- -△- -	- -▲- -
Pre-shaked (63-1-3)	- -□- -	- -■- -

Fig.14 Input Acc. vs. Crest Settlement (Model 63-1)

Notation for Fig.16

Seismic History (Case)	Location P2	Location P5
Virgin (63-1-1～6)	—○—	—●—
Pre-shaked (63-1-2)	- - △ - -	- - ▲ - -

Notation for Fig.15

Seismic History (Case)	Location A2	Location A4	Location A6
Virgin (63-1-1～6)	—○—	—◑—	—●—
Pre-shaked (63-1-2)	- - △ - -	- - ◭ - -	- - ▲ - -

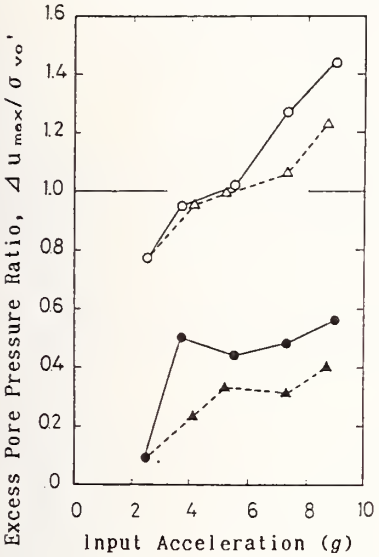

Fig.15 Input Acc. vs. Excess Pore Pressure Ratio (Model 63-1)

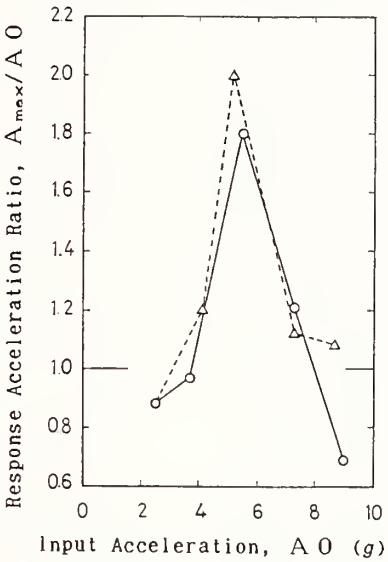

(1) In the side layer

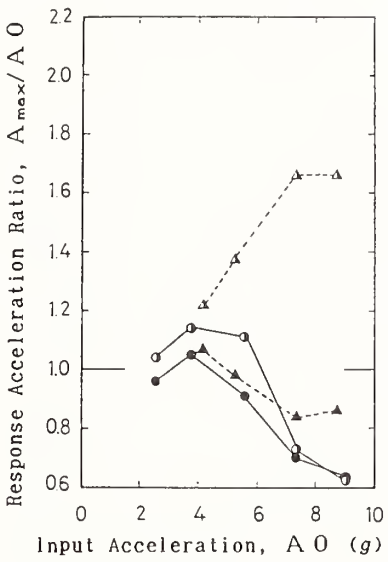

(2) In or below the embankment

Fig.16 Input Acc. vs. Response Acc. Ratio (Model 63-1)

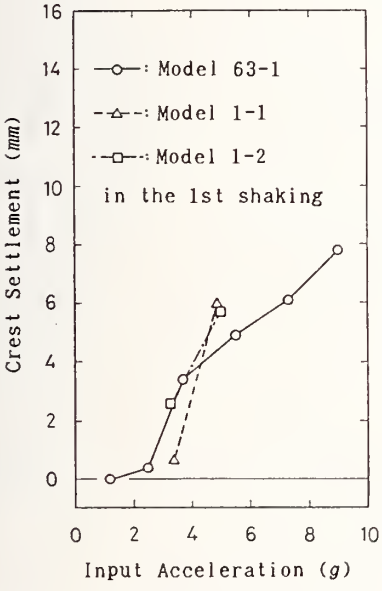

Fig.17 Input Acc. vs. Crest Settlement

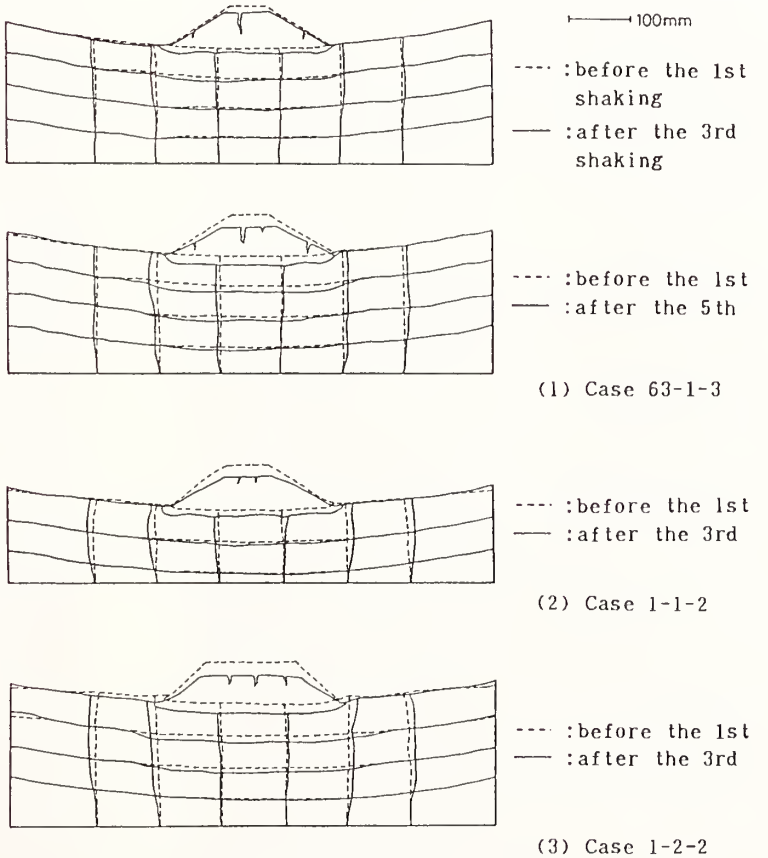

Fig.18 Observed Deformation

Seismic Resistance Requirements of Roller Compacted Dams

by

Alan T. Richardson[1] and Louis H. Roehm[2]

ABSTRACT

Seismic analysis of the U.S. Bureau of Reclamation's (Reclamation) Upper Stillwater Dam is explained as an example of a design method used for evaluation of an RCC dam's seismic resistance. Material strength properties were evaluated by laboratory and field testing. Testing evaluated the weakest link in an RCC structure, the joint between lifts. Computer code EADHI was used to analyze finite element cross-sectional models of the dam for static and dynamic loads. The maximum credible earthquake (MCE) was scaled by spectrum intensity to determine the site response spectrum. Synthetic accelerograms were generated for horizontal and vertical ground motions from the site response spectrum.

Maximum tensile and compressive stresses were determined from the dynamic analysis. Compressive stresses were well below acceptable limits for the RCC. Tensile stresses on the upstream face exceeded the allowable strength of the RCC for 0.10 seconds, indicating cracking of the concrete could occur.

1. INTRODUCTION

Roller compacted concrete (RCC) or a roller compacted dam (RCD), are terms which refer to a construction method for placing mass concrete with large equipment normally used for hauling rock or soil, and compacting the material in place with large vibrating rollers. Time and cost savings achieved by this procedure make it a preferred construction method for concrete dams. Seismic resistance of a dam for a given seismic acceleration depends primarily on the dam's shape, material strength and the stress state existing in the dam. The dam's shape is typically determined by an economic analysis of structurally stable cross sections based on static loads, with shape considerations given for dams located in areas of higher seismicity. Specific material properties for a dam are determined by standard laboratory testing and adjusted for dynamic loads by applying empirically determined factors based on rapid strain rate testing. For RCC dams, material properties testing also requires careful evaluation of the bond strength to be developed between lift lines, since bond strength generally controls the dam's ability to resist vertical tensile stresses. The stress state existing in the dam prior to the dynamic analysis is determined by analysis of static loads on the dam. Dynamic analysis is then used to determine the dam's response to seismic loads.

Upper Stillwater Dam was designed in 1982 by Reclamation. Its design is used here to demonstrate the analysis and evaluation process needed to determine an RCC dam's seismic resistance. Upper Stillwater Dam (figure 1), located in the state of Utah at an elevation of 8,000 feet, was constructed between 1983 and 1987. It has a crest length of 2,700 feet, a maximum structural height of 285 feet and contains a total of 1,600,000 cubic yards of concrete, 90 percent of this total is RCC. Construction was by placing and compacting 1-foot (30 cm) thick lifts between the abutments until the total height of the dam was placed. Both faces of the dam were formed by continuous horizontal slipforming of very low slump conventional concrete. Contraction joints were formed naturally as the dam cooled. The selected dam's cross section minimized the concrete volume while providing the required stability safety factors for static loads. It was then analyzed to determine its ability to resist seismic loads. The dynamic analysis of Upper Stillwater Dam was conducted using the finite element program EADHI [A]. In this program, the complete system is considered as composed of two substructures, the dam represented as a finite element system, and the water in the reservoir treated as a continuum of infinite length in the upstream direction governed by the wave equation. Compressibility of the water is included in the analysis. EADHI is a two-dimensional program including both horizontal and vertical components of ground motion. The program uses an isoparametric

[1] Principal Designer,
U.S. Bureau of Reclamation,
Denver, Colorado 80225
[2] Technical Specialist,
U.S. Bureau of Reclamation,
Denver Colorado 80225

quadrilateral element. The material behavior is assumed to be linearly elastic.

2. MATERIAL PROPERTIES

Reclamation's concrete laboratory conducted an extensive testing program to determine the material properties of RCC [B]. This program included standard structural properties testing of laboratory cylinders and core from a test placement constructed in 1981 at the dam site. Structural testing emphasized the tensile capacity of the joint created between layers of the RCC. Direct tensile tests were conducted on jointed cylinders and at the joint between lifts in cores.

Dynamic properties were not obtained in the laboratory, so static values were increased proportionally according to percentages reported by others [C]. The static compressive strengths of the concrete were increased 20 percent to account for rapid loading effects. This assumption resulted in ultimate dynamic compressive strength of 3,600 lb/in^2 for RCC. The static tensile strength was increased 60 percent to account for rapid loading effects. In addition, the tensile strengths were increased 20 percent to account for nonlinear behavior of the concrete. The analytical models used assume the concrete to be elastic when actually it behaves nonlinearly at failure. Since the stresses computed are therefore artificially high, the assumed tensile strength should be increased accordingly. The ultimate dynamic tensile strength for RCC resulting from these assumptions was 350 lb/in^2. The dynamic modulus of elasti-city for all concrete was assumed to be 2.5 (10^6) lb/in^2, which is 67 percent greater than the static value. This increase is documented by laboratory tests performed by others [C]. The dynamic modulus of deformation of the foundation rock was assumed to be 1.25 (10^6) lb/in^2. This value was based on analytical studies of modulus of 1.0 (10^6) lb/in^2 to be similar to results from studies with several materials in the foundation. Increasing the modulus for dynamic loading resulted in a value of 1.25 (10^6) lb/in^2.

In addition to material properties, the dynamic analyses required a viscous damping constant. Several experimental shaking tests on models and prototypes of concrete dams have indicated values ranging from 2 to 10 percent [D]. The smaller damping values were associated with very low levels of excitation. For earthquake-type vibrations, a value of 10 percent is more representa-tive. For the dynamic analyses of Upper Stillwater Dam, damping was assumed to be 10 percent of critical.

3. INPUT GROUND MOTIONS

In the Reclamation process, two steps are necessary in selecting the seismic loadings to which a dam may be subjected. The first step is to define the magnitudes and locations of the hypothetical earthquakes which could affect the site. The second step is to determine the response spectra and select accelerograms representative of the resulting rock motions.

The earthquake magnitudes and locations estimated for the Upper Stillwater site are listed in the following table.

Richter magnitude			Epicentral	Focal
MCE	100-yr	25-yr	distance	depth
6.0	5.2	4.3	2 km	7 km

The dam was analyzed only for the maximum credible earthquake (MCE) since it would cover the 100- and 25-year events.

Ground motions for use in dynamic analyses were determined as follows: First, historical records with magnitudes and locations similar to the MCE were scaled using spectrum intensity. Spectrum intensity is defined as the area under a velocity response spectrum between 0.1 and 2.5 seconds. Then the average spectral accelerations were calculated for each period of the scaled records. The resulting site response spectrum (SRS) is shown in figure 2.

Once the SRS was determined, synthetic accelerograms were generated. Independent accelerograms were generated for the horizontal and vertical components of the ground motion. The vertical record was computed by scaling one accelerogram by the ratio (0.48) of vertical to horizontal spectrum intensities of the historical records. The horizontal and vertical accelerograms are shown in figures 3 and 4, respectively. Since the Upper Stillwater analysis, Reclamation has refined the spectrum intensity concept (reference E). Computations and field tests have demonstrated that the natural periods of concrete dams are generally less than 0.5 second. Therefore, acceleration spectrum intensity has been introduced and defined as the area under the accelera-tion response spectrum between periods of 0.1 to

0.5 seconds and is an appropriate indicator of the potential response of concrete dams to a given earthquake record.

4. DYNAMIC ANALYSIS

Dynamic studies of Upper Stillwater Dam used the two-dimensional program EADHI. Two models were used in the analyses - one to represent the maximum section and a more typical height section. Hydrostatic loads analyzed were: the normal water surface, elevation 8172.0, and the minimum water surface, elevation 8028.4.

Model grids used in the dynamic studies are shown in figures 5 and 6. Smaller elements were used at elevation 8100, the reentrant corner on the downstream face, to provide better stress definition.

All dynamic studies used only one material model in the dam. The foundation elements used another massless material for rock. Studies made with a homogeneous foundation showed tensile stresses exceeding the capacity of the rock in the foundation element just upstream of the dam. In order to provide a more realistic model, this element was softened by lowering the deformation modulus of the element to 100,000 lb/in^2.

Three different stress output options were used in the EADHI analyses. The first was used to obtain a table of maximum and minimum stresses, and their respective times of occurrence for each element. Secondly, stress histories were generated for particular elements. The third option was used to obtain the stress distributions in the entire dam at specific times corresponding to maximum tensions on both faces. EADHI automatically added static stresses to the dynamic stresses in all analyses.

Several studies were made to determine how much influence individual modes had upon the response of the dam. Up to five modes were included in each study.

5. RESULTS

Each EADHI analysis produced a large amount of output. Only the most significant results are presented. Modal superposition analyses were conducted which included contributions of up to five modes. The following results refer to studies for the first four modes; the fifth mode was judged to have a negligible influence upon the response of the dam. Natural periods for the maximum and typical sections are listed in the following table:

Natural periods - seconds

Mode	Maximum section	Typical section
1	0.462	0.344
2	0.182	0.139
3	0.176	0.125
4	0.094	0.063

The maximum principal stresses occurring at each face are shown on figures 7 and 8.

The maximum tensile stresses of 432 lb/in^2 on the upstream face and about 300 lb/in^2 on the downstream face occur when the water surface is at elevation 8172 (figure 7). For the low water conditions, maximum tensions are about 200 lb/in^2 on each face. At the maximum section, the maximum compressive stress (not shown) is 1,042 lb/in^2. Maximum tensions at the upstream face of the typical section with the normal water surface are about 300 lb/in^2. Vertical stress distributions in the maximum section at particular times related to the maximum tensions on both faces are shown on figure 9. Maximum tensions of about 300 lb/in^2 occur on the upstream face at elevation 8040 with normal and minimum water surface elevations at times 5.19 and 2.23 seconds, respectively, in the response history analyses. Maximum tensions of about 200 lb/in^2 occur on the downstream face at elevation 8095 at times 4.32 and 3.05 seconds for normal and minimum water surface elevations, respectively. As can be seen in figure 9, the stress distribution is almost linear from face to face.

In order to get an indication of the duration and frequency of occurrence of the maximum tensile stresses, several studies were conducted to generate stress histories at selected elements in the maximum section. These elements are 132, which is situated at elevation 8040 on the upstream face, and 167, located at elevation 8095 on the downstream face. Stress histories for element 132 for the analyses including normal and minimum water surface elevations, respectively, are shown on figures 10 and 11. Corresponding stress histories for element 167 are included in figures 12 and 13. Tensile stresses exceed 250 lb/in^2 only in the element 132 for the normal water surface condition; all four

such excursions are of durations less than 0.10 second each.

All dynamic analysis results indicate stress levels in the dam for the minimum water condition are significantly lower than for the normal water surface loading. In addition, stresses from the analyses of the typical section are substantially reduced compared to stresses from the maximum section analysis.

6. EVALUATION

According to Reclamation criteria [F], a safety factor greater than 1.0 is required for the extreme loading combination. The allowable compressive stress for the RCC is 3,600 lb/in^2. The allowable tensile stress for RCC is 350 lb/in^2.

Response history analyses of the normal water condition indicate maximum compressive stresses in the RCC less than 1,100 lb/in^2 which are well below the allowable limit of 3,600 lb/in^2. Tensile stresses in the RCC exceed the allowable limit of 350 lb/in^2 for less than 0.10 second at the upstream face. Except for four excursions of short duration, tensile stresses are generally less than 250 lb/in^2 throughout the dam. When large tensile stresses are present at the upstream face, the downstream half of the dam is in compression. Also, the above-mentioned stresses refer to the maximum section analyses; stresses at the typical section are substantially lower.

Present Reclamation criteria state that "Horizontal cracking should be assumed to occur in a gravity dam wherever the vertical normal stress for dynamic response to an earthquake does not meet minimum safety factor requirements. The depth of crack is assumed to extend along a horizontal section to the point where compressive stress computed without uplift and the internal hydrostatic pressure are equal." These criteria, published in 1974, are based on a pseudo static analysis for earthquake loadings. This method does not account for the rapid cyclic loading of seismic excitation. The analysis method used for this design (EADHI) produces a stress history based on linear elastic theory while accounting for resonance effects in the dam and hydrodynamic interaction. In addition, earthquake-type ground motions are input to the analysis rather than applying peak acceleration values to the concrete and water mass. Consequently, the evaluation of results from the EADHI program requires a different approach than outlined in E.M. 19.

It is important to note that the dynamic tensile strength was exceeded for a short duration on the upstream face. An excursion beyond the elastic limit is not as significant as the general level of repeatable stress at a point. An examination of the stress histories for this analysis shows that the dam responds at repeatable stress levels safely below the dynamic tensile strength. On this basis, it is reasonable to conclude that cracking would not develop through the section. From these observations, the dam's response is predominantly linearly elastic with instants where localized portions of the dam become nonlinear. Therefore, the loading from the MCE could possibly cause cracking of the concrete in a limited area. However, the dam possesses sufficient stability to operate safely during and after the earthquake.

One method of substantiating judgements concerning structural behavior is to observe the actual behavior of similar prototype structures for similar loading conditions. In 1967, Koyna Dam, a 338-foot-high gravity dam located in India, was shaken by a M_s = 6.5 earthquake located at an epicentral distance of 5 miles and a fault break distance of 1.8 miles. The structural damage to the dam was horizontal cracks on either or both faces of a number of monoliths [G, H]. Leakage of water was observed on the downstream face of one monolith, and traces of seepage were observed on five other monoliths. Although the dam cracked, no sudden release of the reservoir took place. The Koyna Dam experience shows that a concrete gravity dam like Upper Stillwater can crack and still retain the reservoir.

Stresses from the low water analyses were substantially reduced compared to stresses of the normal water condition analyses.

In summary, the evaluation of the dynamic analysis of Upper Stillwater Dam indicates that the maximum credible earthquake could cause cracking, but no sudden release of the reservoir will occur. This condition is permissible within the present Reclamation policy.

In August 1984, the Earthquake Engineering Research Center released the program EAGD-84 [I]. This program supersedes EADHI and includes the effects of dam-water-foundation rock interaction and of materials, such as alluvium and sediments, at the bottom of reservoirs. EAGD-84 was run using the Upper Stillwater data. The results indicated that stress values at the heel of the dam were

very similar and maximum values were 100 to 150 lb/in^2 less in the upper part of the dam. This program has become the standard for two-dimensional gravity dam analysis at Reclamation.

9. References

[A] Chakrabarti, P., and A. K. Chopra, "EADHI - A Computer Program for Earthquake Analysis of Gravity Dams Including Hydrodynamic Interaction," Report No. EERC 73-7, College of Engineering, University of California, Berkeley, 1973.

[B] Memorandums from Chief, Concrete and Structural Branch, to Chief, Dams Branch, "Upper Stillwater Dam - Roller Compacted Concrete," April 7, 1982, June 24, 1982, August 30, 1982, and January 13, 1983.

[C] Raphael, J. M., "Tensile Strength of Concrete," Journal of the American Concrete Institute, March-April, 1984.

[D] "Design and Analysis of Auburn Dam," vol. 4, U.S. Department of the Interior, Bureau of Reclamation, 1978.

[E] "Earthquake Ground Motions for Design and Analysis of Dams," Von Thun, J. L. et al., Earthquake Engineering and Soil Dynamics II - Recent Advances in Ground Motion Evaluation, Geotechnical Special Publication No. 20, American Society of Civil Engineers, June 1988.

[F] "Design Criteria for Concrete Arch and Gravity Dams," U.S. Department of the Interior, Bureau of Reclamation, Engineering Monograph 19, Denver, Colorado, February 1974.

[G] Chopra, A. K., and P. Chakrabarti, "The Koyna Earthquake and the Damage to Koyna Dam," Bulletin of the Seismological Society of American, vol. 63, No. 2, April 1973.

[H] Chopra, A. K., "Earthquake Resistant Design of Concrete Gravity Dams," Journal of the Structural Division, American Society of Civil Engineers, June 1978.

[I] Chopra, A. K., and G. Fenves, "EAGD-84 - A Computer Program for Earthquake Analysis of Concrete Gravity Dams," Report No. EERC 84-11, College of Engineering, University of California, Berkeley, 1984.

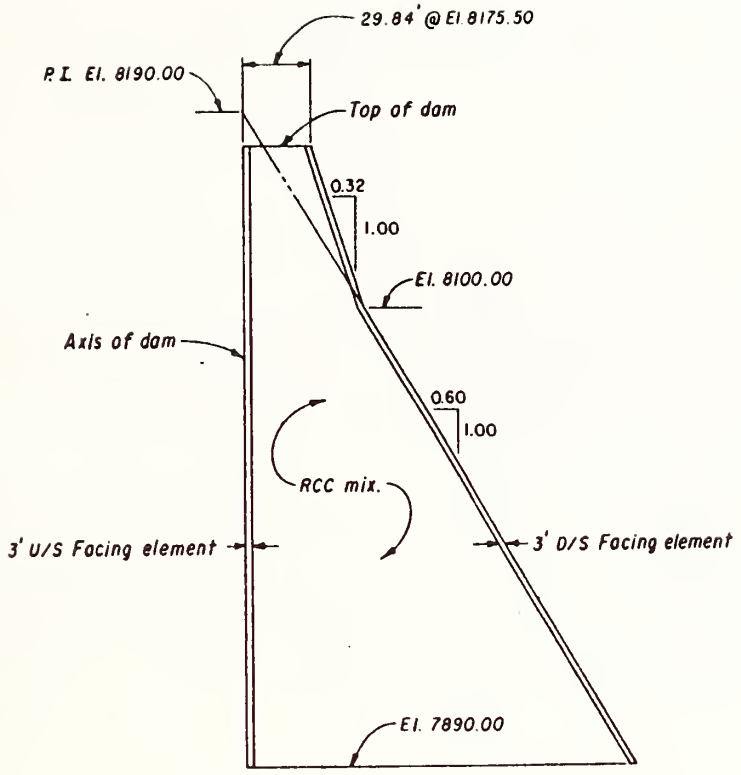

Fig. 1 MAXIMUM DAM SECTION

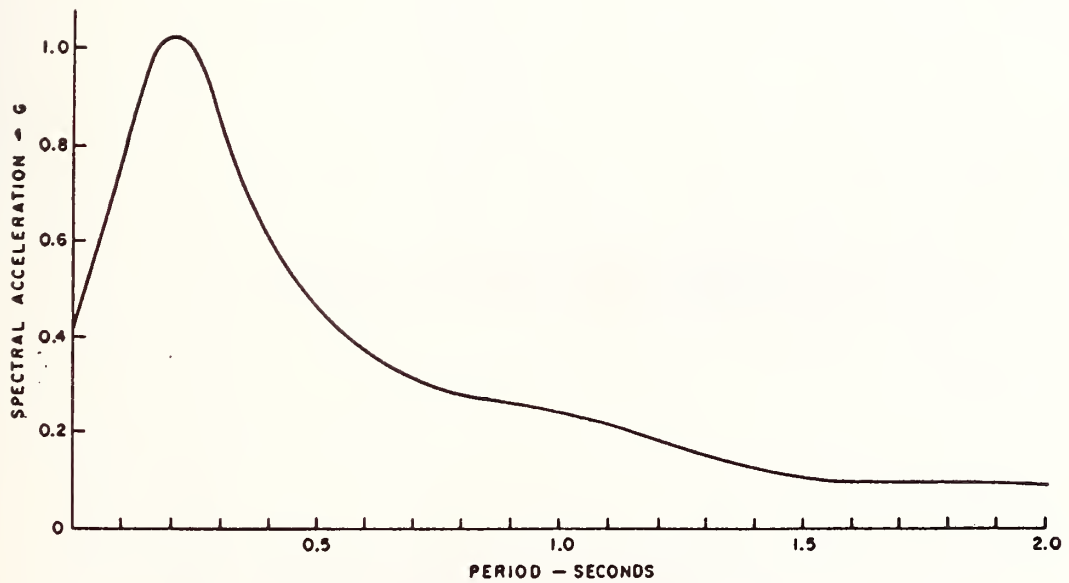

Fig. 2 RESPONSE SPECTRUM
M 6.0 AT 2 KM - 5 % DAMPING

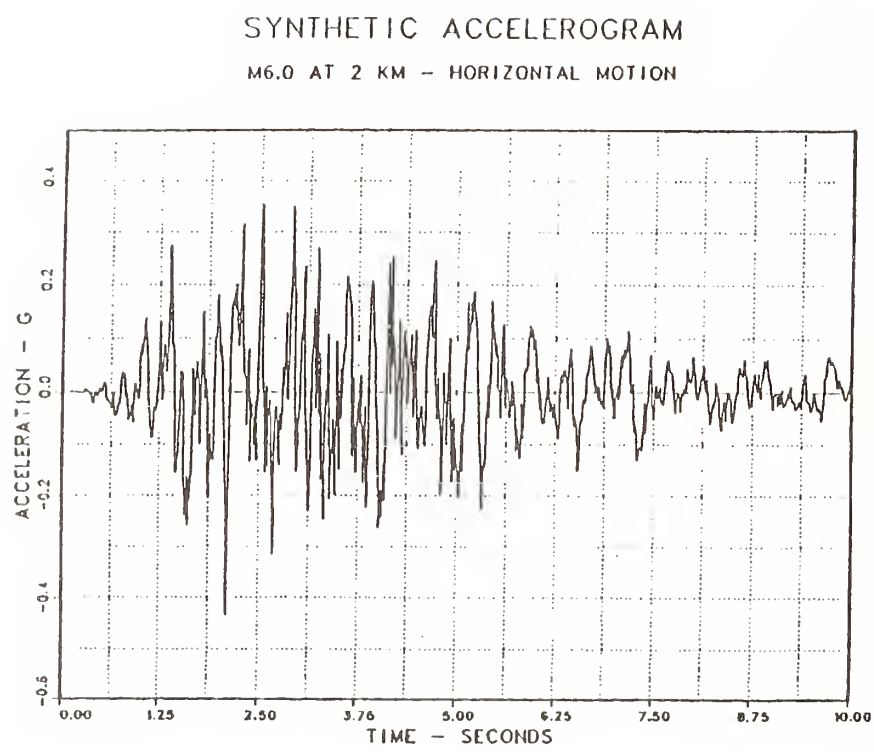

Fig. 3 SYNTHETIC ACCELEROGRAM
HORIZONTAL MOTION

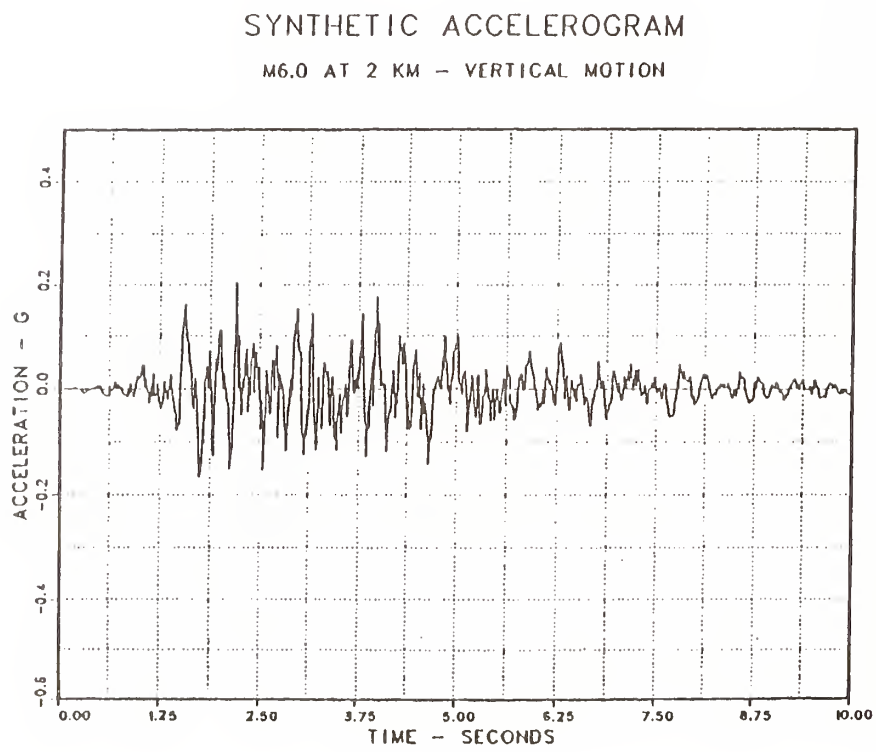

Fig. 4 SYNTHETIC ACCELEROGRAM
VERTICAL MOTION

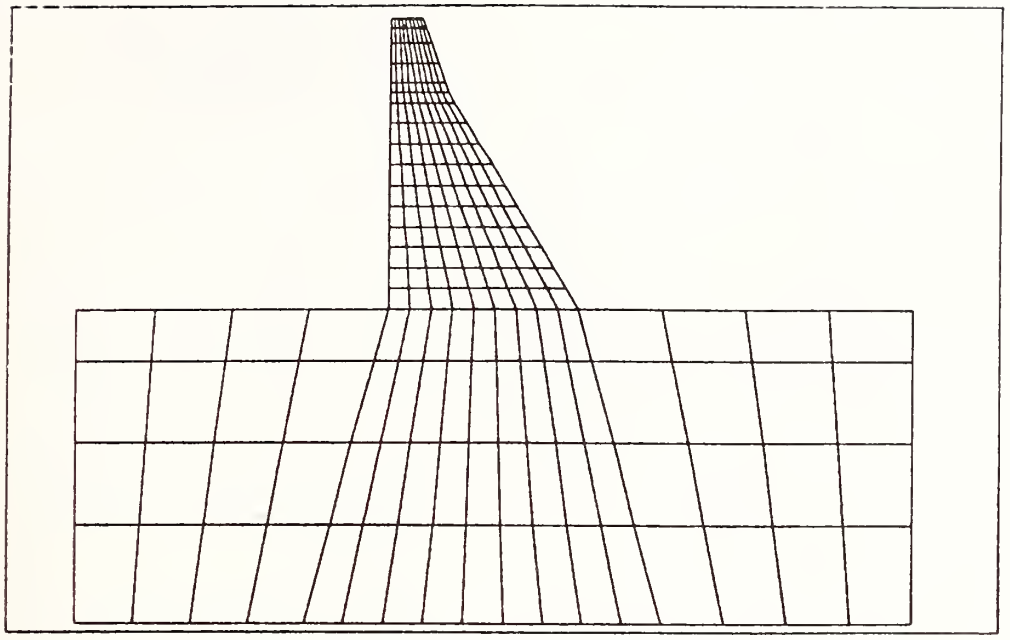

Fig. 5 MODEL GRID
MAXIMUM DAM SECTION

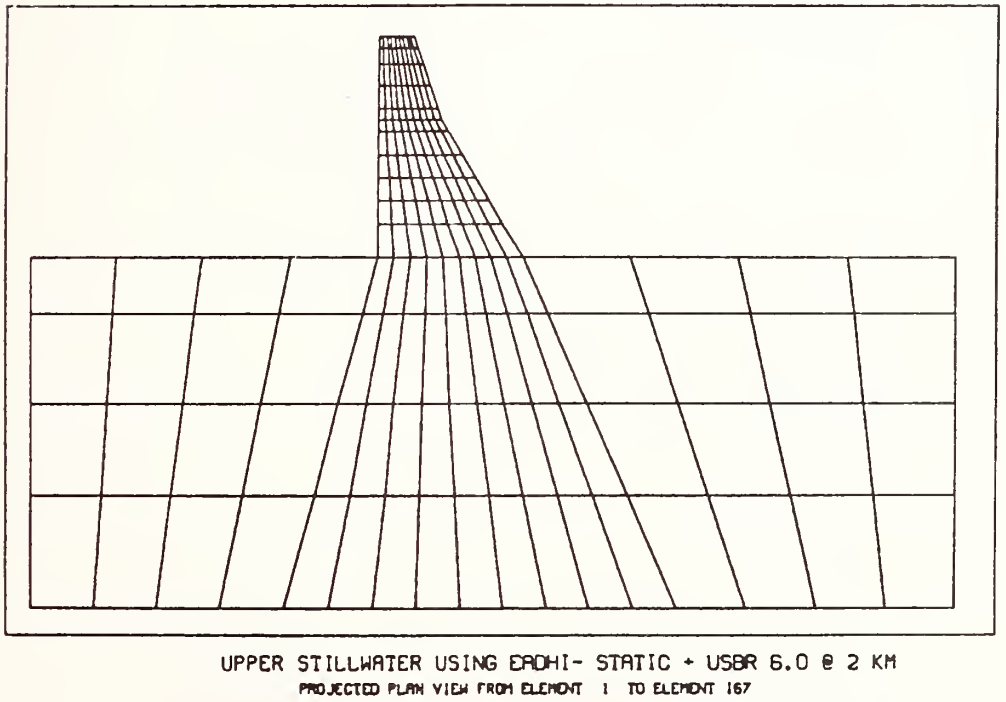

Fig. 6 MODEL GRID
TYPICAL SECTION

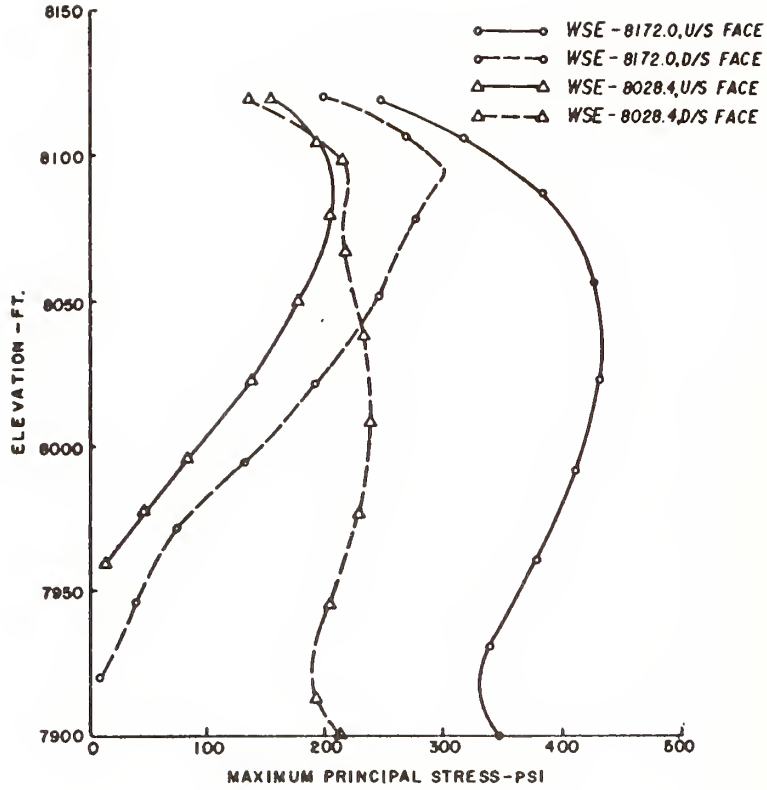

Fig. 7 PRINCIPAL STRESSES - MAXIMUM SECTION
WATER + DEAD LOAD + MCE

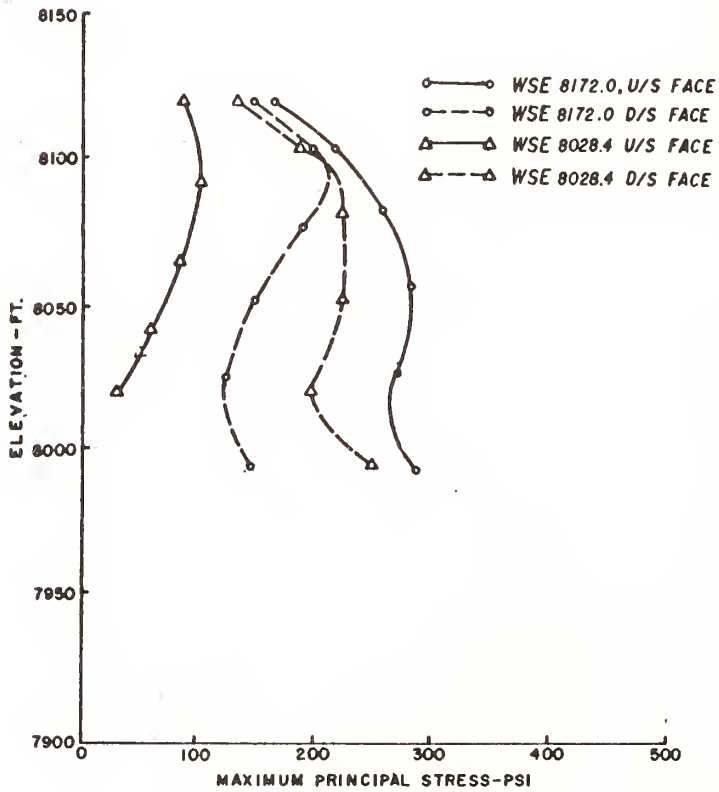

Fig. 8 PRINCIPAL STRESSES - TYPICAL SECTION
WATER + DEAD LOAD + MCE

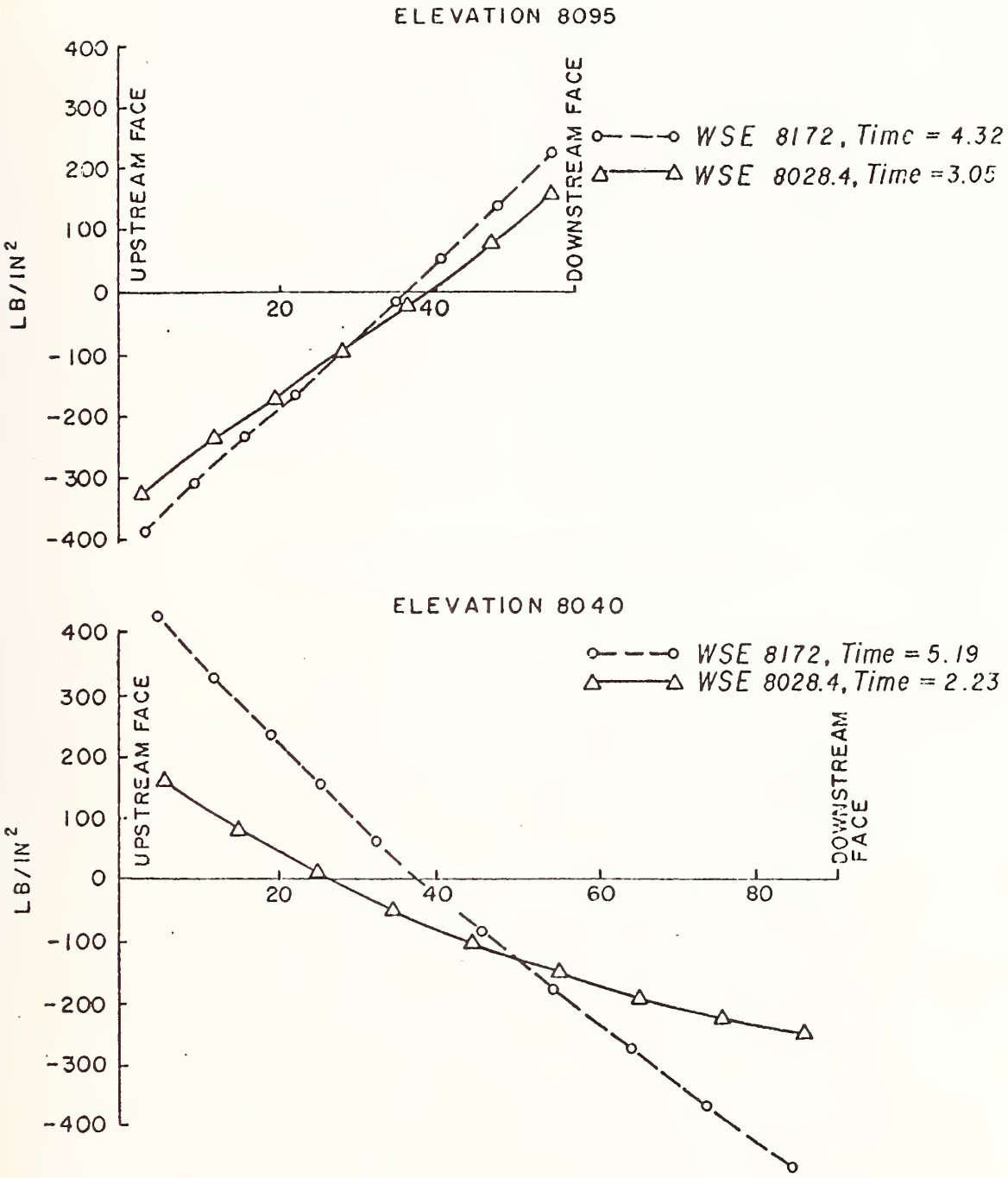

Fig. 9 VERTICAL STRESSES AT MAXIMUM SECTION
WATER + DEAD LOAD + MCE

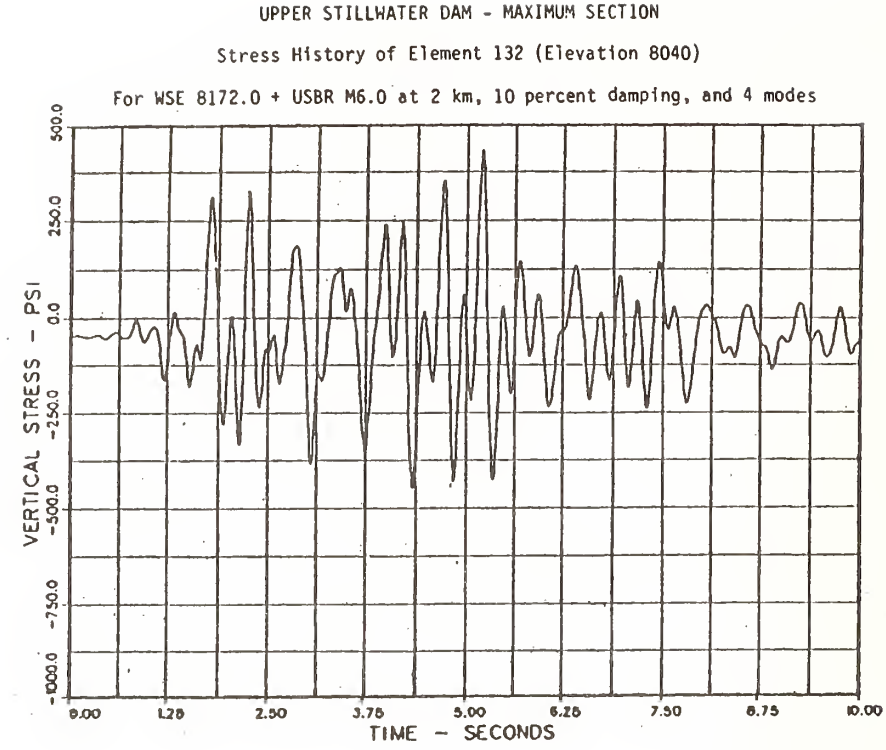

Fig. 10 VERTICAL STRESS HISTORY - MAXIMUM SECTION
UPSTREAM FACE - ELEVATION 8040 - HIGH WATER

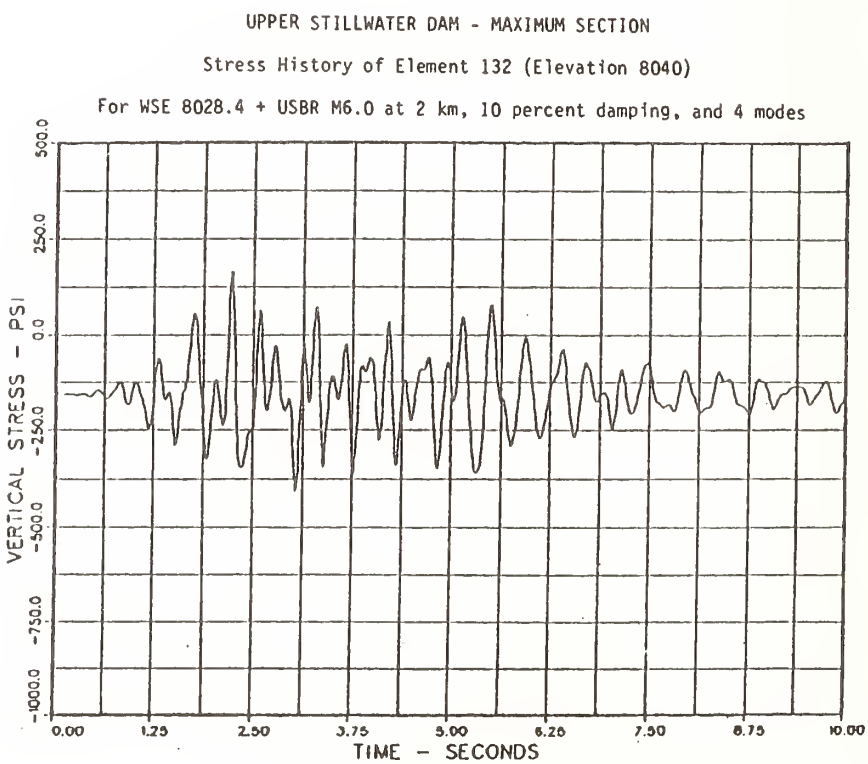

Fig. 11 VERTICAL STRESS HISTORY - MAXIMUM SECTION
UPSTREAM FACE - ELEVATION 8040 - LOW WATER

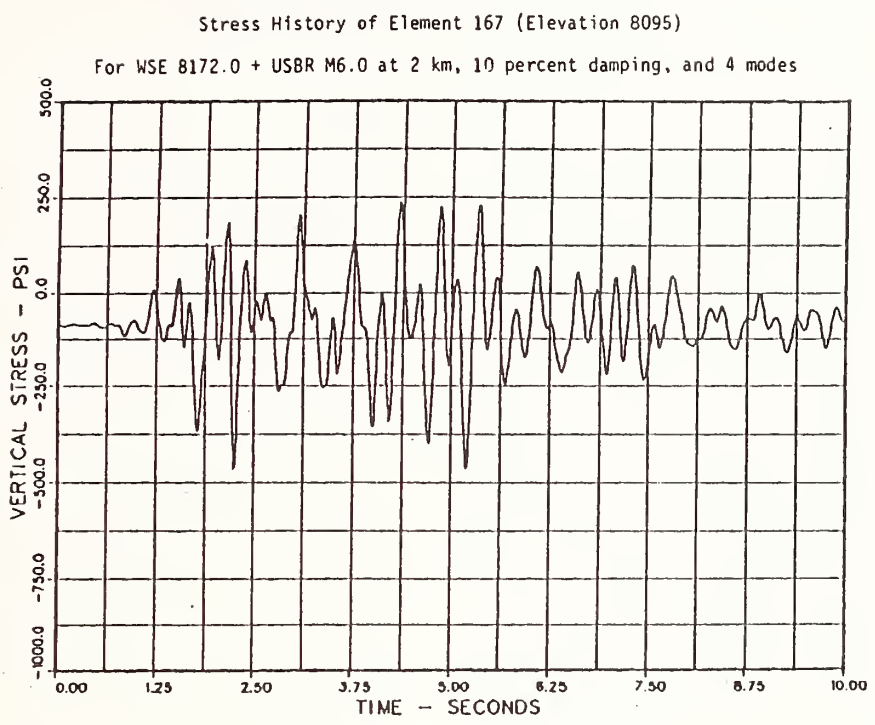

Fig. 12 VERTICAL STRESS HISTORY - MAXIMUM SECTION
DOWNSTREAM FACE - ELEVATION 8095 - HIGH WATER

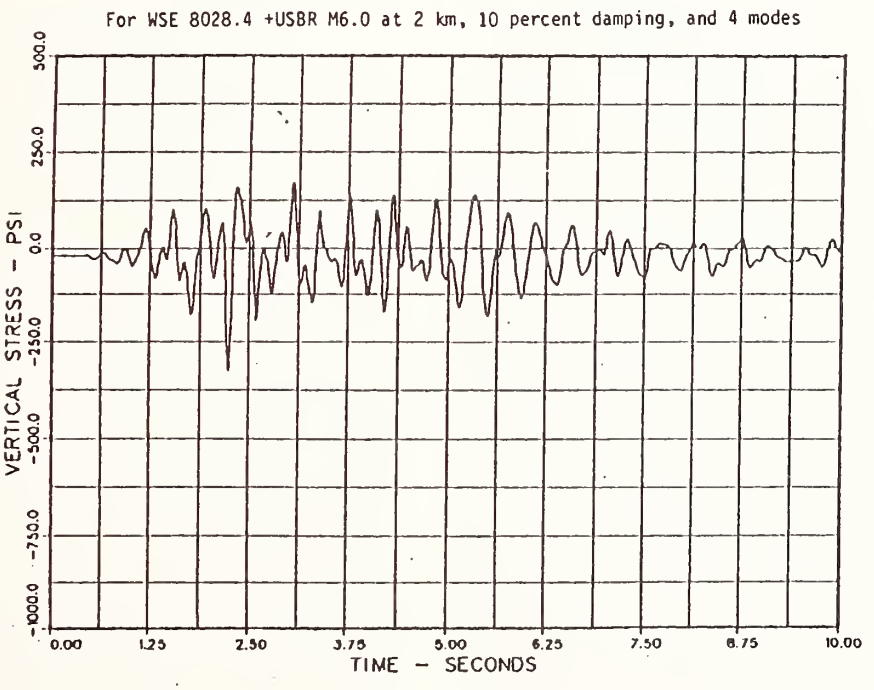

Fig. 13 VERTICAL STRESS HISTORY - MAXIMUM SECTION
DOWNSTREAM FACE - ELEVATION 8095 - LOW WATER

Damage of Soil Liquefaction Caused by Earthquakes and Use of Geomorphological Maps

by

Takekazu AKAGIRI‡

(abstract)

Damage of soil liquefaction caused by big earthquakes have been increasing recent years. The fundamental relationships between soil liquefaction and geomorphological units have been clarified. The author researched soil liquefaction caused by Niigata, Nihonkai-chubu and Chibaken toho-oki earthquakes to review the relationships based on literatures and field survey.

And he concluded that (1)soil liquefaction phenomena were the most remarkably caused in former river courses filled about several ten years ago and banked areas, (2)the qualitative susceptibility to liquefaction for each geomorphological unit has been interpreted using geomorphological maps by Geographical Survey Institute (GSI) and (3)micro-geomorphological maps are available for prediction of liquefaction.

[keywords] soil liquefaction, geomorphological maps, micro-zonation, sub-surface and landform

1.Introduction

Big earthquakes have caused sandy soil liquefaction, collapses of slopes, and other types of ground failures. Many cases of soil liquefaction have been found in the past. Traces of liquefaction caused in 12c. to 19c.. was found in old mounds in the ruins of 5 century in the subsurface layers, which sand boil had not reach the ground surface (Sangawa:1987). And Kanto earthquake (1923, M=7.9) caused soil liquefaction extensively in the lower drainage basin of the Nakagawa river (Gelological Survey 1925, Wakamatsu 1983). Also remarkable soil liquefaction was caused by Niigata earthquake (1964:M=7.5), Miyagiken-oki earthquake (1978: M=7.4), Nihonkai-chubu earthquake (M=7.7), Chibaken-toho-oki earthquake (1987 M=7.5) (fig.1: index map) and others.

Most of plains in Japan have been formed by fluvial process. Material has been transported from mountainous slopes to the lower drainage basin and deposited. Landforms and subsurface ground have been formed by the same process. Thus, it is possible to know subsurface ground condition using micro-landforms.

In this paper, the author reports that it is easy to interpret and predict qualitative susceptibility to the liquefaction using geomorphological maps based on the relationships between landforms and soil liquefaction.

2. Soil Liquefaction Caused by Earthquakes

2-1. Niigata earthquake (1964, M=7.5)

This earthquake induced various kinds of damages in Niigata and its surroundings: tunami, collapses and tilting of houses and buildings, inundation, fire, sudden subsidence and rising of ground surface, crack and sand boil with mud crater and etc.. Among them, soil liquefaction was caused in the extensive area in the lower drainage basin of the river Shinano.

GSI researched the damage using aerial photographs and in the field and compiled maps showing aspects of damage caused by Niigata earthquake and applied geomorphological maps at a scale of 1:10,000 (1964: fig.2,3).

According to the maps, liquefaction was caused remarkably in numbers in the former river courses filled after 1926 along the Shinano river, former river courses in the coastal lowland between the Agano and Shinano, (The area had been a river course during the past 400 years: Wakamatsu 1983), Niigata airport located at artificially changed dunes, interlevee lowlands, edges of natural levees with high ground water level and banked roads in the lowlands (tab.1,fig.3).

Subsurface ground along the Shinano was displaced laterally toward the river about 8m (one side)in the both sides of the river by soil liquefaction and the width of the river became narrower(Hamada et al. 1986). This is clearly found using a set of aerial photographs by GSI, taken before and after the earthquake.

In the subsurface of the damaged areas, Following characteristics were common to the areas in the subsurface of damaged areas: (1)sand deposited thick, which average diameter of the grain size is 0.1～0.5mm, (2)relative density is low and (3)ground water level is high. But, there was no damaged area by soil liquefaction in well developed dunes and natural levees, where ground water level is low and soil is compacted (Japan association of architecture 1964, Aoki, Ogawa, Yagi 1974, GSI: 1964).

2-2. Nihonkai-chubu earthquake (Middle Japan Sea eq.M=7.7)

This earthquake caused intensive damage by tunami from Aomori to Akita: maximum 15m high at the coast, several ten km from north to south along the coast, inundated land area 1km deep inland, various types of ground failures of ground, destruction of houses and buildings, destruction of lifelines and others.

Liquefaction phenomena were caused in many places in the lowlands. Long embankments subsided in the surrounding of the lake Hachirougata. In many places, liquefaction was observed in similar landform units to Niigata in former river courses of the river Omono, banked

‡Geographical Survey Institute

area, edges of sandy landform units (natural levees, sand dune). Lateral displacement of paddy fields was observed(fig.-4, 1984).

And at the edges of sandy landforms, sand was lost at the base of houses too much and damages of houses became larger. But only one house was not damaged at all. According to author's interview with the owner, the house was built up on the basis of enough piles (deep and many) into marshy land because the owner had known that subsurface ground condition had been the worst for housing.

2-3. Chibaken-Toho-Oki Earthquake (1987,M=6.7)

This earthquake hit the neighbor area of Tokyo and caused intensive damages in Chiba and Ibaraki prefectures. Damages are destruction of houses more than about several ten thousands, destruction of life lines, damages of roads, liquefaction in alluvial lowlands and fill along Tokyo Bay, former river courses and banked area in the lowlands of Kujukuri plain, former river courses in the lower drainage basin of the Tone river, and the reclaimed area by draining the lake in Itako Town. And slope collapses were induced in the hill slopes of the Kujukuri coastal area.

Liquefaction phenomena were caused in many places. Fig.5,6,7 are examples in the lower drainage basin of the Tone river. Comparing with liquefied sites and the geomorphological map drawn at a scale of 1:25,000 by GSI, liquefaction was caused in the alluvial lowland(one area), a combination with former river course and slip off slope (5 areas). Most of sand boil were formed in the former river courses. No soil liquefaction phenomena was not observed in undercut slope.

The author researched histories of these liquefied sites using the whole editions of former topographic maps since 1880. According to the maps, liquefied sites had been river courses several ten years ago. And after the construction of short cut in 1915, these sites remained as oxbow lakes where water chestnuts grew thick. And these were filled using river sand of the new channel of Tone river with sandpumps from 1960 to 1967. Later, partly river sand was sold out and backfilled using hilly sand.

Water-chestnuts in the area had deposited at the river floor before fill and came out with sand boil this time. Crack type of sand boil continue intermittently and side by side about several hundreds meters long (fig.5). The distribution coincided with the backfilled hilly sand area.

According to the boring data, which was reseached after the earthquake, by the science and engineering research laboratory of Waseda univ., surface geology consists of the followings: 0-6m:hill sand, river floor sand, 6-10m:fine sand, 10m-:very fine sand. And sand boil consists of fine sand and very fine sand. Then, sand boil came out from deeper layers below hilly sand layer.

Most of liquefaction were caused in the former river courses. Grain sizes are not well sorted. Sand boil was not observed in the former river courses which were filled up by natural processes or by gradual fill without sandpump.

3.Subsurface Condition and Geomorphological Maps

3-1.Geomorphological mapping and subsurface condition

Soil liquefaction is caused by the combination with (1)seismic intensity and duration, (2)density of sand (void ratio, relative density, N value), (3)grain size distribution, (4)ground water level, (5)depth of sand layer. And the phenomena change depend on the combination with these. Among them, except (1), others relates to subsurface condition and it shows that subsurface is indispensable to predict soil liquefaction sites.

Most of plains have been formed by fluvial process in Japan. Landform complex in the upper drainage basin has not changed in a period that microlandforms have been formed in the lower plain in usual. For the reason, in the lower plain, same material, which is transported from the upper drainage basin, has been deposited in specified sites repeatedly and microlandforms have been formed.

This process decides material and types of subsurface ground condition whether a fan develops to a big one or a little scale of boulder fan, and whether the fan consists of gravels or fine sand or silt. Similar type of subsurface have similar characteristics of subsurface condition . Wakamatsu et. al (1980) proposed that qualitative susceptibility to soil liquefaction was decided by the combination with types of plain, characteristics and scale of landform units.

As above mentioned, microlandforms show not only details of relief of plain, but also geomorphological genetic history and have indispensable relations to subsurface condition which are surface geology, soil condition, ground water and so on. Thus, it is naturally possible to make clear subsurface conditions using microlandforms.

As an example showing the relations, there is the distribution of cracks with sand boil in the lowland of Nakagawa river drainage basin in Saitama prefecture to the north of Tokyo, which was caused by 1923 Kanto earthquake (M7.9) in (Gelogical Survey:1925). The distribution coincided with the distribution of natural levees along former river courses. And it is clear that the numbers of liquefaction varied in each kind of geomorphological unit. And recent years, damages of soil liquefaction were caused in artificially changed landforms and subsurface.

Oya, Wakamatsu et al.(1982) compiled a geomorphological map for prediction of flooding and liquefaction in Shonai plain and made clear qualitative susceptibility to liquefaction at each geomorphological unit based on the research how frequently liquefaction was caused at each geomorphologlcal unit subject to seismic ground motion of the J.M.A. intensity V (J.M.A.V corresponds to Modified Mercalli intensity Ⅷ approximately) using the past earthquake. Three months after compilation of the map, Nihonkai-chubu earthquake caused liquefaction near the spring at dune edge where the map had predicted.

Kotoda et al. (1988) clarified peak ground velocity of the past 19 earthquakes at liquefied and non-liquefied sites on various geomorphological units to make clear the quantitative susceptibility to liquefaction. And they got the result of fig.-8,9 which showed critical values causing liquefaction. This does not conflict with the result by Oya et al..

3-2.Prediction of sites using geomorphological maps

Above mentioned geomorphological map was compiled based on the method of Oya's geomorphological map for prediction of flooding at a scale of 1:25,000. And geomorphological map series (1:25,000 land condition map series) by GSI was also based on his method with additional conceptions and legend for prediction of flooding at the beginning. But at this moment it has been being prepared for various purposes including ground failures by earthquake.

A geomorphological map is a map showing microlandforms based on aerial photointerpretation and field check to classify morphological characteristics. Geomorphologically, the objective area is classified into homogeneous units by the combination with form, material, genetic process and period the landform was formed.

Classification consists of three classes: Large units are mountainous area, hill-and-table land, and lowland. Middle units are valley floor, coastal and deltaic plain in the case of lowland. And detailed units are a former river course and a natural levee in the case of deltaic lowland.

In technology, micro-zoning maps for prediction of liquefaction decide susceptibility to liquefaction at each 500m mesh using boring data (geology and N value). The method is a typical quantitative method with an enormous numbers of boring data and the researcher must analyse data at each mesh. And the reliability becomes lower in an area with few boring data. The method is not a preliminary method, but a fundamental research.

The method based on geomorphological mapping is qualitatively. And (1)it is possible to classify pretty extensive area based on aerial photointerpretation in a short period at low cost. And many geomorphological maps covering most of plains have been prepared at middle scales. (2)in comparison with a mesh map, it is possible to draw more suitable boundaries which corresponds with actual boundaries of subsurface conditions using geomorphological maps. (3)even if users do not have enough knowledge of soil engineering and geomorphology, it is easy to interpret subsurface conditions and susceptibility to liquefaction. (4)it is possible to research general condition at a scale of 1:50,000 first, and if necessary, more detailed work can be done at a scale of 1:10,000 or 1:5,000. And quantitative work can be done after it. It means that this method has characteristics as a preliminary research. The National Land Agency has been preparing micro-zonation maps for prediction of liquefaction with geomorphological mapping.

4.Conclusions

(1) The author researched a few earthquakes which caused soil liquefaction and reviewed the relationships between geomorphological units and soil liquefaction. Based on the research of Chibaken-toho-oki earthquake, it was clarified that soil liquefaction was caused in deeper layer than 4m and in the former river courses and fill about several ten years ago. And these sites were shown as specified landform units in the geomorphological maps published by GSI.

(2) The susceptibility to liquefaction for each geomorphological unit based on geomorphological mapping does not conflict with the result that Wakamatsu et.al clarified qualitative susceptibility to liquefaction at every geomorphological unit based on peak ground velocity. And it is reasonably possible to explain conceptions based on fluvial process.

Existing geomorphological maps are available to microzonation for prediction of liquefaction. And the microzonation based on geomorphological mapping is effective as a preliminary research.

Acknowledgment

The author would like to thank Mrs. Kazue Wakamatsu, Waseda Univ. for her helpful suggestion.

References (E):in English

Akagiri,T(1988):Damages Caused by Chibaken-toho Earthquake. Report of GSI(Jihou) vol.67

Oya,M ed.(1983): Method and Development of Geomorphological Mapping. Kokon-shoin Tokyo

Oya, Kotoda, Wakamatsu, Kubo(1982): A geomorphological map for prediction of flooding and liquefaction in the Shonai plain.

GSI(1976):Land condition map series and document of Sawara

GSI(1964): Actual conditions of damages caused by Niigata earthquake and land condition with document 1:10,000 2sheets

Kotoda, Wakamatsu(1988):Liquefaction phenomena and resulting damage to structures during the damages caused by Chibaken-toho Earthquake. Soil and Foundation vol 36-12, pp19-24
Kotoda, Wakamatsu and Mase(1988): Liquefaction phenomena caused by 1987 Chibaken-toho earthquake. part 2. 23rd meeting of soil engineering proceedings. pp959-962
Sunaga, Kumaki(1982):Subsurface damages caused by earthquakes and geomorphological mapping. Report of GSI(Jihou) No.56 pp24-31
First Geographic Division, GSI(1984): Geomorphological map and Damages Caused by Nihonkai chubu earthquake
Geological Survey(1925):Report on Kanto earthquake. part 1. 240p.
Nakano and Oya(1960):The relationships between landforms and high tide flooding. sokuryou. 1960
Hamada, Yasuda, Isoyama and Emoto(1986): Permanent displacement of ground caused by liquefaction. Study on liquefaction induced permanent ground displacements. Civil Association for the Development of Earthquake Prediction pp87
Sangawa(1987):Traces of earthquake found in Hotarudani ruins in Otu city in Shiga pref. Chishitu News No.390.
Wakamatsu,K(1983):Damages caused by earthquakes and geomorphological maps. Oya ed."Method and development of Geomorphological mapping" p157-169
Wakamatsu,K(1980):Geomorphological consideration on site conditions of soil liquefaction caused by earthquake. Asian Profile vol.8, No. 3, 279-297 (E)
Watanabe, Iwata, Yasuda, Sato and Ohashi (1983): 18th meeting of soil engineering. proceedings. pp567-568

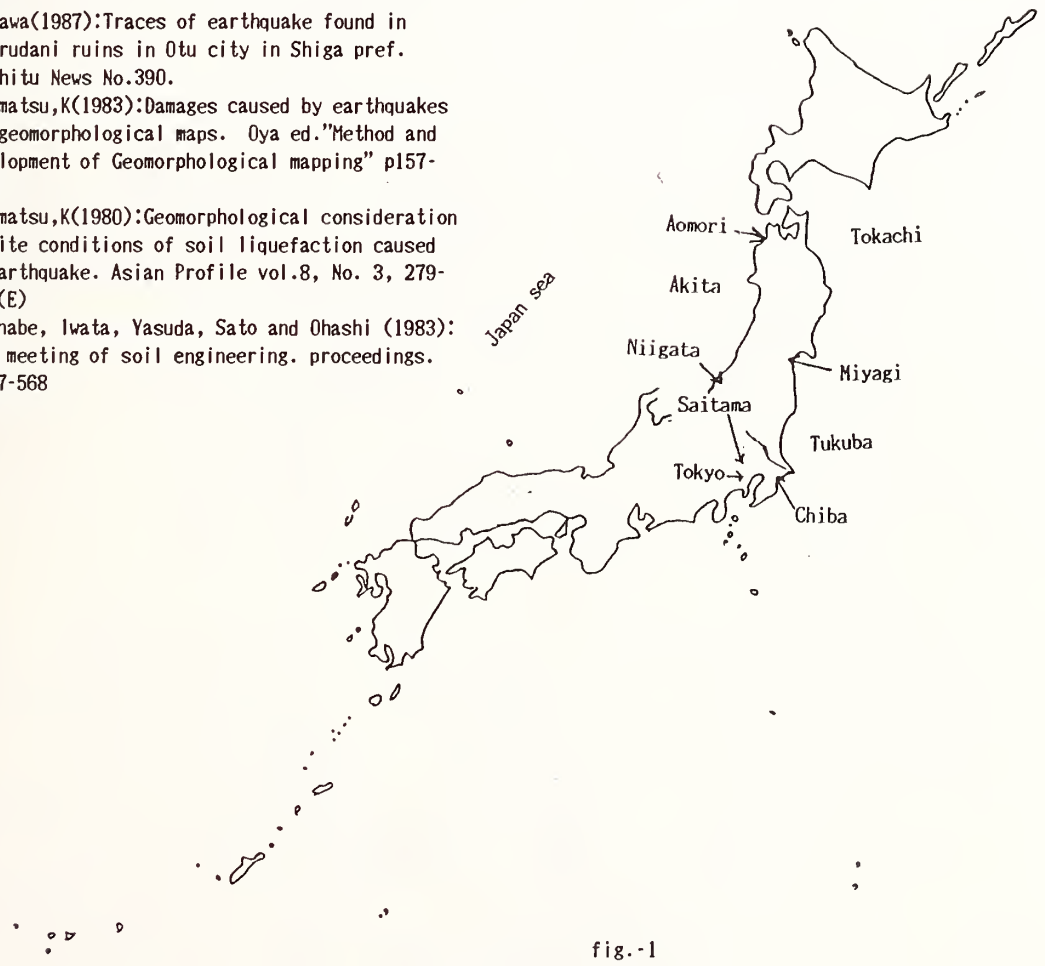

fig.-1

図－1　索引図

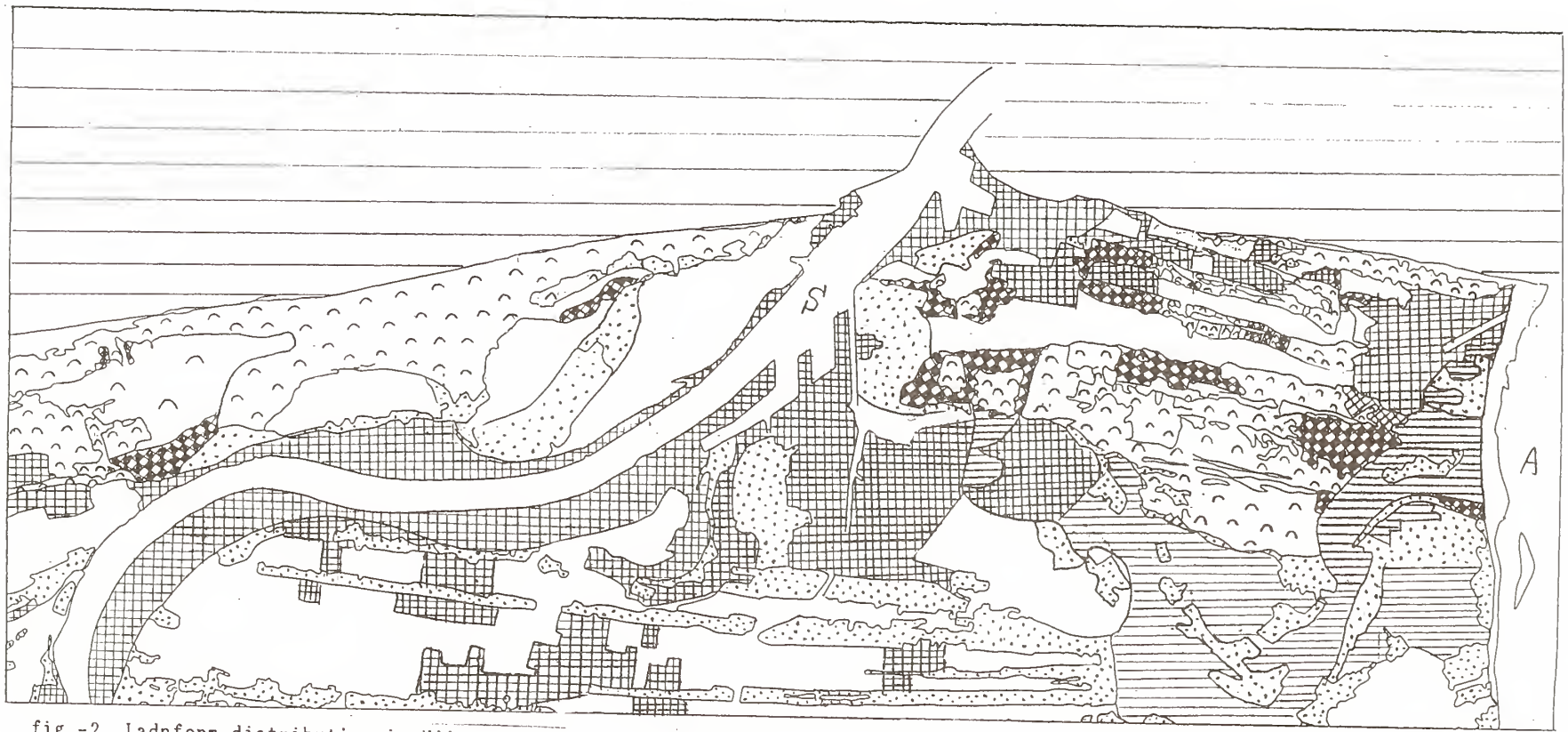

fig.-2 Ladnform distribution in Niigata city
Compiled from "Geomorphological map at a scale of 1:10,000 by GSI". approximate scale 1:50,000

sand dune
砂丘

Shinano river
信濃川 S

coastal lowland
海岸平野

natural levee
自然堤防

beach ridge, bar
砂州・砂堆

former river course
旧河道

banked area
盛土地

fill
埋立地

artificially changed area
人工改変地

Agano river A
阿賀野川

fig.-3 Distribution of cracks and sand boils
Compiled from "Actual condition map on damages caused by Niigata earthquake at a scale of 1:10,000"

凡　例

	地震前の地盤高	G.L. before eaarthquake
	地震後の地盤高	G.L. after eearthquake
	地　割　れ	cracks
	噴砂・噴水	sand boil
	段差のある亀裂	ground crack with vertical gap
	土地の移動方向	lateral displacement
	地震後の耕地界(畦畔)	boundary of paddy field displaced by the eq.

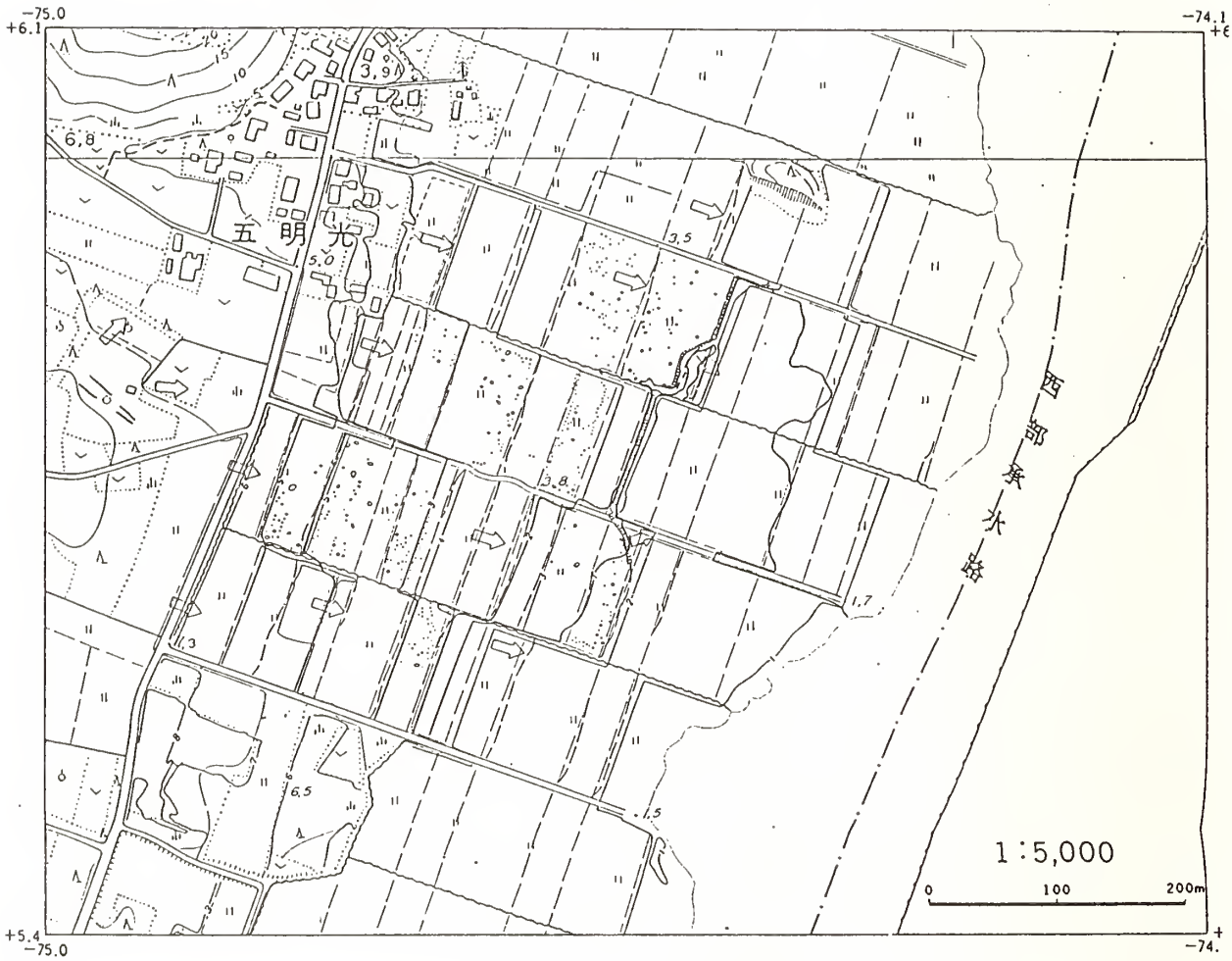

fig.4- Landform change (lateral displacement) at Gomyoukou near Lake Hachirougata in Akita pref. Caused by Nihonkai-Chubu Earthquake, 1983"

by First Geographic Division of GSI(1983)

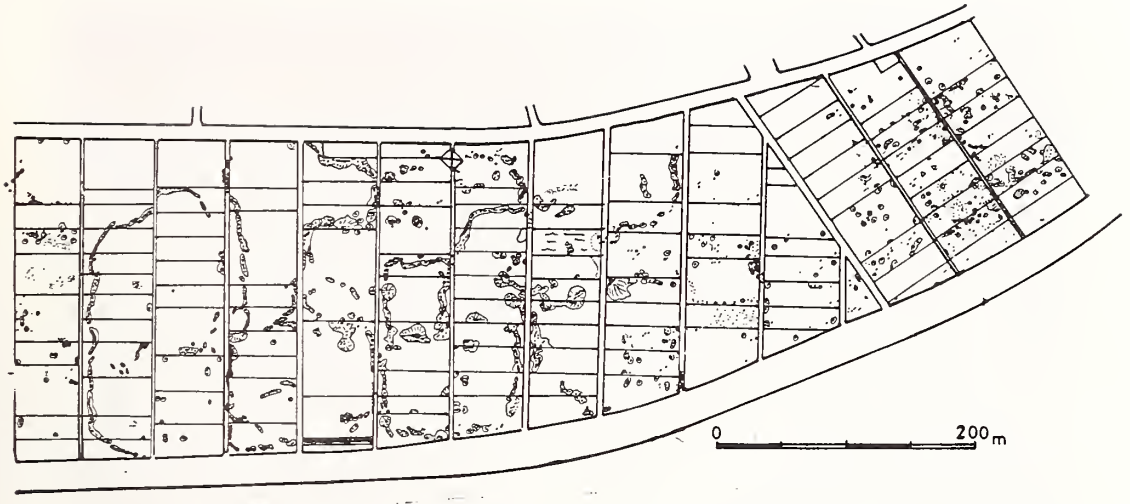

fig.-5 Distribution of Sand Boils in the Lower Drainage Basin of The Tone River

sand boils

horizontal bar
:1 m

horizontal bar
:1.5m

写真12 神崎町向野
群発型の噴砂口，大穴φ2.7m×2.1mが2つ，横棒は検土杖1.5m

fig.6- Distribution of Sand Boils in the Lower Drainage of the Tone River

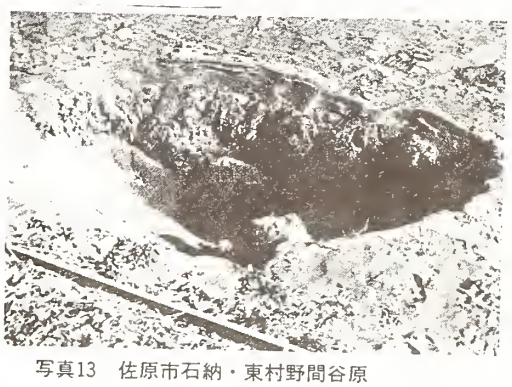

写真13　佐原市石納・東村野間谷原
群発型の最大口径φ2.85m×2.1m，噴砂丘φ27m（写真14にも説明）

fig.7- upper: 1:25,000 geomorphol-gical map
(land condition map) by GSI ×0.5
lower: 1:50,000 topographic map,1975

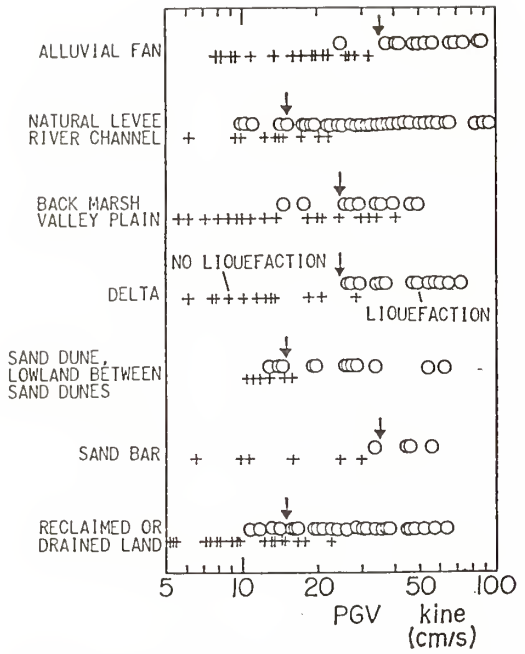

Fig. 8 Peak ground velocity at liquefied and non-liquefied sites on various geomorphological units

fig.9- Peak ground velocity which causes liquefaction

landform	peak ground velocity
fill reclaimed land by draining natural levee river course edge of dune interdune lowland	15cm/s
backmarsh valley floor delta surface	25cm/s
beach ridge fan	35cm/s

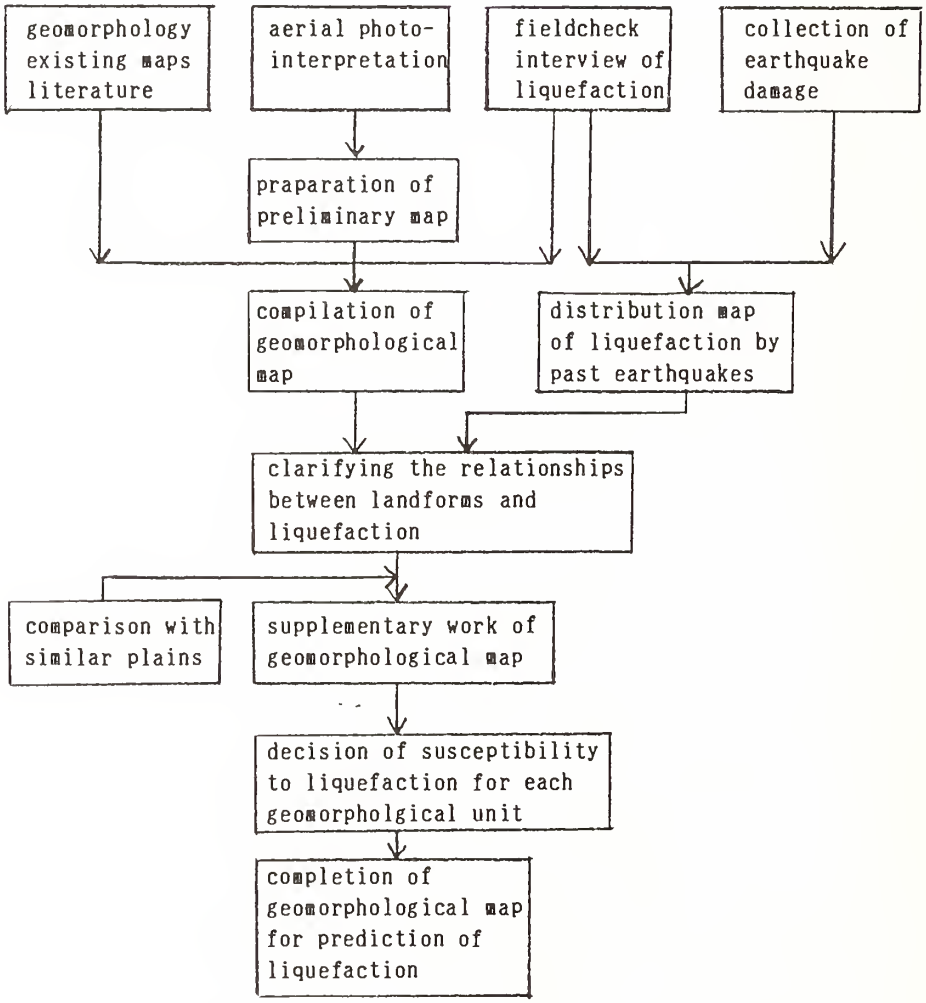

fig.10- A flowchart to compile a geomorphological map for prediction of liquefaction

Dynamic Deformation Characteristics of Compacted Rockfills by Cyclic Torsional Simple Shear Tests

by

Norihisa MATSUMOTO [1] Nario YASUDA [2] Masahiko OHOKUBO [3] Yasushi KINOSHITA [4]

ABSTRACT

Large-scale cyclic torsional simple shear tests (CTSS) were performed to investigate the dynamic deformation characteristics of compacted rockfills (gravels) at wide shear strain range. The effects of confining pressure, void ratio, principal stress ratio and cycle loading frequency on the shear modulus and damping ratio are evaluated. It has been found that shear modulus is expressed as the function of void ratio and confining pressure for compacted rockfill as proposed in the past studies for sands, and damping ratio can be expressed as a linear function of void ratio. The influence of principal stress ratio to shear modulus in the cyclic torsional simple shear test(CTSS) was proven to be different from that at cyclic triaxial test(CTX). Furthermore, the strain dependent curves of normalized shear modulus and damping ratio by CTSS for gravels show similar inclination comparing to those from CTX.

1. INTRODUCTION

It is important for the rational and economical design, and construction of rockfill dams to study the dynamic properties of compacted rockfills (gravels), which occupy a large part of the dam body and contribute greatly the stability. Furthermore it is desirable that these properties be obtained under stress-strain state similar to that of the field.

The cyclic triaxial test using solid specimen of about 30 cm in diameter and 60 cm in height has been frequently conducted due to easy handling. However, the triaxial test, in which the principal stress axes are fixed in vertical and horizontal directions, does not simulate necessarily the stress-strain state of the dam body during earthquakes.

During earthquakes, the shearing vibration is apt to be predominant in the dynamic stress-strain state of rockfill dams with a continuous rotation of principal stress axes. Simple shear test apparatuses of SGI, NGI and Cambridge types can reproduce the stress-strain state of the field elements subject to shear deformations. However, the effects of the end surface of specimen, namely, the shortage of transmitted shear stress and the stress concentration at the inside of specimen are conspicuous in this apparatus. On the other hand , these effects are negligible in CTSS owing to its unlimited cylindrical shape.

A large number of hollow cylindrical torsional simple shear tests have been performed for static and dynamic strength and deformation characteristics of sands to date, only a few tests have been carried out on rockfills. In order to investigate the dynamic deformation characteristics of rockfills (maximum particle size of 38.1 mm) corresponding to grained stress-strain state in the field, the research was conducted for a wide shear strain range by using large-scale cyclic torsional simple shear device with hollow cylindrical specimen.

2. LARGE-SCALE CYCLIC TORSIONAL SIMPLE SHEAR DEVICE

All experiments were performed using large-scale cyclic torsional simple shear device. In this device a hollow cylindrical specimen of 80 cm in height, can apply independently to the specimen axial stress, confining pressure and torsional shear stress. Furthermore, triaxial compression and extension tests can also be carried out by preparing the solid specimen of 40 cm in diameter and 80 cm long in this device.

Fukushima, et al. (1980) investigated the ratio of the outer diameter to height of hollow cylindrical specimens using four different heights of the

1.Chief,Filldam Division,Public Works Research Institute,the Ministry of Construction,TSUKUBA City,Japan
2.Research Engineer, ditto
3.Engineer, ditto
4.Consulting Engineer, C.T.I. Engineering, Co.,Ltd. Formerly visiting researcher of P.W.R.I.

preparing the solid specimen of 40 cm in diameter and 80 cm long in this device.

Fukushima, et al. (1980) investigated the ratio of the outer diameter to height of hollow cylindrical specimens using four different heights of the specimens, with the same outer and inner diameters for dry sands. They reported that the height of specimen was desirable to be larger than the outer diameter to eliminate the disturbance of end constraints. Thus, the ratio of 1.0 has been applied to this large-scale torsional simple shear device as the proportion of a height to a diameter.

3. TEST CONDITIONS AND PROCEDURES

Quartz andesite was used for the specimen materials in this study. The materials were transported from the quarry site of a rockfill dam now under construction to the laboratory of P.W.R.I. The grain size distribution of a specimen is determined so as to resemble that in field, and illustrated in Fig 1. The maximum grain particle size is 38.1 mm resulting from the requirement that maximum particle diameter must not exceed 1/5 of the thickness of the specimen diameter.

All experiments were performed under the air-dried and drained conditions. Table 1 shows test cases conducted this study.

To accommodate the 10 th hysteresis loop of stress-strain under steady state at every 0.01 second, an analog-digital conversion system and data storage system with memory controlled by a personal computer are used for data acquisition.

4. EXPERIMENTAL RESULTS AND ANALYSIS

4.1 Dynamic Test Results

Shear strain dependent curves of modulus G and damping ratio h with void ratio e_c=0.42 and stress ratio σ_1/σ_3 =1.0 are illustrated in Fig. 2. The smooth curves of shear modulus G were obtained at the strain range of 2×10^{-6} ~5×10^{-4}. Usually, dynamic deformation characteristics at the shear strain levels less than 1×10^{-4} was obtained by resonant column test, and those at more than 1×10^{-4} was from cyclic triaxial test (CTX). Both test methods rarely coincided with each other. In this study, dynamic properties at wide shear strain range including strain less than 1×10^{-5} are continuously gained by CTX due to the usage of the ultra-sensitive displacement transducer (Gap sensor).

The effect of confining pressure σ_c on damping ratio were found in the case of sands, however it has not been obvious in rockfills. Otherwise the effect of σ_c on damping ratio was recognized at cyclic torsional simple shear test (CTSS) of this study as described later.

Fig. 3 indicates the relation between shear modulus G and void ratio after a consolidation e_c. G is divided by the function of confining pressure $(\sigma_c)^m$ in order to eliminate the effect of σ_c itself. It is distinct that the void ratio e_c increases, the shear modulus G decreases. The relation of G to e_c for rockfills is well expressed in Eq. 1 proposed by Hardin and Richart (1963) for shear modulus of sands at minute shear strain.

$$\left.\begin{aligned} G &= K(\gamma)\,\alpha\,(\sigma_c)^m \\ \alpha &= \frac{(2.17-e_c)^2}{1+e_c} \end{aligned}\right\} \quad \text{----------(1)}$$

Where, K = constant depending on shear strain, m = power related to confining pressure (depending on shear strain), σ_c = effective confining pressure.

CTSS results of this study are plotted around approximate straight lines from regression analysis as shown in Fig. 3. Kokusho, et al. (1980) also proposed the same slope of approximate straight lines for crushed and round rocks by CTX, so it can be confirmed that the relation between shear modulus G and void ratio e_c for rockfills is independent of testing methods, and can be explained as Eq. 1.

Fig. 4 indicates the relation of shear modulus G to confining pressure σ_c both in logarithmic scales with shear strains as parameters. G at ordinate is divided by Eq. 1 to remove the effect of void ratio. G decreases with the increase of shear strain and increasing with the rise of σ_c. The incline of linear regression line drawn in Fig. 4 becomes gentler according to the smaller shear strain range as well as results from CTX.

Fig. 5 shows the power, m, relating shear modulus G to confining pressure. The power m concerning confining pressure σ_c is a function of shear strain. CTX results of gravel as are

plotted together in this figure with test data of the sand from Kokusho, et al. (1980) and Iwasaki, et al. (1980). It can be seen that power m of rockfills is distributed from 0.65 to 0.85 irrespective of testing method, and is larger than that of sands at wider shear strain range. Consequently, shear modulus G of rockfills can be displayed by Eq. 1 at not only very small but also large shear.

Fig. 6 shows the relation of damping ratio h to void ratio e_c. Damping ratios are also normalized by the function of the confining pressure $(\sigma_c)^n$ to eliminate the effect of the confining pressure in the same way as the case of shear modulus. The relationship has a precise inclination to increase according to the rise of void ratio at shear strain range of $5\times10^{-5} \sim 5\times10^{-4}$. This tendency is attributed to the increase of energy loss by small plastic deformations of the specimen in proportion to the higher void ratio against the same cyclic load. The relationship between damping ratio and void ratio can be expressed by the following equation.

$$\left.\begin{aligned} h &= L(\gamma)\ \beta\ (\sigma_c)^n \\ \beta &= 0.4 + 1.5\ e_c \end{aligned}\right\} \quad \text{----------(2)}$$

Where, L = constant depending on shear strain, n = power related to confining pressure (depending on shear strain).

Fig. 7 illustrates the relation of damping ratio h/β to confining pressure σ_c. Damping ratio is normalized by the function of void ratio e_c to eliminate the influence of e_c as the case of shear modulus. The slopes of linear regression lines become steeper accompanying with the smaller shear strain in opposition to the relation between G and σ_c. The above-mentioned inclination of damping ratio is not often apparent in CTX testing.

Principal stress ratio (σ_1/σ_3, in which σ_1 = major principal stress, σ_3 = minor principal stress) of a rock zone at rockfill dam body ranges from 1.0 to 2.0 according to monitoring of observational instruments at the dam body, and becomes larger inside the body. In this study, CTSS is also performed under two different anisotropic consolidations of σ_1/σ_3 =1.5 and 2.0 besides isotropic consolidation. The relation between principal stress ratio σ_1/σ_3 and Rs, which is the ratio of shear modulus G against shear modulus at σ_1/σ_3 of 1.0 both under the same mean principal stress conditions, is indicated in Fig. 8. Figure is arranged for shear strain of 2×10^{-4} and four levels of mean principal stress σ_m = 1.0, 2.0, 3.0 and 4.0 kgf/cm^2. Rs is less than 1.0 about cyclic torsional simple shear test (CTSS). The results of cyclic triaxial test (CTX) by this apparatus are also shown in Fig. 8, and Rs ranges from 1.2. to 1.4 illustrating the reverse inclination of principal stress ratio in comparison with CTSS. Test result of CTX with solid specimen of ϕ 30 cm in diameter and 60 cm high is conducted by Matsumoto, et al. (1986) using the same quartz andesite and plotted in this figure.

The influence of σ_1/σ_3 to damping ratio is not so clear as that to shear modulus. It is estimated that there is not a significant effect of σ_1/σ_3 upon the damping.

It is generally known that the clay materials are not affected by cyclic frequency of dynamic load except for a large deformation as a creep. Hara and Kiyota (1979) concluded that shear modulus of clean sands is constant value at the frequency range of 0.1 ~ 10.0 Hz. In this study the dependency of frequency for rockfills is investigated about the lower range of 0.01 ~ 0.2 Hz by reason of the limited capacity of testing device. Tests are accomplished for four levels of confining pressure and strain range of $2\times10^{-6} \sim 5\times10^{-4}$, and it is recognized that almost similar shear modulus are observed at each pressure level. (see Fig. 9)

Hardin and Drnevich (1972) proposed that the relation between shear modulus G and damping ratio h is independent of void ratio e_c, confining pressure σ_c and shear strain, and simply expressed as Eq. 3.

$$h = h_{max}\left(1 - \frac{G}{G_0}\right) \qquad (3)$$

Where, G_0 = maximum shear modulus, h_{max} = damping ratio at G=0. Fig. 10 shows the relation of normalized shear modulus G/G_0 to damping ratio h for this testing. Results for specimens at three different void ratios are plotted with their linear regression lines, and the line from the average of whole data. A least squares regression fit is performed to obtain these linear

regression lines. Data of each void ratio scatters around the linear line independent of shear strain and confining pressure σ_c, and high correlation between data and lines are evident. However, h_{max} which shows the slope of linear line, becomes larger according to the increase of e_c as is corresponding to the relation between them in Fig. 6. It has also been shown that h_{max} of sandy soils are determined irrespective of e_c as for average line of several kinds of natural sands drawn in this figure (Tatsuoka, et al. (1978)). Though, gravels have a different inclination according to e_c and indicate lower values comparing with the average line of sands. The effect of principal stress ratio were not evident in this study.

4.2 Strain Dependent Curves of Rockfills

The average degradation curve of normalized shear modulus observed in this laboratory test is shown in Fig. 11 together with the results of rockfills from other researchers. Matsumoto, et al. (1985) conducted cyclic triaxial test (CTX) using crushed angular gravels with the specimen of 30 cm in height and 60 cm in diameter. Reconstituted samples of Tokyo gravel of 90 mm maximum particle size were tested with the same size of specimens in CTX by Hatanaka, et al. (1988). The normalized average degradation curve after Seed, et al. (1984) consists of results from angular and rounded rockfills of several earth and rockfill dams. Hynes, et al. (1988) conducted tests using rounded rockfills from Folsom Dam. The curves obtained by Japanese researchers are about 30 percent higher than those from Seed, et al. (1984) and Hynes, et al. (1988) at strain of 1×10^{-4}.

The strain dependent curves of damping ratio indicate similar inclination in shear strain range of 1×10^{-5} to 5×10^{-4}, though CTX results are expected to show slightly smaller values in larger shear strain except for the results from Seed, et al. (1984).

These divergences may come from the differences of materials, and test equipment and procedures used in both countries, so the further study seems to be necessary in future.

5. CONCLUSION

Air-dried rockfills were tested in a large-scale hollow cylindrical cyclic torsional simple shear apparatus in drained condition. The experiments were conducted under stress controlled condition and about dynamic characteristics at wide shear strain range including less than 1×10^{-5}. the following conclusion can be drawn for rockfills in this study:

1. $K \cdot (2.17-e_c)^2/(1+e_c) \cdot (\sigma_c)m$ can express shear modulus at wide shear strain including initial shear modulus. Power m is distributed from 0.65 to 0.85 independent of shear test method and higher than that of sand.
2. Though the shear modulus of cyclic torsional simple shear test (CTSS) tend to become larger with the increase of principal stress ratio ranging from 1.0 to 2.0, ones of cyclic triaxial compression test (CTX) have an inclination to be smaller under the same stress ratio and mean principal stress.
3. The relation between damping ratio and void ratio is obvious at CTSS and explained as the linear function.
4. Shear modulus relates to damping ratio lineally as proposed by Hardin and Drnevich (1972) and linear regression line has a gentle slope comparing to sands.
5. The strain dependent curves of shear modulus obtained in Japan is 30 % higher than those in the United States.

References

1. Fukushima, S., Nakajima, K. and Tatsuoka, F (1980). "Drained Shear Characteristics of Sand in Torsional Simple Shear Test", The proceeding of 16th Annual Meeting, JSSMFE, pp. 102-105 (in Japanese)

2. Hara, A. and kiyota, Y., (1979). "Study on Dynamic Properties of Soils for Dynamic Analysis of Foundation", The proceeding of 14th Annual Meeting, JSSMFE (in Japanese)

3. Hardin, B. O. and Drnevich, V. P., (1972). "Shear Modulus and Damping in Soils, Design Equation and Curves", Journal of Soil Mechanics and Foundation Engineering, ASCE, Vol, 98, No. SM7, pp.667-692.

4. Hardin, B. O. and Richart, F. E. Jr., (1963), "Elastic Wave Velocities in Granular Soils", Journal of Soil Mechanics and Foundation Engineering, Proceeding of ASCE, Vol.89, No. SMI,

pp.33-35

5. Hatanaka, M., (1975,1976), "Dynamic Behavior of Sand Obtained in Ring Torsion Shear Test", Reports of Committee on Dynamic Properties of Soils, Building Research Institute, Ministry of Construction (in Japanese)

6. Hatanaka, M., Suzuki, Y., Kawasaki, T. and Endo, M., (1988), "Cyclic Undrained shear Properties of High Quality Undisturbed Gravel", Soil and Foundation, Vol.28, No.4, JSSMFE, pp57-68

7. Hynes, M. E., Wahl, R. E., Donaghe, R T. and Tsuchida, T., (1988), "Seismic Stability Evaluation of Folsom Dam and Reservoir Project, Report 4, Mormon Island Auxiliary Dam - Phase I", Technical report GL-87-14, Department of the Army, WES, Corps of engineers

8. Iwsaki, T., Tatsuoka, F. and Takagi, Y., (1976), "Dynamic Properties of Sand at Wide Shear Strain Range", Technical Memorandum No. 1080, Public Works Research Institute, Ministry of Construction, Japan (in Japanese)

9. Iwsaki, T., Tatsuoka, F. and Takagi, Y., (1980), "Experimental Study on Dynamic Deformation Properties of the Ground (II)", Technical Report No.153, Public Works Research Institute, Ministry of Construction, Japan (in Japanese)

10. Kokusho, T. Sakurai, A. and Esashi, Y.,(1979), "Cyclic Triaxial Test of Dynamic Soil Properties for Wide Strain Range", Central Research Institute of Electric Power Industry, Civil Engineering Laboratory, No. 379002, (in Japanese)

11. Kokusho, T. Esashi, Y. and Sakurai, A., (1980). "Dynamic Properties of Deformation and Damping of Coarse Soils for Wide Strain Range", Central Research Institute of Electric Power Industry, Civil engineering Laboratory, Report No. 380002, (in Japanese)

12. Matsumoto, N. Yasuda, N. and Ohkubo, M. (1986), "Measurement of Dynamic Poisson's Ratio of Toyoura Standard Sand", Proceedings of the 21st Annual Meeting, JSSMFE, pp.555-556. (in Japanese)

13. Matsumoto, N. Yasuda, N. and Shiga, M., (1985), "Behaviours of a Rockfill Dam during Earthquakes", The 17th Joint Meeting of U.S.-Japan Panel on Wind and Seismic Effects, UJNR

14. Matsumoto, N. Yasuda, N. and Ohkubo, M., (1986), "Dynamic Shear Modulus, Damping Ratio, and Poisson's Ratio of Coarse-Grained Granular Materials", Civil Engineering Journal, Vol. 28, No. 7, Public Works Research Institute, Ministry of Construction, Japan, (in Japanese)

15. Matsumoto, N. Watanabe, K. and Ohno, K. (1984), "Dynamic Property Tests for Sands and Rockfill Materials by using Large-Scale Shearing Apparatus - Hollow Cylindrical Simple Shear and Cyclic Triaxial shear Test", Technical Memorandum No.2132, Public Works Research Institute, Ministry of Construction, Japan (in Japanese)

16. Ohoka, H. and Itoh, K., (1979), "Stress-Strain Behavior of Dry Sand and Normally Consolidated Clay by Inter-Laboratory Cooperative Cyclic Shear Tests", The 11th Joint Meeting of U.S.-Japan Panel on Wind and Seismic Effects, UJNR, pp.424-453

17. Seed, H. B., Wong, R. T. Idriss, I. M. and Tokimatsu, K., (1984), "Modulus and Damping Factors for Dynamic Analysis of Cohesionless Soils", Report No. EERC 84-14. Earthquake Engineering Research Center, University of California, Berkeley, Ca.

18. Suzuki, Y., Sugimoto, M., Babasaki, R. and Kakita, E. (1976), "Measurement of Poisson's Ratio by Means of Dynamic Triaxial Apparatus", Proceedings of the 11th Annual Meeting, JSSMFE, pp.415-418 (in Japanese)

19. Tatsuoka, F., Iwasaki, T. and Takagi, Y. (1979), "Hysteretic Damping of Sands and Its Relation to Shear Modulus, Soil and Foundations, Vol. 18, No.2, June, 1978

Table 1. Test Cases Conducted (CTSS and CTX)

	Initial Void Ratio	Relative Density (%)	Principal Stress Ratio	Confining Pressure (kgf/cm^2)	Cyclic Frequency (Hz)
1	0.42	70.9	1.0	1.0	0.2
2	0.47	59.2			
3	0.52	47.4		2.0	
4	0.42	70.9		3.0	0.2, 0.1 0.05, 0.01
5	0.42	70.9	1.5	4.0	0.2
6	0.42	70.9	2.0		

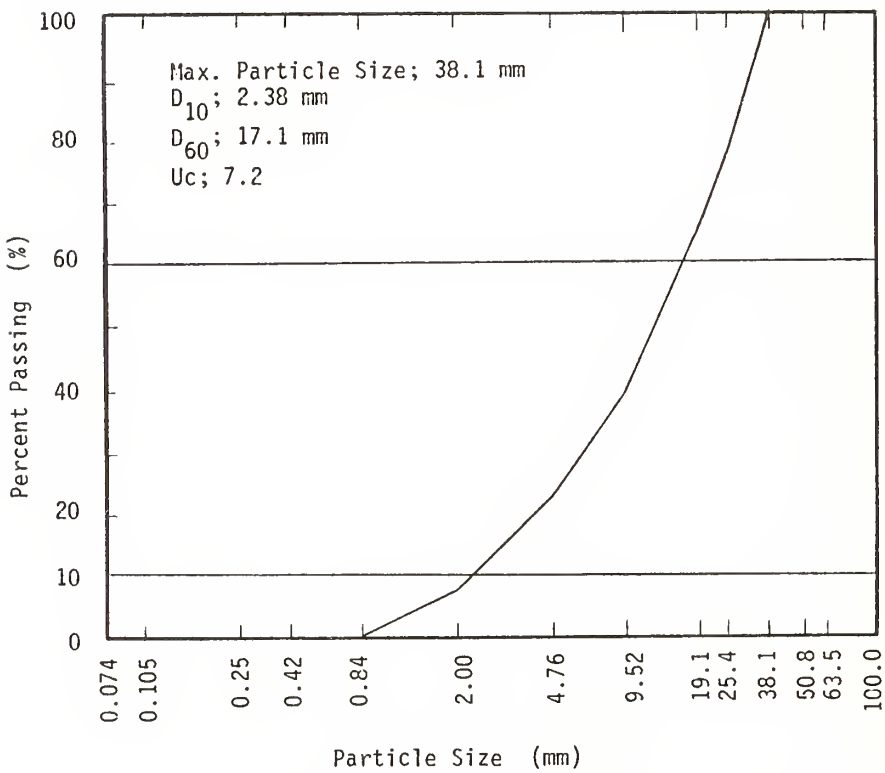

Fig. 1 Grain Size Distribution Curve of Specimen

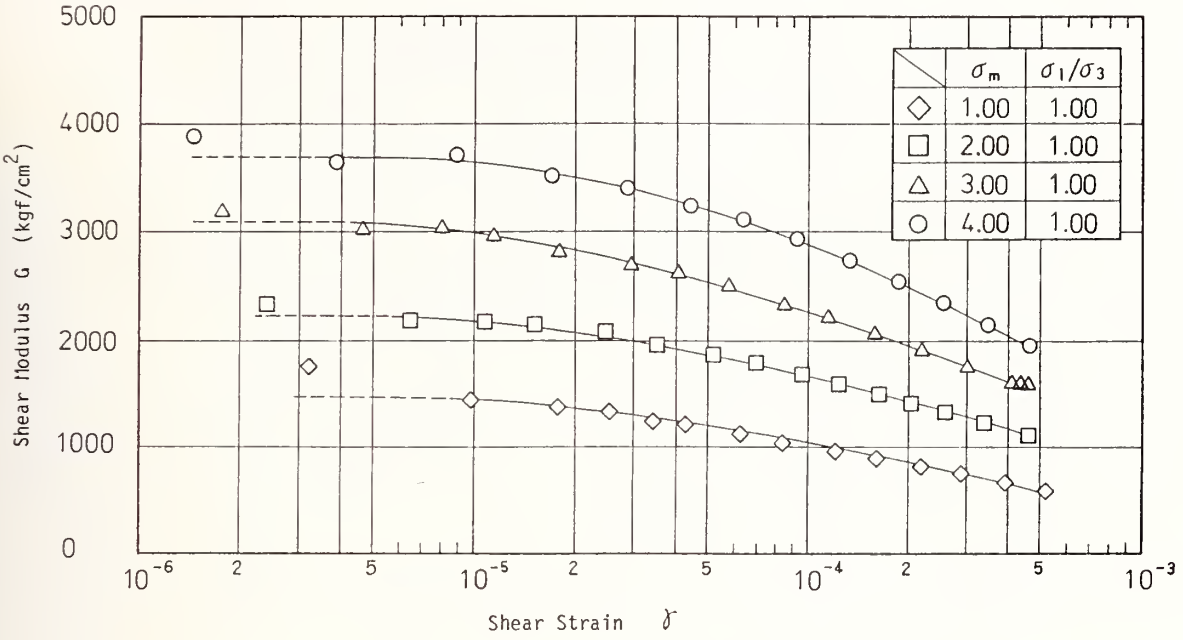

Fig. 2(a) Strain Dependent Curves of Shear Modulus G (CTSS)

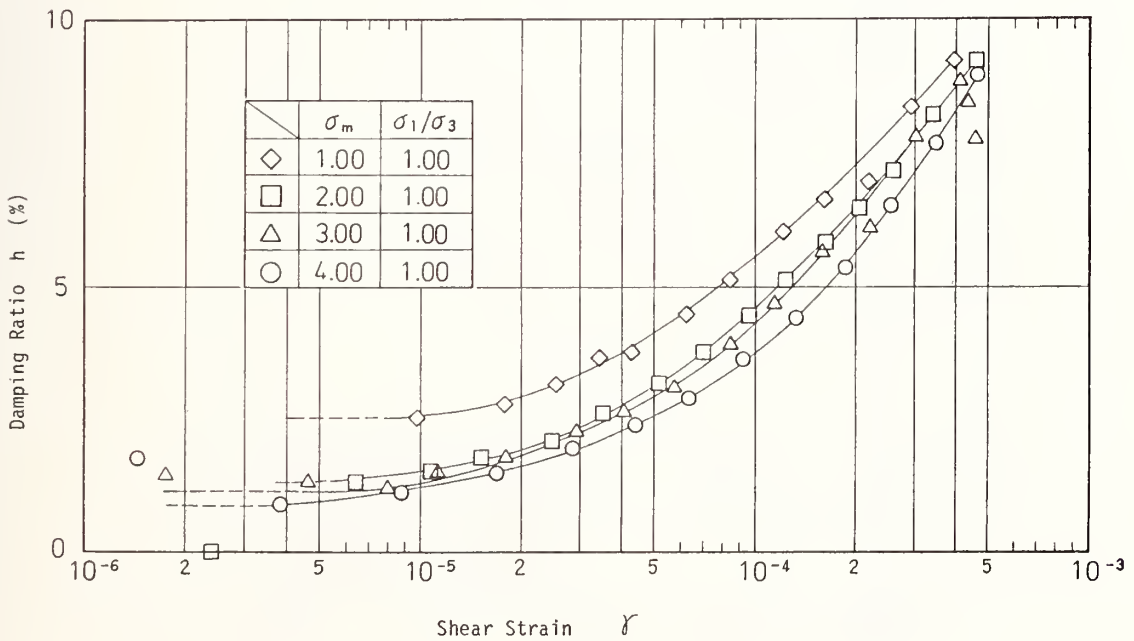

Fig. 2(b) Strain Dependent Curves of Damping Ratio h (CTSS)

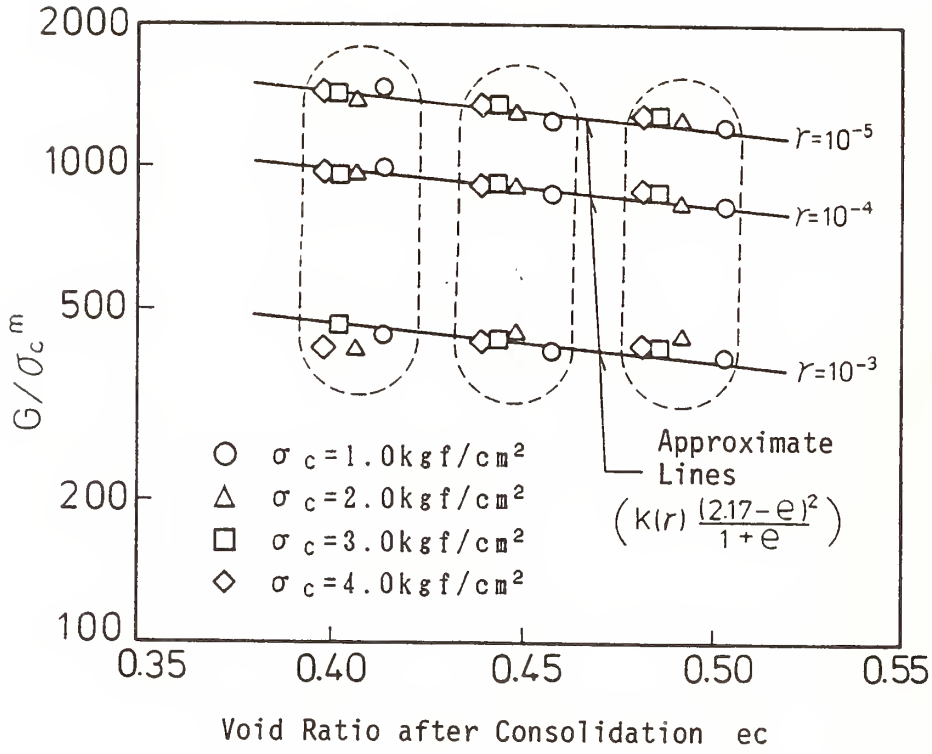

Fig.3 $G/\sigma_c{}^m$ versus Void Ratio e_c (CTSS)

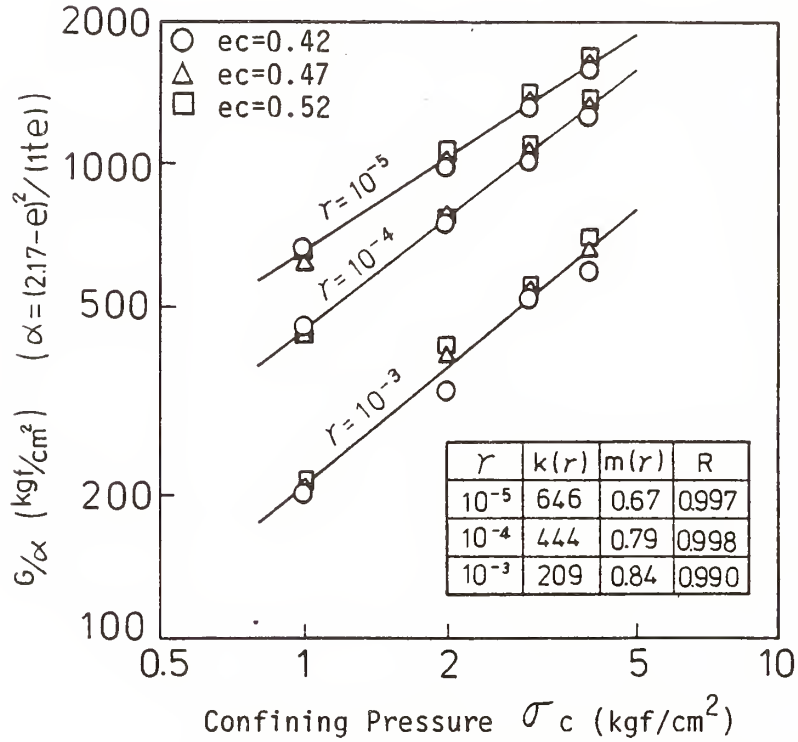

Fig.4 G/α versus Confining Pressure σ_c (CTSS)

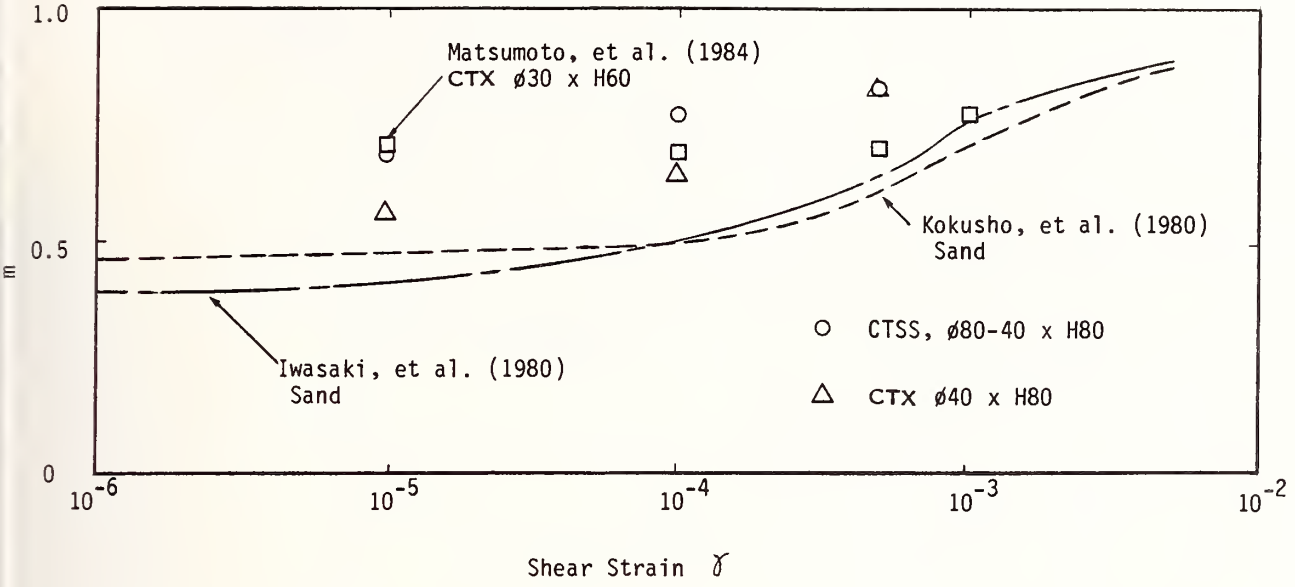

Fig.5 Power Number m versus Shear Strain γ (CTSS and CTX)

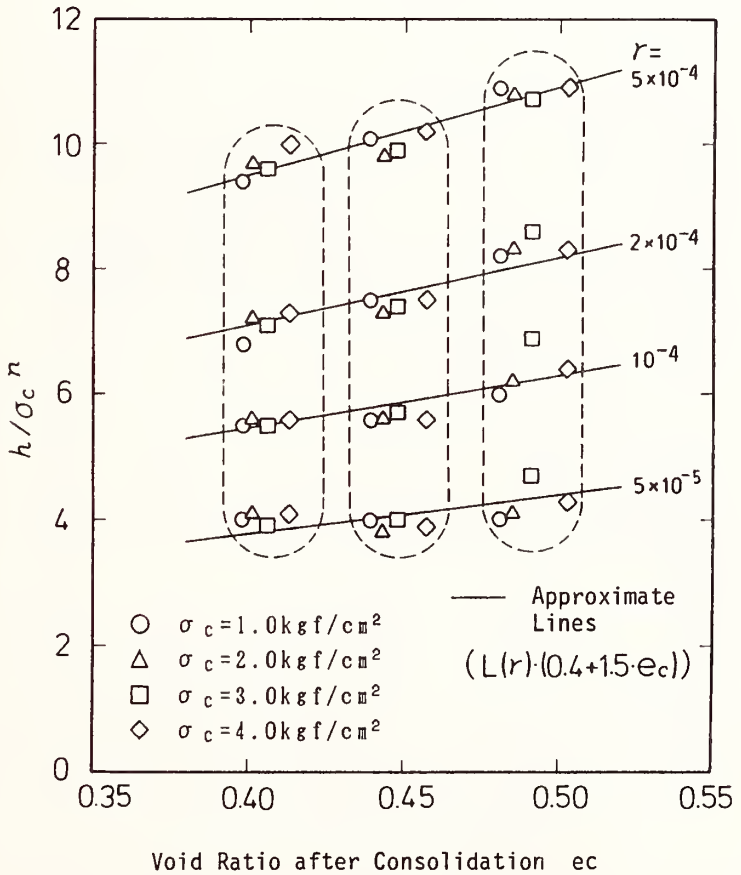

Fig.6 $h/\sigma_c{}^n$ versus Void Ratio e_c (CTSS)

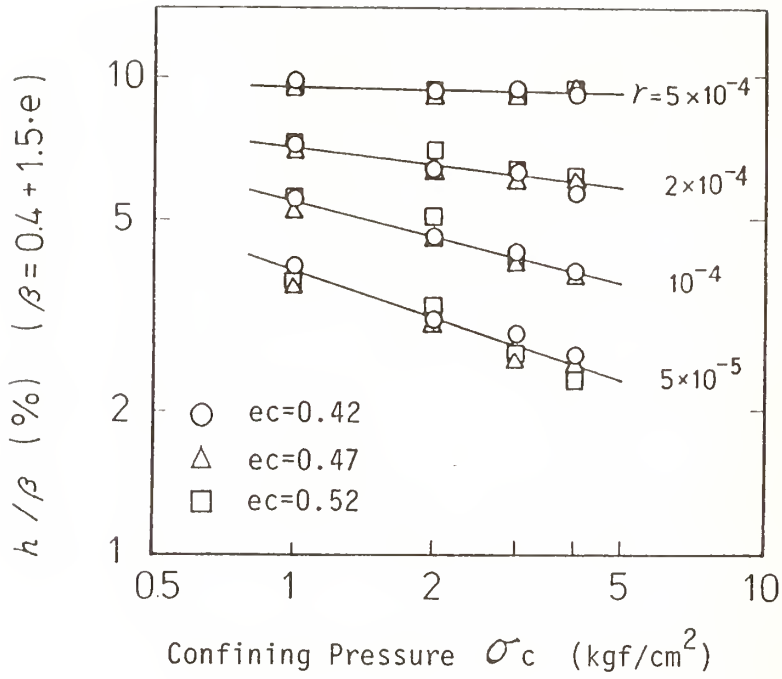

Fig. 7 h/β versus Confining Pressure σ_c (CTSS)

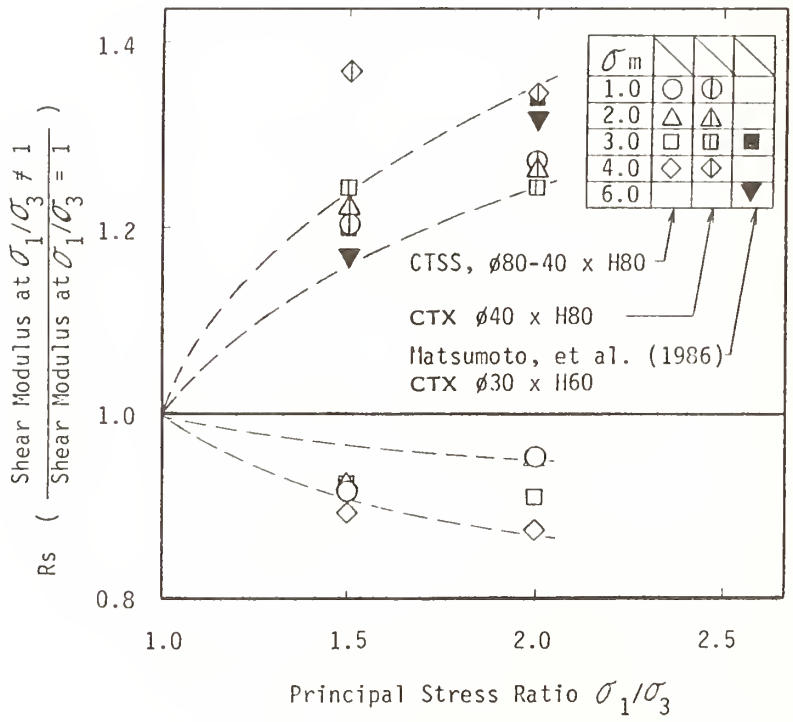

Fig. 8 R_s versus Principal Stress Ratio σ_1/σ_3 (CTSS and CTX)

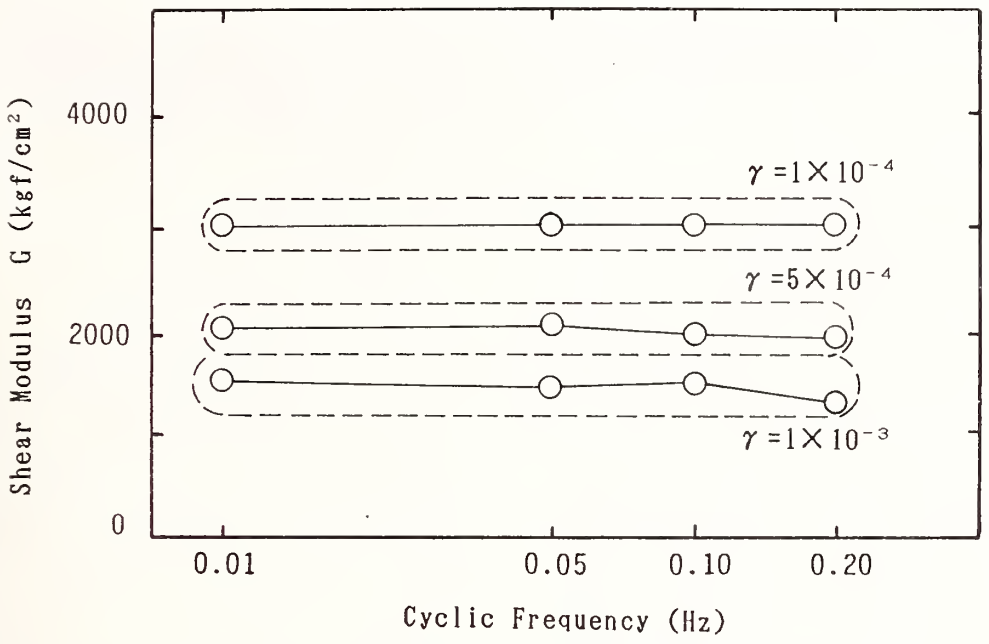

Fig. 9 Shear Modulus G versus Cyclic Frequency (CTSS)

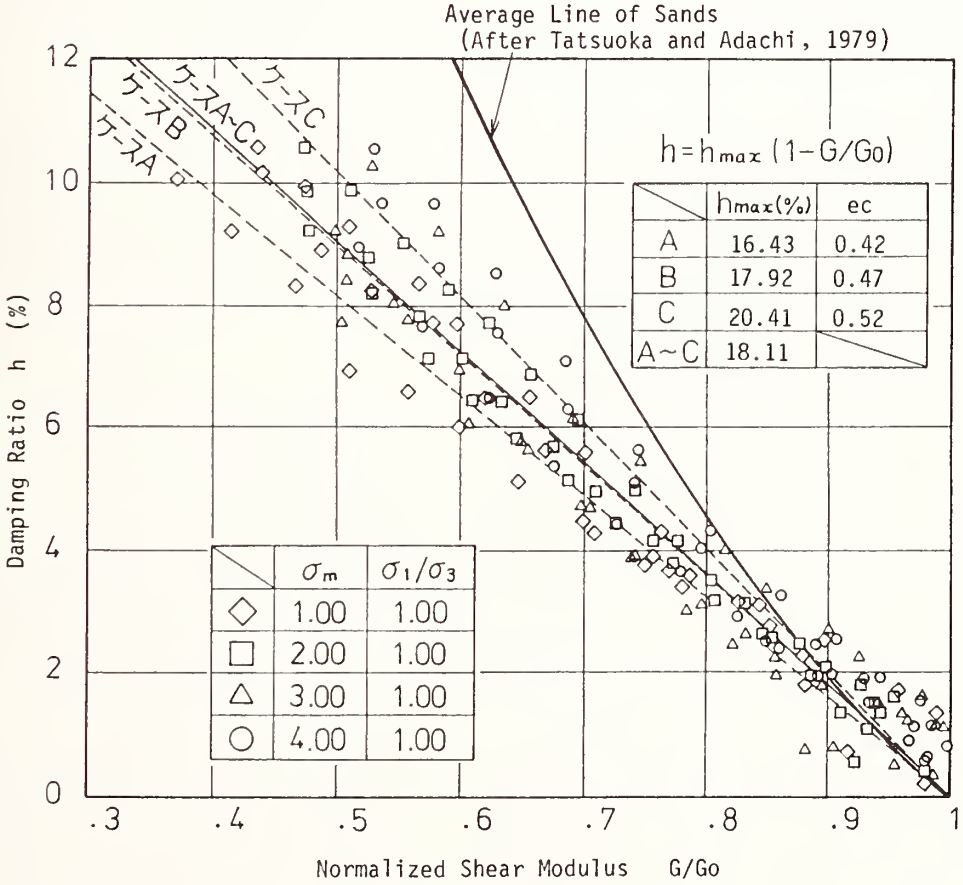

Fig. 10 Damping Ratio versus Normalized Shear Modulus (CTSS)

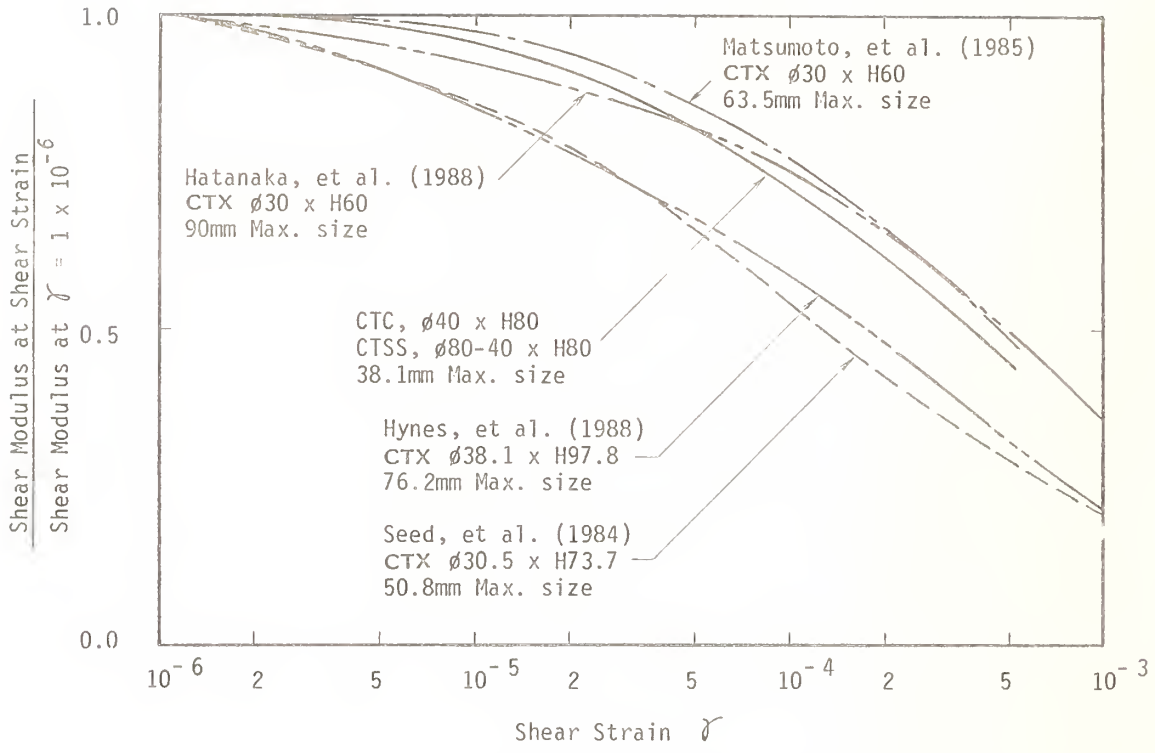

Fig. 11(a) Relationship between Normalized Shear Modulus G/G_0 and Shear Strain γ

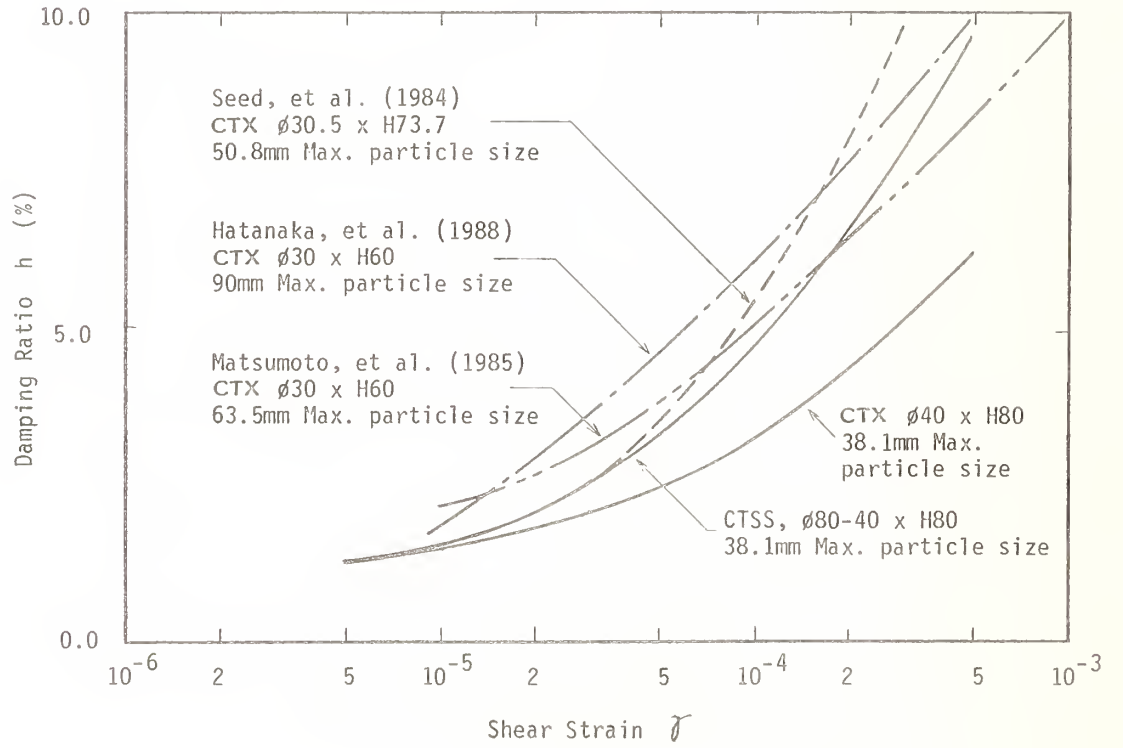

Fig. 11(b) Relationship between Damping Ratio h and Shear Strain γ

Allowable Residual Displacement of Gravity Quaywall Given by Optimum Seismic Coefficient From Economical Viewpoint

By

Tatsuo UWABE[1]

SUMMARY

Cases of earthquake damage to gravity quaywalls were collected for past earthquakes, and the quantity of the earthquake damage which means the residual displacement after earthquakes and the cost of damage was then analyzed. An estimation method to give this quantity of the damage (residual displacement and cost) was presented, using the empirical equation which is the function of the ratio of the corresponding seismic coefficient of the ground acceleration to the seismic coefficient which gives the safety factor of unity in the stability analysis of the design standard. An optimum seismic coefficient from an economical viewpoint and an allowable residual displacement which was defined as an expected seismic damage displacement given by such optimum seismic coefficient were then studied for the rational seismic design, on the basis of the quantitative estimation method of the cost of damage.

Keywords:earthquake resistant design, seismic damage,residual displacement, seismic coefficient, gravity quaywall

1.INTRODUCTION

Currently in Japan, there is a high possibility of the occurrence of a large earthquake in Tokai Area, a central part of Japan, in the near future, and thus many kinds of investigations for earthquake preparedness have been done. One of the investigations related to ports that may become key locations for the transportation of emergency goods immediately after an earthquake, is a survey on the earthquake resistance capability of port facilities to estimate the number of port facilities available after the earthquake. In this survey, the seismic stability of port facilities has been judged by the evaluation method reported by Tsuchida et al[1)]. According to this method there are only the two kinds of analyzed results of no damage, and collapse. However the actual seismic damage of port facilities shows a gradual change from no damage to collapse.

It is now necessary to assess the potential seismic damage quantitatively by the following reasons.

i) If the extent of damage to port facilities is small, they can still serve for the temporary transportation of urgent goods. It is therefore important to know whether the port facilities are available after earthquakes, by prior estimation of the extent of damage.

ii) Because the number of port facilities which are assessed to be damaged is large and because they cannot be reinforced at the same time, it is necessary to decide the priority of reinforcement and an effective reinforcing method according to the extent of potential damage.

With the background described above, the present study is concerned with the development of a quantitative estimation method of seismic damage to port facilities. It is further aimed at establishing the rational earthquake resistant design by utilizing the quantitative estimation method of seismic damage thus developed. In this earthquake resistant design, it is necessary to give an allowable value of seismic damage deformation. The seismic damage deformation means the swelling and settlement of face line of the wharf, the tilting of wall and so on. The allowable value is considered to be given from the viewpoints of the berthing function, the structural stability, the economy and so on. In the present study, the allowable residual displacement from the economical viewpoint is investigated. An optimum seismic coefficient from the

---

[1]Dr.Eng., Chief of Earthquake Disaster Prevention Laboratory, Structural Engineering Division, Port and Harbour Research Institute, Ministry of Transport

economical viewpoint and an allowable seismic damage given by such seismic coefficient is sought for, using the quantitatively estimated potential seismic damage. The structures analyzed in this study are a gravity type quaywall, which is a typical berthing facility in Japan, and a gravity type revetment.
In this report, historical cases of seismic damage to gravity quaywalls are first described. On the basis of these cases, a quantitative estimation method of seismic damage to gravity quaywalls is then presented. Lastly, an optimum seismic coefficient and an allowable residual displacement are derived by applying the quantitative estimation method to several cases of gravity structures with the cost analyses.

2. CASES OF SEISMIC DAMAGE TO GRAVITY QUAYWALLS

2.1 Earthquake, Ports and Gravity Quaywalls

A gravity quaywall is a typical berthing facility to moor ships in Japan. The structural types of gravity quaywalls are classified into the caisson type, the concrete block type, the L-shaped concrete block type, the cellular block type and the wave absorbing vertical wall type. Figure 1 illustrates the caisson type of gravity quaywalls. Table 1 shows the number of port facilities damaged by past earthquakes from 1923 to 1978. The details of these 679 data were shown in the report of Uwabe[2]. In the study on the quantitative estimation of seismic damage to gravity quaywalls the episodes of gravity quaywalls clearly damaged by liquefaction were excluded from this report.

2.2 Quantification of Damage to Gravity Quaywalls

(1) Seismic Damage Deformation

In a survey of seismic damage the swelling and settlement of face line of the wharf, the tilting of wall, the settlement of apron and other factors as shown in Fig.2 was measured, and the length of damaged section in one berth (damage length) was also measured. In this report, these measured values and the damage deformation ratio(the ratio of the maximum swelling to the wall height which is the height between sea bed and wall head) were used as the parameters to quantity the damage deformation.

(2) Cost of Seismic Damage to Gravity Quaywalls

The cost of seismic damage to gravity quaywalls (seismic cost) means the outlay assessed officially as repair work by the government. In this report, the seismic cost was defined as the sum of the repair work cost divided by the damage length of gravity quaywall (unit:1,000 yen/m). In this study, the ratio of the seismic cost to the initial construction cost was also discussed. This ratio is termed the cost rate of seismic damage (seismic cost rate).
The costs shown in the earthquake damage reports are the sums of the day. It was therefore required to convert these costs to same price level. Then, the fluctuation of the past years was investigated in the construction prices, in the wholesale prices of construction materials and in the wages respectively, and the fluctuation was quantified by a price index that is 100 for the prices at the year 1980. The repair cost and the initial construction cost were converted to same price level by this price index[2].

3. QUANTITATIVE ESTIMATION OF SEISMIC DAMAGE TO GRAVITY QUAYWALL BY ANALYSIS OF PAST DAMAGE DATA

3.1 Assessment of Damage Occurrence

A working seismic coefficient means the seismic coefficient which works on structures during earthquakes, and the relation between the working seismic coefficient and the maximum ground acceleration was presented as follows[3].

$$\left.\begin{aligned} K_e &= \frac{\alpha}{g} && (\alpha < 200\ \mathrm{Gal}) \\ K_e &= \frac{1}{3}\left(\frac{\alpha}{g}\right)^{1/3} && (\alpha \geqq 200\ \mathrm{Gal}) \end{aligned}\right\} \qquad (1)$$

where K_e :Working seismic coefficient
α :Maximum ground acceleration (Gal)
g :Acceleration of gravity (980 Gal)

For gravity quaywalls, the stability analysis should aim to derive the sliding and overturning behaviors as well as the bearing strength of the foundation, and also determine the seismic coefficient causing each of these failures under the safety factor of 1. This seismic coefficient is termed the critical seismic coefficient. Critical seismic coefficients are given respectively in three stability examinations mentioned above. When the smallest of these critical seismic coefficients is smaller than the working seismic coefficient, the structure starts to break during earthquakes. This smallest critical seismic coefficient is defined as the breaking seismic coefficient.

A decision on whether or not damage would occur is based on the comparison between the working seismic coefficient and the breaking seismic coefficient. If the breaking seismic coefficient is greater than the working seismic coefficient, the structure is considered safe and earthquake-resistant. Otherwise, the structure is expected to sustain damage due to the earthquake.

3.2 Quantitative Estimation of Seismic Damage to Gravity Quaywall

As mentioned in the last paragraph the structure starts to breaking when the working seismic coefficient(Ke) is greater than the breaking seismic coefficient(Kc), and the quantitative damage that occurs to a structure is considered proportional to the ratio between Ke and Kc. Therefore, a method to estimate the damage extent was presented in this study using this ratio between Ke and Kc. The ratio of Ke to Kc was defined as the risk ratio(Fc). The relationship between the seismic damage deformation and the risk ratio was then investigated on the basis of the regression analysis of the historical seismic damage data. In this analysis, the maximum swelling, the settlement of the face line, the damage deformation ratio and the seismic cost rate were discussed in this report.

Figure 3 shows the relationship between seismic damage deformation ratio (Rg) and the risk ratio (Fc). This figure shows the extent of damage distinguished by the symbols. This extent of damage was classified into five categories between no damage and complete collapse[2]. Table 2 shows the equations representing regressions. The regression formula of Rg and Fc in Fig.3 was then given as follows.

$$Rg = -12.7 + 14.5Fc \qquad (2)$$

As shown in Table 2, correlation coefficients of the regression formula obtained here are not thoroughly high. In order to obtain a high accuracy, it is necessary to reexamine the relationship between the working seismic coefficient and the ground acceleration with higher accuracy, to investigate the relationship between the seismic damage deformation and the risk ratio for each failure mode, considering other factors of the ground condition and so on. However, no one knows whether a large number of damage data for regressions with a higher accuracy will be obtained or not in the near future. Therefore, it may be proper in the present situation to use the regression formula obtained here for this study.

The regression formula that represents the relationship between the seismic cost rate (Cf) of the gravity quaywalls and the risk ratio (Fc) was not obtained with high accuracy because of insufficient number of data covering the cost of seismic damage and result of stability analysis to give the breaking seismic coefficient. Then, the relation between Cf and Fc was presented from the two regression formulae that are the equations of Cf and the damage deformation ratio (Rg) in Fig.4, and that of Rg and Fc in Fig.3. According to these two formulae, the relationship between Cf and Fc can be given as follows.

$$Cf=-62.2+66.2Fc \qquad (3)$$

It was believed that this formula was obtained by means of the best method in the present situation in order to estimate the cost of gravity quaywalls for an optimum seismic coefficient from the economical viewpoint discussed in next chapter.

4. OPTIMUM SEISMIC COEFFICIENT AND ALLOWABLE RESIDUAL DISPLACEMENT FROM ECONOMICAL VIEWPOINT

4.1 Concept of Optimum Seismic Coefficient[4,5] and Allowable Residual Displacement

One of the seismic coefficient given by the rational earthquake resistant design method is the optimum seismic coefficient from the economical viewpoint. The factors to affect the definition of an optimum seismic coefficient from an economical viewpoint are the initial construction cost, the cost of seismic damage to the structures, the utility of repair works to local economics, the effect of port constructions on the environmental and so on. At the present time, it is very difficult to quantify these factors other than the initial construction cost and the cost of seismic damage to structures. Therefore the economical viewpoint in this report focused on these two factors for the first step to define the optimum seismic coefficient.

When the seismic coefficient becomes larger, the expected cost of seismic damage to structures (expected seismic cost:$C_f(k)$) decreases, and the initial construction cost(Ic(k)) increases, as shown in Fig.5. Therefore, it is believed that the sum of the initial construction cost and the expected seismic cost (expected total cost:Ct(k)) shows a raised down curves with the extreme. In this report, the seismic coefficient which gives the extreme of this Ct(k) is defined as an optimum seismic coefficient from an economical viewpoint. And the seismic coefficient in this study is assumed to be the same as the breaking seismic coefficient because the seismic coefficient of the present design method for the gravity quaywall is nearly equal to the breaking seismic coefficient.

An allowable residual displacement for the earthquake resistant design from the economical viewpoint was investigated in this paper as described in Chapter 1. The allowable residual displacement was defined as the expected seismic damage displacement given by the optimum seismic coefficient mentioned in the last paragraph.

The accuracy of estimating the expected seismic costs discussed here is not necessarily very high, considering the scattering of the expected seismic costs and that of the acceleration for the attenuation curves with distance. However, the study on the quantitative estimation of the expected seismic cost is the first stage in earthquake engineering. It was still considered for this study to be currently useful.

4.2 Relation between Initial Construction Cost and Seismic Coefficient

The initial construction cost of a given gravity revetment which was designed for the two kinds of foundation ground of a sand layer and a clay layer, and for several seismic coefficients was estimated[2]. Figure 6 shows this initial construction cost versus seismic coefficient. The vertical axis in Fig.6 is the ratio of the initial construction cost for each seismic coefficient to that for the ordinary condition.

The relationship between the initial construction cost and the seismic coefficient for port facilities had been reported in the study on the economical design of port facilities by Murata, Yagyu and Uchida[6]. Figure 7 shows the initial construction cost against the seismic coefficient for the gravity quaywall where the structure is of the caisson type shown in Fig.8. It is necessary to pay attention to the price level of the year 1976 and the unit of vertical axis that is 10,000yen/m.

4.3 Expected Seismic Cost Rate

(1)Cumulative Distribution Function and Probability Density Function of Maximum Ground Acceleration at Japanese Ports

The probability of the occurrence of the maximum ground acceleration at a given site was studied here based on the report of Kitazawa, Uwabe and Higaki[7]. Figure 9 shows the base rock acceleration against the return period at Tokyo, Niigata and Shimonoseki. These three ports were selected from the viewpoint of probability of earthquake occurrence. According to Fig.9, the maximum base rock accelerations for the return

period of 50 years are about 240 Gal at Tokyo port, about 120 Gal at Niigata port and about 60 Gal at Shimonoseki port.
The cumulative distribution function and probability density function of t durable years were obtained as follows[8,9].

$$F_m(X_m)=\left\{\left(1-\frac{N}{K}\right)+\frac{N}{K}\cdot\exp\left(-m\cdot e^{-\frac{X_m-B}{A}}\right)\cdot\left(\sum_{n=1}^{m}\frac{m^{(n-1)}}{(n-1)!}\cdot e^{-(n-1)\frac{X_m-B}{A}}\right)\right\}^{t} \quad (4)$$

$$f_m(X_m)=\frac{m^m}{(m-1)!}\cdot\frac{t\cdot N}{A\cdot K}\left\{\left(1-\frac{N}{K}\right)+\frac{N}{K}\cdot\exp\left(-m\cdot e^{-\frac{X_m-B}{A}}\right)\cdot\left(\sum_{n=1}^{m}\frac{m^{(n-1)}}{(n-1)!}\cdot e^{-(n-1)\frac{X_m-B}{A}}\right)\right\}^{t-1}\cdot\exp\left(-m\cdot\frac{X_m-B}{A}-m\cdot e^{-\frac{X_m-B}{A}}\right) \quad (5)$$

where, Xm : m-th acceleration
A,B : Constant of Gumbel distribution
N : Number of data
K : Period of earthquake data
t : Durable years
m : Order of extreme

Figure 10 shows the distribution function and the probability density function for Tokyo port. The probability density function of the maximum anticipated acceleration at Tokyo port for the durable years of 50 years is $f_1(x)$ in Fig.10, and the acceleration of about 240 Gal where $f_1(x)$ shows a peak is the same as the expected acceleration for the return period of 50 years in Fig.9.

(2) Expected Seismic Cost Rate

When the distribution function of the m-th extreme is fm(x), the probability of occurrence of the m-th extreme is fm(x)dx. The expected seismic cost rate is derived from fm(x)dx and random D(x)which is the seismic cost rate as follows.

$$P_{cf}=\sum^{m}\int_{(x)}D(x)f_m(x)dx \quad (6)$$

Moreover, D(x) is given by the equation of (3).In case of the expected seismic damage deformation ratio, D(x) is given by the equation of (2). As the extreme of large order had little influence on the expected seismic cost rate, the extremes from 1st to 5th were considered for the calculation of the expected seismic cost rate. Figure 11 shows the expected seismic cost rate of Tokyo port for durable years of 25, 50 and 100.

4.4 Optimum Seismic Coefficient and Allowable Residual Displacement

Optimum seismic coefficients to minimize the expected total cost were calculated for Tokyo port, Niigata port and Shimonoseki port. The number of durable years was 50, and the extremes from 1st to 5th were considered. The relations between the initial construction cost and the seismic coefficient in Figures 6 and 7 were used. As the amount of the initial construction cost in Fig.6 was not shown, it was supposed that the initial construction cost of the ordinary condition was 1,000,000 yen/m. As the year of the price level in Fig.7 is the year 1976, the amount of the expected seismic cost was converted in the price level of the year 1980.
Results of calculation are shown in Fig.12 for the gravity revetment and in Fig.13 for the gravity quaywall (Caisson type). The solid lines with symbols of X in Figures 12 and 13 show the initial construction cost. The solid lines with closed circles, open circles and squares show the expected seismic cost. The dotted lines show the expected total cost. Table 3 shows the optimum seismic coefficient to minimize the expected total cost in Figures 12 and 13.
The optimum seismic coefficients obtained here, were compared with the expected maximum ground acceleration with a return period of 50 years. Table 3 shows the seismic coefficients transformed from the expected maximum ground accelerations for a return period of 50 years in Fig.9, using Eq.(1). In the case of gravity revetments, the optimum seismic coefficients were larger than the seismic coefficients for a return period of 50 years. In the case of gravity quaywalls, the optimum seismic coefficients were the same as the seismic coefficients at Tokyo port and were slightly larger than those at Niigata port and Shimonoseki port.
Figures 12 and 13 show the expected maximum swelling calculated from

Eq.(2). The height of structures is 5 m for the gravity revetment and is 14m for the gravity quaywall. The expected maximum swellings of the optimum seismic coefficient are as follows. In the case of the gravity revetment, the expected values of maximum swelling were 5 cm at Tokyo port, 10cm at Niigata port and 1 cm at Shimonoseki port. The reason why the expected maximum swelling at Tokyo port is smaller than that at Niigata port is that the increasing rate of the initial construction cost between 0.15 and 0.2 is larger than that between o.2 and 0.25.In the case of the gravity quaywall, the expected values of the maximum swelling were 67 cm at Tokyo port, 50 cm at Niigata port and 10 cm at Shinomoseki port. This displacement is an allowable residual displacement, when defined from an economical viewpoint. In addition to the displacement discussed here, an allowable displacement from the viewpoint of the berthing function, the structural stability and so on should be examined for the rational earthquake resistant design.

5. CONCLUSION

Data on cases of seismic damage to gravity quaywalls were collected. Then the quantification of the earthquake damage and the quantitative estimation method of seismic damage to gravity quaywalls were investigated. The relation between the damaged deformation ratio and the risk ratio which is the ratio of the working seismic coefficient to the breaking seismic coefficient, and the relation between the seismic cost ratio and the risk ratio were obtained on the basis of the seismic damage data of gravity quaywalls in past earthquakes.
Moreover, the procedure to give an optimum seismic coefficient from an economical viewpoint and the allowable residual displacement which was defined as the expected seismic damage displacement given by such optimum seismic coefficient was presented, using the method for estimating the cost of seismic damage to gravity quaywalls. The optimum seismic coefficients and the allowable residual displacement of the gravity revetments and quaywalls were obtained from the expected total cost with the durable period of 50 years at Tokyo port, Niigata port and Shimonoseki port. The results of a comparison between these optimum seismic coefficients and the working seismic coefficient calculated from the expected maximum ground accelerations for the return period of 50 years were as follows. In the case of gravity revetments the optimum seismic coefficient was larger than the working seismic coefficient with the return period of 50 years. In the case of gravity quaywalls the optimum seismic coefficients were same as the working seismic coefficient at Tokyo port and were slightly larger than those at Niigata port and Shimonoseki port. The working seismic coefficient in Table 3 are nearly equal to the seismic coefficient used in the present design method of gravity quaywalls for each port. As the seismic coefficient of the present design method had been established empirically on the base of the past earthquake damage, it seems that the result of this study on the optimum seismic coefficient shows the validity of the empirical engineering judgment from the economical viewpoint for the seismic coefficient.

REFERENCES

1) Tsuchida, H., Noda, S., Inatomi, T., Uwabe, T., Yagyu, T. and Murata, T. :Method of Evaluation for Seismic Stability of Port and Coastal Facilities, Technical Note of the Port and Harbour Research Institute(PHRI), No.336, June 1980
2) Uwabe, T.:Estimation of Earthquake Damage Deformation and Cost of Quaywalls based on Earthquake Damage Records, Technical Note of PHRI, No.473, Dec.1983
3) Noda, S., Uwabe, T. and Chiba, T.: Relation between Seismic Coefficient and Ground Acceleration for Gravity Quaywall, Report of PHRI, Vol.14, No.4, Dec.1975, pp.67-111
4) Nonaka, M., Inokuma, Y. and Katayama, T.:Studies on Seismic Damage Rate and Optimum Seismic Coefficient Determination of Highway Bridges, Proc. of JSCE, No.340, Dec. 1983, pp.87-96
5) Matsuo, M.:Reliability in Geotechnical Engineering Design, Gihodo Press, March 1984

6) Murata, T., Yagyu, T. and Uchida, T.:Some Consideration on Profitable Designing for Port and Harbour Facilities, Proc. of 1980 Annual Research Presentations of PHRI, Dec.1980, pp.233-276
7) Kitazawa, S., Uwabe, T. and Higaki, N.:Expected Values of Maximum Base Rock Accelerations along Coasts of Japan, Technical Note of PHRI, No.486, July 1984
8) Gumbel, E.J.:Statistics of Extremes (Japanese translation version),Seisan-Gijyutsu-Senta-Shinsya, June 1978
9) Uwabe, T. : Study on Quantitative Estimation of Seismic Damage to Gravity Quaywall, Technical Note of PHRI, No.548, June 1986

Table 1 Data of seismic damage to port facilities

Number of Earthquakes	Number of ports	Structural type	Number of damage data
17	100	Quaywall	
		Gravity type	275(77)
		Steel sheet pile type	161(56)
		Cellular type	11(7)
		Piled pier type	31(17)
		Breakwater	40(11)
		Other types	161(39)
		Total	679(207)

Figures within parentheses are no damage data and are included in total of each type.

Table 2 Results of regression analysis

Criterion variables	Regression formula	Correlation coefficient	standard deviation
Maximum swelling (Dx,cm)	Dx=-113.8+124.4Fc	0.559	59.1
Settlement of face line (Sp,cm)	Sp= -50.9+ 57.1Fc	0.667	20.0
Damage deformation ratio (Rg,%)	Rg= -12.7+ 14.5Fc	0.445	9.1

Predictor variable (Fc):Risk Ratio(Ke/Kc)

Table 3 Optimum seismic coefficient and allowable residual displacement

Name of port	Optimum seismic coef.		Seismic coef. (Return period of 50 years)	Allowable residual dis.(cm	
	Revetment	Quaywall		Revetment	Quaywall
Tokyo	0.23	0.21	0.21	5	67
Niigata	0.15	0.13	0.12	10	50
Shimonoseki	0.10	0.08	0.06	1	10

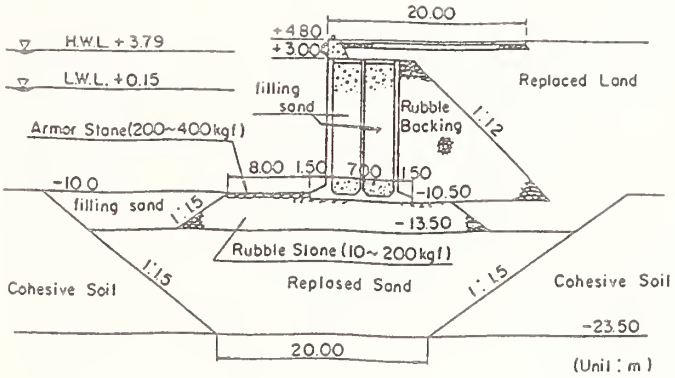

Fig.1 Gravity Quaywall(Caisson Type)

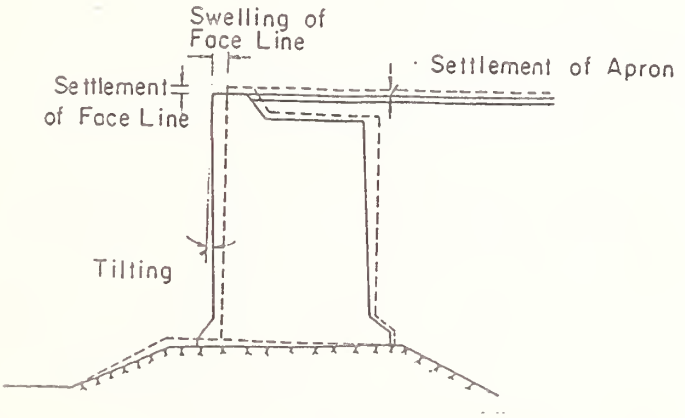

Fig.2 Seismic Damage Deformation

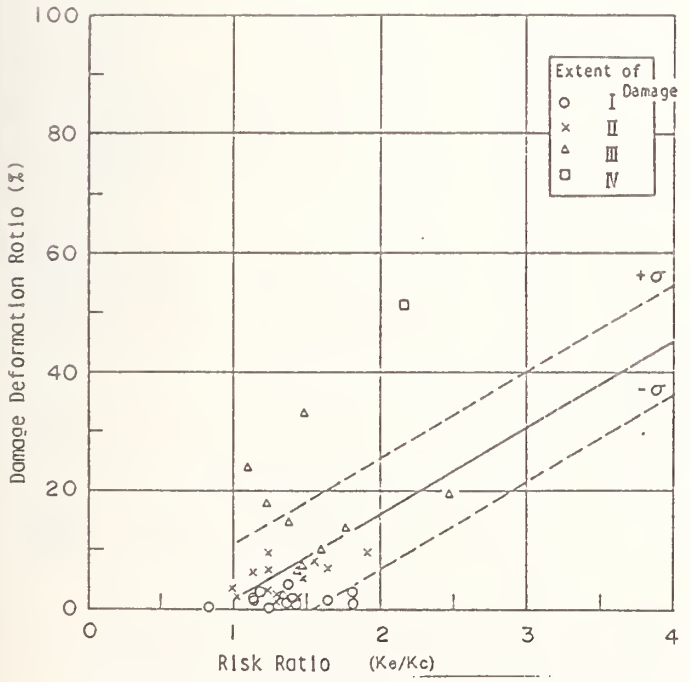

Fig.3 Damage Deformation Ratio versus Risk Ratio

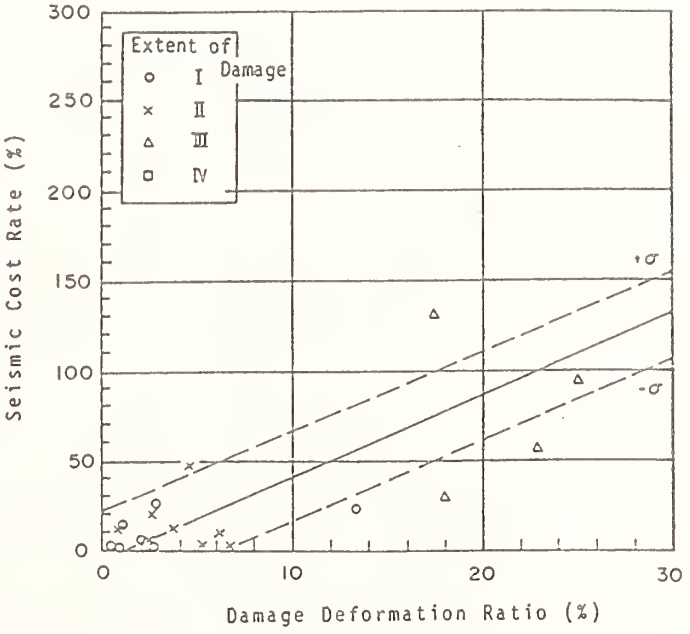

Fig.4 Seismic Cost Rate versus Damage Deformation Ratio

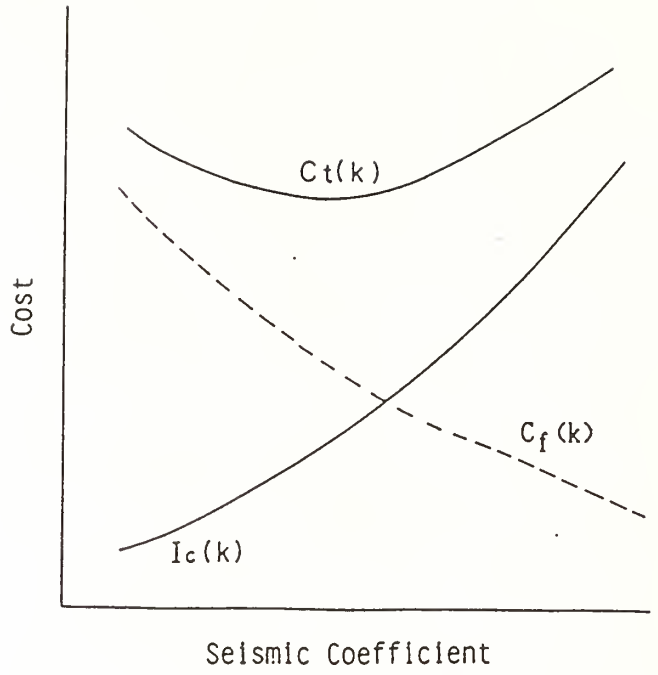

Fig.5 Relation between Cost and Seismic Coefficient

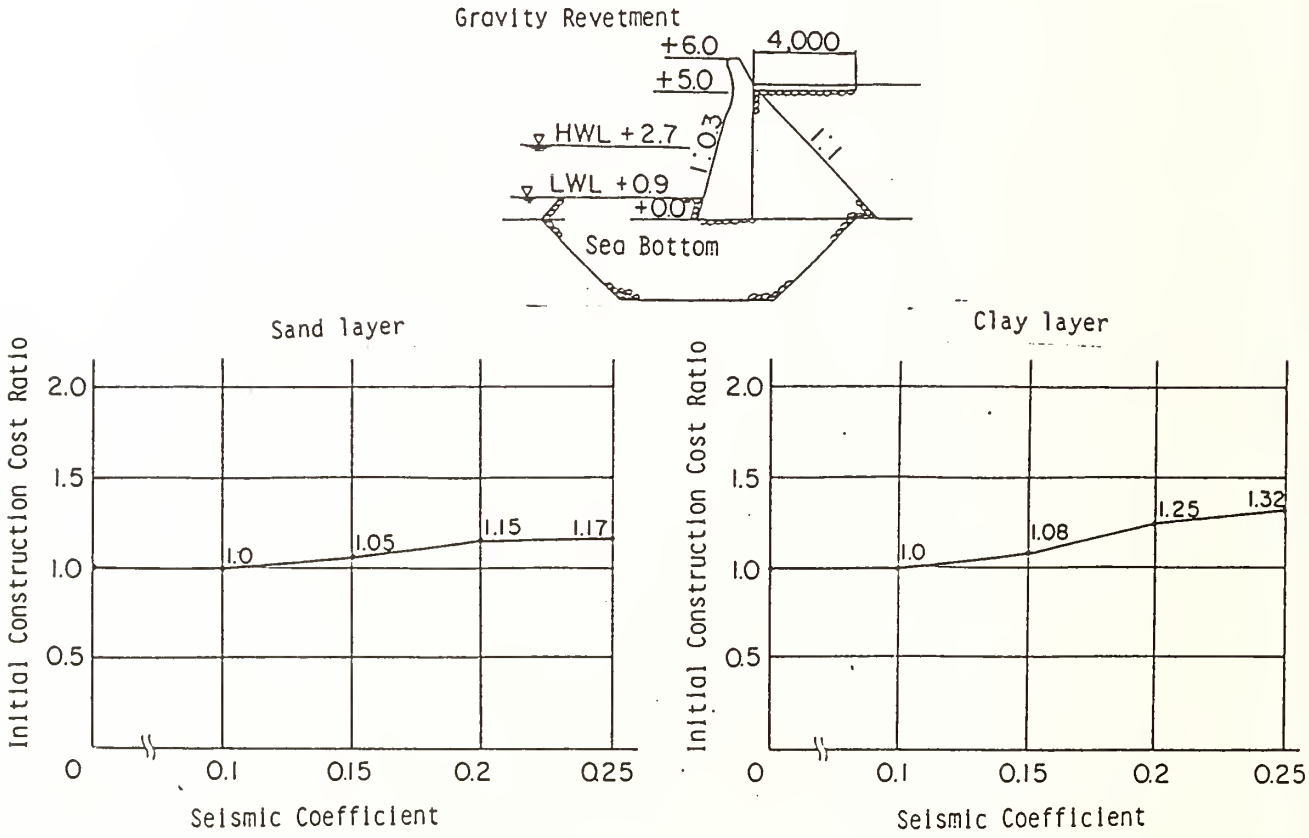

Fig.6 Initial Construction Cost versus Seismic Coefficient (Gravity Revetment)

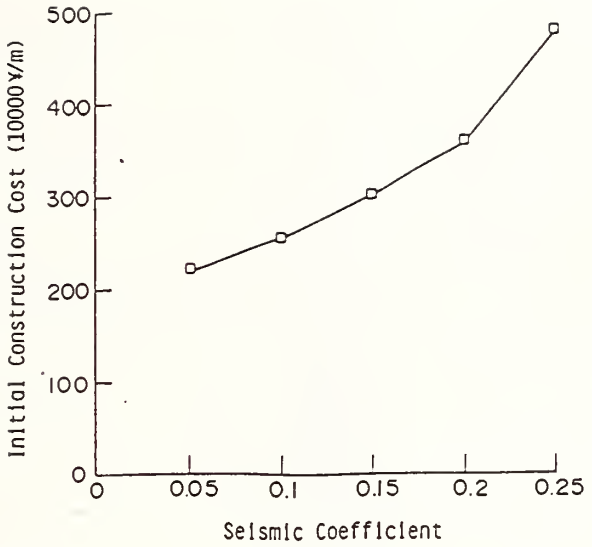

Fig.7 Initial Construction Cost versus Seismic Coefficient(Murata et al.[6])

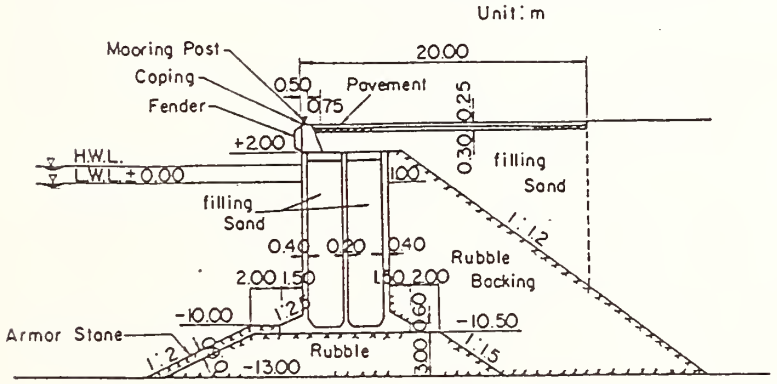

Fig.8 Standard Section of Caisson Type Quaywall (Murata et al.[6])

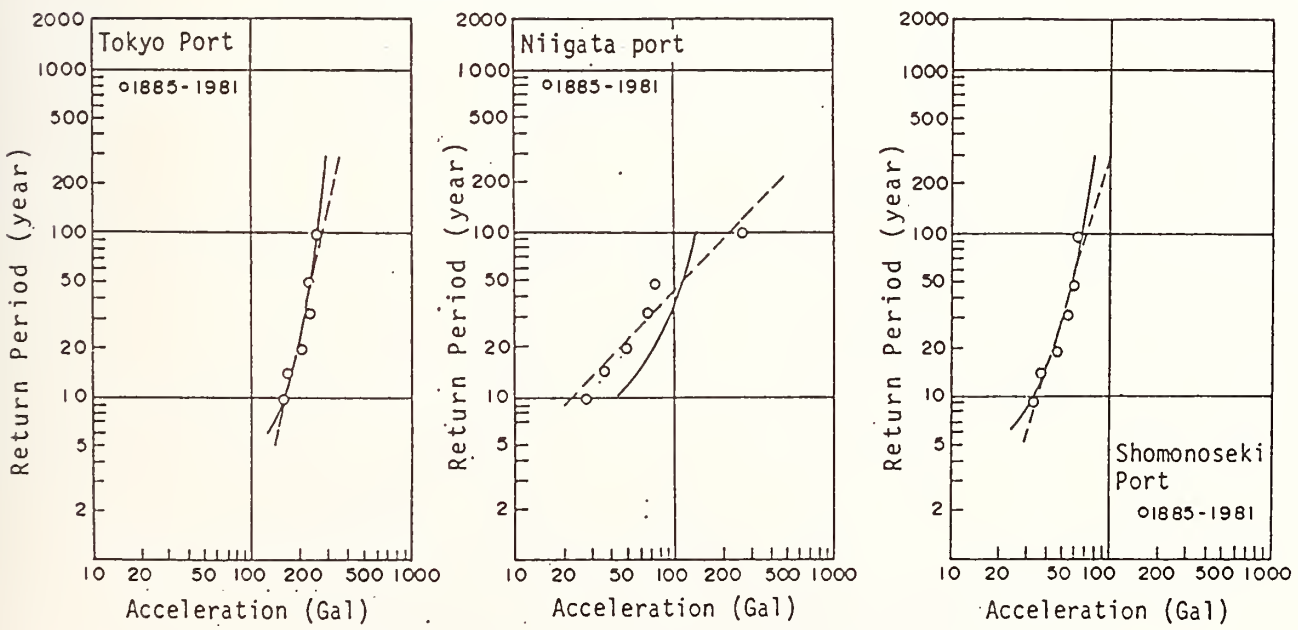

Fig.9 Maximum Base Rock Acceleration versus Return Period

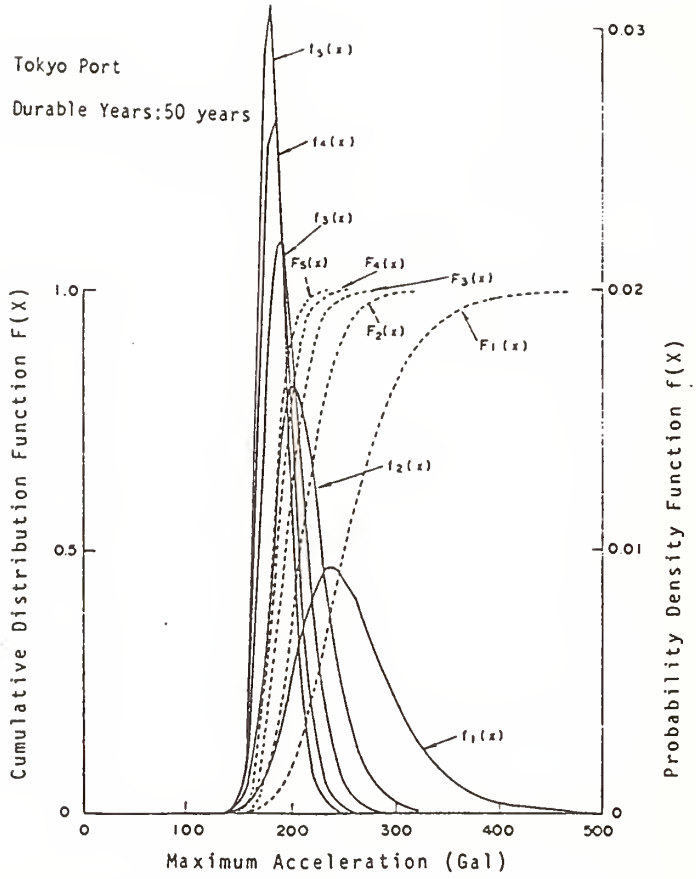

Fig.10 Distribution Function and Probability Density Function(Tokyo Port)

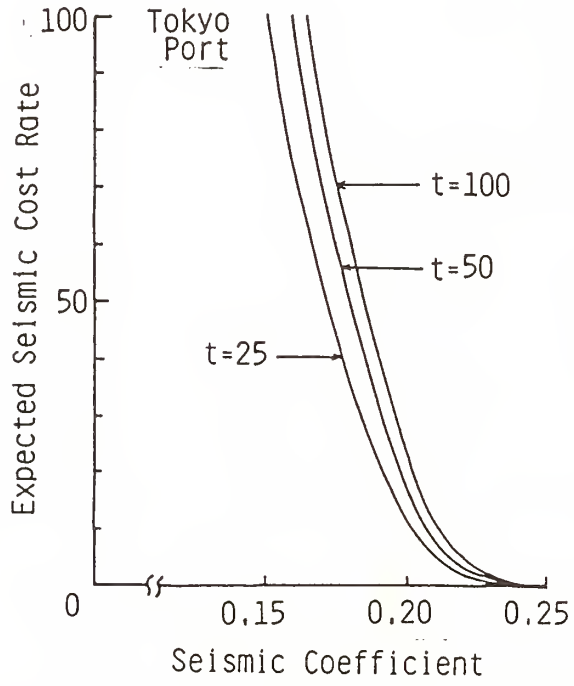

Fig.11 Expected Seismic Cost Rate versus Seismic Coefficient

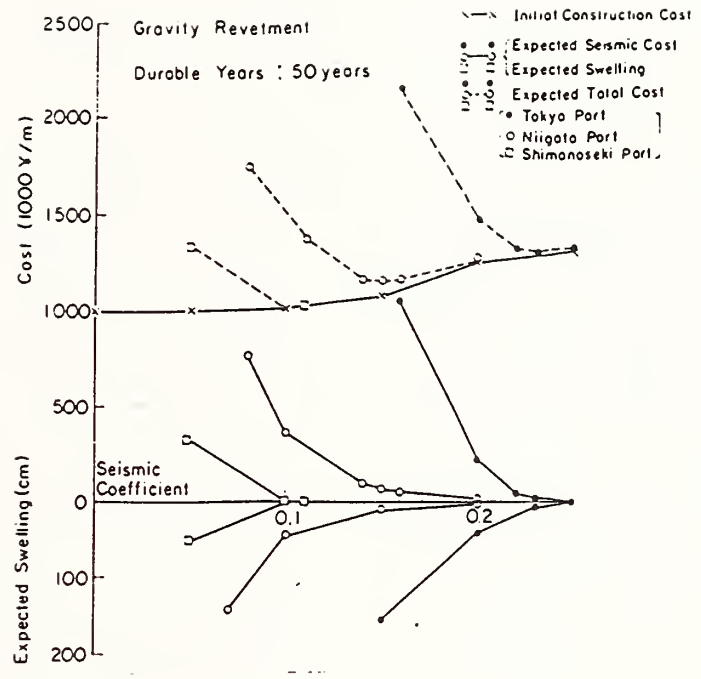

Fig.12 Expected Total Cost versus Seismic Coefficient(Gravity Revetment)

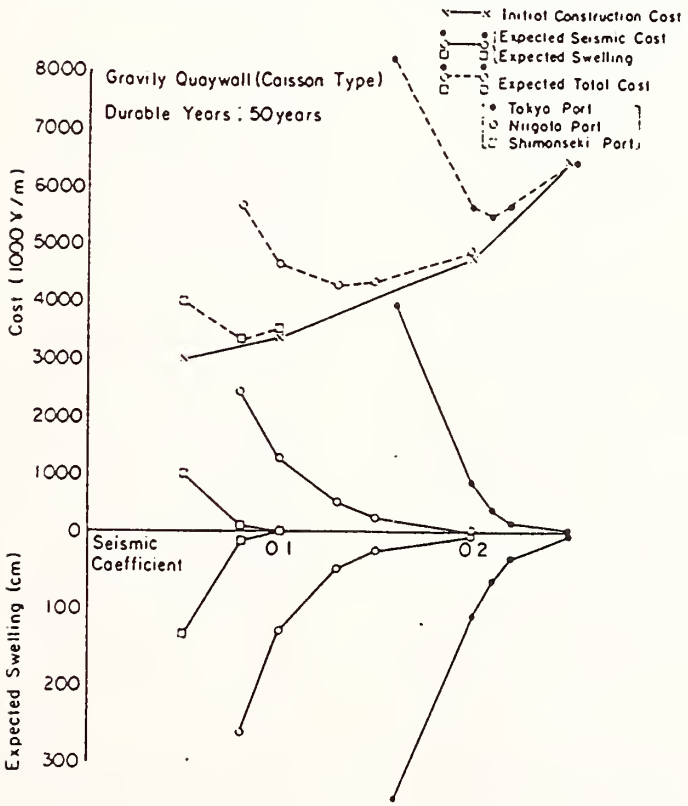

Fig.13 Expected Total Cost versus Seismic Coefficient(Gravity Quaywall)

The Relation Between the Building Damages and the Vibration Properties of Ground (In the Case of Spitak Earthquake)

By

Keiichi OHTANI[1], Hiroyoshi KOBAYASHI[2]

SUMMARY

The tragic earthquake of December 7, 1988 (Spitak earthquake) occurred near Spitak, Armenia, USSR. The earthquake resulted severe damages of buildings at the northern part of Armenia. And that earthquake also resulted in a loss of life estimated at greater than 45,000. The buildings, especially the reinforced concrete apartment houses were suffered very severe damages.

The causes of this disaster were mainly estimated that (1) the very strong ground motion was attacked to the hazard area, and (2) the natural period of building was consisted with the predominant period of ground.

This paper described that the estimation of the intensity of ground motions by assuming a fault-rupture model and by considering geological conditions, and the relation between the building damages and the dynamic properties of ground by the data of microtremor.

KEY WORD

Spitak earthquake, Seismic intensity, Building damages, Dynamic behaviour of ground, Microtremor measurement.

1. INTRODUCTION

The tragic earthquake of December 7, 1988 occurred near Spitak, Armenia, USSR. The earthquake resulted severe damages of structures, especially the apartment housing buildings, at Leninakan, Spitak, Kirovakan, Stepanavan in the north-western part of Armenia. And, this earthquake also resulted in a loss of life estimated at greater than 45,000; the actual death toll may be significantly higher. The damages of structure were concentrately occurred to the buildings, especially the apartment houses of reinforced concrete structures.

The lessons learned from past damaging earthquakes have pointed out that there is an evident relation between earthquake damages and geological conditions, because the intensity and characteristics of ground motions depend on geological conditions.

The objectives of this paper are to estimate the intensity of ground motions due to Spitak Earthquake by assuming a fault-rupture model and by considering geological conditions and to discuss the relations between their results and the causes of damages due to Spitak Earthquake by using the microtremor data on buildings and ground surfaces.

2. ESTIMATION OF SEISMIC INTENSITY

2.1 Parameters of earthquake and distribution of after shocks

The parameters of Spitak earthquake as reported by the Soviet Academy of Science are:

Magnitude;	M=6.8 - 7.0
Origin time;	December 7, 1988 11hr41min,local time 07hr41min(GMT)
Latitude(deg);	40.9N
Longitude(deg);	44.2E
Depth;	10km

Based on the recorded data at Earthquake Research Institute, Armenia Academy of Science, the fault plane solution is shown in Fig. 1(c). This solution was the reverse fault with right lateral component, the strike and dip angle of the fault were estimated to N60 W, 60 , respectively.

The Figs. 1(a) and 1(b) which were measured by Armenia Earthquake Research Institute are shown the distributions of aftershocks. The Fig. 1(a) is shown the distribution of aftershocks which were measured within the duration between December 7, 1988 and January 15, 1989, and the Fig. 1(b) is shown the distribution of aftershocks within December 7, 1988, because the shape of fault corresponds to the distribution of aftershocks measured within 24 hours after a mainshock. The center and radius of circles in those figures are shown the location and magnitude of earthquakes, respectively. From these figures of distribution of aftershocks, the shape of earthquake fault was

---

*1 Head, Earthquake Disaster Prevention Laboratory, National Research Center for Disaster Prevention, Science and Technology Agency

*2 Professor Emeritus, Tokyo Institute of Technology

estimated as follows:
Length; L=35km, Width; W=12km
Dip angle; 60 , Strike; N60 W.
These values are coincided with the values by Armenia Earthquake Research Institute.

The fault slips were discovered in the hill area on the west of Spitak. The maximum vertical and horizontal components of the fault slips which were discovered, are the value of 2.0 m and 1.8 m, respectively.

2.2 Estimation of seismic moment

The seismic moment of the earthquake is the value of $2.5X10^{26}$ dyne cm which is calculated by the parameters of L=35km, W=12km and D=1.5m (mean value). By using this seismic moment, it can be introduced to the magnitude of M=6.8 (Table 1). The parameter of D=1.5m is chosen as the mean value based upon the discovered fault slips.

Fig. 2 shows the location and parameters of the earthquake fault. The rectangle and double-lined part in this figure are illustrated to the location and scale and the shallow part of the fault, respectively. And, the black circle is illustrated to the epicenter.

2.3 Maximum Accelerations and Seismic Intensity

The maximum accelerations at each place are calculated as the product of those of the incident waves from the seismic bedrock and amplification factors by using the method of Drs. Midorikawa and Kobayashi.[1] We assumed the rupture velocity (V_R) is 2.5 km/sec by experience. The surface-soil conditions at each place are incorporated on the basis of Armenia geological map (1/6,000,000) as shown in Fig. 3. The amplification factors to the seismic bedrock at each place are shown in Table 2, considering the surface geological conditions. The seismic intensity (MSK) are evaluated on the basis of the maximum accelerations which are reduced to about 80% levels of the calculated ones. The reduction factor depends on the experimental relation between maximum accelerations and seismic intensity in Japan.[1] The results are shown in Table 3.

The maximum acceleration level of Spitak 2 in Table 3 is expressed as more than 600gal, as the past results show good agreement in the range of maximum accelerations less than 600gal or so, in case the calculation is carried out in the elastic manner adopted here.[1] The maximum acceleration level of Gukasyan is expressed as more than 228gal, as the geological condition is assumed as hard rock because of the insufficient information.

2.4 Appraisal of the seismic intensity

The relations between the calculated results of seismic intensity by the assumption of fault-rupture model and the reported seismic intensity and the earthquake damages are summarized as follows:

(a) The maximum acceleration levels of Gukasyan and Yerevan agree with those of available accelerograms recorded in Gukasyan and Yerevan which are about 210gal and 61gal, respectively.

(b) The seismic intensity are 10 in Spitak, 9-10 in Leninakan, 8-9 in Kirovakan, 6 in Yerevan in terms of MSK scale and agree with the estimated ones in Armenia.

(c) The results are supposed to explain that the intensity of ground motions in Kirovakan more close to the epicenter is lower than that in Leninakan far from the epicenter, although the final judgement requires the exact seismic source mechanism and geological condition.

2.5 Comments on the Seismic Zoning Map for the seismic design

The seismic zoning map for the seismic design is used generally in Armenia. But, the method of seismic zoning map, which is adopted in Soviet, is similar to based upon the method of seismic macro zoning map in Japan. Therefore, the method in Soviet does not considered the method of the micro zoning, namely based upon the dynamic properties of ground. It is seemed that the method of macro zoning map is mainly based upon the statistical result of the occurrence of historical earthquakes, and is not considered the Seismotectonics, which is strongly insisted by the Soviet Academy of Science in former times.

This Armenia region is located the very active seismic zone, where the Anatoria fault is closed to the west side of Armenia and the Zakros seismic belt is connected to the south-eastern direction of Armenia through the Azerbaizian. The present zoning map of Armenia is difficult to understand for the considering with the face of geological structures.

We hope that the seismic zoning map will

be corrected based upon the results of the distribution of the seismic intensity of each city at this earthquake and the seismotectonics of these area.

3. DYNAMIC PROPERTIES OF BUILDINGS

3.1 Microtremor measured on buildings

The buildings which were suffered severe damages were concentrated to the uniformly produced reinforced concrete apartment houses. Therefore, the microtremor measurement on buildings were conducted to the research for the change of dynamic behaviour between the undamaged and slightly damaged buildings and the relation of the occurrence of damages. For the measurement of undamaged buildings, we conducted in Yerevan, the capital of Armenia. For the measurement of slightly damaged buildings, we conducted in Leninakan and Kirovakan.

The structural types of measured buildings were selected to the 9-story precast reinforced concrete frame buildings, 9-story large-size panel buildings, 5-story stone-masonry buildings with reinforced frame and 4 and 16-story site-casted reinforced concrete buildings.

3.2 Natural periods and critical damping coefficients of building

The microtremor on the buildings were measured 19 sites in Yerevan, Leninakan and Kirovakan. The measurement in Yerevan were recognized for the dynamic properties of undamaged buildings. The measurements in Leninakan and Kirovakan were recognized for the properties of slightly damaged buildings. The measurement results are shown in Table 4.

The change of dynamic properties between damaged and undamaged buildings for 3 structural types are appointed out as follows:

1) 5-story Stone-Masonry Building : The natural periods and critical damping coefficients of undamaged buildings are 0.28 - 0.33 sec. and 2.2 - 7.2 %, respectively. The natural periods and critical damping coefficients of damaged buildings are 0.21 - 0.55 sec., 1.9 - 4.4 %, respectively. The difference of the natural periods of damaged and undamaged buildings are so large, because it is guessed that this causes is based upon the deteriorative effects of walls.

2) 9-story Precast Reinforced Concrete Frame building : The natural periods of undamaged buildings in the longitudinal direction and transverse direction are 0.61 - 0.63 sec. and 0.46 - 0.53 sec., respectively. The natural periods of damaged buildings in the longitudinal and transverse directions are 0.83 - 1.07 sec., 0.81 - 1.00 sec., respectively. The natural periods of damaged buildings are increased about 30 - 40 % compared with the periods of undamaged buildings. The critical damping coefficients of damaged buildings are 25 % larger than those of undamaged buildings.

3) 9-story Large-Size Panel Building : The natural periods and critical damping coefficients of undamaged buildings are 0.38 - 0.39 sec. and 1.2 - 2.5 %, respectively. The natural periods and critical damping coefficients of damaged buildings are 0.40 - 0.46 sec. and 2.6 - 4.5 %, respectively. The natural periods are not so changed between undamaged and damaged buildings, but the critical damping coefficients of damaged buildings are almost 2 times those of undamaged buildings.

3.3 Relation between the building damages and the dynamic behaviour of buildings

Every structural types of building were suffered heavy damages during this earthquake. The degree of building damages was decided by the relation between the dynamic properties of building and ones of ground, instead of the difference of structural systems. However, by the inspection of damaged feature, the most damaged buildings were constructed by the uniformly procedure, and had the almost same degree of aseismic capacities. Then, it is supposed that the building damages were concentrately occurred by the passage the some level of strong earthquake motion.

For the construction of uniformly housing complex, it is important that the buildings have the sufficient aseismic capacities and the wide resistant performance to earthquake by considering with the dynamic property of ground. We considered that this earthquake hazard is seemed to the one example of warning to the building which is constructed by the standard design.

4. DYNAMIC BEHAVIOUR OF GROUND AND RELATION OF BUILDING DAMAGES

4.1 Measurements of microtremor on ground surface

The dynamic properties of surface ground are well known to effect the damage degree of buildings during earthquake. And also, the shapes of Fourier spectrum of microtremor are well known to similar to the shapes of Fourier spectrum of strong motion earthquake. The amplitude of Fourier spectrum of strong motion earthquake is equivalent to the amplitude of Fourier spectrum of microtremor.

The measurement of microtremor on the ground surface are done for the grasping of the dynamic properties of ground. The measurements were made to the following two objectives:

1) The damaged buildings have the natural periods of around 0.5 sec. of precast reinforced concrete frame buildings in Leninakan and the natural periods of around 0.3 sec. of stone-masonry buildings in Spitak and Kirovakan. Therefore, the microtremor were measured by the short period seismometer (the natural period of pendulum is 1 sec.).

2) The microtremor by the long period seismometer (the natural period of pendulum is 3 sec.) were measured for the estimation of deeper ground structures in Leninakan.

4.2 Microtremor measured in and around Leninakan

The microtremor of ground were measured at 12 points in and around Leninakan. The measured points are shown in Fig. 4.

The wave forms of microtremor are shown in Fig. 5. Fig. 5(a) shows the six points (11, 1, 3, 6, 9, 10) which are lined from north to south direction of Leninakan city. Figs. 5(b), 5(c) and 5(d) show the 5 points (11, 12, 4, 7, 10) from north to south of different line of Fig. 5(a), 4 points (2, 1, 12, 5) and 3 points (6, 7, 8) from west to east direction, respectively. The Fourier spectrum of each point are shown in Fig. 6(a) and Fig. 6(b).

The relation between mean period of microtremor and degree of building damages in Leninakan was summarized as follows:

1) In the northern area of Leninakan (north part from Lenin square): The mean period of microtremor of ground is around 0.5 sec., and this period is close to the natural period of 9-story precast reinforced concrete frame buildings. So it is guessed that this fact might be one of causes of making damages of this kind of buildings more seriously.

2) In the central area of the city: The mean period of microtremor of ground is 0.2 - 0.3 sec., and this period is close to the natural period of low-rise stone masonry buildings. This fact might be one of causes of making damages of this kind of buildings more seriously. It is necessary to implement the more detailed survey, because there are under ground flows of river.

3) In the southern area of Leninakan: The mean period is close to the period in the northern area, but it's amplitude is larger than of the northern area.

4) General trend of dynamic properties of ground in and around Leninakan: Leninakan city is located on the deep sedimentary layer, and the predominant periods of microtremor are effected by the local sedimental condition of surface layer. And so, the amplitude of microtremor of some areas have remarkably large according to the material of surface ground at the very shallow part. These fact might be caused the degree of damages of buildings.

4.3 Microtremor measured in and around Spitak

The microtremor of ground were measured at 10 points in and around Spitak. The measured points are shown in Fig. 7.

The wave forms of microtremor of each points are shown in Fig. 8, and the Fourier spectrum are shown in Figs. 9(a) and 9(b).

The relations between mean period of microtremor and degree of building damages in Spitak are summarized as follows:

1) Seismic bedrock of Spitak: The predominant period is very short (less than 0.1 sec.) at the foot around the hill, where a monument was constructed at the top of this hill. The seismic bedrock is located at the very shallow in these area. Therefore, the dynamic properties does not appeared in the microtremor, and the amplitude during the earthquake was comparatively small.

2) The predominant periods in the heavy damaged area of Spitak are the range between 0.2 sec. and 0.4 sec., and these periods are close to the natural period of destructed buildings. So it is guessed that this fact might be one of

causes of making damages of this kind of buildings more seriously. And then, the other cause of making damages is very strong earthquake motion itself.

3) New developing area of Spitak: The predominant period in new developing area of Spitak is almost close to that in the damaged area of Spitak. Therefore, it is necessary to construct the more reinforced and more stiffened buildings.

4.4 Microtremor measured in and around Kirovakan

The microtremor of ground were measured at 5 points in and around Kirovakan. The measured points are shown in Fig. 10.

The wave forms and the Fourier spectrum of microtremor of each point are shown in Fig. 11 and Fig. 12, respectively.

The relations between mean period of microtremor and degree of building damages in Kiravakan are summarized as follows:

1) The amplitude of microtremor at the just front of the City-Office is about 1/3 times of the amplitude in heavy damaged area. The predominant period in heavy damaged area, where is located very close to the City-Office, is 0.2 - 0.4 sec. This fact might be one of causes of making damages of buildings more seriously.

2) New developing area of Kiravakan: The predominant period in new developing area of Kirovakan is a little longer than the period in the damaged area of Kirovakan.

4.5 Relation between the ground properties at the narrow valley and the earthquake damages

At the city area, which is located at the comparatively narrow valley in the mountain zone (for example, the area of Spitak or Kirovakan), the relations between the ground properties and the earthquake damages will be generally appointed as follows;

1) At the area of outcrop part of seismic bedrock or on the very shallow sedimentary layer, the damages of buildings were not so severe. The amplitude of microtremor is small at the range of short periods, but is relatively large at the range of longer periods. (example: the hill area of Spitak, point 7. the central area of Kirovakan, point 2)

2) The building damages were more severe by the more thickness of the sedimentary layer. But, it is very clear to find the relation between the damage and the selectivity of predominant period. The amplitude of microtremor is remarkably large at the range of short period, but is not so remarkable at the range of longer period. (example: the housing complex area of northern part of Spitak, point 2. the housing complex area of north-western part of Leninakan, point 1)

4.6 Properties of longer period microtremor in Leninakan

The microtremor by long period seismometer (the natural period of pendulum is 3 second) in the new developing area of northern Leninakan find the predominant period of 3 - 4 sec. The 3 measured points, as illustrated A1, A2 and A3, are shown in Fig. 4. The wave forms of longer period microtremor at each point are shown in Fig. 13.

This long predominant period is caused by the very deep sedimentary layer on the seismic bedrock. This fact shows that the seismic bedrock of Leninakan area will be located at the several kilometres bellow the ground surface. The long predominant period in the new developing area of southern Leninakan is close to the period in the northern part area. Therefore, the seismic bedrock in and around Leninakan area is located at almost same depth.

4.7 Relation between the earthquake damages and the seismic microzoning

The one of the causes of heavy damage of buildings is able to explain the coincidence between the predominant period of ground and the natural period of building. The other cause is very strong earthquake motion itself. Therefore, it is necessary to more consideration of dynamic properties of ground for the Seismic Microzoning. The measurements of microtremor on ground and building are very effective procedure to estimate the predominant period of ground and the natural period of building, respectively.

ACKNOWLEDGMENT

Measuring of the microtremor were carried out by the apparatus of Tokyo Institute of Technology and great cooperation on the digitization and analysis were obtained from Dr. Kazuoh SEO, Associated Professor and Mr. Takanori SAMANO, Assistant, Tokyo

Institute of Technology. The cooperation are deeply acknowledged.

REFERENCE

1) S. MIDORIKAWA and H. KOBAYASHI; "Isoseismic Map in Near-Field with regard to Fault Rupture and Site Geological Conditions" Proceedings of 7th World Conference on Earthquake Engineering, Istanbul, Turkey, Sept., 1980.

Table 1 Parameters of Fault-Rupture Model

Fault Dimension	L=35 km W=12 km D=1.5 m (mean value)
Dip Direction	N60°W
Dip Angle	60°
Rupture Velocity	2.5 km/sec

Table 2 Geological Conditions and Amplification Factors

Geological conditions	Amplification Factors
Thick Sediment	4.5
Hard Sediment	3.5
Tertiary Period	2.5
Paleogene Period	2.0

Table 3 Maximum Acceleration and Seismic Intensity at Each Place

Place Name	Maximum Acceleration	Seismic Intensity (MSK)	Remarks
SPITAK 2	More than 600 gal	10	Sediment(Deposit)
LENINAKAN 1	530 gal	10	Northern Area
SPITAK 1	520 gal	10	Hard rock
LENINAKAN 2	470 gal	9	Southern Area
STEPANAVAN	460 gal	9	
APARAN	370 gal	9	
KIROVAKAN 2	360 gal	9	Sediment(Deposit)
KIROVAKAN 1	250 gal	8	Central Area
GUKASYAN	More than 228 gal	8	Unidentified Geology
YEREVAN	65 gal	6	

Table 4 Dynamic Properties of Damaged and Un-damaged Buildings

Type of Structure and No. of Story	Damage ※1	Translation				Torsional			
		Longitudinal		Transverse		Longitudinal		Transverse	
		T sec	h %	T sec	h %	T sec	h %	T sec	h %
Stone Masonry 5	U	0.30	4.8	0.33	7.2	0.35	2.6	0.35	4.6
	U	0.28	2.2	0.28	4.6	0.23	1.8	0.23	1.1
	D	0.49	4.0	0.28	1.9	0.41	4.7	0.41	3.6
	D	0.44	2.6	0.21	1.9	0.40	3.6	0.40	4.5
	D	0.52	4.0	0.52	7.4	0.55	3.2	0.56	4.1
	D	0.55	3.4	0.55	4.4	0.56	5.9	0.59	4.7
Precast Frames 9	U.U	0.57	1.6	0.79	1.1	0.50	9.3	0.54	15.0
	U.U	0.43	11.1	0.63	1.4	0.41	9.9	0.41	4.7
	U	0.61	3.2	0.46	1.7	0.41	0.6	0.42	2.5
	U	0.63	0.5	0.53	2.3	0.55	3.4	0.55	3.4
	D	0.93	---	0.93	---	0.87	---	0.85	---
	D	1.07	---	0.96	---	0.95	---	0.95	---
	D	1.00	---	0.81	---	0.80	---	0.77	---
	D	0.83	---	1.00	---	0.77	---	0.78	---
Large Pnel 9	U	0.38	2.2	0.38	1.2	0.30	2.3	0.30	0.5
	U	0.38	1.8	0.39	2.5	0.29	1.4	0.29	0.5
	U	0.46	4.5	0.40	2.6	0.46	3.4	0.45	1.8
Monolithic 4	U	0.51	2.6	0.32	2.2	0.27	0.9	0.27	2.9
Monolithic 16	U	1.10	7.8	1.00	6.1	0.96	1.9	1.18	1.3

--- unknown ※1 U:Undamaged D:Damaged U U:Undamaged and Under Construction

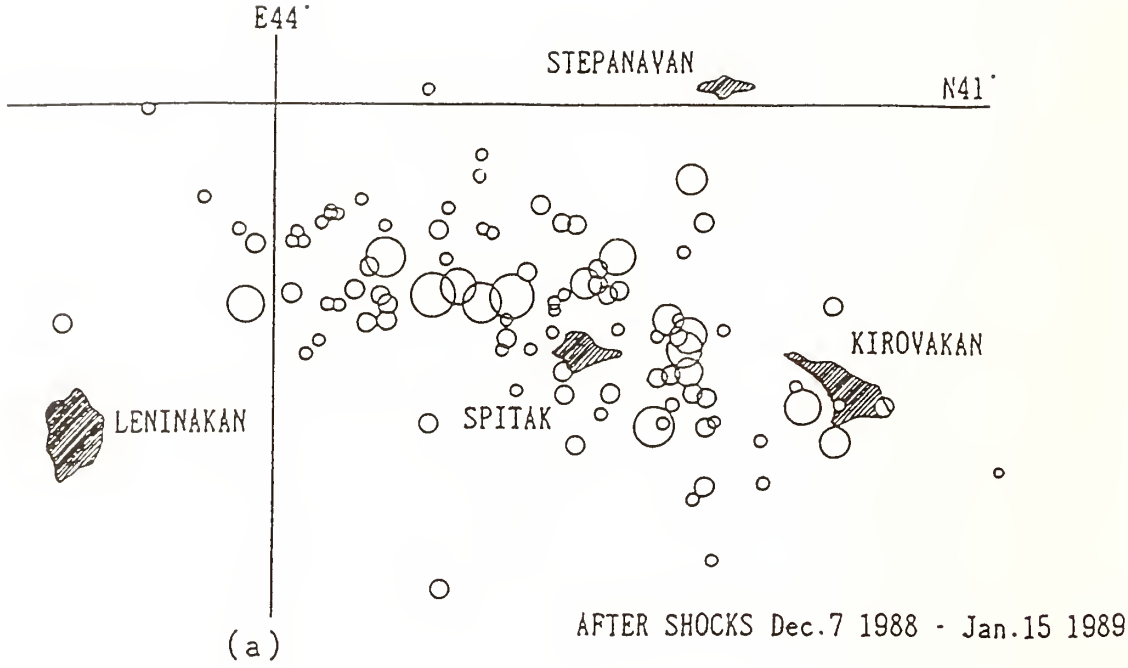

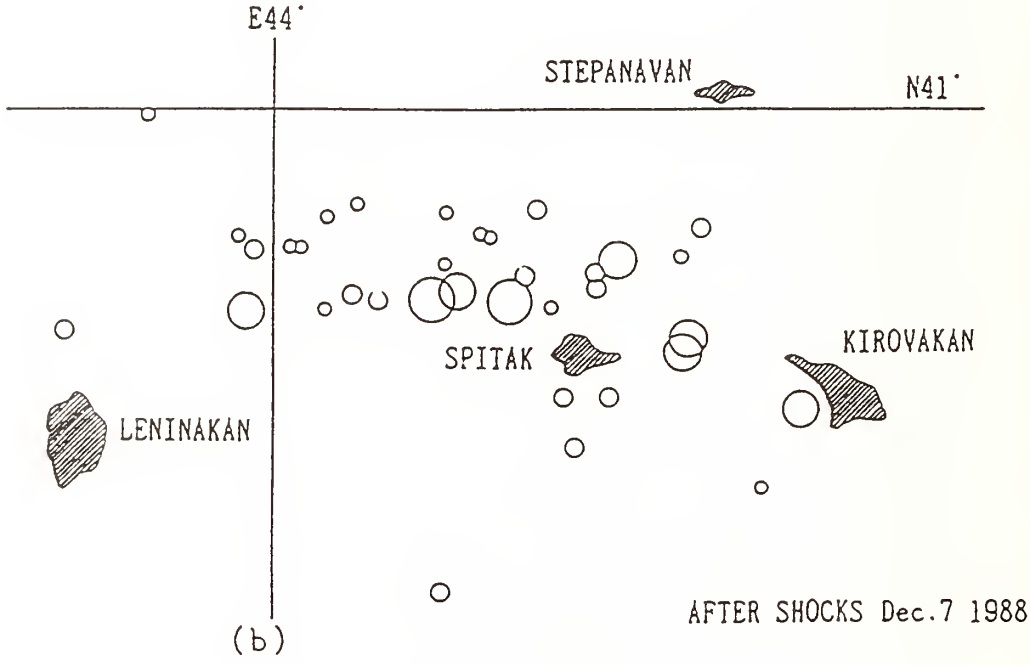

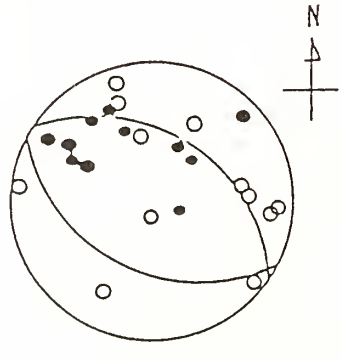

Fig. 1 Distribution of After Shocks and Source Mechanism

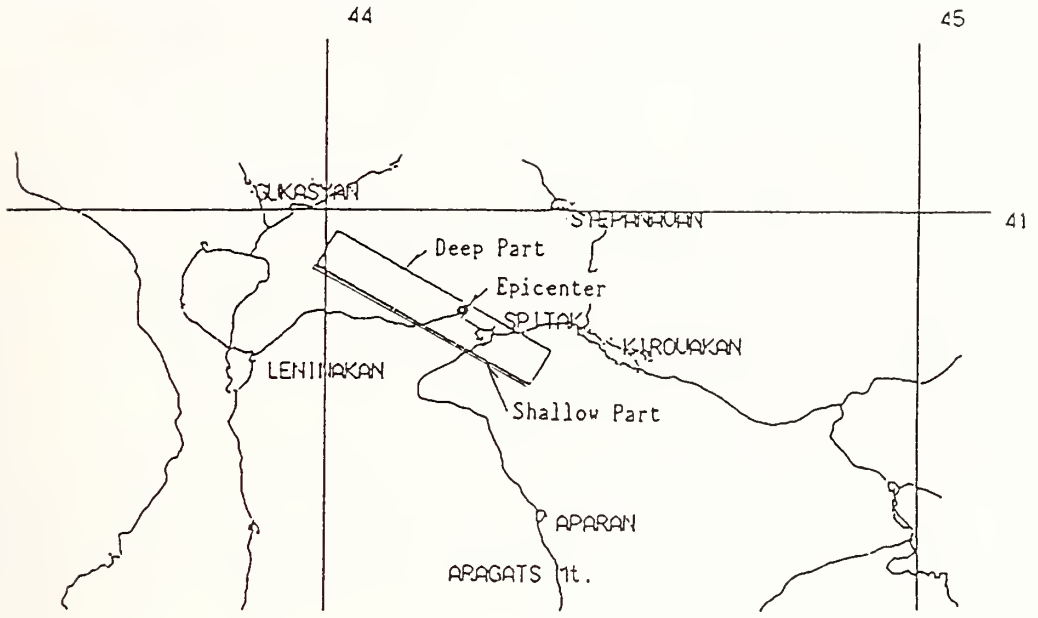

Fig. 2 Location of Fault-Rupture Model

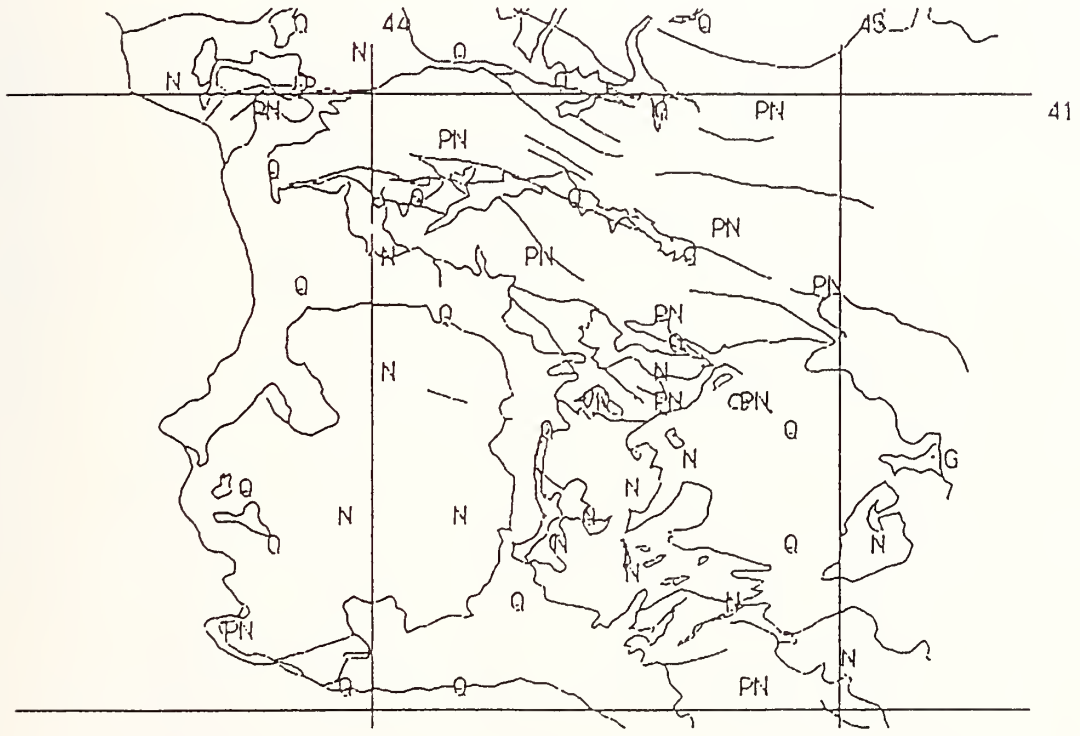

Fig. 3 Geological Map of ARMENIA

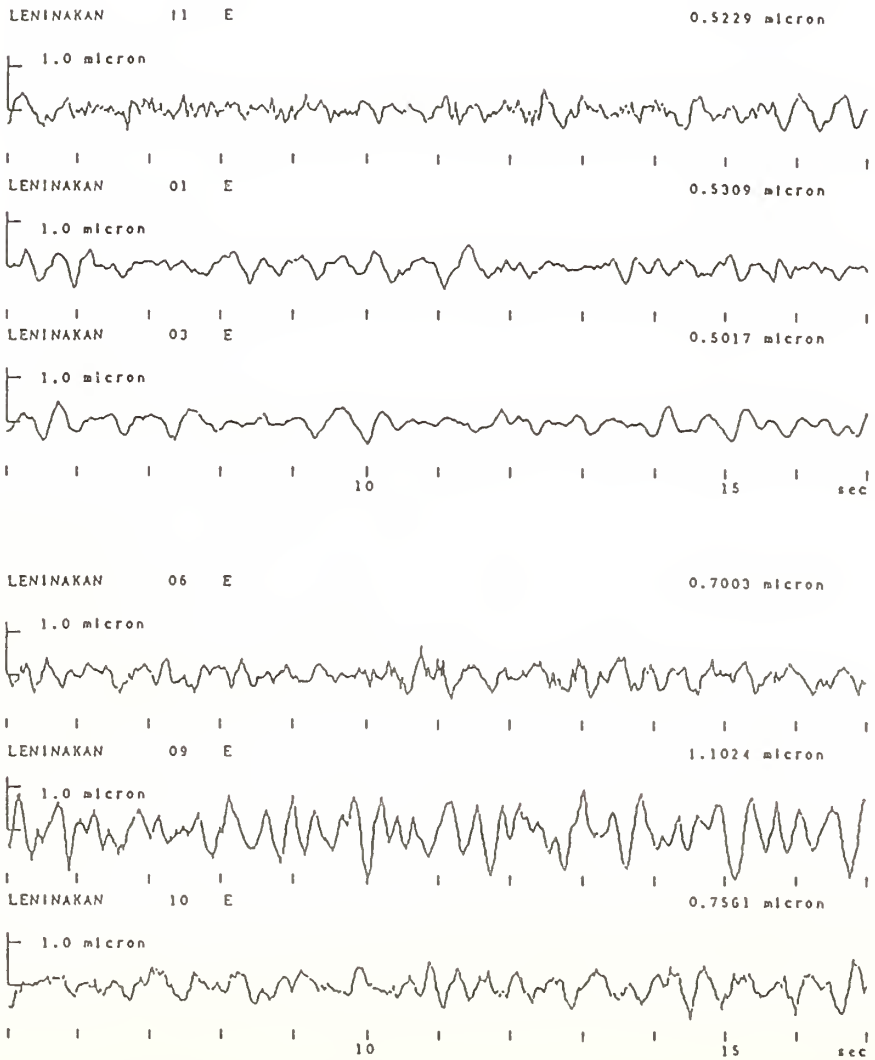

Fig. 5(a) Wave Forms of Microtremor in LENINAKAN

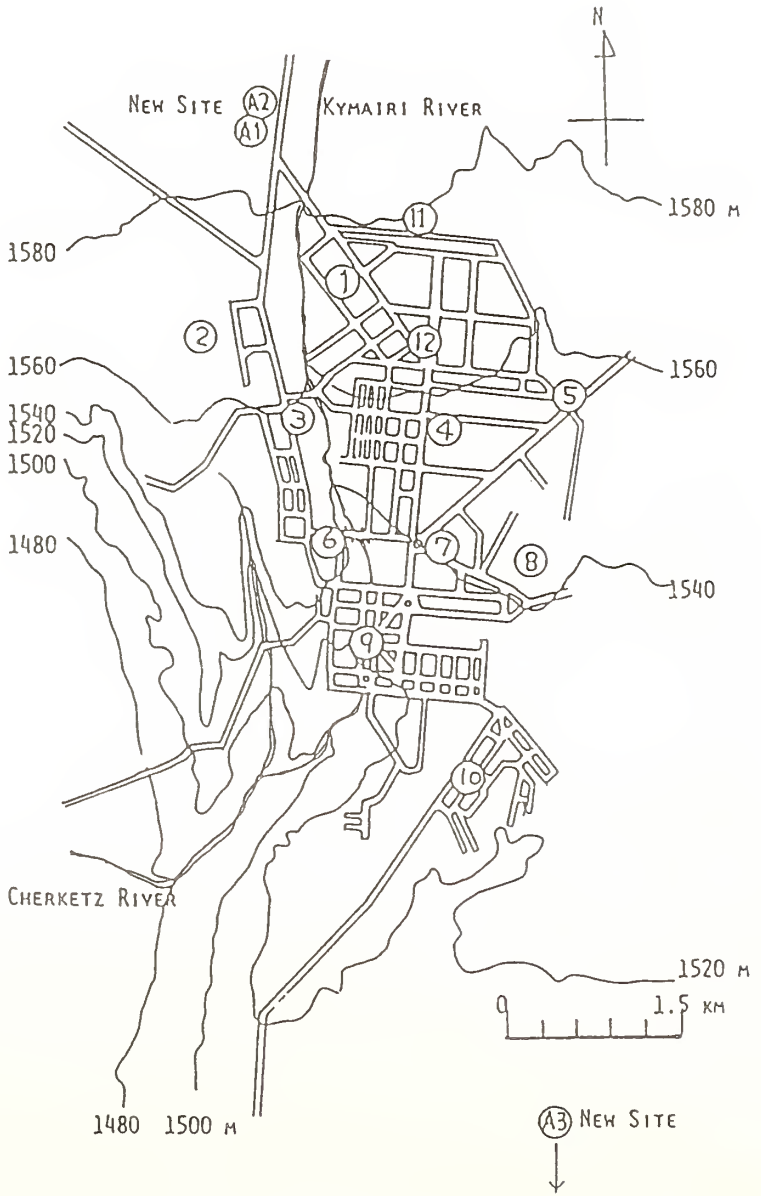

Fig. 4 Measured Points of Microtremor in LENINAKAN

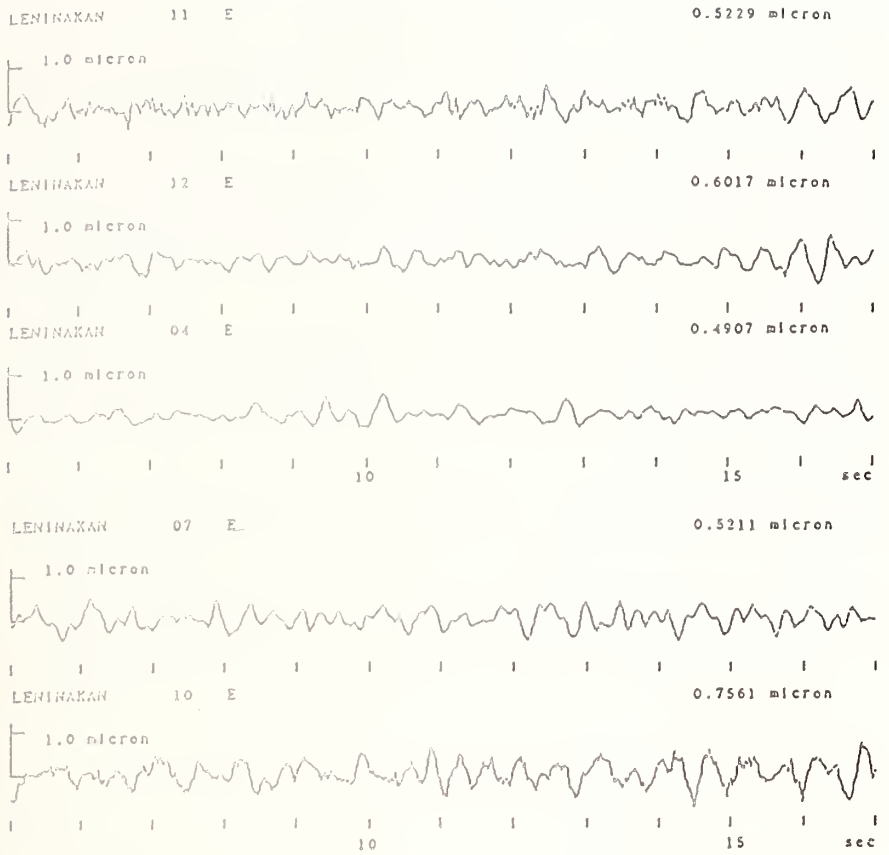

Fig. 5(b) Wave Forms of Microtremor in LENINAKAN

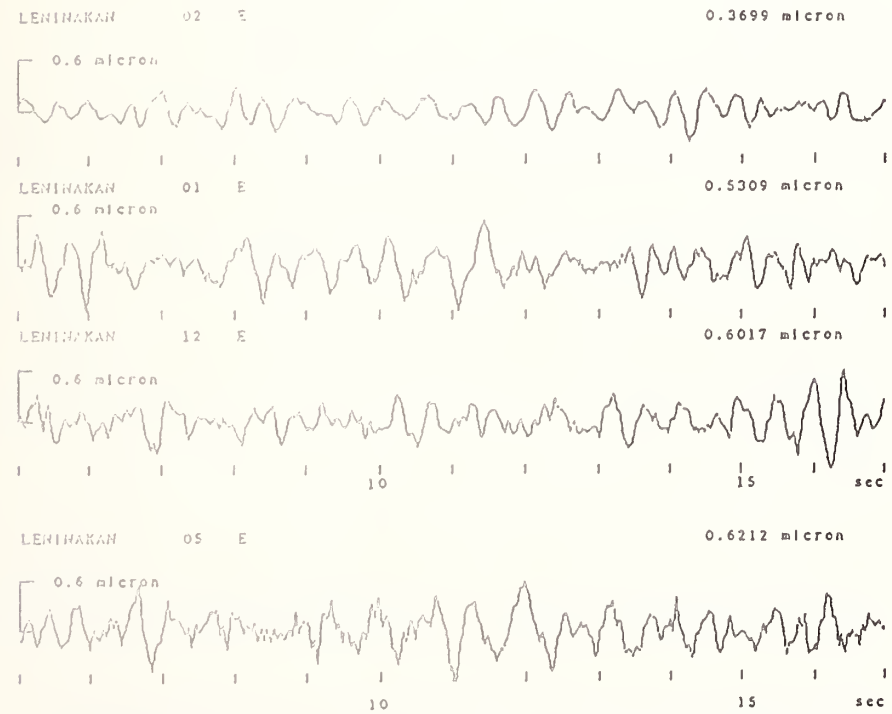

Fig. 5(c) Wave Forms of Microtremor in LENINAKAN

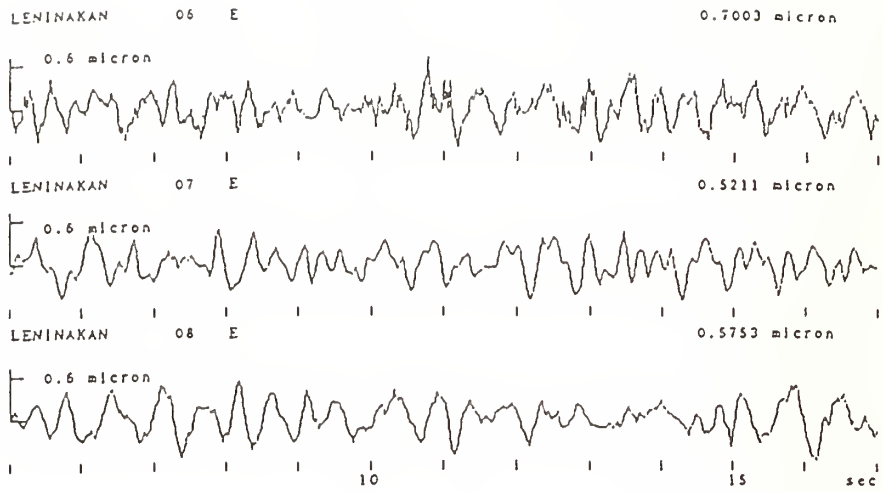

Fig. 5(d) Wave Forms of Microtremor in LENINAKAN

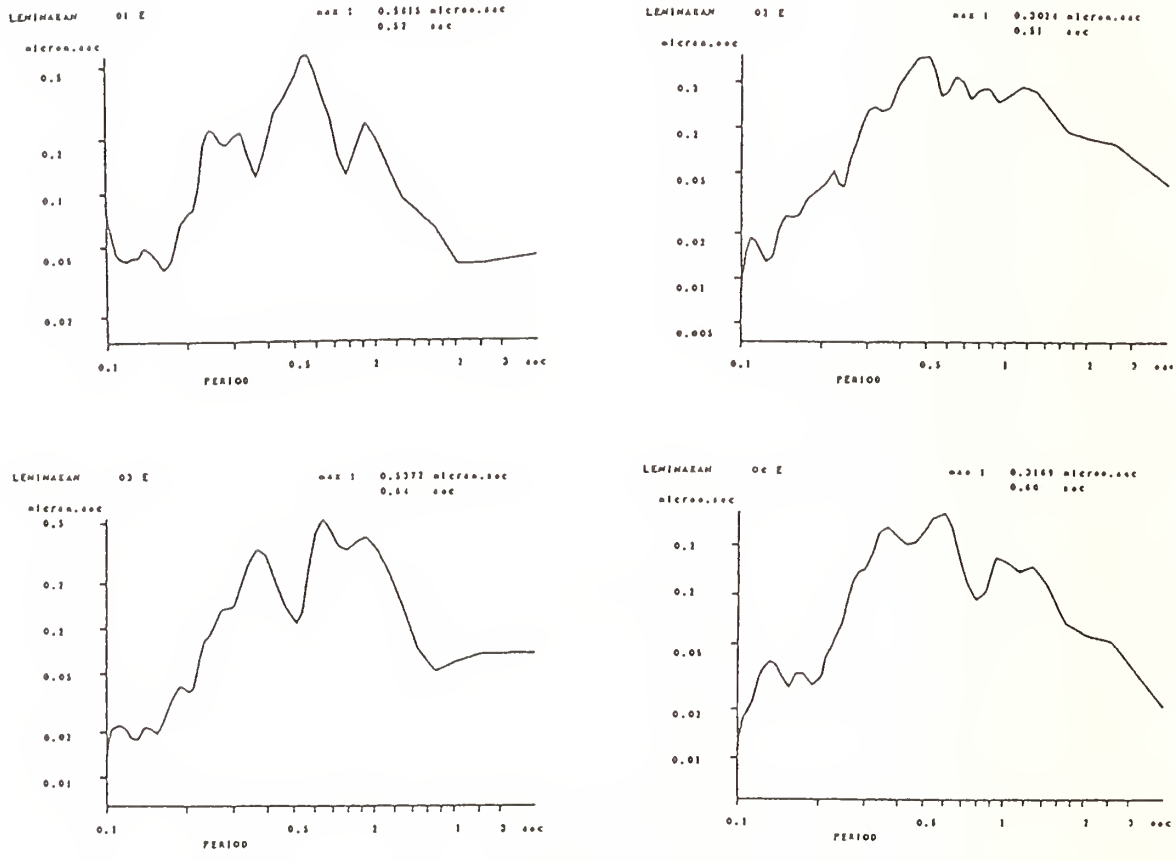

Fig. 6(a) Fourier Specta of Microtremor in LENINAKAN

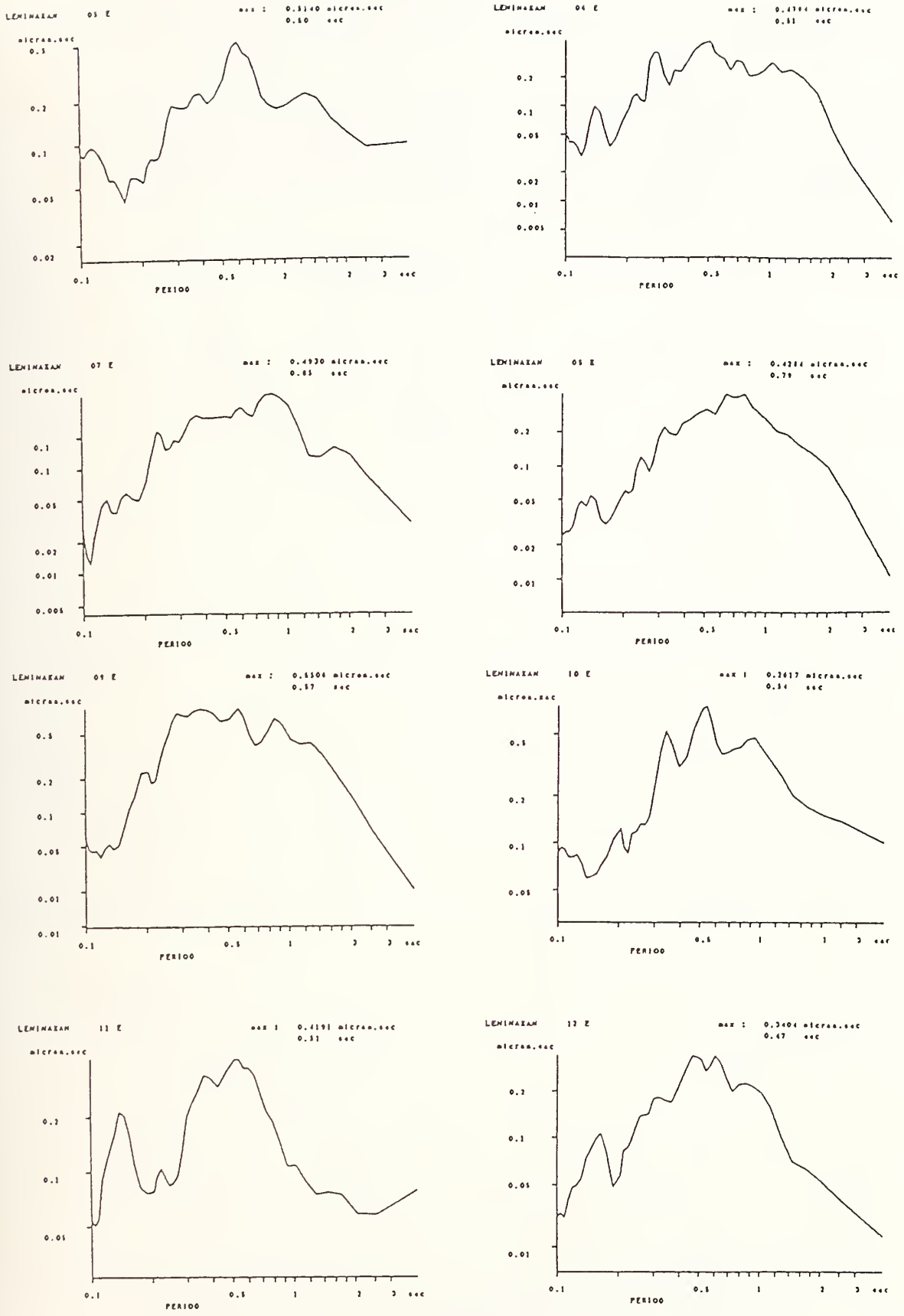

Fig. 6(b) Fourier Spectra of Microtremor in LENINAKAN

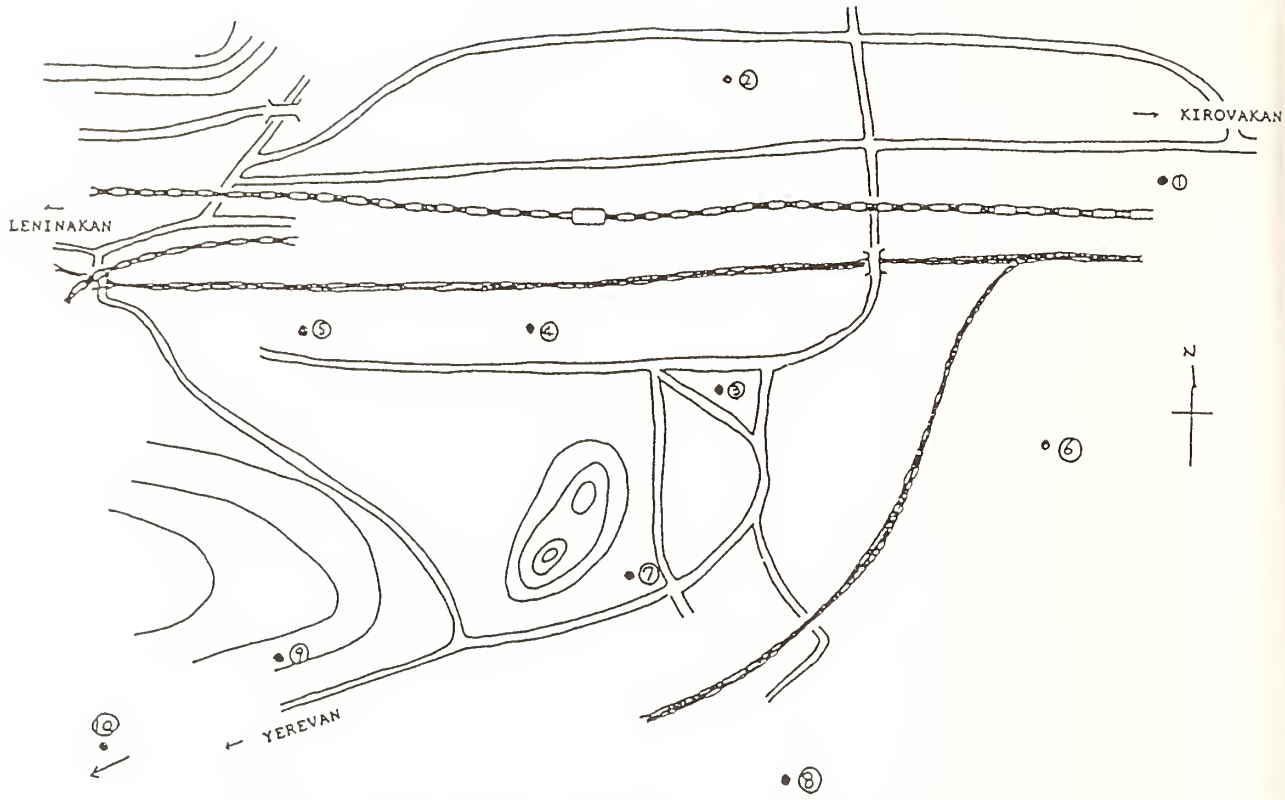

Fig. 7 Measured Points of Mictrotremor in SPITAK

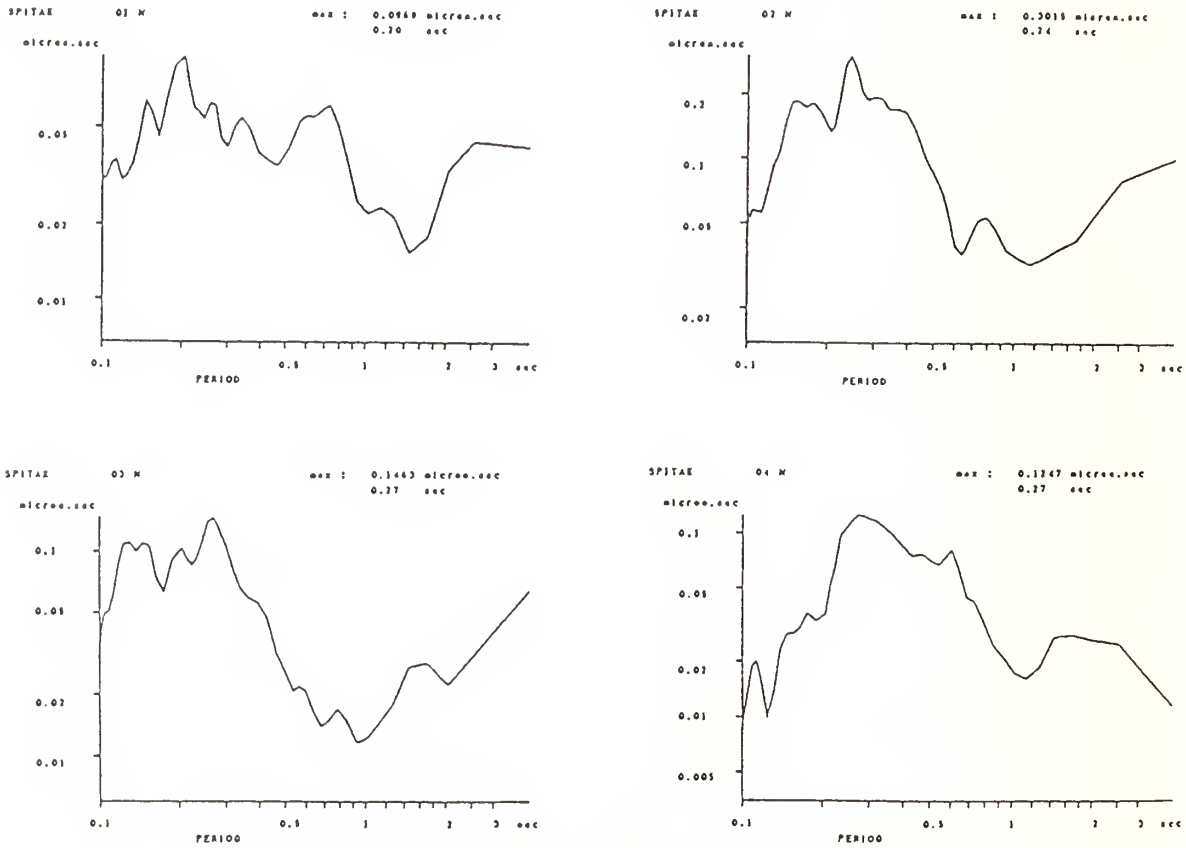

Fig. 9(a) Fourier Spectra of Microtremor in SPITAK

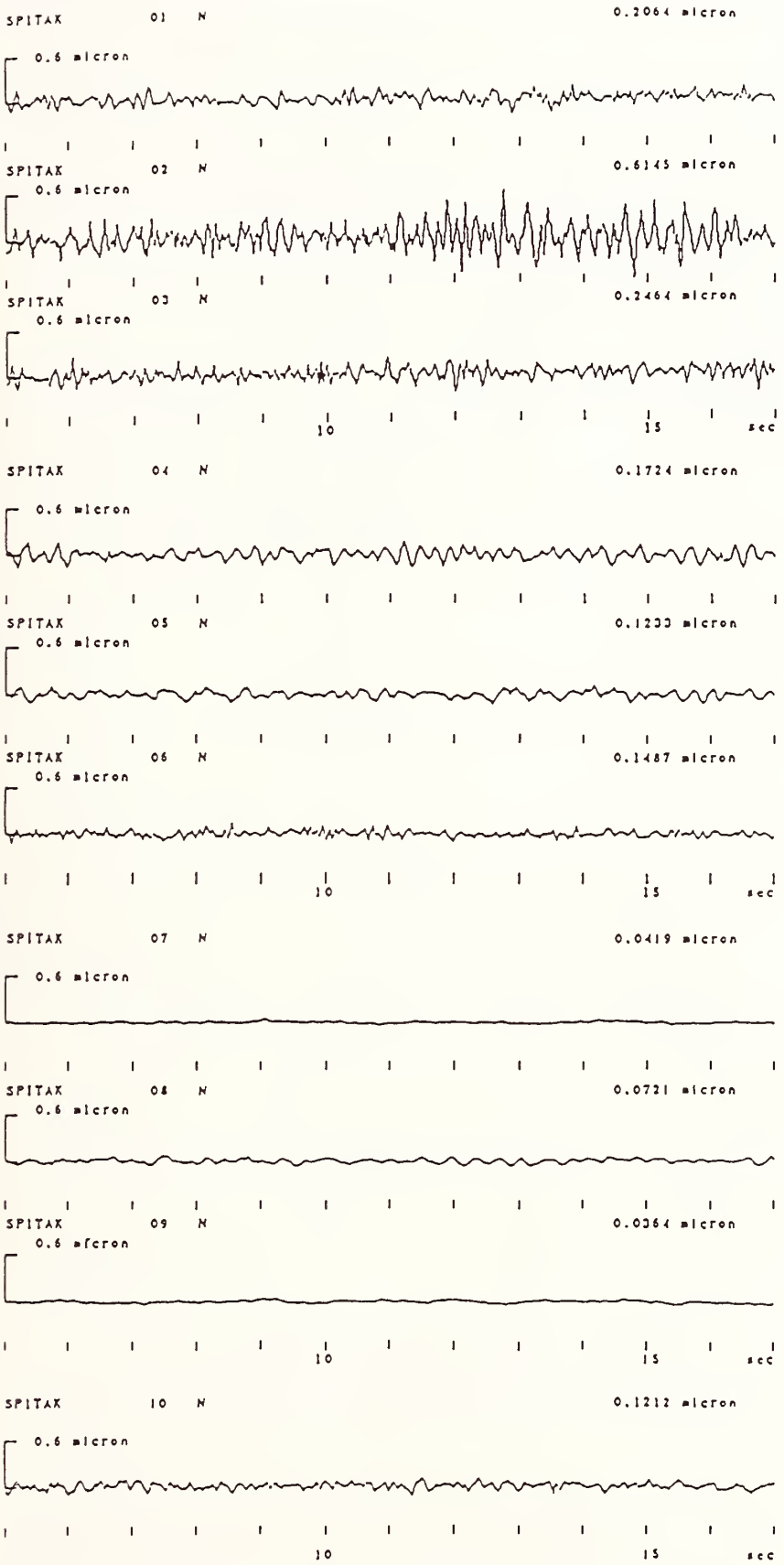

Fig. 8 Wave Formes of Microtremor in SPITAK

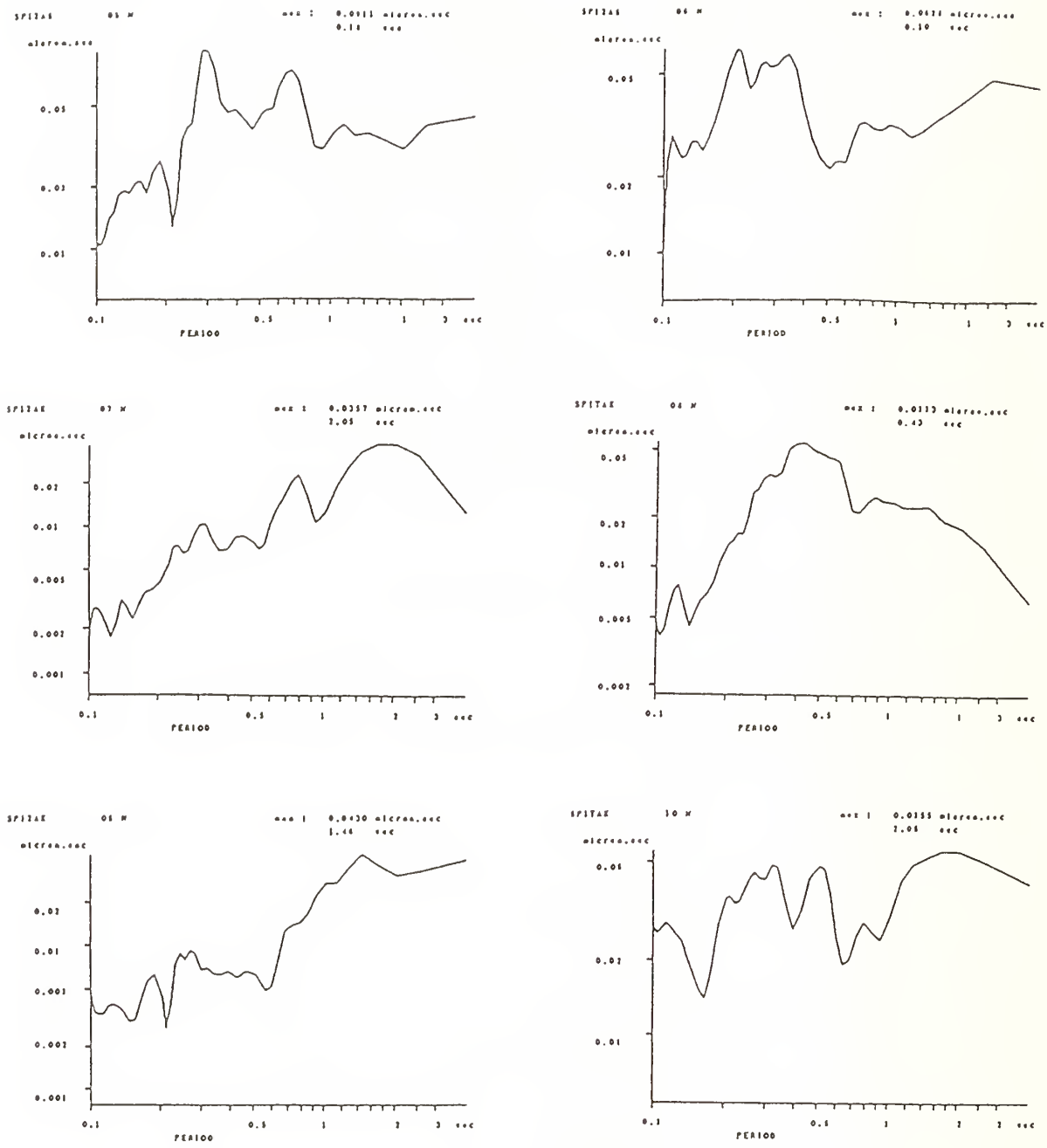

Fig. 9(b) Fourier Spectra of Microtremor in SPITAK

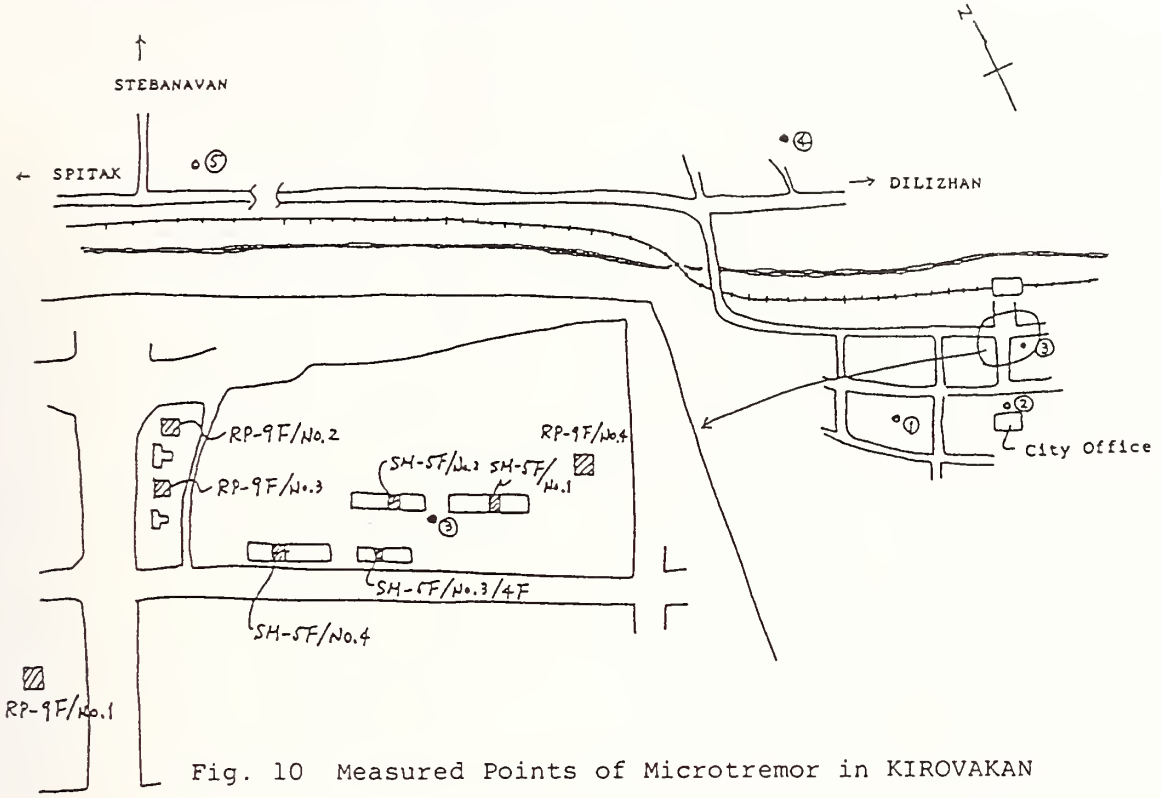

Fig. 10 Measured Points of Microtremor in KIROVAKAN

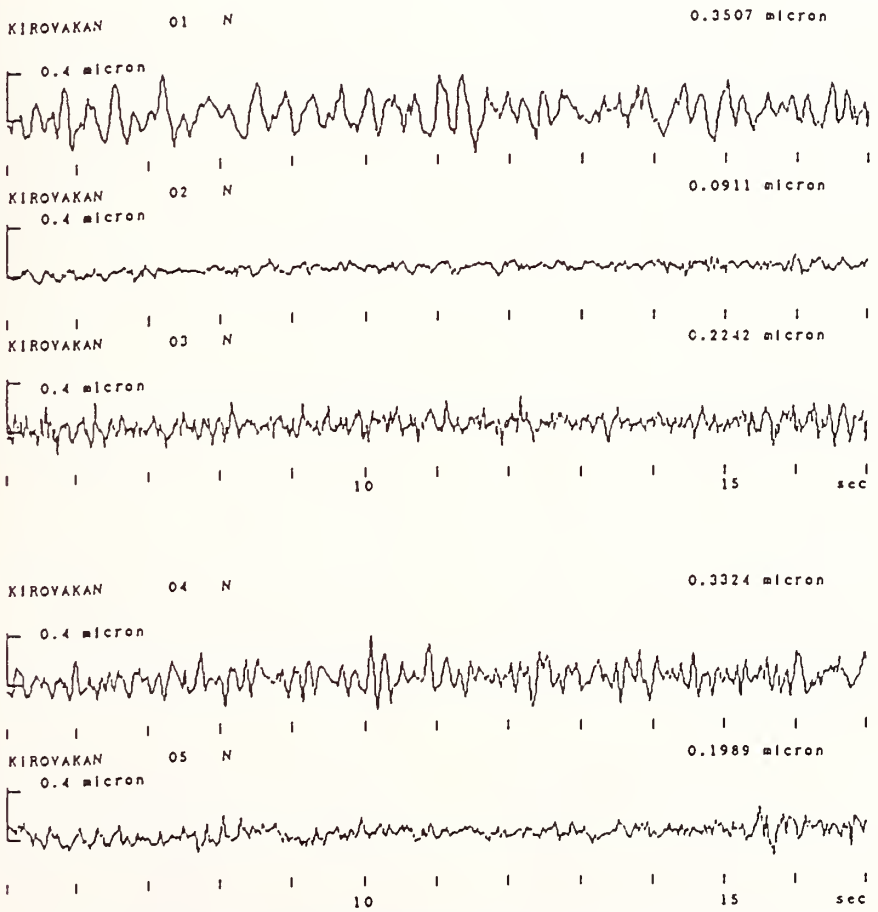

Fig. 11 Wave Forms of Microtremor in KIROVAKAN

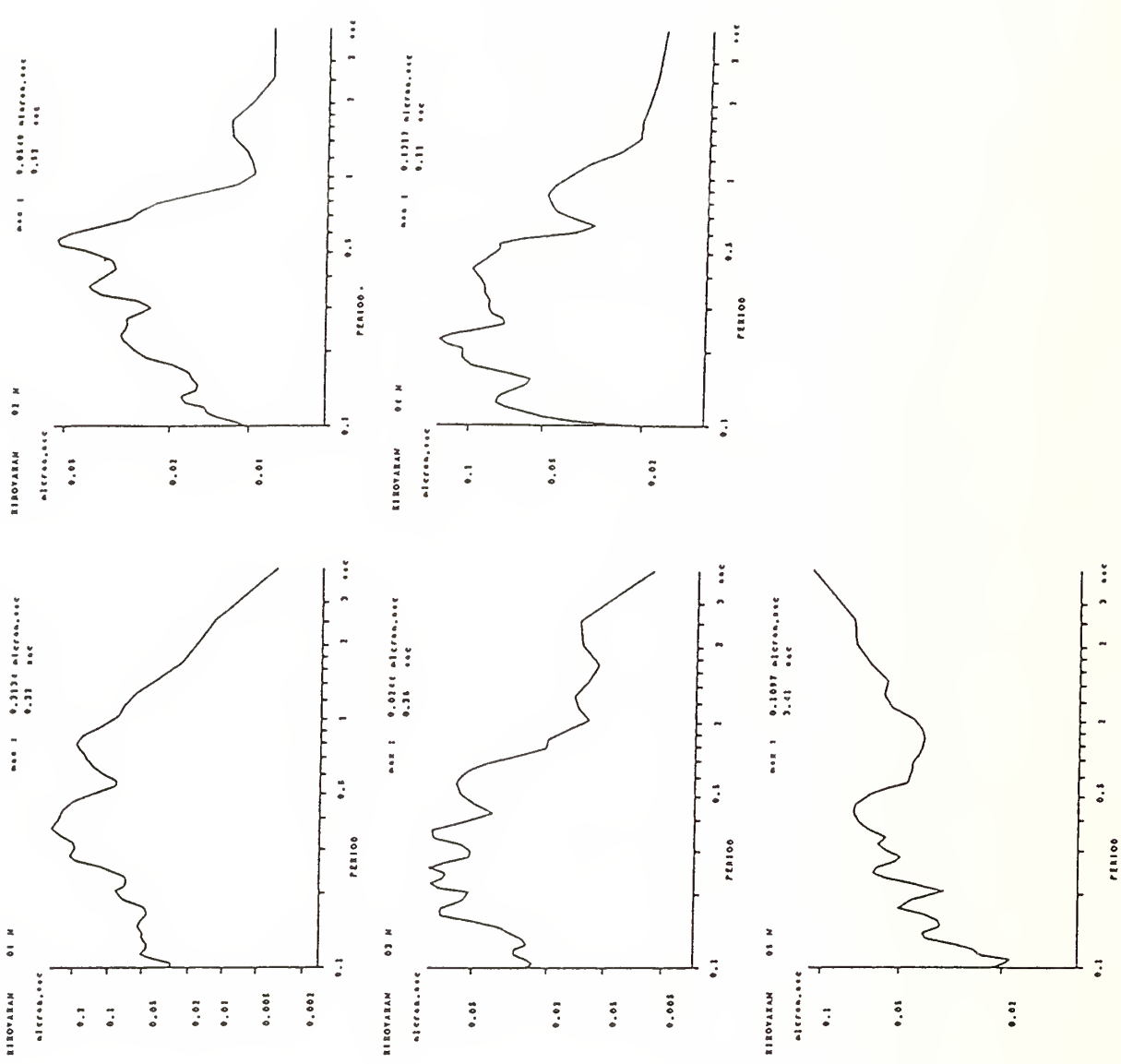

Fig. 12 Fourier Spectra of Microtremor in KIROVAKAN

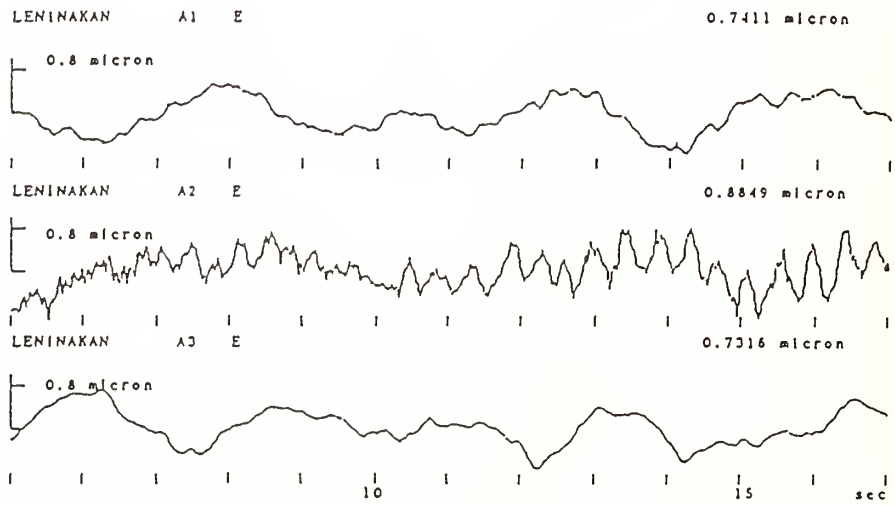

Fig. 13 Wave Forms of Microtremor in LENINAKAN
(by Long Period Seismometer)

New Seismic Design Specifications of Highway Bridges in Japan

By

Toshio IWASAKI[1], Kazuhiko KAWASHIMA[2] and Kinji HASEGAWA[3]

ABSTRACT

Introduced are the new Seismic Design Specifications of Highway Bridges in Japan issued on February 1990. Main items of the revision including the seismic lateral force, evaluation of inertia force considering structural response, check of bearing capacity for lateral load for reinforced concrete pier and dynamic response analysis are presented.

KEY WORDS

Seismic Design, Design Method, Highway Bridge

1. INTRODUCTION

First requirement on lateral force for design of road bridge in Japan was included in "Draft Details of Road Structure" issued in 1926 with considerations of the damage caused by the Kanto Earthquake in 1923. It was stipulated in the draft details that the maximum lateral force expected to develop at the site shall be considered in seismic design. After experiencing significant damages during strong earthquakes seismic regulations were reviewed and amended several times as shown in Table 1. "Design Specifications of Steel Road Bridges (Draft)" were issued in 1914, and "Design Specifications of Steel Road Bridges" and their revised version were issued in 1934 and 1939, respectively. Although a requirement for lateral force was stipulated in these specifications, first comprehensive seismic design stipulations were issued in 1971 in a separate volume exclusively for seismic design as "Seismic Design Specifications of Road Bridges". It was described in the specifications that lateral force shall be determined depending on zone, importance and ground condition in seismic coefficient method and structural response shall be further considered in the modified seismic coefficient method. Evaluation on soil liquefaction was firstly incorporated in view of the damages caused by the Niigata Earthquake in 1964. The 1971 specifications were revised in a form of "Part V Seismic Design" of "Design Specifications of Road Bridges" in 1980. A rational evaluation method for soil liquefaction as well as practical countermeasures against the liquefaction was included in the specifications.

Since 1985 extensive efforts have been undertaken to establish more rational seismic design criteria for road bridges, with consideration of recent advantages of earthquake engineering and lessons gained from recent earthquakes. New specifications were were completed in 1990.

This paper outlines the new specifications (JRA, 1990) for seismic design of road bridges with emphasis on the stipulations revised.

2. BASIC PRINCIPLES FOR DEVELOPING NEW SPECIFICATIONS

Road bridge is a vital component of road, and it has to be safe enough against an earthquake so that function of road be maintained. It can be used without loosing any structural functions against small to moderate earthquakes with high to moderate possibility to occur at the site. Critical failure causing total collapse of the bridge has to be avoided even during a significant earthquake such as the Kanto Earthquake in 1923. Seismic design method has been gradually improved with consideration on damage experiences and advantage of earthquake engineering. Based on such improvement of seismic design method as well as various countermeasures against an earthquake, it is considered that seismic damages of road bridge have been decreasing as a total in recent years as shown in Table 2. However it is also important to note that new damages which have not been identified in the past earthquakes have been seen in recent earthquakes, due to improvement of seismic design method. This obviously shows that the countermeasures aiming only to minimize the damages developed in the past earthquake do not give a credit to avoid new type of damage in the future earthquake. In revising the design specifications, it is required to take account of such new type of

---

1) Director General, Public Works Research Institute
2) Head, Earthquake Engineering Division of Earthquake Disaster Prevention Department, Public works Research Institute
3) Research Engineer, ditto

damage patterns.

In view of the understanding on the damage patterns of road bridges in recent earthquakes and advances of earthquake engineering, the following revisions were included in the New Seismic Design Specifications.

1) modification on classification of ground condition
2) unification of seismic coefficient method and modified seismic coefficient method including the revision of the seismic coefficient
3) evaluation method of inertia force for continuous bridges
4) improvement on strength of sandy soils against liquefaction
5) evaluation of bearing capacity of reinforced concrete piers for lateral force (ductility check)
6) design ground motion for dynamic response analysis as well as an analytical model

Table of content of the new specifications is the following :

Chapter 1 General
Chapter 2 Basic Principle of Seismic Design
Chapter 3 Load and Design Condition in Seismic Design
Chapter 4 Seismic Coefficient
Chapter 5 Bearing Capacity for Lateral Force of Reinforced Concrete Piers
Chapter 6 Dynamic Response Analysis
Chapter 7 Structural Details in Seismic Design
Chapter 8 Device to Expect Reduction of Lateral Force

〈Appendix〉
I. References on Liquefaction
II. Examples of Classification of Ground Condition
III. References on Design Ground Motion
IV. Example of Calculation of Natural Period and Inertia Force
V. Reference on Bearing Capacity of Reinforced concrete Piers for Lateral Force
VI. Practices of Structural Details

Table 3 shows the revised part or newly introduced parts in the new specifications, and **Fig. 1** shows the flow-chart of seismic design.

3. CLASSIFICATION OF GROUND CONDITION

Classification of ground condition was changed from four groups to three groups as shown in **Table 4** by combining the group 2 and group 3 into same group. The classification of the ground condition is made base on the characteristics value at the site specified as

$$T_G = 4 \sum_{i=1}^{I} \frac{H_i}{V_{si}} \qquad (1)$$

where
T_G : characteristic value (sec)
H_i : thickness of i-th subsoil layer (m)
V_{si} : shear wave velocity of i-th sublayer (m/sec)
I : sublayer's number counted from ground surface

The change was made because most of the seismic damage of road bridge in the past earthquake was likely to be developed on the group 4 with the difference between the ground group 2 and 3 being practically very small, and because difference of ground motion characteristics in terms of response acceleration spectra is few between the ground group 2 and 3. It was also taken into account that the classification of the ground condition based on the difference of characteristic value of only 0.2 second is practically quite hard in view of the fact that shear wave velocity is generally estimated from an empirical formulae based on N-value of standard penetration test.

4. SEISMIC COEFFICIENT

In the previous specifications, the seismic coefficient method was used for the bridges with pier height less or equal to 15 m and the modified seismic coefficient method was used for the bridges with pier height larger than 15 m. The modified seismic coefficient method was originally intended to apply to bridges with the natural period longer than 0.5 second. However, as various foundations becomes to be adopted on wide range of soil conditions, even bridges with pier height less than 15 m is likely to have the natural period longer than 0.5 second. This always caused confusion in selecting the seismic design method.

Therefore, the seismic coefficient method

and the modified seismic coefficient method was unified, and this is referred to as seismic coefficient method.

In the seismic coefficient method, the design seismic coefficient shall be determined by Eq.(2), but no less than 0.1.

$$k_h = c_z \cdot c_G \cdot c_I \cdot c_T \cdot k_{h0} \qquad (2)$$

where

k_h : design horizontal seismic coefficient,

k_{h0} : standard design horizontal seismic coefficient (=0.2),

c_z : modification factor for zone (refer to Fig. 2),

c_G : modification factor for ground condition (refer to Table 5),

c_I : modification factor for importance (refer to Table 6), and

c_T : modification factor for structural response (refer to Table 7). For computing inertia force associated with the weight of soils and dynamic earth pressure, c_T has to be 1.0.

In Eq.(2) the modification factors c_z and c_I are the same with the value specified in the previous specifications. The modification factor c_G was changed associated with the change of ground condition classification. The modification factor c_T, which represents the difference of lateral force due to structural response, corresponds to the modification factor β in the previous specifications. The modification factor β was formulated based on an analysis of 44 components of strong motion records obtained in Japan. The new modification factor c_T was determined from an analysis of earthquake response spectra base on 394 components of strong motion records obtained in Japan. Considerations that the seismic damage was likely to occur in bridges with short natural period were also included.

Fig. 3 shows an comparison of the seismic coefficient between the previous and new specifications assuming that $c_z = c_T = 1.0$.

5. EVALUATION METHOD OF INERTIA FORCE

In the previous specification, for computing an inertia force associated with dead weight of superstructure, which is to be used in seismic design of substructure, the bridge is divided into several structural segments consisting of a substructure and the part of superstructure which is vertically supported by the substructure considered. Then, the inertia force (lateral force) used for the seismic design of substructure of the i-th structural segment is assumed to be determined as

$$F_{ai} = k_{hi} R_i \qquad (3)$$

where

F_{ai} : inertia force associated with dead weight of superstructure for design of i-th substructure

k_{hi} : seismic coefficient considered for i-th structural segment

R_i : reaction force developed at i-th substructure due to dead weight of the part of superstructure supported by the i-th substructure.

However as various type of bridge structures become to be constructed, it became apparent that the inertia force determined by Eq.(3) assuming that the bridge can be divided into several structural segments is inadequate, because the inertia force at each substructure significantly depends on flexibility and height of the substructure and type of the superstructure. Therefore, more rational method to evaluate the inertia force induced in the superstructure for the purpose of seismic design of substructure was required. The same demand also arises in the bridge where the superstructure and the substructure are not separated by means of bearing supports.

Therefore, in stead of the structural segment, a definition of seismic design structural unit, defined as the structural unit which can be considered to develop the same response during an earthquake, was newly introduced in the new specifications. Table 8 shows examples how the seismic design structural unit be selected for typical combinations of structural type and direction for evaluating the inertia force.

Natural period and the inertia force shall be determined as:

1)Seismic design structural unit consisting of a substructure and a part of superstructure supported by the substructure

In this case, there is essentially no difference with the previous specifications. Inertia force shall be determined by Eq.(4), and the natural period shall be computed as

$$T = 2.01 \sqrt{\delta} \qquad (4)$$

where

T : natural period, in second, of the seismic design structural unit

δ : lateral displacement, in meter, of

the substructure subjected to a lateral force equivalent with 80 % of the dead weight of a substructure above the ground surface assumed in seismic design and the dead weight of a part of the superstructure supported by the substructure.

It should be noted here that only the substructure on the ground surface assumed in seismic design shall be subjected to inertia force because the seismic force below the ground surface assumed in seismic design is disregarded in seismic design. The ground surface assumed in seismic design is generally taken as the bottom plane level of the footing in case of pile foundation. However, when the soil layers whose soil constant is assumed as zero due to possible soil failure such as liquefaction, the bottom of these layers is regarded as the ground surface assumed in seismic design.

2)Seismic design structural unit consisting of substructures and a part of superstructure supported by these substructures.

This is the case newly introduced in the new specifications. Natural period and the inertia force shall be evaluated in accordance with **Fig. 4**, i.e.,

i)idealize a seismic design structural unit by a linear elastic frame model

ii)apply a lateral force equivalent with the dead weight of superstructure and substructure above the ground surface assumed in seismic design, and compute the natural period as

$$T = 2.01 \sqrt{\delta} \qquad (5)$$

$$\delta = \frac{\int w(s)u(s)^2 ds}{\int w(s)u(s) ds} \qquad (6)$$

where

$w(s)$: dead weight of the seismic design structural unit (superstructure and substructure above the ground surface assumed in seismic design) at point s (tf/m)

$u(s)$: lateral displacement developed in the seismic design structural unit at point s (m) when subjected to w(s) in a direction considered in design.

III)determine the seismic coefficient k_h depending on the natural period T.

iv)compute inertia force as

$$F_d = k_h \times F \qquad (7)$$

where

F_d : shear force (tf) / bending moment (tfm) due to inertia force

k_h : seismic coefficient

F : force developed in the seismic design structural unit when subjected to a lateral force equivalent with dead weight of seismic design structural unit above the ground surface assumed in seismic design (tf/tfm)

For substructure supporting girder bridges, shearing force developed at the center of gravity of superstructure shall be regarded as the lateral force for seismic design. However, when the inertia force computed by Eq.(7) is smaller than the inertia force computed by Eq.(3), the latter shall be adopted for design. This needs some explanations. The inertia force computed by Eq.(7) is approximately proportional to the stiffness of each substructure. This implies that the inertia force concentrates to the substructures with high stiffness, while reverse is true for the substructure with low stiffness. Inertia force takes even negative value when the stiffness of the substructure is extremely small as compared with other substrctures. However, when failure of the structure such as bearing supports occurs, the contribution of each substructure for supporting the inertia force of superstructure could be changed from the distribution computed by Eq.(7). Base on such considerations, lower limit for the inertia force evaluated by Eq.(7) was included.

6. STRENGTH OF SANDY SOIL LAYER FOR LIQUEFACTION

For saturated alluvial sandy layers within 20 m from the ground surface which have the water table within 10 m from the ground surface, and have D_{50}-value on the grain size accumulation curve between 0.02 and 2.0 mm, the liquefaction potential during an earthquake has to be checked. For those soil layers required for the check of liquefaction, liquefaction potential shall be evaluated in terms of liquefaction resistance factor F_L as

$$F_L = R/L \qquad (8)$$

where

F_L : liquefaction resistance factor

R : resistance of soil elements against dynamic load

L : dynamic load induced in soil ele-

ments during an earthquake

In the previous specifications the resistance R of soil elements against dynamic load was evaluated from N-value of standard penetration test and D_{50}-value. Because fine sand content is found an important factor, It was included for evaluating R.

7. CHECK OF BEARING CAPACITY OF REINFORCED CONCRETE PIERS FOR LATERAL FORCE

Even for a significant earthquake, the bridge has to avoid critical failure. Reinforced concrete pier which is the most important member for preventing critical failure of bridge has to have the required ductility as well as the strength. The check of bearing capacity for lateral load was introduced to avoid brittle failure of reinforced concrete piers in inelastic range. Check of bearing capacity for lateral load is advised for the reinforced concrete piers with small concrete section.

Fig. 5 shows a flow-chart of the check of bearing capacity of reinforced concrete piers for lateral force. Main steps of this check are the following :

1) Judgement of bearing capacity for lateral force

Bearing capacity for lateral force shall be checked as

$$P_a > k_{he} W \qquad (9)$$

where

P_a : bearing capacity of reinforced concrete pier for lateral force (tf)

k_{he} : equivalent horizontal seismic coefficient for check of bearing capacity for lateral load

W : equivalent dead weight (tf), and shall be determined as

$$W = W_u + c_P W_p \qquad (10)$$

$$c_P = \begin{cases} 0.5 & P_u \leqq P_s \\ 1.0 & P_u > P_s \end{cases} \qquad (11)$$

W_u : dead weight of a part of superstructure supported by the rein forced concrete pier (tf)

W_p : dead weight of the reinforced concrete pier (tf)

P_u : bearing capacity of reinforced concrete pier for flexural failure (tf)

P_s : bearing capacity of reinforced concrete pier for shear failure (tf)

When the check for the bearing capacity for lateral force by Eq.(9) cannot be satisfied, modification of the design has to be made so that the modified section, which is designed in accordance with the seismic coefficient method, satisfies Eq.(9). it is generally advised to increase the concrete section with decreasing the amount of reinforcement.

2)Equivalent horizontal seismic coefficient for check of bearing capacity for lateral force

Equivalent horizontal seismic coefficient for check of bearing capacity for lateral force shall be determined as

$$k_{he} = \frac{k_{ho}}{\sqrt{2\mu - 1}} \qquad (12)$$

$$k_{ho} = c_Z \cdot c_I \cdot c_R \cdot k_{hcD} \qquad (13)$$

where

k_{he} : equivalent horizontal seismic coefficient for check of bearing capacity for lateral force

k_{hc} : seismic horizontal coefficient for check of bearing capacity for lateral force

μ : allowable ductility factor

c_Z : modification factor for zone (refer to **Fig. 2**)

c_I : modification factor for importance (refer to **Table 6**)

c_R : modification factor for structural response (refer to **Table 9**)

K_{hcD} : standard horizontal seismic coefficient for check of bearing capacity for lateral force

The standard horizontal seismic coefficient k_{hcD} was determined so that it can represent a realistic ground motion developed during a significant earthquake with magnitude as large as 8.

3)Bearing capacity for lateral force and allowable ductility factor

Bearing capacity for lateral force P_a and the allowable ductility factor μ shall be determined based on the failure mode as :

a)Flexural failure

$$P_a = P_y + \frac{P_u - P_y}{\alpha} \qquad (14)$$

$$\mu = 1 + \frac{\delta_u - \delta_y}{\alpha \delta_y} \qquad (15)$$

where

P_u, δ_u : bearing capacity (tf) and ultimate displacement (m) for flexural failure

P_y, δ_y : yielding force (tf) an yielding

displament (m) for flexural failure

α : safety factor (=1.5)

b)Shear failure

$$P_a = P_s \quad (16)$$

$$\mu = 1 \quad (17)$$

where

P_s : bearing capacity (tf) for shear failure

8. DYNAMIC RESPONSE ANALYSIS

As number of bridges with complex dynamic response characteristic increases, unified stipulations for dynamic response analysis become required. Although only general consideration for selecting the input ground motion was described in the previous specifications, a simplified but practical input ground motion as well as an analytical model and evaluation of the results of the dynamic response analysis was introduced in the new specifications.

In principle, dynamic response analysis shall be made by means of response spectral analysis with use of an analytical model which simulates dynamic characteristics of the bridge. Acceleration response spectrum for the response spectrum analysis shall be determined as

$$S = c_Z \cdot c_I \cdot c_D \cdot S_0 \quad (18)$$

where

S : response spectrum for response spectrum analysis (gal)

c_Z : modification factor for zone (refer to **Fig. 2**)

c_I : modification factor for importance (refer to **Table 6**)

c_D : modification factor for damping, and shall be determined based on modal damping ratio h_i as

$$c_D = \frac{1.5}{40h_i + 1} + 0.5 \quad (19)$$

S_0 : standard response spectrum for response analysis method (gal) (refer to **Table 10**)

When the time history analysis is required, strong motion records which have the similar characteristics with S by Eq.(18) shall be used with the consideration on site condition and structural response of the bridge. Three ground acceleration records which were modified so that their response characteristics match with S_0 in Eq.(18) are provided in Appendix III. They can be used as the standard ground motions for the time history analysis.

Because the results of the dynamic response analysis highly depend on the analytical model and the properties assumed in the analysis, indiscriminate evaluation of the results is quite difficult. Therefore it is required to use the overall result of the analysis considering accuracy of the properties and the analytical model used in the analysis. It is stipulated in the new specifications that the results obtained by the dynamic response analysis shall be used for the check of seismic safety of the bridge based on the allowable stress and displacement which are referred in the seismic coefficient method.

9. CONCLUDING REMARKS

The proceeding pages presented the outline of the main points of the new Seismic Design Specifications for Highway Bridges issued in February 1990. In the new specifications, seismic coefficient method by combining the previous seismic coefficient method and the modified seismic coefficient method is adopted, and based on the allowable design approach this method is regarded as the basic seismic design method. Besides the design by means of the seismic coefficient method, for those bridges which require the check of ductility, the check of bearing capacity of reinforced concrete piers for lateral force is made. Dynamic response analysis can be made for the bridges which require precise analysis considering structural response.

REFERENCES

1) Kawakami,K., Kuribayashi,E., Iwasaki,T. and Iida,Y.: On Specifications for Earthquake Resistant Design of Highway Bridges, 7th Joint Meeting, Panel on Wind and Seismic Effects, UJNR, Tokyo, Japan, 1975

2) Kuribayashi,E., Iwasaki,T., and Ueda,O.: New Specifications for Earthquake Resistant Design of Highway Bridges in Japan, 12th Joint Meeting, Panel on Wind and Seismic Effects, UJNR, Washington, D.C., U.S.A., 1980

Table 1 History of Design Loads for Highway Bridges in Japan

Year	Name of Regulations	Design Live Loads				Impact Loads	Seismic Loads k: Horizontal Seissmic Coefficient	Major Earthquake
		Class	Truck Roller Loads Streetcar	Uniform Loads	Line Loads			
1) 1886	Order No. 13 Ministry of Home Affairs (MHA)		.	U-454 kg/m	–	not considered	not considered	
2)	Order MHA		R-13.6 t S-12.7	U-400 600 kg/m (carnage way) U-270 400 kg/m (footway)		not considered	not considered	
3) 1919	Road Laws MHA		R-13.6 t T-11.2 t S-30 t	Same as 2)	–	not considered	not considered	
4) 1926	Specifications for Design of Roads, Road Laws, MHA	1st 2nd 3rd	T-12 t T-8 T T-6 t	U-600 kg/m U-500 kg/m U-500 kg/m	–	considered	Seismic Coefficient Method K=0.15–0.4 depending on location and ground condition (k≧0.3 advised in Toyo, Yokohama)	
5) 1939	Specifications for Design of Steel Road Bridges, MHA	1st 2nd	T-13 t T-9 T	U-500 kg/m U-400 kg/m		considered	Seismic Coefficient Method k_s=0.2, k_s=0.1	1946. Nankai (M=8.1) 1948. Fukui (M=7.3) 1952. Tokachi-oki (M=8.2) 1964 Niigata (M=7.5)
6) 1956 (and 1964)	Revision of Specifications for Design of Steel Road Bridges, JRA	1st 2nd	T-20 t T-14 t	– –	L-20 (5t m) L-14 (3.5 t/m)	considered	Seismic Coefficient Method k=0.1~0.35 depending on location and ground conditions	
7) 1964 to 1971	Specifications for Design of Substructure of Road Bridges, JRA	Same as 6)					Same k as (6) Detailed calculation methods	
8) 1971	Specifications for Earthquake-Resistant Design of Highway Bridges, JRA	Same as 6)					Seismic Coef. method k=0.1~0.24 (Rigid) Modified SCM. K=0.05~0.3 (Flexible)	
9) 1980 Modified SCM	Part V Seismic Design Specifications for Highway Bridges IRA	Same as 6)					Seismic Coef. Method k=0.1~0.24 (Rigid) k=0.05~0.3 (Flexible) Earthquake Response Analysis (Very Flexible Bridges)	1978 Miyagiken-oki (M=7.4)
10) 1990	Same as 9)	Same as 6)					Seismic Coefficient Method k=0.1~0.3 Bearing Capacity of RC Piers for Lateral Load Dynamic Response	1982 Urakawa-oki (M=7.1) 1982 Nihon-kai-chubu (M=7.7)

Table 2 Seismic Damage in Recent Earthquakes

Year	Major Earthquake	Change of Major Seismic Damage	Seismic Design Method	Seismic Inspection and Retrofitting
1920	1923 Kanto Earthquake (M7.9)	Failure of Superstructure due to Tilting/Movement of Foundation		
1930			1926 Initiation of Seismic Design (Stipulations for Road Construction)	
1940	1946 Nankai Earthquake (M8.1)	Failure of Concrete around Fixed Bearing	1939 Introduction of Standard Seismic Coefficient (Specifications for Steel Bridge)	
1950	1948 Fukui Earthquake (M7.3) 1952 Tokachi-oki Earthquake (M8.1)	Damage due to Liquefaction		
1960	1964 Niigata Earthquake (M7.5)	Failure of RC Piers, and Bearing	1956 Seismic Coefficient depending on Zone and Ground Condition (Specifications for Steel Bridge)	
1970	1978 Miyagi-ken-oki Earthquake (M7.4)		1971 • Seismic Coefficient depending on Zone, Ground Conditions, Importance and Structural Response • Introduction of Evaluation Method for Liquefaction (Specifications for Seismic Design)	1971 Seismic Inspection 1976 Seismic Inspection
1980	1982 Urakawa-oki Earthquake (M7.1) 1983 Nihon-kai-chubu Earthquake (M7.7)		1980 • Part V Seismic Design, Specifications for Design of Highway Bridge • Introduction of New Evaluation Method for Liquefactions	1979 Seismic Inspection 1986 Seismic Inspection
1990			1990 Part V Seismic Design, Specificatins for Design of Road Bridge	

Table 3 Table of Contents of 1990 Seismic Design Specifications of Highway Bridges

Contents		Same as 1980 Specs.	Modified		Newly Introduced
			Slightly	Completely	
Chapter 1	General 1.1 Scope	○			
	1.2 Definition of Term		○		
Chapter 2	Basic Principle for Seismic Design		○		
Chapter 3	Design Load and Design Condition in Seismic Design 3.1 Design Load and Load Combination in Seismic Design		○		
	3.2 Effect of Earthquake	○			
	3.3 Inertia Force 3.3.1 General			○	
	3.3.2 Calculation of Natural Period			○	○
	3.3.3 Calculation of Inertia Force			○	○
	3.4 Earth Pressure during Earthquake	○			
	3.5 Hydrodynamic Pressure during Earthquake		○		
	3.6 Classification of Ground Condition in Seismic Design		○		
	3.7 Soil Layers Whose Bearing Capacities are Reduced in Seismic Design 3.7.1 General				○
	3.7.2 Sandy Layer Vulnerable for Liquefaction		○		
	3.7.3 Very Soft Clayey and Silty Layer	○			
	3.7.4 Treatment of Soil Layers Whose Bearing Capacities are Reduced in Seismic Design	○			
	3.8 Ground Surface Assumed in Seismic Design	○			
Chapter 4	Design Seismic Coefficient 4.1 General	○			
	4.2 Design Horizontal Seismic Coefficient			○	
	4.3 Factors for Modifying Standard Design Horizontal Seismic Coefficient			○	
Chapter 5	Check of Bearing Capacity of Reinforced Concrete Pier for Lateral Load 5.1 General				○
	5.2 Check of Safety				○
	5.3 Horizontal Seismic Coefficient for Check of Bearing Capacity for Lateral Load 5.3.1 Equivalent Horizontal Seismic Coefficient for Check of Bearing Capacity for Lateral Load				○

Contents		Same as 1980 Specs	Modified		Newly Introduced
			Slightly	Completely	
Chapter 5 (cont't)	5.3.2 Design Horizontal Seismic Coefficient for Check of Bearing Capacity for Lateral Load				○
	5.4 Bearing Capacity for Lateral Load 5.4.1 Bearing Capacity for Lateral Load Allowable Ductility and Equivalent Natural Period				○
	5.4.2 Displacement and Lateral Load at Yielding and Ultimate Stage				○
	5.4.3 Bearing Capacity for Shear Failure				○
Chapter 6	Dynamic Response Analysis 6.1 General				○
	6.2 Analytical Method and Analytical Model 6.2.1 Analytical Method				○
	6.2.2 Analytical Model				○
	6.3 Input Motion for Dynamic Response Analysis 6.3.1 Acceleration Response Spectral Value for Response Spectral Analysis				○
	6.3.2 Grond Motion for Time History Analysis				○
	6.4 Check of Safety				○
Chapter 7	General Provisions for Structural Details in Seismic Design 7.1 General		○		
	7.2 Devices for Preventing Superstructures from Falling 7.2.1 General		○		
	7.2.2 Stoppers at Movable Bearing		○		
	7.2.3 Length between End of Girder and Edge of Substructure		○		
	7.2.4 Devices for Preventing Superstructure from Falling		○		
	7.3 Structural Details at Bearing		○		
Chapter 8	Devices Expecting to Reduce Seismic Effects			(○)	
Appendices	I. References on Liquefaction		○		
	II. Examples of Classification of Ground Condition		○		
	III. Reference on Design Ground Motion			○	
	IV. Example of Calculation of Natural Period and Inertia Force			○	
	V. Reference on Bearing Capacity of Reinforced Concrete Pier for Lateral Load and Example of Calculation				○
	VI. Practices of Structural Details		○		

Table 4 Classification of Ground Conditions

1980 Specifications			1990 Specifications	
1	$T_G < 0.2$	(Rock)	I	$T_G < 0.2$
2	$0.2 \leqq T_G < 0.4$	(Diluvium)	II	$0.2 \leqq T_G < 0.6$
3	$0.4 \leqq T_G < 0.6$	(Alluvium)		
4	$0.6 \leqq T_G$	(Soft Alluvium)	III	$0.6 \leqq T_G$

Table 5 Ground Condition Factor c_G

Ground Group	I	II	III
c_G	0.8	1.0	1.2

Table 6 Importance Factor c_I

Group	c_I	Definition
1st class	1.0	Bridges on expressway (limited access highways), general national road and principal prefectural road. Important bridges on general prefectural road and municipal road.
2nd class	0.8	Other than the above

Table 7 Structual Response Factor c_T

Ground Group	Structural Response Coefficient c_T		
Group I	$T < 0.1$ $c_T = 2.69T^{1/3} \geqq 1.00$	$0.1 \leqq T \leqq 1.1$ $c_T = 1.25$	$1.1 < T$ $c_T = 1.33T^{-2/3}$
Group II	$T < 0.2$ $c_T = 2.15T^{1/3} \geqq 1.00$	$0.2 \leqq T \leqq 1.3$ $c_T = 1.25$	$1.3 < T$ $c_T = 1.49T^{-2/3}$
Group III	$T < 0.34$ $c_T = 1.80T^{1/3} \geqq 1.00$	$0.34 \leqq T \leqq 1.5$ $c_T = 1.25$	$1.5 < T$ $c_T = 1.64T^{-2/3}$

Table 8 Seismic Design Structual Unit

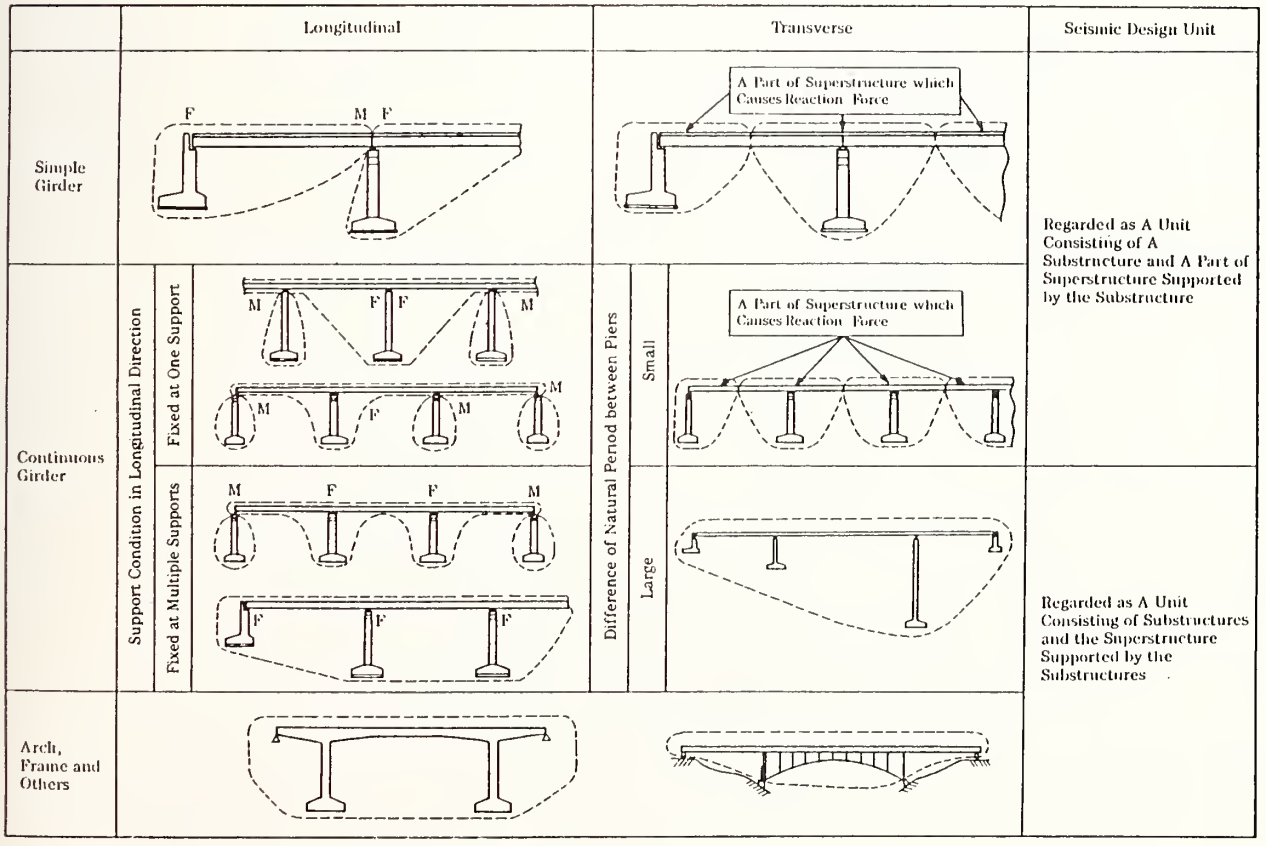

Table 9 Structual Response Factor c_R

Ground Group	Structural Response Coefficient c_R		
Group I	$T_{EQ} \leqq 1.4$ $c_R = 0.7$		$1.4 < T_{EQ}$ $c_R = 0.876T_{EQ}^{-2/3}$
Group II	$T_{EQ} < 0.18$ $c_R = 1.51\ T_{EQ}^{1/3} \geqq 0.7$	$0.18 \leqq T_{EQ} \leqq 1.6$ $c_R = 0.85$	$1.6 < T_{EQ}$ $c_R = 1.16T_{EQ}^{-2/3}$
Group III	$T_{EQ} < 0.29$ $c_R = 1.51T_{EQ}^{1/3} \geqq 0.7$	$0.29 \leqq T_{EQ} \leqq 2.0$ $c_R = 1.0$	$2.0 < T_{EQ}$ $c_R = 1.59T_{EQ}^{-2/3}$

Table 10 Structual Response Spectral Value S_O

Ground Condition	S_O (gal)		
Group 1	$T_i < 0.1$ $S_O = 431T_i^{1/3} \geqq 160$	$0.1 \leqq T_i \leqq 1.1$ $S_O = 200$	$1.1 < T_i$ $S_O = 220/T$
Group II	$T_i < 0.2$ $S_O = 427T_i^{1/3} \geqq 200$	$0.2 \leqq T_i \leqq 1.3$ $S_O = 250$	$1.3 < T_i$ $S_O = 325/T_i$
Group III	$T_i < 0.34$ $S_O = 430T_i^{1/3} \geqq 240$	$0.34 \leqq T_i \leqq 1.5$ $S_O = 300$	$1.5 < T_i$ $S_O = 450/T_i$

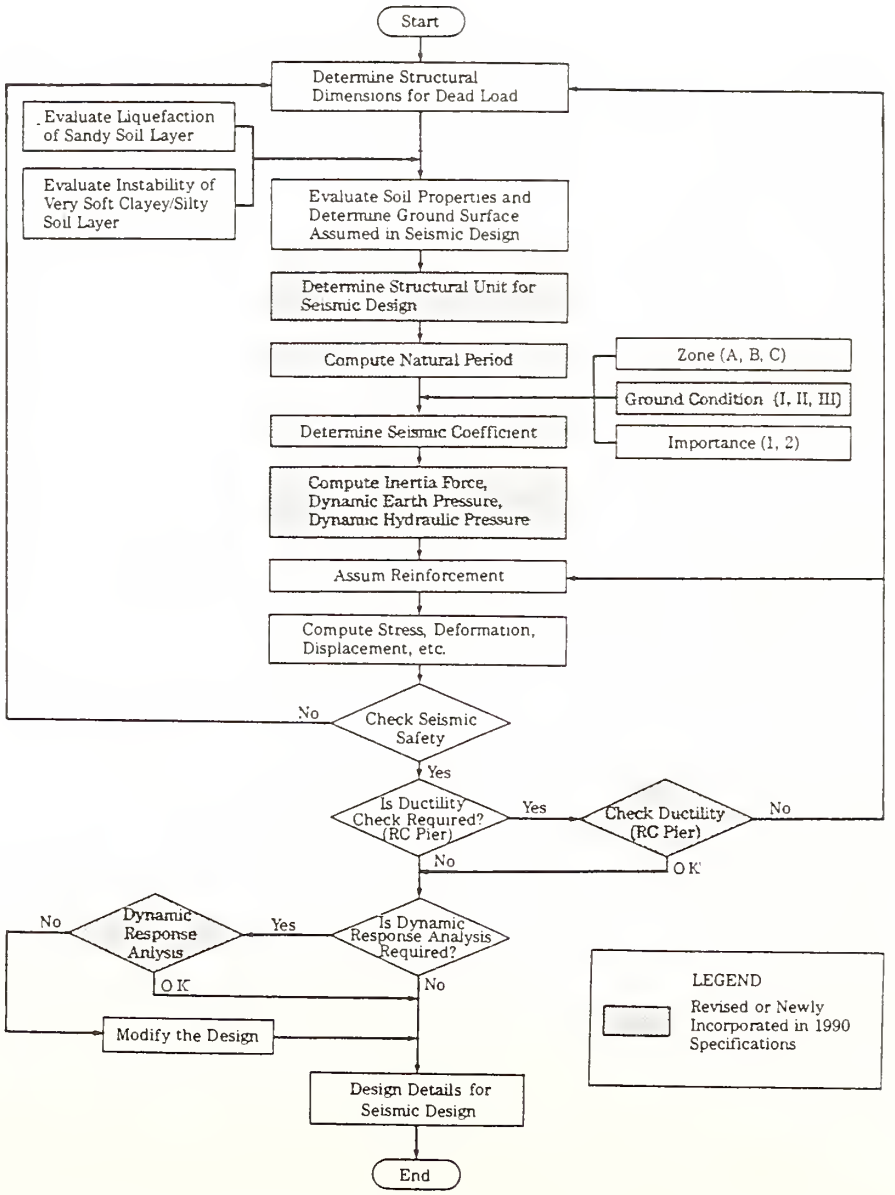

Fig.1 Flow of Seismic Design of Highway Bridge

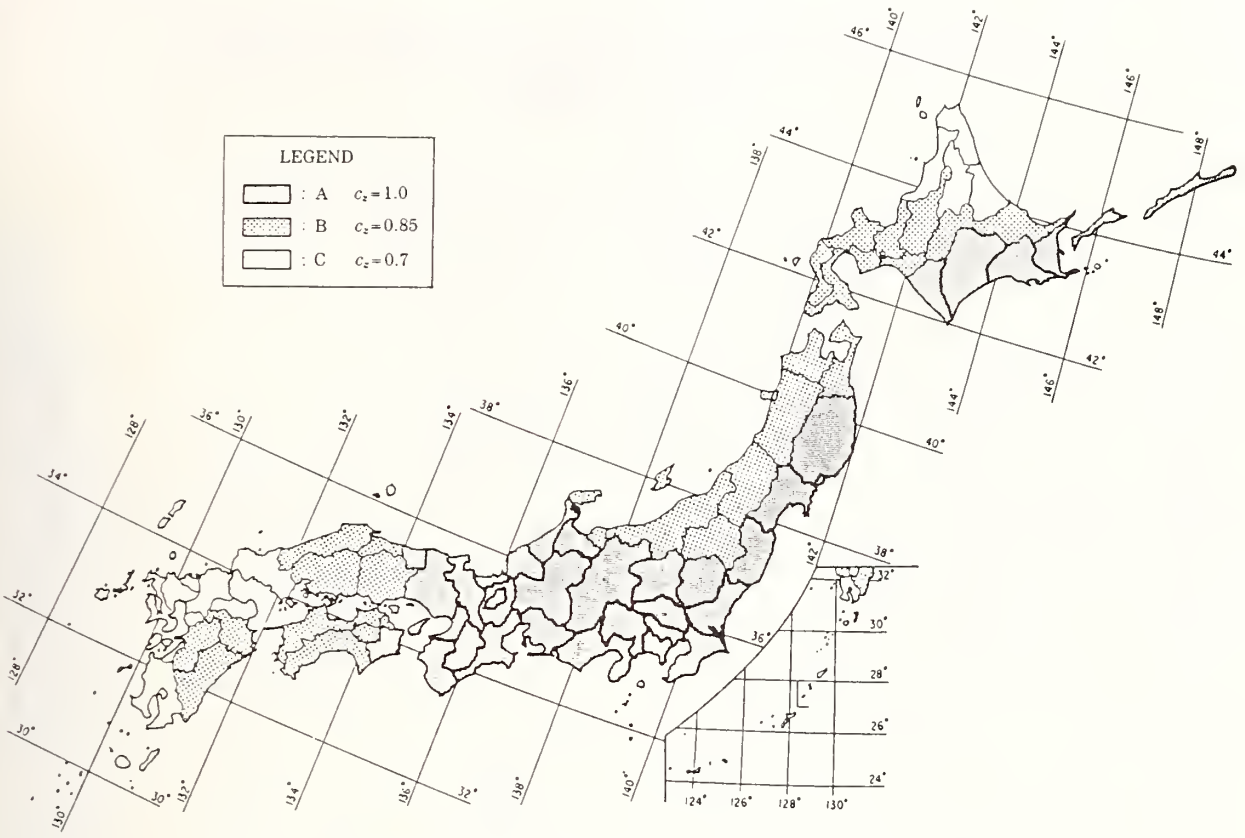

Fig.2 Seismic Zoning Map and Modification Coefficient c_Z

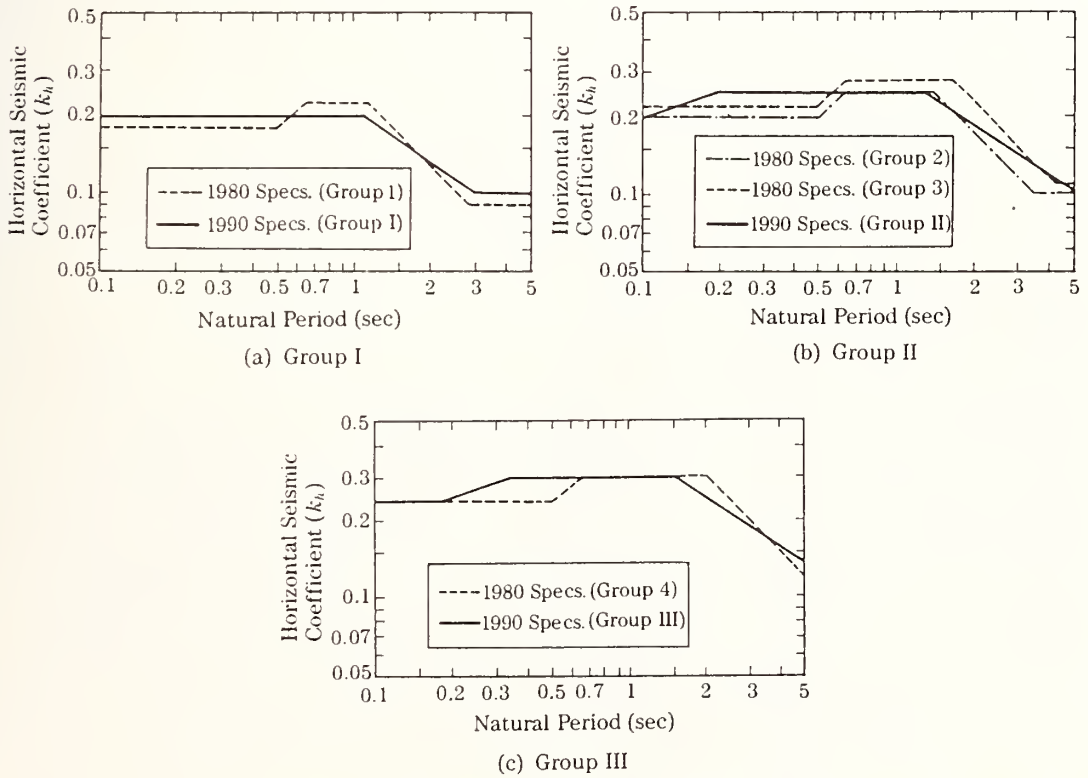

(a) Group I

(b) Group II

(c) Group III

Fig.3 Comparison of Seismic Coefficient between 1980 and 1990 Specifications

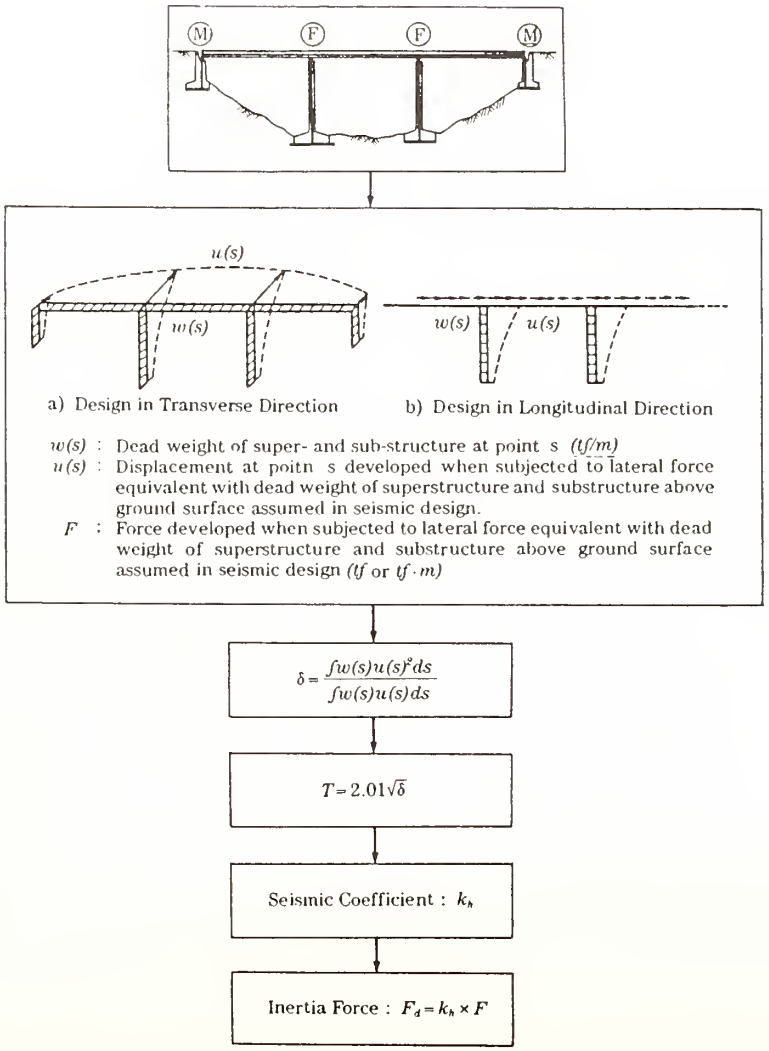

Fig.4 Determination of Inertia Force

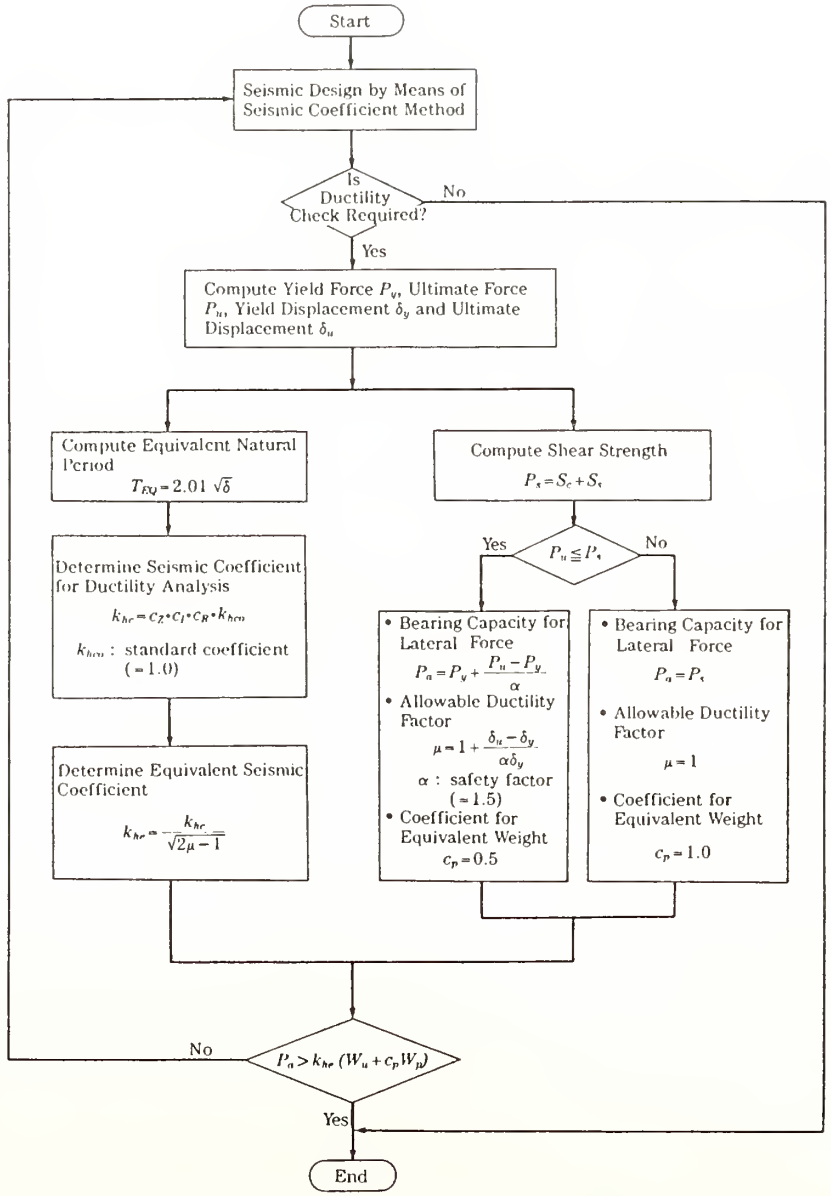

Fig.5 Check of Bearing Capacity of Reinforced Concrete Pier for Lateral Force

Scatter on Mechanical Properties of Structural Steels Recently Supplied in Japan

By

Hirofumi AOKI*1 Hiroyuki YAMANOUCHI*2 Ben KATO*3

[Summary]

Statistical investigations are carried out on mechanical properties of structural steels and the causes of the scatter are presumed. Higher yield ratios of steel give unfavourable influences on failure modes at the ultimate limit states of steel structures, as well as the scatter of yield strengths. The present paper emphasizes that upper limits of not only yield strengths but also yield ratios should be specified in the appropriate industrial standards in order to reduce the deviations.

Furthermore,it is necessary that accurate measurement and standardized expression on stress-strain curves of steels. Such statistical data are expected to be accumulated internationally.

[Key words]

Structural steel,yield strength,yield ratio, Scatter of mechanical properties, ultimate limit states, stress-strain relations

1. Introduction

It is a worldwide prevalency that structural design criteria are transferring from allowable stress design to limit state design based on reliable engineering. Subsequently to Canada, Europe and the U.S. [1], `Standard for Limit State Design of Steel Structures (draft)´ [2] was published in this February by Architectural Institute of Japan. In such a limit state design, load and resistance are treated as nondeterministic. Therefore, statistical data with respect to various factors are important to estimate the safty of structures.

As uncertainty of the resistance, three factors are generally considered, that is, material, fabrication and professional[3]. The present paper concentrates a focus on randomness at the main stuctural material of steel structures. First of all, statistical features on mechanical properties of structural steels recently produced in Japan are surveyed. Secondly, it is recomfirmed that plastic deformation capacity of structural elements which determines the ultimate limit state of steel structures is strongly dependent on yield ratios of steels. Finally, standing a view of point from structural engineers, some reversions for the industrial standards of materials are proposed.

2. Statistics with respect to mechanical properties of steels recently supplied in Japan

The statistics on mechanical properties of steels in the United States have been investigated by Garambos et al[4]. The statistical features on yield strength (This is a term for yield point and off-set yield stress.) and yield ratio which is defined as yield strength by tensile strength were recently clarified in Japan by analyzing the data by collecting mill

*1 Professor, Yokohama National University
*2 Head, Building Research Institute
*3 Professor, Toyo University

sheets which are issued as inspection certificates from mill makers with blust furnaces[5～7].

Fig.-1 indicates the distributions of yield strength, tensile strength and yield ratio of plates SS41 with less than 40mm in thickness (24 kgf/mm^2 is the minimum yield strength and 41～52 kgf/mm^2 is the range of the tensile strength) which are most used as general structural steels. Referring to this figure, the mean value of the yield strength is around 31 kgf/mm^2, which is about 1.15 times of the specified minimum value. The coefficient of variation is as much as 3.5%.

Fig.-2 also shows the distributions of SM50 (33 kgf/mm^2 is the minimum yield strength and 50～62 kgf/mm^2 is the range of the tensile strength) which is the most popular high tensile strength steel adopted for steel building structures in Japan.

Fig.-3 demonstrates those of steel tubes with a circular or rectangular hollow section. The yield strength of such a tube rises higher caused by as cold-formed. As the result, the yield ratio also becomes higher.

Furthermore, by analysis for these data in detail, it becomes clear that yield strengths are correlated with the thickness of plates, as shown in Fig.-4. And, Fig.-5 shows the difference of the distributions due to makers. Therfore, the distributions shown in Figs.-1～3 can be variable if the composion of the thickness of the plates or production ratio of the makers varies.

Above results can be summarized as follows.

1) Yield strengths of the plates with thinner thickness is higher than that with thicker one.
2) The distribution of tensile strengths is normal, on the other hand, that of yield strengths is approximately logarithmic normal.
3) Scatter of yield strengths is large in contrast with that of tensile strengths.
4) There exists a weak but positive correlation between yield strengths and tensile strengths. Yield ratios are strongly correlated with yield strengths, however, there is no relation with tensile strengths.

The finishing temperature at the final rolling for thinner plates is inclined to be lower. This makes the yield strength dependent on the thickness of plates. Above 2) and 3) result from that the upper limit of yield strengths are not specified in the industrial standard of materials.

3. Yield ratios of steel and Plastic Deformation Capacity of Steel Elemewnts

It is indispensable to safty of structures that the absolute values of yield strength and tensile strength are secured as sufficient values. On the other hand, scatter of the full plastic moments of members is caused by scatter of yield strengths. Therefore, it is pointed out that if the scatter of yield strengths is larger, the real collapse mechanism of the frame becomes different from one which is predicted at the design analysis[6].
However, the yield ratio of structural steels is a more essential factor for ultimate limit states of steel structures. That is, it strongly influences on the plastic deformation capacity of structural elements[7]. If the yield ratio is neally equal to 1.0, a premature failure may occur at the statically indeterminate structure. Because redistribution of the moments is impossible owing to extremely small rotation capacity at the plastic hinges.

Fig.-6 demonstrates the ultimate limit states of cantilevers by comparing two different materials which yield ratios are 0.5 and 0.8, where buckling phenomena are

not considered. By observing this figure, it can be easily found out that areas of the plastic zones are different in spite of the fact that the maximum moments at the ends of the members are same. As a result, the plastic rotation capacity of the member with higher yield ratio becomes smaller. A statically indeterminate structure composed by such members with higher yield ratio may fracture before the collapse mechanism completes, as shown in **Fig-7**.

Observing the statistical features of yield ratios at **Figs.-1～3** , the range of yield ratios for SS41 is 0.55～0.85 and for SM50 is 0.60～0.90. That for steel tubes is especially large, because of effects of cold-forming.

As clarified at the previous section, yield ratios are strongly correlated with yield strengths. Therefore, controlling the scatter of yield strengths smaller is most efficient for making the scatter of yield ratios smaller. In other words, upper limits of yield strengths and yield ratios should be specified in the industrial standards of materials. **Table-1** lists representative specifications for mechanical properties of structural steels. Unfortunately in this table we cannot find any standard which specifys an upper limit of yield strengths or that of yield ratios.

Under international negotiations, these specifications are expected to be realized.

4. Standardized stress-strain relations

A stress-strain relation of mild steel under uniaxial tension loading has a clear upper yield point as shown in **Fig.-8**. The yield ratio can be definitely defined by the ratio of the yield point to the tensile strength. However, yield ratio of over 60 kgf/mm^2 high tensile strength steel is ambiguous, because the srtress-strain curves of this kind steel is so-called round house type. That is, off-set strength is often used as the yield strength. It has been pointed out that plastic deformation capacity cannot be predicted properly by such ambiguous yield ratios based on off set strengths, otherwise that sufficient complimentary energy is required for such steels[9]. By other expression, the shape of the stress-strain curve is also very important factor as well as yield strength and tensile strength. Therefore, it is insisted that stress-strain curves under uniaxial tension loading should be measured accurately up to the maximum load. With these points as background, a tension testing, specified standard shapes of specimens and strain rates, has been proposed by RILEM TC/83-CUS[11]. According to this method, stress-strain relations of SS41 and SM50 are tried to be standardized. **Fig.-9** and **Fig.-10** are the results and **Table-2** lists the characteristic values which determine the standard curves[12].

5.Conclusive remarks

Statistical features on mechanical properties of steels are investigated, especially with respect to not only yield strengths but also yield ratios which are most important factors for ultimate limit states of steel structures. The results are summarized as follows.

1. Concerning with yield strengths,

a)The scatter of yield strengths is due to the differences of production instruments, technical level and quality control at mill makers.

b)Yield strengths are dependent on the thickness of plates.

c) Yield strengths of the marerial as cold-formed indicate very high compared with the values specified in the design codes.

2. Concerning with yield ratios,

a)The scatter of yield ratios are larger than that of yield strengths.
b)However, it is mainly caused by the scatter of yield strengths.
c)Cold-formed members have very high yield ratios.
d)The shape of the stress-strain curves or complimentary energy rather than yield ratio is an important factor for steels without a clear upper yield point.

Considering above conclusions, following points are proposed.

1.The upper limit of yield strengths should be specified in the industrial standards of structural steels.
2.The upper limit of yield ratios also should be specified.
3.Full stress-strain curves measured accurately up to the maximum tension load should be accumulated.

[References]

[1] AISC :Load and Resistance Factor Design Specification for Structural Steel Buildings, Sep.,1986
[2] AIJ :Standard for Limit State Design of Steel Structures (Draft), Feb.,1990
[3] Ravindra,M.K.and Galambos,T.V.:Load and Resistance Factor Design for Steel,ASCE, Vol.104,No.ST9,Sep.,1978
[4] Galambos,T.V. and Ravindra,M.K.:Properties of Steel for Use in LRFD,ASCE,Vol. 104,ST9,Sep.,1978
[5] Aoki,H.and Murata,K. :Statistical Study on Yield Point, Tensile Strength and Yield Ratio of Structural Steel, Trans. AIJ No.335,1984
[6] Aoki,H.and Masuda,M.:Statistical Investigation on Mechanical Properties of Structural Steel Based on Coupon Tests, Trans.AIJ No.358,1988
[7] Yamanouchi,H., Kato,B. and Aoki,H.:Statistical Features of Mechanical Properties of Current Japanese Steels, Material and Structures,24,1990
[8] Kuwamura,H. and Sasaki,M. :Effect of Randomness in Members' Yield Strengths on the Failure Mechanism of Multi-Story Rigid Frames,J.of Structural Engr. Vol. 34B,1988
[9] Kato, B. and Okumura, T. :Structural Behaviour Including Hybrid Construction, 10th Congress of IABSE,Tokyo,Sep.,1976
[10]Kuwamura, H. and Kato, B. :Inelastic Behaviour of High Strength Steel Members with Low Yield Ratio, Pacific Structural Steel Conference, May,1989
[11]RILEM TC/83-CUS :Tension Testing of Metallic Structural Materials for Determining Stress-strain Relations under Monotonic and Uniaxial Tensile Loading,Material and Structures,23,1990
[12]Kato, B., Aoki, H. and Yamanouchi,H. :Standardized Mathematical Expression for Stress-strain relations of Structural Steel under monotonic and Uniaxial Tension Loading, Materials and Structures,23,1990

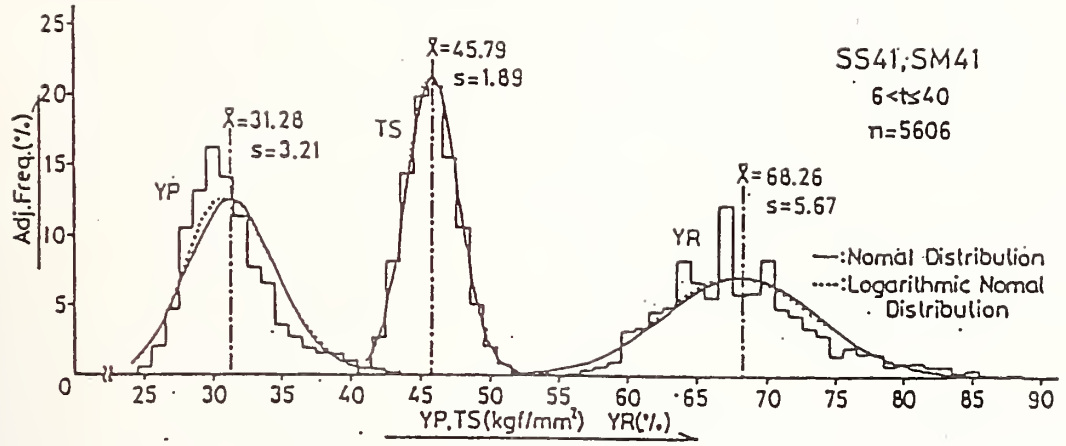

Fig.-1 Histogram of Mechanical Properties for SS41 and SM41 (6 mm$<t\leq$40 mm)

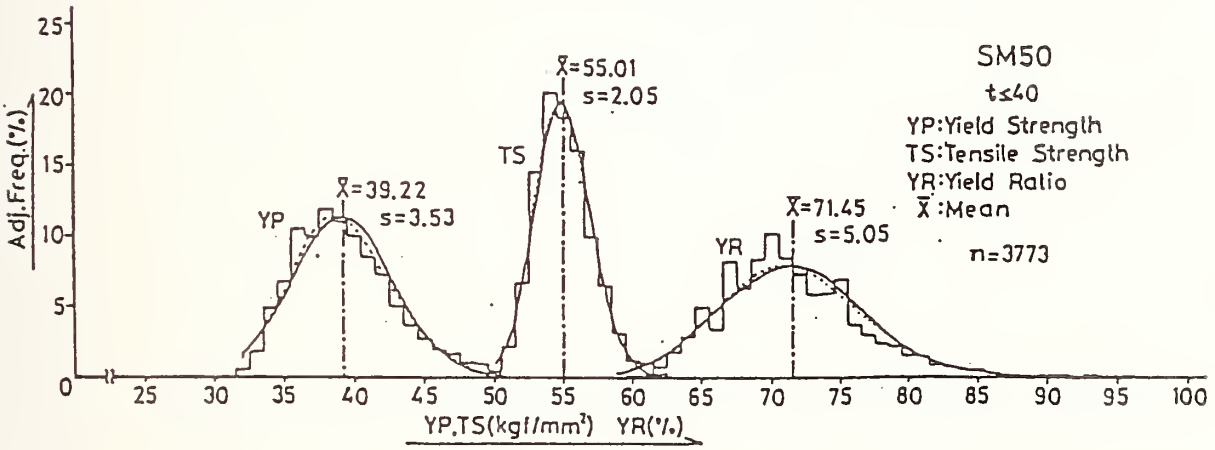

Fig.-2 Histogram of Mechanical Properties for SM50

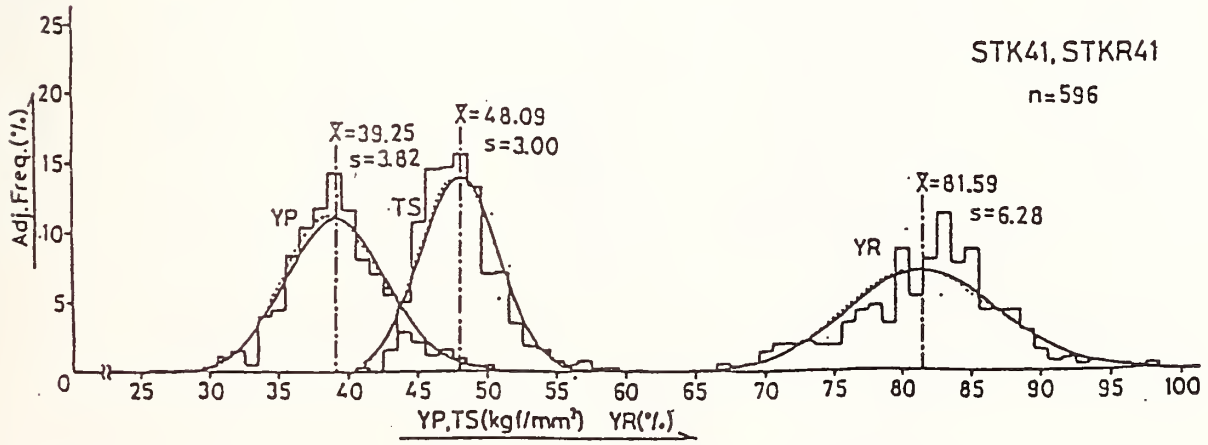

Fig.-3 Histogram of Mechanical Properties for STK41 and STKR41

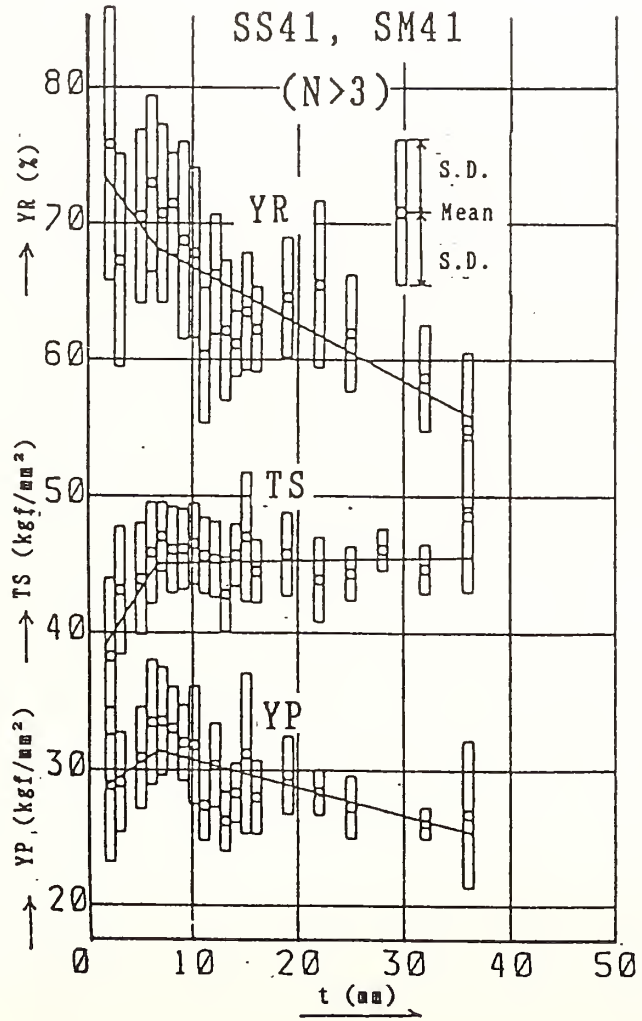

Fig.-4 Relations between Thickness and YP,TS,YR

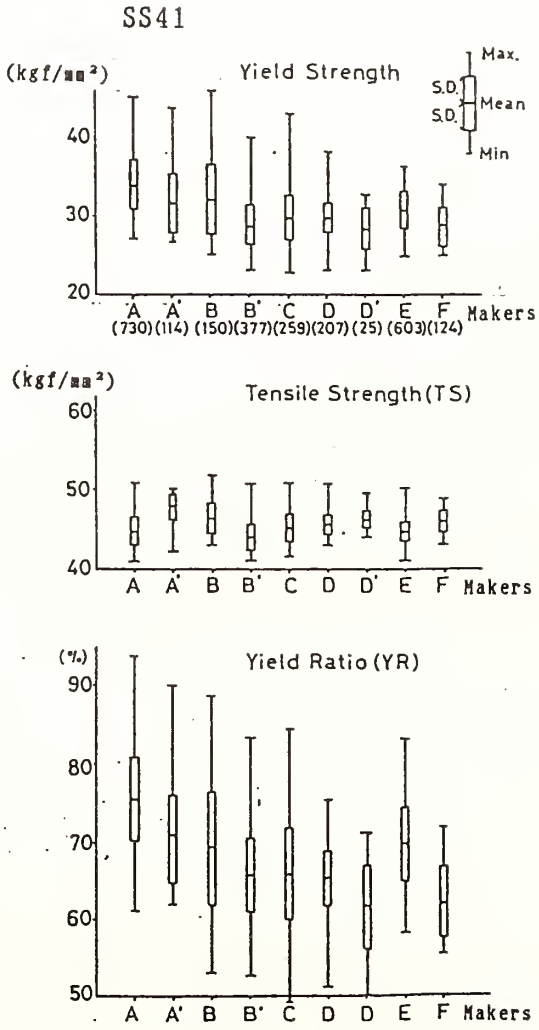

Fig.-5 Distributions of Each Producer

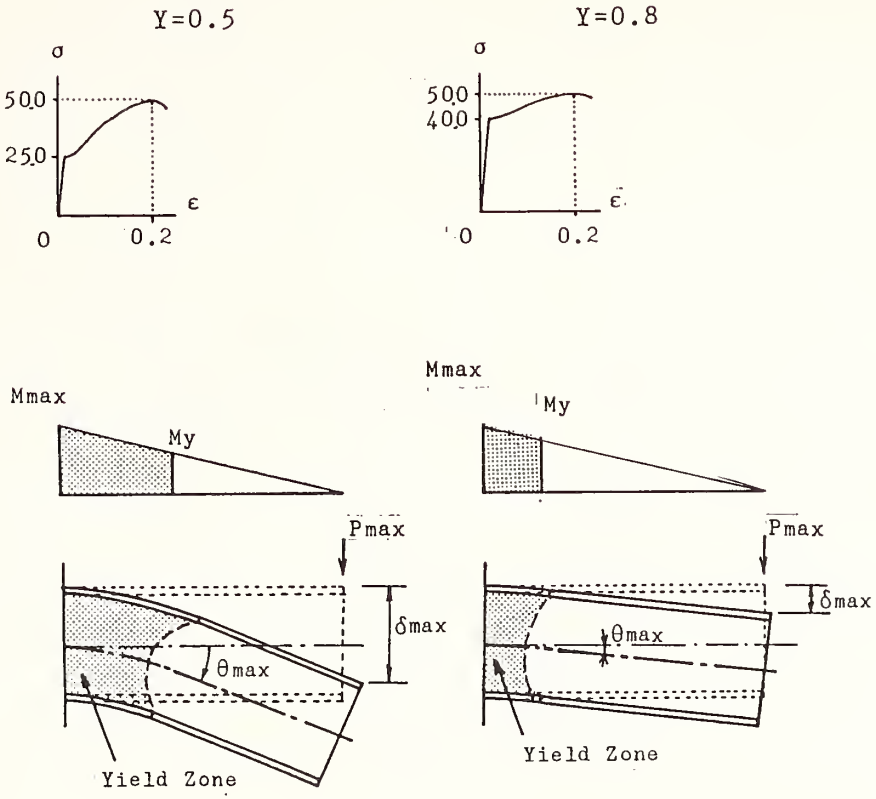

Fig.-6 Plastic Deformation Capacity of Cantilevers with H-shape Section

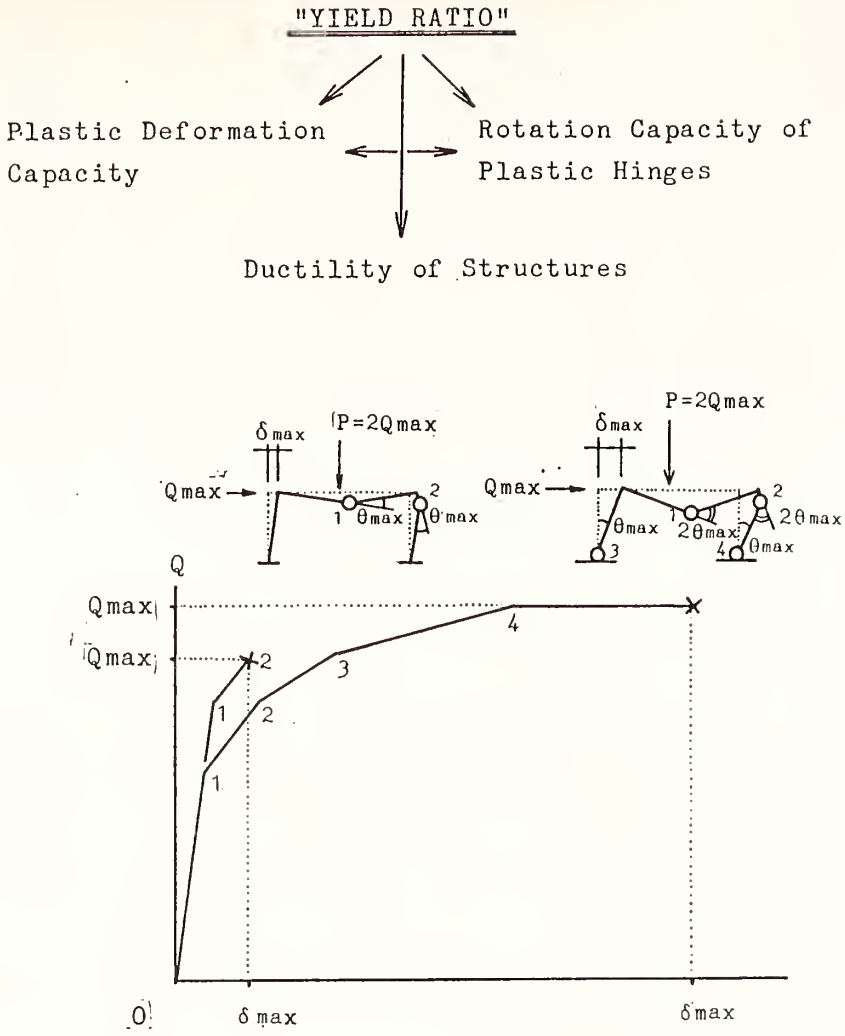

Fig.-7 Collapse Mechanism of Rigid Frames

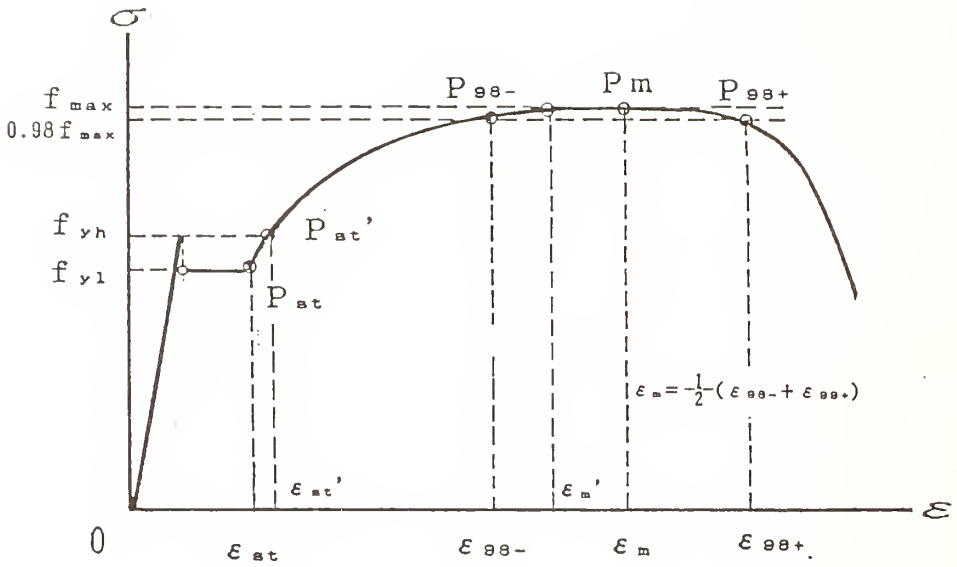

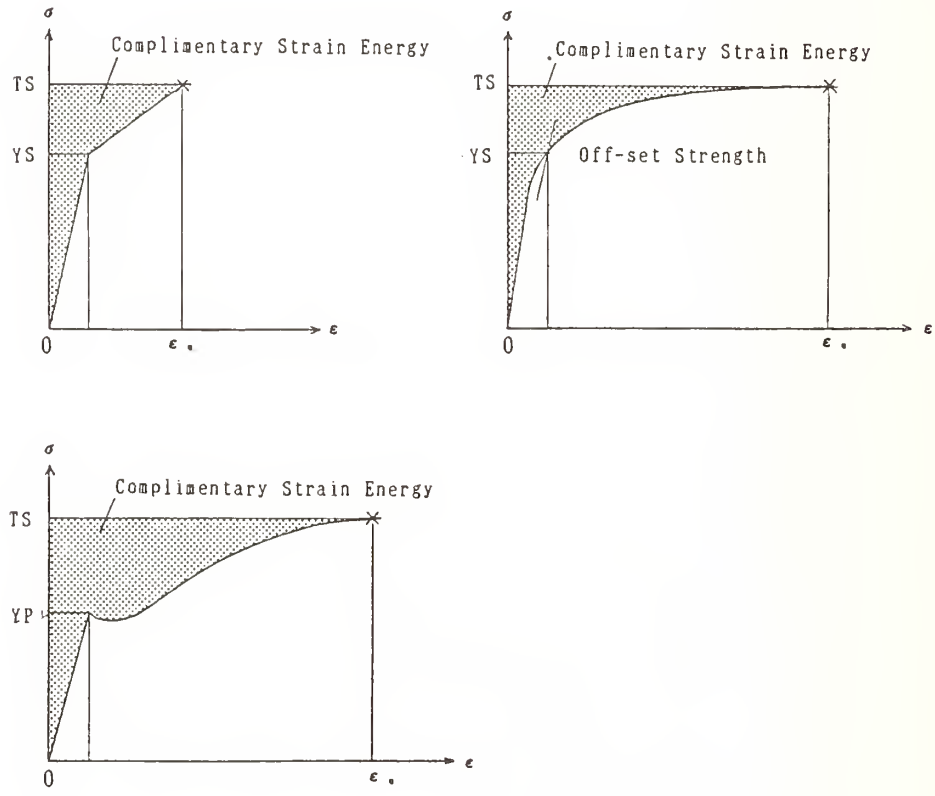

Fig.-8 Shapes of Stress-Strain Curves

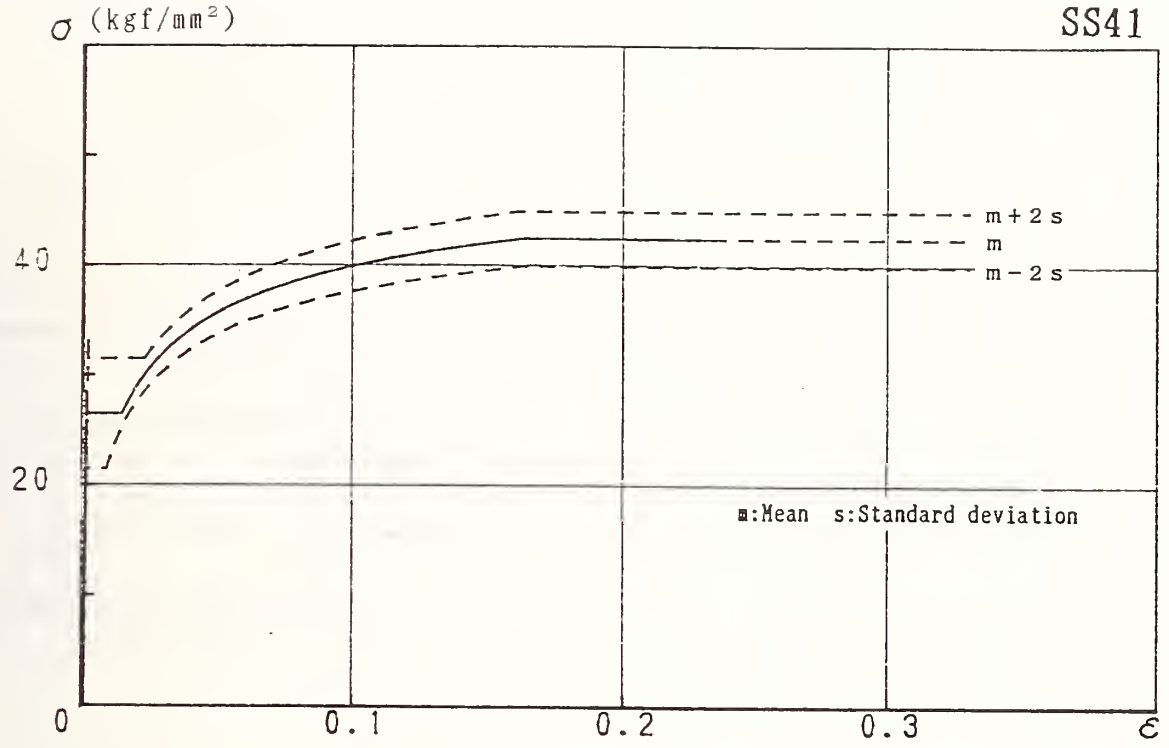

Fig.-9 Standardized Stress-strain Relations for SS41

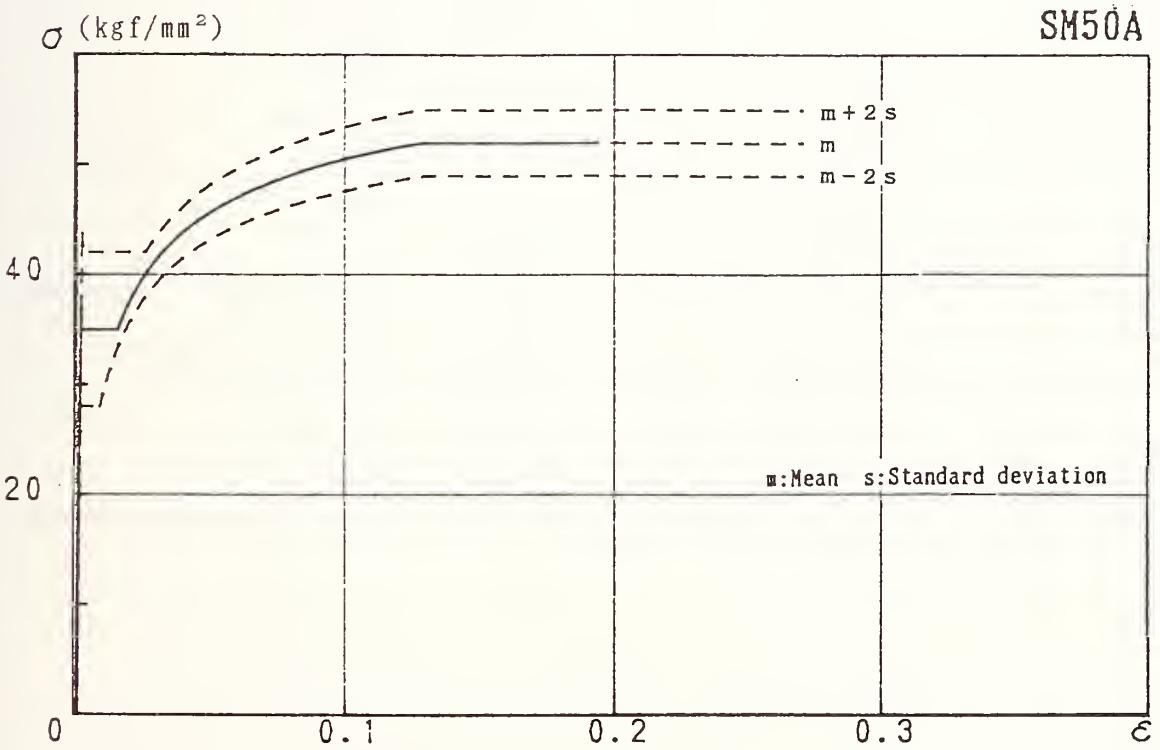

Fig.-10 Standardized Stress-strain Relations for SM50

Table-1 List of Standards

Country	Standards	Designation	Min. Yield Stress MN/m²	Tens. Strength MN/m²	Y*	Remarks
INTERNATIONAL	ISO	Fe 42	245	412 ~ 490	0.594	
		Fe 52	343	490 ~ 608	0.70	
ENGLAND	BS 4360	Grade 40	230	400 ~ 480	0.575	
		Grade 50	345	500 ~ 620	0.69	}Columbium and/or Vanadium
		Grade 55	430	550 ~ 700	0.782	
FRANCE	NFA 35-501	Grade E24	235	363 ~ 441	0.647	
		Grade E30	294	461 ~ 559	0.637	
		Grade E36	353	501 ~ 608	0.692	
		Grade A50	294	490 ~ 588	0.60	
		Grade A60	333	588 ~ 706	0.567	Impact tests Not Req'd. Limited Weldability
		Grade A70	363	686 ~ 833	0.530	
JAPAN	JIS G - 3101 ~ 3106	SS41, SM41	235	403 ~ 510	0.583	
		SM 50A, B	315	490 ~ 607	0.642	
		SM 50Y	353	490 ~ 607	0.72	Columbium and/or Vanadium
		SM 53	353	520 ~ 642	0.678	
		SM 58	452	570 ~ 718	0.794	
	WES	HW 70	686	785 ~ 932	0.874	
		HW 80	785	864 ~ 1030	0.908	
		HW 90	883	951 ~ 1130	0.93	
U.S.A.	ASTM	A 36	248	400 ~ 552	0.62	
		A242, A441, AA441	317	462	0.686	A242: weathering steel
		A572 Gr 45	310	414	0.748	
		50	345	448	0.77	Columbium and/or Vanadium
		55	379	483	0.785	
		60	414	517	0.8	
		A 588	345	483	0.713	Weathering Steel
		A 514	690	793 ~ 930	0.87	
WEST GERMANY	DIN 17100	st 37.283	240	370 ~ 450	0.647	
		st 46.223	290	440 ~ 540	0.658	
		st 52.3	360	520 ~ 620	0.691	

* Y = Yield Ratio; not specified in these standards.

Table-2 Material Constants for Standardized Curves

GRADE OF STEEL		kgf/mm²			ε_{98-}	ε_m	ε_{98+}	R	(γ)
		fyh	fyl	fmax					
SS41	m+2S	34	32	45	0.14	0.235	0.33	0.50	(1.28)
	m	29	27	43					(1.27)
	m-2S	24	22	41					(1.26)
SM50A	m+2S	43	41	56	0.11	0.19	0.27	0.57	(1.23)
	m	37	35	53					(1.22)
	m-2S	31	29	50					(1.21)

m: Mean value s: Standard deviation

$0 \leqq \varepsilon \leqq \varepsilon_y$ $\sigma = E \cdot \varepsilon$, $\varepsilon_y = f_{yh}/E$

$\varepsilon_y \leqq \varepsilon \leqq \varepsilon_{st}$ $\sigma = f_{yl} = f_{yh} - 2$

$\varepsilon_{st} \leqq \varepsilon \leqq \varepsilon_m'$ $\sigma =$ (1)

$\varepsilon_m' \leqq \varepsilon \leqq \varepsilon_m$ $\sigma = f_{max}$

$$\sigma = \frac{E}{\left\{1 + \left(\frac{\varepsilon}{\varepsilon_0}\right)^{R}\right\}^{1/R}} \varepsilon \qquad (1)$$

$$\varepsilon_0 = \gamma \cdot f_{max}/E \qquad (2)$$

Development of Effective Use of New Metallic Materials for Building Structures

by

Hiroyuki Yamanouchi[1], Hirofumi Aoki[2]
and
Tatsuo Murota[1]

ABSTRACT

The Japanese Ministry of Construction has initiated a five-year research and development program on "Effective Utilization of Advanced Materials for Construction" from the fiscal year of 1988. As part of the national program, new metallic materials for building structures are also adopted. This paper describes the outline of the metal phase of the program and issues to be solved in the future work.

KEYWORDS: New metallic materials; building structures; technology of effective use.

1. INTRODUCTION

Recently in Japan, it is widely recognized that buildings and facilities having high quality and good performance should be constructed to establish more durable and usable social capital. As a necessary consequence, this trend requires building materials to be more durable, fire-protective, mechanically excellent and beautiful. These days, thus, new materials having new function or performance have come to be partly or fully used for buildings, even if these materials have also higher cost.

The national program intends to support technically the above recent trend and then to lead to new technologies that enable new materials to be effectively used for buildings.

As part of the program, some new metallic materials for building structures are targeted for developing new building technologies. This paper describes the outline of the metal phase of the program and identifies technical issues to be solved in the course of the program

2. PRELIMINARY STUDY

Before discussing the topic on each new metallic material, we should describe briefly preliminary studies which were carried out to choose new materials to be targeted in the future work of the program. As is well known, there are all kinds of new materials which have been developed in many industrial fields. Thus, as the first step of the program, it was strongly needed to find out new metallic materials highly applicable to building structures; these materials should also be under a feasible outlook on developing technologies for effective use within the limited period of the program. In the first year of the program, the following ten materials were then chosen for the preliminary studies;

1) Structural steel with high strength and low yield ratio (high quality steel)
2) Stainless steel
3) Aluminum alloy
4) Laminated high-damping steel plate
5) Ultra mild steel
6) Cables
7) Clad steel
8) Steel-concrete composite material
9) Steel-rubber laminated bearing for base isolation
10) Titanium alloy

Regarding these materials, the present condition of development or production, material properties and applicability to building structures were studied through hearing from specialists of production areas and with extensive literatures.

3. TARGETED MATERIALS

On the basis of the preliminary studies, we finally determined the materials to be adopted in the program. In the selection, the following criteria were adopted; a material coming under at least one of the criteria should be eliminated:

1) Design manuals or specifications are well established.
2) Administrative treatment is now necessary rather than research and development.
3) The cost is too high for application to building structures.
4) The production system is not fully completed.
5) The material has low usability for major structural members.
6) Production and user sides have less concern over the use of the material.

Some of the above items should be explained in more detail. That is, materials

---

1 Building Research Institute, Structure Department
2 Yokohama National University

applicable to the item 1 have good design manuals or specifications on the basis of basic research. Thus, there is almost no need of a further study in this program; this can be said even if those manuals or specifications were established by unofficial groups. Also in the case of item 2, necessary technical development has been almost finished so that an administrative treatment is now needed for general use in building structures. Materials coming under the item 3 should be eliminated from target materials since building structures use a large amount of material in general. Thus the use of such materials would extremely boost the total cost of the buildings. Regarding the item 4, more stable and wider supply should be considered. For instance, if only one maker can produce the material, it is not appropriate to develop a utilization technology for the material in the national program.

By applying the criteria to the ten materials mentioned in the preceding section, the following five materials were selected as target materials in this program:

1) Structural steel with high strength and low yield ratio (high quality steel)
2) Stainless steel
3) Aluminum alloy
4) Laminated high-damping steel plate
5) Steel-rubber laminated bearing for base isolation

Here, the reason for eliminating the rest five materials should be briefly noted. That is, the "ultra mild steel" which has the lower yield strength around 10kg/mm^2 and high ductility can be supplied by only one steel makers; this material corresponds to the item 4 of the criteria. However, this material would be usable as a material for "damping devices". It is thus hoped that more steel makers produce this type of steel for stable supply. The "cable" has already good design manuals in the field of bridges in Japan. In the field of building structures, thus, an administrative consideration is now needed to make the material generally usable. The "clad steel" has also well-established standards in the field of chemical plants and machinery. In the world of building structures, however, the need for this material is not dug up as yet. Thus it is too early to pick up this material as a target. The "steel-concrete composite material" is in a somewhat different category from the other materials because this material has already been used widely in building structures. However, regarding some types of structural members made of this material, for instance steel tubular columns filled with concrete, there exists a significant discrepancy in evaluating member strength, between the design recommendations of the Architectural Institute of Japan and the Enforcement Orders of Japanese Building Standard Law. However, this different view does not need more research and development, but probably a careful administrative treatment for general use. The "titanium alloy" is too much expensive, about fifty times as costly as ordinary steel, whereas this material has very excellent performance. Then, the usability of this material may be very low for general building structures. However, this material would be useful for localized use in structures under special environment such as an offshore condition. In fact, titanium alloy bolts have been developed for the use under such severe conditions.

4. ISSUES TO BE SOLVED

In this section, we describe the present proceeding of the program and issues to be solved for each targeted material.

1) High quality steel

This steel has considerably high strength (60kg/mm^2 in maximum tensile strength), but the yield ratio, defined as the ratio of yield strength to maximum tensile strength, is less than 0.8. Furthermore, the yield strength is well controlled with the range of 48±3 - 5kg/mm^2. Japanese major mill makers have already been able to produce this type of steel by the Thermo Mechanical Control Process (TMCP) which is applied in the latter stage of rolling.

By a trial-design study in the program, it is found that 10 to 20 percent of the amount of steel can be saved when this new steel is used in lieu of normal steel with the yield strength of 24kg/mm^2. However, this saving would not always ensure the spread of this steel because the cost of the steel is expected to increase by 10 percent or more. Furthermore, the cost of building structures themselves, now in general, amounts to around 20 percent of the total building cost. On the other hand, the use of the new steel can give a considerable advantage to structural engineers since the steel would provide building structures having good performance. However, this kind of merit cannot be easily understood by building owners. Then, the key points for effective use of the new steel would be as follows;

1) Development of new structural systems by using the new steel
2) Simplification of structural design and shortening of construction terms

Regarding the first item, it is necessary to develop new design requirements which reflect

the peculiarity of the new steel. The second item is related to the smaller scatter band of the yield strength of the new steel than that of normal steels. It is a key point whether or not the well-controlled yield strength would make design procedures simple and also make inspection work easy.

2) Stainless steel

As is well known, stainless steel has not only higher corrosion resistance but also larger ductility and lower heat conductivity, than normal carbon steels. On the other hand, a weak point of this material for general use is its higher cost; at present, four to five times as expensive as normal structural steels. Probably for this reason, stainless steel is not prevailing so far for structural members.

Stainless steel has a lot of kinds corresponding to the combination of chemical components. Then, the two thirds of all product in Japan is the JIS grade of SUS304 (18Cr-8Ni) which is austenetic stainless steel and may be most suitable for structural members. In other grades, the grade of SUS304N2, which includes nitrogen, and the grade of SUS329J2L, which is austenetic-ferritic duplex phase stainless steel, are also applicable to structural members as high strength stainless steels, whereas these two grades have some problems in welding and forming.

The first problem in making use of stainless steel for structural members is whether or not stainless steel members can be used without fire resisting covering; designers would desire to make the best use of the fine surface of stainless steel. For this, first, thermal characteristics of stainless steel members should be carefully investigated. Second, the Japanese method for fire resisting design should be revised so that the thickness of fire resistive covering can be determined corresponding to the thermal stress and the surface temperature of members. Yet, since this is a drastic change in the fire protective and resistant design philosophy of Japan, it will take a long period over the remaining years of this program.

The second key is directly related to the cost of stainless steel. The present cost is even higher than ordinary structural steel as mentioned before. According to the preliminary study, there is little prospect of being able to cut the cost by a large margin even after ten years. Thus, it may not be reasonable to build a structure fully with stainless steel. Otherwise, stainless steel may be used partially in structural members to make use of its high ductility; for instance, in ordinary steel members, portions at which hinge formation is expected may be replaced with stainless steel to gain more hinge rotation.

The third point at issue is in the present fabricating and constructing system of stainless steel structures in Japan. At present a few fabricators can deal with stainless steel to make up building-structural members. Even these fabricators have not always good quality control system in their factories. Furthermore, a qualifying match system of welding workers is not established as yet. Now, in order to diffuse stainless steel as structural members, the establishment of a fabrication and construction system sufficiently assured is urgent business of concerned areas.

3. Aluminum alloy

Japan now imports about 90 percent of all aluminum alloy ingot which is processed in Japan. From thirty years ago, the Japan Light Metal Association has dealt with how to make good use of aluminum alloy for structural members. On the other hand, before the above activities, the Japanese Architectural Institute published "Design Guidelines for Aluminum Alloy Structures" as a draft version. Unfortunately, however, these activities did not effectively spread the material in the field of building structures, in particular in the use for major structural members; aluminum alloy is not yet approved as a material for major structural members in the Japanese Building Standard Law. As recent examples of aluminum structures in Japan, we can cite a covering frame over a heated pool, top-light frame, greenhouse frame and sunroom frame; nevertheless major structural members are made of steel in most cases. The keys for developing utilization technologies on aluminum alloy are similar to those on stainless steel. Here the problem of fire protection and resistance for aluminum alloy is more serious than for stainless steel, since the melting point of aluminum alloy is even lower than that of stainless steel; that is, around 620°C.

On the other hand, regarding the fabrication and construction of aluminum structures, aluminum extruding companies have sufficiently covered this area so that there exists almost no problem such as poor quality of work. As a technical point, finally, an advantage that free sectional shapes can be obtained by extruding should be effectively used. For instance, a wall structure comprised of a thin walled wall-like box section including inside stiffener plates, may be a structural system pertinent to

aluminum alloy.

4. Laminated damping steel plate

This damping plate is comprised of two thin steel plates and a thin layer of viscoelastic polymer that is adhesively sandwiched between the plates. When the damping plate vibrates, vibrational energy is transformed into thermal energy by a shear deformation in the polymer, resulting in the vibration highly damped. In particular, the damping plate seems to be most effective in preventing a solid-propagating noise. Stainless steel is also used for the thin steel plates.

In Japan, major mill makers are producing the damping plate for the use of floor plates, roofing plates and exterior stairs. As the present problems in fabricating the damping plate, there is some difficulty in welding owing to combusion of polymer and in press forming owing to spring-back which disturbs, in particular, right-angle forming at corners. Then, the keys for effective and wide use are to determine a common testing method for evaluating damping characteristics, and to standardize a method for evaluating the performance of each used portion in building.

5) Laminated steel-rubber bearing

Laminated rubber bearing is made of thin steel plates and rubber sheets by pasting one over the other alternatively. In Japan, major rubber-tire makers have initiated to produce this type of bearing for the use of seismically base-isolated buildings. By using the rubber bearings, natural vibration period of a building can be made extremely longer since the bearing has a low horizontal (shear) stiffness; the bearings support the building weight with high vertical stiffness owing to the steel plates in the bearing. The types of the bearing are classified as follows:

1. Ordinary type mentioned above
2. Lead-rubber bearing
3. High damping rubber bearing

The first type bearings have low inherent energy absorption so that additional dampers are usually needed to form a base-isolated structure. The lead-rubber bearing contain a lead plug inserted in the center hole of the bearing as an incorporated damper. The rubber itself of the third type bearings has high inherent damping capacity enhanced by mixing filler.

In Japan, most research and development are being made to summarize design guidelines or to accomplish safety assessment methods in the following organizations:

1. Tri-partite R & D among the Housing Bureau of the Ministry of construction, the Building Research Institute and the Building Center of Japan; to develop a safety assessment method for technical approvement of base-isolated buildings
2. The Architectural Institute of Japan; to summarize design recommendations for base-isolated buildings
3. The Public Works Research Institute; to make progress in the technology of base-isolated highway bridges.

On the basis of the above progress, the significant keys in our new program in then to standardize the testing method for characterizing rubber bearings, to grasp the scatter of performance characteristics of products, and to evaluate aging characteristics and degradation of rubber. In these activities, it is hoped to reflect requirements of structural engineers as the user side.

5. SUMMARY

The program status and future work are briefly introduced concerning each new metallic material for building structures. As initial conclusions on the basis of preliminary studies, the following three keys are found to be significant commonly for all materials:

1. Development of new structural systems using new materials
2. Cost implications
3. Control and assurance of quality of products, and fabrication and construction work

The program is now in the beginning of the third year so that many sorts of experimental studies are in progress to draw design recommendations on structural members with new concerned materials. After three years, then, some of those materials will be recognized as "existing" materials not only by structural engineers but by the building administration.

Theme V

Loma Prieta Earthquake

Initial Overview of the San Francisco Bay and Santa Cruz Mountains Ground Motion

by

A. Gerald Brady[1]

ABSTRACT

The strong-motion accelerograms from the Loma Prieta earthquake are analyzed for their long-period content in order to obtain a clearer picture of the long-period wave propogation details. Shear waves having periods in the 3.5 to 4 sec, and 5 to 7 sec ranges travel across four groups of stations with satisfactory coherency. Displacement accuracies are of the order of 0.5 cm for most of this data, with signal amplitudes an order of magnitude higher than the noise. Resonances associated with shear waves of 1.5 sec period are responsible for about 3/4 of the differential displacement necessary to unseat the 15 m section of the Bay Bridge.

KEYWORDS: Bay Bridge; coherency, displacements; earthquake; shear waves.

1. INTRODUCTION

Strong motion accelerographs from at least 139 stations were triggered by the M_S7.1 main shock of the Loma Prieta, California, earthquake occurring at 0004:15.24 GMT, on 18 October 1989[1,2,3,4]. The hypocentral depth was 18.5 km, deeper than most events on the San Andreas in this region. During the 7 to 10 seconds following initiation, the rupture spread bilaterally along the fault, and upwards towards the ground surface on the 70° downward-dipping fault. The total ruptured section is estimated from aftershock studies to be 40 km in the northwest-southeast direction, equispaced about the hypocenter, and 13 km deep, failing to reach the ground surface by about 5.5 km. In the hypocentral region the relative motion along the fault is estimated to be 2 m horizontally and 1.2 m vertically; the southwestern side moved northwestward and upward with respect to the other side. The right-lateral displacement is typical of San Andreas movement; the vertical displacements are not, although the non-vertical dip and the slight bend in the San Andreas alignment in this region will have contributed to this effect. The vertical displacements are certainly coordinated with the building of the Santa Cruz Mountains, in which the ruptured segment lies.

Although the 139 stations with triggered accelerographs are scattered throughout the San Francisco Bay area and areas to the east and south of the epicenter, some specific groups of stations afford the opportunity to study the transmission of long-period waves along the ground surface, or upwards from the rock below. This study is based on the appearance of waves with displacement amplitudes of several tens of centimeters and periods of several seconds during the routine processing search for a long-period (low-frequency, low-cut) filter that leaves relatively untouched those frequency components whose signal levels are well above noise levels.

Part of this search for a long-period filter relies on the fact that over an array of stations of small enough geographical dimension, waves of sufficient wavelength (period times wave velocity) must appear coherent as they cross the array, that is, they must retain closely their shape and amplitudes, although they may be offset in arrival times by small amounts.

Another of the more important criteria used in determining the long-period filter is a comparison between the Fourier amplitude spectrum (FAS) of a signal including its noise and the spectrum of a representative noise sample. At the long period where these spectra merge, noise is clearly prominent and a lower period must be chosen for a final processing filter.

Processing of the Loma Prieta strong-motion data continues at both the California Division of Mines and Geology's Strong-Motion Instrumentation Program (CSMIP)[3] at Sacramento, and the U.S. Geological Survey's Cooperative Network of Strong-Motion Instruments (USGS)[4] at Menlo Park. This investigation studies the processed data from arrays shown in Figure 1, at:

1.1 Anderson Dam, 27 km from the epicenter, on a line perpendicular to the San Andreas through the epicenter, and covering several kilometers;

1.2 Gilroy Array, Numbers 1, 2, 3, 4, 6, and 7, centered approximately 31 km east of the epicenter, but spanning from 15 to 28 km from the nearest part of the rupture, measured along a line approximately straight and transverse to the San Andreas.

1.3 Stanford, Palo Alto, and Menlo Park. A triangular array 51 km in a northwesterly direction from the epicenter, and centered 7.3 km from the closest point of the San Andreas, although the rupture did not reach this point. The triangular array, with one station at its center, has sides between 6 and 7 km long.

---

[1]U.S. Geological Survey, Menlo Park, California, 94025 USA

1.4 San Francisco to Oakland. This array spans 15 km from the Franciscan rock in San Francisco to the Recent Alluvium in Oakland, roughly following the line of the Bay Bridge. This line is approximately 97 km from the epicenter, and is aligned transverse to the radial direction. Its center lies 20 km from the nearest point of the San Andreas.

All processed data from these stations are available from CSMIP (CDMG, 630 Bercut Dr., Sacramento, California) and the USGS (Menlo Park, California). Table 1 contains the details of the stations and instruments in the arrays, with their routinely processed long-period limit.

2. ACCURACY OF DISPLACEMENTS

The accuracy of displacements calculated by integration from digitized accelerograms has been the subject of many investigative efforts, ever since routine processing of accelerograms was performed at Caltech in the early 1970s[5]. A description of the accuracy of the long-period amplitudes is required for a study of the displacement histories at more than one station as waves traverse a specific array. These displacements are characterized by long-period content. Consequently long-period errors are of interest. The discussion is confined to errors derived from the broadband white noise errors in acceleration during the digitizing process. The causes of these errors include accuracy in the selection of the centerline of the trace and round-off error associated with the least count in the Y-direction[6].

Sources of error in the digitized acceleration trace that are removed by subtraction of a digitized reference trace include inaccurate or non-rectilinear film transport during recording, distortion during film processing, and inaccurate but consistent and stable digitizing hardware. These hardware problems include transportation of the digitizing mechanism relative to the digitized film, and optics problems including parallax. The reference trace to be subtracted is assumed to be placed close to the data trace. These errors are not discussed further.

The CSMIP data discussed here is produced on a rotating drum raster scanner whose optimum operational characteristics incorporate a pixel size in the Y-direction of 50 micron. A film trace sensitivity of 1.9 cm/g results in a least count of 2.6 cm/sec^2. Descriptions of tests on this system indicate that the RMS error is of the order of one count, or 2.6 cm/sec^2. The USGS data reported on here is produced on a trace-following laser scanner, whose least count in both directions is one micron, corresponding to 0.052 cm/sec^2. Digitization of very small amplitude records[7] and of typical reference traces confirms that the RMS error, depending to some extent on the quality of the focusing of the traces, varies between 5 and 15 micron. The great majority of traces have very high quality, with an RMS error of 5 micron, corresponding to 0.26 cm/sec^2.

These RMS errors in acceleration can be translated into RMS errors in displacement. The FAS of a digitized reference trace, treated as acceleration, is relatively flat throughout the entire frequency range of this study, 25 Hz to 10 sec, including particularly 0.1 to 0.25 Hz, and the displacement spectrum would consequently fall off approximately with the inverse square of the frequency. This results in the RMS displacement errors in Table 2 for the two digitizing procedures, at periods between 4 and 10 seconds. These errors are not necessarily those in listed peak displacements; they indicate the error in oscillatory displacement amplitudes during oscillations at the listed periods. These expected errors must be recognized in the following sections.

3. DISPLACEMENTS ACROSS SPECIFIC ARRAYS

3.1 Anderson Dam

Processing the Anderson Dam records permits a full description of the decisions made on the long-period content. These are representative of all the processing in this study. The processed film records are from instruments at the crest, left abutment, and downstream of the earth and rockfill structure, 64 m high with a crest length of 422 m. The abutment and downstream instruments are approximately 300 m and 250 m, respectively, from the crest instrument.

An accurate measure of the long-period noise effects can be obtained in the spectral domain as follows. When a reference trace is subtracted from a data trace the result is effectively the sum of the noise-free signal and a quantity equal to the difference between two random error histories. At long enough periods, the noise will be dominant, and the FAS will so indicate, with increasing amplitudes. A close approximation to the spectral content of this difference between two random error histories can be obtained by subtracting the relevant reference trace from a second digitized reference trace, preferably closely placed on the original record. At long enough periods, this spectrum will therefore have the same increasing amplitudes as the previous one. The spectra meet and coalesce at periods where noise is dominant over the signal. Figure 2 compares the FAS of the left abutment 243° component (with no filtering, but with reference trace subtraction and mean value subtraction) with the FAS of another reference trace from the same film, prepared in the same way. The spectra have barely merged at 40 sec (0.025 Hz), a period equal to the record length. At 10 sec (0.1 Hz) there is at least an order of magnitude between these spectra.

Filtering at a series of long-period cut-offs,

namely, 4, 6, 10, and 40 sec, showed that 10 sec waves crossing this 3-station array remained coherent. This is shown in Figure 3, where the displacements at the three stations are offset appropriately in the Y-direction for clarity and in the X-direction for alignment in time -- these instruments are not wired for simultaneous triggering or common timing marks. Comparison of these displacements with the value for the USGS RMS error of 10-second waves, namely 0.66 cm, is good. Another feature illustrated by this figure is the shape of the corrected displacement waves at the time of triggering. The bi-directional Butterworth filter performs with no obvious distortions and no ringing; the displacements from the non-simultaneous triggered records line up well.

The shear waves arrive at Anderson Dam 3.5 sec after the first instruments triggered. Although shear waves of all periods arrive at practically the same time, the 10-sec filtered displacements exaggerate the waves of longest period. The 340° component, along the dam crest and approximately parallel to the San Andreas, shows a probable shear wave of period 5 to 7 seconds, having initial motion in a direction close to southeast. Radial motion, not clearly associated with these shears, also has prominent 6 sec periods.

3.2 Gilroy Array

The long-period limit chosen for these CSMIP records is 6 sec, using a filter whose response falls to zero in the interval between 6 and 12.5 sec. The north and east components of all six stations indicate a sharp shear wave arrival in the northeast direction, 3 sec after triggering at #1, and 5 sec after triggering at #6. This is probably a transverse shear wave, initial motion in the NE direction, the wave front moving down the fault in the SE direction. The amplitude of the northeasterly swing in displacement reaches 22 cm in the alluvium deposits in that part of the array closest to the San Andreas, and falls to a few centimeters at the array's eastern end, 28 km from the fault.

This shear pulse provides the prominent long-period ground motion to the southeast of the earthquake. The displacement plots indicate that at each station, after the initial ground motion to the northeast, a number of waves with specific periods were prominent. With the help of the FAS plots, these periods are found to be 1.4, 3 and 5 sec.

3.3 Standard, Palo Alto and Menlo Park

Four stations forming a triangle with a central point provide records that illustrate the ground motion in the vicinity of Stanford University. Triaxial sensors at ground level recorded the motion at a Stanford parking garage (SPG), the central point, 51.3 km in an approximate northwesterly direction from the epicenter. The stations at Stanford SLAC, the Menlo Park VA Hospital, and the Palo Alto VA Hospital are each approximately 4 km from SPG. Three of the stations indicate that ground motion during the passage of a 3.5 sec wave was transversely aligned with the epicenter; a small vertical component to the motion is also present. The peak displacements at the four stations depend on local geology effects, resonant amplifications and waves at shorter periods, but the amplitude of this specific long-period wave lies in the range of 12 cm at SLAC, closest to the San Andreas, to 8 1/2 cm.

Coherence is more difficult to identify in the accelerations. Several occurrences of 1 Hz content is identifiable across all four stations in their most east-west trending components. Peak accelerations, however, are associated with higher frequencies than this, affected also by local geology, resonances, simultaneous arrivals of peak amplitudes from higher frequency waves, interaction with the structure housing the instrumentation and other nearby structures, and other considerations.

3.4 San Francisco to Oakland

The longitudal motions of the eastern portion of the Bay Bridge between Yerba Buena Island (YBI) and Oakland are estimated from the main shock records from accelerographs at YBI, the Oakland Outer Harbor Wharf (OHW) and the Pacific Park Plaza at Emeryville (EMV). YBI is on Mesozoic sediments of the Franciscan formation and the recorded long-period motion may be considered representative of the western abutment of the cantilevered section of the Bay Bridge and also representative of the lowest levels of the concrete piers under the cantilevered section and the steel truss section in contact with this same hard rock. OAK and EMV are on filled land overlying Recent Alluvium; their motion is representative of the eastern abutment of the Bay Bridge in Oakland and the lowest levels of the piers supporting the bridge near the abutment which are in contact with the same sediments.

The records were filtered at a long-period limit of 6 seconds, and rotated to an 80° alignment. Only OAK had radio time (trigger time was 0004:35.0 GMT on 18 October 1989) so that alignment in the X direction was made instead on the arrival of the S wave, using the accelerogram traces and concentrating on 3 to 4 Hz content. At the same instant, the displacement plots show the arrival of a long-period wave of 3.5 to 4 sec period, 5.8 cm amplitude, transversely aligned with the epicenter, that is, longitudinal to the bridge. The hard rock sites in San Francisco (namely Pacific Heights and Rincon Hill), YBI, OHW and EMV all contain this ground movement with remarkable coherency. A higher frequency wave (period 1.5 sec) is also barely present, riding on the 3.5 to 4 sec wave, on the rock sites. At EMV and OHW this has resonated to

amplitudes of 8.6 and 12.7 cm, respectively, still riding, now in an overpowering way, on the longer wave. If the assumption is made that OHW is representative of the longitudinal abutment motion, subtraction of YBI from OHW yields a differential displacement peaking at 11 cm between the two bridge abutments (Figure 4). Caltrans measurements[8] indicate that the ends of the two trusses, where the 15 m bridge deck slabs failed, separated by 26 cm and returned 13 cm. The bearing seat was only 15 cm wide. As reported here, measurements from the records indicate that 11 cm of separation occurred at the foundation level. Structural dynamics during the earthquake must account for the remaining Caltrans separation.

4. CONCLUSIONS

Although ground accelerations recovered from strong motion accelerograms provide a means for calculating the forces suffered by the structures affected by the Loma Prieta earthquake, a better understanding of the overall ground motions emanating from the epicentral area has been obtained by considering the long period content portrayed most clearly by integrated displacements. Estimates of the total rupture duration are 7 to 10 sec, but the most prominent components are shear waves of 5 to 7 sec travelling northeast with ground motions parallel to the fault, and shear waves of 3.5 to 4 sec travelling to the northwest and southeast with ground motions transverse to the fault.

Amplifications and resonances at 1.5 sec are clearly responsible for some of the more impressive damage to the Bay Bridge.

TABLE 1. INSTRUMENTS IN THE ARRAYS

Array	Station	Cooperative Network	Long Period(s)
1.	Anderson Dam Crest, Left Abutment, Downstream	USGS	10
2.	Gilroy #1, 2, 3, 4, 6, 7	CSMIP	6
3.	Stanford SLAC Stanford Parking Palo Alto VA Hospital Menlo Park VA Hospital	USGS	4
4.	San Francisco: Pacific Heights San Francisco: Rincon Hill Yerba Buena Island Oakland: Outer Harbor Wharf Emeryville	CSMIP CSMIP CSMIP CSMIP USGS	6

TABLE 2. DISPLACEMENT ERRORS

RMS error in accln. (cm/sec^2)	RMS error in displacement (cm) 4 sec	6 sec	8 sec	10 sec
2.6	1.0	2.4	4.2	6.6
0.26	0.1	0.24	0.42	0.66

5. REFERENCES

1. Ward, P. L., and R. A. Page; The Loma Prieta Earthquake of October 17, 1989; U.S. Geological Survey Pamphlet (1989).
2. Plafker, George and J. P. Galloway (editors); Lessons Learned from the Loma Prieta, California, Earthquake of October 17, 1989; U.S. Geological Survey Circular 1045 (1989).
3. Shakal, A. and others; CSMIP Strong Motion Records from the Santa Cruz Mountains (Loma Prieta) California, Earthquake of 17 October 1989; Report No. OSMS 89-06 (1989).
4. Maley, R. and others; U.S. Geological Survey Strong-Motion Records from the Northern California (Loma Prieta) Earthquake of October 17, 1989. U.S.G.S. Open-file Report No. 89-568 (1989).
5. Brady, A. G.; History of Accelerogram Data Processing Proceedings, Golden Anniversary Workshop on Strong-Motion Seismomatry, USC, Los Angeles (1984).
6. Trifunac, M. D., F. E. Udwadia and A. G. Brady; Analysis of errors in digitized strong-motion accelerograms; Bull. Seis. Soc. Am., 63, 1, pp 157-187, 1973.
7. Fletcher, J. B., A. G. Brady and T. C. Hanks, Strong-Motion Accelerographs of the Oroville Aftershocks: Data Processing and the Aftershock of 0350 August 6, 1975; BSSA, 70, 1, p 243-267 (1980).
8. Lew, H. S. (editor); Performance of Structures During the Loma Prieta Earthquake of October 17, 1989. NIST Special Publication 778 (1990).

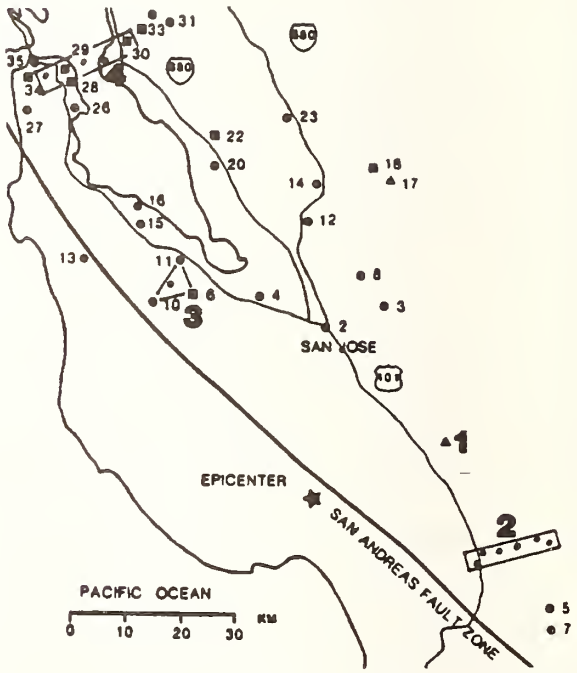

Figure 1. Location of 4 arrays. Other USGS stations and CSMIP stations in the arrays are shown.

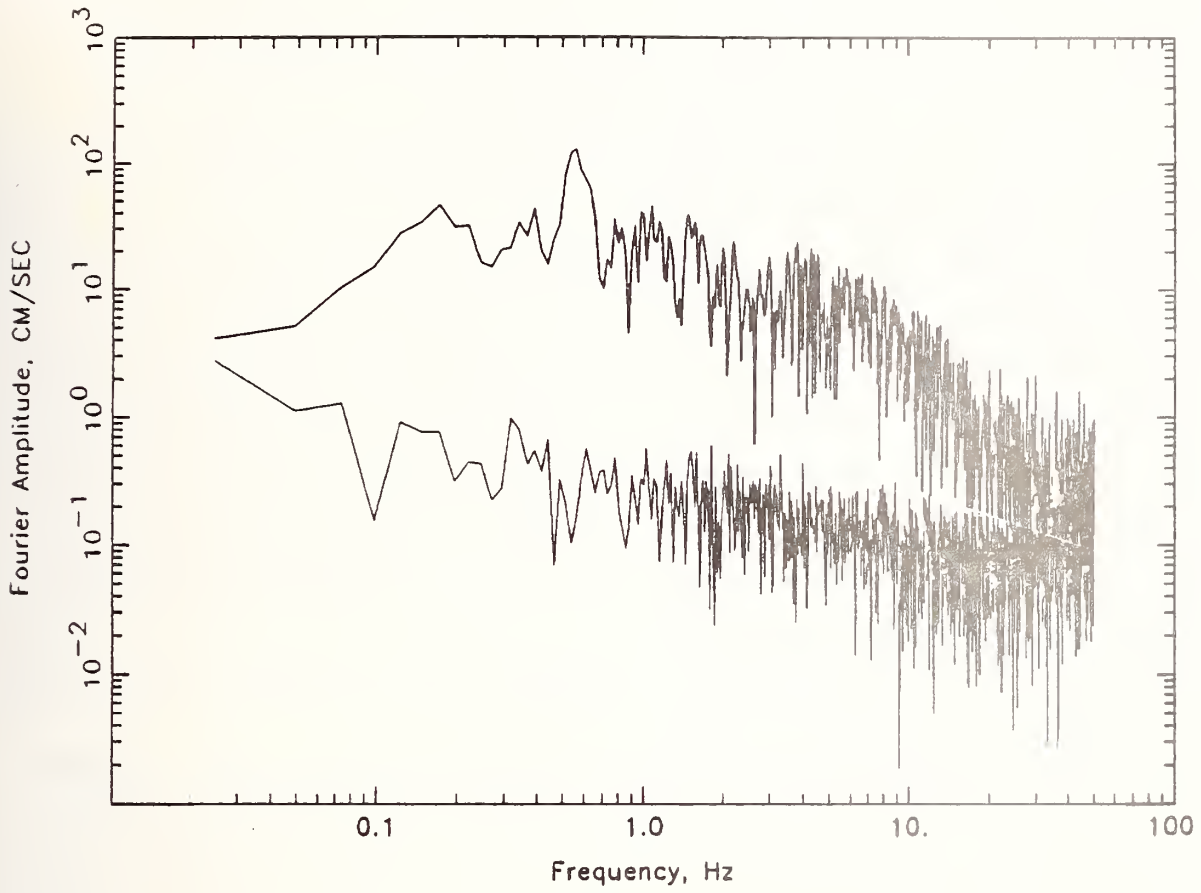

Figure 2. Fourier amplitude spectra of Anderson dam, left abutment, 243° component (upper) and a reference trace processed identically (lower); no long-period filter, subtraction of fixed trace, and subtraction of mean.

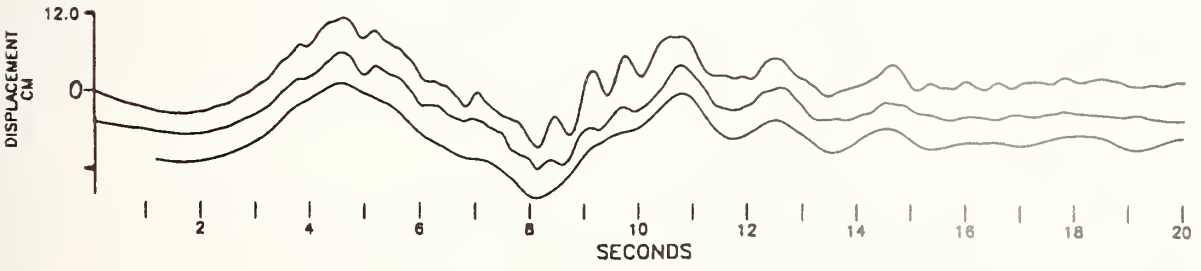

Figure 3. Anderson Dam, 243° components, at crest (upper), downstream and left abutment (lower); Y-direction offsets are for clarity, X-direction offsets align the long periods.

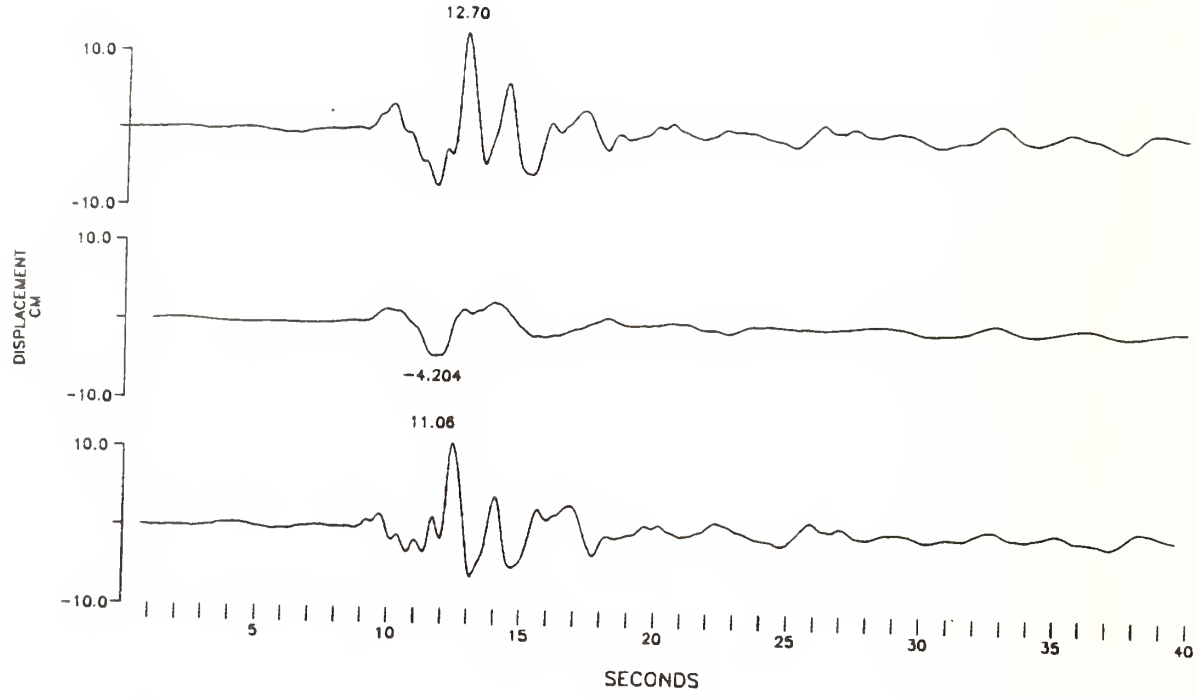

Figure 4. Calculated displacements at Oakland Outer Harbor Wharf (upper), Yerba Buena Island, and their difference (lower), in the 80° direction, approximately in the longitudinal direction of the Bay Bridge.

The Loma Prieta Earthquake: Site Response and Liquefaction

by

Ellis L. Krinitzsky[1]
A. G. Franklin[1]

ABSTRACT

During the magnitude 7.1 Loma Prieta earthquake of October 17, 1989, damage was widespread in the mountains and towns near the epicenter, but otherwise was concentrated in pockets around the margin of San Francisco Bay. These pockets occurred where vulnerable structures were founded on deposits of bay mud, which amplified the ground accelerations in the east-west direction by an average factor of 2.8, and in the north-south direction by 4.2. Occurrences of liquefaction outside the epicentral area typically were in artificial fill materials placed on bay mud. The combination of thick bay mud deposits and liquefiable sandy fill was particularly devastating in the Marina District of San Francisco.

KEYWORDS: Earthquake; liquefaction; site response

1. INTRODUCTION

The Loma Prieta earthquake was a magnitude 7.1 event that occurred at 5:04 p.m., California Daylight Saving Time, on October 17, 1989. The earthquake is believed to have been generated by movement on a segment of the San Andreas fault with "sympathetic" activation of branch faults. However, there is no evidence of relative movement on the surface trace of the San Andreas fault. The epicenter, principal active faults in the region, and the area of microearthquakes that were recorded by the U.S. Geological Survey within two days following the event, are shown on Figure 1 (from Plafker and Galloway, 1989). The microearthquakes indicate the extent of fault rupture in the subsurface. The inclusive area that is represented is approximately 150 km by 60 km and includes all of the metropolitan area from San Jose to San Francisco and Oakland. Within this area there was appreciable but localized damage to structures from shaking, soil liquefaction, and ground displacements.

2. EXTENT OF DAMAGE RELATED TO LIQUEFACTION

Earthquake effects were widespread in the mountains and towns near the epicenter and in small isolated pockets throughout the San Francisco Bay area. The greatest property damage occurred in the towns of Santa Cruz and Watsonville and in the Marina district of San Francisco. There were numerous fatalities, pronounced highway damage, and dislocation of traffic principally in Berkeley and Oakland on Interstate-80 and Interstate-880, closure of the San Francisco Oakland Bay Bridge, destruction of the bridge at Struve Slough on Highway 1 at Watsonville, and extensive damage to Highway 17 north of Santa Cruz. Additionally, there was runway damage at the Alameda Naval Air Station and the Oakland International Airport, damage in the terminal building of the San Francisco International Airport, plus damage to property and roads from earth movements and landslides throughout the Santa Cruz mountains. Minor landslides occurred along the Pacific Coast, posing potential hazards where Highway 1 and urban developments lie in close proximity to the coast, as at Half Moon Bay, Pacifica, and Pescadero.

Liquefaction effects were observed around the margins of San Francisco Bay at several locations on bay muds, especially at sites where sandy fill had been placed over the bay mud. Such occurrences include the San Francisco Marina District, the Oakland International Airport, the Alameda Naval Air Station, and the Port of Oakland. Outside the Bay area, liquefaction occurred in young alluvial deposits near the epicenter, notably on the Pajaro and San Lorenzo Rivers.

2.1. San Francisco - Oakland Area

In the San Francisco - Oakland area, there were disruptive and costly damages to bridges, freeways, wharves, buildings and the major airports. The center of this area is about 90 km from the epicenter of the earthquake, a distance at which the ground motions due to the earthquake should have been greatly attenuated. Reference to Figure 1 shows this area as Modified Mercalli (MM) intensity zones VI and VII. Within these zones are several intensities VIII and IX that are in the form of localized, anomalous intensities. The MM intensities in this range may be generalized as:

VI	Essentially no structural damage
VII	Negligible structural damage
VIII	Threshold of damage to good construction
IX	Significant damage to good construction

The anomalous intensities in Figure 1 are clearly the result of locally unfavorable conditions such as bay muds and artificial fill; all of the anomalies are in such areas. Figures 2 and 3 show thicknesses and depths of younger bay mud; figure 4 shows the depth to bedrock. In figure 4, the Marina District is shown as a deep embayment. The contours on figures 2 to 4 are from Goldman (1969).

The bay muds are composed mostly of marine clays that are intermixed with lesser quantities of silts and fine sands. Additionally, there is organic

[1] U.S. Army Engineer Waterways Experiment Station, Vicksburg, Mississippi 39180

matter including some peat. Upper layers of the mud are unconsolidated and may be semi-fluid. The Marina District is one of the areas in which rubble from the 1906 San Francisco earthquake was dumped and later covered with sand.

2.1.1. The Interstate - 880 Collapse

A section of I-880 in Oakland, known both as the Nimitz Freeway and as the Cypress Avenue Expressway, suffered a collapse in almost 2 km of the upper deck during rush hour traffic. The earthquake motions caused the reinforced concrete columns to crack leaving the hinge joints supporting the decks unstable. As the columns buckled, the decks slid and dropped.

Damage to the freeway is almost the only damage in that area. The buildings are mostly intact, as are the other elevated sections of highway in the area. A few collapsed chimneys and brick facings were observed. The I-880 collapse occurred entirely in a segment that was founded on bay muds. Horizontal motions in this area for rock, alluvium and bay mud during a magnitude 4.1 aftershock (Borcherdt and Hough, 1989) show that the bay mud had the effect of amplifying the motions by a factor of about 5 compared to rock and about 2 compared to alluvium. Amplification of motions in the bay mud also has a spectral effect observed in longer predominant periods of motion.

Earthquake motions recorded in the free field on bay muds nearby at Emeryville during the Loma Prieta earthquake had a peak horizontal acceleration of 0.25 g.

2.1.2. The Bay Bridge

A single span of the San Francisco - Oakland Bay Bridge collapsed during the earthquake. The bridge was otherwise structurally intact. Lateral movement on the order of several feet appears to have occurred in the piers. The movement sheared bolts in the upper structure holding the support beams, thus permitting the upper deck to crash down. Again the culprit appears to be in the greater excitation that was generated in this portion of the foundation soils. The bay muds have a thickness of approximately 40 ft according to the interpretation in figure 2.

In aerial photographs made the day after the earthquake (figure 5), sand extrusions characteristic of liquefaction can be seen on the approaches to the toll plaza on the Oakland side of the Bay Bridge. These deposits of sand were smaller in extent, but otherwise similar to, those seen on the runways of the Alameda Naval Air Station and the Oakland International Airport.

2.1.2. The Marina District

The Marina District in San Francisco is an area that suffered a concentration of costly damage that included a fire resulting from a burst gas main. Figure 6 shows the Marina area on 18 October 1989, the day following the earthquake. The burnt-out area is in the center of the picture. On an opposite corner is a building that was twisted off its foundations. In the rest of the area the damage is generally less spectacular though on the ground one can see much damage in the first stories and in the pavements and streets.

Figure 7 shows the boundaries of the area in which major damage occurred in the Marina District. As seen in figure 4, the area is underlain by deep deposits of bay mud. On top of the bay mud is artificial fill over which sand has been placed. Additionally there are areas of naturally occurring sands from beaches and dunes. Since the area is nearly at sea level and essentially flat, much of the near-surface sand was water saturated.

The combination of foundation conditions was ideal to assure serious damage in a strong earthquake: a deep, soft soil column to amplify the bedrock motions; dumped fill and liquefaction-susceptible sand overlying it; and a high water table to assure saturation of the sand.

Figure 8, from Plafker and Galloway (1989), shows the effect of soil conditions in amplifying ground motions during a magnitude 4.6 aftershock of the Loma Prieta earthquake. The accelerograph locations are shown in figure 7. The vertical velocities were measured on sandstone, dune sand, and artificial fill. The water-saturated dune sand shows peak motions more than 5 times as great as in the adjacent sandstone outcrop.

Some effects of soil liquefaction are seen in figures 9 to 11. Figure 9 shows sand extrusion with blow holes in the Marina Green. Figure 10 shows sand extrusions which ran out from under a garage door and over the sidewalk. Numerous cases of sand extrusions into basements were reported. Lateral translation of the pavements riding on liquefied sand caused the buckling and breakup of the sidewalks and streets in figure 11.

2.1.3. The Port of Oakland

The port facilities in Oakland suffered considerable damage from shaking and from soil liquefaction. Damage to the wharves occurred from shaking of the pile foundations whereas liquefaction was the chief cause of damage in the adjacent soil areas. Liquefaction was observed at distances of up to 35 m inland. Pavements were dropped in those areas relative to the docks by up to 45 cm.

2.1.4. Alameda Naval Air Station and Oakland International Airport

Runways at the Alameda Naval Air Station and at the Oakland airport suffered spectacular effects from liquefaction. Figure 12 shows sand extrusions on the runways at the Alameda Naval Air Station, one of which, in the center of the photo, is 120 m in length and 30 m in maximum width. There is a linearity in the alignment of these liquefaction occurrences. The soils were placed as fill materials. In the areas marked with crosses considerable cracking took place in the pavements. Damages in

the pavements at the Oakland airport were similar.

2.2. Santa Cruz

The experiences in the Marina District of San Francisco, where damage resulted from a combination of liquefaction in the foundation soils and weaknesses of unsuitably built structures, were repeated in other areas. The business district of Santa Cruz was severely damaged as a result of unfavorable construction, in this case unreinforced masonry, ground motion amplification in alluvial soils, and possibly liquefaction in the foundations.

The depth of soft soils varies from 7 to 165 m and contains very young alluvial deposits. The area of severest property damage is adjacent to the present course of the San Lorenzo River. Some deposits of soil which might have been extruded by liquefaction were observed, but they could have resulted from broken water lines. No gross distortion of pavements, such as that seen in the Marina District, was observed here.

Santa Cruz was close to the epicenter of the earthquake and experienced peak motions that were measured nearby at 0.60 g vertical and 0.54 g horizontal.

Figure 13 shows fissures and undulating displacements in the levee along the San Lorenzo River near the business district of Santa Cruz. Figure 14 shows the pattern and extent of these fissures. The levees were severely damaged throughout their lower reaches. Ground displacements were mostly in the form of elongate fissures that paralleled the length of the levees. Eyewitness accounts of the earthquake describe large ground waves that moved through this area of very thick, unconsolidated alluvial deposits in which the water table is near the surface. After the earthquake, sand extrusions adjacent to the levee were apparent over much of its length, indicating liquefaction of the foundation soils under the levees.

2.3. Watsonville

Downtown Watsonville had a concentration of damage in the business district similar to that which occurred in Santa Cruz. The causes were the same: unreinforced masonry construction on very thick, unconsolidated soils with a high water table resulting from the local situation in a valley along the Pajaro River. There was also widespread damage in residential areas, mostly due to collapse of chimneys and inadequate lateral bracing at the foundation connections.

Levees on the Pajaro River in and near Watsonville were damaged extensively, much as in Santa Cruz. Figure 15 shows elongate fissures in the levees downstream from Watsonville. Some of these fissures were measured at 2.0 to 2.3 m maximum depth, which makes them slightly deeper that the levees are high. Sand extrusions in a plowed field adjacent to the levee are shown in figure 16. There is a linear rupture with extrusion of sand and multiple vent holes along the alignment. Other occurrences of sand extrusion were common in the vicinity of the levees.

3. EARTHQUAKE GROUND MOTIONS

Figures 17 and 18 compare peak horizontal accelerations at hard and soft sites respectively as measured during the Loma Prieta earthquake with the Krinitzsky-Chang-Nuttli (1988) curves for a M = 7.0 earthquake. The data were obtained from reports of the U.S. Geological Survey (see Maley and others, 1989) and the California Division of Mines and Geology (see Shakal and others, 1989). The curves are for mean and mean plus one standard deviation. The distances shown are focal distances.

A hard site, as distinguished from soft, has a shear wave velocity greater than 400 m/sec and surficial soft cover is less than or equal to 15 m. Values at hard sites from the Loma Prieta earthquake (figure 17) are in general agreement with the Krinitzsky-Chang-Nuttli curves.

Values at soft sites have a much greater spread in values, almost a full order of magnitude at a focal distance of 80 km. The hard sites have half of this spread. Figure 18 indicates which values are for bay muds. Eight of the nine bay mud locations provided records that have peaks well above the mean plus one standard deviation for magnitude 7. Anomalously high values such as these were observed for motions in the soft lake deposits in Mexico City during several earthquakes. Amplification factors there were as much as 5 times for soft versus hard ground (Krinitzsky, 1987).

Figure 19 compares Loma Prieta accelerograph records for a granite and a bay mud site at roughly similar distances, 52 versus 67 km, from the earthquake source. The amplification factor for the bay mud in this instance is about four times. There is also a change in the spectral composition of the bay mud record whereby there is a shift to a longer predominant period, in this case about two seconds. This effect is further illustrated by the data in Table 1, in which ground motions at hard sites are compared with those at several soft sites with comparable focal distances.

Compared with hard sites, peak horizontal accelerations at bay mud sites were amplified an average of 2.8 times in the east-west direction and 4.2 north-south. An extreme amplification of 9.7 times (north-south) occurred in Oakland harbor.

4. CONCLUSIONS

Outside of the epicentral region, severe damage and liquefaction during the Loma Prieta earthquake occurred in localized pockets in which the Modified Mercalli intensity was as much as two levels higher than in the surroundings. These anomalous pockets of damage were characterized by the existence of vulnerable structures founded on deposits of bay mud, in which the ground accelerations were amplified by an average of 2.8 times in the east-west

direction and 4.2 times in the north-south direction. Occurrences of liquefaction were also characterized by the presence of sandy artificial fill overlying the bay mud. The Marina District of San Francisco, the San Francisco - Oakland Bay Bridge, the Cypress Expressway on I-880, the Port of Oakland, the Alameda Naval Air Station, and the Oakland International Airport were affected.

Existing distance-magnitude-motion curves do not account for the high values of ground motions at these sites, although similar occurrences have been observed on very soft sites during past earthquakes, notably in Mexico City.

5. ACKNOWLEDGEMENT

The work reported in this paper was carried out under funding provided by the U.S. Army Corps of Engineers, and is published by permission of the Office of the Chief of Engineers.

6. REFERENCES

Borcherdt, Roger D., and Hough, Susan E. 1989. "Mud May Have Contributed to the Collapse of Nimitz Freeway during the Loma Prieta Earthquake," Earth in Space, Vol. 2, No. 4, pp 6-8.

Goldman, Harold B., ed. 1969. Geologic and Engineering Aspects of San Francisco Bay Fill, Special Report 97, California Division of Mines and Geology, San Francisco, California.

Krinitzsky, E.L. 1987. "Empirical Relationships for Earthquake Ground Motions in Mexico City," in The Mexico City Earthquakes - 1985, Factors Involved and Lessons Learned, American Society of Civil Engineers, New York, 474 pp.

Krinitzsky, E.L., Chang, Frank L., and Nuttli, Otto W. 1988. "Magnitude-Related Earthquake Ground Motions," Bulletin of the Association of Engineering Geologists, Vol XXV, No. 4, pp. 399-423.

Maley, R., Acosta, A., Ellis, F., Etheredge, E., Foote, L., Johnson, D., Porcella, R., Salsman., M., and Switzer, J. 1989. U.S. Geological Survey Strong-Motion Records from the Northern California (Loma Prieta) Earthquake of October 17, 1989, U.S. Geological Survey Open File Report 89-568, Menlo Park, California, 85 pp.

Plafker, George, and Galloway, J.P., eds, 1989. Lessons Learned from the Loma Prieta, California, Earthquake of October 17, 1989, U.S. Geological Survey Circular 1045, Washington, D.C. 48 pp.

Shakal, A., Huang, M., Reichle, M., Ventura, C., Cao, T., Sherburne, R., Savage, M., Darragh, R., and Petersen, C. 1989. CSMIP Strong-Motion Records from the Santa Cruz Mountains (Loma Prieta), California, Earthquake of 17 October 1989, California Division of Mines and Geology, Report OSMS 89-06, Sacramento, California, 156 pp.

Table 1. Amplification of ground motions due to local site conditions

HARD SITE	Focal Dist km	Accel g EW	Accel g NS	BAY MUD SITE	Focal Dist km	Accel g EW	Accel g NS	Amplification EW	Amplification NS
Hayward CSUH	71	.08	.08	San Francisco Airport	79	.33	.24	4.13	3.00
				Foster City:					
				Redwood Shores	63	.29	.26	3.63	3.25
				Redwood City	63	.23	.28	2.88	3.50
				Foster City	66	.11	.12	1.38	1.50
Yerba Buena Is.	95	.07	.03	Treasure Is.	98	.16	.10	2.29	3.33
				Oakland Wharf	95	.27	.29	3.86	9.67
				San Francisco 18-Story	95	.14	.17	2.00	5.67
Berkeley, Strawberry Canyon	98	.08	.04	Emeryville	97	.26	.22	3.25	5.50
				Larkspur	115	.14	.10	1.75	2.50
							AVERAGE AMPLIFICATION:	2.8	4.2

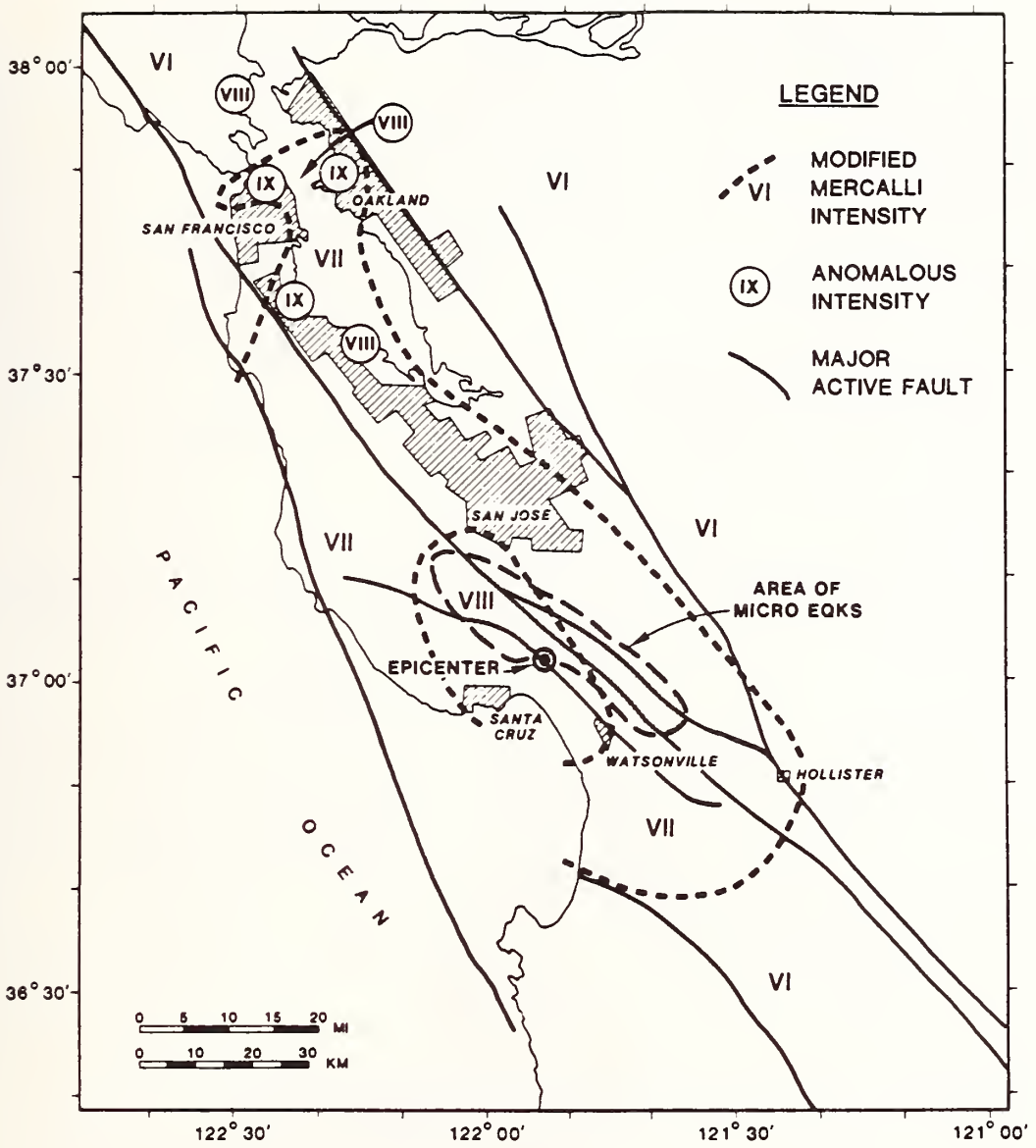

Figure 1. Location map for the Loma Prieta earthquake, showing Modified Mercalli intensities from Plafker and Galloway (1989) and anomalous intensities noted in the San-Francisco - Oakland Bay area.

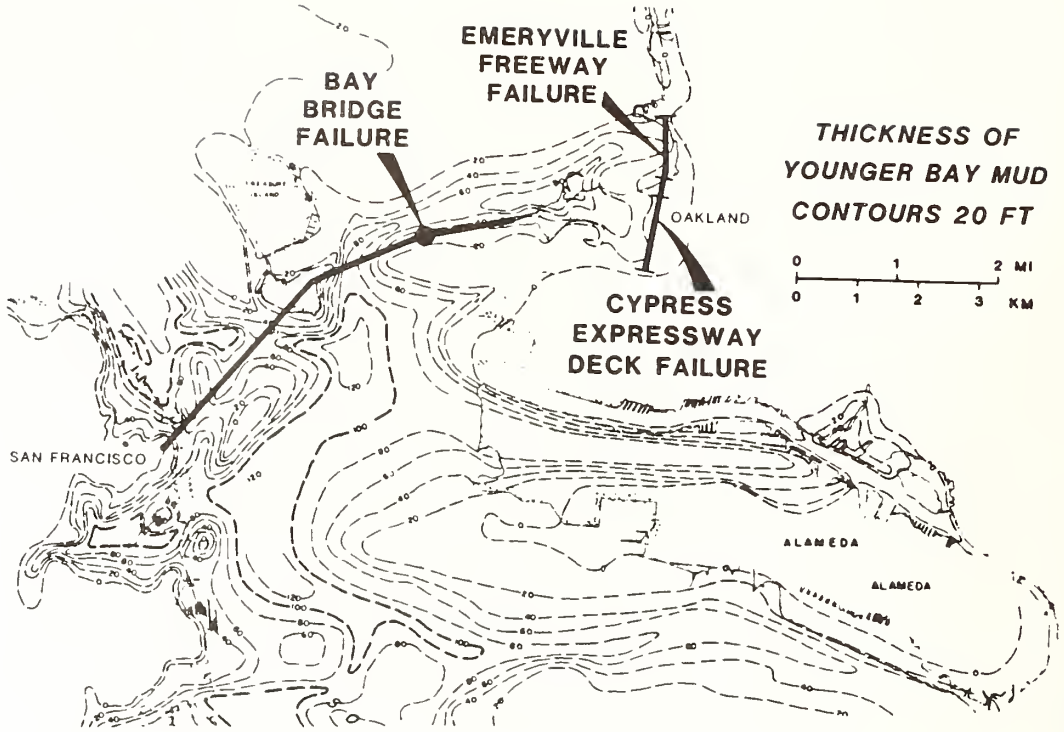

Figure 2. Thickness of the younger bay mud with locations of Cypress Expressway deck failure, the Emeryville Freeway failure and the Bay Bridge failure. Contours are from Goldman (1969).

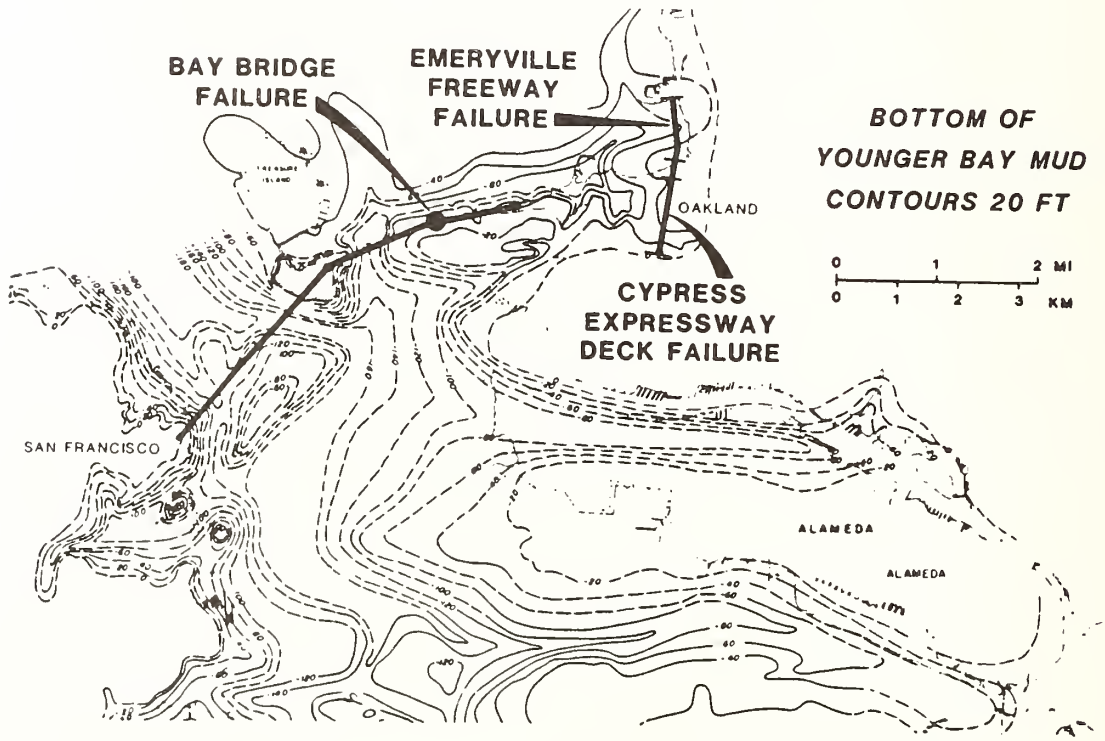

Figure 3. Bottom of younger bay mud with locations of Cypress Expressway deck failure, the Emeryville Freeway failure and the Bay Bridge failure. Contours from Goldman (1969).

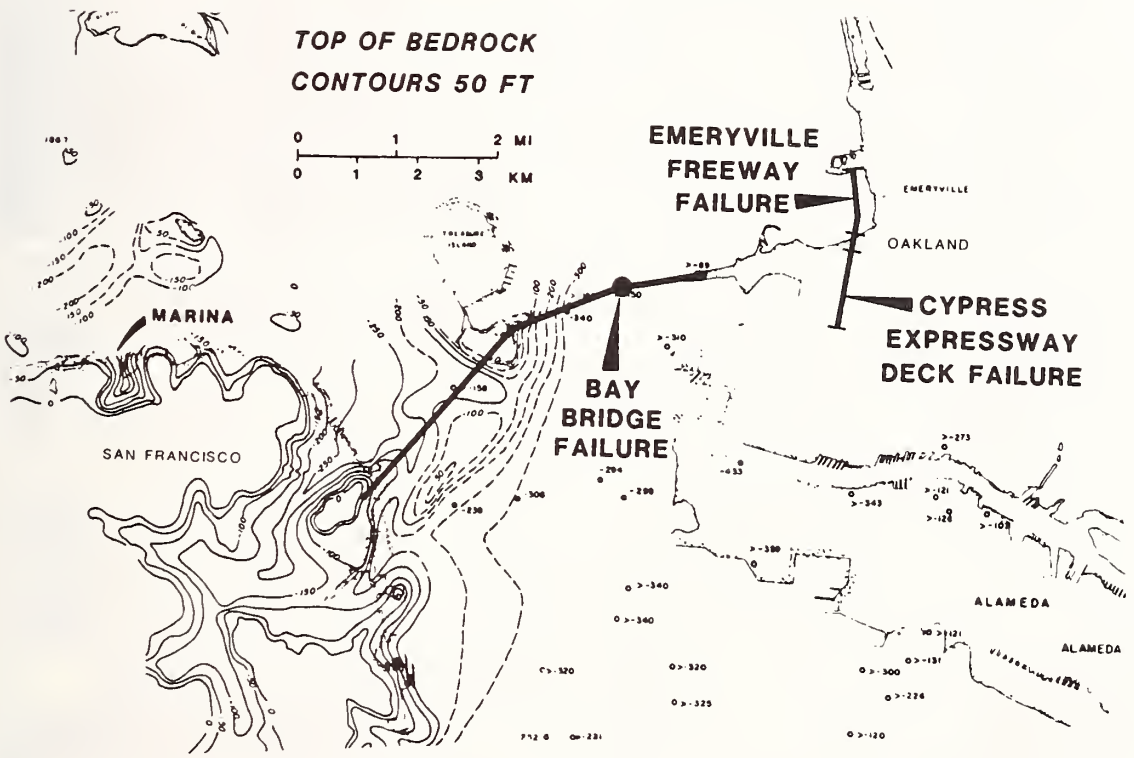

Figure 4. Top of bedrock with locations of the Marina District in San Francisco, the Cypress Expressway deck failure, the Emeryville Freeway failure and the Bay Bridge failure. Contours from Goldman (1969).

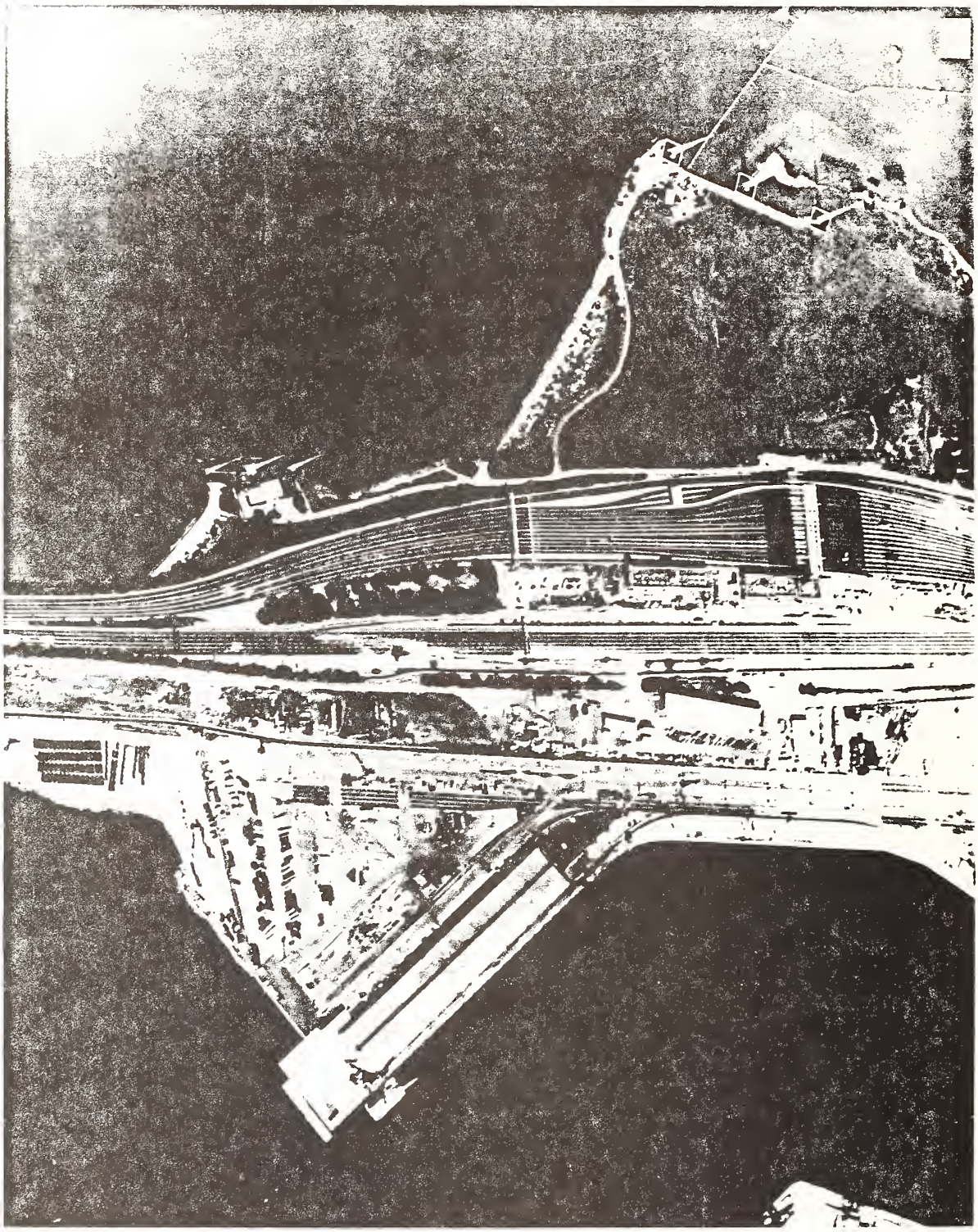

Figure 5. Aerial view of the toll plaza on the Oakland side of the Bay Bridge, showing sand extrusions on pavements. Taken on the day following the earthquake.

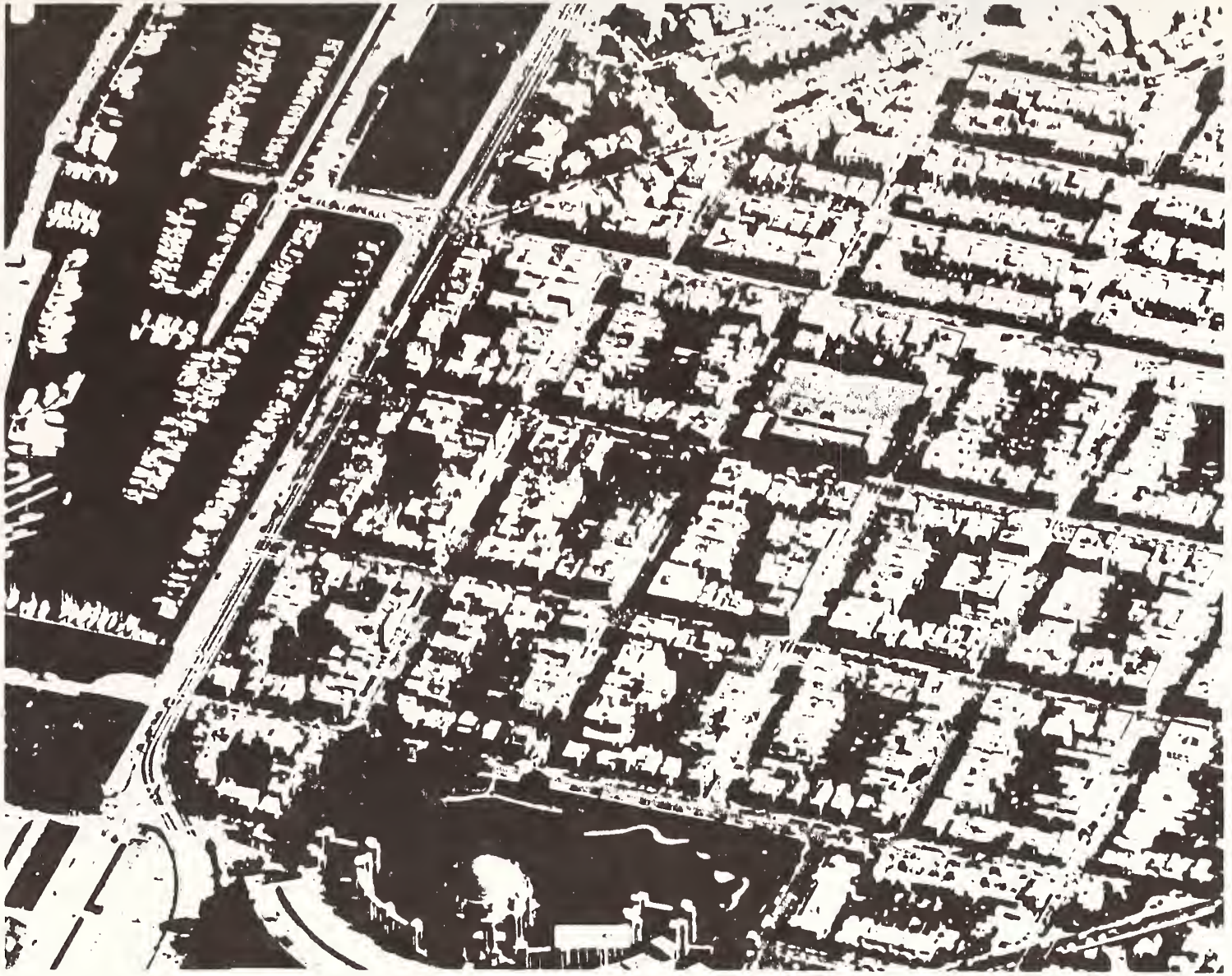

Figure 6. Aerial view of the Marina District in San Francisco on the day following the earthquake.

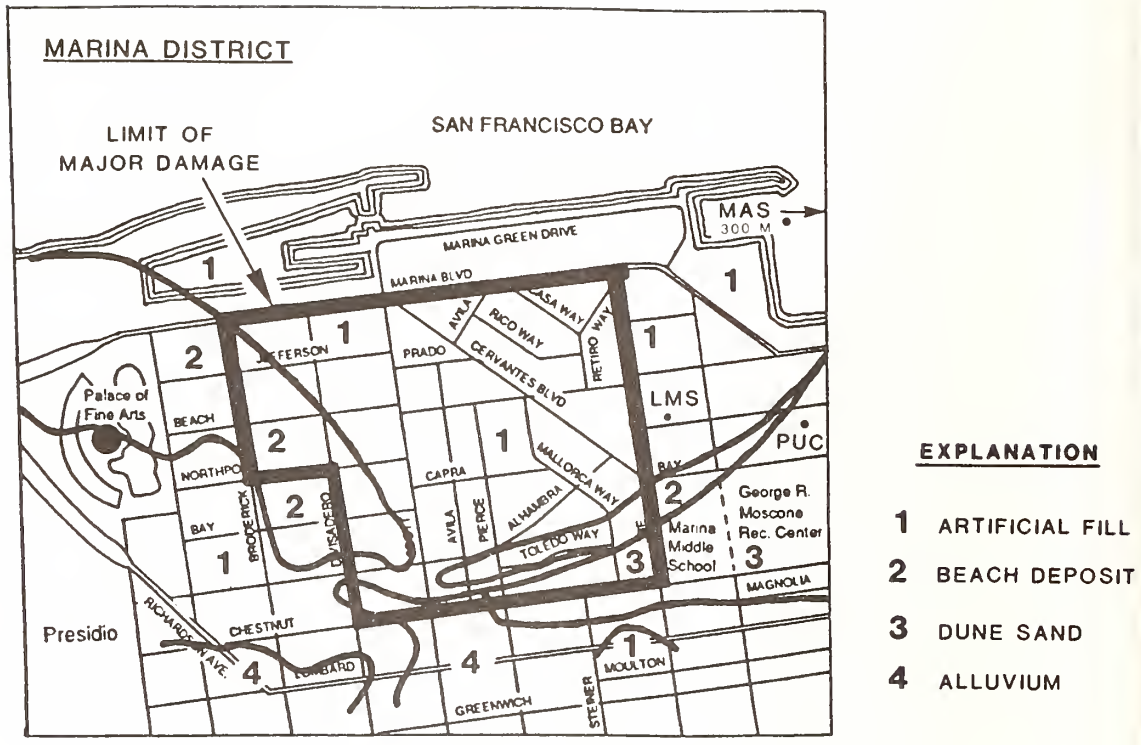

Figure 7. Limits of major damage in the Marina District, and types of underlying soil deposits.

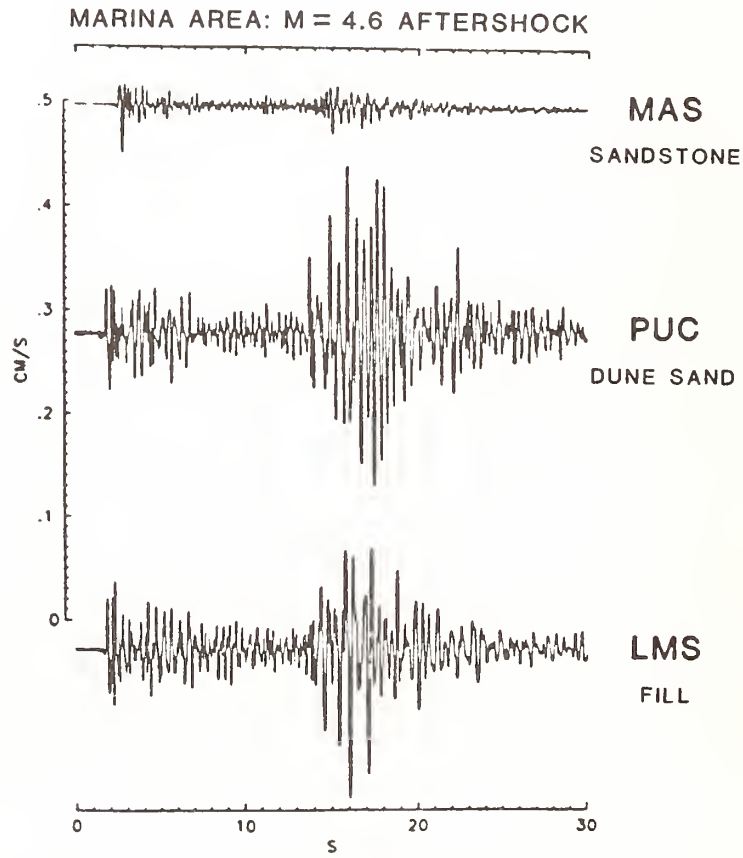

Figure 8. Vertical velocities on sandstone, dune sand, and fill in the Marina District during a M = 4.6 aftershock (Plafker and Galloway, 1989).

Figure 9. Sand boil from sand liquefaction in the Marina Green, San Francisco.

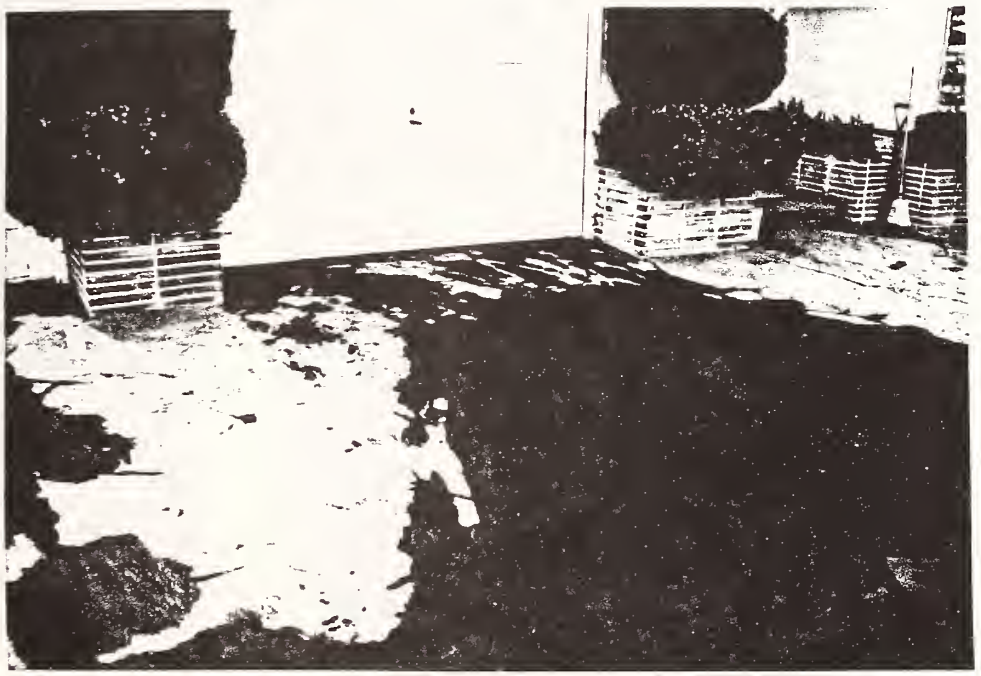

Figure 10. Sand extrusion flowing out of garage and over sidewalk, in the Marina District.

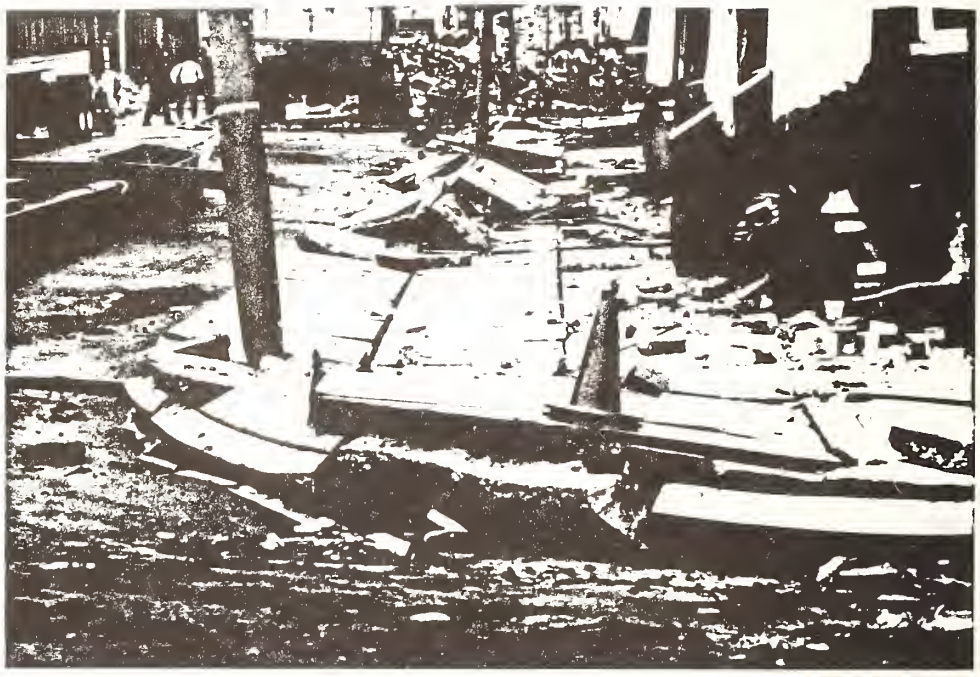

Figure 11. Buckled and broken sidewalks and street pavement resulting from soil liquefaction, in the Marina District.

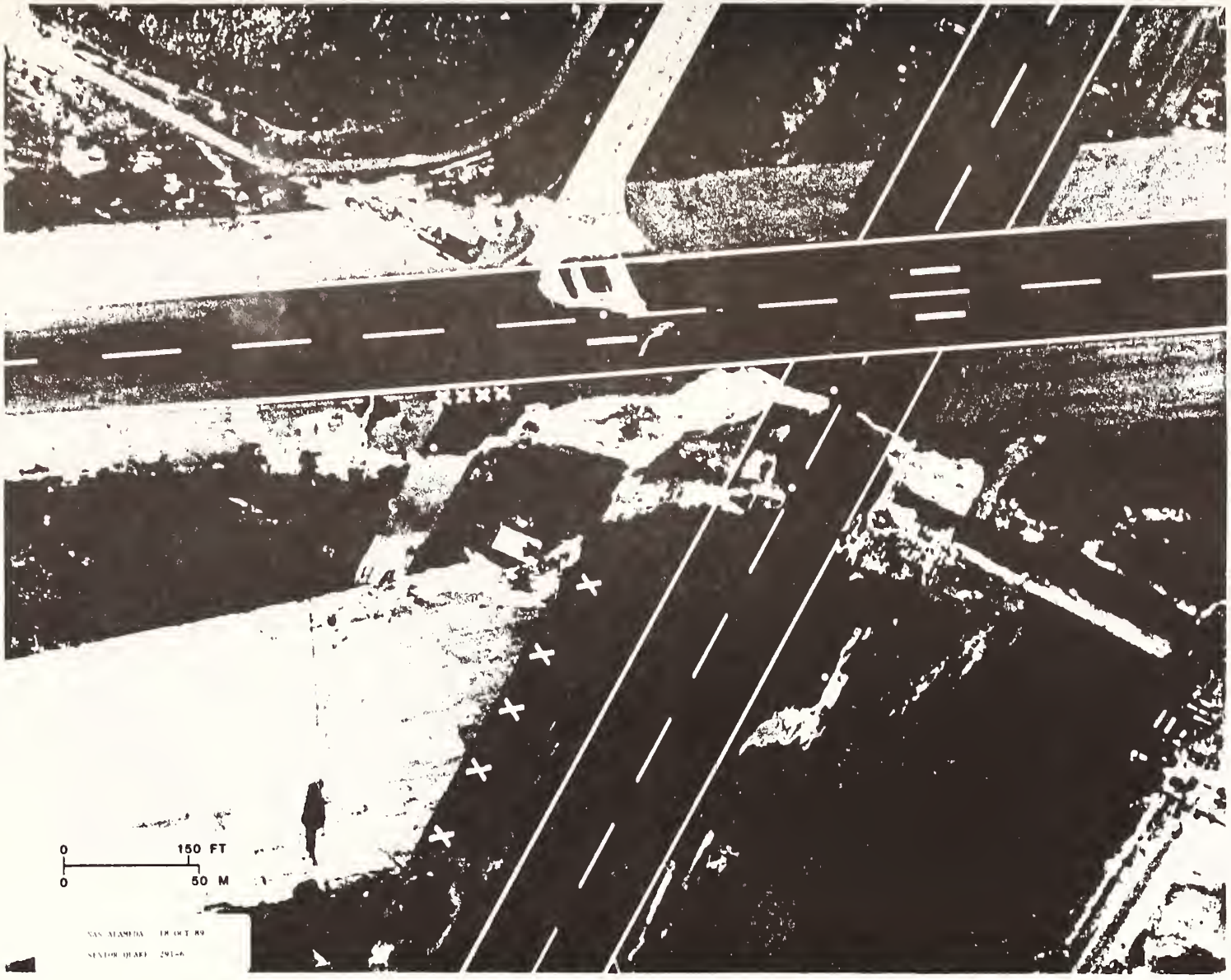

Figure 12. Large-scale soil liquefaction in fill materials at the Alameda Naval Air Station.

Figure 13. Cracking and slumping of levee along the San Lorenzo River in downtown Santa Cruz, resulting from liquefaction of foundation soils.

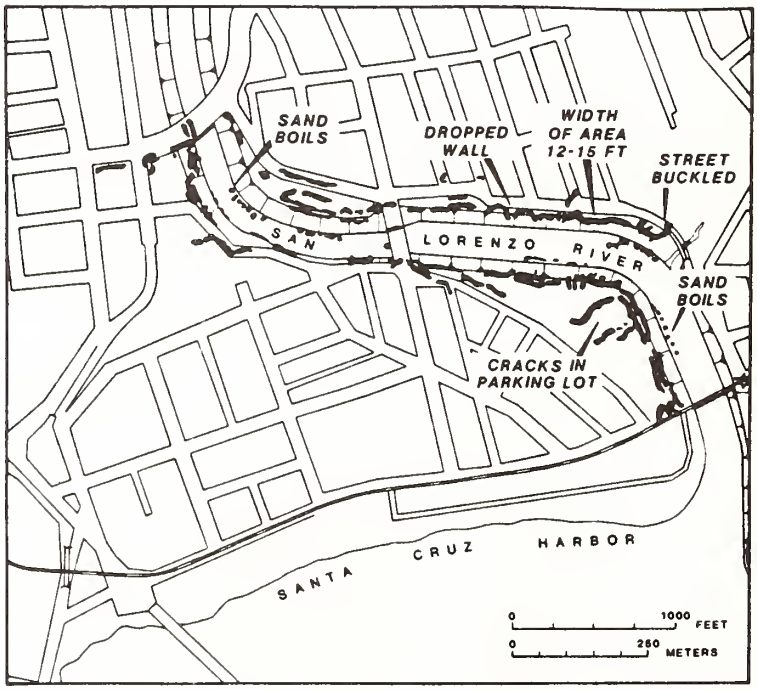

LIQUEFACTION AT LEVEES, MAPPED 20 OCT, 1989

SANTA CRUZ, CA

Figure 14. Patterns of fissures in the levees of the San Lorenzo River in downtown Santa Cruz.

Figure 15. Liquefaction-induced fissures in levee of the Pajaro River, near Watsonville. The fissures were deeper than the height of the levee.

Figure 16. Liquefaction in a field adjacent to the Pajaro River levee near Watsonville. Sand extruded from a linear ground break, with multiple vent holes.

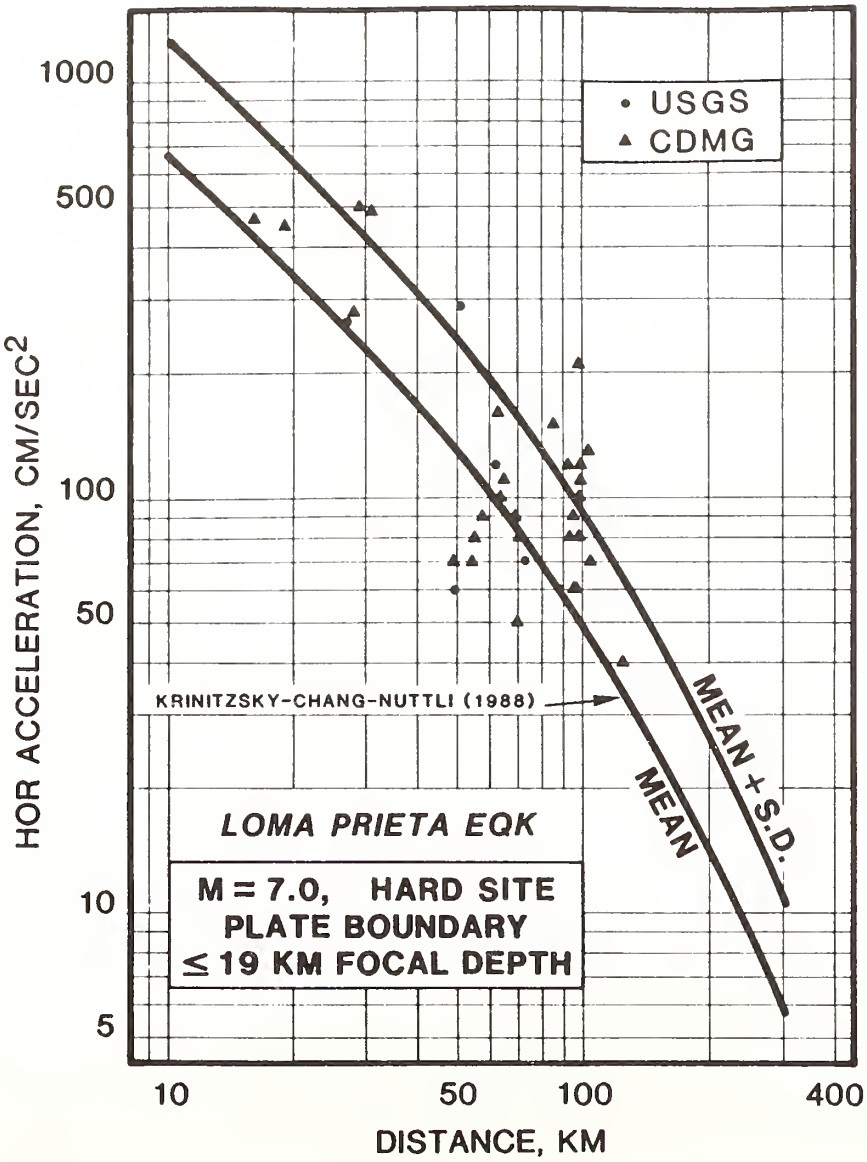

Figure 17. Comparison of Loma Prieta peak horizontal accelerations for hard sites with Krinitzsky-Chang-Nuttli curves for a M = 7.0 earthquake.

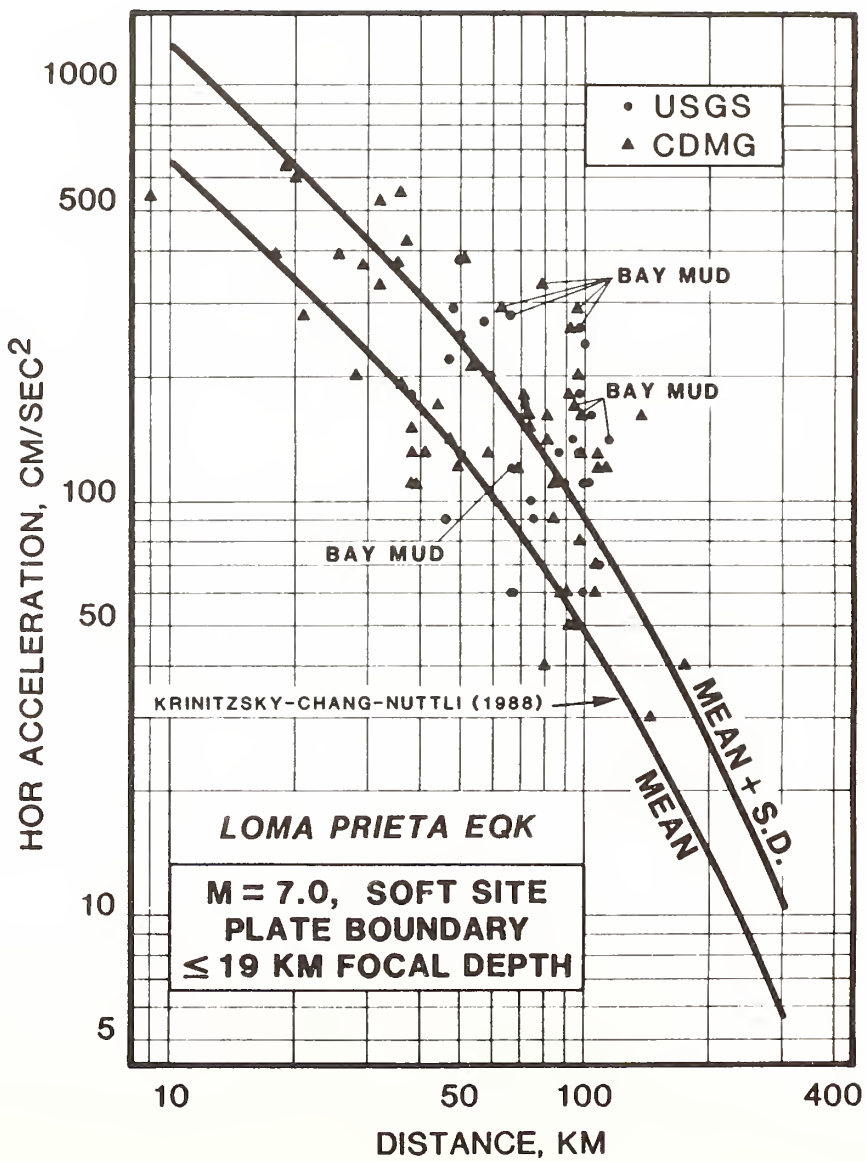

Figure 18. Comparison of Loma Prieta peak horizontal accelerations for soft sites with Krinitzsky-Chang-Nuttli curves for a M = 7.0 earthquake.

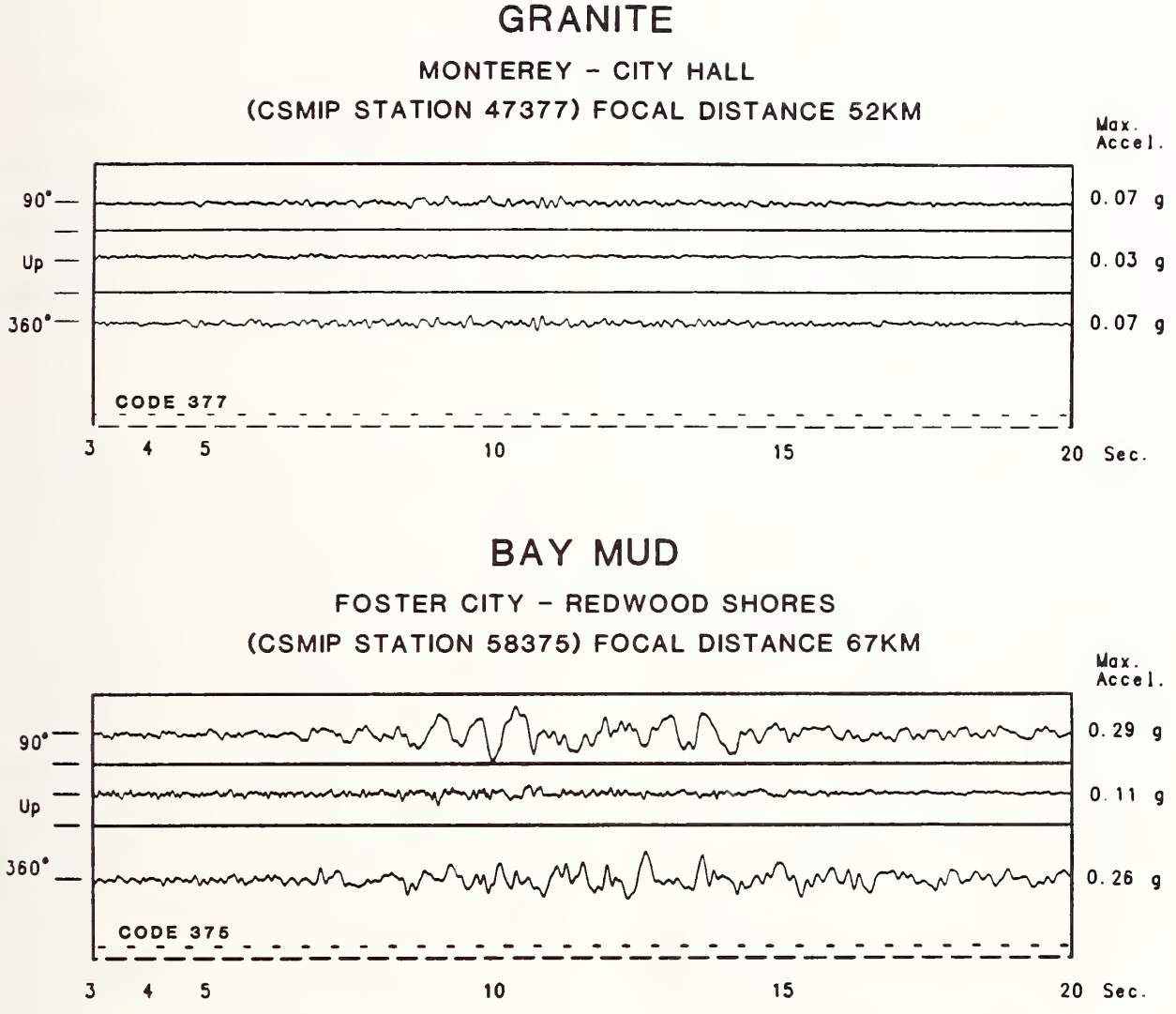

LOMA PRIETA EQK, 1989

Figure 19. Comparison of Loma Prieta accelerograph records for a granite and a bay mud site.

Dam Performance During the Loma Prieta Earthquake of October 17, 1989

by

Robert B. Mac Donald[1]

ABSTRACT

Several dams were damaged and numerous others had records of strong ground motions as a result of the October 17, 1989, magnitude 7.1 Loma Prieta earthquake. The tabulated results of a survey on damage and recorded ground motion are presented. Maximum dam sections and locations of strong motion instruments are shown where possible.

KEWORDS: Dam; earthquake; earthquake damage; Loma Prieta earthquake; strong motion

1. INTRODUCTION

Shortly after 5:00 p.m. on October 17, 1989, the Loma Prieta earthquake (Ms = 7.1) initiated along the San Andreas fault. Shaking from the earthquake was felt over a wide region in west-central California. About a dozen embankment dams near to the epicenter suffered strong shaking; numerous others received only minor shocks. The strong motion phase of shaking lasted only about 12 seconds. There are about 100 dams of various sizes, most of them embankment dams, in a 100-kilometer radius from the epicenter.

Considering the numerous dams in the vicinity, damaged dams were few in number. Numerous strong motion records were recovered from dams in the area; however, some of the severest shaking was not recorded due to lack of instruments. This paper describes the performance of both damaged and undamaged dams. Selected maximum dam sections and locations of strong motion instruments are illustrated where possible. Physical data and performance are tabulated in Tables 1, 2, and 3.

Not all as-built changes from original designs may be shown in the dam sections. In addition, not all instrument records, mapping of cracks and possibly related geologic features, foundation information, and dam design were available at the time of this writing (January-March, 1990).

2. ANTICIPATED TYPICAL PERFORMANCE OF DAMS

Embankment dams are more numerous than concrete dams, hence more records of embankment performance during earthquakes are available. After strong shaking, many embankments exhibit settlement and longitudinal cracks in the crest area. Transverse cracks near to abutments are also common. Changes in seepage and piezometer levels or pressures are not unusual, and over a period of time these earthquake-induced changes often return to "normal."

In general, embankments built of compacted clayey materials, when on a sound foundation, appear to be fairly resistant to earthquake damage. Conversely, embankments of poorly consolidated sands or silts, tailings dams, and dams on liquefiable foundations are highly susceptible to damage.

The record of performance during earthquakes for concrete dams is limited compared to embankments. However, all principal types of concrete dams, including arch, multiple arch, gravity, and buttress, have experienced high peak accelerations, and all types have had at least one example of serious cracking (the arch without earthquake loading). Improvements in design for seismic loading probably would have prevented much of the known concrete dam damage. Foundation conditions appear to have been satisfactory in those concrete dams experiencing damage.

3. RECORDED PERFORMANCES OF DAMS AFFECTED BY THE LOMA PRIETA EARTHQUAKE

The locations of selected dams with some record of performance or close proximity to the earthquake are shown in Figure 1. The names, types, heights, and epicentral dis-

[1]U.S. Bureau of Reclamation
Code D-3610, Building 67
DFC, Denver, CO 80225

tances of these selected dams, are tabulated in Table 1, while damage is tabulated in Table 2.

3.1 Williams Dam

Williams Dam was 10 km from the earthquake epicenter, and this is the shortest epicentral distance for any dam of moderate to large size. The dam is a 21 meter-high concrete gravity dam with a crest length of 27 m and a crest width of 3 m. The upstream face is vertical and the downstream face curves from the crest to the 19 meter-wide base. The dam is on jointed, but sound, conglomerate and it is only 0.6 km from the surface trace of the San Andreas fault. The reservoir is basically silted up and is not fully performing its original function of water storage.

The dam must have experienced strong shaking. It did not have strong motion instruments. There was no damage to the dam; however, shallow rock falls occurred on the abutments.

3.2 Austrian Dam

Austrian Dam, Fig. 2, is a 56 meter-high embankment located 12 km from the earthquake epicenter. Austrian Dam was originally designed as a zoned embankment, but was constructed as a homogeneous dam. It had more damage than any other dam affected by the Loma Prietra earthquake. During the earthquake, the embankment settled up to 85 cm over the right two thirds of the dam, while the right end of the dam moved 37 cm downstream. A maximum upstream movement of 15 cm was recorded at the left quarter point of the crest. Longitudinal cracks up to 4-1/2 meters deep formed on the upper 25 percent of the upstream dam face, while shallower longitudinal cracks covered much of the downstream face. Transverse cracks occurred in the embankment near both abutments, and were the only cracks in the dam crest. Right-side transverse cracking near the spillway was 4-1/2 meters deep. It is felt that this transverse cracking is more severe than would be expected for the amount of settlement.

On the right abutment, a reinforced concrete spillway, with its left wall in contact with the embankment, suffered severe to minor cracking throughout its entire length (headworks, chute, and terminal structure). Due to tension cracks transverse to the spillway axis as well as downstream movement, the entire spillway structure seems to have elongated by about 30 cm. Excavations along the left spillway wall revealed that at least part of the spillway chute and spillway wall separated from the foundation and the embankment probably because of side-to-side rocking. In addition, some voids were created under the upper spillway floor (as determined by drilling). The 8 meter-high spillway wall may have accentuated the rocking.

The embankment and spillway were thoroughly investigated by surface mapping, trenching, and drilling, and by checking piezometers and surface measuring points. Coincidentally, measurement surveys had been run the day before the earthquake. Dam settlement, lateral movements, and piezometric changes due to the earthquake are shown in Figs. 2 and 3.

Significant rises in the water levels, Fig. 2, in four piezometers in the dam were noted after the earthquake. Piezometer No. 6 rose to above the existing reservoir level. The water levels were trending back to "normal" by late October; however, subsequent construction activities on the dam damaged some of the piezometers and further water level observations are incomplete. The cause of the water rise in the piezometers is not known, but it is speculated that embankment pore water was expelled into the piezometer pipes because of high pore pressures dynamically induced during the earthquake shaking. The piezometers consist of slotted pipe with a sand filter sealed in 5-foot intervals with a 3/4-inch open riser pipe to the surface. Rainfall was not a factor in the water level changes, because the observations were made several days apart when there was no rain.

Perched water is known to exist in the dam, probably a consequence of layering in the embankment and former high reservoir levels. Water was observed to have gushed out of the embankment in several of the post-earthquake investigation trenches, and is generally attributed to the perched water trapped in the layers.

Since the start of the rainy season was imminent, repair to the embankment and spillway were expedited. In early November a temporary repair of the spillway was initiated. Epoxy grouting was used in spillway cracks where feasible; however, where cracks were too wide, Portland cement grout was used. Many of the cracks have had only a surface treatment, but drill core samples indicate good penetration of the epoxy grout. The spillway damage will be reevaluated in 1990 and there is a potential of more repair or even replacement.

Cracked embankment material and cracked foundation near the spillway was excavated and replaced by compacted embankment. Material to a depth of nearly 8 meters was removed on the right and left sides of the embankment near the abutments. Minor curtain grouting was done in the left abutment.

A 1972 analysis estimated that 1-1/2 to 3 meters of settlement would result during strong motion occurring during a magnitude M = 8.3 earthquake. The maximum 85 cm of settlement for a magnitude M = 7.1 earthquake reasonably approximated the 1972 estimate; however, the transverse cracking was more severe than expected.

3.3 Almaden Dam

Almaden Dam, Fig. 4, is a 34 meter-high embankment built in 1936 and located 15 kilometers from the epicenter. It has an upstream impervious zone covered with reinforced concrete paving and a downstream pervious zone. Earthquake damage was negligible. Minor longitudinal cracking was found in the upstream embankment face near the edge of the concrete face paving. No repairs were necessary.

3.4 Guadalupe Dam

Guadalupe Dam, Fig. 5, is a 43 meter-high embankment built in 1935 and located 18 kilometers from the epicenter. It has an upstream impervious zone faced with reinforced concrete slabs and a downstream pervious zone. A modification was made to the dam in 1972 by removing concrete slabs from the upstream toe and placing a lightly-compacted, clayey buttress berm against the upstream slope. This berm, not shown in Fig. 5, was placed up to elevation 570 feet, which just overlaps the concrete slabs facing the upper part of the slope.

The earthquake caused primarily longitudinal cracking up to 2 1/2 cm wide on the upper 4 meters of the berm. These longitudinal cracks had a maximum depth of about 1.3 meters. By the time repair work was initiated, some of these cracks were 10 cm wide. Transverse cracks occurred in the embankment crest near the right and left abutments. Discontinuous minor longitudinal cracks occurred on the crest and were confined to 60 cm downstream from a crest floodwall. Minor cracking, spalling, and offset occurred in the concrete panels on the upstream face. Settlement amounted to 20 cm and there was 5 cm of transverse movement upstream.

The cracked berm material was subsequently removed, replaced, and recompacted.

3.5 Newell Dam

Newell Dam, Fig. 7, is a 55 meter-high embankment built in 1960 and located 19 km from the epicenter. Newell Dam has a central impervious core with an upper pervious and a lower random zone upstream and a random zone downstream. The spillway is on the left abutment. A sloping intake structure for the outlet works is along the left side upstream dam face and connects to the former diversion conduit in the dam base.

During the earthquake, longitudinal cracks developed high in the upstream slope (Fig. 7). Minor spalling occurred inside the sloping outlet works intake structure; in addition, there was local separation of the intake structure and embankment. Embankment and foundation seepage measured at the downstream toe was found to have increased.

Since the earthquake, excavation and recompaction of the cracked area has been completed. The spalling that occurred in the intake structure will not be repaired at this time. The foundation seepage has nearly returned to normal.

3.6 Elmer J. Chesbro Dam

Elmer J. Chesbro Dam, Fig. 6, is a 29 meter-high embankment built in 1955 and located 19 km from the epicenter. Elmer J. Chesbro Dam is a compacted "homogeneous" earthfill embankment with more-pervious materials selected for upstream and less-impervious selected for dowmstream. It has a 1.2 meter-thick riprap shell on the upstream slope and a loose rockfill berm at the downstream toe. The rockfill in the berm is separated from the earth embankment by a 1.2 meter-thick gravel drain. The outlet works under the dam is basically a 1.4 m (56 inch) I.D. welded steel pipe in a reinforced concrete jacket and placed on rolled embankment material. The detached spillway is on the right abutment.

During the earthquake, a 97 meter-long discontinuous longitudinal crack, up to 10 cm wide and 2.4 meters deep, occurred on the upstream shoulder of the dam crest. Vertical offset along the crack was 6 cm down on the upstream side. The cause of the crack is attributed to settlement of the cohesionless upstream riprap shell. Transverse cracks up to 1.4 m deep occurred at the right end of the crest. Transversely oriented cracks also occurred in the natural ground of the

spillway approach near to a steep shoulder of the right abutment. An outlet works inspection after the earthquake disclosed cracks in welds in two joints of the steel pipe; however, these cracks appeared to be of pre-earthquake origin. Crest settlement was up to 11 cm.

The cracked embankment was excavated and, together with added material, replaced and recompacted.

3.7 Lexington Dam

Lexington Dam, Fig. 8, is a 62 meter-high embankment built in 1953 and located 21 km from the epicenter. Lexington Dam has a thick central impervious core. The upstream zone, originally intended to be a pervious zone, is actually a random zone containing impervious materials, as allowed by a specification change. Downstream is a zone of random semi-pervious materials. A narrow filter zone with its base on a French drain lies between the core and downstream semi-pervious zone. The outlet works extends under the embankment. Bedrock consists mostly of Franciscan sandstone and shale.

During the earthquake, transverse cracks occurred in the embankment and natural ground at both abutments. On the left side along the downstream groin a 58 meter-long, discontinous, transverse, embankment crack system, with individual cracks up to 2 cm wide averaged about 2 m deep. This cracking appears to have been controlled by the steep abutment-embankment contact. On the right side transverse cracks were both upstream and downstream of the crest, but were confined to natural ground (colluvium and highly weathered rock). A continuous primary crack on the right side from downstream to upstream of the crest reached a maximum width of 2 cm, averaged about 2 m in depth, and was about 137 meters long. Further upstream from this primary crack, other cracks were discontinuous for another 85 m. Minor longitudinal cracks were found on both upstream and downstream faces of the embankment. Maximum crest settlement was 26 cm and downstream movement was 8 cm. An outlet works inspection after the earthquake disclosed a 9 meter-long bulge in the 1.5 meter (50 inch) steel pipe; however, the bulge was determined to be of pre-earthquake origin. A temporary rise in foundation hydrostatic pressure was reported.

Excavation, replacement, and recompaction of the cracked areas have been completed.

The Loma Prieta earthquake shaking is well-documented at Lexington Dam by an extensive array of strong motion instruments. The layout and maximum accelerations recorded by these instruments are shown in Fig. 8. The maximum crest accelerations transverse and parallel to the dam axis were 0.45g and 0.40g, respectively.

3.8 Vasona Percolation Dam

Vasona Percolation Dam, Fig. 9, is a 10 meter-high embankment, built in 1935 and located 24 km from the epicenter. Vasona Percolation Dam has an upstream impervious zone with a cutoff trench that is deep relative to the dam height. The upstream slope of this impervious zone has a concrete facing. Several pervious to semi-pervious zones are downstream.

During the earthquake, some transverse cracking occurred in the embankment near the right abutment. The cracking pattern was primarily longitudinal; cracks up to 6 meters long formed along 146 m of the right embankment crest. All of the cracking was found to be relatively shallow (maximum depth = 1.7 m) and the dam remained in a normal operation mode.

The cracked embankment was excavated and recompacted.

3.9 Rinconada Reservoir Embankment

The offstream embankment for Rinconada Reservoir is 12 m in height and was built in 1969. This reservoir is 26 km from the epicenter.

The embankment was undamaged during the earthquake. However, the outlet works, which is located on natural ground apart from the embankment, incurred damage near its intake. The walls of a vault, having a nozzle intake from the reservoir, were cracked. The cracks in the asphalt-coated concrete walls of the vault allowed water to pass from the vault into pervious backfill.

The reservoir was drained and repairs to the walls of the vault have been completed.

3.10 Leroy Anderson Dam

Leroy Anderson Dam, Fig. 11, is a 72 meter-high embankment built in 1950 and located 27 km from the epicenter. Leroy Anderson Dam has an upstream impervious zone, and semi-pervious and pervious zones downstream.

During the earthquake longitudinal cracks occurred in the asphalt crest roadway. The cracks may be related to a transition zone between the impervious zone upstream and more pervious zones downstream that underlies the crest. The cracks were about 1/2 cm wide at their maximum and had a maximum depth of about 61 cm. This damage is very slight. Pavement sealing by patching has been completed.

The dam is well-instrumented to record strong motion (Fig 11). The maximum transverse acceleration recorded on the crest was 0.43g and at the toe was 0.23g.

3.11 Coyote Dam

Coyote Dam is a 42 meter-high rolled earth and rockfill embankment built in 1936 and located 31 km from the epicenter. There was no damage at the dam from the earthquake. Coyote Dam has, however, strong motion instruments associated with it. A southwest "abutment" site recorded a maximum acceleration of 0.49g. A downstream site had a maximum acceleration of 0.19g.

3.12 Cherry Flat Dam

Cherry Flat Dam is an 18 meter-high embankment completed in 1936 and located 42 km from the epicenter. There was no damage at the dam from the earthquake. An orthogonal self-contained strong motion instrument was in operation on the left abutment. The instrument recorded maximum accelerations of 0.09g, 0.07g, and 0.06g in directions parallel to the dam axis, transverse to the dam axis, and up, respectively.

3.13 San Justo Dam

San Justo Dam, Fig. 10, is a 46 meter-high zoned embankment completed in 1987 and located 46 km from the epicenter. There was no damage to the dam nor any found in the immediate area of the reservoir; however, measurements from survey points located along the crest of the dam indicate that up to 4 cm of settlement occurred during the earthquake. A temporary rise in foundation hydrostatic pressure was reported.

The dam has an array of strong motion instruments (Fig. 10). Maximum axial acceleration occurred in the center of the crest and was 0.39g while axial acceleration at the downstream toe was 0.16g. Maximum transverse acceleration was also at the center of the dam crest and was 0.50g while transverse acceleration at the toe was 0.26g.

3.14 Del Valle dam

Del Valle Dam is a 68 meter-high embankment completed in 1968 and located 66 km from the epicenter. There was no earthquake damage in the area of the dam. Strong motion instruments are located on the dam crest and at the downstream toe. Maximum axial accelerations were 0.08g on the crest and 0.06g at the downstream toe. The maximum transverse accelerations were 0.08g at the crest and 0.04g at the toe; the axial accelerations were 0.08g at the crest and 0.06g at the toe.

3.15 Lower Crystal Springs Dam

Lower Crystal Springs Dam (Fig. 12) is a 43 meter-high concrete gravity structure completed in 1888 and located 69 km from the epicenter. There was no earthquake damage in the area of the dam. Strong motion recording instruments are on the crest, left abutment, downstream toe, and downstream as shown on the plan and section in Fig. 12. The maximum crest acceleration was a transverse acceleration of 0.10g near the left abutment; the accelerometer in the center of the crest malfunctioned. At the downstream toe of the dam, both the axial and transverse maximum accelerations were 0.05g.

4. CONCLUSIONS

Considering the proximity of numerous dams to the epicenter of the major Loma Prieta earthquake, very few of these structures were adversely affected. Eight dams or their appurtenant structures sustained damage, which ranged from serious to very minor. The greatest damage occurred at Austrian Dam where large settlements and cracks occurred and the spillway was badly damaged.

There were two factors which contributed to the limited damage. The first was the short period of strong motion shaking, only about 12 seconds. The second was the timing of the earthquake. The earthquake occurred in the third year of below-average rainfall as well as in fall when reservoirs were drawn down to low levels to satisfy water demands of the warm summer season.

Certain effects consistent in the performance of embankment dams during earthquakes were documented. Longitudinal cracking and embankment settlement, two common responses to strong earthquake shaking at earthen and rockfill structures, occurred at a number of dams close to the epicenter of the Loma Prieta earthquake. Many transverse cracks also occurred, and these features are of some concern to dam safety. Temporary

fluctuations in piezometric levels were documented for Austrian Dam and reported for two other dams. Two concrete gravity dams that are discussed had no damage.

5. ACKNOWLEDGEMENTS

The author is appreciative of field notes and information from Don Babbitt, Dapartment of Water Resources, State of California, and gratefully acknowledges the information and reports provided by Robert Tepel of the Santa Clara Valley Water District.

6. REFERENCES

1. Maley, R. et al, 1989, U.S. Geological Survey strong-motion records from the northern California (Loma Prieta) earthquake of October 17, 1989: U.S. Geological Survey Open-file Report 89-568.

2. Meigh, A. C., 1980, Geotechnical Invesigations for Dams, Proc. of International Symposium on Geotechnical Problems and Practice of Dam Engineering, Asian Institute of Technology, Bangkok, 163-181.

3. Plafker, George, and Galloway, John P., Editors, 1989, Lessons learned from the Loma Prieta, California, earthquake of October 17, 1989: U.S. Geological Survey Circular 1045.

4. Shakal, A. et al, 1989, CSMIP strong-motion records from the Santa Cruz Mountains (Loma Prieta), California earthquake of 17 October 1989: Report No. OSMS 89-06, California Strong Motion Instrumentation Program.

5. R. L. Volpe & Associates, 1990, Investigation of SCVWD Dams Affected by the Loma Prieta Earthquake of October 17, 1989, Los Gatos, CA.

6. USCOLD Committee on Earthquakes, Performance of Dams During Earthquakes, in preparation.

Table 1. List of Selected Dams

Dam Name	Type Dam	Height		Epicentral Distance		Year Complete	Damage	Strong Motion Record
		ft	m	mi	km			
Williams	Concrete Gravity	69	21	6	10	1895	None	No
Austrian	Embankment	185	56	7	12	1950	Severe	No
Almaden	Embankment	110	34	9	15	1936	No	No
Guadalupe	Embankment	142	43	11	18	1935	Yes	No
Newell	Embankment	182	55	12	19	1960	Yes	No
Elmer J. Chesbro	Embankment	95	29	12	19	1955	Yes	No
Lexington	Embankment	205	62	13	21	1953	Yes	Yes
Vasona Percolation	Embankment	34	10	15	24	1935	Yes	No
Rinconada Reservoir	Embankment	40	12	16	26	1969	Yes	No
Leroy Anderson	Embankment	235	72	17	27	1950	Minor	Yes
Coyote	Embankment	140	43	19	31	1936	No	Yes
Cherry Flat	Embankment	60	18	26	42	1936	No	Yes
San Justo	Embankment	147	46	29	46	1987	No	Yes
Del Valle	Embankment	222	68	41	66	1968	No	Yes
Lower Crystal Springs	Concrete Gravity	140	43	43	69	1888	No	Yes

Table 2. Earthquake Effects on Embankments

Dam Name	Cracks		Maximum Settlement	Maximum Transverse Movement	Other
	Longitudinal	Transverse			
Austrian	u/s & d/s faces	in embank. near both abutments	85 cm	37 cm d/s 15 cm u/s	piezometer level rise, spillway cracking and separation from foundation
Almaden	minor on u/s embank. face	none	not known	not known	
Guadalupe	on u/s berm, minor along crest	in embank. near both abutments	20 cm	2 cm d/s 5 cm u/s	concrete facing slabs u/s have minor cracking, spalling, and offset
Newell	high on u/s slope	none	not known	not known	interior spalling and local separation from foundation of sloping intake structure
Elmer J. Chesbro	along u/s crest shoulder	at contact of crest and right abutment	11 cm	0.3 cm d/s 1.5 cm u/s	crack in natural ground of left abutment along shoulder of steep abutment
Lexington	minor on u/s & d/s faces	in embank. left side, in natural ground on rt. side	26 cm	7.6 cm d/s 4.3 cm u/s	cracking near boathouse, near spillway bridge, along spillway, and in natural ground near intake structure, foundation hydrostatic pressure rise reported
Vasona Percolation	right side embankment crest	minor in embankment near right abutment	5 cm	3 cm d/s none u/s	
Rinconada Reservoir	none	none	not known	not known	cracked walls in separate outlet works vault
Leroy Anderson	intermittent along crest	none	4 cm	2 cm d/s 1.5 cm u/s	
San Justo	none	none	4 cm	not significant	temporary peizometer water level rise reported

Table 3. Maximum Accelerations (g) Experienced at Instrumented Dams

Dam Name	Direction	Crest	Toe	Other
				Left Abutment
Lexington	Axial	0.40	None	0.41
	Transverse	0.45		0.45
	Vertical	0.22		0.15
				Left Abutment (rock)
Leroy Anderson	Axial	0.32	0.18	0.08
	Transverse	0.43	0.23	0.07
	Vertical	0.16	0.16	0.05
				Left Abutment
Coyote	Axial		0.17	0.15
	Transverse		0.19	0.49
	Vertical		0.10	0.08
				Left Abutment
Cherry Flat	Axial			0.09
	Transverse			0.07
	Vertical			0.06
				Embankment near Left Abutment
San Justo	Axial	0.39	0.16	0.30
	Transverse	0.50	0.26	0.24
	Vertical	0.32	-	0.24
Del Valle	Axial	0.08	0.06	
	Transverse	0.08	0.04	
	Vertical	0.07	0.03	
				Left Abutment
Lower Crystal Springs	Axial	None	0.05	0.07
	Transverse	0.10	0.05	0.09
	Vertical	0.03	-	0.03

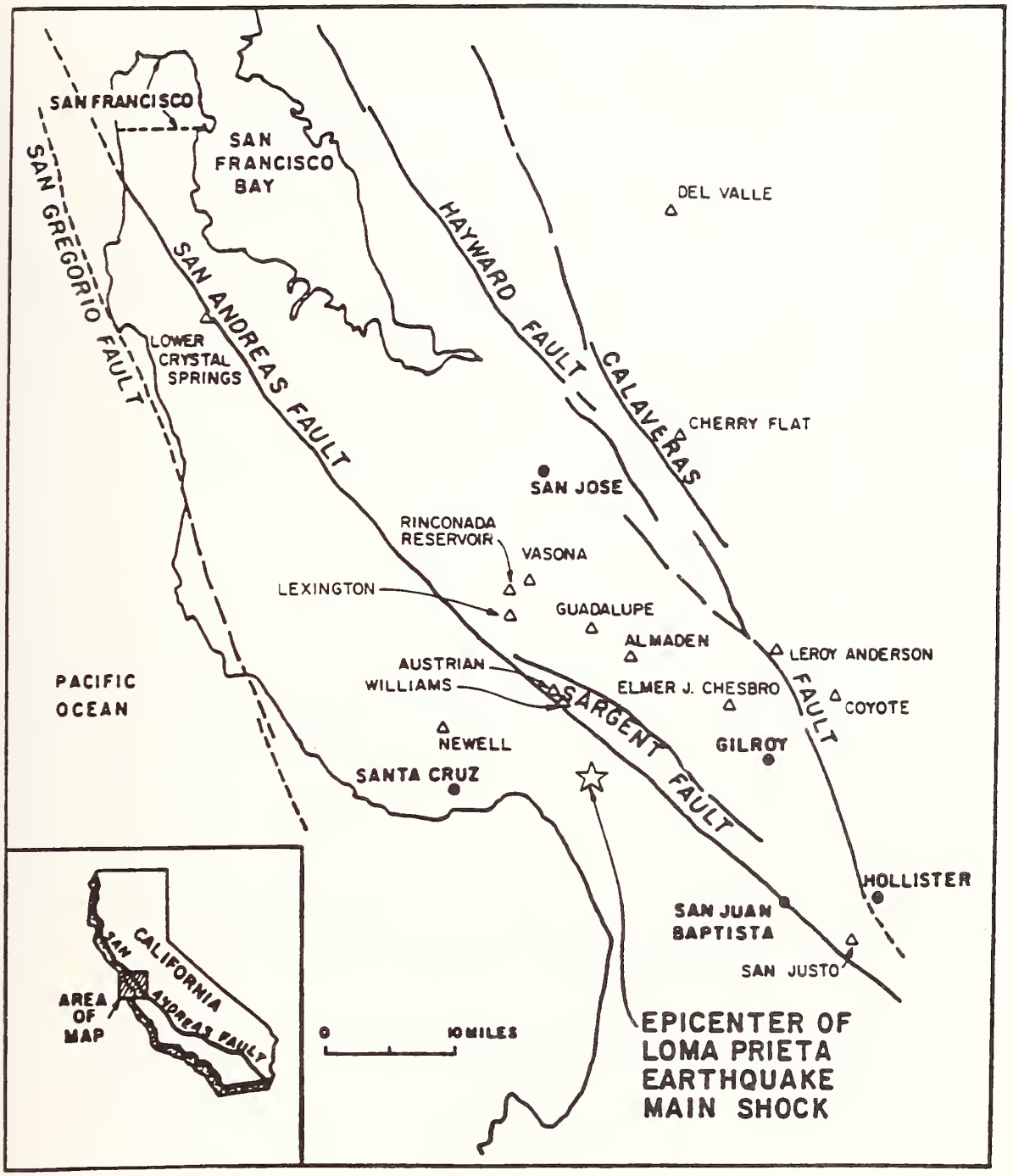

Fig. 1. Location of selected dams affected by the October 17, 1989, Loma Prieta earthquake with the earthquake epicenter shown. The earthquake was caused by rupture along the San Andreas fault. The epicenter is to the southwest of the fault since, in this area, the fault dips about 70 degrees southwest and the initiating rupture was at a depth of 18 km.

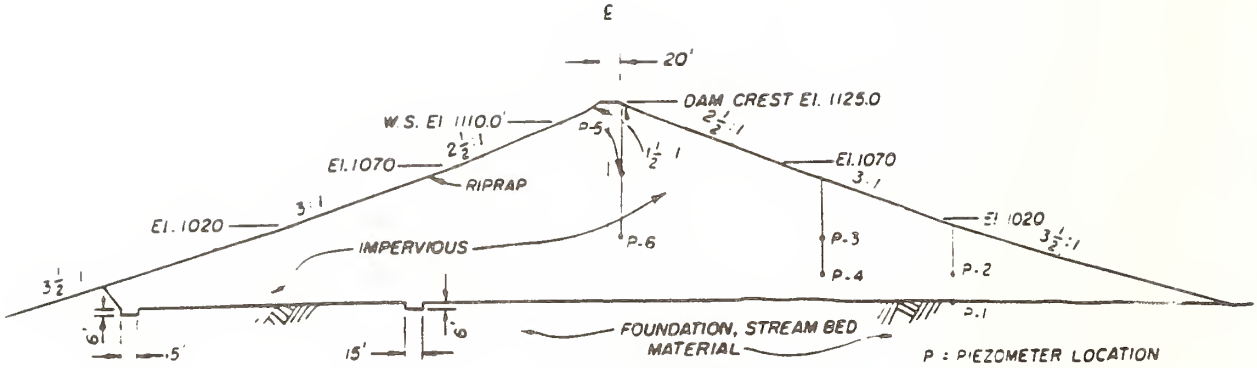

a.

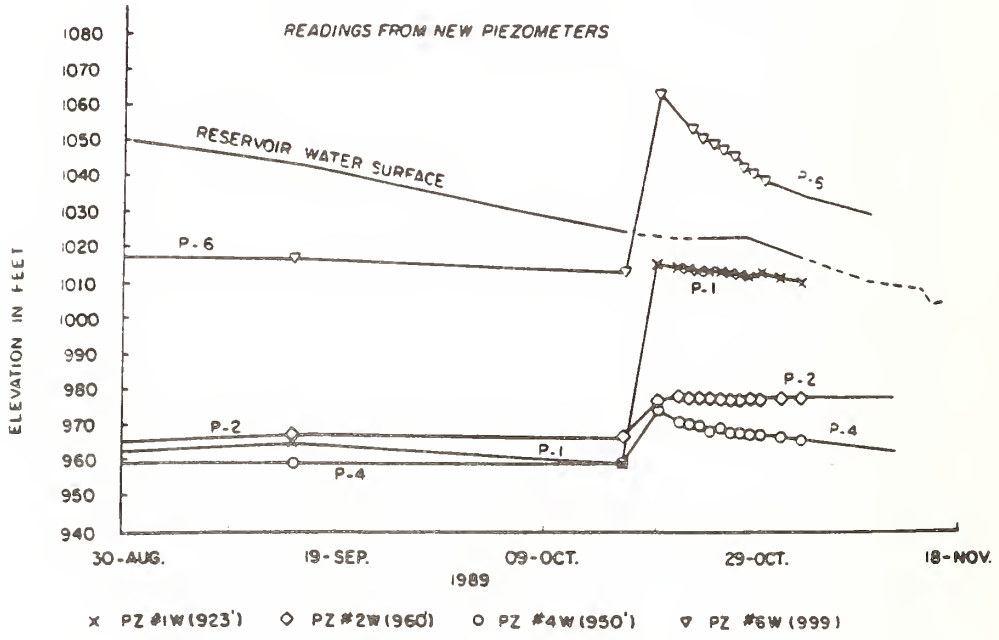

b.

Fig. 2. Austrian Dam. a. shows typical section and b. shows piezometer readings before and after earthquake.

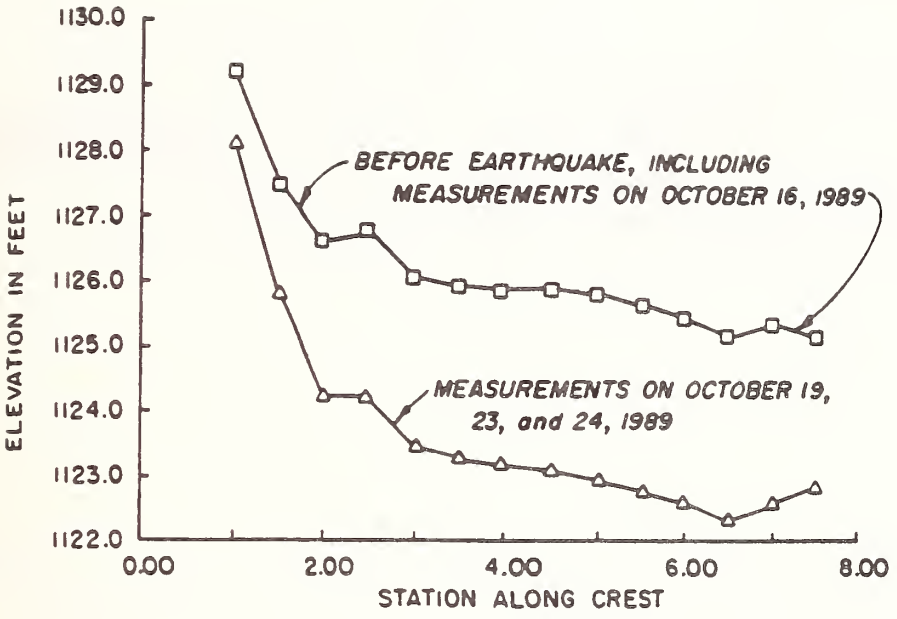

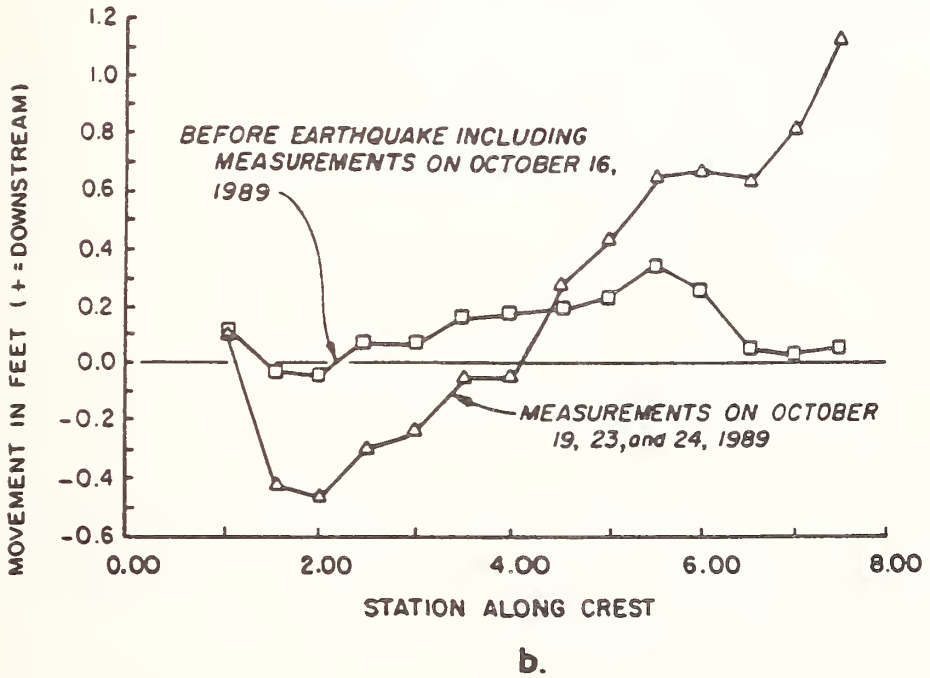

Fig. 3. Austrian Dam. a. Shows cumulative settlement along dam crest just before and after October 17, 1989, earthquake. b. Shows horizontal transverse movements of crest survey points just before and after earthquake.

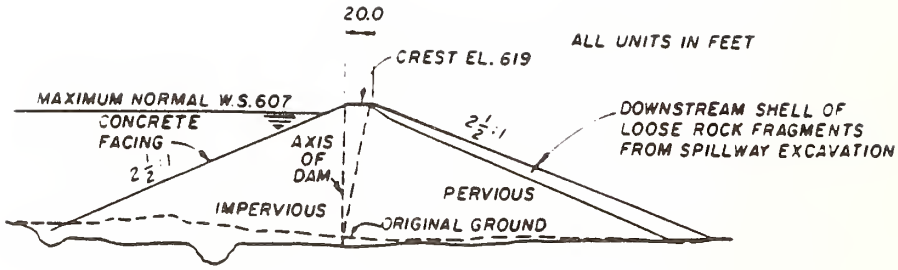

Fig. 4. Almaden Dam. Typical section.

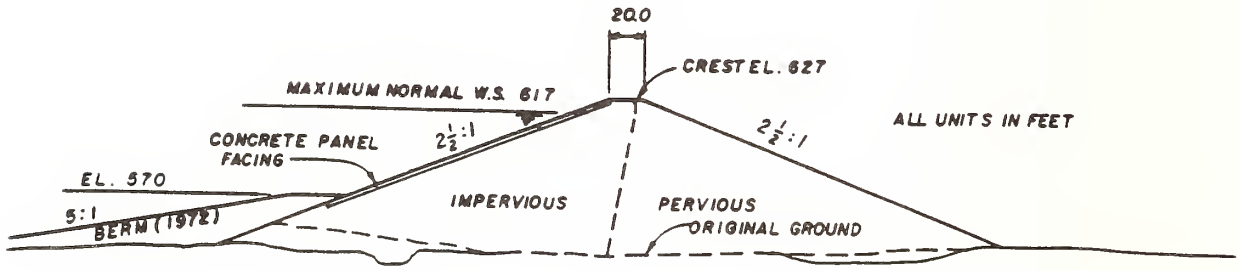

Fig. 5. Guadalupe Dam. Typical section.

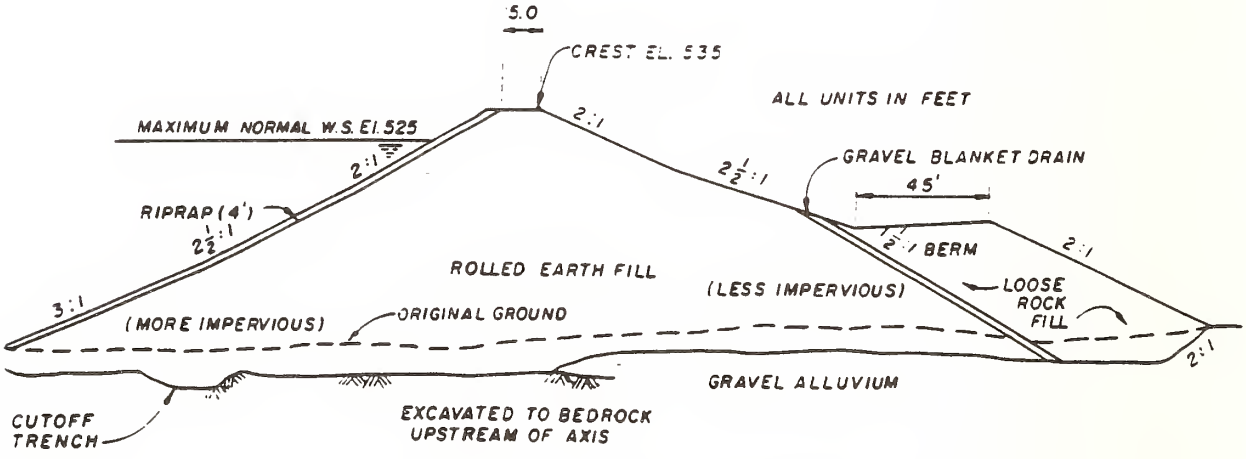

Fig. 6. Elmer J. Chesbro Dam. Typical section.

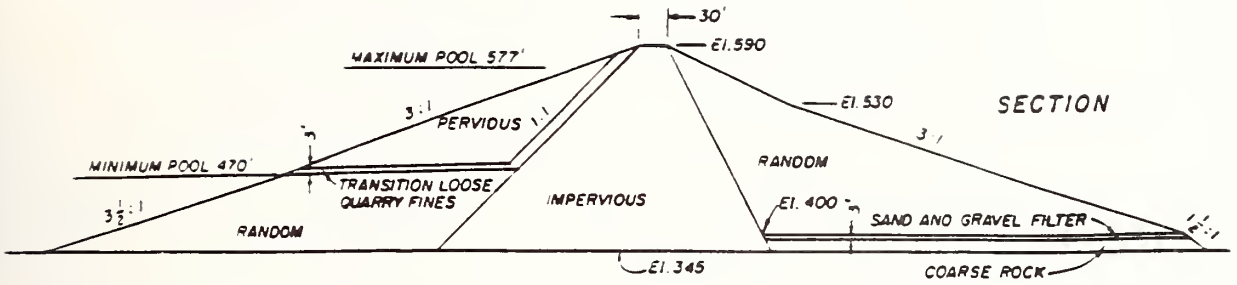

a.

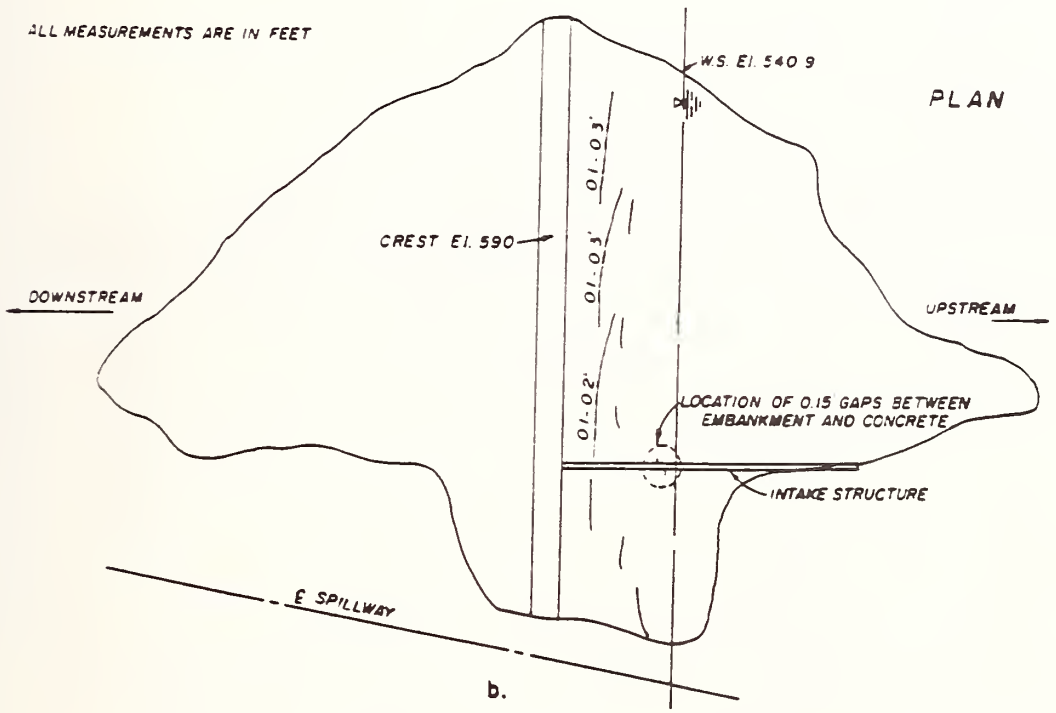

b.

Fig. 7. Newell Dam. a. Typical section. b. Plan of dam showing longitudinal cracks along upper upstream face.

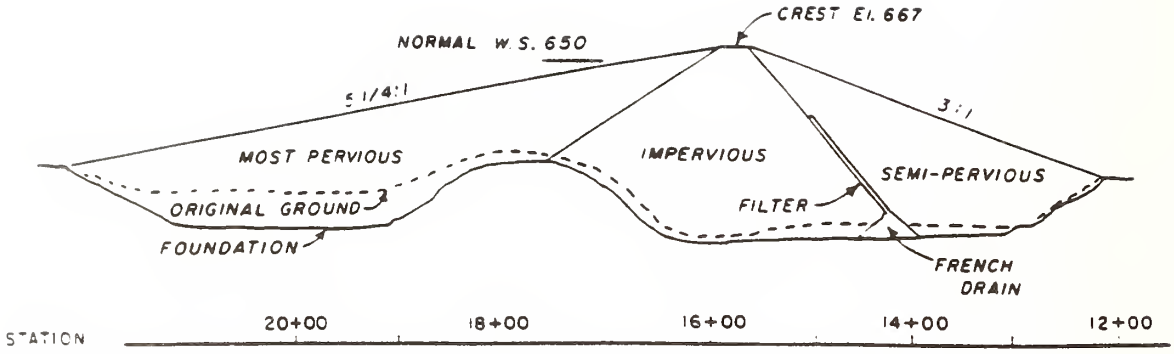

a.

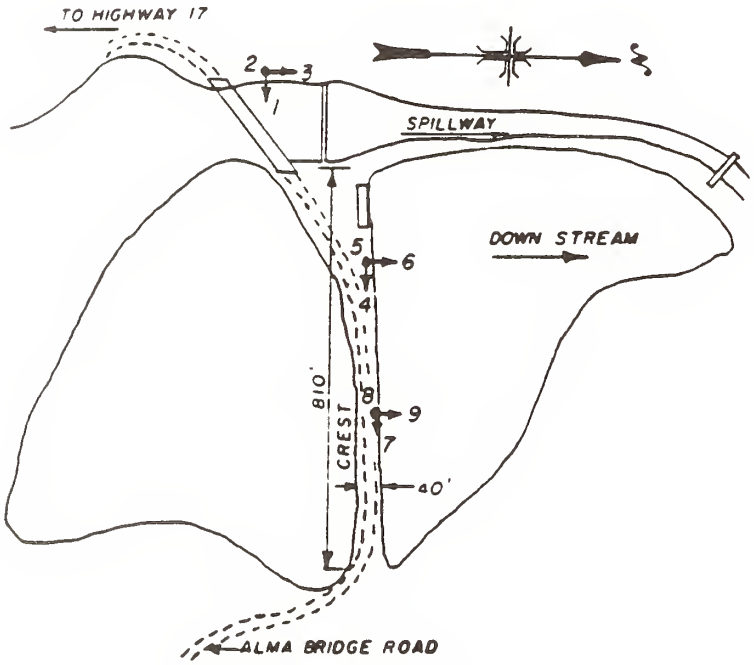

SENSOR NO.	MAX ACCEL. (g)
1	0.41
2	0.15
3	0.45
4	0.40
5	0.22
6	0.39
7	0.34
8	0.20
9	0.45

b.

Fig. 8. Lexington Dam. a. Typical section. b. Plan of dam showing location of strong-motion instruments and table of maximum accelerations of strong-motion instruments.

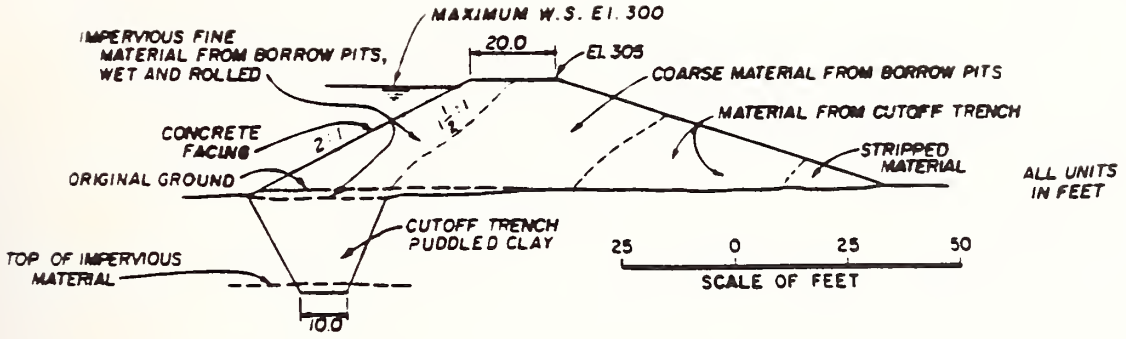

Fig. 9. Vasona Percolation Dam. Typical section.

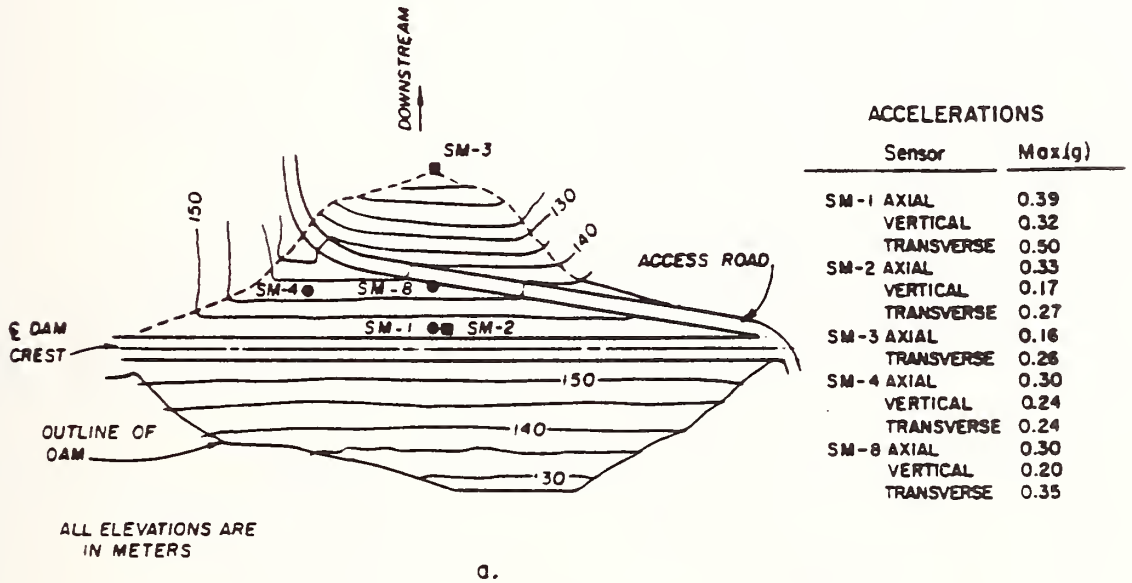

a.

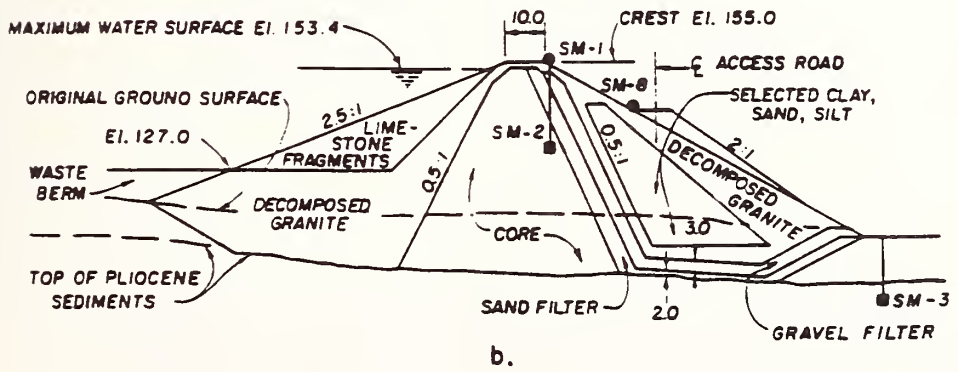

b.

Fig. 10. San Justo Dam. a. Plan view showing location of strong-motion instruments and table of maximum accelerations during the October 17, 1989, main earthquake event. b. Typical section, also showing location of strong-motion instruments.

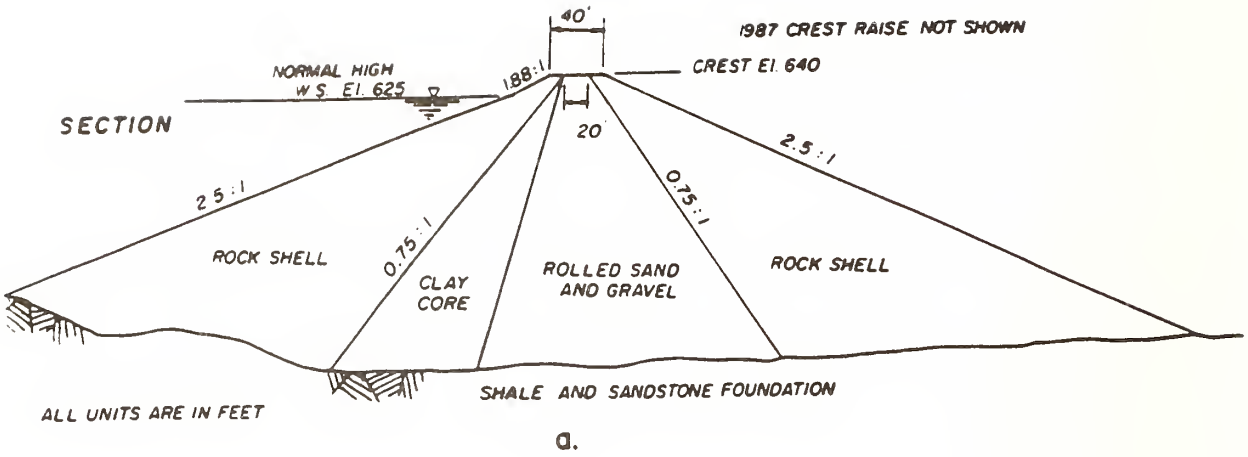

a.

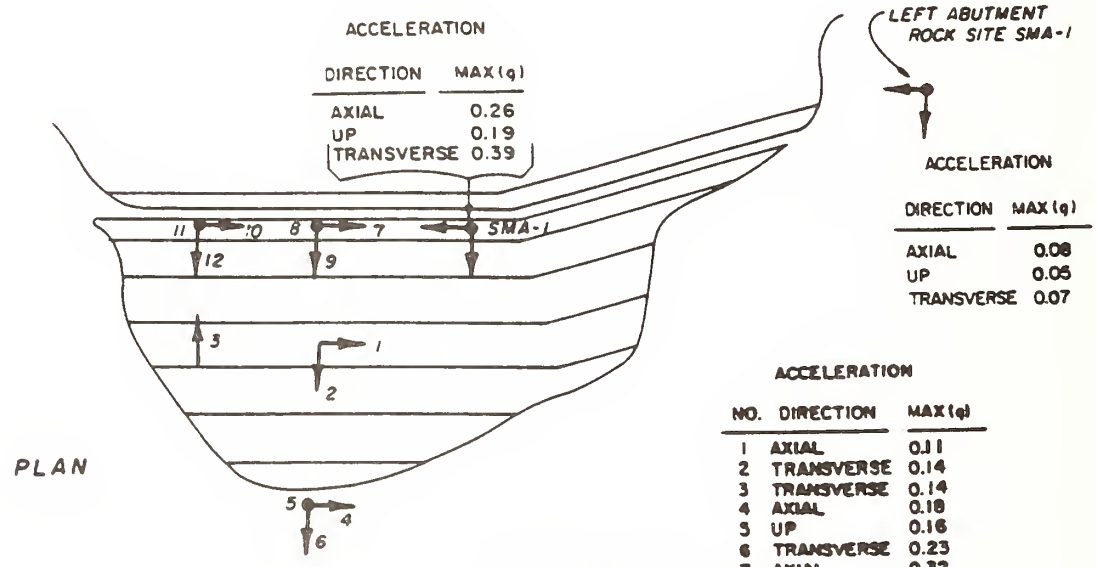

b.

Fig. 11. Leroy Anderson Dam. a. Typical section. b. Plan of dam showing locations of strong-motion instruments and tables showing maximum accelerations during the October 17, 1989, earthquake.

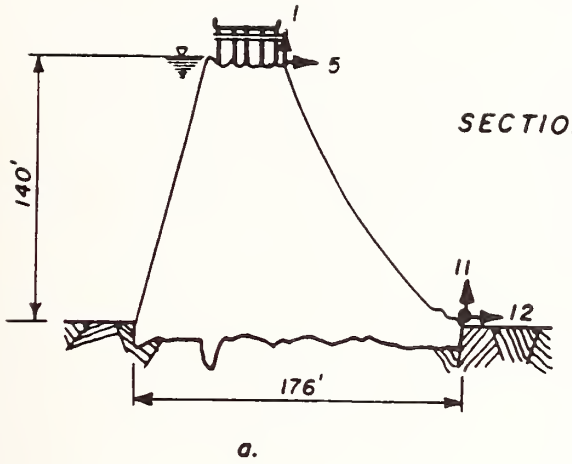

a.

SENSOR NO.	MAX ACCEL. (g)
1	0.03
2	0.07
3	0.10
4	0.07
5	Malfunction
6	0.07
7	0.06
8	0.03
9	0.09
10	0.05
11	Malfunction
12	0.05
13	0.09
14	0.03
15	0.07

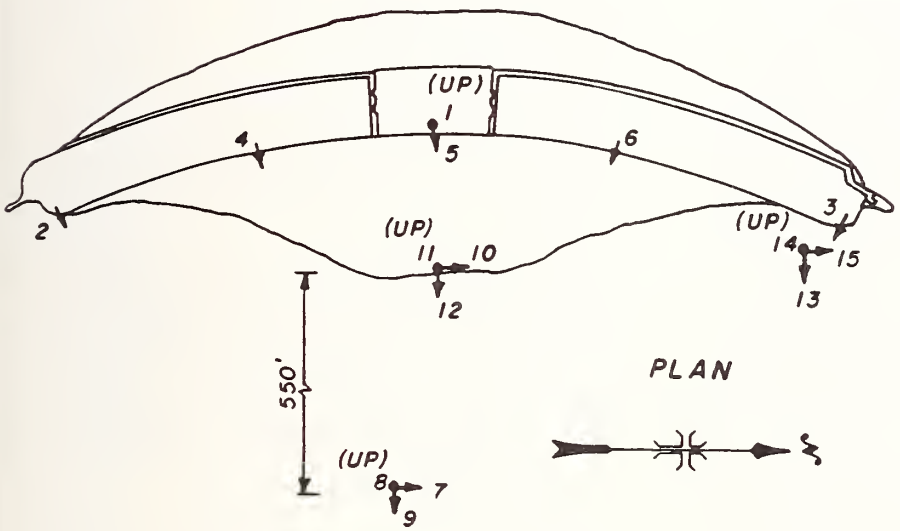

b.

Fig. 12. Lower Crystal Springs Dam. a. Typical section showing locations of strong-motion instruments and table of maximum accelerations during the main event of the October 17, 1989, earthquake. b. Plan of dam showing locations of strong-motion instruments.

Performance of Wood-Framed Structures in the Loma Prieta Earthquake

by

John Tissell, P.E.[1]

ABSTRACT

The performance of wood-framed buildings in the Loma Prieta earthquake was investigated by a team of engineers from the Technical Services Division of the American Plywood Association. The purpose of the investigation was to determine if deficiencies in the building code were a factor in building damage. All of the damaged buildings examined were either built prior to the addition of seismic requirements to the code or were constructed with obvious nonconformance to building code requirements. Most failures were caused by lack of connections to the foundation, or lack of lateral stiffness in the first floor or in short "pony" or cripple walls between the foundation and the first floor.

KEYWORDS: Building Code; Connections; Earthquake; Shear Walls; Wood-framed.

1. INTRODUCTION

In the late afternoon of October 17, 1989 a strong earthquake was felt throughout the San Francisco Bay area. The earthquake, subsequently known as the Loma Prieta earthquake, registered 7.1 on the Richter scale. Much publicity was given to the collapse of a section of the double-decked Nimitz freeway in Oakland where the majority of fatalities occurred, and to the Marina district in San Francisco where a number of outdated residential buildings were destroyed, either by the earthquake or by the ensuing fire resulting from broken gas lines.

Other areas reporting heavy damage were Santa Cruz County, location of the earthquake's epicenter, and the town of Los Gatos, near the Santa Cruz Mountains. Farther north on the San Francisco peninsula, several homes in the Los Altos Hills area received heavy damage.

On October 23, a team of three engineers from the Technical Services Division of the American Plywood Association traveled to the San Francisco Bay area to spend several days observing the effects of the earthquake on wood construction. Those participating were Daniel H. Brown, John R. Tissell and William A. Baker. The primary objective was to determine if deficiencies may exist in building codes published subsequent to the Sylmar quake in the San Fernando Valley of California in 1971. The Sylmar earthquake resulted in several building code changes designed to strengthen buildings against severe lateral forces.

The team discovered in short order that damage was quite widely scattered. Vast areas between the highly publicized damage zones appeared to have little or no structural damage from the earthquake.

2. CONVENTIONAL WOOD-FRAMED BUILDINGS

The epicenter of the earthquake was located in the Santa Cruz Mountains near the Loma Prieta school. The quake opened up several ground fissures of considerable length. The fissures were in the proximity of Summit Road and necessitated pavement repairs in several places where they crossed the road. In this area, primarily populated with wood-frame residences, the extremes of no apparent structural damage whatsoever to complete destruction were observed. Even in areas where damage was high, many wood-frame "success stories" were encountered. The house pictured in Figure 1 appeared to sustain no structural damage other than the collapse of the masonry chimney. The house was two stories on a sloping lot, with a wood-framed daylight basement to the rear and was sided with plywood panels which acted as bracing. It was located approximately 100 feet from a ground fissure, and undoubtedly was shaken rather severely. In fact, it was located about 200 yards from the house shown in Figure 8 which was completely destroyed in the earthquake.

Dennis J. McCreary, staff engineer with the International Conference of Building Officials, promulgators of the Uniform Building Code, visited Santa Cruz County shortly following the earthquake. He observed, "It appeared that where there were failures in wood-frame buildings, they were due to inadequate connections, or lack of structural continuity in design."

2.1 Cripple Walls

"Cripple" or "pony" walls appeared to have been the source of failure in a number of damaged homes. Cripple walls are typically stud walls which spring from the foundation to the first floor framing. They are often used on stepped foundations in buildings built on sloping sites and are usually short, but can be as much as full story height. When cripple walls have a

---

1. American Plywood Association, Tacoma, Washington 98411

stud height exceeding 14 inches, the Uniform Building Code requires that they be considered first-story walls for the purpose of determining the bracing required. The code also requires that cripple walls exceeding 14 inches shall be framed with studs not less in size than that of the studding above and, when they exceed 4 feet in height, cripple walls shall be framed of studs having the size required for an additional story. These requirements clearly indicate that such walls are required to provide resistance to lateral forces, and are not merely skirting.

Several instances were observed where houses had been moved laterally off their foundations. In every case of this type which was observed, the cripple walls were laying flat on their sides as shown in Figure 2. Although these walls were typically sheathed or sided with plywood panels, nailing was typically much sparser than required by the code. Thus, the panels themselves could not provide sufficient lateral resistance to prevent racking of the cripple walls. No instance was observed where a cripple wall collapsed which was nailed in accordance with code requirements.

In the Los Altos Hills area, one house was observed where a rather long section was built over a garage on a sloping site. Nearly all the side walls of the garage, which supported the first floor, can be considered a cripple wall. Two-foot-wide plywood walls (veneered with stone masonry) were built on either side of the garage door opening. During the earthquake, this section of the house appeared to rotate counterclockwise, resulting in detaching the room over the garage completely from the rest of the house and laying over the narrow walls beside the garage door opening about one foot (see Figure 3). At the location where the room detached from the rest of the house, there appeared to be no structural continuity, as shown in Figure 4. Here, again, nailing of the sheathing along the cripple walls was less than that required by code. In addition, the garage door header, which supported a portion of the first floor, was not adequately tied to the supporting walls. Further, the narrow walls beside the garage door opening were not anchored with hold-downs appropriate for shear walls. Still, the room above the garage, complete with unbroken picture window, moved as a unit and was undamaged except for where it separated from the rest of the house.

2.2 Houses Without Cripple Walls

In an older section of Los Gatos, many houses were observed that had slipped laterally off their foundations. The age of these houses would indicate that they were board sheathed and the foundations appeared to be unreinforced masonry. Due to the age of the houses, and that they were obviously constructed before modern building codes, no detailed inspections were made by the team.

In the same area, the house shown in Figure 5 was seen. Even though it has a double garage in the ground floor, it appeared undamaged. This house appeared to be built under recent building codes.

The two-story house with basement garage shown in Figure 6 showed no indication of damage even though it was very near two houses that were badly damaged (one of which is shown in Figure 12).

Figure 7 is a house near Summit Road and north of Highway 17. Ground movement in the area is evidenced by buckled blacktop in the road near the house and several broken buried water lines. Even though the entire end of the house is taken up by a double garage door, this house did not show any indication of damage. There was an approximately one-inch crack in the walkway between the street and the house, which indicated shifting of ground in this area.

2.3 Major Framing Connections

Two of the badly damaged houses that were examined showed very little connection between the major floor framing members and the foundation. While both of these houses had stepped foundations, each had one side where the floor framing bore directly upon the sill plate which was well bolted to the concrete foundation.

In the rectangular house where the 2x floor joists were on the sill plate, there was no evidence of fasteners between the joists and the plate. The Uniform Building Code requires three 8-penny nails per joist for this connection. The perimeter band joist was nailed to each joist; however, the band joist was fastened to the sill plate with toe nails approximately 4 feet on center.

The second house was octagonal in shape, and the floor was framed with 4-inch-wide beams (see Figure 8). A careful examination of the sill plate showed at the most only one toe nail connecting the floor joists to the sill plate. Again, the floor framing members were nailed to the perimeter band joist and, in this case, the perimeter band joist was anchored to the foundation using hold-down anchors with lag screws into the band joist. The earthquake movement was such that the lag screws failed in withdrawal from the band joist.

2.4 Construction in the Marina District

The portion of San Francisco known as the Marina district is an area where the rubble from the 1906 earthquake was dumped and then subsequently filled with sand dredged from the bay. During the 1989 earthquake the fine sand liquified and, in many cases, flowed up through cracks in the road or sidewalk. In other instances, the sidewalks were badly distorted by pressure from the sand.

The typical building in this area is a four-story apartment consisting of three floors above ground floor garages. Around the most badly damaged buildings, inspection was possible only by observations from outside the police barricades.

The large number of garage door openings on the ground floor of these buildings resulted in only a very small length of exterior wall for racking resistance. These walls were typically concealed by masonry veneer; however, in many instances, the masonry had fallen away exposing the sheathing. The sheathing was typically horizontal boards and in the one building where the sheathing had fallen off with the masonry, there was cut-in 2 x 4 diagonal bracing. The few interior partitions that were visible in the garages were sheathed with gypsum wallboard.

While several of these apartment buildings did collapse, many more showed evidence only of distortion at the first floor. Figures 9 and 10 show one of these buildings. House movers were already at work placing shoring and steel beams to prevent further collapse and to enable jacking up of the buildings and restoring the ground floor.

The small, approximately 2-1/2-story apartment building shown in Figure 11 was entirely sheathed with plywood. On this particular building the exterior damage was superficial, with a small 2-foot-high brick veneer wall falling away from the building. Investigation showed no ties between the brick and the building. Upward ground movement was sufficient to completely jam the garage door, so the owner found it necessary to saw off the bottom of the door to open it after the quake. The concrete garage floor was totally destroyed and will have to be replaced, but the building above showed no evidence of damage.

At another location, a contractor was adding plywood sheathing to the interior of a garage to add lateral resistance to a relatively undamaged apartment building. The contractor pointed out that there were no anchor bolts from the sill plate to the foundation, so his first step was to drill in anchor bolts. He then added blocking between the studs and was applying 3/8" plywood horizontally to the walls.

One large apartment complex in the Marina district was destroyed by fire initiated when natural gas lines were broken due to the earthquake. This can also be related to lateral load resistance of buildings. According to Franklin Lew, Manager of Seismic Safety Program for the city and county of San Francisco, "Wood-frame buildings designed to provide lateral resistance are less likely to sway and drift in an earthquake. This limits breakage of electrical, gas and water lines within the building, thus reducing the chance for catastrophic fires."

3. CHIMNEYS

The chimney damage shown in Figure 1 was common to many houses whether or not they were further damaged. The chimneys typically were not reinforced and were not tied sufficiently to the structure. Chimney failures were seen in many of the areas observed. Some residences constructed in the last 15 or 20 years have utilized insulated steel chimney flues enclosed by decorative plywood siding. A number of these were observed, and none had collapsed except for one which was not well fastened to the house and also was sheathed with heavy stone veneer.

4. POLE-SUPPORTED BUILDINGS

There were many pole-supported houses located on steep slopes in the town of Los Altos Hills - about 25 miles from the epicenter.

Some of these suffered extensive damage, and the one shown in Figure 12 appeared to be a total loss. The damage seemed to be due to two factors: 1) inadequate connections between the floor system and the pole foundation, and 2) unequal stiffness of the poles.

The first deficiency caused the floor systems to shift relative to the poles. This movement was sufficient in some cases to cause the floor framing to lose support from the poles.

The second deficiency was due to the unequal height of the poles. Even if the floor system successfully tied the poles together so they acted as a unit, their varying stiffness meant that the connections between the floor and the shortest poles carried the greatest lateral forces during the earthquake. Those connections would be the first to overload and fail, then the next shortest pole/floor connection and so on.

Poles under some houses had been braced with diagonal cables, and these structures appeared to be undamaged. Repairs underway at one home included the addition of diagonal cables.

5. INDUSTRIAL BUILDINGS

During the 1971 Sylmar, California earthquake there were numerous failures due to masonry and concrete walls pulling away from roof systems. The failures were initiated by weak connections between the walls and the roof framing. The Uniform Building Code was subsequently improved to correct this situation by requiring a positive tie between the walls and roof framing.

A small industrial building in Campbell, about 20 miles from the epicenter, had minor damage of this type. A 4x12 timber ledger was bolted to the masonry wall.

The plywood sheathing of the panelized roof was the only tie to the wall capable of resisting outward (tension) forces acting on the wall. The nails holding the plywood to the top of the ledger held, but the ledger split along the bolt lines. The splits in the ledger were apparently caused by cross-grain bending. As mentioned above, this detail is no longer permitted by the Uniform Building Code. In spite of the damage, the plywood roof diaphragm functioned satisfactorily, preventing damage to the masonry walls.

6. MASONRY BUILDINGS

Masonry buildings typically perform poorly in earthquakes, particularly those that are unreinforced. Without reinforcement, masonry buildings fail in a brittle fashion. In the town of Los Gatos, about 15 miles from the epicenter, an entire block of one - and two-story masonry stores had been severely damaged and will undoubtedly be demolished.

Unlike wood construction, which is light in weight, masonry is heavy. Its greater weight leads to greater lateral forces to resist than wood construction.

7. SUMMARY AND CONCLUSIONS

A team of engineers from the American Plywood Association visited the San Francisco Bay area shortly following the Loma Prieta earthquake of October 17, 1989. Damage from the earthquake occurred in scattered locations within the region. Within these locations, the heaviest damage appeared to be to buildings with unreinforced masonry walls. All observed wood-framed buildings which were damaged were either built before the 1973 Uniform Building Code introduced updated earthquake regulations, or incorporated critical construction features but with inadequate connections, or other features which were not nailed or stapled in accordance with minimum code requirements.

It is the conclusion of the investigators that framed construction built to meet current code provisions performed very well. No code deficiencies for this type of construction were observed. However, greater attention must be paid to design and installation of connections and fasteners, and to structural continuity, especially in small buildings which may not be engineered.

Figure 1. Two-story house with wood-framed daylight basement located about 100 feet from ground fissure in Santa Cruz Mountains. No apparent structural damage except collapsed masonry chimney.

Figure 3. House in Los Altos Hills rotated counterclockwise in portion over garage due to inadequate nailing of sheathing and connections at narrow walls beside garage door opening. Rooms above appeared to move as a unit and remain sound.

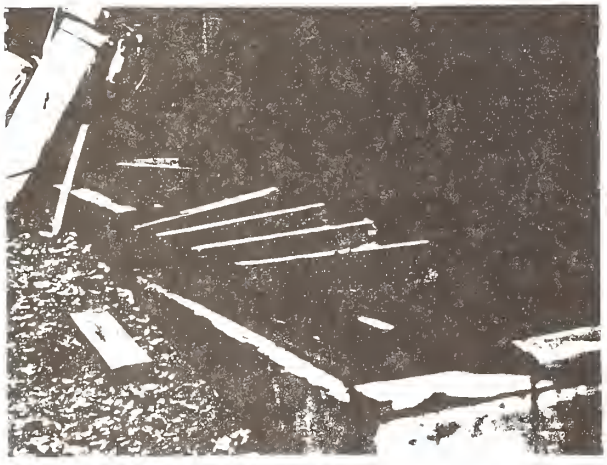

Figure 2. Collapsed cripple wall on house in Santa Cruz Mountains. Plywood sheathing on all cripple walls was inadequately fastened, allowing house to shift off foundation which split the sill plate along the bolt line.

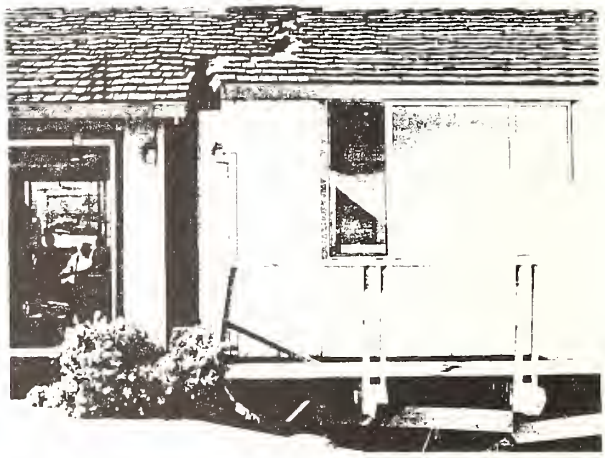

Figure 4. Break in house between kitchen and recreation room. The kitchen floor was wood framed over a crawl space. At the right end of the house, the crawl space became the garage. All of the major floor and wall framing members had unspliced joints at the break.

Figure 5. Undamaged split level house located in area of Los Gatos where many older one-story houses slipped laterally off their foundations.

Figure 7. Undamaged house in area of sufficient ground movement to buckle blacktop road and break water lines.

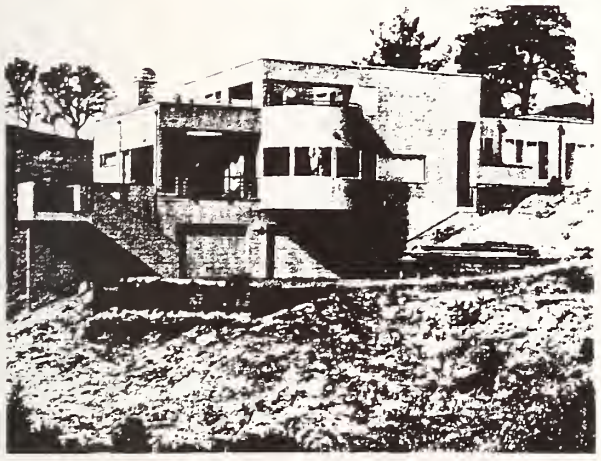

Figure 6. Well constructed split level house with no apparent damage. Two nearby single level homes were damaged, one beyond repair.

Figure 8. Lateral displacement of floor at completely destroyed house in Santa Cruz County. The lag screws connecting the band joist to the anchors failed in withdrawal. Other than a single toe nail, no fasteners were found tying the floor joists to the sill, which was bolted to the concrete foundation.

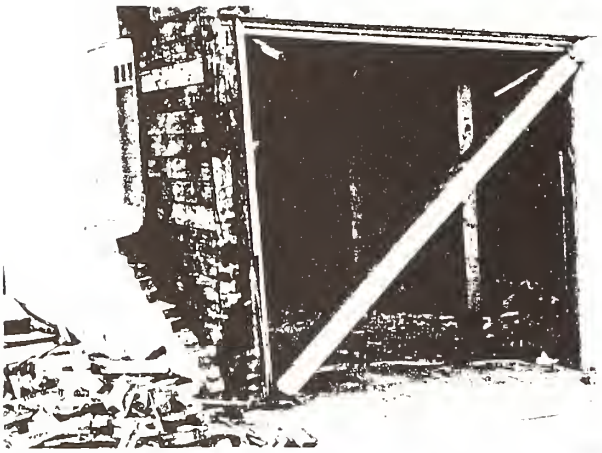

Figure 9. Corner apartment building in the Marina district. The masonry veneer was anchored to the sheathing by nails embedded in the mortar.

Figure 11. Plywood sheathed and sided apartment building near the building shown in Figure 9. Except for the badly damaged concrete garage floor, this building had minor damage.

Figure 10. Corner apartment building in the Marina district. House movers have shored the garage level in preparation for restoring the building.

Figure 12. A badly damaged house in the Los Altos Hills area, supported on poles. The few connections between the poles and the floor framing failed due to poor quality welds. The floor joists were steel under the center portion of the house and wood at the edges. there appeared to be a lack of continuity between the two types of framing.

Seismic Performance of Nonstructural Elements During the Loma Prieta Earthquake

by

T.T. Soong[1]

ABSTRACT

For nonstructural elements, some of the national and statewide (California) provisions have only recently been applied to newly constructed facilities and to upgrading of existing nonstructural systems. The Loma Prieta earthquake provided a good opportunity for assessing whether these newly instituted standards have provided added margin of safety to these systems under strong earthquake disturbances.

Seismic performance of a selected class of nonstructural elements during the Loma Prieta earthquake is assessed in this paper. Emphasis is placed on their performance evaluation with respect to the criteria under which they were designed, upgraded or constructed.

KEYWORDS: Building codes; earthquake resistant structures; ground motion; nonstructural damage; pressure piping.

1. INTRODUCTION AND BACKGROUND

Nonstructural elements of a building are generally considered as those materials that are not a part of the structural system. They include equipment, architectural elements and building contents. The importance of nonstructural element issues in seismic design and performance evaluation is now well recognized by researchers as well as practicing engineers. The subject received special attention after the San Fernando earthquake of 1971 when it became clear that damage of nonstructural elements not only can result in major economic loss, but also can pose real threat to life safety. For example, an evaluation of various VA hospitals following the San Fernando and other previous earthquakes revealed that many facilities still structurally intact were no longer functional because of loss of essential equipment and supplies (Veterans Administration, 1976). Economic loss due to seismic nonstructural damage can also be considerable. A case in point is the seismic damage sustained by a seven-story hotel during the 1971 San Fernando earthquake. Of $143,000 in total damage in 1971-value dollars, only $2,000 was structural damage while the remaining 98.6% was nonstructural (Murphy, 1973). Recent federal estimates of earthquake property damage after selected future major earthquakes in California are given in Table 1 (FEMA, 1981).

In practice, nonstructural elements are treated independently in the seismic design and evaluation of building structures. They are considered as being subjected to forces applied by the structures to which they are attached. Today, major building codes and seismic design guidelines exist which address the seismic force input to various nonstructural elements.

Nationally, the Uniform Building Code (ICBO, 1988) is widely used for seismic design standards for structures and nonstructural elements, from which local jurisdictions and some federal agencies have developed similar seismic design requirements. The UBC formulates the design force for nonstructural systems as an equivalent static lateral force applied to the approximate center of gravity of the system being analyzed. It is given by

$$F_p = ZIC_pW \tag{1}$$

where F_p is the lateral design force and Z is the seismic zone factor, taking values of 0, 3/16, 3/8, 3/4 and 1 for seismic zones 0, 1, 2, 3 and 4, respectively. I is the importance factor which takes the value of 1 for most structures, 1.25 for buildings with room occupancy loads of 300 or more and 1.5 for essential buildings such as fire stations and hospitals. W is the weight of the nonstructural system and C_p is the lateral force coefficient. A portion of the C_p-table stipulated in Title 24 of the California Administrative Code is reproduced in Table 2 (State of California, 1985).

Some variations and refinements of the basic formula (1) are found in other codes depending on whether they consider earthquake response characteristics of the ground, attachment details, and vibrational characteristics of the structural-nonstructural systems. The Applied Technology Council (ATC), for example, has developed some more elaborate guidelines. For seismic design of electrical and mechanical equipment, the formula is (ATC, 1978)

$$F_p = AC_pMW_pPm \tag{2}$$

where A is the effective peak ground acceleration, C_p is the lateral force coefficient, M is the equipment amplification factor, W_p is the equipment weight, P is the performance level coefficient, and m is the attachment amplification factor.

The exception, it appears, is the nuclear power industry where much more stringent and rigorous standards are recommended. For example, in seismic qualification class 1E equipment for nuclear power generation stations, the recommended qualification methods consist of (IEEE, 1987):

(a) Predicting the equipment's performance by analysis, including dynamic analysis of the combined structure-equipment system and nonlinear equipment response.

[1] National Center for Earthquake Engineering Research and Department of Civil Engineering, State University of New York at Buffalo, Buffalo, New York 14260

(b) Testing the equipment under simulated seismic conditions.

(c) Qualifying the equipment by the combination of test and analysis.

(d) Qualifying the equipment through the use of experience data.

Some of the provisions mentioned above have only recently been applied to newly constructed facilities and for upgrading of precode nonstructural elements. Hence, the Loma Prieta earthquake provided a good opportunity for assessing whether or not these new provisions and standards represent a significant step forward in terms of improved seismic nonstructural performance.

For this purpose, rather than covering a broad spectrum of nonstructural damage due to the Loma Prieta earthquake, this paper focuses on a selected list of nonstructural systems with emphasis placed on their performance evaluation with respect to the criteria under which they were designed, upgraded or constructed. These systems are (a) hospital facilities; (b) facades, panels and glazing; and (c) pressure piping.

2. HOSPITAL FACILITIES

Following the 1971 San Fernando earthquake, in which several modern hospital buildings and equipment sustained significant damage, the State of California gave control to the State to develop hospital construction standards and regulations, to assume responsibility for overseeing construction, and to perform design plan checking. The California Administrative Code, discussed in Section 1, is the first to link geology, seismology, structural design and nonstructural system design. As a consequence, all hospital-related projects have been subjected to review by the State and have been made to conform to the requirements of the 1985 Triennial Edition of the State Building Code, Title 24, Part 2.

It is thus of special interest to observe seismic damage to hospital facilities due to the Loma Prieta earthquake in order to assess whether these State-imposed provisions have provided added margin of safety to these structures and their contents.

A survey of 60 hospitals in the affected six-county area shows that all hospital facilities performed well during the event (Staehlin, 1990). Most, if not all, of the reported damage was limited to those facilities that had not been upgraded to the above-mentioned provisions.

Minor damages to the nonstructural elements, however, were widespread. Numerous pieces of equipment broke loose from their attachments and separated from duct work or piping, causing some problems for the affected facilities. Older vibration isolators and machine mounts in some cases literally exploded during the event. Figures 1 and 2 show such instances at the Watsonville Community Hospital.

Elevators in these facilities posed a separate problem. Of the 428 elevators in the survey, 2[illegible] or 65.9% were tripped by motion detectors and out of service for between 10 minutes to three weeks, 50 of these sustained damage ranging from loosened bolts attaching the guide rails to twisted rails due to vibration of the counterweights.

3. FACADES, PANELS AND GLAZING

Preliminary observations indicate relatively good response of newer engineered buildings with corresponding minor damage to nonstructural elements such as facades, claddings and glazing. In downtown San Francisco, severe glazing damage occurred at a retail building which is new in appearance. However, it was in fact constructed in 1946 as one of the first hermetically sealed buildings in the city (EERI, 1989).

In older engineered buildings, some patterns of damage to facades and claddings are apparent. Many buildings showed loss of brick masonry facades and parapets. Figures 3 and 4 give an example of such damage to a building in San Francisco's Mission District. Indeed, hundreds of multi-story masonry structures in San Francisco and elsewhere suffered extensive cracking and loosening of mortar. It is estimated that about 10,000-20,000 unreinforced masonry structures in San Francisco sustained damage during the Loma Prieta earthquake.

Widespread damage to glass panels (Fig. 5), gypsum board partitions, and suspended ceilings and floors (Fig. 6) was observed. This type of damage was common in steel buildings with masonry infill panels (A. Elnashai et al, 1989). Such structures are typically more flexible than reinforced concrete structures and therefore impose large displacements on nonstructural elements.

As reported in (EERI, 1989), while nonstructural damage is considered relatively minor for each building in this event, the overall amounts to a large sum for area-wide damage. Some large corporations, such as Pacific Bell and Pacific Gas and Electric, report nonstructural damage of up to $45 million or $50 million.

4. PRESSURE PIPING

The performance of steel piping at the Moss Landing Power Plant of the Pacific Gas and Electric provided an opportunity to observe the effect of the Loma Prieta earthquake on many piping systems and their supports. The piping system at Moss Landing was designed in accordance with the pressure piping industry's construction code (ASME ASA (now ANSI) B31.1 Code) in effect at the time of construction. The provisions of the Uniform Building Code was followed in the application of the lateral force criteria. The piping system was fabricated from carbon and low alloy (chrome-molybdenum) steels and it is believed that such piping systems should perform satisfactorily in an event of this intensity without loss of pressure retaining integrity, except where relative support motions exceed the cyclic strain limits of the materials.

Figures 7 and 8 illustrate some of the more important observations at this site. Although pipe support deformations are evidently well into the plastic range, pipe supports appear to have performed well with no evidence of loss of pressure retaining integrity or of damage to the pressure boundary. Figure 7 appears to sug-

gest that earthquake loads on pipe support elements might be allowed to induce "effective" stresses that are well above current typical allowable stresses, i.e., perhaps some multiple of the material yield strength (Haupt and Curtis, 1989).

These figures also show thermal saddles acting as bumpers between the support steel and the pressure boundary. These saddles are commonly used to spread the earthquake loads occurring from the pipe impact on lateral supports over a larger area of the actual pressure boundary element. The saddles shown and other bumpers performed as expected.

Finally, several support elements broke entirely free from the structure to which they were attached due to the impact of the pipe on the support. Where this occurred, however, it was subsequently found that the supports had been attached to the structure by tack welds (Haupt and Curtis, 1989).

5. CONCLUDING REMARKS

As in the past, nonstructural damage due to the Loma Prieta earthquake is difficult to assess partly because it is largely internal and invisible from the outside and partly because of the lack of a systematic procedure for inventory and reporting of this type of damage. One general observation that can be made is that nonstructural damage in this event is not as serious as originally feared due in part to the satisfactory performance of more recently engineered buildings. It is pointed out in (EERI, 1989) that the Loma Prieta earthquake produced ten to fifteen seconds of strong shaking with peak horizontal ground accelerations ranging from 0.67g near the epicenter to approximately 0.25g in the Oakland-San Francisco area. Had the ground motion duration been significantly longer, a great deal more damage would have resulted from this event.

As observed earlier, a significant amount of nonstructural damage was a result of support failure, which could have been prevented had relatively simple protective procedures been instituted. Furthermore, observed damages sustained by vibration isolators and machine mounts underscore the continued existence of a serious conflict between the need to anchor heavy machinery to the structure to avoid earthquake damage on the one hand, and the requirement that vibrating equipment be isolated from the structure for vibration and acoustical control on the other. One possible solution to this problem may be the installation of braces which would not touch the equipment base or piping system during normal operation but become effective when excessive motions take place (Ayres et al, 1973).

6. ACKNOWLEDGEMENT

Some of the photographs used in this paper were supplied by Professor Barry J. Goodno of the Georgia Institute of Technology, Mr. Ronald Haupt of the Pressure Piping Engineering Associates, Inc., and Mr. William Staehlin of the Office of Statewide Health Planning and Development, the State of California. Their generosity and assistance are greatly appreciated.

This work was supported in part by the National Center for Earthquake Engineering Research under Grant No. NCEER-89-2002A.

7. REFERENCES

1. Ayres, J.M. et al, 1973, "Nonstructural Damage to Buildings," *The Great Alaska Earthquake of 1964: Engineering*, National Academy of Sciences, Washington, D.C.

2. EERI, 1989, *Loma Prieta Earthquake, October 17, 1990, Preliminary Reconnaissance Report 89-03*, El Cerrito, CA.

3. Elnashai, A. et al, 1989, *The Loma Prieta Earthquake of 17 October 1989: Seismological, Geotechnical and Structural Field Observations*, ESEE Research Report No. 89/11, Imperial College of Science and Technology, London.

4. FEMA, 1981, *An Assessment of the Consequences and Preparations for a Catastrophic California Earthquake*, Washington, D.C.

5. Haupt, R. and Curtis, D., 1989, *Performance of Industrial Facilities*, Pressure Piping Engineering Associates, Inc., Foster City, CA.

6. IEEE, 1987, *Recommended Practice for Seismic Qualification of Class 1E Equipment for Nuclear Power Generating Stations*, IEEE, New York, NY.

7. International Conference of Building Officials, 1988, *Uniform Building Code*, Whittier, CA.

8. Murphy, L. (Ed.), 1973, *San Fernando, California Earthquake of February 9, 1971*, Vol. 1A, NOAA, Washington, D.C.

9. Staehlin, W., 1990, *A Report to the Building Safety Board on the Performance of Hospital Buildings in the Loma Prieta Earthquake of October 17, 1989*, Sacramento, CA.

10. State of California, 1985, *California Administrative Code, Title 24 Building Standards*, Sacramento, CA.

11. Veteran Administration, 1976, *Study to Establish Seismic Protection Provisions for Furniture, Equipment and Supplies for VA Hospitals*, Washington, D.C.

Table 1. Estimated Loss in Major Future Earthquakes
(Taken from FEMA, 1981)

Fault	Loss to buildings ($ in billions)	Loss of contents ($ in billions)	Total loss ($ in billions)
Northern San Andreas	25	13	38
Hayward	29	15	44
Newport–Inglewood	45	24	69
Southern San Andreas	11	6	17

Estimates uncertain by a possible factor of two to three.

Table 2. Horizontal Force Factor C_p
(Taken from State of California, 1985,
Table No. 2-23J, Part B)

Category	Direction of horizontal force	Value of C_p
1. Mechanical and electrical components:		
a. All mechanical and electrical equipment or machinery which is a part of the building service systems.	Any direction	0.33
b. Tanks (plus contents) and support systems.		0.33
c. Emergency power supply systems in public school buildings. Essential communication equipment and emergency power equipment in hospitals, such as engine generators, battery racks and fuel tanks necessary for operation of such equipment.	Any direction	0.50
d. Hospital piping, electrical conduit, cable trays and air handling ducts.	Any direction	0.50
2. Hospital equipment when permanently attached to building utility services such as: surgical, morgue and recovery room fixtures, radiology equipment, medical gas containers, food service fixtures, essential laboratory equipment, TV supports, etc.	Any direction	0.33
3. a. Storage racks with the upper storage level more than 5 feet in height (plus contents).	Any direction	0.30
b. Floor supported cabinets and bookstacks more than 5 feet in height (plus contents).	Any direction	0.30
4. Wall hung cabinets and storage shelving (plus contents).	Any direction	0.30
5. Suspended ceiling framing systems	Any direction	0.30
6. a. Suspended light fixtures.		
b. Surface mounted light fixtures.	Any direction	1.00

Fig. 1. Failure of Vibration Isolator, Watsonville Community Hospital

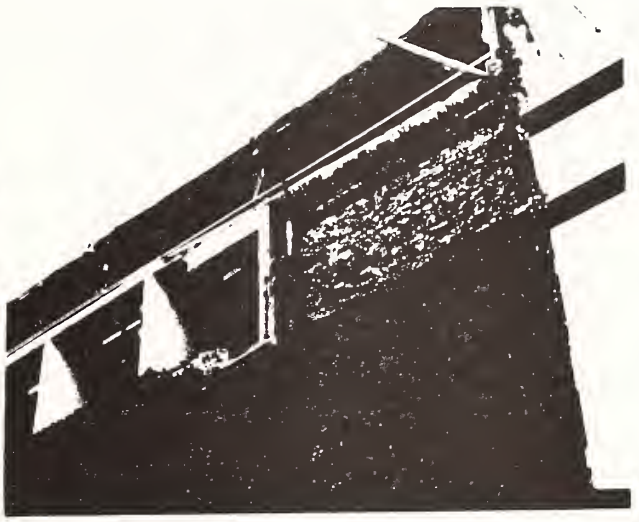

Fig. 3. Loss of Masonry Facade and Parapet, Mission District, San Francisco

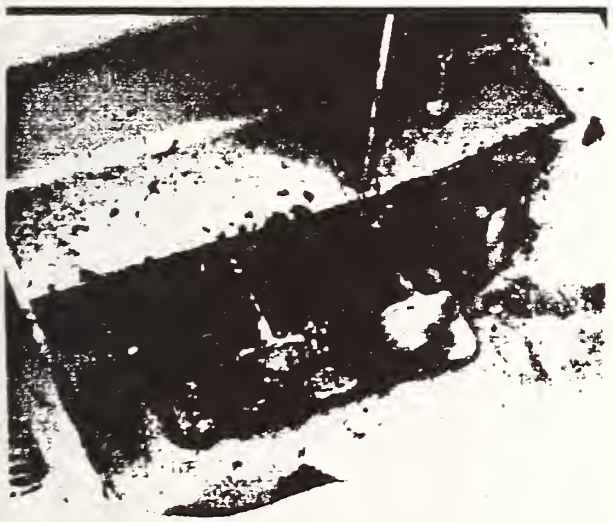

Fig. 2 Broken Mount of Emergency Generator, Watsonville Community Hospital

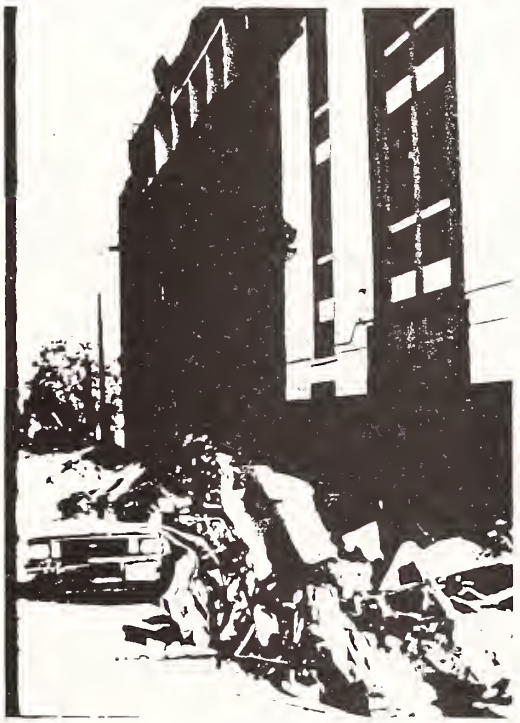

Fig. 4. Cars Crushed by Fallen Masonry, Mission District, San Francisco

Fig. 5. Loss of Glass to Building, Oakland

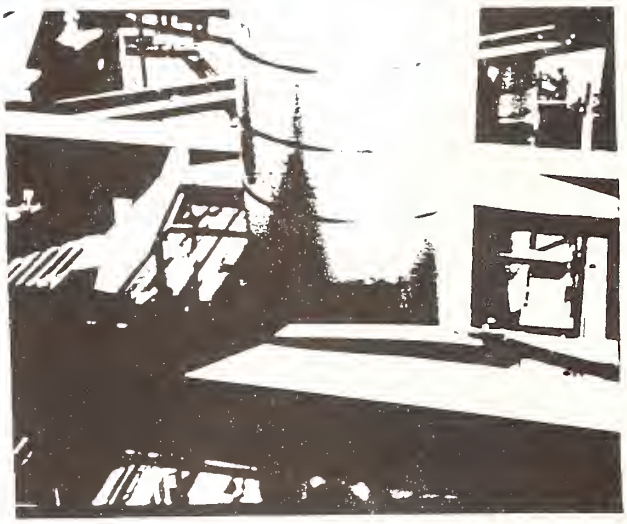

Fig. 7. Laterally Deformed Support at Moss Landing Power Plant

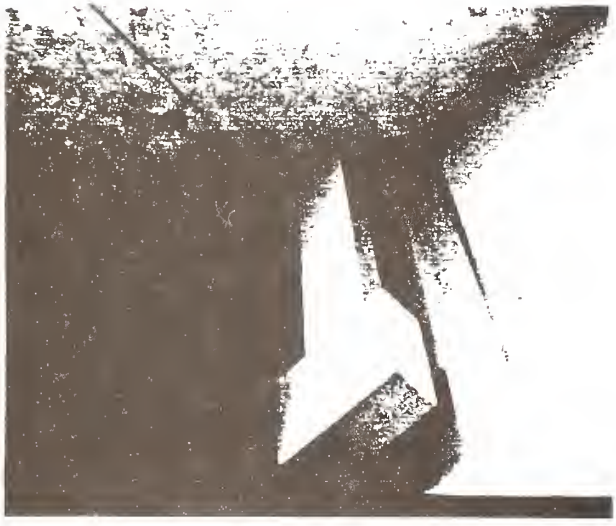

Fig. 6. Damage to Suspended Floor in Building, San Mateo

Fig. 8. Laterally Deformed Support at Moss Landing Power Plant

Socio-Economic Impacts of Lifeline Performance Related to the Loma Prieta Earthquake

by

Maryann T. Phipps[1] and Ronald T. Eguchi[2]

BSTRACT

feline performance during the October 17, '89 Loma Prieta Earthquake was evaluated d documented in the paper entitled "Lifelines erformance During The October 17, 1989 oma Prieta Earthquake" (Khater, et al., 1990). his companion paper examines the socio-onomic impacts of lifeline performance. felines considered are: transportation, ater, sewage, power, gas, and communication stems. Among the most prominent cioeconomic impacts directly related to eline performance are those resulting from rthquake damage to the transportation twork. The impacts on both individuals and sinesses are discussed. As damage to other elines was limited, so too were the related cioeconomic impacts. Observations related to e impacts of each lifelines on the community d regional economy are presented.

INTRODUCTION

ifelines, by definition, are critical systems sential for the well being of a community. ften, the performance of a lifeline system is easured not by the direct effects resulting om system damage but by the indirect effects at result from its inability to function. ritical services such as emergency water supply r fighting fires, electric power for business d industry, communication services for ordination of response and recovery efforts, d transportation routes for import of needed mergency supplies or evacuation are all rvices essential for the rapid recovery of a ty after a major earthquake.

Economic and social losses as a result of lifeline failures may indeed account for a large percentage of the losses experienced after an earthquake. Unfortunately, there is no convenient way of quantifying or tracking such losses. Some of the reasons for this difficulty are:

1. Lack of adequate measures for quantifying social losses, i.e., inconvenience.

2. No systematic effort to collect data such as the number of homeless or relocations due strictly to failures of lifelines.

3. Difficulty, in general, in quantifying secondary losses, e.g., business interruption losses.

4. Difficulty in categorizing social and secondary economic losses by facility type, i.e., building losses vs. lifeline losses.

5. Lack of systems models that account for the interaction and interdependence between different lifeline systems and businesses that depend on lifeline services.

Fortunately, the resiliency of lifeline systems and communities, in general, is such that in

---

[1]H.J. Degenkolb Associates, San Francisco, CA 94104
[2]Dames & Moore, Los Angeles, CA 90017

moderate earthquakes, many temporary repairs can be made to restore partial service to an affected community. Because of this resiliency the impact of lifeline failures in recent U.S. earthquakes has not been as catastrophic as it could be. In large earthquakes, such as a repeat of the 1906 San Francisco earthquake, socio-economic losses as a result of lifeline failures would be expected to increase significantly. Resources that are normally available under mutual aid agreements may not be available because these outside resources may also be affected by the earthquake. Furthermore, earthquake damage will be more severe, and in many cases, large portions of lifeline systems may require complete replacement.

It is important that future research efforts record and attempt to quantify these socio-economic losses. Performance models should be developed that can provide even order-of-magnitude estimates of these losses. Breakdown of these losses by source, such as lifeline failures, would also be important.

The following discussion summarizes, on a quantitative basis, the socio-economic effects caused by lifeline failures in the October 17, 1989 Loma Prieta earthquake. More work needs to be conducted in order to collect important data for measuring socio-economic losses, and more research should be devoted to developing socio-economic models.

2. SOCIO-ECONOMIC IMPACTS OF LIFELINES PERFORMANCE

2.1 Transportation Systems

Of all the lifeline systems damaged by the earthquake, none was damaged as severely and dramatically as the transportation network. Damage to highway structures was the most significant cause of life loss and also carried with it the greatest socio-economic impact on the region. The collapse of the I-880 Cypress Street structure, the collapsed span of the Oakland-Bay Bridge, damage to freeway accesses leading into San Francisco, and damage to Highway 17 in Santa Cruz forced a temporary, yet overwhelming restructuring of regional transportation systems and clearly illustrated the region's economic dependence on its transit system.

Physical losses to the highway system are estimated at $1 billion. The physical losses are only one indicator of the economic impacts on the region, however. Economic losses due to business disruption and personal hardship also accompanied the physical damage.

For the most part, alternate transportation routes and/or transportation modes were developed to bypass each of the devastated highway segments. Consequently, major societal impacts resulting from the damaged highway system were averted. Socioeconomic impacts were generally limited to modifications to commute habits, longer transit times, and business losses.

The socio-economic impacts related to the collapsed Bay Bridge serve to demonstrate some of the societal impacts. The Bay Bridge collapse required that 250,000 commuters a day seek alternate transportation to San Francisco and/or develop alternate work patterns. Because BART, the regional heavy rail system, was essentially undamaged during the earthquake, there was a transit system available to accommodate commute traffic between San Francisco and the East Bay. Most commuters chose BART as an alternate. This shift in commute patterns was effected by an unprecedented cooperative effort among transit agencies. Regional bus and train systems, ferry service and BART formed a partnership to assist the community at large. For example, bus routes were modified to permit easy access to BART stations and ferry terminals. Representatives from all key agencies met regularly to monitor, adjust and improve transit

service. Local newspapers and television maintained a key communication link between the transit agencies and the public.

Commute habits were substantially altered for the short term. To accommodate the crowds encountered on BART during peak commute hours many riders altered their schedules to permit early commuting. Companies encouraged such changes by adopting "flex schedules". Some pre-earthquake commuters shifted their offices to branches located near their homes. The cooperative efforts of public agencies and the flexibility of employers and employees overcame the obstacle posed by the loss of the Oakland-Bay Bridge. Consequently, the San Francisco-East Bay link was maintained and potential economic losses were minimized.

During several months following the reopening of the Oakland-Bay Bridge, commute patterns were observed to be somewhat of a blend of pre- and post- earthquake patterns. Six months after the earthquake, however, commute patterns have generally returned to pre earthquake days.

Some short term economic losses can be directly or indirectly attributed in whole or in part to the damaged highway transportation system. Examples of the economic impacts, focusing primarily on San Francisco, include the following:

Decline in Retail Sales - The inability to drive directly to San Francisco from East Bay locations, crowding of the BART system, and general fear invoked after the earthquake caused people to postpone or redirect shopping trips which were originally destined for San Francisco. Both large and small San Francisco retail enterprises suffered substantial revenue declines immediately after the earthquake. Because of the regional redistribution in retail sales, large retail enterprises with branches outside of San Francisco did not to suffer appreciably. However, for those small businesses without such branches the losses were significant and unrecoverable.

Decline in Tourism - San Francisco's number 1 industry, tourism, suffered markedly after the earthquake. Tourists were afraid to travel to San Francisco fearing another earthquake would hit and uncertain of the City's ability to overcome the recent devastation. The hotel industry - a key barometer of tourism - suffered significant earthquake-related losses. In October, San Francisco hotels lost nearly $32 million in revenues. Since October, convention business has once again been restored. "Discretionary" travel to San Francisco, which accounts for half of all out-of-town tourism, has dropped by as much as a third. (Examiner)

Decline in Restaurant Business - Restaurants were forced to bear the brunt of decreases in tourism as well as a decrease in the flow of Bay Area residents into San Francisco. Many residents of the region grew accustomed to not coming to San Francisco during the month-long Bay Bridge closing and hence, the earthquake has had some short term as well as long term impacts on the restaurant industry. In a two-week period after the quake business in San Francisco County declined 30 to 40 percent; some restaurants lost up to 90% of their revenues. More than a month after the quake, restaurant business on average was down 15% to 25%. At least one restaurant closed permanently. In Santa Cruz County one week after the quake, business was down 60 percent. In November and December, business was still down 60 percent. (Examiner)

Increase in Unemployment - Damage to property coupled with the economic impacts on tourism and related industry as described herein led to substantial increase in unemployment. In October, San Francisco's unemployment claims were 50 percent higher than the City's monthly average, while in November the claims soared by 84 percent. In Santa Cruz County where physical damaged to

property was the primary cause for unemployment, the number of claims quadrupled and in November they were twice that of the county's average. (Examiner)

Lower Productivity - People missed work for several days after the earthquake. Upon returning, productivity was limited for many reasons.

Some long term impacts of the damaged transit system can also be identified.

Decline in Retail Sales One of the potential long term impacts of the damage to the highway system is demonstrated by the earthquake's effects on merchants in Chinatown. While the Bay Bridge was restored to service one month after the earthquake, two bridge approach ramps which direct riders to Chinatown, Fisherman's Wharf and North Beach, all popular San Francisco tourist spots, are still closed. These highway structures are of construction similar to the I880 Cypress structure, suffered moderate structural damage during the earthquake, and are likely to remain closed for a number of years.

Chinatown businesses are claiming that, six months after the earthquake, business is still down approximately 25% from that prior to the earthquake. They claim that this decline is due primarily to the lack of direct access to the area. Visitors driving to Chinatown must now travel through many local streets, often in bumper-to-bumper traffic. The Chinatown businesses cannot support themselves with local traffic only. Businesses rely on an infusion of people from outside the City. An economic study of the area is currently underway.

Enhanced Communication Among Regional Transit Agencies Regional transit agencies joined together after the earthquake to serve the public need. Since that time, agencies are meeting regularly to discuss regional transit issues and plan for the future.

Increased Spending on Seismic Safety The State of California Department of Transportation had requested state funds for seismic strengthening of highway structures to mitigate the known seismic hazard posed by numerous existing highway structures. In the seventeen years prior to the earthquake, $54 million of state funds had been appropriated for this purpose. Shortly after the earthquake, state legislators appropriated $80 million for seismic retrofit of state highway structures. The funding was generated from a quarter percent increase in the state sales tax. Additional proposed legislation could lead to the appropriation of up to $400 million to complete the seismic strengthening of all known hazardous highway structures (Roberts).

2.2 Electric Power Systems

Nearly one million PG&E customers lost electrical power immediately after the earthquake. Service was restored to 600,000 customers within 12 hours after the quake and to another 300,000 within 36 hours. Physical losses to PG&E totaled $1 million.

Because power outages were generally limited in duration, the related socio-economic impacts were likewise limited. In general, business activities were suspended by most businesses until full power was restored. Large businesses and public agencies were equipped with emergency generators to assist in recovery efforts until power was fully restored. Some companies obtained generators from outside the area. Many small businesses simply waited until commercial power was restored, incurring the related business losses in the interim. The loss of power contributed, in part, to local unemployment.

Some businesses, which rely heavily on commercial power for the manufacture of "high-tech" goods lost substantial inventory as work in progress was damaged. Those businesses dependent on power for the preservation of

food or other items, lost inventory when power was lost.

The interdependence of utilities was dramatically demonstrated after the earthquake. For example, the loss of commercial power caused innumerable communications problems. One common cause of telephone service disruption was the lack of emergency power for private branch exchanges (PBX). These PBX systems are connected to outside telephone lines but rely on in-house power. Where reliable in-house emergency power was not available, phone service to these systems was lost for the duration of the commercial power outage.

A similar interdependence of utilities was demonstrated by some gas detection systems which reportedly malfunctioned as a result of the power outage. (Sherman)

The socio-economic impacts of power outages after the Loma Prieta Earthquake appear to be limited to the direct loss of foregone production of goods and services. Long-term impacts appear minimal. PG&E's customers will generally fund the cost of repair, which in this earthquake is relatively small and will not have a dramatic impact on utility bills.

2.3 Natural Gas Transmission Systems

The Pacific Gas and Electric (PG&E) Company service region covers most of northern and central California and includes the entire earthquake-affected area. PG&E receives the majority of its gas through large diameter transmission lines that enter California at the Oregon and Arizona borders. There are gas storage fields at various locations in the service area; however, the two storage fields closest to the earthquake epicenter were both well over 60 miles away.

The gas transmission lines and large-diameter distribution mains experienced only three leaks due to the earthquake. Unstable soil in the Marina District of San Francisco caused damage that resulted in the replacement of approximately ten miles of cast-iron and steel distribution mains with polyethylene plastic pipe. Also in the Marina, 1,500 services to 5,400 individual meters were replaced in less than five weeks. Three miles of distribution mains were replaced in Los Gatos and Watsonville. Other damage was scattered and minor.

PG&E restored service to over 150,000 customers whose gas service had been turned off. A total of 1,100 service personnel participated in the relighting process, including approximately 400 from other utilities in the West. Within a week, service was restored to all customers with undamaged piping.

Socio-economic losses as a result of gas disruption were minimal in this event. Like most of California, winters in the Bay area are generally mild; thus lack of heating fuel did not pose a serious health threat. Lack of natural gas does affect other daily functions, e.g., cooking and bathing. In at least one severely damaged area, i.e., the Marina District, PG&E set up temporary bathing facilities for residents until all repairs to water and natural gas facilities had been completed.

Economic losses to industries requiring natural gas as a fuel source are not known by the authors at this time. However, gas service was restored to most areas within several days. Areas affected by longer outages, e.g., the Marina District, Los Gatos, are largely residential areas with relatively little industry. Watsonville may be an exception.

2.4 Communications

Pacific Bell is the primary provider of local telephone service in the Bay Area. For the most part, damage to Pacific Bell facilities was minor and did not affect service.

Overload of the system immediately after the quake led to "slow dial tone". Pacific Bell reduced the number of incoming calls to the area to provide maximum available service to local residents. In most areas the impact of phone service was to require waiting on the order of a minute to receive dial tone.

For some businesses with Private Branch Exchanges, power loss meant the loss of their means of communication as discussed previously. Some businesses had alternate communication systems in place. However, shortcomings in these systems were clearly identified. For example, internal radio systems were often rendered useless because of overloading, i.e. too many companies were using the same frequency. Some radio systems were disabled when remote equipment was damaged.

The interdependence of utilities was again demonstrated by Pacific Bell's reliance on commercial power. Pac Bell's central offices generally have electric-generators to recharge batteries which maintain phone service for extended periods, without commercial power. While only one central office was temporarily disabled due to malfunctions of the back-up energy supply, the need for a closer working relationship between PG&E and Pacific Bell was well-demonstrated. The need to interconnect Emergency Operations Centers with PG&E and Pacific Bell was also demonstrated.

The short-term socioeconomic impacts of loss of communications included the emotional strain of being unable to reach loved ones to determine their well being, loss of business revenue and delay in overall recovery efforts. Every business, utility and public agency impacted by the earthquake has gained an appreciation for their dependence on uninterrupted sources of power and communications. Improved alternate communications means are likely to develop.

2.5 Water and Sewage Facilities

In general, most of the damage to water supply systems was to pipelines. Areas that were severely affected included the Marina District in San Francisco, the South of Market area in San Francisco, parts of the East Bay (e.g., Oakland), cities in the South Bay (San Jose, Cupertino, Campbell, Los Gatos and Los Altos), and cities in the Monterey Bay area (Watsonville, Pajaro, Hollister and Sunny Mesa). Loss of electric power also affected the operation of some pump facilities.

Water service was available to most communities after the earthquake. The greatest concern for communities affected by pipeline breaks was contamination of water suppplies. The following communities issued advisories to boil water after the earthquake (TCLEE, 1990):

- Los Gatos
- Watsonville
- Hollister
- Santa Cruz
- Scotts Valley

In general, no serious problems were encountered with sewage and wastewater systems. Power outages affected the operation of some sewage treatment and pump stations, and the loss of power resulted in some untreated sewage being dumped into the San Francisco Bay.

3. CONCLUSIONS

Lifelines are indespensible to the vitality and viability of an economy. They are vital to life safety in the immediate aftermath of a destructive earthquake and are necessary in the subsequent reconstruction period. Direct damage to lifelines also leads to secondary

effects including reduced business productivity, loss of income, reduced employment, lower consumer spending, and decreased property and sales tax revenue. Each of these effects was realized, to some extent, after the Loma Prieta Earthquake.

Because the interruption of lifelines was in general, limited in duration, the impacts that lifeline damage caused by the Loma Prieta Earthquake had on the Bay Area economy were similarly limited. It is estimated, that in aggregate, income loss over in the twelve months following the earthquake is likely to amount to less than one percent of the region's total output. Unemployment directly resulting from the earthquake is expected to amount to a fraction of one percent of the region's total employment of 3 million jobs (Munroe).

The only lifeline severely impacted by the earthquake was the transportation network. Both short and long term socioeconomic impacts have been observed.

4. ACKNOWLEDGEMENTS

Partial funding for this limited investigation was sponsored by the National Science Foundation and the National Center for Earthquake Engineering Research. This support is gratefully acknowledged.

5. REFERENCES

(1) Khater, M., Scawthorn, C., Isenberg, J., Lund, L., Larsen, T., and M. Shinozuka, "Lifeline Performance During the October 17, 1989 Loma Prieta Earthquake," Proceedings of the 22nd Joint Panel Meeting on Wing and Seismic Effects, May 14-25, 1990.

(2) Munroe, Tapan, The Economic Impact of the Loma Prieta Earthquake of 1989: A Preliminary Look, Pacific Gas and Electric Company, 1990.

(3) Roberts, James E., Caltrans, Manager, Division of Structures, Personal Communication, 1990.

(4) The San Francisco Examiner, January 14, 1990.

(5) Sherman, William J., Intel Seismic Program Manager, Personal Communication, 1990.

(6) Technical Council on Lifeline Earthquake Engineering (TCLEE), ASCE, Contribution to Earthquake Engineering Research Institute (EERI) Reconnaissance Report, 1990.

Lifelines Performance During the October 17, 1989 Loma Prieta Earthquake

by

M. Khater[1], C. Scawthorn[1], J. Isenberg[2], L. Lund[3], T. Larsen[1] and M. Shinozuka[4]

ABSTRACT

Lifelines performance during the October 17, 1989 earthquake was evaluated and documented. Lifelines considered are: transportation, water, sewage, power, gas, and communications systems. The Loma Prieta earthquake has demonstrated that earthquakes can still cause severe damage to modern urban areas. Even though only few building were actually destroyed, major lifeline damage resulted, demonstrating that the highway system can be damaged, electric power can be lost to large areas, water mains can be severed, gas lines broken, sewer lines ruptured and vital services lost. Among the most catastrophic seismic-induced events were the collapse of the elevated Cypress Street section of Interstate 880 in Oakland, the collapse of a section of the San Francisco-Oakland Bay Bridge, multiple building collapses in San Francisco's Marina district, and the collapse of several structures in Santa Cruz and other areas in the epicentral region. Damage and business interruption losses were estimated as high as $ 6 billion. Human losses were severe.

KEYWORDS: Seismic damage; Lifelines performance; interaction.

1. INTRODUCTION

On October 17, 1989 at 5:04 p.m. local time, a M_S 7.1 earthquake occurred due to approximately 40 km rupture along the San Andreas fault. The epicenter of the 20 seconds earthquake was located near Loma Prieta in the Santa Cruz Mountains about 16 km NE of Santa Cruz, 30 km south of San Jose and about 100 km south of San Francisco (Figure 1).

Major damage included the collapse of the elevated Cypress Street section of Interstate 880 in Oakland, the collapse of a section of the San Francisco-Oakland Bay Bridge, multiple building collapses in San Francisco's Marina district, and the collapse of several structures in Santa Cruz and other areas in the epicentral region. Damage and business interruption losses were estimated as high as $ 6 billion. Human losses were severe: 62 people died, 3,700 people were reported injured and over 12,000 were displaced. At least 18,000 homes were damaged, 960 were destroyed and over 2,500 other buildings were damaged and 145 destroyed.

The Loma Prieta earthquake has demonstrated that earthquakes can still cause severe damage to modern urban areas. Even though only few buildings were actually destroyed, major lifeline damage resulted, demonstrating that the highway system can be damaged, electric power can be lost to large areas, water mains can be severed, gas lines broken, sewer lines ruptured and vital services lost. In order to put these effects into perspective, this paper records the performance of different lifelines (transportation, water, sewage, power, gas, and communications systems) during the Loma Prieta earthquake.

1. EQE Engineering, 595 Market St., San Francisco, CA 94105.
2. Weidlinger Associates, 4410 El Camino Real, Suite 110, Los Altos, CA 94022
3. Consulting Engineer, formerly Los Angeles Dept. Water and Power (ret.)
4. Department of Civil Engineering and Operation Research, Princeton University, Princeton, NJ 08544

2. LIFELINES PERFORMANCE

2.1 Transportation Systems

A major effect of the Loma Prieta Earthquake was on the transportation system, with the highway network suffering the worst damage.

2.1.1 Highway

Several major highways and overpasses were damaged and rendered useless some for only a short time, other for as much as a few years. Figure 2 shows the major highways and overpasses which were closed due to earthquake damage.

The collapse of more than a mile of the Cypress Street elevated section of I-880 was the largest contributor of deaths in the earthquake. The double-deck Cypress Street overpass structure consisted of box girder decks supported by concrete frames (Figure 3A). Support columns contained large amounts of vertical reinforcing steel (typically # 18) which provided ample vertical load-resisting capacity. However, only #4 bars, spaced at 12 inches, were used to tie the vertical steel and provide shear resistance for the columns. These ties provided very little shear capacity, resulting in very sudden brittle failure of the overall beam/column system (Figure 3B). Contributing to this failure were the relatively large number of hinges in the frames, typically reducing the structure to a deterministic structure (i.e., redundancy). These hinges were introduced due to concerns over shrinkage in the prestressed girders.

The 53-year old Bay Bridge (San Francisco-Oakland Bridge) is the major surface link between the northern San Francisco Peninsula and the East Bay. Approximately 300,000 commuters traverse the bridge each day. The loss of a 50-ft span of the upper deck of this bridge and subsequent damage to the lower deck caused major transportation problems. The Bay Bridge is a complex structure composed of back-to-back suspension structures on the west section, the world's largest single-bore tunnel, and a cantilever truss bridge followed by a curved incline section to the east. During the earthquake the cantilever and incline sections displaced longitudinally, resulting in the gap increasing beyond the beam seat capacity of 5 inches, dropping the upper span onto the lower span as shown in Figure 4.

Roads which were closed after the earthquake are given in Table 1 and shown in Figure 2.

2.1.2 BART

The Bay Area Rapid Transit District (BART) is a 71.5 mile, automated rapid transit system serving over 3 million people in the three BART counties of Alameda, Contra Costa, and San Francisco, as well as riders from northern San Mateo County.

Due to the earthquake the transition structure located just west of the Oakland West Station was damaged. The transition structure is a cast-in-place reinforced concrete structure leading from the east end of the bay tube to the adjacent elevated structure. The track grade is 3.98%. There are four stringer beams, which line up with the rails. At each bent, there are four concrete piles under the bent cap beam. There are five spans, and each is forty feet long as shown in Figure 5. The stringer and bent cap beam for the second and fourth spans are cast monolithically with reinforcement extending from the top on the pile. This design provides a rigid frame in the longitudinal direction for these spans. The third span is a floating span, and is supported from the second and fourth spans by a bracket on the side of the bent cap beam.

In the third span, which is the floating span, the ends of all of the cap beam brackets were severely damaged. At pier 4 (Fig. 5) south side (the sliding joint) about half the width of the bracket has broken out and fallen. The break extends back from the end of the bent cap about four feet. On the north end, there was a vertical crack which penetrated the full depth of the bracket and could seen on the bottom for about 2 feet along the length. The third span was temporarily supported by shoring on timber cribbing. The damage to the transition structure was most probably caused because the sliding joint did not function as intended, and the reinforcing steel did not come all the way to the face of the bracket.

The transbay tube (Figure 6) performed very well during the earthquake. The profile was checked immediately after the earthquake and little change was observed. The track alignment was excellent. The San Francisco side experienced a little movement, and the Oakland side moved about .75 in. longitudinally. The tube has a capacity of +/- 3.25 in. movement in the longitudinal direction, and

has a capacity of ±6 in. movement in the vertical and horizontal directions.

BART set its highest ever patronage records during the closure of the San Francisco Oakland Bay Bridge. Weekday trips averaged 347,122, compared to 257,500 trips after the bridge opened, or an increase of approximately 40%.

2.1.3 Port Facilities

This Section summarizes the damage to the marine facilities of the Port of Oakland. There are five ports in the Bay Area (Oakland, San Francisco, Redwood City, Richmond, and San Jose) but only Oakland sustained significant damage. Initially after the earthquake, total damage to the Port of Oakland was estimated to be on the order of $100 million, with approximately 60% of that corresponding to damage sustained to the airport (the air facilities portion of the Port of Oakland). In an interview with port officials in March, 1990, this estimate has been revised down to between $50 and 60 million, with the airport damage approximately $20 million of the total. Thus, the total damage to the marine facilities is estimated to be between 30 and 40 million dollars. This figure is primarily for the repair and/or the replacement of facilities and infrastructure components. The cargo handling components are primarily owned and maintained by the tenants.

The peak ground acceleration at this site is assumed to have been on the order of 20% of gravity. The collapsed portion of the Cypress viaduct is within 1/2 mile of a considerable portion of the marine facility.

Damage to the Oakland marine facilities is most easily examined by looking at the damage to the components. The cargo handling operations sustained minimal damage, emerging from the earthquake substantially operational. The facilities sustained a significant amount of damage, with temporary fixes necessary in some areas. The infrastructure was damaged to a degree, but was fundamentally functional soon after the earthquake.

CARGO HANDLING OPERATIONS: The cargo handling operations consist of items such as liquid storage tanks, bulk storage elements, container storage elements, cranes, etc. The cargo handling operations sustained minimal damage, emerging from the earthquake substantially operational. Estimated damage to cranes is 0.5% of their value, and the estimated damage to the remainder of the cargo handling operations is negligible.

Total damage to the 23 cranes is estimated to be on the order of $1 million. Assuming a value of $8 million per crane ($184 million total), this corresponds to a damage ratio of approximately 0.5%. Damage to the cranes was limited to minor racking and pounding, with no incidence of loss of stability. Not all of them are 100% functional presently, but that is due to the settled condition of the dike, and not to crane damage. The rails upon which these cranes are supported are supported on piles. Differential settlement between the rails varied from zero to 2 feet. It is estimated that these cranes could operate with a differential settlement of 8 inches.

Cargo containers in the facility did not overturn. Container storage in the marine facility consist of both containers on chassis and stacked containers. Stacked containers were both in grouped stacks, and free standing, with no adjacent stacks. Stacked trailer chassis did overturn, but were not damaged.

There are no major liquid or bulk storage elements within the marine facilities. Much of the bulk cargo is break bulk. This cargo is not known to have sustained much damage. It is the opinion of the Port that damage to goods in transit was minimal.

FACILITIES: The facilities at the Port of Oakland consist of items such as buildings, berthing structures, retaining structures, hydraulic fill, etc. The facilities sustained a significant amount of damage, with temporary repairs necessary in some areas to allow operations to continue. Damage to buildings varied, but was very minimal. The berthing structures underwent the greatest damage, attributed to the use of batter piles. Settlement of the hydraulic fill in the port area disrupted the use of the facility.

Damage to buildings varied. There is an estimated $1 million damage to the office structure in the APL Terminal (berths 60-63). This is a reinforced concrete

frame structure, with damage primarily limited to failure of the unreinforced masonry infill in the stairwells. The container freight station at berth 10 had minimal damage, with some broken studs in the walls, and minor spalling of the columns. One container freight station is slated for demolition, but this is primarily due to the need to rebuild the wharf structure underneath it (Howard Terminal, Berth 69). The remainder of damage to buildings is minimal.

Damage to the berthing structures is substantial, and the cost to repair these facilities is a significant portion of the total repair costs. Damage is primarily due to the use of batter piles upon the wharfs. The batter piles were inadequately connected to the wharf structure, and this connection was typically heavily damaged, with very little or no residual strength. Differential settlements, both laterally and vertically, leave the wharfs pulled away from the dike in many places from 2 to 8 inches. Wharfs with all vertical piles performed considerably better, with very minor cracking of the piles. Piles are primarily concrete, with a few concrete jacketed timber piles. New construction is slated to utilize all vertical piles.

All of the wharf structures have been surveyed since the earthquake, with damage tabulated, including a map of all the piles, and the damage sustained. One wharf structure (Berth 26) sustained damage at the interface where the structural system changed from batter piles to an all vertical system.

The use of retaining walls is not very prevalent in the Port of Oakland. There was one cracked concrete retaining wall at berth 69 (Howard Terminal). All wharfs are on individual piles and there are no sheet piles used at this facility.

The settlement of the hydraulic fill varied. By far the greatest settlement was near the end of the Seventh Street Terminal, where the fill settled up to 5 feet. This terminal is directly above the transbay BART tube, which may have accounted for some of the settlement. The Seventh Street Terminal was perhaps the most damaged portion of the entire facility, with many other extensive vertical displacements ranging up to 2 feet, and lateral displacements ranging up to 1 foot. Settlements in some areas preclude the continued usage of the large container cranes. The effects of ground settlement and liquefaction were present generally throughout the port. These effects included sand boils, settlements, and large cracking of the pavements.

INFRASTRUCTURE: The infrastructure consists of roadway and rail transportation (tracks, pavements, tunnels, bridges, causeways, signals, etc.); utilities (power, communication, water, natural gas, etc.; pipelines, etc. The infrastructure was damaged to a degree, but was fundamentally functional soon after the earthquake. Roadways were mostly undamaged, and only a small portion of the railways were unusable, mostly due to excessive ground settlement. Underground water pipes broke, but there is no indication of any major damage to other underground pipes. Emergency services were mostly untested, there were no fires or life-threatening collapses.

By and large, the roadways in the Port area were undamaged. The roads are used for extra heavy loads, with allowable axle loads greater than on most roads. This extra strength may have been a factor in their satisfactory performance.

Rail facilities underwent varying amounts of damage. At the Bay Bridge Terminal (Berth 9), railroad tracks buckled both horizontally and vertically. At the Seventh Street Terminal, rails going onto the wharf structure were damaged from differential settlement of the wharf and the piles supporting the rails. Damage at the two intermodal yards (Southern Pacific and Union Pacific) was reported as being minor.

One 18" water main burst, and was eventually shut off (Berth 20). Upon the resumption of service, several more (estimated at about 20-30) leaks were discovered. The capacity of the water supply after the earthquake remained mostly untested. In the event of a fire, they would have had to leave the burst water pipe in the circuit, having to deal with a large loss of pressure and water volume.

The facility was without power after the earthquake, due to damage distant from the facility. Power was restored without any problems.

There were no reported fuel leaks. The facility does not have any oil storage tank or underground fuel pipes. Ship fueling is performed via barges from Richmond.

2.2 Electric Power Systems

The electric power systems in the earthquake-affected ares are operated by the Pacific Gas and Electric Company (PG&E). Figure 7 shows the electric power facilities and the transmission routes in the earthquake-affected area. About 1.4 million customers lost electric service in the minutes after the earthquake. Most of them were in San Francisco, San Mateo, Santa Clara, Santa Cruz, San Benito, Alameda and Contra Costa counties. Within 48 hours, service to all but 26,000 customers was restored. In San Francisco, a 217-megawatt unit at Potrero Power Plant and two 106-megawatt units at the Hunter's Point Power Plant tripped off line when the quake hit. The U.S. Navy loaned PG&E the services of the frigate USS Lang to provide emergency steam to heat the feedwater for the Potrero Unit. The two Hunters Point Units that tripped off the line were returned to service as the electric load began to climb on October 19. In San Jose and San Mateo, two key substations (Metcalf and San Mateo substations) suffered major damage, contributing to the interruption of electric service in San Francisco and the area south of San Jose. At Metcalf substation in south San Jose, heavy damage occurred in the 500,000-volt switchyard. The San Mateo substation is an important link in the system that delivers bulk power into San Francisco. Damage to a transformer sharply reduced the amount of power that could move north. At Moss Landing Power Plant on Monterey Bay 30 miles south of the quake epicenter, a 750-megawatt generating unit was damaged and went down, as were the high-voltage switchyards connecting the plant to the transmission system. the Diablo Canyon Nuclear Power Plant near San Luis Obispo, about 140 miles south of the epicenter, had no damage and continued to operate without any interruption.

Emergency repairs reconnected the transmission links serving San Jose and San Francisco and new substation equipment was flown in with the help of the U.S. Air Forces.

2.3 Natural Gas Transmission Systems

Two major natural gas transmission routes feed the San Francisco Bay Area system, with some systems dating back to the 1940s. From the south through the Santa Clara Valley, supply is via two large diameter pipes; and from the east, three lines are used for supply. Other transmission lines are used to feed the outlying areas.

There were only three failures reported to gas transmission and large distribution lines. There were leaks in a 20-in. semi-high-pressure welded steel distribution line in Oakland, a 12-in. line in Hollister, and an 8-in. line in Santa Cruz. In the sandy fill soil of San Francisco's Marina District, gas lines were subjected to greater stresses and were severely damaged. Damage was distributed throughout the city with more than 400 breaks in mains, service, and meter locations. A construction force of over 300 workers worked to rebuild about 10 miles of gas line at an estimated cost of $20 million, which was completed in about three months.

In the epicentral area in the Santa Cruz Mountains, distribution system damage was restricted to three small line leaks. Two of these occurred at locations where gas lines were attached to bridge structures that suffered damage. A third leak occurred in a section of old line constructed in 1948. This line was in the process of being replaced. Los Gatos, Watsonville, Hollister, Richmond, San Jose, Oakland and Alameda also reported damage to either mains or services.

In the hours after the quake, about 153,000 customers shut off gas service to their homes or businesses. Where customers shut off their gas service, a PG&E service person checked for possible leaks, re-opened the service line, checked again for any problems, then re-lit pilot lights where necessary. PG&E service personnel used gas "sniffing" devices to check for leaks from natural gas lines. If escaping gas was noted, lines were uncovered and either replaced or repaired. In the hard-hit areas, inspectors checked for pockets of gas before allowing re-occupancy, and before electric service could be restored.

Gas service was essentially back to normal throughout the system in four days except for San Francisco's Marina District and hard hit areas in the Santa Cruz, Watsonville, Los Gatos area. The heavy damage to the gas system in downtown Los Gatos was repaired within two weeks after the quake.

2.4 Communications

Pacific Bell is the primary provider of local telephone service in the affected area. The damage to Pacific Bell facilities was minor and did not affect service. In general, telephone systems performed

better than expected, especially considering the seismic forces that equipment in the epicentral area had to withstand. For example, in Watsonville a four-story reinforced concrete shear-wall structure built in the 1950's was subjected to peak ground acceleration of 0.39g in the horizontal direction and 0.66g in the vertical direction. The peak horizontal acceleration on the roof was 1.24g. The building contains three floors of telephone switching equipment. In addition, it has extensive piping, cable trays, and heating and ventilating systems. During the earthquake, when off-site power was lost, the emergency diesel generator started up immediately and it and the batteries in the building kept the system on-line through the major aftershocks.

The loss of commercial power caused some communication problems. Telephone systems are designed to run on batteries for several hours. Central offices usually have electric-generators to recharge the batteries so that phone service can be maintained for extended periods without commercial power. There were some problems with electric-generators and in one case service at an office had to be reduced until additional backup power could be obtained.

A more common cause of telephone service disruption was the lack of emergency power for private branch exchanges (PBXs) which are privately owned phone systems used by companies and large organizations for telephone service within a facility. These connect to outside lines provided by the local telephone company and use building power when this was lost, so was telephone service.

2.5 Water and Sewage Facilities

Water supply for the Bay Area is primarily imported via long aqueducts from the Sierra Nevada or the Sacramento Delta. A small portion of the supply, especially for Santa Cruz and Monterey Counties is pumped from local groundwater basins or collected as local surface water from steams and springs. Wastewater treatment facilities for most of the area are both secondary and tertiary treatment facilities and discharge treated water into the San Francisco Bay, Pacific Ocean, Monterey Bay, or sewage lagoons.

A preliminary survey of earthquake damage was conducted by members of the American Society of Civil Engineers, Technical Council on Lifeline Earthquake Engineering, Earthquake Investigation Committee, who contacted 25 water agencies and 12 sewer entities, only a portion of the total number of agencies in the area.

The most significant impact on water and sewage lifeline systems of the Loma Prieta Earthquake was the loss of commercial power for a long period of time. Those agencies without emergency power were without power from a few hours to several days. Commercial power, which is supplied by one utility, had significant damage to several high voltage substations which caused most of system in the earthquake area to lose power. The power supply was restored carefully and slowly to service areas and only after checking for gas leaks to avoid the potential for fire. Some of the emergency power supplies had problems because of limited fuel capacity or failed to operate because they had not been tested.

There was no reported damage to any of the four major aqueducts or any of the aqueduct storage reservoirs supplying the area. There was minor damage to a few local reservoirs consisting of earth embankment and abutment cracks and concrete spillway cracks. Repairs were made by excavation and recompaction and epoxy grouting. All the reservoirs were at a low level at the time of the event because of the third-year drought conditions in California and all have been authorized for filling.

There were approximately 800 to 1,000 water main breaks due to the earthquake primarily in the unstable areas along the shore of San Francisco Bay and along the rivers and estuaries entering Monterey Bay. Most of these areas suffered from liquefaction. In general, breaks were longitudinal and circumferential and occurred in small diameter cast iron (sand cast) with fixed (cement or lead caulked) bell and spigot joints pipe; and were due to tension, compression, and bending due to differential settlement. Corrosion of pipe and fittings also played a part in some of these breaks.

In the San Francisco Marina District, the 4-, 6-, and 8-inch mains were installed in the 1930's and were replaced following the earthquake with ductile iron pipe with rubber gasket joints. It is estimated that

100 of the 150 breaks in the San Francisco system occurred in the Marina area. A majority of the main breaks in Alameda occurred on 4- and 6-inch diameter welded steel pipe and were due to corrosion at the joints. Leaks occurred in the San Jose-Los Gatos area on mains ranging in size from 4- to 37-inches of steel, cast iron, asbestos cement, and ductile iron; three-quarters of which were in 25- to 30-year old steel pipe with limited corrosion protection. The types of leaks were holes in the pipe due to corrosion, pulled joints and circular breaks. More than one-half of the leaks were due to holes in the pipe due to corrosion.

In the Monterey Bay area damage to water mains also occurred to mains in unstable areas due to liquefaction. Failure modes included bell cracking, circumferential, longitudinal cracking and push-on joint failures. A majority of the breaks occurred in cast iron pipe with lead caulked joints and small diameter galvanized iron pipe at the threads. It was reported that ductile iron pipe and asbestos cement pipe with rubber gasket joints performed well. It is not known how much of these kinds of pipe is in the older areas subjected to liquefaction.

Service connection breaks occurred in galvanized iron, copper, and polyvinyl chloride pipe.

Relatively few sewer breaks have been identified, because most sewers are gravity flow and water does not appear at the surface of the ground unless there is a blockage. It may be assumed, however, there are at least as many sewer main breaks as water breaks, especially in the same areas of unstable ground. Contacts with sewage agencies indicate they are in the process of performing television (video camera) surveys of the mains to determine the extent of the damage. Breaks in sewer pressure lines (force mains) were identified when power was restored to the sewage pumping stations.

There was little damage reported to pumping stations and pumping wells, except for outages due to the loss of commercial power. Three wells constructed without gravel pack became sanded near Santa Cruz and have been redrilled and another well in Watsonville had a broken discharge pipe.

There was significant damage to small (10,000 to 100,000 gallons) bolted steel, welded steel and redwood tanks, especially in the Santa Cruz Mountains. The damage consisted of collapses, shell buckling (elephant foot), roof buckling and inlet/outlet problems of tanks which had little or no seismic considerations in the design. A 1.1 million gallon post-tensioned concrete tank failed at the vertical joint. The tank was constructed of precast vertical wall panels wrapped with post-tensioned wire and coated with gunite. There was evidence of corrosion which may have contributed to the failure.

In two instances, undamaged water storage tanks were drained. In Hollister, an unreinforced masonry building collapsed onto an adjacent building which had a wet (fire) standpipe. The debris from the collapsed building pulled a coupling on a 6-inch private fire service releasing an uncontrolled flow of water which almost drained a 2 million gallon tank before it could be controlled.

In San Francisco, the Auxiliary Water Supply System (AWSS) provides high pressure supply for emergency fire protection. This system relies on local reservoirs and tanks for supply and is completely separate from the municipal system. A water main on this separate system broke several miles away from a 750,000 gallon tank, which led to temporary loss of pressure in the system (see Scawthorn and Blackburn, 1990). These two events indicate the need for monitoring and controlling the outflow from the storage system after a disaster such as an earthquake.

Damage occurred to a number of water and wastewater treatment plants due to wave action (sloshing) in the South San Francisco Bay area. A laboratory person in Los Gatos reported the wave action almost reached the top of a 30-inch protective railing around a clarifier basin. The damage at an 80 mgd plant was due to the differential movement between the up-flow center feed clarifier and the rectangular walls of the basin. The launderers (wires) pulled away from the wall or pounded against the wall. Some of the launderers fell to the bottom and jammed the sludge scrapers. At a 40 mgd wastewater treatment plant wave action caused fiber glass scum troughs to be damaged in rectangular clarifier basins. The troughs were attached to the concrete wall with a fabricated fiber glass bracket that broke at the angle point. The troughs fell to the bottom and jammed the sludge sweeping scraper. Both plants continued operations

by placing basins not in use back in service.

The major lessons learned from the Loma Prieta earthquake were to continue to use flexible joints in water and sewage piping, provide emergency power for essential facilities, monitor the storage level in tanks and reservoirs to control outlet flow and to consider wave action in the design of treatment plants.

3. OBSERVATIONS OF PIPELINE RESPONSE AT PARKFIELD, CALIFORNIA

An experiment to measure pipeline response to travelling wave effects and to lateral offsets is located on the San Andreas Fault at Owens' Pasture near Parkfield, California approximately 175 km to the south of the epicenter of the October 17, 1989 Loma Prieta Earthquake. A magnitude 6 earthquake is predicted by the U.S.G.S. to occur here within the next few years. The experiment involves an array of welded steel and ductile iron pipe segments which are placed across a strand of the fault. Instrumentation includes strong-motion accelerographs, strain gages on the welded steel pipes, and relative displacement transducers at the joints of the ductile iron pipes. The threshold trigger levels for recording were set at 2 gal. to record foreshocks of the predicted Parkfield-Cholame earthquake and other low amplitude seismic events. Useful records of pipeline strain and ground motions were obtained from the Loma Prieta earthquake, which caused 20 gal. peak accelerations at Owens' Pasture.

3.1 Observed Response in Loma Prieta Earthquake

Peak accelerations of about 20 gal. were recorded in both surface (0-40 sec) and body wave (about 40-80 sec) phases. A triangular region of ground defined by the three seismographs is assumed to deform with constant strain. When the measured horizontal components of ground displacements are imposed on vertices of a constant strain finite element, peak transient values of ground strain of order .001 are found.

Time histories of strains were recorded on the welded steel pipe segments beginning in the interval 34-40 seconds after the start of the ground motion records, which corresponds to the surface wave phase. It is possible that the body wave phase did not induce pipe strains high enough (20 microstrain) to trigger the memory of the data logger; it is also possible that peak strains exceeded 20 microstrain during the body wave phase but at a frequency too high to be resolved by the data logger whose upper limit is currently about 1 hz.

The maximum strains in the tension pipe segment are tensile because transient compressive and tensile strains are superposed onto permanent tensile strain induced by right lateral strike slip; transient compressive and tensile strains in the compression segment are superposed onto permanent compressive strain. The amount of offset that would cause the observed permanent pipe strains is about 1.3 mm. Coseismic creep derived from the U.S.G.S. creepmeter XPK1 is about 1.8 mm. Apparently, some slip occurred at the pipe-soil interface.

The data also illustrate the following points:

1. The pipeline strains on opposite sides of the springlines are approximately equal. This shows that, at least in the horizontal plane, direct extension or compression dominates and bending is less significant.

2. The frequency content of the direct ground strain and of the pipe strain time histories agree closely. In the interval between 34 and 50 seconds, the ground and pipe strains at a number of stations are nearly the same with peak and valleys of the same amplitude occurring almost simultaneously.

3. The shifts in the amplitudes of the pipe strain time history records correspond to the development of a permanent ground strain that appears to occur between 40 and 50 seconds. It is apparently associated with lateral offset as measured in the creepmeter XPK1.

4. CASE STUDY ON SEISMIC PERFORMANCE OF LIFELINE SYSTEMS

As mentioned above, lifeline systems serving the Bay Area performed reasonably well under the Loma Prieta Earthquake, even though isolated failure were significant. It is anticipated, however, that, given time, earthquakes with larger magnitudes will occur, possibly at a more unfavorable location in the Bay area. Therefore, a case study has just been initiated under the sponsorship of the National Center for Earthquake Engineering Research (NCEER). The case study purpose is to investigate how lifeline systems such as water, power and gas delivery systems, telecommunication and transportation systems serving a community performed under the Loma Prieta Earthquake. A community will be chosen for the case study most probably among Los Gatos, Watsonville, or Santa Cruz, taking into consideration the extent of damage, size of community in terms of geography and population, number of lifeline systems involved, degree of utility and governmental cooperation, etc.

The following NCEER researchers are participating in this project: A.H-S. Ang (University of California, Irvine), T. Ariman (University of Tulsa), B. Jones (Cornell), J. Isenberg (Weidlinger Associates), M. Khater (EQE Inc.), F. Kozin (Polytechnic University of New York), M. O'Rourke (RPI), T. O'Rourke (Cornell), M. Phipps (H. J. Degenkolb Associates) and C. Scawthorn (EQE Inc.) (Table 2). There are six specific tasks, some of which can be performed simultaneously. First, physical and operational information on each system will be gathered and documented. Second, on the basis of the information thus gathered and documented, physical and operational models will be developed for the system. Using these models, the state of damage and that of unserviceability will be simulated for each system under the Loma Prieta Earthquake and compared with the actual states of damage and unserviceability for model verification. Third, performance interaction among lifeline systems will be reconstructed on the basis of available data and also modeled. Fourth, the nature and extent of seismic preparedness on the part of governments, utilities, industry, and citizens will be examined as well as to what extent such preparedness, if implemented, indeed mitigated the seismic disaster. Fifth, an analytical model recently developed by Kozin for resource allocation to implement repair and restoration of damaged lifeline systems will be tested against what actually happened, and revised if necessary. Finally, the societal impact of simultaneous and multiple lifeline system failures will also be investigated. Each of these tasks are listed in the attached table together with the names of investigators and brief comments on the task contents.

It is believed this case study will provide valuable insight into the physical, operational, governmental, and societal consequences of lifeline system failure caused by earthquakes for the community as a whole. Lastly, study of the system interaction issue is also of substantial interest from both the technical and societal points of view.

5. REFERENCES

C. Scawthorn and F. Blackburn. *Performance of the San Francisco Auxiliary and Portable Water Supply Systems in the 17 October 1989 Loma Prieta Earthquake.* Fourth U.S. National Conference on Earthquake Engineering. May 20-24, 1990. Palm Springs, California.

6. ACKNOWLEDGMENT

We are indebted to Dr. Jim Gates and Mr. Jerome Houke from Caltrans, Mr. Sy Mouber and Mr. W. Belding from BART, Dr. Edward Matsuda and Mr. William Rowe from PG&E, and Mr. Gerald Serventi and Mr. Thomas Daniels from the port of Oakland for their assistance in documenting the performance of lifelines during the Loma Prieta earthquake. Support from the National Center for Earthquake Engineering Research, SUNY-Buffalo, is also gratefully appreciated.

Table 1

MAJOR ROADS CLOSED AFTER THE EARTHQUAKE

- Martinez-Benicia Bridge closed to trucks in both directions
- I-80 and I-880 closed between Berkeley and I-980 in Oakland due to the collapsed Cypress section
- Bay Bridge closed because of structural damage
- Embarcadero Freeway closed due to earthquake-induced damage
- Interstate 280 closed from U.S. 101 to downtown San Francisco
- U.S. 101 northbound at Highway 92 overpass closed due to debris
- Highway 9 closed at the San Lorenzo River Bridge (near Santa Cruz) due to structural damage
- Highway 17 closed from Scotts Valley to Highway 9 due to landslides
- Highway 1 north closed at Struve Slough Bridge due to a collapsed bridge
- Highway 129 closed at Aromas Road
- Highway 25 closed from U.S. 101 to 15 miles south of Hollister due to rockslides

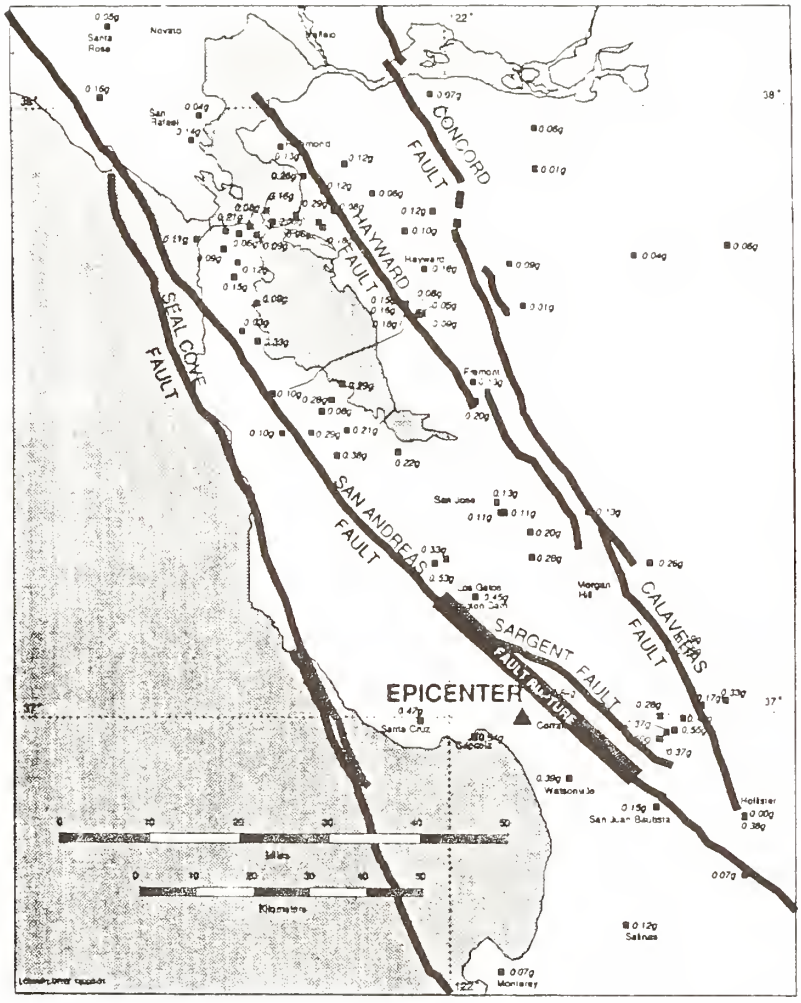

Figure 1: Epicenter of the Loma Prieta Earthquake

Table 2

CASE STUDY ON SEISMIC PERFORMANCE OF LIFELINE SYSTEMS SERVING A COMMUNITY SUBJECTED TO LOMA PRIETA EARTHQUAKE

Project #	Project Title	Investigator(s)	Comments
1	Description of lifeline systems	M. Khater & J. Isenberg	Information gathering and documentation at site
2	Modeling of lifeline systems and verification ■ Vulnerability	A. Ang (Power & Telecommunications), T. Ariman (Gas & Oil) M. Grigoriu (Water),	Use existing models upon adjustments. If not, develop models.
	■ Serviceability	M. O'Rourke (Transportation), T. O'Rourke (Geotechnical).	Simulate states of damage and serviceability and compare with observation
3	Lifeline System Interaction ■ Observation ■ Modeling & Verification	J. Isenberg, M. Khater	Document and model lifeline performance interaction and verify models.
4	■ Preparedness and emergency response	M. Phipps F. Kozin & C. Scawthorn	Preview and recommend preparedness and emergency response measures
5	■ Restoration		Document and model restoration process
6	Societal Impact	Barclay Jones	Evaluation of societal impact of lifeline system failures

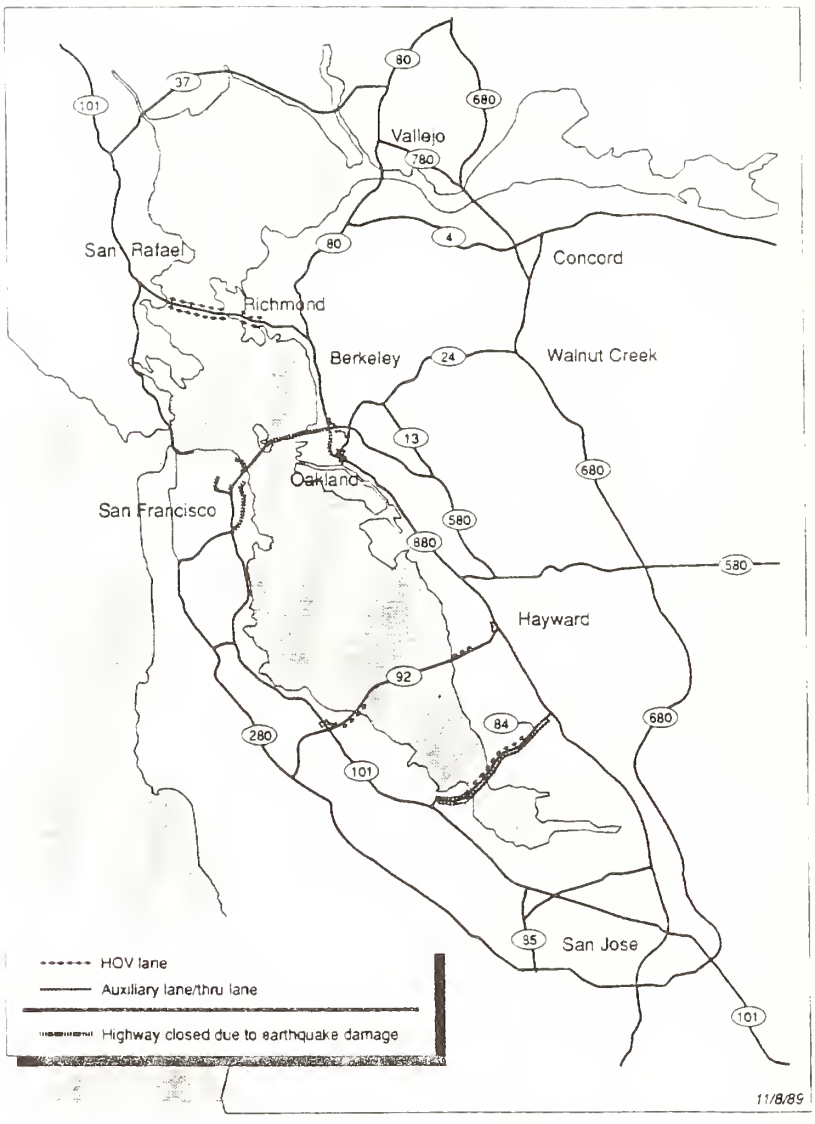

Figure 2: Earthquake Traffic Management Projects (after Caltrans)

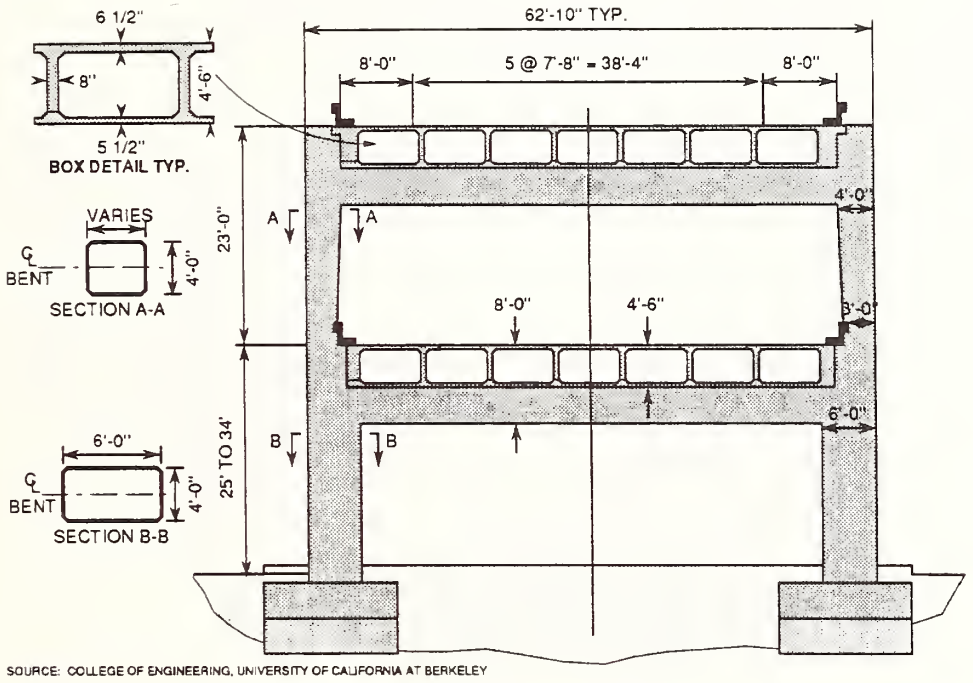

SOURCE: COLLEGE OF ENGINEERING, UNIVERSITY OF CALIFORNIA AT BERKELEY

Figure 3A: Typical concrete frame supporting the double-deck Cypress Street overpass structure

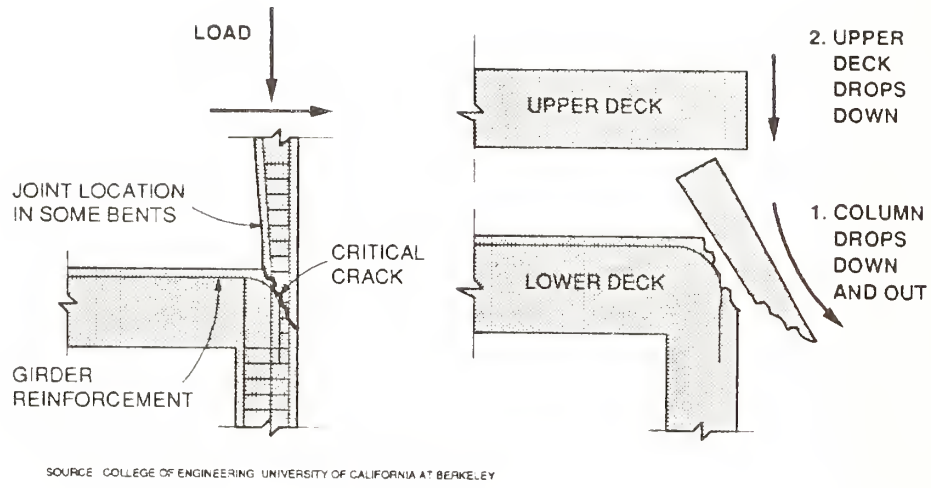

Figure 3B: Poorly detailed and inadequate horizontal ties were primarily responsible for the Cypress section column failures

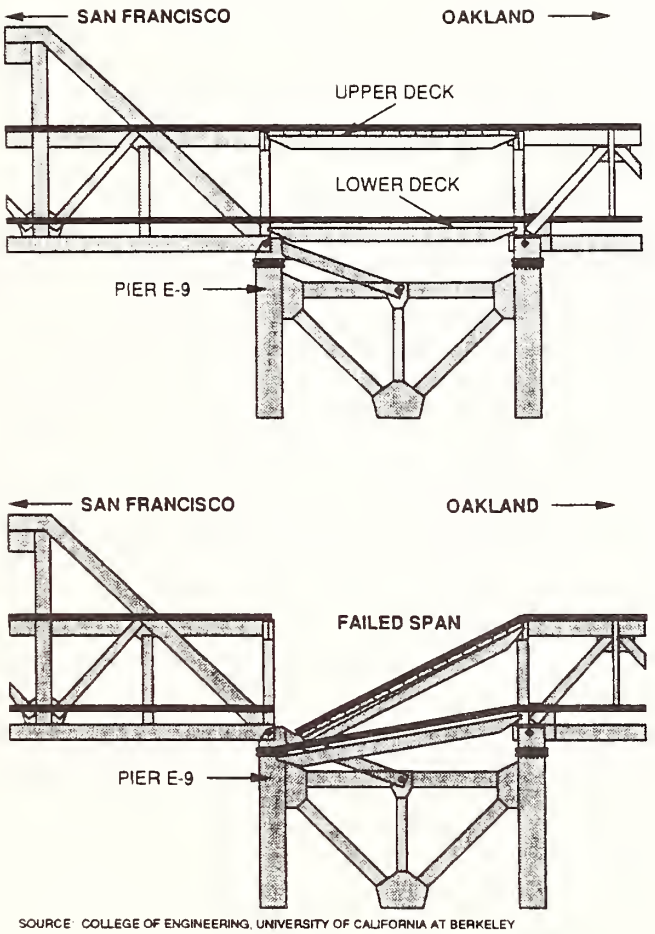

Figure 4: Failure of the Bay Bridge during the Loma Prieta Earthquake

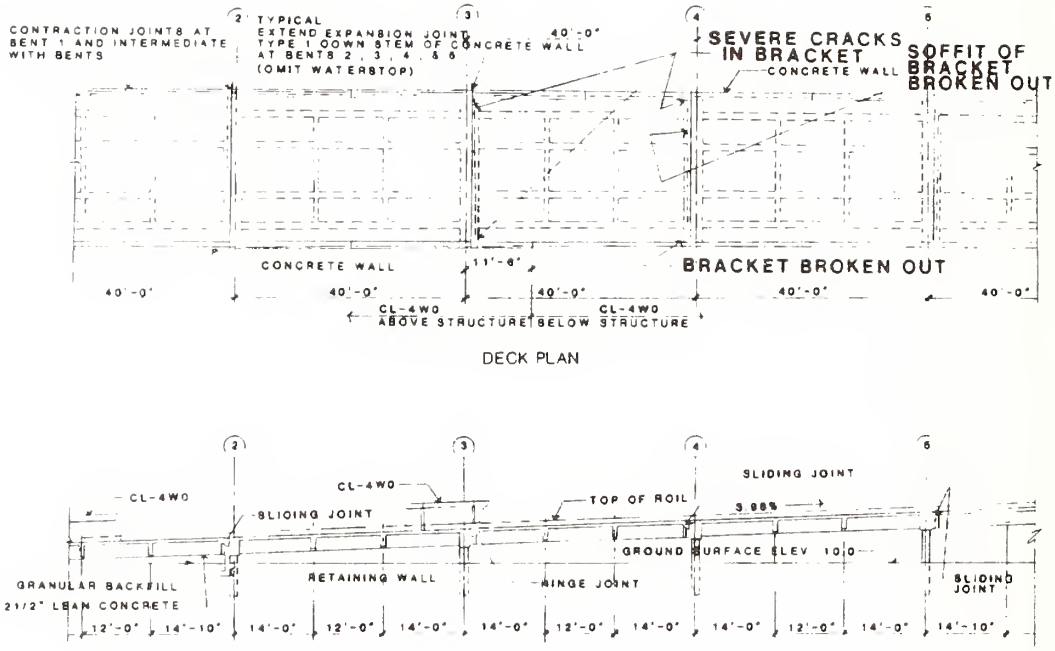

Figure 5: Trans-bay line Oakland approach aerial transition deck plan and profile

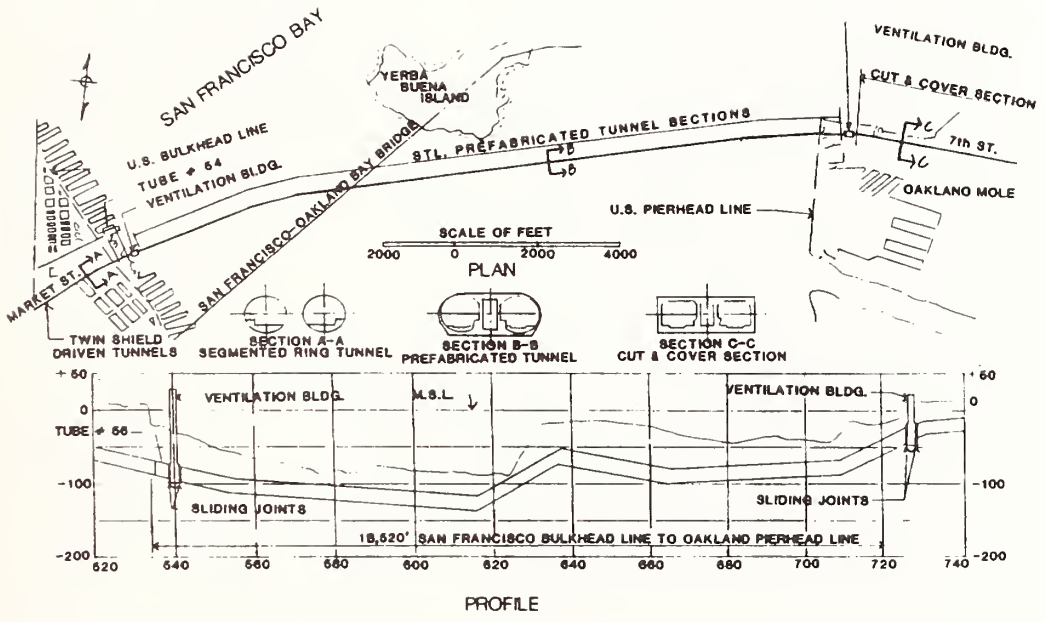

Figure 6: Plan and profile of trans-bay tube

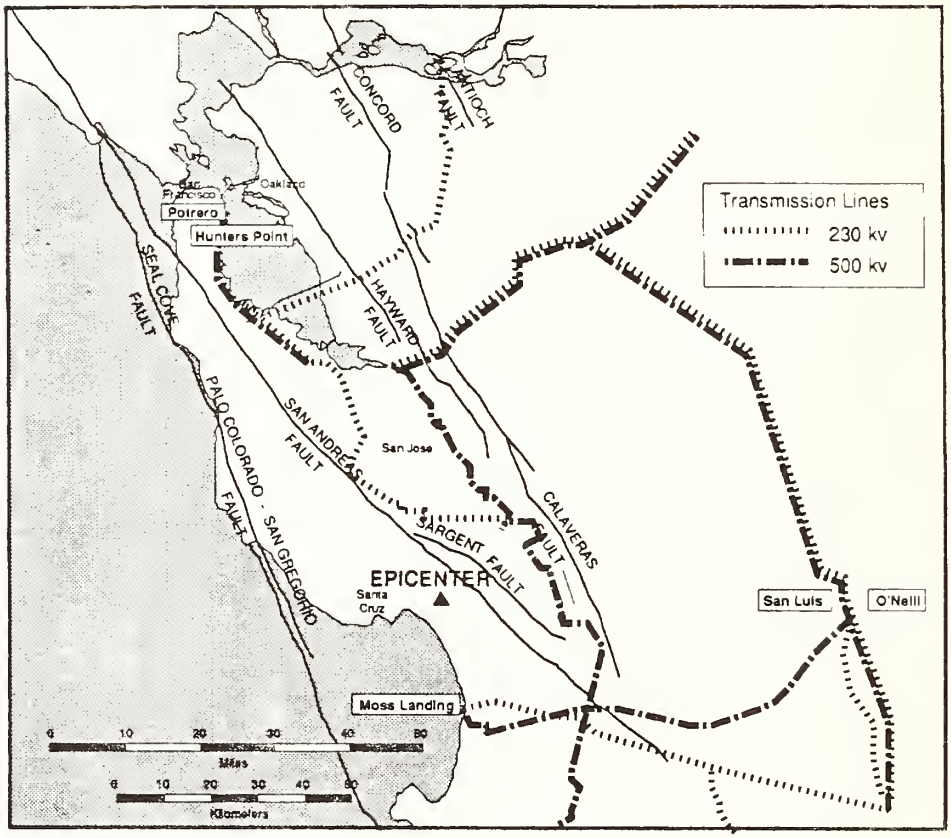

Figure 7: Electric power system in the earthquake-affected areas

Summary Report on the Loma Prieta Earthquake of October 17, 1989

by

Toshio IWASAKI*)

ABSTRACT

On October 17, 1989, the Loma Prieta Earthquake struck the Santa Cruz region, California, U.S.A. The Japanese government sent a study team for the purpose of investigating characteristics of damages caused by the earthquake. This paper presents a summary of the full report prepared by the study team, and emphases on the outline of the damage, strong motion observation, liquefaction, slope failures, damage to lifeline facilities, measures against disaster, voluntary activities by the residents and lessons learned from the earthquake.

KEYWORDS : Loma Prieta Earthquake, Earthquake Disaster, Strong Motion Observation, Liquefaction, Slope Failure, Lifeline Facilities, Measures against Disaster

1. INTRODUCTION

The Loma Prieta Earthquake with magnitude of 7.1 occurred in the Santa Cruz region, California, U.S.A., at 5:04 p.m. (Pacific Daylight Saving Time) on October 17 (Tuesday), 1989. The earthquake struck not only the epicentral region but also San Francisco Bay area located about 90km north of the epicenter. As a result of the earthquake, 62 persons lost their lives and important public facilities and buildings were heavily damaged.

The Japanese government sent a study team consisting of 16 experts of the concerned organizations and institutions in order to contribute to development of the measures against earthquake disaster not only in Japan but also in world-wide countries where occurrences of earthquakes are great threat. The investigation started from mid-November for two weeks just after finishing emergency rescue activities for suffered people. An investigation on the damages in the epicentral region and San Francisco Bay area was made with a great assistance and support of many organizations concerned with disaster prevention including U.S. federal organizations, the California state government, local (county and city) governments and private firms.

The investigation by the Japanese team was successfully completed with a great deal of supports by Dr.R.N.Wright, the U.S. Chairman of the Panel on Wind and Seismic Effects, UJNR, Mr.N.J.Raufaste, Secretary-General of the Panel, and Dr.H.S.Lew, Dr.A.G.Brady, and Mr.J.H.Gates (members of the Panel).

The original full report (in Japanese, about 300 pages) was published in January 1990. The contents of the report are as follows:

Preface
1. Introduction
2. Natural Conditions and Social Conditions
3. Systems of Earthquake Prediction and Precursors of the Loma Prieta Earthquake
4. Outline of the Event, Crustal Movements and Strong Motion Observations
5. Soil Liquefaction and Slope Failures
6. Damages to Roads and Bridges
7. Damages to Buildings
8. Damages to Lifeline Facilities (Except Roads and Bridges)
9. Disaster Preparedness Administrations and Emergency Measures
10. Public Responses (Voluntary Activities and Contributions of Volunteers, and Public Education)
11. Closing Remarks (Summary of Findings, Discussions with U.S. Experts, Proposals, and Acknowledgments)

This paper presents a summary of the report with an emphasis on the outline of the damages, ground failure, strong motion data, damages to lifeline facilities (road facilities and others), measures for disaster prevention and voluntary activities by the residents and conclusions (lessons learned from the earthquake).

2. OUTLINE OF DAMAGES

Fig.1 shows the epicentral region and San Francisco Bay area affected by the Loma Prieta Earthquake. Major damages were developed in the region of Watsonville located south of the epicenter to Martinez located north of Richmond.

FEMA (U.S. Federal Emergency Management Agency) and OES (Office of Emergency Service, State of California) reported an estimation of damages as

1)Number of death : 62 persons
(Besides a few lives were lost by indirect effects such as heart attack)

*) Director General, Public Works Research Institute, Ministry of Construction

2)Number of the injured : 3,208 persons
3)Total cost of damages :
estimated as 70 to 80
billion dollars
(An official estimate by the Federal or State governments has not yet released)
4)Suffered people : about 55,000 persons

3. OUTLINE OF THE LOMA PRIETA EARTHQUAKE

Since the San Andreas fault and several active faults run through the California state, California is one of earthquake prone regions similar to Japan. The Loma Prieta Earthquake is a medium size earthquake with magnitude of 7.1 along the San Andreas fault. Any particular forecasts for the occurrence of the earthquake were not made.

USGS (United States Geological Survey) reported that the epicenter was located at 37.036° N. latitude, 121.883° W. longitude. The focal depth was 18km, and this is said rather deep than normal ones so far observed along the San Andreas fault. Geodetic surveys following the earthquake indicate that a slip at the hypocenter region had a right-lateral horizontal component and vertical component that caused a total oblique-slip displacement of 2.3 m. The area of the fault surface was estimated to be 13 km wide and 40 km long. Since the epicenter was relatively deep, any fault has not been observed on the ground surface.

In the epicentral region, due to an extremely strong ground motion (horizontal acceleration over 0.7 g) extensive ground fissures and slope failures as well as deformations of ground surfaces were developed.

4. STRONG MOTION RECORDS

Intensified strong motion observation have been made in the State of California by mostly USGS and CDMG (California Department of Mines and Geology). During the earthquake, strong motion records were obtained at 135 stations (38 stations by USGS, 93 stations by CDMG and 4 stations by the University of California at Santa Cruz).

Fig.2 shows acceleration records and response acceleration spectra obtained at city of Corralitos closest to the epicenter (epicentral distance is 7km, and the distance to the fault is only 1 km). Peak accelerations are 0.5 g and 0.64 g in two orthogonal horizontal directions and 0.47g in vertical direction. The records can be characterized as the large peak acceleration and relatively long predominant period of 0.7 seconds. This may be one of the reasons to cause heavy damages in San Francisco Bay area.

Fig.3 shows the distribution of peak accelerations on ground surface level and first floor level of buildings. Stations ① to ④ located north-east of the city of San Francisco are on the rocky bed, and peak accelerations recorded are in the range of 0.06 g to 0.09 g. On the other hand, peak accelerations recorded at stations ⑤ to ⑨ are within the range of 0.16 g to 0.26 g (0.33 g at San Francisco International Airport) which are 2.5 to 3 times larger than those on the rocky bed. It should be noted that accelerations were largely amplified by the effects of soft ground.

Fig.4 shows the relationship between epicentral distances and peak accelerations obtained through the analyses of strong motion data (excluding the data recorded at buildings and building basements). In the figure, empirical formula (for ground condition II) proposed by PWRI[4] is also shown.

$$a_{max} = 232.5 \times 10^{0.31M} \times (\Delta + 30)^{-1.218} \quad (1)$$

where, a_{max}, M and Δ represent peak acceleration in gal (cm/sec^2), magnitude of earthquake (7.1) and epicentral distance in km. Since Eq.(1) shows a mean attenuation derived from a statistical analysis of strong motion records on the ground surface with moderate to hard soil conditions (ground group II specified in the Seismic Design Specifications of Highway Bridges), actual data disperse along the mean value expressed by Eq.(1). Two curves showing the variation of a standard deviation (1σ) from the mean value are also shown in Fig.4.

This figure indicates that peak accelerations recorded varies widely even for the same epicentral distance. However, since peal acceleration recorded during the Loma Prieta Earthquake are within the range of the mean value $\pm 1\sigma$, the attenuation with distance can roughly be explained by Eq.(1). It is often suspected that a special ground vibration called as echo phenomena occurred in the bay area because heavy damage was developed not in the epicentral region but in the bay area far from the epicenter. But, excluding the fact that rather long period ground motion was developed from the fault, it should be emphasized that the propagation of the ground motion was not extraordinary from the viewpoint of the fact that peak accelerations attenuate with distance in a quite natural way predicted from the past Japanese experiences.

5. LIQUEFACTION, GROUND FISSURES AND SLOPE FAILURES

Liquefaction, ground fissures and slope failures were found at several places. Damages caused by liquefaction concentrated in the cities of Santa Cruz and Watsonville located south of the epicenter, at alluvial soil ground along rivers and coasts , and at reclaimed lands in San Francisco Bay area.

Although various structures were heavily affected by liquefaction in some areas (Marina district in San Francisco, Oakland Port, Oakland Airport, cities of Santa Cruz and Watsonville), liquefaction did not affect strongly structures in other districts.

Ground fissures occurred in the epicentral region. Particularly in the region about 8km long and 2.5km wide which is located south-west of the San Andreas fault and west of State Highway 17, several ground fissures occurred and caused heavy damages to some residential houses.

Landslides were also found in several places in the epicentral region. Some roads were closed to public traffic. Photo.1 shows the largest landslide on State Highway 17. It took about one month to completely reopen this potion to the public traffic.

6. DAMAGES TO ROAD FACILITIES

6.1 OUTLINE OF DAMAGES TO ROAD FACILITIES

CALTRANS (Department of Transportation, State of California) reported that damage of road facilities is estimated as $ 18 billion which corresponds to 22.5% of the total property damage of $ 80 billion caused by the Loma Prieta Earthquake. The damage to road facilities includes damages to bridges, cracks of pavement, falls of rocks and soils, slope failures along the roads. The damages of bridges were most serious among them.

According to CALTRANS, there are about 1,500 bridges managed by the State and the almost same number of bridges managed by counties and cities in the affected region. Three bridges were critically damaged and fell down, 9 bridges were heavily damaged, 13 bridges were moderately damaged and 65 bridges were slightly damaged. Damages to three fallen bridges are described in details in the following.

6.2 Cypress Viaduct (Interstate 880)

The Cypress viaduct consists of a bi-level concrete decks with length of about 2km on the Cypress Street of I-880 through the city of Oakland. It was designed so as to resist a lateral earthquake force of seismic coefficient of 0.06 in 1953 and 1954, and its construction was completed in 1957. The Cypress structure consists of three-span continuous RC cellular box girders with span length of 24m. The ends of the girders were interconnected using expansion joints and the structure was equipped with cable restrainers at each transverse expansion joint between the longitudinal box girders.

Bridge columns were made of reinforced concrete and hinged connections were provided at the bottom of the columns. Three types of column configurations were employed as shown in Fig.5. Type-1 was generally used, and Types 2 and 3 were employed at the sections which had a wider lateral beam, such as ramp and skew sections, and sections to be widened in the future. On Types 2 and 3, lateral beams of upper girder were made of prestressed concrete using unbonded PC steel bars.

Bridge columns were supported by rafts and pile foundations, and columns and rafts were interconnected using hinged joints. The Cypress Viaduct passed through the transition area of ground conditions between reclaimed soft ground, which was a hinterland-damp ground before 1956, and well-compacted sand layer of diluvial soil. Soft silty and clayey layers were piled up almost to 20m in maximum in the reclaimed zone. The 2-km section of Cypress Viaduct heavily damaged was demolished soon after the earthquake. The 1.2-km section of the Cypress Viaduct between the interchange I-80 and the crossing point with 18th street fell down. This section was found to be in the reclaimed area as shown in Fig.6. Peak acceleration in that area was estimated to be about 0.26 g and the damage should be caused by the fact that the seismic design coefficient of 0.06 was smaller than the acceleration actually acted.

Photos.2-4 show typical damages in which the upper deck completely fell down on the lower deck. Fig.7 shows an estimated collapsed mechanism of Type-1 column. This figure indicates that shear failure occurred by excessive lateral load at lower portion of hinged joints which supported upper columns and girders. At the same time, flexural cracks were developed at the corners between lateral beams and columns of upper girders, and then the corners were tore up. Finally upper decks fell down.

The hinged portion which supported upper columns was installed at the higher portion than lateral beam of lower deck, as shown in Fig.8(a). However, the reinforcement in the portion was not enough when compared with that in lateral beam, because small seismic design coefficient of 0.06 was considered. Therefore, when lateral force was imposed at the hinge, shear cracks easily developed. Then when cracks reached to the axial reinforcement at the ends of cross sections of columns of the lower decks, it was easy to shift to failures as tearing up the axial reinforcement. Furthermore, fixing length of U-shaped anchorage reinforcement, which was arranged to restrict longitudinal reinforcement at the top portion of columns for preventing this type of failure, was not long enough. It was also estimated that the sufficient performance of the portion could not be expected because of this inadequate arrangement of reinforcement at the hinge portion.

On the other hand, the most of reinforcement at the bottom of upper lateral

beams terminated and the reinforcement which was anchored to the columns was almost one fourth of those in the bottom. The haunch was not provided at the corner of beam-column connection as shown in Fig.8(b). Besides, the reinforcement in the bottom of lateral beam was not bent down into the column and anchorage length was not long enough, either. Hence, when the bending moment was imposed at the corner and then flexural crack reached to the reinforcement at the bottom of lateral beam, failure occurred at the corner and the reinforcement was easily pulled out of the column. Therefore, it was estimated that both of upper columns opened towards the outside because the two legs were forced to open, and that finally upper decks fell down onto the lower decks.

6.3 Bay Bridge (Interstate 80)

The Bay Bridge is a double-decked highway bridge with total length of 13.4 km connecting cities of San Francisco and Oakland, and consists of twin suspension bridges between Yerba Buena Island and San Francisco (west side) and truss bridges including cantilever structures between Yerba Buena and Oakland (east side). The bridge was designed in consideration of a seismic design coefficient of 0.1 and its construction was completed in 1936.

A deck span with the length of 15 m fell down on E9 steel pier as shown in Photos.5 and 6, provably due to out-of-phase longitudinal vibration between the bridges of east side (Oakland side) and west side (San Francisco side).

Although ground soils near Pier E9 consist of mainly silty and clayey layers which partially include sand layers, the surface layer is not particularly thick at the Pier E9 site. Bed rock can not be found at least up to 35m under the bottom of the sea.

The Pier E9 is of a four-column diagonally braced steel tower which was designed as laterally fixed supports for both of a truss with 154 m long in the east bay side and a truss with 88 m long in the west bay side. The fallen girders for supporting the upper and lower decks connect two truss bridges on the Pier E9. One more girder was provided under lower deck for installing an electric transformer. The fallen girders were supported by I-beams with a seat length of 12.7cm, and the east side of girders was bolted to these seats. Although the length between the end of the girder and the edge of I-beam was not long enough, fallen girders were designed so that they connect two truss bridges which were fixed at Pier E9. As the relative displacement between two truss bridges was designed not to be developed, it seems that the falling of the girders during the earthquake was not predictable.

During the earthquake all of 24 bolts (ϕ 25.4mm) at the Pier E9 connecting shoes of the east side truss bridge were sheared off as shown in Photo.7, and the girders moved about 14 cm to the east and about 2 cm to the north. Because of this excessive displacement the upper deck fell down and struck the lower deck. Although the shoe seats for the lower deck were damaged by the shock of the fallen upper deck, the girder supporting the electric transformer prevented the two-layer girders from falling down completely into the sea.

After the earthquake, two damaged decks were removed and new girders were designed and erected. The residual morements of 13-span truss bridges (total length of 1,140 m) were replaced, one by one, using jacks at each span. Although the restoring work of the girders was estimated to take at least a few months, the work was completed and reopened to public traffic on November 17, just one month after the earthquake. A great deal of efforts of CALTRANS should be highly applauded.

6.4 Struve Slough Bridges (State Highway 1)

Struve Slough Bridge, crossing a damp soft soil zone located on State Highway No.1 south of Watsonville, is a 21-span continuous RC girder bridge. Three gerber hinges (expansion joints) were located in each bridge. Although the abutment at both ends of the bridges were supported on stiff ground, piers were built in the damp soft soil (ground water level of -0.8m). The piers consisted of pile bents (ϕ 38 cm) which were fixed to the lateral beam of the deck. The bridges were designed in 1961 according to the former seismic design code, and the construction was completed in about 1965.

As shown in Photos.9 and 10, the center section about 100 m long of the bridge, which has a total length of about 232 m, moved residually about 80 cm in maximum in the transverse direction and fell down. Four piles punched out through the deck slab and the head of piles stick out from the slab as long as 1.2 m to 1.8 m.

Photo.11 shows the damage to the connection of piles to lateral beam. The heads of the pile bents completely failed and the some axial reinforcements ($6 \times \phi$ 20mm) were seriously bent and broken. The pile bents were completely failed at their heads and dislodged from the lateral beam, crashed to the deck slab, and seriously inclined. Some pile bents completely fell down onto the ground. The 4 pile bents punched out through the deck slab by the falling-off energy of the deck slab as shown in Photo.10, which implies that vertical bearing capacity of the piles was estimated high enough. Since a gap about 60 cm wide in the transverse direction between piles and ground surface can be found, it seems that the piles largely moved.

Although the portion of the pile over the ground level was made of reinforced concrete, portions under the ground level are estimated to be cast-in-place plain concrete piles, so called dropped-in-shell piles which are one type of Raymond piles. This type of pile has not been employed in Japanese bridges.

It is considered that an excessive earthquake lateral force over the one considered in the design may be a major reason for such a critical damage. It is also considered that the ground acceleration was at least more than 0.2 g at the site, and that the substructure consisted of 4 pile bents, which connected to lateral beam, could not resist the lateral force in the transverse direction. Furthermore, it is supposed that the plain concrete portions of the piles under the ground level failed during the earthquake, judging from appeared damage of the piles.

7. DAMAGES TO LIFELINE FACILITIES (EXCEPT ROAD FACILITIES)

This section briefly summarizes damages to lifeline facilities (except road facilities above mentioned) such as water supply and sewer facilities, electric communication facilities, electric power supply facilities, gas supply facilities, broadcasting facilities, data communication and computer facilities, harbor and airport facilities, subway, and river facilities.

The serious damages to water supply and sewer facilities were not developed except some damages at Marina District and South Market area in San Francisco.

Although slight damages to cables, antennas of automobile phones and electric power apparatus were found, physical damages to electric communication facilities, were not found, either. However, since a large number of phone calls from not only domestic but also world-wide countries rushed to the region (7 times for receiving and 2 times for sending, when compared with the ordinary numbers), congestion of the phone communication continued for two days because of exceeding the dealing capacity by far. Communication companies in the affected region restricted a considerable number of calls (especially for receiving) for two days.

Electric power supply stopped for a day or two mainly in some areas in San Francisco, due to damages to power generation, transformer sub-station, and power distribution facilities. The power failure seriously affected the normal living of the residents, and interrupted functions of various facilities, which depend on electricity.

Gas supply facilities in three cities close to the epicenter and some other areas (with soft reclaimed ground) in San Francisco were damaged. In particular, cast-ironed pipes were damaged due to liquefaction of ground in Marina District in San Francisco. The gas mains of total length of about 16 km and distribution pipes to houses were renewed after the earthquake.

Although broadcasting facilities were affected by the power failure, direct damages were slight and therefore broadcasting continued. It seems that the continuation of broadcasting greatly contributed to security and ease of the residents.

Electric power failure and damage to buildings caused losses of functions of data communication and computer systems in San Francisco. However, little damages to physical facilities were found.

Subsidences of grounds and damages to buildings of harbor and airport facilities, mostly caused by liquefaction of ground, were found in Oakland Harbor and San Francisco International Airport.

Although the BART subway (including a section of submerged tunnel) operated in San Francisco Bay area were affected by the power failure, and a little increase in leakage of water at approach sections of the tunnel was observed. Operation of the subway restarted within a few hours after performing quick inspections and temporary repair works. The BART subway as well as ferryboats played an important role for public transportation until Bay Bridge reopened to public traffic.

Several damages to river embankments, such as subsidences, were found in the epicentral region. Minor cracks at the surfaces of upper and lower sides of earth dams were also found.

8. MEASURES AGAINST DISASTER AND VOLUNTARY ACTIVITIES

Twenty two fires occurred in San Francisco. No fires were big. In the worst case 4 houses were burned down. It should be recognized that usual disaster drill and education on earthquake disaster for the residents prevented big fires and occurrences of panic. In despite of the power failure, the public order was maintained after the earthquake, with helps by volunteers. Therefore, no critical problems happened to public security or traffic flow.

Emergency measures against disaster were implemented by the federal, state and local governments in the same buildings (in some cases). Each role of these organizations was shared clearly. Various measures for the sake of suffered people were conducted.

It should be particularly emphasized that people of the U.S. have voluntary spirits since the foundation of the nation, and that the voluntary activities by private sectors

such as the Red Cross and the Salvation Army played important roles in reducing disasters. This is an important suggestion to improve Japanese situations of measures and policies against disasters.

9. CONCLUDING REMARKS

Although the Loma Prieta Earthquake was medium in size with magnitude of 7.1, San Francisco Bay area was heavily affected. This happened since the great San Francisco earthquake of 1906 (magnitude of 8.3) which affected most seriously in the history of U.S.A. It is said that the Loma Prieta Earthquake was a first experience in which a medium size earthquake struck a modern highly information-oriented and densely populated city.

The earthquake indicates how seismic performance of lifeline facilities (such as road, electric power and information communication facilities) is important. The earthquake caused fatalities of 62 lives and heavy structural damages. However, the effects of the earthquake have not ended yet and will happen in various forms. In California state, sales tax has been raised as much as 0.25% for 13 months of the period from Dec. 1, 1989 to Dec. 31, 1990, and an increase in state revenue of $8 millions is expected to spend for restoring. Furthermore, federal government will spend the ordinary budget of 3 times as much as state one for the purpose of restoring public facilities (namely, federal and state governments shared 75% and 25% of the budget for the restoring public facilities, respectively).

It is indicated that frequencies of occurrences of large earthquakes in Japan are higher than those in U.S. Although it is not appropriate to directly apply the experiences of the Loma Prieta Earthquake to Japan (because seismic design methods of structures including the seismic forces are not same), it is essential to constantly promote and improve measures against disasters caused by large earthquakes.

10. ACKNOWLEDGMENTS

Great supports and efforts were given, from both U.S. and Japan, to the Japanese Government Study Team for the Loma Prieta Earthquake. The author, on behalf of the team members expresses our appreciations to following organizations and individuals

From the Japan side, the team got a great deal of supports and cooperations from the Ministry of Foreign Affairs, Consulate-General of Japan in San Francisco, Disaster Prevention Bureau of National Land Agency (especially Mr.Ichiro Ichikawa, Chief of the Bureau), Ministry of Construction, Japan Highway Public Corporation, Metropolitan Expressway Public Corporation and Honshu-Shikoku Bridge Authority. The author would like to greatly appreciate to the concerned persons of the above organizations. And Mr.Hideaki Oda, Sub-leader of the team, and other members of the team are acknowledged for a great contribution to field investigations and preparation of the report.

A great deal of appreciations are also directed to Dr. R.N.Wright (Directer of Center of Building Technology, National Institute of Standards and Technology and also U.S. Chairman of the Panel on Wind and Seismic Effects, UJNR), Mr.N.J.Raufaste (Secretary-General of the Panel, NIST), Dr.H.S.Lew (member of the Panel, NIST), Dr.A.G.Brady (member of the Panel, United States Geological Survey, Department of the Interior), Mr.J.D.Cooper (member of the Panel, Federal Highway Administration), and Mr.J.H.Gates (member of the Panel, CALTRANS) for providing a great deal of supports with regards to 1) invitation of the team, 2) arrangement for the field investigation, 3)joint investigation of the affected structures, and 4) offer of many information including valuable photographs and slides.

11. References

1) Japanese Government Study Team for the Loam Prieta Earthquake (T. Iwasaki, H. Oda, et. al.) : Report on the Damage by the Loma Prieta Earthquake, Disaster Prevention Bureau, National Land Agency, January, 1990 (in Japanese).

2) Iwasaki, T., Kawashima, K., Itoh, Y., Akimoto, Y. and Tatsumi, M. : Reconnaissance Report on Damage by the Loma Prieta Earthquake, Civil Engineering Journal. Vol.32, No.2, February, 1990 (in Japanese).

3) Iwasaki, T. and Kawashima, K., Damages to Bridges during the Loma Prieta Earthquake, Journal of Roads, No.1990-2, February, 1990, Japan Road Association. (in Japanese)

4) Kawashima, K., Aizawa, K. and Takahashi, K. : Attenuation of Peak Ground Acceleration, Velocity and Displacement Based on Multiple Regression Analysis of Japanese Strong Motion Records, Earthquake Engineering and Structural Dynamics, Vol.14, 1986

5) Lew, H.S. (editor), Performance of Structures during the Loma Prieta Earthquake of October 17, 1989, NIST Special Publication 778, NIST, January, 1990.

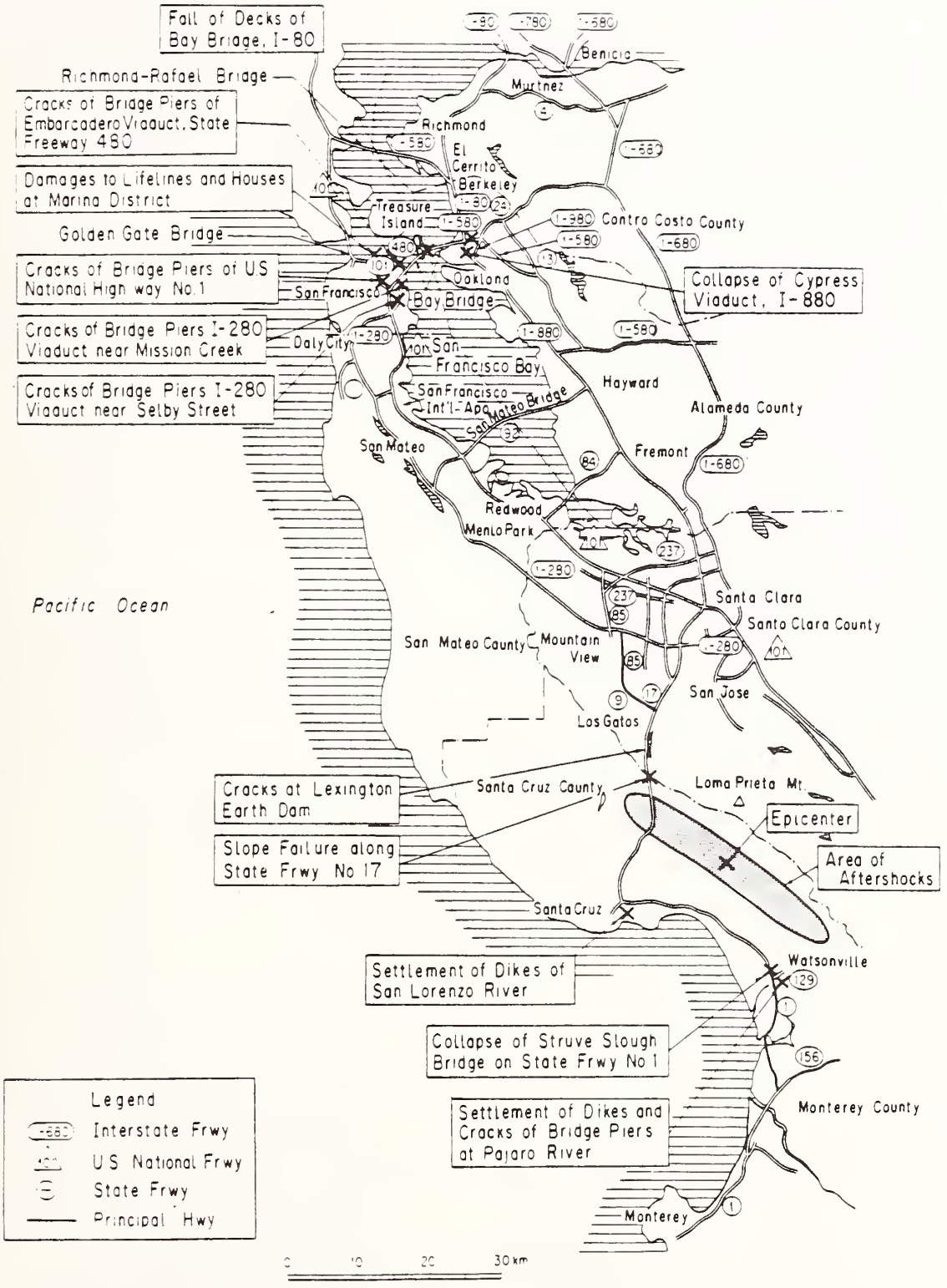

Fig. 1 Map of Affected Area

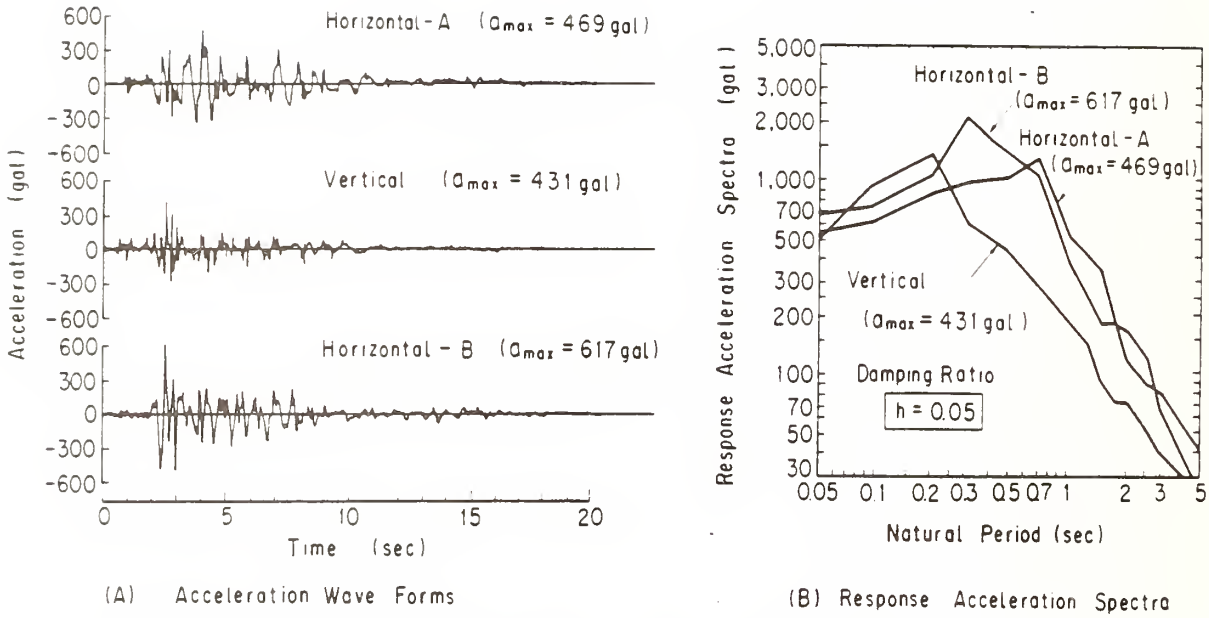

(A) Acceleration Wave Forms

(B) Response Acceleration Spectra

Fig. 2 Acceleration Wave Froms and Response Acceleration Spectra (for Damping Ratio of 5%) Recorded at Corralitos Closest to the Epicenter (from CDMG)

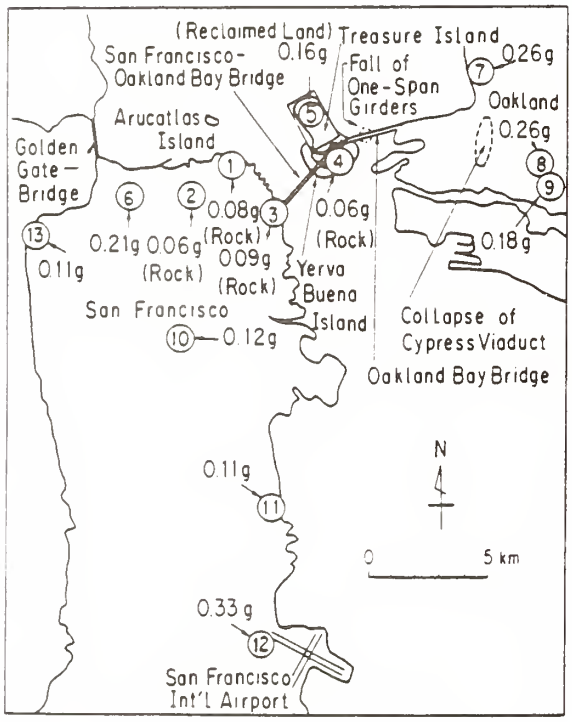

Fig. 3 Distribution of Peak Accelerations on Ground Surfaces and First Floors of Buildings (from USGS and CDMG)

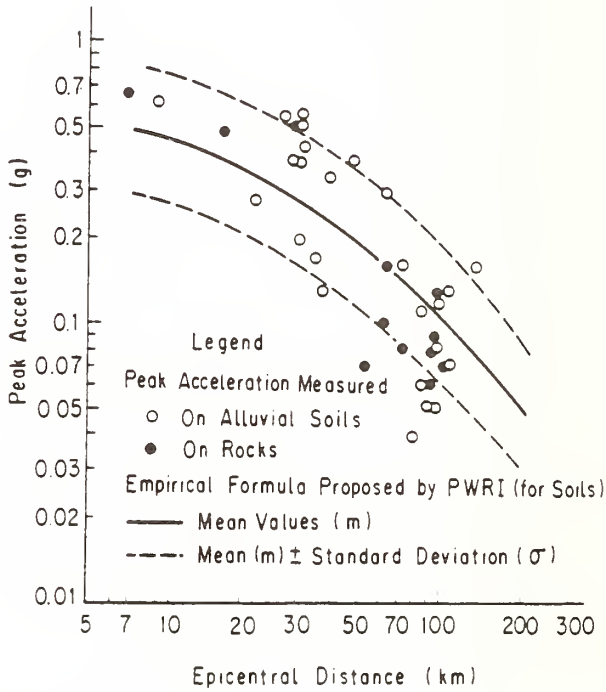

Fig. 4 Relationship between Epicentral Distances and Peak Accelerations

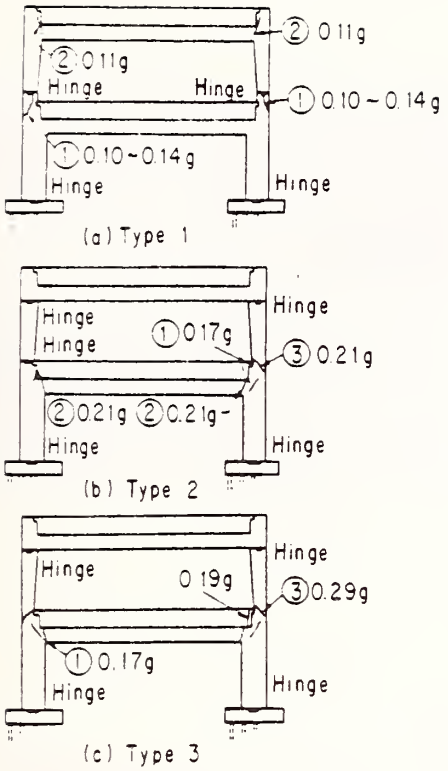

Fig. 5 Three Typical Types of Piers of Cypress Viaduct (Accelerations indicated correspond to those which cause failures at respective locations, estimated by Prof. Priestley, Univ. of Calif. at San Diego)

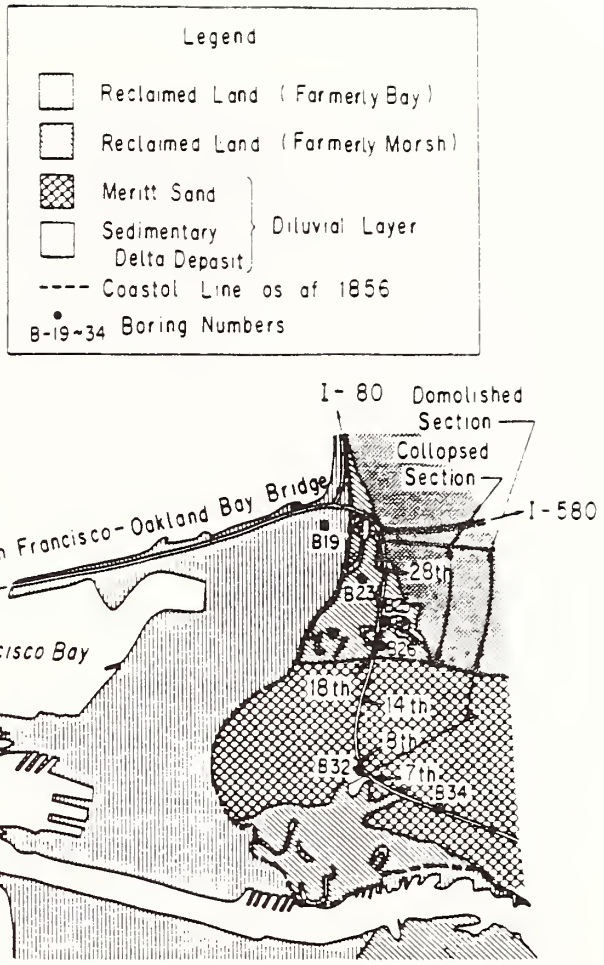

Fig. 6 Location and Geological Conditions of Cypress Viaduct

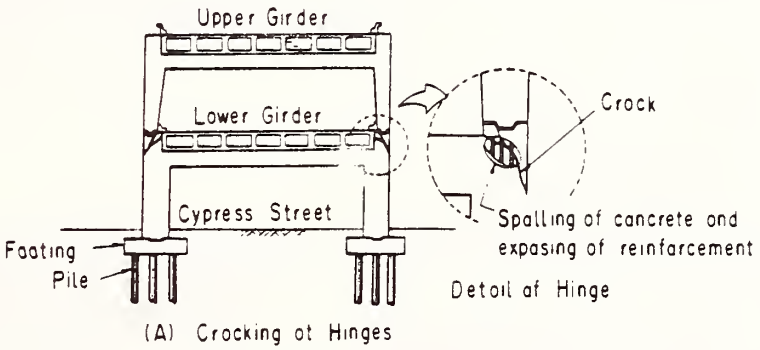

Fig. 7 Estimated Collapse Mechanism of Cypress Viaduct (Type 1 Pier)

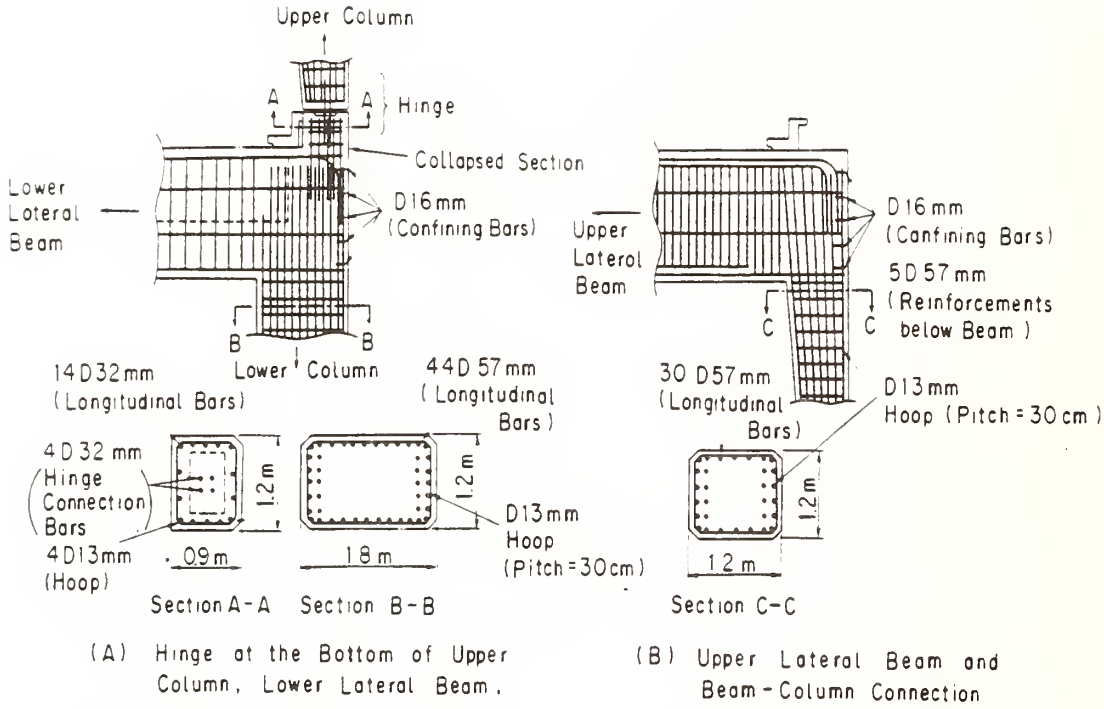

Fig. 8 Structural Details of Hinge and Beam-Column Connection at Cypress Viaduct

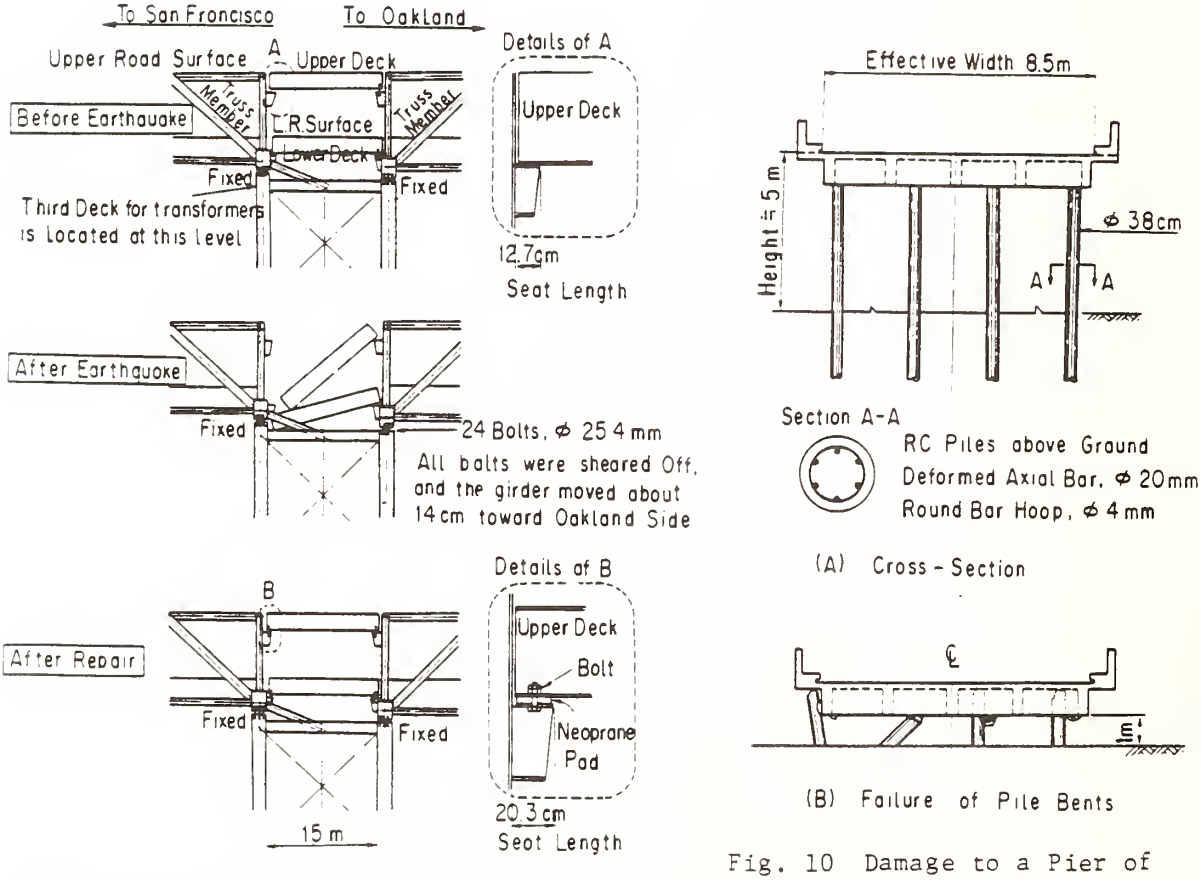

Fig. 9 Fall of One-Span Decks on Pier E9 of Bay Bridge and Outline of Its Repair

Fig. 10 Damage to a Pier of Struve Slough Bridge

Phote. 1 Slope Failure along State Freeway No.17 (One of Largest Landslides caused by the Earthquake with Height ≒ 20m and Length ≒ 100m; It took one month to completely open this portion to the public traffic. This photo was taken in the end of November, 1989 after repair works finished.)

Photo. 2 Collapse of Cypress Viaduct on 32nd Street, Oakland. Typical damage to Type 1 piers (from CALTRANS).

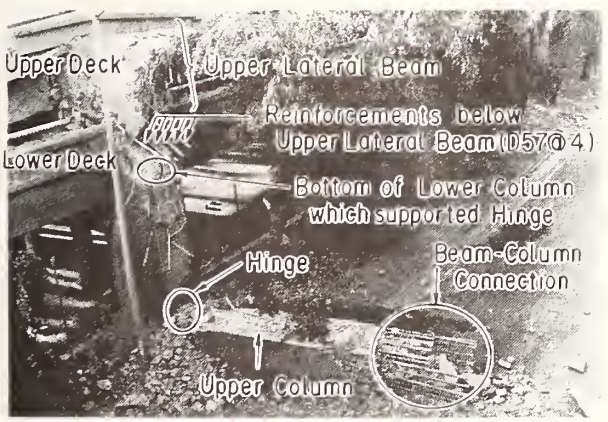

Photo. 3 Collapse of Type 1 pier of Cypress Viaduct. Upper Deck completely fell down onto lower deck due to failures at hinge at the bottom of the upper column and at beam-column connection (from CALTRANS).

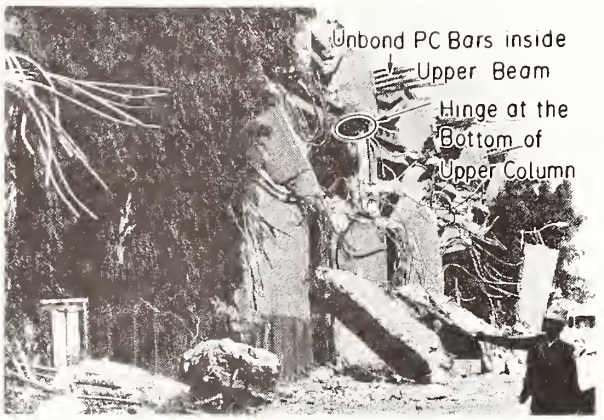

Photo. 4 Collapse of Type 2 pier of Cypress Viaduct. Upper columns fell down due to failures at upper hinges. Reinforcements at the bottom of columns are seen. Unbond PC bars are seen atop (from CALTRANS).

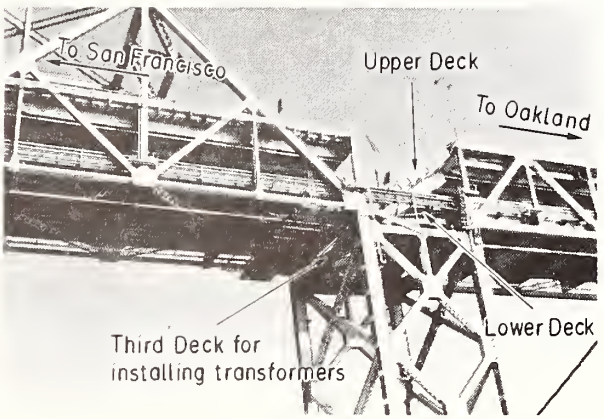

Photo. 5 Fall of one-span decks on steel pier E9. Upper and lower decks fell down, but fortunately those two decks stopped on the third deck which install transformers (from CALTRANS).

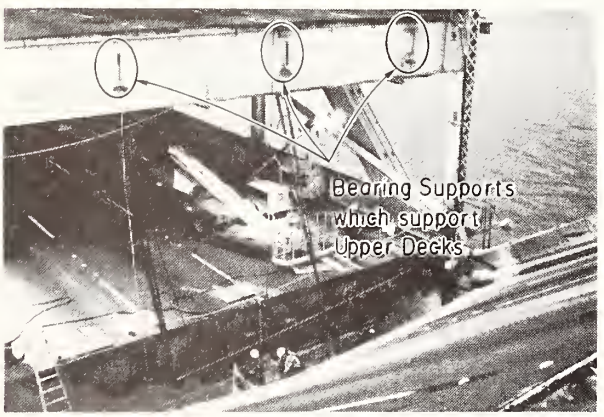

Photo. 6 Removal of fallen decks. Bearing supports for upper deck are seen. The length of bearing seat is 12.7 cm (from CALTRANS).

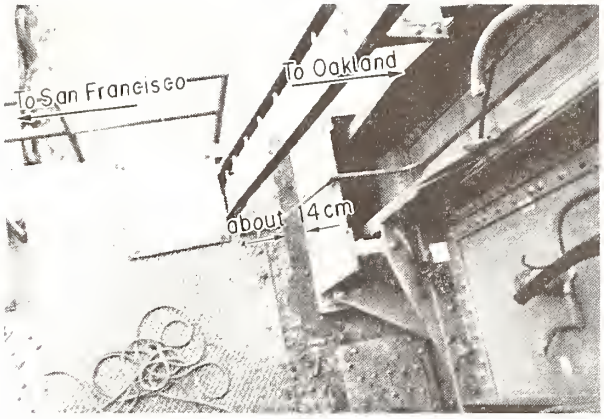

Photo. 7 Movement of the fixed bearing support on the east (Oakland) side of pier E9. Bolts were shear off, and the support moved about 14 cm to Oakland side. Due to this movement the upper deck (with bearing seat length of 12.7cm) dislodged from the supports, and fell down (from CALTRANS).

Photo. 8 Due to the impact of the fall of the upper deck onto the lower deck, the lower deck fell down onto the third deck which install transformers (from CALTRANS).

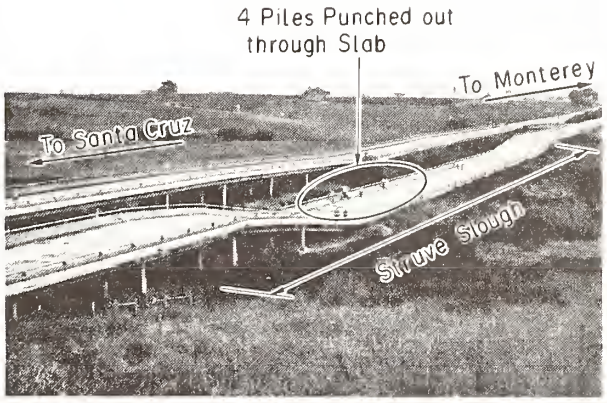

Photo. 9 Overall view of Struve Slough bridge, RC girder bridge with 21 spans and about 232m long, crossing over Struve Slough. There are 3 girder hinges along the longitudinal direction.

Photo. 10 4 Pile bents punched out (up to 1.2 to 1.8m) through slab at Struve Slough bridge.

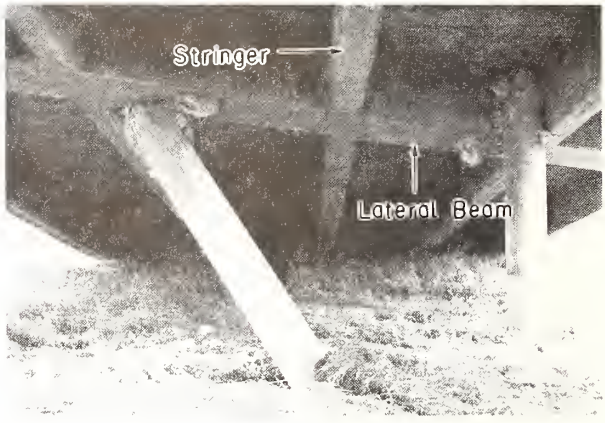

Photo. 11 Heads of pile bents completely failed and dislodged from the lateral beam. The superstructure moved about 80cm in the transverse direction (left in the photo.).

Photo. 12 Pile bent largely moved, causing a big hole surrounding the bent. Peat soils of high water content with high water table of 80 cm below the ground surface look very soft.

Manuscripts Authored for Panel Meeting but Not Presented Orally

Experimental Study on Lateral Flow of Ground Induced by Soil Liquefaction

by

Yasushi SASAKI*, Ken-ichi TOKIDA**
Hideo MATSUMOTO*** and Shoichi SAYA****

SUMMARY

A series of shaking table tests are carried out on the lateral flow of the ground caused by liquefaction. The model grounds are 6.0 m long, 0.8 m wide and their average height is 1.2 m. The slopes of ground surface and the lower boundary condition of liquefiable layer are varied. The deformation of model grounds, excessive pore water pressure of the liquefied layer, and the acceleration of the grounds are monitored. Based on the test results, the influence of the slope, the input motion and the thickness of liquefied layer to the ground flow is examined.

KEY WORDS : Liquefaction, Sloped Ground, Ground Flow, Shaking Table Test

1. FORWARD

The soil liquefaction has caused severe damages for structures during the past earthquakes in Japan. Hamada et. al. (1986) pointed out that the fairly big amount of lateral flow of ground could be seen broadly in the areas in Niigata and Noshiro where the soil liquefaction of the ground apparently took place during the Niigata Earthquake and the Nihonkai-chubu Earthquake respectively.
Therefore it becomes necessary to consider two types of effect induced by soil liquefaction for the earthquake resistance design of structures; the loss of bearing capacity of ground and the influence of ground flow. However the mechanism of ground flow and predicting method of this phenomena are not yet clarified at present.
Under these circumstances, the authors conduct a series of shaking table tests to study the mechanism of ground flow and to establish the procedure for estimating ground flow. This paper describes the essential factors causing lateral flow of ground due to liquefaction from the experiments.

2. METHOD OF EXPERIMENTS

Shaking table tests on eight model grounds (Model-1 ~ 8) are carried out. The grounds except for Model-7 and Model-8 basically consist of three layers. The lowermost sand layer is compacted enough not to liquefy during shaking, the middle layer is loose sand which is expected to liquefy, and at the top of them is set the unsaturated sloped uppermost layer. The Model-7 dose not have the uppermost layer, instead the lower boundary of liquefiable layer is inclined. The Model-8 does not have the lowermost layer. Eight models are shown in Fig. 1 and Table 1.
The thickness of liquefiable layer (H_L), the slope of surface (θ_s) and lower boundary of liquefiable layer (θ_b) are varied to have different conditions in order to examine the influence of these factors to the lateral flow. Furthermore, for Model-5, 6 and 8, shot of lead or gravel is used as the unsaturated uppermost layer to give the larger overburden pressure and lesser cohesion. The water level is set equally to the upper boundary of liquefiable layer. The characteristics of the materials for ground models are indicated in Table 2.
In each test, constant sinusoidal acceleration with a frequency of 2 Hz is employed for 20 seconds (40cycles), and several levels of maximum acceleration are applied stepwise to the shaking table as an input motion. The measured maximum accelerations of the shaking table and the results of lateral displacement at surface are summarized in Table 3.
As shown in Fig. 1, accelerometers, pore water pressure meters, strain gage meters and displacement meters are installed in or on the ground models to measure the time history of acceleration, pore water pressure and displacement of layers during shaking. Vertical marked lines are also installed at the side of each model grounds in order to monitor the deformation of the layers.

* Directer, Earthquake Disaster Prevention Department, Public Works Research Institute, Ministry of Construction
** Head, Ground Vibration Division, Earthquake Disaster Prevention Department, ditto
*** Research Engineer, Ground Vibration Division, ditto
**** Ground Vibration Division, ditto

3. RESULTS OF EXPERIMENTS

From the above described shaking table tests, principal characteristics of lateral ground flow due to liquefaction and factors concerning to the ground flow are drawn as follows.

3.1 DISTRIBUTION OF GROUND FLOW

Fig. 2 shows the typical distribution of lateral displacement at the surface (Model-4 and 6). From this figure, it can be seen that tensile strains occur at the upper part of slope (right hand side in Fig. 2), the lower part of slope seems to be compressed.
Fig. 3 shows successive change of vertical marked lines during excitation at the Step-2 in the cases of Model-4 and 6. This figure is drawn from photographs taken through the transparent glass window on the side of the container. Based on this figure, it can be noted that the deformations of ground surface is induced by the deformation of the liquefied layer but not by the deformation of the uppermost layer. The displacement at the lower boundary of liquefied layer is almost zero, and increases upwards in the liquefied layer.

3.2 RELATION BETWEEN ACCELERATION, EXCESSIVE PORE WATER PRESSURE AND GROUND FLOW ON TIME HISTORY DURING EXCITATION

Fig. 4 shows the typical relation of time histories between acceleration, excessive pore water pressure in the liquefied layer and lateral displacement at the surface,at the Step-2 in the case of Model-6. From this result, it can be seen that the acceleration in the liquefiable layer becomes spiky just before the excessive pore water pressure in liquefiable layer approaches to the effective overburden pressure, and decreases after the complete liquefaction in the layer is obtained.
On the other hand, Fig.5 shows the relation of time history between the lateral displacement at the surface and the excessive pore water pressure in liquefied layer at Section A, B, C and D respectively. From this figure, the displacement at the ground surface begins to increase gradually just after the excessive pore water pressure ratio ($\Delta u / \sigma'_v$) approaches to the range of 0.6 to 0.8, and also continues to increase gradually during excitation after the complete liquefaction in the subground layer is attained.

3.3 RELATION BETWEEN DURING AND AFTER EXCITATION

Fig. 4 also shows the behavior after stopping excitation. After excitation, the excessive pore water pressure keeps the pressure by seepage pressure for about 2 minutes, and it takes about 20 minutes for high excessive pore water pressure to decrease to almost zero. On the other hand, the displacement at the ground surface increases a little after excitation, but it is very little comparing with that during excitation. From the site observation on the liquefaction and lateral ground flow in the past earthquakes, sand boils, water springs and ground movements are reported to continue for a while after the earthquake. The cause of the difference on ground flow induced by liquefaction between the actual phenomena at sites during earthquakes and experiments can not be cleared at present.

3.4 RELATION BETWEEN INPUT MOTION AND GROUND FLOW DIRECTIONS

Fig. 6 shows the direction and quantity of ground flow at the surface measured by the bench mark points, against the direction of input motion, at the Step-2 in the case of Model-8. From this figure, the surface of the semi-corn shaped slope and the neighboring horizontal ground seems to move almost uniformly and radially, that is, in the direction of slope.
Judging from these characteristics concerning the ground flow, it seems that whichever the direction of the excitation is, the liquefaction induces the ground flow towards the direction of the initial shear stress in the liquefiable layer enforced by sloped overburden load.

3.5 EFFECTS OF SURFACE SLOPE AND LOWER BOUNDARY SLOPE

Fig. 7 shows the influence to ground flow at the surface by slopes of both surface and lower boundary of liquefiable layer. As seen in the figure, the influence of the slope of the lower boundary of liquefiable layer to the ground flow seems very small. However, when both ground surface and lower boundary of liquefiable layer are sloped as the case of Model-3, the slope of the lower boundary of liquefiable layer is likely to increase the ground flow.

3.6 ESTIMATION OF GROUND FLOW

From the above mentioned test results, it is reduced that the slope of surface (θ_s), the thickness of liquefied layer where the excessive pore water pressure ratio ($\Delta u / \sigma'_v$) is almost equal to 1.0 (H) and the duration time of excitation while the ratio ($\Delta u / \sigma'_v$) is almost 1.0 (T), can be considered as the main factors relating to the quantity of ground flow measured at the surface (D). Fig. 8 shows the relation between the parameter D/(T·H) and the slope of surface(θ_s) in the Sections A, B, C and D at the Step 1 and Step 2 for all Models excepting Model-8. Based on this figure, it can be seen that the parameter D/(T·H) has a tendency to increase according to the increase of the slope θ_s.

CONCLUSION

Based on the above-mentioned results for shaking table tests, the following can be concluded:

(1) The pore water pressure increases firstly during excitation, preceding the lateral ground deformation, and the lateral displacement of the sloped ground begins to increase remarkably when excessive pore water pressure ratio in the underlying layer exceeds about the range of 0.6 ~ 0.8.

(2) The lateral deformation occurs only in the liquefied layers, and the surface layer is displaced according to the deformation of underlying liquefied layers.

(3) The ground seems to be deformed by shear force during excitation and the deformation mode of ground in the direction of depth differs according to the position and the lapse of exciting time.

(4) Just after stopping the excitation, the excessive pore water pressure in the liquefied layer keeps the pressure by seepage for a while and begins to decrease gradually. On the other hand, the lateral ground flow almost stops.

(5) The lateral ground flow is affected severely by the slope of ground surface, and however is very small in case that the ground surface is flat even though the lower boundary of the liquefiable layer is sloped.

(6) The direction of excitation has no significant influence to the lateral flow of ground, and the lateral ground deformation is related to the direction of the slope of surface.

(7) The lateral ground flow at the ground surface in this series of experiments can be expressed by the slope of surface, thickness of perfectly liquefied layer and the duration time of excitation after almost complete liquefaction.

As mentioned above, characteristics on ground flow induced by liquefaction are clarified and principal factors which cause liquefaction induced ground flow are qualitatively summarized by Fig 8.

REFERENCES

1) Hamada, M., Yasuda, S., Isoyama, R. and Emoto, K. "Study on Liquefaction Induced Permanent Ground Displacements," Association for the Development of Earthquake Prediction, 1986.
2) Sasaki, Y., Matsumoto, H. and Saya, S. "Shaking Table Tests on Ground Flow Induced by Liquefaction", Technical Memorandum of Public Works Research Institute, No. 2768, February, 1989 (in Japanese).

Table 1 Characteristics of Ground Models

Model No.	Slope of Surface θ_s(%)	Slope of Lower Boundary of Liquefiable Layer θ_b(%)	Thickness of Liquefiable Layer H_l(cm)	Liquefiable Layer	Unsaturated Surface Layer	
				Unit Weight γ_{t1}(tf/m^3)	Unit Weight γ_{t2}(tf/m^3)	Materials
1	5	0	70	1.93	1.49	sand
2	7.5	0	35	1.88	1.37	sand
3	5	5	5～35	1.93	1.57	sand
4	5	0	35	1.90	1.49	sand
5	2.5	0	35	2.06	5.71	shot of lead
6	0～5	0	35	2.00	1.48	gravel
7	0	5	35～65	1.93	———	———
8	15	0	25	1.84	1.36	gravel

Table 2 Characteristics of Materials used for the Experiments

1) Sand (Mt. Sengen-yama Sand)

Specific Gravity of Soil Particle G_s	2.655
Maximum Void Ratio e_{max}	0.976
Minimum Void Ratio e_{min}	0.596
Maximum Grain Size (mm)	4.76
Mean Grain Size D_{50}(mm)	0.27
Coefficient of Uniformity U_c	1.37

2) Shot of Lead

Specific Gravity of Soil Particle G_s	11.34
Mean Grain Size D_{50}(mm)	2.00

3) Gravel

Maximum Grain Size (mm)	9.52

Table 3 Input Motion to the Shaking Table and Lateral Displacement at Surface after Excitation

Model No.	Shaking Step No.	Maximum Acceleration at Table α_{max} (gal)	Lateral Displacement at Surface (Section B) (mm)
1	1	80	61
	2	110	169
	3	160	118
	4	220	56
2	1	65	28
	2	110	144
	3	155	165
	4	105	62
3	1	65	68
	2	110	156
	3	90	87
	4	85	35
4	1	65	6
	2	95	72
	3	140	142
	4	190	44
5	1	60	1
	2	101	4
	3	152	210
	4	154	69
6	1	60	1
	2	104	101
	3	153	106
	4	154	54
7	1	64	−2
	2	103	17
	3	154	11
	4	151	6
8	1	51	14
	2	94	11
	3	95	5

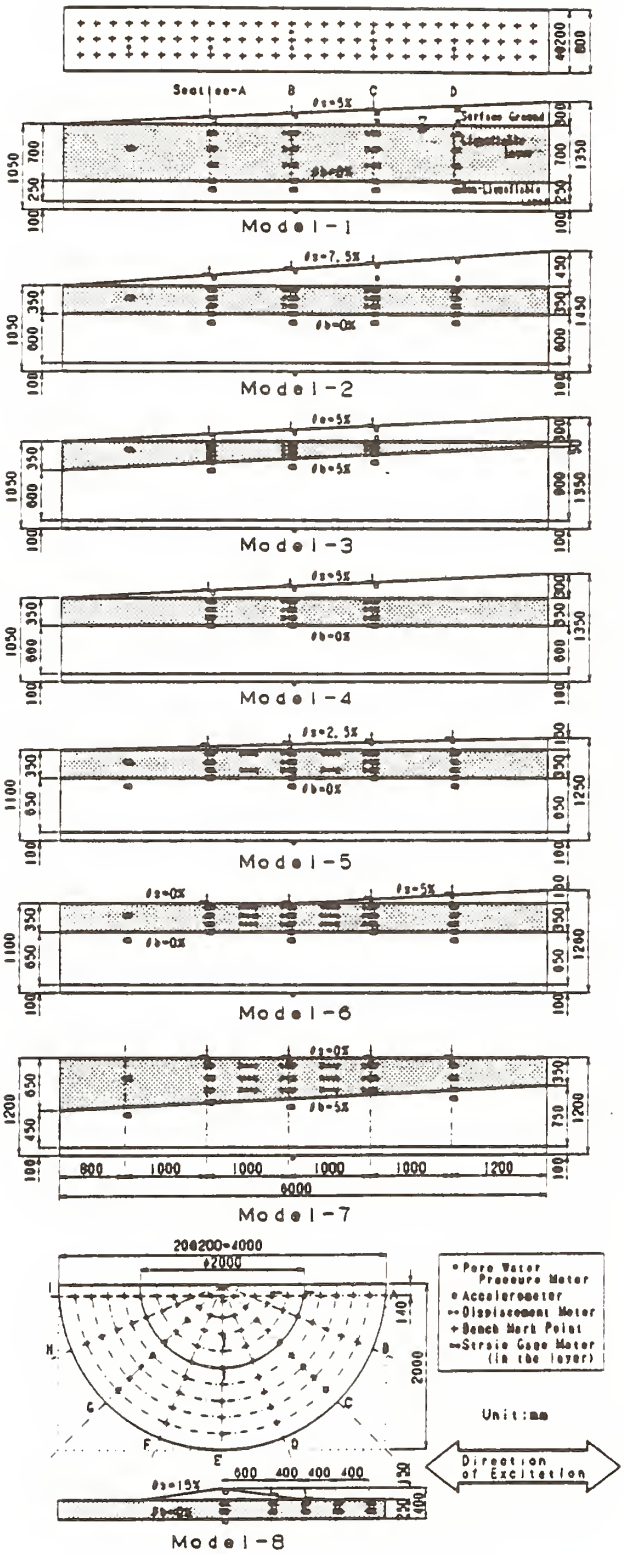

Fig. 1 Ground Models and Measurements

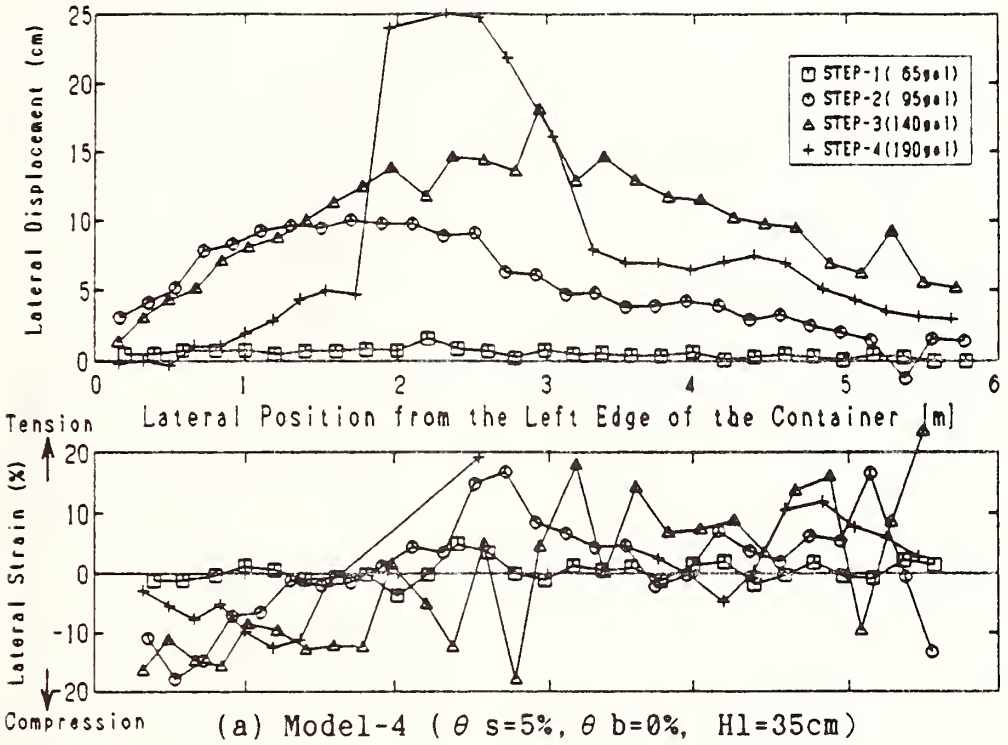

(a) Model-4 (θ s=5%, θ b=0%, Hl=35cm)

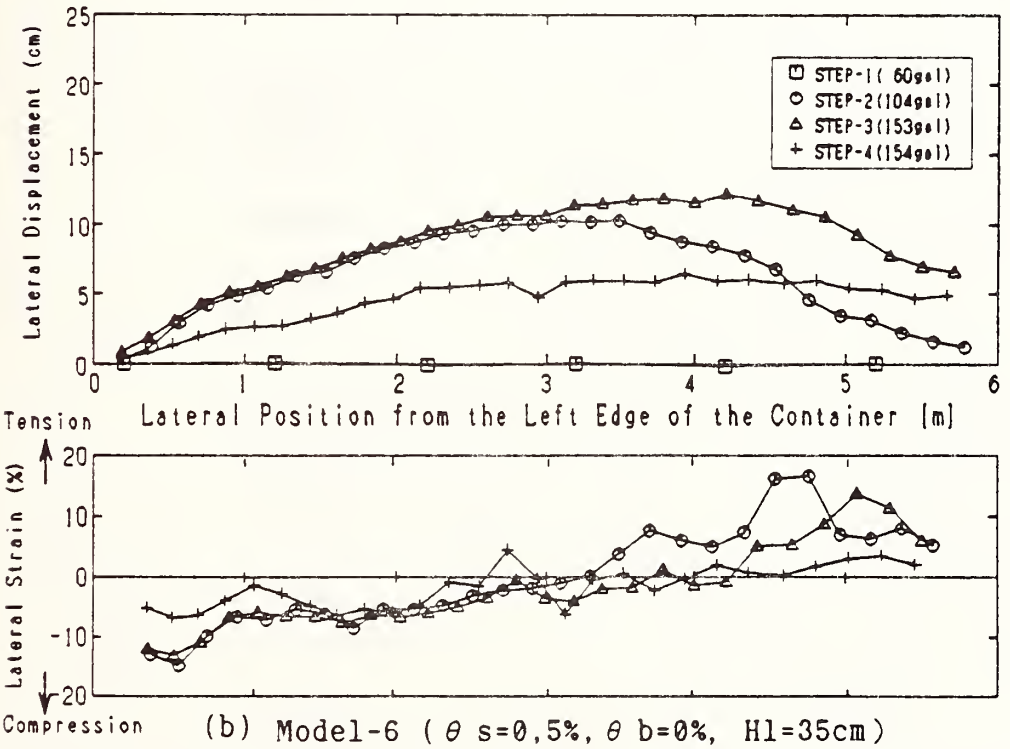

(b) Model-6 (θ s=0,5%, θ b=0%, Hl=35cm)

Fig. 2 Lateral Deformation of Ground Surface Resulted from Bench Mark Points

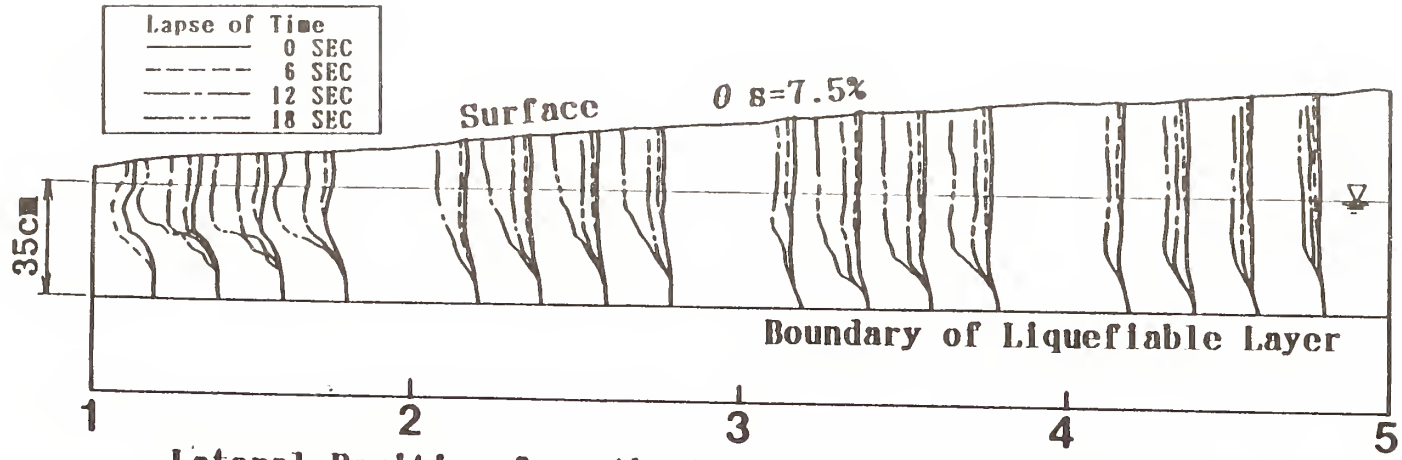

(a) Model-2 (Step-2: α max=110gal)

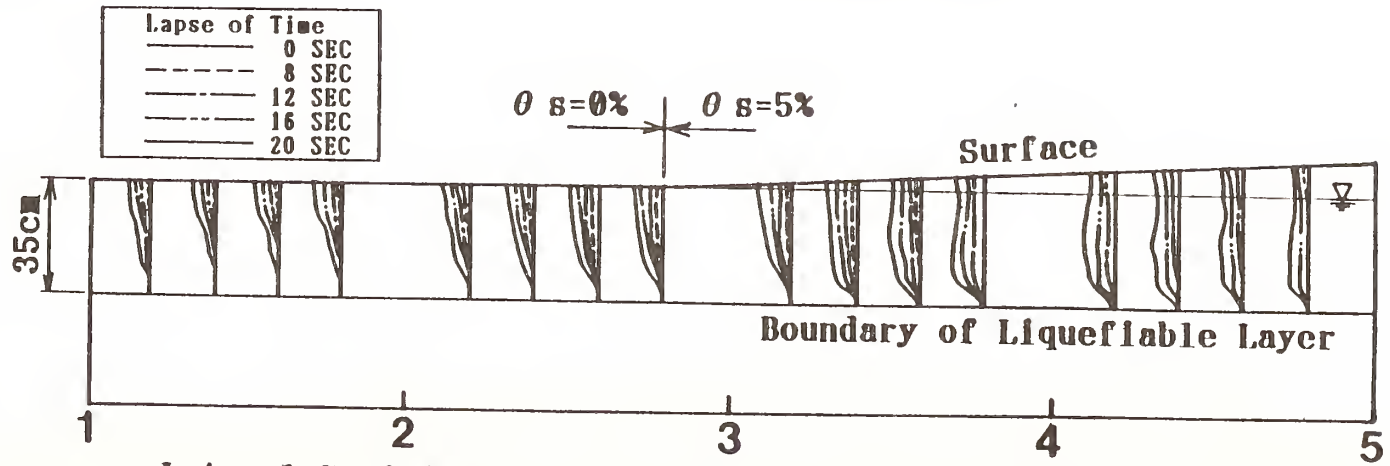

(b) Model-6 (Step-2: α max=104gal)

Fig. 3 Time History of lateral Deformation

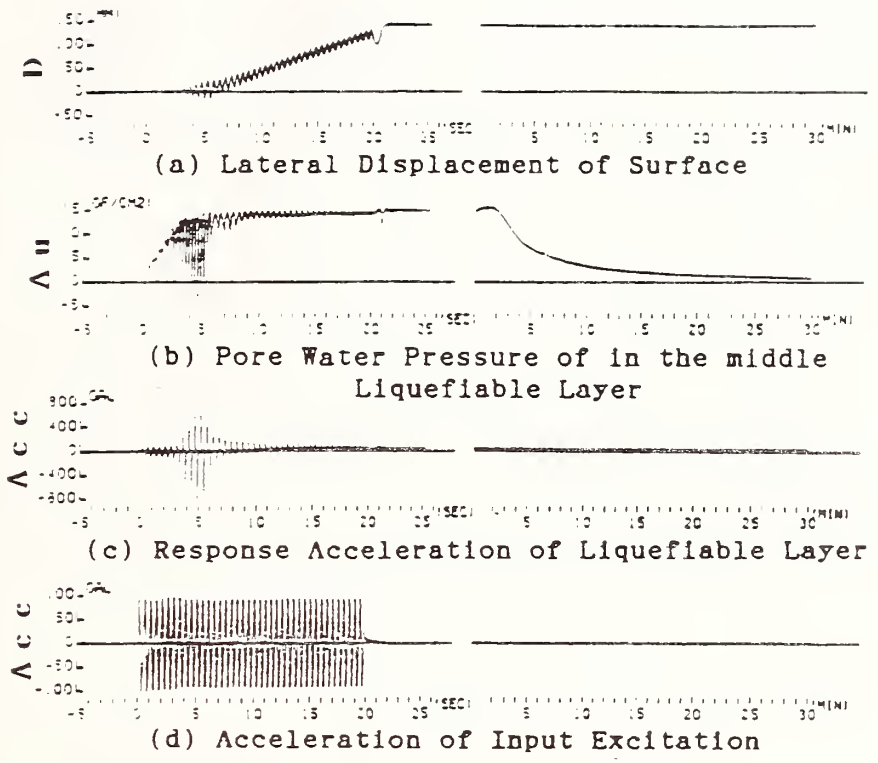

Fig. 4 Relation Between Lateral Displacement of Surface, Pore Water Pressure and Acceleration of Liquefiable Layer (Model-6, Step-2, Section-A)

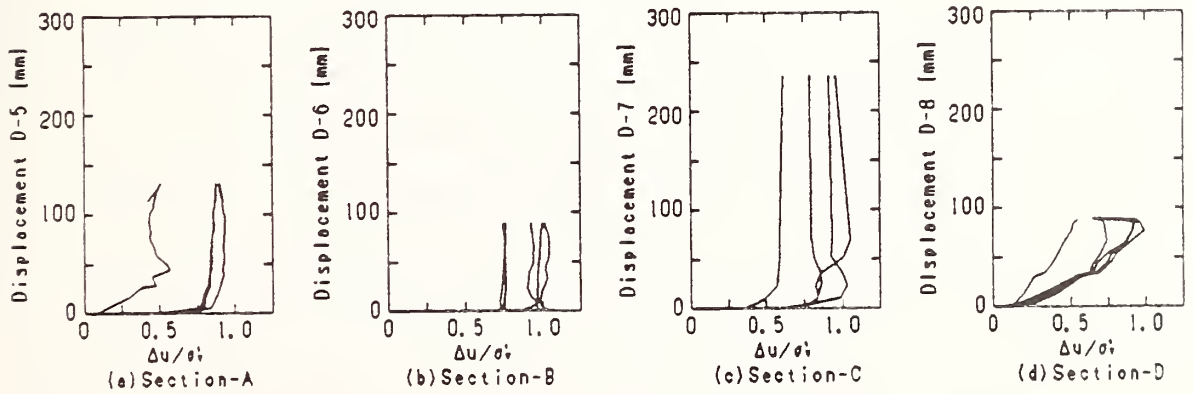

Fig. 5 Relationship between Pore Water Pressure Ratio and Displacement of Surface (Model-6,Step-2: α max=104gal)

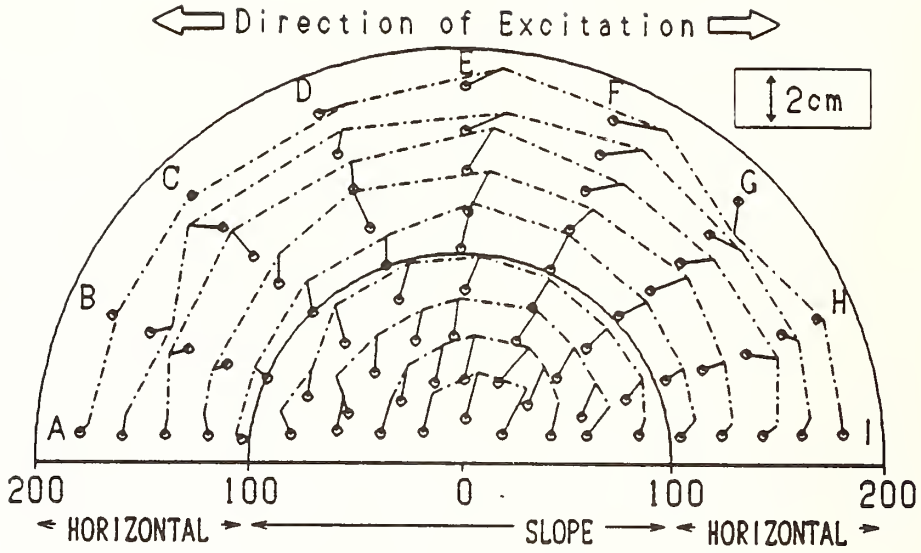

(a) Direction of Ground Flow

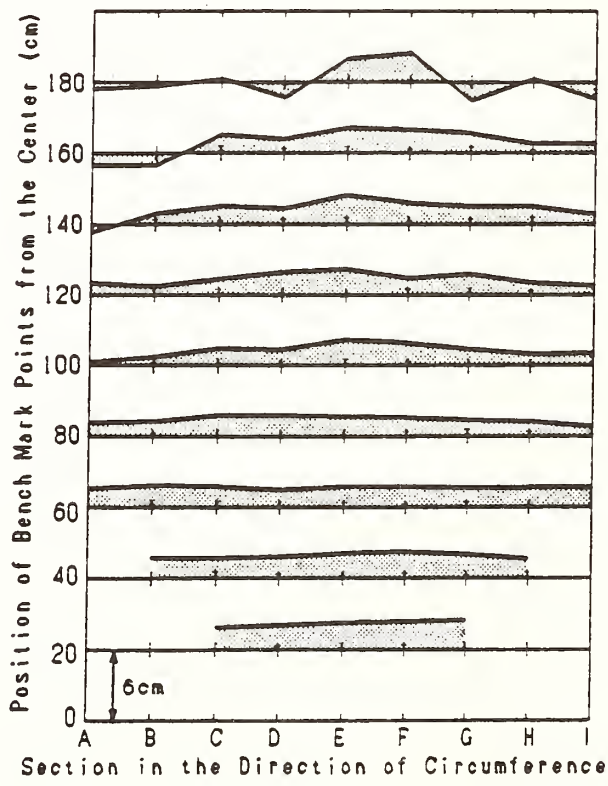

(b) Distribution of Ground Flow

Fig. 6 Relationship between the Direction of Ground Flow and the Director of Input Motion (Model-8,Step-2: α max=94gal)

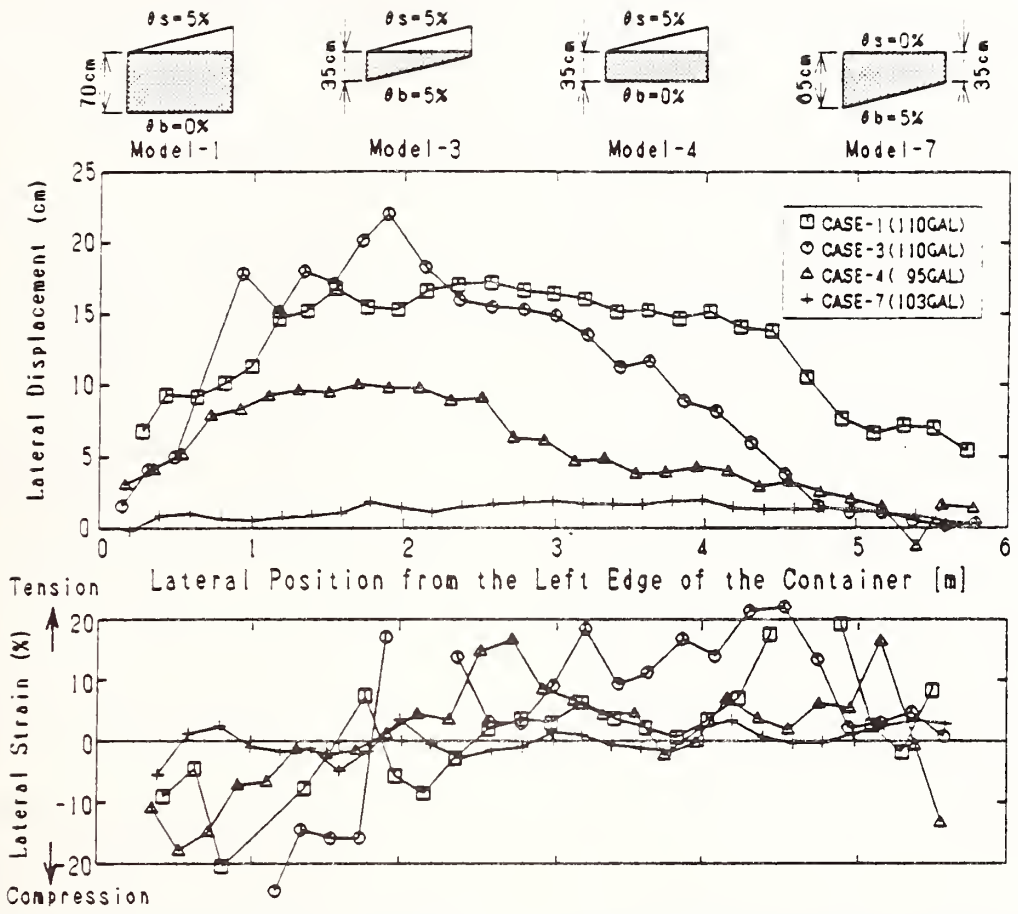

Fig. 7 Influence by Slopes of Ground Surface and Boundary of Liquefiable Layer for Ground Flow

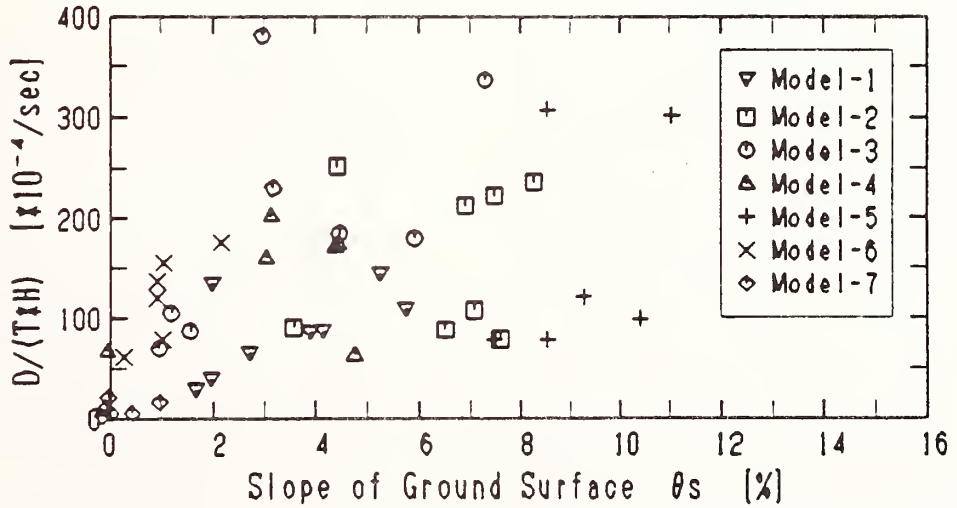

Fig. 8 Relation between Lateral Flow and Slope of Surface (Section A,B,C,D)

Development of Advanced Reinforced Concrete Buildings Using High-Strength Concrete and Reinforcement

by

Tatsuo Murota [1], Hisahiro Hiraishi [2],
Takashi Kaminosono [3], Masaomi Teshigawara [3] and Hitoshi Shiohara [4]

ABSTRACT

This paper lists research subjects conducted in 1989 in MOC's five-year research project on reinforced concrete buildings using high strength and high-quality concrete and reinforcing steel. This project is simply referred as to "New RC". The paper also describes the outlines of some of important research subjects related to structural performance.

1. INTRODUCTION

Reinforced concrete (hereafter referred as to "RC") has widely been used for medium scale buildings because of the low cost, excellent durability and easy maintenance, so on. However, it is impossible to realize the super high-rise buildings and buildings with long spans which are currently required from the social point of view, if the material strength remains within ordinary ones.
The Project aims to produce high strength concrete of the specified strength of from 300 kgf/cm^2 – 1,200 kgf/cm^2 (30 – 120 MPa) and high strength and high quality reinforcing steel bars of the yield strength of 4,000 kgf/cm^2 – 12,000 kgf/cm^2 (400 to 1,200 MPa), and to develop new fields of RC buildings by utilizing them.

2. RESEARCH SUBJECTS CONDUCTED IN 1989

The following researches were conducted in 1989.

1. Researches on Concrete
   - (a) Quality examination of cement for high strength and super high strength concrete
   - (b) Quality examination of the aggregate for high strength and super high strength concrete
   - (c) Quality standard and application criteria of the admixture for high strength and super high strength concrete
   - (d) Development of the binder for high strength and super high strength concrete
   - (e) Design method of mix proportion for high strength and super high strength concrete
   - (f) Evaluation method of workability of high strength and super high strength concrete
   - (g) Evaluation of mechanical properties of high strength and super high strength concrete
   - (h) Evaluation of long-term properties of high strength and super high strength concrete
   - (i) Evaluation of compressive strength of concrete in structures
   - (j) Evaluation of durability of high strength and super high strength concrete
   - (k) Development of essential construction techniques for high strength and super high strength concrete
   - (l) Evaluation of fire resistance of high strength and super high strength concrete
   - (m) Evaluation method of quality reliability of high strength concrete in structures
2. Researches on Reinforcing Steel Bars and Confined Concrete
   - (a) Production techniques of high strength and super high strength reinforcing steel bars and their mechanical properties
   - (b) Development of standard hooks for lateral reinforcement
   - (c) Effect of lateral confinement on compressive behavior of columns
   - (d) Behavior of columns subjected to axial force and bending moment
   - (e) Analytical modeling for stress vs. strain relations of concrete and steel, and bond characteristics
   - (f) Development of computer program using finite element analysis method
   - (g) Yield criteria of concrete under biaxial compression
   - (h) Deterioration characteristics in compressive capacity of cracked concrete
   - (i) Tension stiffening of cracked reinforced concrete
   - (j) Anchorage strength of longitudinal reinforcing steel bars in beams bent inside exterior beam column joint panel
   - (k) Bond characteristic of longitudinal reinforcing steel bars in beams and columns
3. Researches on Structural Performance of Members
   - (a) Deformation capacity of column under high-axial force
   - (b) Deformation capacity of Beams
   - (c) Bond splitting failure of beams beyond flexural yielding
   - (d) Flexural behavior of shear walls
   - (e) Shear behavior of shear walls
   - (f) Shear capacity of beams

[1] Director, Structural Engineering Department, Building Research Institute
[2] Head, Structural Division, Structural Engineering Department, Building Research Institute
[3] Senior Resarch Associate, Large Scale Structure Testing Division, Production Department, Building Research Institute
[4] Research Associate, Structural Division, Structural Engineering Department, Building Research Institute

(g) Shear capacity of columns

(h) Shear capacity of interior beam column joint panels

(i) Shear capacity of exterior beam column joint panels

4. Researches on Structural Design

(a) Structural design examples and their discussions
- A sixty-story frame building and that with shear walls
- A forty-story building with double tube and a forty-story building with tube core system
- A medium-high-rise office building

(b) Frame work of design method

(c) Design criterion

(d) Literature survey for input ground motion for structural design

(e) Structural systems of foundations and their structural performance

3. Research on Reinforcing Steel Bars and Confined Concrete

3.1 Production of High Strength reinforcing bar

Several steel makers have developed three types of high strength steel, the specified yield strength of which was 7,000 kgf/cm^2 – 10,000 kgf/cm^2 (700 MPa – 1,000 MPa). The mechanical properties seemed to satisfy the criterion determined in the Project. The total amount of the supplied steel bars were sixteen tons until March 1990, which were used for tests in the Project.

3.2 Pull-out Strength Test of Standard Hooks for Stirrups

Pull-out tests of seventy standards hooks which were embedded in high strength concrete were carried out. The shape of standard hooks used were in accordance with JASS5 (AIJ Standard Specification for Reinforced Concrete Construction), which is permitted to apply only to normal strength concrete. Figure 1 shows the specimens and loading method.
Test parameters include (1) type of hook (90 deg. bent and 135 deg. bent), (2) concrete compressive strength (400, 800 and 1,200 kgf/cm^2(40, 80 and 120 MPa)) and (3)diameter of stirrups (D10 and D13).
From the test results it is revealed that the hooks with yield strength of 8,000 kgf/cm^2 (800 MPa) have enough pull-out strength beyond yield stress of the steel bar, if they are embedded in high strength concrete with compressive strength more than 800 kgf/cm^2 (80 MPa), using the specification cited in JASS5.

3.3 Failure Criterion of High Strength Concrete under Biaxial Compression

High strength concrete panels with dimension of 200 × 200 × 50 mm were loaded to failure under biaxial compression. The test conditions were similar to the test of Küpfer et al. [1]. The panels were subjected to monotonically increasing load, maintaining the ratio of principal stresses (1) 0.0, (2) 0.2, (3) 0.52, (4) 0.75 and (5) 1.0. In order to prevent the effect of confinement of loading plate, tefron seats with cup grease were inserted between loading plate and specimen. Stress-strain relations were measured and failure criterion are examined.
Figure 2 shows the failure criterion of the principal stress. The tests results show that the strength increases more than thirty percent than strength under uniaxial compression, although the increase of compressive strength decrease to zero in case of the ratio of 1.0.

3.4 Development of Longitudinal Bar in Beam of Beam Column Joint Panel

Pull out tests of 90 deg. hooked bar anchorage used for development of longitudinal bar of beam in exterior beam column joint panel were conducted. The specimens were column with dimension of 300 × 300 × 1,500 mm and a pair of hooked bar anchored in them. The test parameters were (1) concrete strength (800 and 1,200 kgf/cm^2 (80 and 120 MPa), (2) amount of transverse reinforcement in column, (3)Diameter of anchor bar, (4)thickness of cover concrete and (5) effect of multi-layer of bar anchorage. The test results showed failure due to splitting of the cover concrete in all specimens.
The pull out strength observed were compared with existing Equation as (1) (see Fig. 4);

$$P = w d_b f_{bear} \sin\theta \frac{h}{h-j} \qquad (1)$$

where, $w = \beta\sqrt{2}r\cos(\pi-\theta)$, $\theta = \tan^{-1}(l_{dh}/j)$, $l_{dh} = l_1 + r + d_b$, $\beta = (r/3d_b) - 0.84$, $f_{bear} = \alpha\gamma\sqrt{\sigma_B}$, $\alpha = 16.1C_0/d_b$, $\gamma = 1 + 30A_s/(l_j s)$, d_b = diameter of anchor bar in cm, h = distance between two contraflexure points of column in cm, r = rudius of bent in cm, σ_B = concrete compressive strength in kgf/cm^2, l_1 =development length in cm, A_s =sectional area of a set of transverse reinforcement in cm ^{2}, s = space of transverse reinforcement in cm, j = distance between tensile reinforcement and concrete compressive force resultant and C_0 = concrete cover thickness from surface of column to center line of steel bar.
The average and standard deviation of ratio of observed strength to calculated strength are 1.11 and 0.11, respectively.

4.1 Flexural Behavior of Column under High Axial Stress

Experimental study on columns was performed to investigate the relationships between the amount of hoops and deformation capacity of the column subjected to bonging moment and shear force under high axial stress. The effects of amount and details of hoops on the deformation capacity of columns were discussed based on the test results
Eight columns (250 mm × 250 mm in section and 1,000 mm in height) with loading stubs at each end of the column, were designed to fail in compression after flexural yielding (see Table 1). Parameters in the tests were selected from the factors which would affect on the deformation capacity of column. Those are 1) amount of hoops, 2) strength of hoops, 3) diameter of hoops, 4) tie reinforcement in core section, 5) arrangement of longitudinal steel bars, and 6) axial stress level (η_c = axial force divided by

compressive strength of concrete and cross sectional area of column).
Compressive strength of concrete was 1,015 kgf/cm^2 (104 MPa).
Tensile yield strength of longitudinal steel bars were 3,870 kgf/cm^2 (395 MPa) and 3,460 kgf/cm^2 (353 MPa), for D13 and D19, respectively.
Tensile yield strength of hoops were 3,500 – 11,500 kgf/cm^2 (364 – 1,173 MPa).
Bending moment and shear force were applied to the specimen in alternate direction with controlling the deformation of the specimen and keeping the loading stubs parallel to each other. Constant axial load the stress level η_c of which was 0.35, was applied to the Specimens B1-B7. Variable axial force, whose axial stress level (η_c) is from 0.0 to 0.5, was applied to the Specimen B8.
Conclusions listed bellow were obtained
1) The New RC column have a large deformation capacity if the high strength reinforcement for hoops are properly arranged.
2) The column with tie reinforcement in core section has larger deformation capacity than that without tie reinforcement. Although both of the columns have the same amount of confinement.
3) The column whose longitudinal steel bars are arranged in the centers of the sides of the section shows larger deformation capacity than that with longitudinal reinforcements only at the four corners of the section.

4.2 Flexural Behavior of Shear Wall

Static loading test was carried out on the lower part of the shear wall in the high-rise (40 stories) New RC building. The objective is to clarify the typical restoring force characteristics of high strength concrete shear wall failed in flexure.
Two shear wall Specimens, NW–1 and NW–2, were tested. NW–1 is 150cm in span length, 20cm x 20cm column in section, 8cm in wall thickness, and 300cm in height. NW–2 has the same dimension as NW–1 except the height is 200cm. Compressive strength of concrete was 894 kgf/cm^2 (91MPa) for NW–1, 955 kgf/cm^2 (97 MPa) for NW–2, respectively. Tensile yield strength of steel bars were 7,914 kgf/cm^2 (808 MPa), 10,216 kgf/cm^2 (1,042 MPa), and 12,846 kgf/cm^2 (1,311 MPa) for longitudinal steel bars of column, reinforcement in wall panel, and hoops of column respectively.
Horizontal force was applied to the top of the specimen with the axial force of 180 tonf equivalent to the axial force of the assumed 40-story New RC building. Shear span ratio were 2.0 for NW–1 and 1.33 for NW–2, respectively.
The following conclusions are obtained

1. Longitudinal steel bars of a boundary column of NW–1 ruptured at the drift angle of 0.025 rad. Compressive failure in wall panel occurred at 0.015 rad. in the Specimen NW–2. But columns of the specimens were stable and could sustain the axial force.
2. The restoring force characteristics were "S" shape with poor energy absorption type hysteretic loops.
3. Flexural strength of New RC shear wall was estimated by the same equation for normal strength shear walls.
4. Shear strength of New RC shear wall was underestimated by the same equation for normal strength shear walls.

4.3 Shear Strength of Beam

Objective of this study is to examine the equation to estimate the shear strength of beams using high strength concrete of 1,200 kgf/cm^2 (122 MPa). The results will be used for the future research plan to establish the equation for shear strength of beams applicable to wide-range of concrete strength.
Four specimens were tested. The specimens are 15 cm x 30 cm in section and 90cm in span length and have concrete stubs for loading at each side of the specimen. Compressive strength of concrete was 1,136 kgf/cm^2 (116 MPa). Tensile yield strength of reinforcement was 10,160 kgf/cm^2 (1037 MPa) for longitudinal steel bars (D16) and 2,953 – 7,993 kgf/cm^2 (301– 816 MPa) for shear reinforcements (D16 to D8) (see Table 2).
Static loading in one direction was applied to the specimen.
Conclusions listed bellow were obtained.

1. Empirical equation proposed by prof. T. Arakawa underestimates the shear strength of New RC beams.
2. Shear strength of New RC beams could be estimated accurately by the A–Method [2] proposed by the Architectural Institute of Japan using the effective compressive strength of concrete proposed by CEB [3].

4.4 Shear Behavior of Exterior Beam Column Joint Panel

Objective is to clarify the effect of concrete strength, amount of hoops in joint, and axial force in column on the shear strength and restoring force characteristics of beam column joint subassembledges.
Four specimens were the 1/3 scaled exterior beam column joint subassembledges of full scale frame with 3.5 m in story height, 7.15m in bay span, 75 cm x 75 cm in section of column, and 60 cm x 75 cm in section of column. Compressive strength of concrete was 525 kgf/cm^2 (54 MPa) – 907 kgf/cm^2 (93 MPa) . Tensile yield strength of steel bars was 11,100kgf/cm^2 (1133 MPa) for longitudinal steel bars (D13) of column and beam, and 8,400 kgf/cm^2 (857 MPa) for longitudinal steel bars (D10) of beam (see Table 3).
The following conclusions were obtained.

1. At least 17 % of compressive strength of concrete can be expected for shear strength of exterior beam column joint panel using concrete that is less than 800 kgf/cm^2 (82 MPa) in compressive strength.
2. The effect of axial force on the shear strength of New RC exterior beam column joint panel is little if the axial stress is less than 30 % of compressive strength of concrete.
3. Shear crack strength can be estimated by the principal stress method.

5. Research on Structural Design

5.1 Structural Design and the Check of Their Seismic Behaviors

Traial designs of sixty-story moment resisting frame structure and wall-frame structure, forty-story double tube structure and tube-core structure, and fifty-story structure with long span were carried out and seismic behaviors of the buildings were examined.
Key plan of 60 story moment resisting frame structure is illustrated in Fig. 12. Interstory height and dimensions of structural members are tabulated in Table 4 and 5, respectively.
Span length of 6 m and building height and stance are 175.6 m ($1FL = GL + 0.5$ m) and 36 m, respectively. The ratio of building height to building stance is 4.88.
The maximum dimension is 85 cm × 85 cm for column and 45 cm × 90 cm for beam. Material strength is listed in Table 6. Concrete strength is from 630 to 990 kgf/cm^2 (64 – 101 MPa), and Steel yield strength is 7,000 or 8,000 kgf/cm^2 (714 – 816 MPa). The main results of design and seismic behavior are summarized in Table 7. In the structural design using New RC materials, allowable permanent axial stress for column, allowable interstory drift at the design base shear, shear stress of beam column joint panel, will be important factors to dominate the building design. However, shear stress of beams, or columns are very small, and, non-linear earthquake response analysis showed relatively small values of the drift. Super high-rise moment resisting frame structures will be easily designed if New RC material merits are used. The following items should be discussed to propose and establish design method for New RC buildings.

1. The characteristics in long period range (more than 3 second) of earthquakes motion.
2. Safety for column subjected to up-down component as well as two direction components of earthquake motion.

Fifty-story office buildings with long span need structural elements such as shear wall to stiffen buildings. One percent drift is commonly used as the building drift limitation against earthquake motions with the maximum velocity of 50 cm/sec.. This limitation for fifteen through twenty-story buildings need to be discussed still more.

5.2 Foundation system

It is difficult to use large diameter RC pile in site, although the foundation of New RC building is subjected to large axial force and span is small comparing with that of steel buildings.
The foundation system of three trial designed buildings (60-story moment resistant frame and wall-frame structure, and 40-story double tube structure) are examined. Following three foundation systems are concluded to be suitable for New RC buildings.

1. wall type pile
2. foundation mat with small diameter pile
3. foundation using upper two systems together

CONCLUDING REMARKS

This paper described the outstanding research results mainly concerning to structural performance conducted in second year of five years New RC Project. The research products to this time seems to indicate that the objectives expected early in this program will be fruitfully completed. Much cooperation and assistance to the Project is highly appreciated.

ACKNOWLEDGMENT

The Project is going to be conducted by great effort of peoples in universities, private companies, etc., under the Technical Coordinating Committee chaired by Prof. H. Aoyama, University of Tokyo.
Their works and cooperation are greatly acknowledged.

References

[1] H. Kūpfer, H. K. Hilsdorf, and H. Rusch, "Behavior of Concrete under Biaxial Stresses, " 1969, Aug. ACI Journal, pp.656–666.

[2] Architectural Institute of Japan, "*Design Guideline for Earthquake Resistant Reinforced Concrete Buildings Based on Ultimate Strength Concept* " , May 1988 (in Japanese).

[3] Comite Euro-International du Beton/Federation Internationale de a Precontrainte, "*CEB-FIP Model Code for Concrete Structures* ," 3rd Edition, Paris, 1978.

Table 1: Lists of Column Specimens

ID	Longitudinal Re-Bars	Ratio of Axial Stress	Hoops			
			Arrangement	pw	wσy	pw wσy
B1	12-D13	0.35	4-5φ @60	0.50	7892	39.5
B2	12-D13	0.35	4-5φ @40	0.75	7892	59.2
B3	12-D13	0.35	4-5.5φ@60	0.61	3570	21.2
B4	12-D13	0.35	4-5φ @60	0.50	11482	57.4
B5	12-D13	0.35	2-5φ @30	0.50	7892	39.5
B6	12-D13	0.35	2-7φ @60	0.50	8738	43.7
B7	4-D19	0.35	2-5φ @30	0.50	7892	39.5
B8	12-D13	0-0.5	4-5φ @40	0.75	7892	59.2

Ratio of Axial Stress = Axial force/(bDσB)

pw : Ratio of Hoops (%) wσy : Yield Stress of Hoops (kgf/cm2)

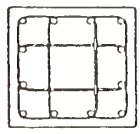

SPECIMEN B1-B4,B8

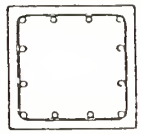

SPECIMEN B5,B6

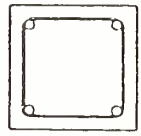

SPECIMEN B7

Table 2: Lists of Beam Specimens

ID	Hoops			
	Arrangement	pw	wσy	pw wσy
PB-1	4-D6 @100	0.85	4275	36.5
PB-2	4-D8 @50	2.64	2953	78.0
PB-3	4-D6 @100	0.85	7993	67.9
PB-4	4-D8 @50	2.64	7413	195.7

pw : Ratio of Hoops (%)

wσy : Yield Stress of Hoops (kgf/cm2)

Table 3: Lists of Exterior Beam Column Joint Assemblage Specimens

ID	Concrete Strength (kg/cm2)	Ratio of Axial Stress	Joint Hoop pw (%)
J1	525	0.0	0.60
J2	834	0.0	0.60
J3	886	0.0	0.23
J4	907	0.3	0.60

Ratio of Axial Stress = Axial force/(bDσB)

pw : Ratio of Hoops (%)

Table 4: Story Height

Story	Story height(clear height)
60F - 41F	2.90m (2.20m)
40F - 21F	2.90m (2.15m)
20F - 2F	2.90m (2.15m)
1F	4.00m (3.10m)

Table 5: Dimensions of Member

(a) Column

Story	Dimension
60F - 51F	75×75cm
50F - 41F	75×75cm
40F - 31F	80×80cm
30F - 21F	80×80cm
20F - 11F	85×85cm
10F - 1F	85×85cm

(b) Beam

Story	Dimension
RF - 52F	40×70cm
51F - 42F	40×70cm
41F - 32F	40×75cm
31F - 22F	40×75cm
21F - 12F	45×75cm
11F - 3F	45×75cm
- 1F	45×90cm

Table 6: Materials

(a) Concrete

Story	Concrete specified strength F_c in kgf/cm^2
60F - 51F	$F_c = 630$
50F - 41F	$F_c = 630$
40F - 31F	$F_c = 810$
30F - 21F	$F_c = 810$
20F - 11F	$F_c = 990$
10F - 1F	$F_c = 990$

(b) Steel

Diameter in mm	Specified yield strength σ_y in kgf/cm^2
D10(d_b=10) - D16(d_b=16)	SD80(σ_y=8,000)
D19(d_b=19) - D32(d_b=32)	SD70(σ_y=7,000)
D35(d_b=35) - D41(d_b=41)	SD70(σ_y=7,000)

Table 7: Main Results of Structural Design and Their Discussion

Design method		Ultimate strength design
Fc (kgf/cm^2) σ_y (kgf/cm^2)		990 7,000 8,000 (for hoop)
Design base shear coefficient (C_B)		0.0684
Drift angle at C_B	1st. story Max.	1/355 1/113 (32F)
Drift angle at yield mechanism	Base shear 1st. story Max.	0.074[3] 1/238 1/88 (33F)
Parmanent axial stress level of column (N/BD, kgf/cm^2)	Interior Exterion Corner	0.249Fc 0.204Fc 0.152Fc
Max. steel ratio in column	Interior Exterion Corner	1.32% 2.38% 3.79%
Max. tensile steel ratio in beam		1.39%
Shear stress of column (Q/BD, kgf/cm^2)	Static Dynamic[2]	18.6 14.9
Shear stress of beam (Q/BD, kgf/cm^2)	Static Dynamic[2]	23.2 Ductility factor=0.7
Additional axial force of column (ΔN/BDFc)	Static Dynamic[2]	0.511Nu[4] (Corner) 0.188 (Taft EW)
Dynamic response[1]	Drift of 1F Max. R C_B Ground motion	1/716 1/227 (45F) 0.040 Taft EW 1952
Dynamic Response[2]	Drift of 1F Max. R C_B Ground motion	1/444 1/186 (25F) 0.0541 Taft EW 1952
Natural period (sec.)	1st. 2nd. 3rd.	4.02 1.28 0.69
Max. shear stress and bond stress in joint panel (kgf/cm^2)	Shear stress Bond stress	105.5 (3.35 $\sqrt{Fc}$) less than 4 $\sqrt{Fc}$[5]

1) Max. velocity of input ground motion is modified to 25 cm/sec.
2) Max. velocity of input ground motion is modified to 50 cm/sec.
3) The second reflection point on the diagram of shear v.s. deformation relationship.
4) $Nu = 0.85(B*D-Ag)Fc+Ag\,\sigma y$
   Ag : total amount of steel in column
5) Bond stress is calculated as $1.3(1.1\,\sigma y)d/(4Dc)$
   d : diameter of steel
   Dc: depth of column

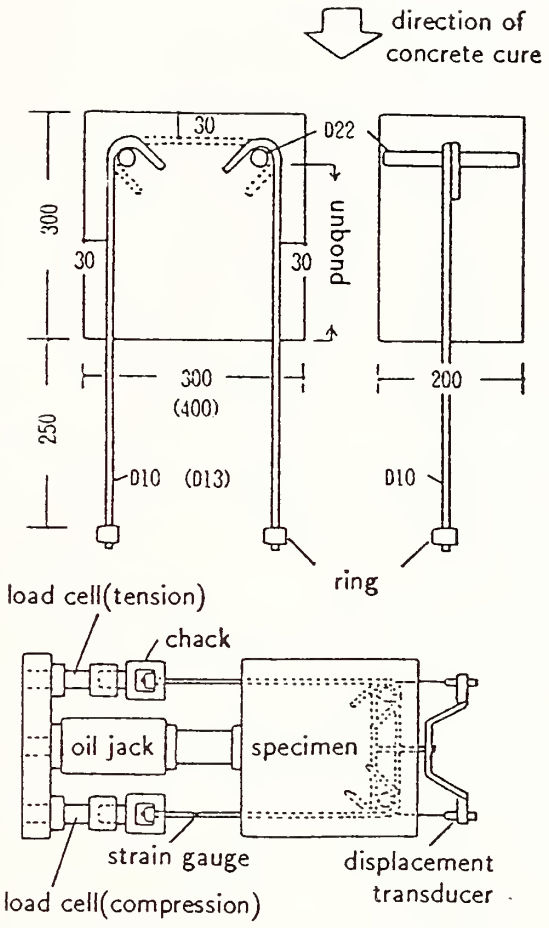

Figure 1: Loading Apparatus for Pull Out Test of Standard hooked Anchorage

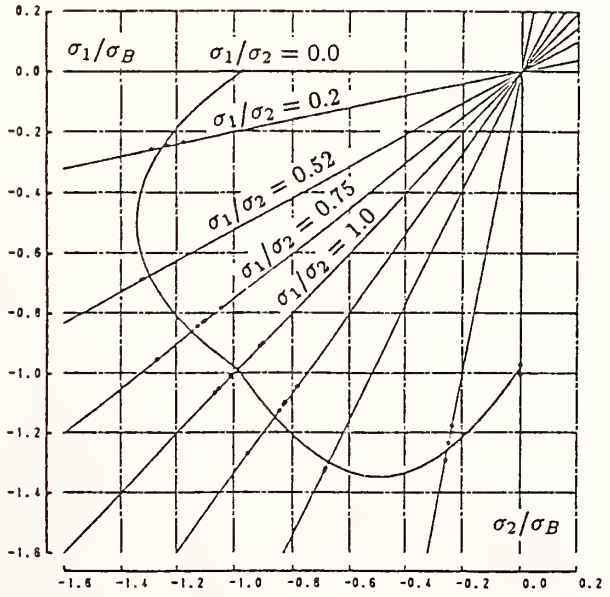

concrete compressive strength $\sigma_B = 63$ MPa

Figure 2: Failure Criterion of High Strength Concrete

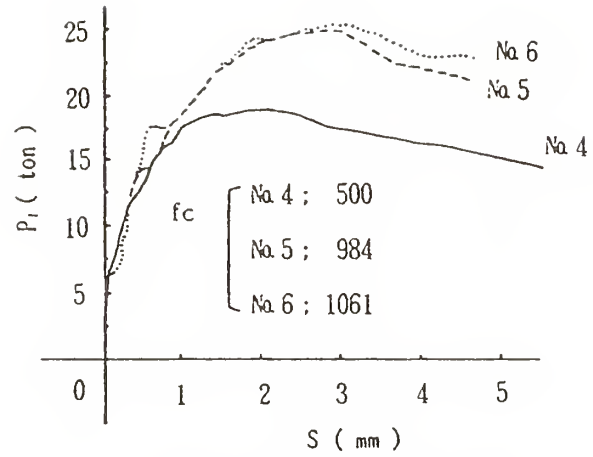

(a) Effect of Concrete Strength

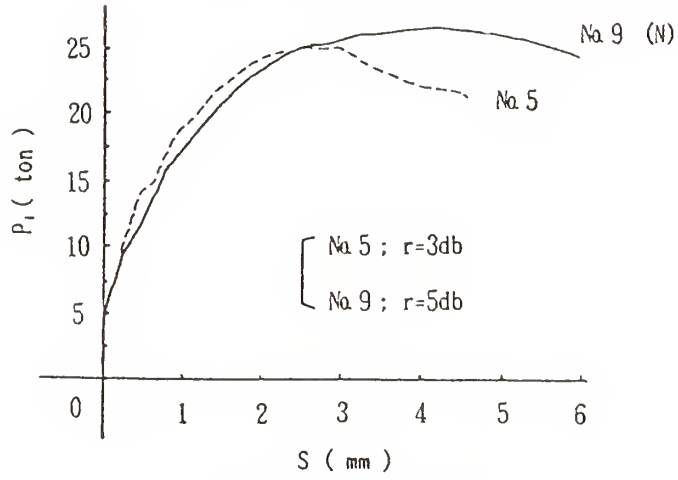

(b) Effect of bent radius

Figure 3: Pullout Load – Slip Relations of 90 deg. hooked anchor

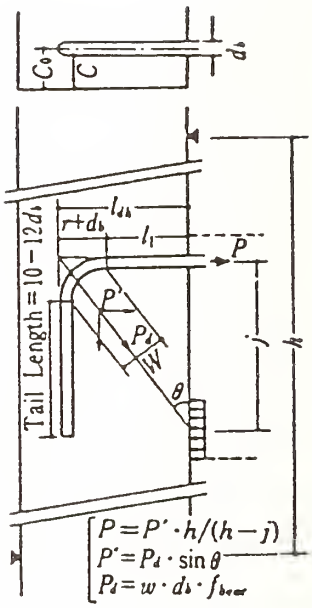

Figure 4: Schematic Mechanism of anchorage of 90 deg. hooked anchor

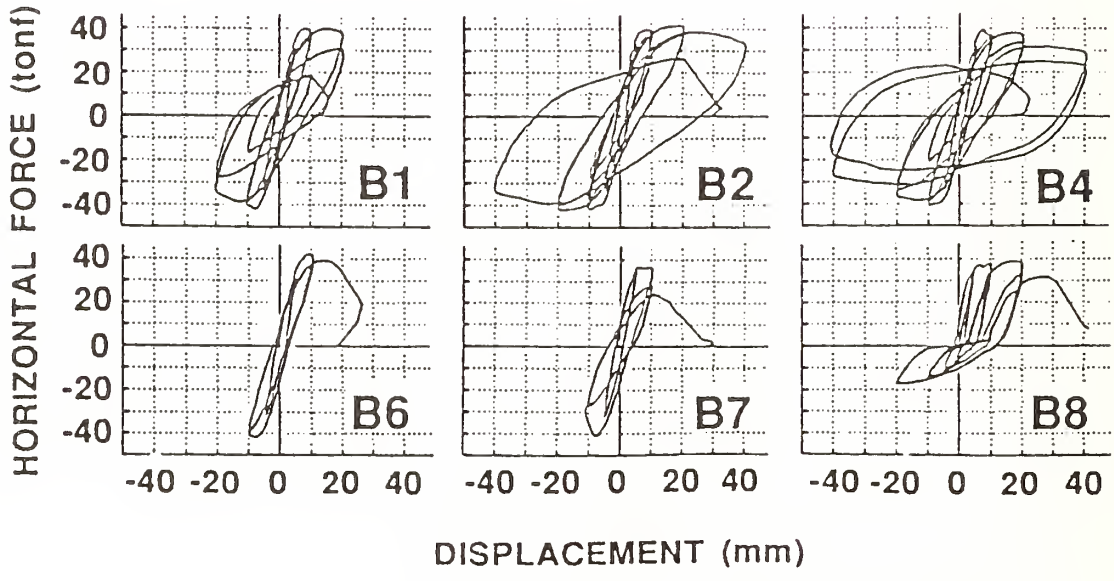

Figure 5: Horizontal Force and Displacement Relationships

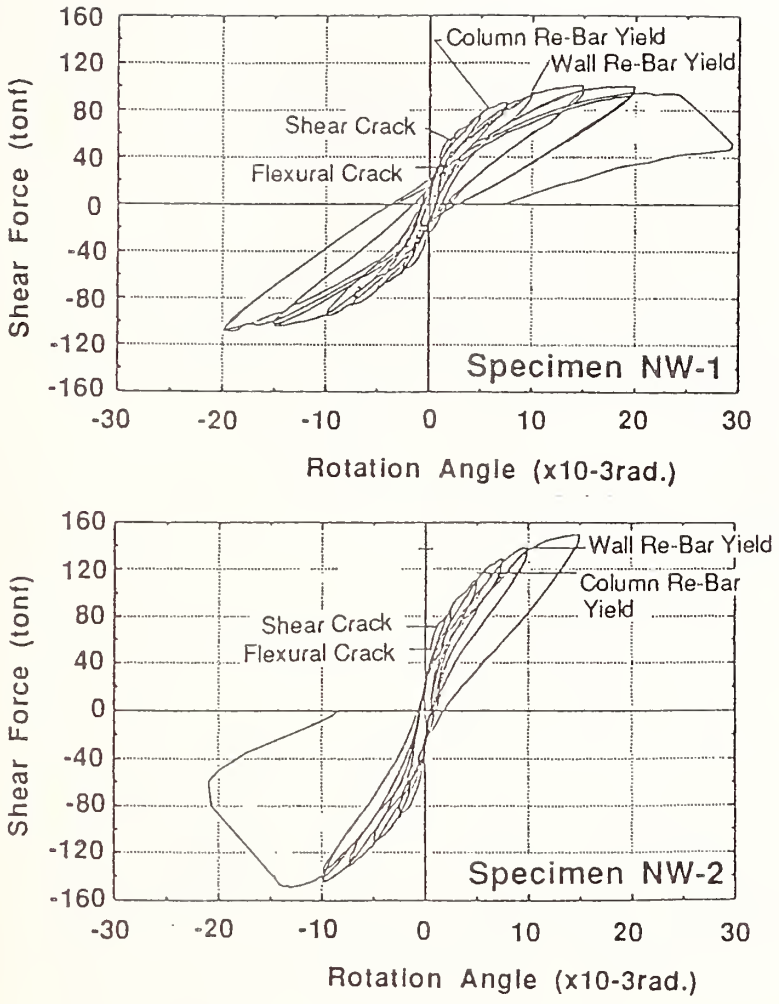

Figure 6: Shear Force vs. Rotation angle Relationship

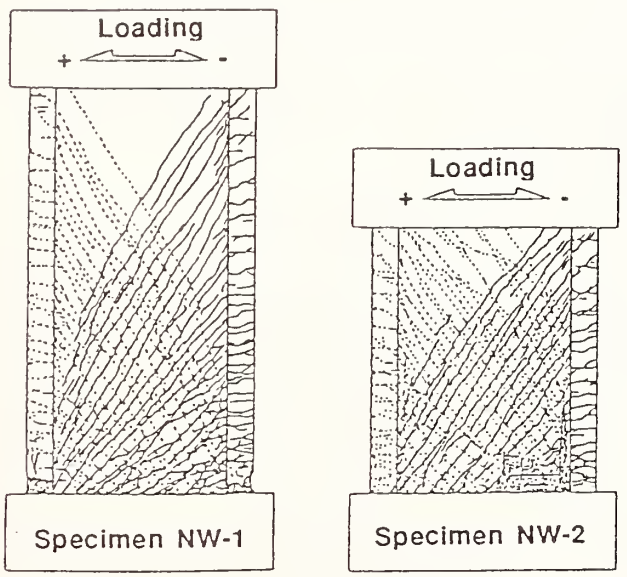

Figure 7: Crack Pattern

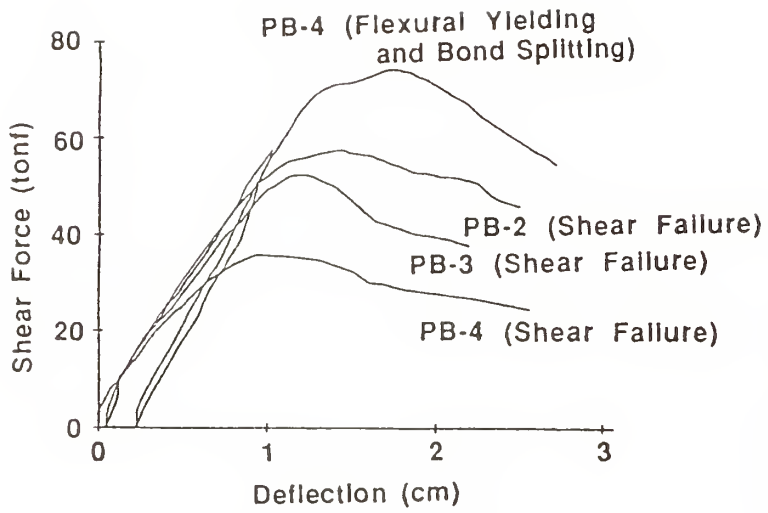

Figure 8: Shear Force vs. Deflection Relationships

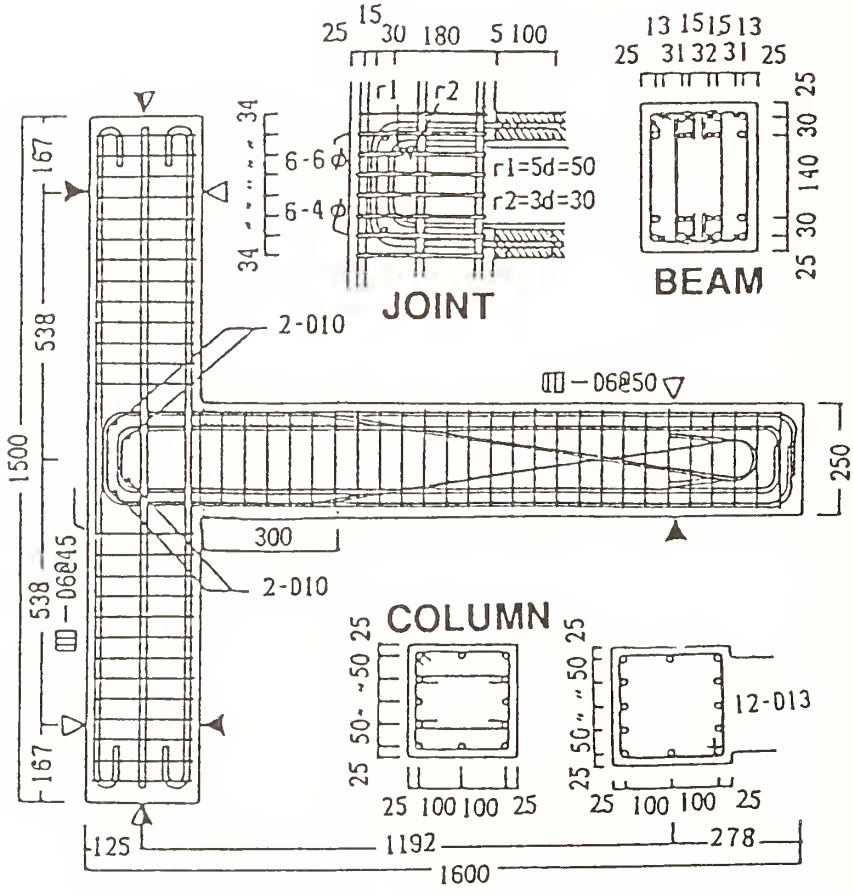

Figure 9: Specimen

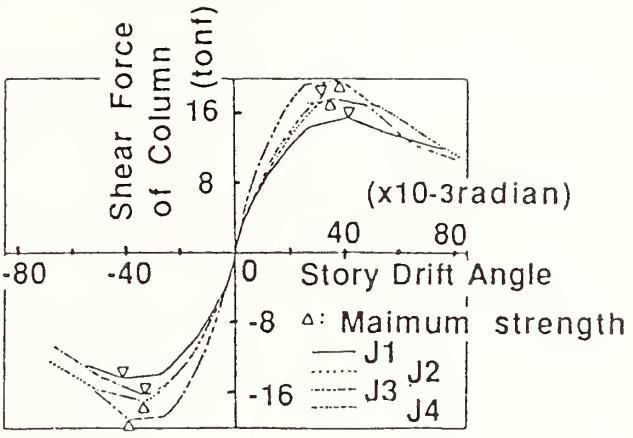

Figure 10: Skeleton Curves of Shear Force of column vs. Story Drift Angle

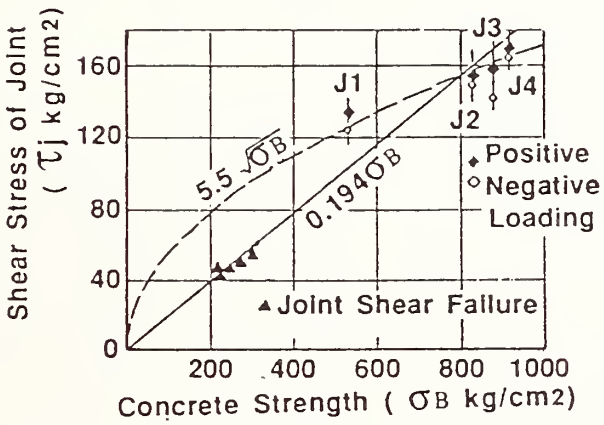

Figure 11: Relationship of Maximum Shear Stress vs. Concrete Strength

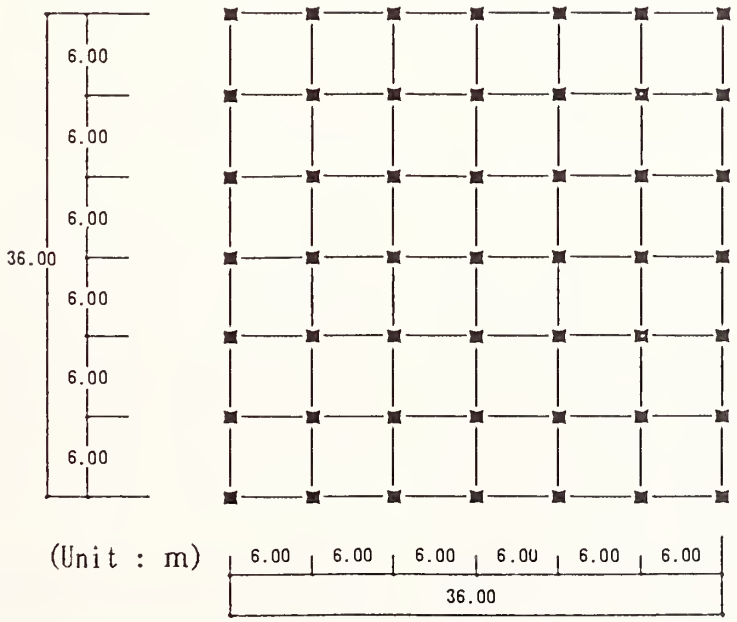

Figure 12: Plan

Characteristics of Supplemental Dampers for Earthquakes

by

Robert D. Hanson[1]

ABSTRACT

A number of imaginative approaches to improved earthquake response performance and damage control have been developed and others will be forthcoming. These can be divided into two groups, Passive Systems of which base isolation and supplemental mechanical damping are examples and Active Systems which require active participation of mechanical devices whose inputs depend upon measured building response. The discussion in this paper focuses on only passive supplemental mechanical damping systems. It is hoped that as a result of the information summarized in this paper the reader will be able to conclude that supplemental damping can provide performance and economical advantages for the earthquake resistant design for some new buildings and provides other advantages when developing strengthening systems for existing buildings. The advantages and disadvantages among the damping devices discussed is left to the reader. However, information necessary to make decisions between the use of supplemental damping systems, base isolation or active control systems is beyond the scope of this paper.

KEYWORDS: Damping, Damping devices, Structural response, Supplemental damping

1. INTRODUCTION

The building motions and damage caused by the Chilean and Mexican earthquakes of 1985 have amply demonstrated that single measures of earthquake motions, such as peak ground acceleration, do not provide an adequate basis from which to anticipate building response amplitudes or building damage. Even the use of multiple measures of ground motion as incorporated in the Response Spectra do not explain the survival or failure of buildings subjected to different earthquake ground motions. Many engineers believe that the duration of the ground motion is an important factor in exciting the response and causing damage to a building. Some have suggested that an additional design parameter is need to complement the current Response Spectral procedure (Code Lateral Force procedure). Earthquake input energy is currently being investigated as a logical complementary consideration for the design of earthquake resistant buildings.

Simultaneously, the expectations of building owners and engineers are increasing. That is, they expect that their buildings will not experience serious damage in a large earthquake, such as occurred in Mexico City in 1985, and that the buildings will continue to be operational following moderate earthquake ground motions, such as the Whittier event in 1987 and in San Francisco during the Loma Prieta earthquake of 1989. Limits on lateral drift calculated for code seismic forces are being used implicitly to control building damage. These greater expectations for the behavior of our earthquake resistance building designs should be faced directly with knowledge and imagination rather than indirectly through implicit methods.

The paper is divided into two main sections. The first summarizes analytical studies of the earthquake response of buildings with added supplemental damping in both the elastic and inelastic range of response. The results are presented in a form of response spectra modifications which are appropriate as damping is added to the building. Although data also exists for presentation as energy input spectra modifications, that data is not included in this paper. The second section of the paper discusses the characteristics of the two most practical classes of supplemental energy dissipation devices for earthquake resistant design utilization and illustrates some of the commercially available devices. Experimentally determined characteristics for several of these devices are given. It is

[1]National Science Foundation, Washington, DC 20550

concluded that added damping can provide significantly improved earthquake response performance and that practical commercial damping devices are available.

2. EFFECT OF ADDED DAMPING ON SEISMIC RESPONSE

The displacement response spectra, SD, is a key parameter in estimating the maximum displacement responses in each mode of a building for past earthquakes or for a specified design spectra. This spectral displacement decreases as damping increases. Ashour (1987) developed a relationship for the change in SD of elastic system with changes in damping and correlated these with results obtained from existing earthquake accelerogram records.

2.1 Elastic Response.

The natural period, Tn, used in the study were 0.5, 1.0, 1.5, 2.0, 2.5, and 3.0 seconds which covers a representative range of natural periods. Three real and twelve artificial earthquake records were used for excitation input. Damping values used were 0, 2, 5, 10, 20, 30, 50, 75, 100, 125 and 150 percent of critical. The values of SD for a given Tn and damping factor were normalized with respect to the SD at Tn for zero damping for each earthquake record and were than averaged over the 15 records to obtain a mean value for each period and fraction of critical damping. Figure 1 shows the resulting relation for the mean value of SD as a function of period and damping for zero and five percent damping normalizations.

These curves can be represented by simple decaying functions,

$$R = [\{1 - e^{-\beta B}\}/\{\beta B\}]^{1/2}$$

where β is the selected fraction of critical damping and B is a coefficient which was evaluated for zero initial damping normalization to be 24 for the upper bound and 140 for the lower bound, Figure 2(a). For an initial elastic spectral normalization of α, the simple decaying function can be expressed by

$$R = [\alpha \{1 - e^{-\beta B}\}/\beta\{1 - e^{-\alpha B}\}]^{1/2}$$

The system damping must be greater than or equal to the initial elastic spectral normalization damping to use this equation. For five percent (5%) damped spectra normalization, set $\alpha = 0.05$. Ashour (1987) found the upper bound B = 18 and the lower bound B = 65 for this case, Figure 2(b).

2.2 Inelastic Response.

The inelastic response evaluations are more difficult to establish on a comparative basis. Wu (1987) used one artificial and nine real earthquake records to study the elastic-plastic response of single degree systems. One form for presentation of his conclusions uses the peak ground parameters as a basis to derive the inelastic response spectra. Figure 3 gives the Response Spectra amplification factor in the acceleration region at periods of 0.1 second and 0.5 second for damping from 10 to 50 percent and ductilities from one to six. The effect of increasing damping and ductility can be seen. The amplification factor in the velocity region is shown in Figure 4 and in the displacement region at periods of three seconds and ten seconds in Figure 5. In these figures β is the fraction of critical damping and μ is the structural ductility factor. Thus, it can be seen that supplemental damping can effectively reduce structural yielding demands of an earthquake.

It is interesting to note that these amplification factors can be divided into terms which include the viscous damping of the system and separate terms which include the structural inelastic yielding. The inelastic deamplification factors for the three regions of concern are plotted in Figure 6 with the corresponding data including damping from 10 to 50 percent of critical. The relatively small scatter of the data with changes in damping illustrates the point that spectral modifications for high damping and for inelastic action can be considered separately. Thus previous experience with inelastic spectral modifications can be retained while incorporating modifications for higher damping.

As will be seen later steel yielding hysteretic characteristics are generally curvilinear and can be reasonably represented by equivalent viscous damping as was assumed in the previous studies. Friction and lead yielding characteristics are box shaped with sharp corners; for large motions equivalent viscous damping which changes with amplitude can be used, but for small motions the behavior is more of a stick-slip nature for which equivalent linear modelling is not very accurate. For these reasons most of the friction (and lead yielding) analytical studies have used nonlinear

models to represent the damping device characteristics.

Filiatrault (1988) described a design procedure for simple friction damped braced frames. The system used the Pall friction damping device located at midpoints of diagonal braces, Figure 7. They assumed that the key parameters in the design process were the expected peak ground acceleration, a_g; the predominate period of the ground motion, T_g; the period of the unbraced building, T_u; the period of the braced building (no slip of the devices), T_b; the mass of the building, m = W/g; and the friction slip load, V_o. Using a stochastic representation of the ground motion in a parametric study they develop the simple friction slip load design spectrum illustrated in Figure 8.

Given the weight of the building, its fundamental unbraced period, the expected braced frame period (with no slip), the expected peak ground acceleration, and the expected predominate period of the ground; the design friction slip load is determined using the curves of Figure 8. There are several parameters which can greatly influence the selected slip load. First, the design slip load is selected to be directly proportional to the expected peak ground acceleration and the weight of the building. Second, the ratio of the ground motion period to the unbraced frame period has significantly different characteristics for different period ratios: For T_g less than T_u the design slip load changes rapidly with T_u. For T_g greater than T_u the design slip load is relatively independent of T_u, but is dominated by the ratio of the braced period to the unbraced period.

Studies at the University of British Columbia on the Pall friction damper have used the minimum elastic energy of the structure (sum of instantaneous strain and kinetic energy of the structure) as a key parameter in setting the optimum slip load for the friction devices. Using the first six seconds of the El Centro 1940 NS accelerogram a curve showing the variation in maximum system elastic energy as a function of slip load is given in Figure 9. It can be seen that the system energy is sensitive to the selected optimum slip load. At zero slip load the structure behaves as an unbraced frame and at very high slip loads it behaves as a concentrically braced frame. Thus, the selection of the appropriate slip load must consider both the expected moderate earthquake motions for damage control and the potential severe earthquake motions for safety.

3. DAMPING DEVICES

Damping devices can be classified into four primary types on the basis of the material used to transform mechanical energy to heat: (i) Velocity proportional viscous material which can be liquid, such as silicon oil, or solid, such as special rubbers or acrylics; (ii) Friction devices in which the resisting forces are a constant which depends upon the interface contact pressures and the interface materials. Steel to steel, copper with graphite to steel, or brake pad to steel interface materials are most common; (iii) Metallic yielding devices in which the resisting forces depend upon the nonlinear stress-strain characteristics and geometrical configuration of the material. Mild steel and lead are the two most commonly used materials; and (iv) Magnetic damping devices. The following discussion will concentrate on the friction and metallic yielding devices because they appear to be more practical for earthquake resistance applications.

3.1. Friction Devices

3.1.1 Cylindrical Device (Sumitomo Metal Industries) The standard device (Figure 10) has a 10 ton (22 kips) maximum slip capacity and an 8 cm (3 inch) double amplitude stroke range (Figure 11). This device saw its initial application as the shock absorber for the Japanese "bullet" train. The potential use of this device in a 31 story building was reported by Teramoto (1988).

3.1.2. Pall Friction Braced Frame Device (Pall Dynamics) The direct slip device uses brake pad material against steel. The normal pressure which controls the slip force is maintained by a spherical springs. The device is located in the structure as illustrated in Figure 7. The characteristics of the device have been reported earlier (Pall, 1982; Pall, 1986). It was reported that the device has been installed in a building in Canada.

3.1.3 Rotary Friction Device (Hazama-Gumi) The device uses sintered metal brake pads against stainless steel to provide the friction force. Because the rotational characteristics of the device the direction of the input forces causes a slight asymmetry of the frictional resistance (Takai, 1988). This device was developed for use with base isolation systems, but could be adapted for in structure use.

3.2. Metallic Devices

3.2.1 Lead Damper (DSIR-New Zealand, Oiles Corporation, (Fujita, 1988)) The piston lead damper (Figure 12) was developed in New Zealand for bridge uses and has been licensed in Japan by Oiles Corporation. A different lead damper uses a lead post containing 12 steel wires to ensure pure shear deformation in the lead (Figure 13). Sample data shown in Figure 14 illustrates that the lead hysteretic characteristic is very similar to the friction damper characteristic.

3.2.2 Steel Plate Damper (Bechtel Corp., CounterQuake Corp.) The device was originally developed for pipe restraints in nuclear power plants. The concepts were extended to building structures (Scholl, 1987). The configuration of the device (Figure 15) is selected to maximize the amount of material yielding without excessive localized strains. Experimental data on smaller sized ADAS devices have been reported (Bergman, 1987; Bergman, 1988) and are illustrated in Figure 16. Three story steel frame shaking table tests using these devices has been recently completed at the University of California at Berkeley (Whitaker, 1989).

3.2.4 Steel Post Dampers (Kajima Corp., Oiles Corp.) The basic concept of these devices uses cantilever beam yielding. The dimensions and cross-sectional shape along the height are unique. The Joint Damper (JD) by Kajima is used to connect separated structures at the atrium roof level. The connection provides stiffness and energy dissipation characteristics. The Oiles Steel Bar Damper is used to provide vibrational isolation and hysteretic damping during excessive motions.

4. REMARKS

Analytical studies have demonstrated that supplemental damping can effectively control the response of buildings during earthquakes. These studies have shown that the response of a highly damped building is not sensitive to the peculiarities of specific earthquakes. Thus the added viscous type damping effectively decreases response variability and uncertainty from a broad spectrum of earthquake inputs; thereby improving the performance of the building and reducing the risk of severe damage.

A large number of damping devices are currently available and others under development. This is a tribute to the imagination of earthquake engineers. While most of the devices developed in Japan are intended for use with base isolation systems for the nuclear power industry, application to commercial and residential buildings is moving rapidly.

5. CONCLUSIONS

The following conclusions are the result of a number of analytical studies and the information summarized herein:

5.1. The incremental effect of adding supplemental damping devices is greater when the total damping is small than when the total damping is high.

5.2. The combined effect of added damping and inelastic response of the structure can be separated into the effects resulting from higher damping and the effects resulting from member yielding.

5.3. Supplemental damping devices are more effective in reducing the corresponding earthquake response spectral values in the mid period region (velocity region) than in the low (acceleration controlled region) and high (displacement controlled region) period regions. Nevertheless additional damping makes the structures less sensitive to earthquake peculiarities.

5.4. The selected damping devices should be dependable and require a minimum amount of maintenance. The delivered devices should have quality controlled manufacturing to ensure that the characteristics established through testing programs and specified by the designers is achieved in field installations.

6. ACKNOWLEDGEMENTS

This paper is based upon research supported by National Science Foundation Grants ECE-8512726 and CES-8821735, and by the Bechtel Power Corporation. The opinions expressed herein are those of the author and do not necessarily represent the opinions of the sponsors. Much of the analytical and experimental research summarized was obtained by Samir Ashour (Ashour, 1987), David M. Bergman, Yung-feng Su (Su, 1990) and Jian-ping Wu (Wu, 1987) in conjunction with their Ph.D. studies at the University of Michigan. Their originality and contribution to this effort are gratefully

acknowledged. Portions of this paper were prepared for the 1988 SEAOC Annual Convention (Hanson, 1988).

7. REFERENCES

Ashour, Samir A., (1987) Elastic Seismic Response of Buildings with Supplemental Damping, Ph.D. Dissertation, Department of Civil Engineering, University of Michigan, January.

Bergman, David M. and Subhash C. Goel, (1987) Experimental Characteristics of the ADAS Device, Department of Civil Engineering, University of Michigan, Report UMCE 87-10, November.

Bergman, David M. and Robert D. Hanson, (1988) Characteristics of Mechanical Dampers, Ninth World Conference on Earthquake Engineering, Tokyo/Kyoto, Japan, August, (#6052).

Filiatrault, Andre and Sheldon Cherry, (1988) Seismic Design of Friction Damped Braced Frames, Ninth World Conference on Earthquake Engineering, Tokyo/Kyoto, Japan, August, (#5145).

Fujita, Satoshi, Takafumi Fujita, Yukio Sasaki, Shigeru Fujimoto, Noboru Narikawa and Chiaki Tsuruya, (1988) Earthquake Isolation Systems for Buildings of Industrial Facilities Using Various Types of Damper, Ninth World Conference on Earthquake Engineering, Tokyo/Kyoto, Japan, August.

Hanson, R.D., D. M. Bergman and S.A. Ashour, (1986) Supplemental Mechanical Damping for Improved Seismic Response of Buildings, Third USA National Conference on Earthquake Engineering, Charleston, SC, August, Vol. II, pp. 1129-1140.

Hanson, Robert D., (1988) Energy Dissipation Systems, Proceedings of the 1988 Structural Engineers Association of California Convention, Kona, Hawaii, October

Pall, A.S. and C. Marsh, (1982) Response of Friction Damped Braced Frames, Journal of the Structural Division, ASCE, Vol. 108, No. 6, June, pp. 1313-1323.

Pall, A.S., (1986) Energy-Dissipation Devices for Aseismic Design of Buildings, Proceedings, ATC Seminar on Base Isolation and Passive Energy Dissipation, Applied Technology Council, Redwood City, CA, March, pp. 241-250.

Scholl, Roger E., (1988) Added Damping and Stiffness Elements for Earthquake Damage and Loss Control, Proceedings of Conference XLI: A Review of Earthquake Research Applications in the National Earthquake Hazards Reduction Program: 1977-1987, U.S. Geological Survey, Open File Report No. 88-13-A, San Diego.

Su, Yung-feng, (1990) Seismic Response of Building Structures with Mechanical Damping Devices, Ph.D. Dissertation, Department of Civil Engineering, University of Michigan, Ann Arbor, January.

Takai, Hidehiro, Tetsuo Uno and Kiyoshi Nagai, (1988) Study on the Friction Damper as the Device of a Base Isolation System, Ninth World Conference on Earthquake Engineering, Tokyo/Kyoto, Japan

Teramoto, Takayuki, Haruyuki Kitamura, Kenji Araki and Kiichi Takada, (1988) Application of Friction Damper to Highrise Buildings, 13th Congress, International Association for Bridge and Structural Engineering, Helsinki, Finland, June, pp.753-758.

Whittaker, A.S., V.V. Bertero, L.J. Alonso, and C. Thompson, (1989) Earthquake Simulator Testing of Steel Plate Added Damping and Stiffness Elements, Report No. UCB/EERC-89/02, Earthquake Engineering Research Center, University of California, Berkeley, January.

Wu, Jian-ping, (1987) Statistical Study of the Inelastic Response of Structures with High Damping Subjected to Earthquakes, Ph.D. Dissertation, Department of Civil Engineering, University of Michigan, Ann Arbor, November.

Wu, Jian-ping, and Robert D. Hanson, (1989) Inelastic Response Spectra with High Damping", Journal of the Structural Division, ASCE, Vol. 115, No. 7, July, pp. 1675-1696.

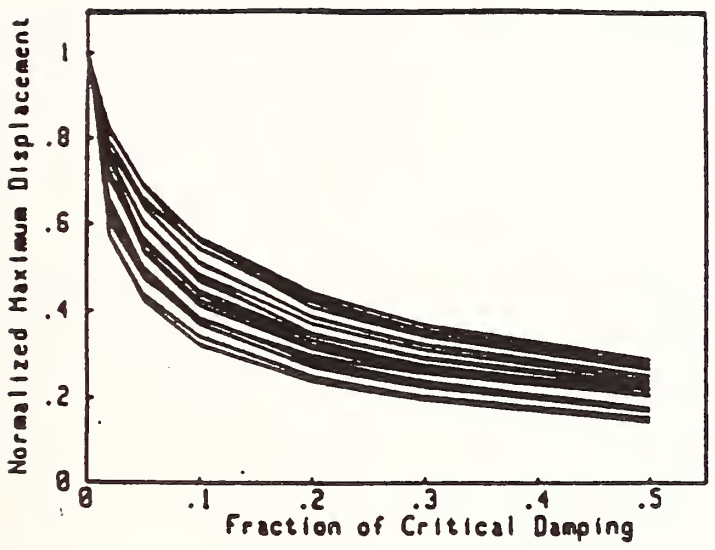

(a) Zero Damping Normalization

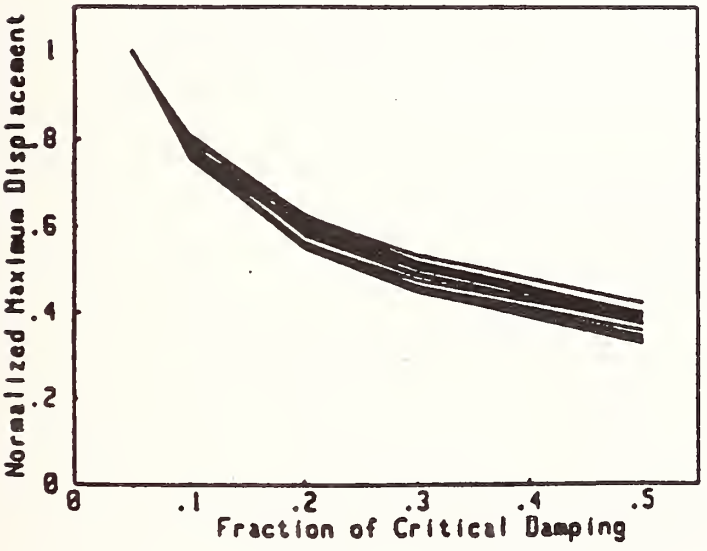

(b) Five Percent Damping Normalization

Figure 1. Normalized Mean Displacement for Spectra of 15 Earthquake Records [from Ashour (1987)]

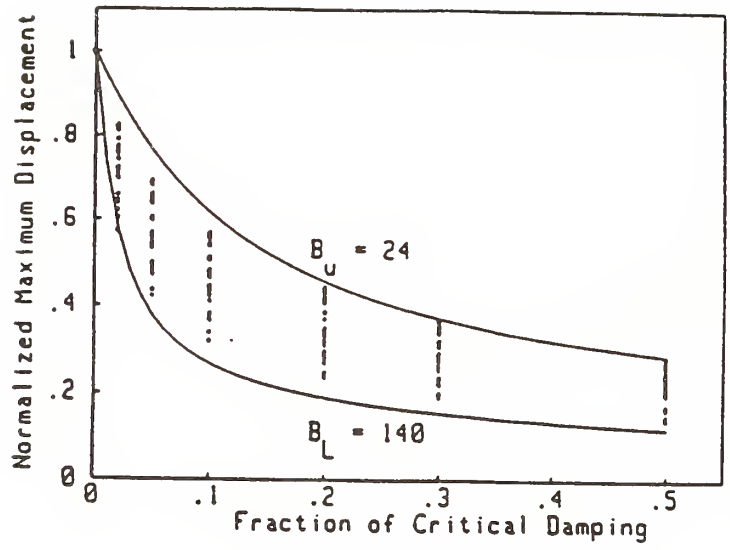

(a) Zero Damping Normalization

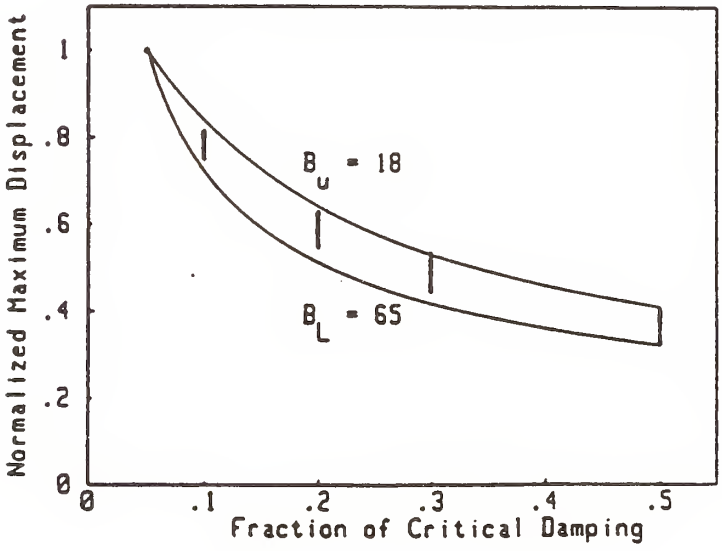

(b) Five Percent Damping Normalization

Figure 2. Envelope of Normalized Mean Displacement Response [from Ashour (1987)]

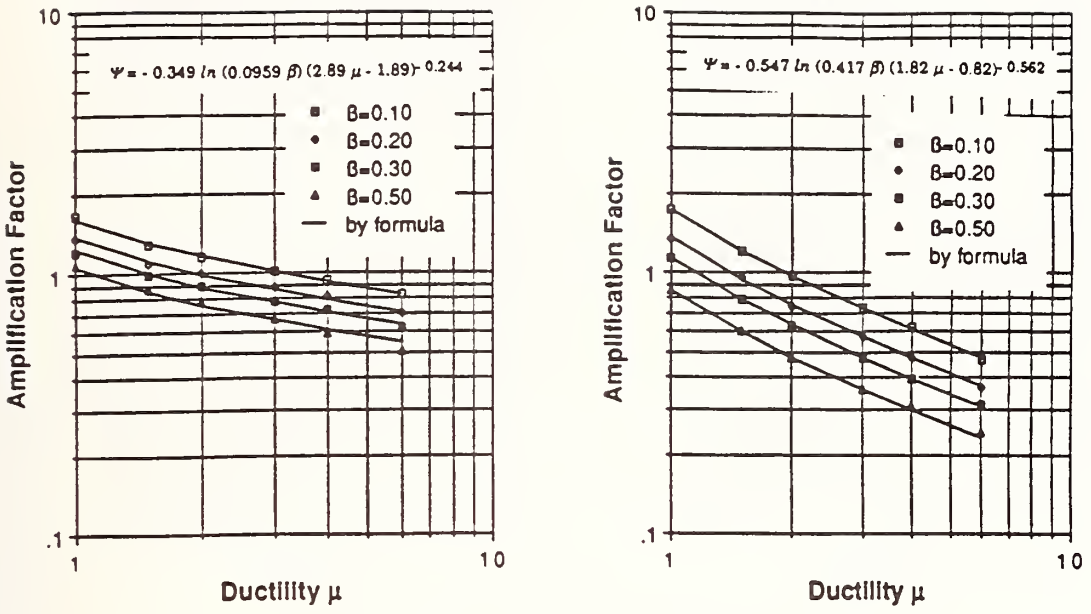

(a) At 0.1 sec Period (b) At 0.5 sec Period

Figure 3. Amplification Factors in the Acceleration Region
[from Wu (1987)]

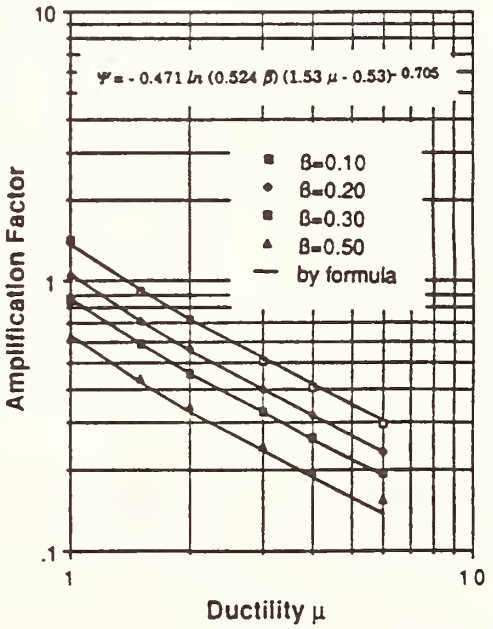

Figure 4. Amplification Factors for PSV_{max} in the Velocity Region
[from Wu (1987)]

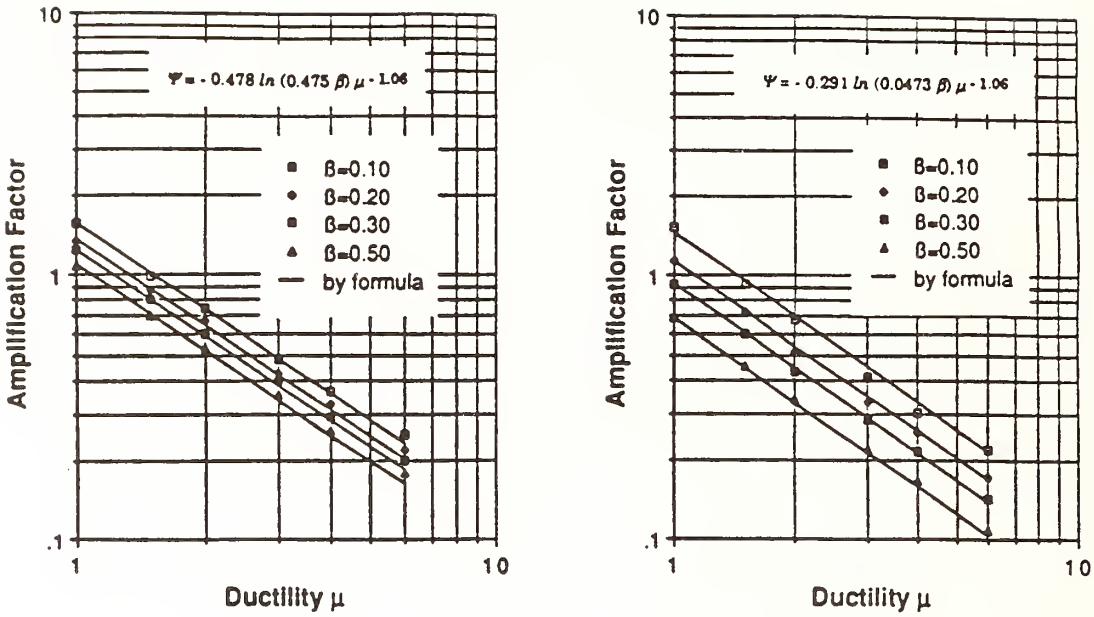

(a) At 3.0 sec Period (b) At 10.0 sec Period

Figure 5. Amplification Factors in the Displacement Region
[from Wu (1987)]

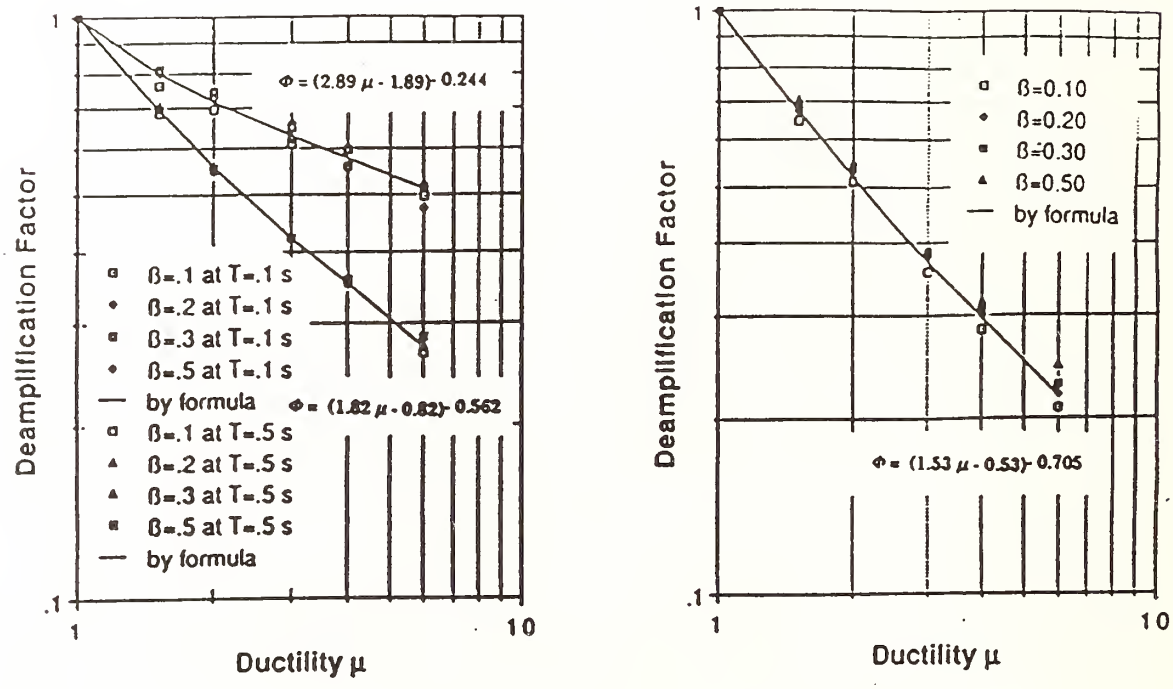

(a) In the Acceleration Region (b) In the Velocity Region

Figure 6. Deamplification Factors in the Three Regions
[from Wu (1987)]

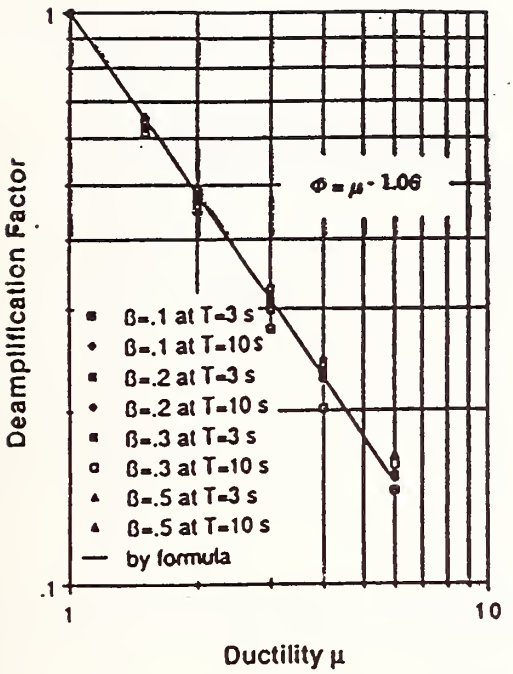

(c) In the Displacement Region

Figure 6. Deamplification Factors in the Three Regions [from Wu (1987)]

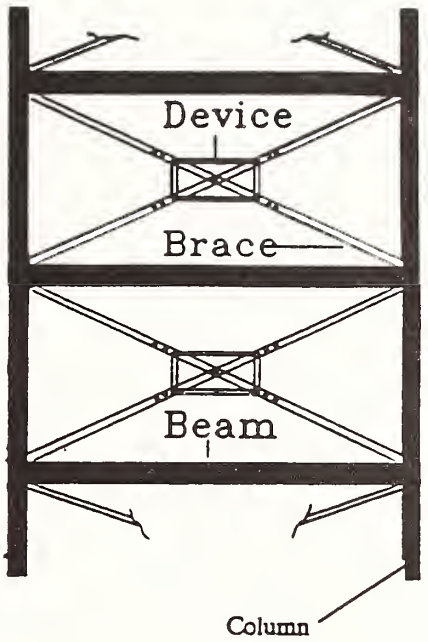

Figure 7. Pall Friction Device Installation [from Filiatrault (1988)]

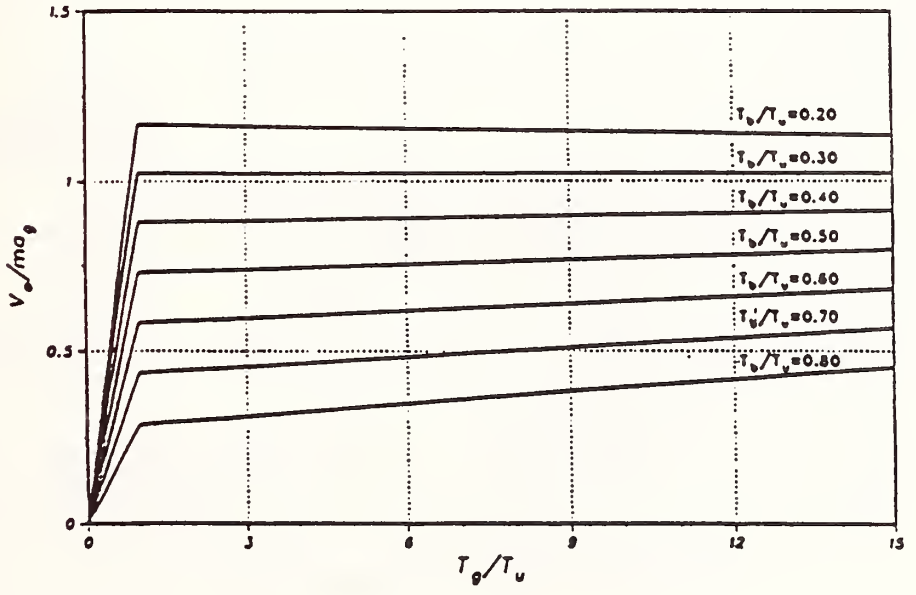

Figure 8. Design Slip Load Spectrum for Single Degree System [from Filiatrault (1988)]

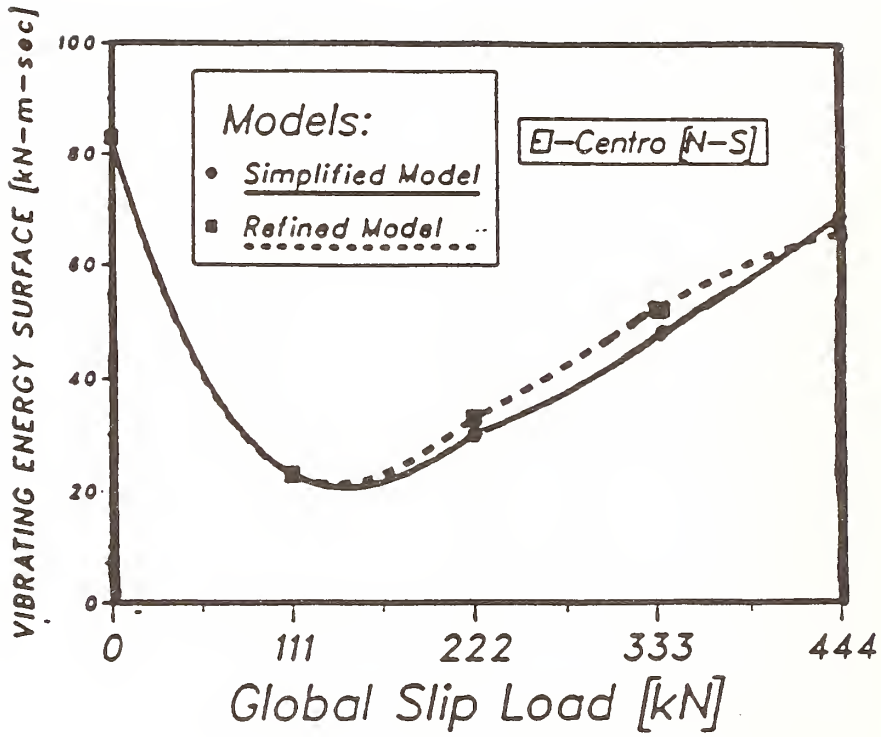

Figure 9. Optimum Slip Load for Friction Damped Braced Frames Subjected to Six Seconds of El Centro 1940 Accelerogram [adopted from Univ. of British Columbia]

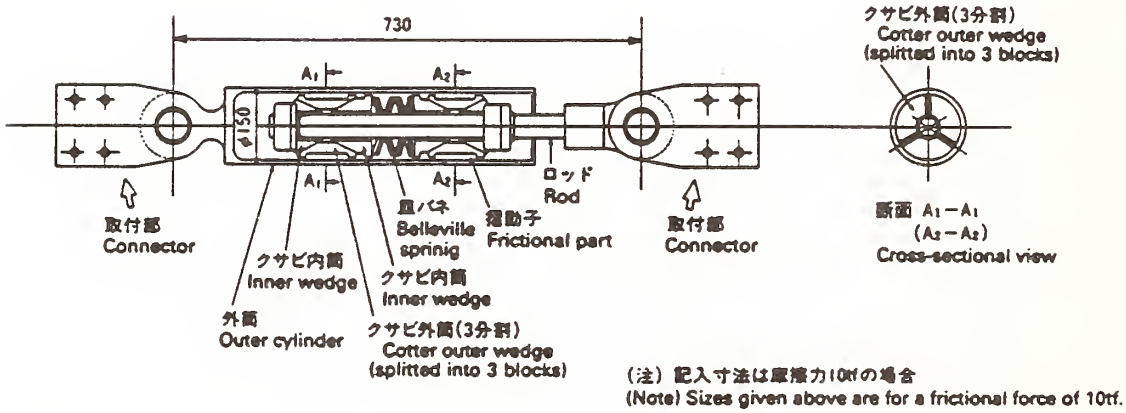

Figure 10. Cylindrical Friction Damper

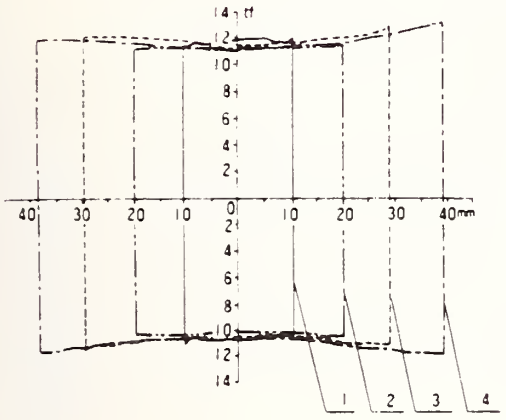

供試ダンパー Specimen	F - 1
周 辺 温 度 Peripheral temperature	R . T
波 形 Wave form	正弦波 Sine wave
周 波 数 Frequency	0.33HZ

		振 幅 Amplitude	ダンパー温度 Temperature of damper
1	———	10mm	58℃
2	——·——	20	62
3	- - - - - -	30	60
4	——··——	38	64

Figure 11. Hysteresis Characteristics for Cylindrical Friction Damper

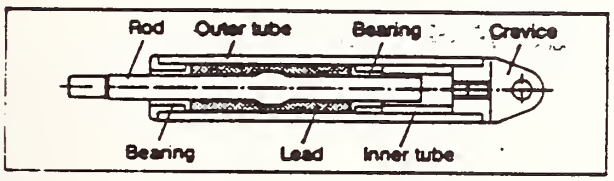

Figure 12. Piston Lead Damper

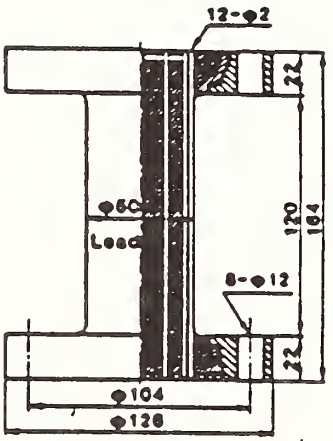

Figure 13. Cylindrical Lead Damper with Steel Wires

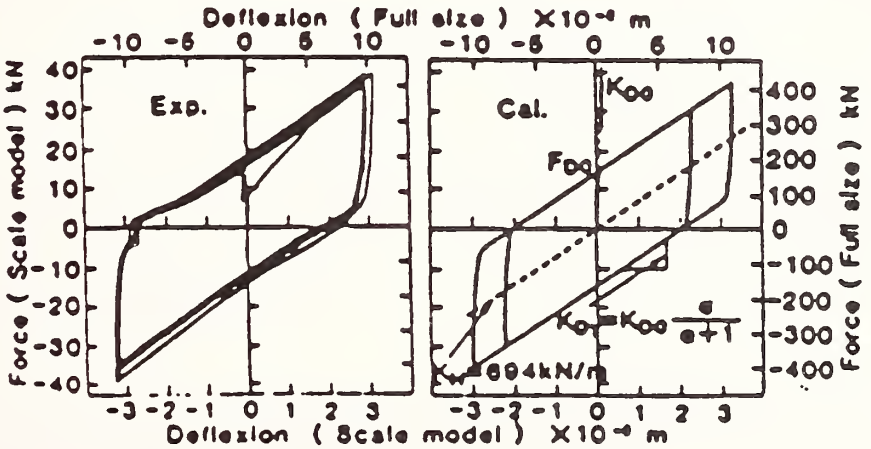

Figure 14. Hysteresis Characteristics for Lead Damper Shown in Figure 13 [from Fujita (1988)]

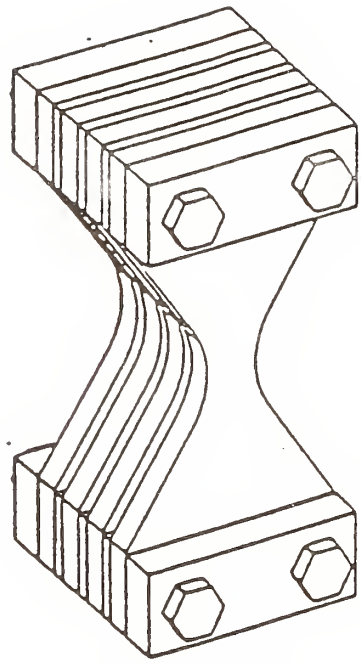

Figure 15. Added Damping and Stiffness (ADAS) Steel Plate Damper [from Bergman (1987)]

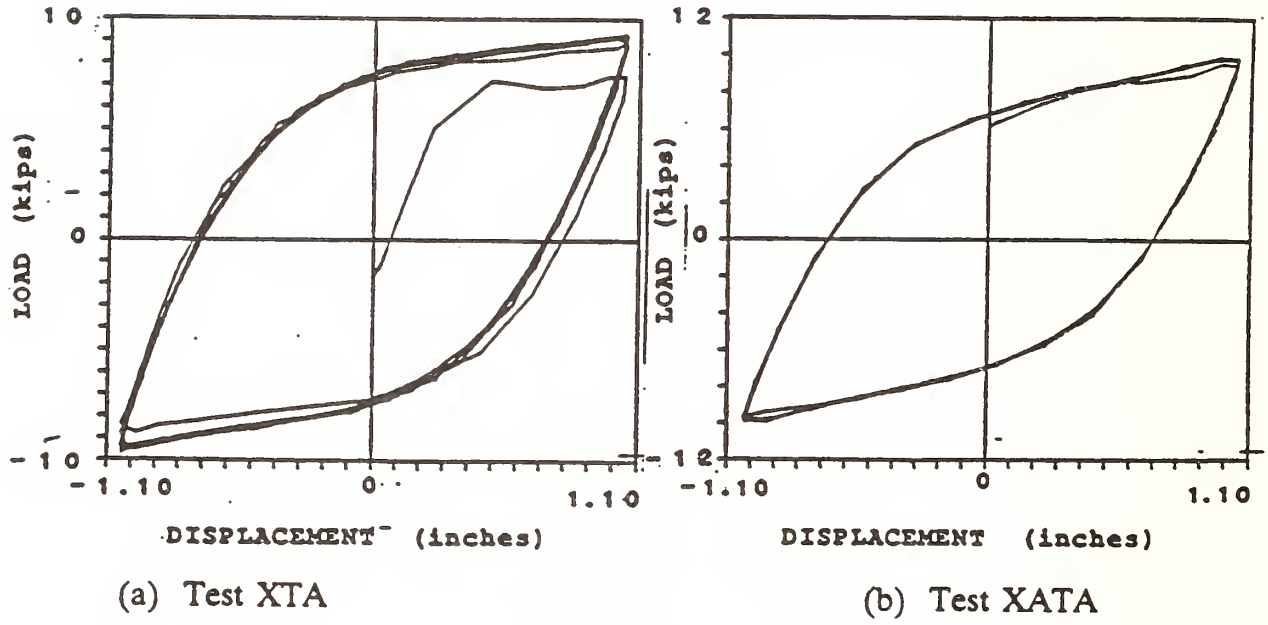

(a) Test XTA

(b) Test XATA

Figure 16. Characteristic Hysteresis Curves for Seven Plate, Five Inch High, 5/16 Inch Thick ADAS Device [from Bergman (1988)]

An Economic Analysis of Laminated Rubber and Steel Bearing Base Isolation System for Buildings

by

Tingley K. Lew[1]

ABSTRACT

The economics of laminated rubber and steel bearing base isolation system for buildings is determined from the very limited data available. The incremental costs for installing the base isolation system for a four-story concrete frame and six-story steel frame building are compared with the benefits from reduction in structural and non-structural costs, and the present worth of reduction in expected future earthquake damage over the service life of the base isolated building. Based on the results of the analysis, conclusions and recommendations are given.

KEYWORDS: Base isolation system; earthquake damage; incremental cost; isolation bearings; percent cost.

1. INTRODUCTION

The lateral force resisting systems of conventional fixed-base buildings are generally designed to resist seismic forces by having the necessary strength and ductility. Due to the relative large seismic design forces especially in zones of high seismic activity, it is generally not economical nor practical to design the lateral force resisting systems of buildings to respond elastically under extreme earthquake loading. Hence, the lateral force resisting systems of conventionally designed buildings are expected to respond inelastically under the maximum earthquake-induced forces during their service lives.

Such inelastic deformations of the building's lateral force resisting system generally produce significant structural damage. In addition, large interstory displacements (story drift) accompanying such deformations cause nonstructural damage in the building. Dynamic response of the building's structural system generally amplifies the earthquake ground motions at the upper levels of the building. Such dynamic amplification of the ground motions causes nonstructural damage unless adequate seismic anchorage and supports are provided. Nonstructural damage include the overturning and sliding of the building contents and subsequent impact of the contents (for example, bookshelves, sensitive mechanical and electronic equipment, filing cabinets, etc.).

The intent of any base isolation system is to reduce the earthquake-induced accelerations at the various levels of the building and, hence, the base shear demand on the building (Figure 1) by increasing (shifting) the fundamental period and damping of the fixed-base building, adjusting and/or controlling the response mass, or some other means. Historical development of the base isolation system for buildings and its implementation are given in References 1 through 6. Some of the more recent analytical and experimental studies on base isolation for building structures may be found in References 7 through 12. The friction pendulum system (Ref 9) appears to be most promising. This simple system allows the engineer/designer relatively fine control over the period shift of the fix-based building and is rather insensitive to torsional response of buildings with asymmetrical mass and/or stiffness distribution compared to the other base isolation systems. Base isolated building structures in Japan are given in Reference 13.

In current U.S. practice, base isolation is generally accomplished by introducing lateral flexibility by way of isolation bearings/energy dissipators at the base of the building, thereby shifting the fundamental period of the building away from the range where the earthquake ground shaking energy is dominant and accompanied by large demands (Figure 1). Thus, the dynamic response of the base isolated building is greatly reduced as compared to the fixed-base building.

Base isolation is most suitable for structures located relatively close to the potential earthquake sources in high seismicity areas with large seismic design forces. Furthermore, the suitability of base isolation depends on the intended occupancy of the building. Certain occupancy demands an increase in safety above those obtainable from conventional design, e.g., hospitals, fire stations, police stations, telephone exchanges, telecommunication and computer centers[2] housing essential services, and/or expensive equipment.

Structures with low fundamental periods (<0.7 to 1.0 second) benefit the most from the increase in period by base isolation. Generally, most of the earthquake ground shaking energy input to the base of the buildings on stiff to intermediate soil sites is concentrated in periods ranging between 0.1 and 1.0 second. Base isolation is generally best suited for relatively stiff, squat, low- to medium-rise buildings with

[1]Naval Civil Engineering Laboratory Code L51, Port Hueneme, CA 93043-5003

[2]The cost of equipment housed in such facilities can be up to several times the cost of the building. By contrast, the cost of the contents of a typical commercial building is about 10% of the cost of the building.

between three to ten stories and fixed-base fundamental periods less than about 0.7 to 1.0 second. Base isolation is not likely to benefit taller or more flexible buildings whose fixed base period is in the range where the demand from the earthquake site response spectrum is relatively low and decreases relatively slowly with increasing periods (the right most portion of the curve in Figure 1).

Earthquake base isolation is best suited for buildings located on stiff to intermediate stiff soil sites. Sites with soft soil profiles tend to filter out the high frequency components of the earthquake ground motion and may provide some reduction of the seismic forces transmitted to short period structures. Relatively deep (deeper than about 5 feet or 1.5m) soft soil deposits at the site can amplify the relatively long period (> 0.30 second) components of ground shaking from nearby earthquakes and/or large magnitude distant earthquakes and defeat the intent of base isolation (e.g., acceleration data recorded in soft clay sites in the San Francisco Bay area during the 1989 Loma Prieta northern California earthquake). By contrast, sites with stiff soil profiles tend to amplify the low period components of the ground motion. A base isolation system on such a site will filter out these low period components of earthquake ground shaking energy and be more effective than on a soft soil site.

The current application of base isolation to buildings is made difficult by the limited data on the range expected earthquake ground motion characteristics for a particular site relatively close to the energy source and the uncertainties about the inelastic structural response under relatively large loads from a major earthquake. Thus, most of the existing base isolated buildings are designed to remain essentially elastic with a small amount of localized yielding in noncritical structural framing members for safety and serviceability.

To reduce the contribution from their higher modes, base isolated buildings are generally designed to be relatively stiff in the lateral directions. The principal dynamic response characteristics of a base isolated building are illustrated by the mode shapes and modal shear distribution shown in Figure 2 for a base isolated shear beam type building.

- The relatively high flexibility and damping of the base isolated building results in a long first mode period and, thus, low demand (loading) from the site response spectrum.

- The relatively high lateral flexibility of the base isolated building system ensures a low modal participation factor for the second and higher modes. This reduces the horizontal accelerations and seismic forces on the building and its contents.

- The energy dissipation capacity of the base isolation system reduces the seismic forces, the associate base isolator displacement, and building deformations.

- Base isolation provides a more uniform seismic shear force distribution over the lower levels of the building.

Although base isolation reduces the horizontal accelerations of the building, it increases the horizontal displacement of the building system as a whole. The story drift of the base isolated building is reduced. However, the horizontal displacement of the building over its height can be relatively large, with most of the displacement concentrated at the base of the building. The base isolation system and the utility connections at the isolator level must be designed to accommodate the anticipated base isolator displacement (possibly as large as 12 to 16 inches for some systems) and remain functional.

Due to the lateral flexibility introduced by the base isolation system, wind loading becomes one of the dominant factors in the design of a base isolation system. Theoretically, a base isolation system can be designed to reduce the maximum floor accelerations to one-tenth or less than the maximum horizontal earthquake ground acceleration at the site. In practice, this reduction is limited by the lateral displacement capacity of the base isolation bearings, the wind loading at the site, and the amount of hysteretic energy dissipation required by the base isolation system. The laminated rubber and steel isolation bearings must be designed to remain stable in the vertical direction under the maximum earthquake-induced horizontal ground displacement at the site. This indirectly controls the lateral stiffness of the bearings and, hence, the seismic load transmitted to the structure. Wind restrain is needed for the base isolation system to minimize personnel discomfort from the relatively frequent wind-induced displacements of the building and the resulting fatigue damage to piping and other utility connections in the building. For high seismicity sites, the base isolation system is generally designed to yield at between 3% and 6% of the weight of the building to satisfy wind restrain requirements. Although some researchers have suggested that 5% is optimal, the three base isolated buildings that use a laminated rubber and steel bearing with a vertical cylindrical lead plug energy dissipator in Reference 4 through 6 have a design yield of about 7% of the weight of the isolated structure.

To provide an adequate amount of energy dissipation capacity, the hysteretic energy dissipators of the base isolation system must have a sufficiently high yield capacity to provide the needed energy dissipation.[3] A highly ductile energy dissipator with a low design yield level is unlikely to

[3]The energy dissipation capacity of the hysteretic energy dissipator is proportional to the area under its force displacement curve. Ductility is the ratio of the maximum displacement to the displacement at yield.

provide the needed energy dissipation to limit the maximum horizontal displacement of the isolation bearings to reasonable values. The effective combined lateral stiffness of the laminated rubber and steel bearing and the yielding lead plug energy dissipator controls the seismic forces transmitted to the building and the maximum horizontal displacement of the building. A 2-inch-thick shell of rubber covers the outside of the isolation bearing (Figure 3) to provide about 3 hours of needed fire protection. This layer of rubber also protects the steel plates of the bearing from atmospheric corrosion. A properly designed base isolation system will generally result in an equivalent base shear of between 0.2g and 0.25g for the building with a maximum horizontal design earthquake acceleration of about 0.5g.

For a fixed-base building with an effective period of less than about 0.7 second, the input maximum earthquake ground accelerations at the site are amplified at the upper floor levels by average[4] factors of about 3.5 and 2.5, respectively, for 2% and 5% damping. By contrast, both analytical results (Ref 14 and 15) and experimental results for a one-third scale building model (Ref 16) have shown that a properly designed base isolation system can generally reduce the dynamic accelerations of the building and, hence, base shear demand on the building by a factor of about five, as compared to the fixed-base building. A three-bay, five-story, one-third scale model steel frame building, with and without laminated rubber and steel/lead plug isolation bearing/energy dissipation system was tested at Berkeley (Ref 16). The model was subjected to the 1940 El Centro earthquake time-history, scaled to a peak value of about 0.55g. The experimental results are shown in Figure 4. From the curves in the figure, it can be seen that the maximum table acceleration for the fixed-base building is amplified by a factor of about 5 at the fifth floor level. The average acceleration for all the floor levels is about 1.25g. By contrast, all the floor accelerations for the isolated building are only about 0.25g, one-half of the maximum shake table acceleration. Consequently, potential earthquake damage to structural and nonstructural elements in the base isolated building is expected to be much less than that of the fixed-base building.

Results of analytical studies, laboratory experiments on scale models of steel frame buildings on a shake table, and field performance of prototype buildings[5] indicate that the usage of laminated rubber and steel/lead plug isolators for earthquake base isolation is technically feasible. The only question that remains is whether earthquake base isolation for buildings is cost effective. For this economics analysis, the base isolated building is divided into three subsystems (Figure 5):

- Building System
  - Structural frame
  - Bottom floor slab
  - Isolation bearing connections
- Base Isolation System
  - Isolation bearings/energy dissipators
  - Bearing connections to foundation
  - Foundation
  - Water/gas/electrical connections
- Soil System
  - Soil profile and properties
  - Earthquake ground motion input

In the building system, the bottom floor slab and isolation bearing connections are additional cost items as compared to a conventional fixed-base building.

In the base isolation system, the isolation bearings, the bearing connections to the foundation, the additional excavation required to provide the gap around the perimeter of the building to accommodate building movement at its base and sliding grills to cover over this gap, and the retaining wall around the perimeter of the gap are extra cost items. In addition, special detailing for facial panel anchorage, stairs, elevator, and mechanical shafts are required at the isolator level and are extra cost items.

In the soil system, the different soil layer thicknesses and stiffness and strength properties modify the dominant periods of the earthquake ground motions input into the base of the building. To be effective, the base isolation system must shift (increase) the fundamental period of the fixed-base structure to a period range where the earthquake ground motion input energy is relatively low. The soil subsystem together with the characteristics of the incoming earthquake ground motions control the period range in which the earthquake ground shaking energy is dominant.

The potential benefits from base isolation of a building include:

- Savings in the cost of the lateral force resisting system and nonstructural system due to reduction in the seismic design forces.
- Reduction of potential structural and nonstructural damage over the service life of the building. Minimizing damage to essential equipment, services, and other nonstructural elements.

---

[4]Some of the larger amplification factors can be 1.5 times or larger than the average factors.

[5]To date, none of the known prototype base isolated building has been subjected to severe earthquake ground shaking near its upper design level.

- Reduction of potential down time required for repairs of earthquake damage.

- Ensures that the structure and its contents remain functional during and after a major earthquake.

The last two items are important in an economic analysis and can be quantified in dollars for civilian buildings where losses from potential down time can be estimated from available operating cost and revenue data. However, the U.S. Navy is a nonprofit organization and the corresponding operating cost and revenue data are not readily available. For this study, the last two items are considered as intangible benefits from base isolation.

The purpose of this paper is to determine the economics of laminated rubber and steel bearing base isolation system for buildings from the very limited data available.

2. ESTIMATED COST OF LAMINATED RUBBER/ LEAD PLUG, ISOLATION BEARINGS

The cost of the base isolation bearings depends on the weight of the building excluding its foundation. This is because the isolation bearings must support the weight of the building under ordinary conditions. In addition, the bearings must be able to resist the earthquake-induced inertia forces of the isolated building. These inertia forces increase with the weight of the building supported by the isolation bearings. Hence, the cost of the base isolation bearings is expected to be smaller for the lighter steel buildings as compared to the heavier reinforced concrete buildings.

In this study, estimated costs of the bearings expressed as a percentage of the unit cost (cost per square foot) of newly constructed steel frame and concrete frame office buildings in southern California.

The typical seismic design floor loads for steel frame and concrete frame office buildings are as follows:

Steel Frame		Concrete Frame	
Finish	1.0 lb/ft²	Floor covering	1 lb/ft²
Steel deck	3.1	Concrete frame	129
Concrete fill	32.0	Partitions	20
Steel bearing girders	5.9	Ceiling	5
Columns	1.5	Mech and Elect	5
Partitions	20.0	Exterior wall	4
Ceiling	10.0	Misc.	4
Mech and Elect	5.0		168 lb/ft²
Misc.	1.0	Seismic L.L.=50/4=	13
	79.5 lb/ft²		181 lb/ft²
Seismic L.L.=50/4=	12.5		
	92.0 lb/ft²		

For practical purposes, the typical seismic design floor load for concrete frame buildings is about twice that for steel frame buildings. For reference, the typical seismic design floor load for small stucco and wooden frame apartment or office buildings is about 44 lb/ft², or about one half of that for steel frame buildings.

The estimated cost of the laminated rubber and steel/lead plug base isolation bearings for modern commercial buildings is about $21/ton or $0.0105/lb of supported weight (Ref 6). Multiplying the latter by the seismic design floor loads gives unit costs for base isolation bearings at $0.97/ft² and $1.90/ft², respectively, for steel frame and concrete frame buildings. Base isolation is more attractive for buildings with smaller design floor loads.

Based on the 1986 construction costs given in Reference 17, the estimated unit costs for different types of new construction in southern California are given in Table 1. Due to the difference in construction required to satisfy functional requirements, the unit costs for hospital, telephone exchange, and medical clinics are much higher than the unit costs for steel frame and concrete frame office buildings. Similarly, the unit costs for wood framed apartments or office buildings, reinforced masonry or steel framed warehouses or industrial buildings are less than those for steel framed or concrete framed office buildings.

The unit cost of the base isolation bearings for steel frame and concrete frame buildings expressed as a percent of their corresponding unit construction cost are 1.1% ($0.97/ft² / $88/ft²) and 2.2% ($1.90/$88), respectively.

For steel frame and concrete frame hospitals, these percent costs for the base isolation bearings are 0.6% ($0.97/$166) and 1.1% ($1.90/$166), respectively. These values are about one-half of those values for steel frame and concrete frame office buildings. The percent costs of the base isolation bearings for the other buildings shown in Table 1 can be determined in a similar manner.

The percent cost of the base isolation bearings decreases with increasing unit construction cost of the building. Thus, base isolation tended to be economically more attractive for buildings with high unit construction costs than those with low ones.

3. ESTIMATED INCREMENTAL COST FOR INSTALLATION OF THE BASE ISOLATION SYSTEM

The incremental cost associated with the installation of a base isolation system in a building is the difference between the added cost for the base isolation system and the savings from the reduction in structural and nonstructural costs.

3.1 Added Cost

The added cost for the base isolation system includes the cost of the isolation bearings, basement slab above the base isolators, retaining wall around the perimeter of the gap (see Figure 5), extra excavation for the gap, sliding cover for the gap, flexible utility connections, etc.

The William Clayton Building is a four-story (including basement) reinforced concrete frame building of 97 meters (318 feet) by 40 meters, (131 feet) in plan with column spacing at 7.2 meters (24 feet), on centers constructed in New Zealand (Ref 4). It is the first building fitted with a laminated rubber and steel/lead plug base isolation system. The building was designed for 1.5 times maximum ground motion time-history from the 1940 El Centro earthquake, i.e., a peak horizontal acceleration of about 0.52g. The base isolation system cost was about 4% of the total building cost. With the base isolation system, the reinforcing detailing for the beam-to-column joints were relaxed somewhat. Otherwise, beams 200 mm deeper would be necessary to accommodate the full joint shear reinforcement detailing required. However, no definite indications were given in the reference on whether the building was more or less expensive than a conventional building. Hypothetically, if there were no savings in structural and nonstructural costs, the William Clayton Building would cost 4% more than a conventional building. The building would be economical only if the base isolation system reduced the present worth of expected future earthquake damage to the building by equal to or greater than 4%. The cost of the base isolation bearings for concrete frame office buildings given earlier is 2.2% of the total building cost. Subtracting this from the added cost of the base isolation system of about 4% gives 1.8% as the approximate added cost of the base isolation system, excluding the cost of the bearings.

Kelly and Hodder (Ref 16) reported the estimated added costs of the base isolation system and the savings in structural and nonstructural costs for a six-story 170,000 ft², steel frame medical building. A figure showing the building and the itemized costs from the reference is reproduced here as Figure 6. The cost of the 46 base isolators is given as $46,000. The author believes that a more probable cost should be about 170,000 ft² x $0.97/ft² = $165,000 for the isolation bearings. In addition, a miscellaneous cost of $40,000 would be more appropriate than the $30,000 shown, due to the increase in isolation bearing cost. The author's estimated total cost for the building is $14.96 x 10^6 (170,000 ft² x $88/ft²). The modified added costs for the base isolation system are:

	Cost	% of Building Cost
46 Base Isolators	$165,000	1.1%
Retaining Wall	144,000	0.9
Basement Slab Separation	57,000	0.4
Miscellaneous	40,000	0.3
Total	$406,000	2.7%

The added cost for the base isolation system excluding the cost of the base isolation bearings is 1.6%. This is approximately equal to the corresponding 1.8% determined earlier for the four-story concrete frame building. The slightly higher percentage for the William Clayton Building might be expected because it has only four stories as compared to the six stories for the building above. The fixed portion of the added cost for the base isolation system excluding the bearings is distributed over a smaller number of stories and, hence, smaller total floor area. Thus, the resulting added cost percentage is expected to be somewhat larger.

3.2 Savings in Structural and Nonstructural Cost

Because base isolation reduces the seismic forces on the building, the cost for providing seismic resistance to structural and nonstructural elements is expected to decrease as compared to a fixed-base building. However, the cost reduction is not expected to be great for two reasons.

First, the current practice is to design the base isolated building to remain essentially elastic for an equivalent base shear[6] of between 0.20 and 0.25g associated with a maximum ground acceleration of about 0.5g. This is approximately equal to the code design base shear for seismic Zone 4 (e.g., UBC, SEAOC, NAVFAC P-355). The structural detailing for base isolated buildings can be relaxed somewhat. However, to fulfill the intent of base isolation - to minimize the building and its contents from damage due to major earthquakes - the base isolated building is generally designed to remain essentially elastic and with as much reserve ductility and energy absorbing capacity as possible. This is done to provide an extra margin of safety in the rare event that the earthquake ground motions at the site are larger than or much different from the characteristics of design ground motions. If the actual maximum earthquake ground acceleration is much larger than the design acceleration, the laminated rubber and steel/lead plug base isolation system would still remain functional, but the seismic forces transmitted to the building would be much increased (Figure 7). The ductility and overstrength capacity (above the elastic) of the lateral force resisting system of the building will resist the increase in seismic forces by inelastic defor-

[6]Dynamic analysis procedures should be used for the design and analysis of base isolated buildings.

mation as in a conventional fixed-base building.

Second, the cost for providing seismic resistance to the structural system of a multistory building is only a small fraction of the total building cost. For illustration, a listing of the structural and nonstructural costs for a 13-story steel frame building (from Ref 18) is shown in Table 2. The total structural cost including seismic provisions for Zone 4 is about 30% of the total building cost. About one-fifth (5.7%) of this 30% goes to providing seismic structural resistance. About 2.3% of the total building cost (near the bottom right corner of the table) goes to providing seismic resistance to nonstructural elements. Thus, the cost of providing seismic resistance to structural and nonstructural elements of a steel frame building is approximately equal to 8% of the total cost for a conventional building. Any savings by base isolation would have to come from this 8%. Because of the desire for essentially elastic response of the building, base isolation is expected to reduce this percentage by only a small amount. Most of the actual savings, however, would probably come from the reduction in the sizes of the structural elements and reduction in bracing and anchorage of the electrical and mechanical components had the building been designed to remain essentially elastic under a maximum earthquake design ground acceleration of between 0.4g and 0.5g without base isolation[7]. For reinforced concrete frame buildings, the cost of providing seismic resistance to structural and nonstructural elements in seismic Zone 4 is about 10% (Ref 18).

It is hypothesized that to satisfy the essentially elastic criterion, the 8% and 10% seismic construction cost for steel frame and concrete frame buildings, respectively, could only be reduced by about one-third as a result of base isolation. Hence, the savings in the structural and nonstructural cost for steel frame and concrete frame buildings by using isolation are estimated to be about 2.7% and 3.3%, respectively.

The corresponding estimated reduction in structural and nonstructural cost given for the six-story steel frame building in Figure 6 is $384,000, or about 2.6% ($384,000/ $14.96 x 10^6) of total building cost. This compares favorably with the 2.7% estimated previously. About six-tenths (1.5%) of this 2.6% cost savings is due to reduction in the structural requirements that include the elimination of the shear walls required to reduce interstory drift and the reduction in requirements for floor and roof diaphragm connection requirements. The remaining 1.1% savings is due to the reduction in seismic bracing for mechanical and electrical components. Although a reinforced concrete frame building would probably not require shear wall bracing to reduce story drift or special floor and roof diaphragm connections, savings in the structural cost would come from a reduction in structural member sizes and steel reinforcement, and a slight relaxation of the beam-to-column joint reinforcement detailing requirement. It seems reasonable to expect a comparable savings in the structural cost for base isolated concrete frame buildings of about 1.9% [(1.5/2.6) x (3.3%)]. The savings for the nonstructural cost of the concrete frame building is about 1.4%.

3.3 Incremental Cost

For the four-story concrete frame William Clayton Building, the estimated incremental cost is about 0.7%. That is, the estimated cost for the base isolated building is about 0.7% larger than a conventional building without base isolation. For the six-story steel frame building, the estimated incremental cost for the base isolation system is about 0.1%. Due to the approximate numbers used, this incremental cost is rounded off to zero percent.

Base isolation for the four-story concrete frame William Clayton Building would be economical only if base isolation could reduce the present worth of the expected earthquake damage over the service life of the building by 0.7% or more.

4. REDUCTION IN EXPECTED FUTURE EARTHQUAKE DAMAGE OVER SERVICE LIFE OF THE BUILDING

Reference 20 presented the present worth of expected future earthquake damage to buildings, based on average historic building damage versus earthquake intensity data (Ref 21) using the probability versus maximum ground acceleration curve for an intermediate soil site in California with a maximum ground acceleration of 0.4g, with 80% probability of not being exceeded in 50 years.[8] The interest rate used was 10%.

The present worth of all the expected future earthquake damage in 50 years for steel frame and concrete frame buildings with seismic design is 2.7% and 4.2%, respectively, of the replacement cost of the building.

Assuming that base isolation is effective in reducing the expected earthquake damage by two-thirds, the present worth of the reduction in expected future earthquake damage by base isolation for steel frame and concrete frame buildings is 1.8% and 2.8%, respectively. Because both of these values are larger than the corresponding incremental costs of 0% and 0.7% for the steel frame and concrete frame buildings analyzed, respectively, base isolation is economical for both buildings.

---

[7]This is a requirement only for essential facilities that must remain functional during and after a major earthquake. See NAVFAC P-355.1 (Ref 19).

[8]This corresponds to a typical site in seismic Zone 4 (Ref 19).

A summary of the costs and benefits for the base isolated four-story concrete frame and six-story steel frame buildings analyzed is shown in Table 3. The total benefits are 6.1% and 4.4%, respectively, for the concrete and steel buildings. The larger benefit for the concrete building is due to its greater reduction in structural and nonstructural costs for expected future earthquake damage by base isolation. The total added costs for the base isolation system are 4.0% and 2.7%, respectively, for the concrete and steel buildings. Apparently, the larger cost for the concrete building is due primarily to its greater isolation bearing cost because of its greater dead weight. The benefits minus costs are 2.1% and 1.7%, respectively, for the concrete and steel buildings. This suggests that base isolated concrete or steel frame essential buildings are economically competitive if their cost is not greater than about 2% of their conventional fixed base counterparts.

The main benefits of earthquake base isolation for buildings are the reduction of the expected future earthquake damage to the building over its service life, ensuring that the building and its contents remain functional during and after a major earthquake, and reducing the potential down time required for repairs. Base isolation appears to be most attractive economically and functionally for essential facilities, particularly those facilities that contain sensitive equipment whose cost is greater than the cost of the building. For the latter buildings, the benefits from reducing future earthquake damage to the building are magnified by the ratio of building plus contents cost, divided by the cost of the building without contents, see Table 3.

5. CONCLUSIONS

Based on the results of the analysis presented, the following conclusions are drawn:

1. Base isolation is economically more attractive for lighter buildings with smaller design floor loads.

2. Base isolation is economically more attractive for building structures with average or above average unit cost.

3. Base isolation is economical for low-rise steel frame and concrete frame office buildings.

4. The main benefits of earthquake base isolation for a building are the reduction of the expected future earthquake damage over its service life, ensuring that the building and its contents remain functional during and after a major earthquake, and reducing the potential down time required for repairs after a major earthquake.

5. Base isolation appears most attractive for essential facilities such as hospitals, telephone exchanges, telecommunication centers, and computer centers, especially those facilities that contain sensitive equipment that costs more than the facility itself.

6. RECOMMENDATION

It is recommended that earthquake base isolation be considered as an alternative to conventional fixed-base design and construction for essential facilities located near potential earthquake sources that must remain functional during and after a major earthquake, particularly those that contain sensitive equipment which costs more than the facility itself.

7. ACKNOWLEDGMENTS

The continual support by Mr. J.V. Tyrrell (Retired NAVFAC Code 04BO), Mr. H. Nickerson (NAVFAC Code 04B2), and Mr. J. Cecilio (NAVFAC Chief Engineer) is appreciated.

This paper was sponsored by the Naval Facilities Engineering Command.

8. REFERENCES

1. Lee, D.M., and Medland, I.C. "Base isolation - an historical development, and the influence of higher mode responses." Bulletin of the New Zealand National Society for Earthquake Engineering, vol 11, no. 4, Dec 1978, p. 219-233.

2. Kelly, J.M. Earthquake Engineering Research Center. Report No. UCB/EERC-81/01: Control of seismic response of piping systems and other structures by base isolation. University of California at Berkeley, Berkeley, Calif., Jan 1981.

3. Skinner, R.I. "Base isolated structures in New Zealand," in Proceedings of the Eighth World Conference on Earthquake Engineering, San Francisco, Calif., 1984. Earthquake Engineering Research Institute, vol V, Berkeley, Calif., p. 927-934.

4. Megget, L.M. "The design and construction of a base isolated concrete frame building in Wellington, New Zealand," in Proceedings of the Eighth World Conference on Earthquake Engineering, San Francisco, Calif., 1984. Earthquake Engineering Research Institute, vol V, Berkeley, Calif., p. 935-942.

5. Kelly, J.M. "Aseismic base isolation: Review and bibliography," Soil Dynamics and Structural Engineering, 5, 1986, p. 202-216.

6. Walters, M. and Elsesser, E. "Base isolation of the existing city and county building in Salt Lake City," paper given at seminar on Implementation of Base

Isolation at the San Bernardino County's Foothill Community Law and Justice Center. Sponsored by ASCE/County of San Bernardino/California Seismic Safety Commission, San Bernardino, Calif., Feb 1986.

7. Chung, L.L., Lin, R.C., Soong, T.T., and Reinhorn, A.M. "Experimental study of active control for MDOF seismic structures," Journal of Engineering Mechanics, American Society of Civil Engineers, 111, 1989, p. 1609-1627.

8. Mostaghel, N. and Khodaverdian, M. "Dynamics of resilient-friction base isolator (R-FBI)," Earthquake Engineering and Structural Dynamics, 15, 1987, p. 379-390.

9. Zayas, V. Low, S., Bozzo, L., and Mahin, S. Earthquake Engineering Research Center Report No. UBC/EERC-89/09: Feasibility and performance studies on improving the earthquake resistance of new and existing buildings using the friction pendulum system. University of California, Berkeley, CA, Sep 1989.

10. Su, L., Ahmadi, G., and Tadjbakhsh, I.G. "A comparative study of base isolation systems," Journal of Engineering Mechanics, American Society of Civil Engineers, 115, 1989, p. 1976-1992.

11. Su, L., Ahmadi, G., and Tadjbakhsh, I.G. "A comparative study of performances of various base isolation systems, Part I: Shear beam structures," Earthquake Engineering and Structural Dynamics, 18, 1989, p. 11-32.

12. Su, L., Ahmadi, G., and Tadjbakhsh, I.G. "A comparative study of performances of various base isolation systems, Part II: Sensitivity analysis," Earthquake Engineering and Structural Dynamics, 19, 1990, p. 21-33.

13. Kitagawa, T.Y. and Hirosawa, M. "Base isolated building structures in Japan," proceedings of the 20th Meeting of the U.S.-Japan Cooperative Program in Natural Resources Panel on Wind and Seismic Effects, N.J. Raufaste, Editor, NIST SP 760, National Institute of Standards and Technology, Gaithersburg, MD., Jan. 1989.

14. Lee, D.M. and Medland, I.C. "Estimation of base isolated structure responses," Bulletin of New Zealand National Society for Earthquake Engineering, vol 11, no. 4, Dec 1978, p. 234-244.

15. Megget, L.M. "Analysis and design of base isolated reinforced concrete frame building," Bulletin of New Zealand Society for Earthquake Engineering, vol 11, no. 4, Dec 1978, p. 245-254.

16. Kelly, J.M. and Hodder, S.B. Earthquake Engineering Research Center. Report No. UCB/EERC-81/16: "Experimental study of lead and elastomeric dampers for base isolation systems." University of California at Berkeley, Berkeley, Calif., Oct 1981.

17. R.S. Means Co., Inc., "Building construction cost data 1986," 44th Edition, Kingston, Mass., 1985.

18. Leslie, S.K. and Biggs, J.M. Massachusetts Institute of Technology. Report No. 341: Optimum seismic protection and building statistics, Mass., May 1972.

19. Departments of the Army, Navy, and Air Force. Army Technical Manual No. 5-809-10-1, NAVFAC P-355.1, and Air Force Manual No. 88-3, Ch. 13.1, Final Manuscript: Seismic design guidelines for essential buildings (a supplement to Seismic Design for Buildings), prepared by URS/Jon A. Blume and Associates, Engineers. Washington, DC, Mar 1985.

20. Lew, T.K. Naval Civil Engineering Laboratory. Technical Memorandum TM 51-86-10: Present worth of expected earthquake damage based on historic and rapid seismic analysis data. Port Hueneme, Calif., May 1986.

21. Sauter, F.F. "Damage prediction for earthquake insurance," in Proceedings of the Second U.S. National Conference on Earthquake Engineering, Stanford University, Standford, Calif., 22-24 Aug 1979. Earthquake Engineering Research Institute, Berkeley, Calif., 1979, p. 99-108.

Table 1.
Typical 1986 Unit Costs for New Construction in Southern California (from Ref 17)

Building Description	Estimated Cost ($/ft²)
Steel framed office building	88
Concrete framed office building	88
Hospital	166
Telephone Exchange	149
Police Station	128
Medical Clinics	94
Fire Station	88
Small stucco and wood frame apartment or office building	44-59
Reinforced concrete block warehouse or industrial building	31-45
Steel framed warehouse or industrial building	29

Table 2.
Cost Increase for Increasing Seismic Force Design Levels (after Ref 18)

Item	Percentage Total Cost of Item	Increase Over Original Total Construction Cost (%) for Zones	
		3	4
Structural			
Structural Steel[a]	12.5	2.68	5.4[b]
Foundation[a]	1.2	0.162	0.162
Concrete Walls and Slab[a]	3.7	0.09	0.102
Composite Deck[a]	5.8		
Total Structural	23.2	2.93	5.66[b]
Nonstructural			
Masonry Core[a]	5.0	0.55	0.71
Precast Panels[a]	4.73	0.033	0.067
Plumbing	3.6	0.022	0.022
HVAC	18.8	0.15	0.197
Electrical (including lights)	8.5	0.104	0.104
Elevators	4.8	0.131	0.165
Window Systems	4.5		0.627[c]
Partitions	4.45	0.163	0.163
Acoustical Ceilings	2.2	0.114	0.163
Miscellaneous Metals	3.7	0.089	0.089
Total Nonstructural	60.28	1.36	2.31
Total Code Design (code design items)	32.93	3.51	6.44[b]
Maximum Design[d]	83.48	4.29	7.97[b]

[a]Code design.
[b]Using built-up members.
[c]New window system.
[d]Total structural and nonstructural items.

Table 3.
Summary of Costs and Benefits of Base Isolated Buildings Analyzed

Building Description	Benefit (%)*		Cost ($)*		Benefit-Cost (%)*
William Clayton Building four-story reinforced concrete frame	Reduction in structural and nonstructural costs	3.3	Isolation bearings	2.2	
	Reduction in future earthquake damage	2.8	Base isolation system excluding bearings	1.8	
		6.1		4.0	2.1
Six-story steel frame medical building	Reduction in structural and nonstructural costs	2.6	Isolation bearings	1.1	
	Reduction in future earthquake damage	1.8	Base isolation system excluding bearings	1.6	
		4.4		2.7	1.7

*Percent of total cost of building excluding contents.

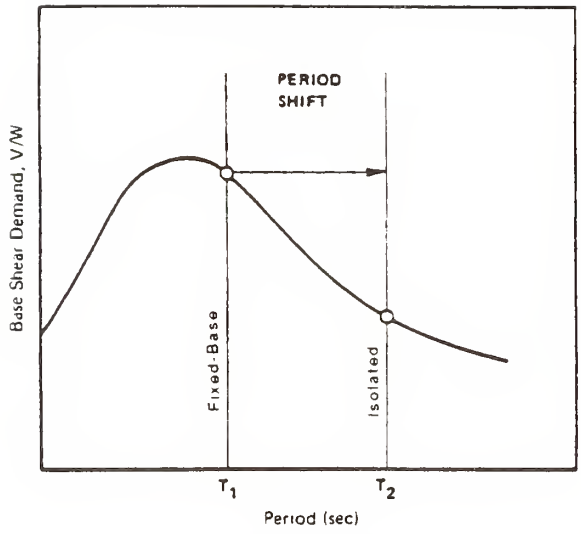

Figure 1. Idealized base shear demand versus period curve.

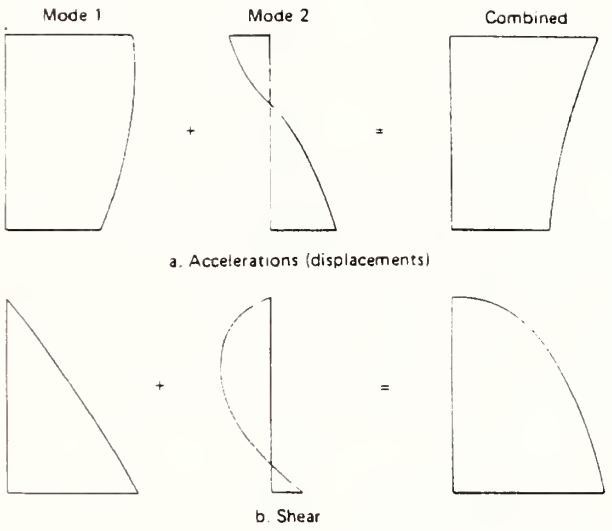

Figure 2. Modal and combined response of a base isolated shear beam type building.

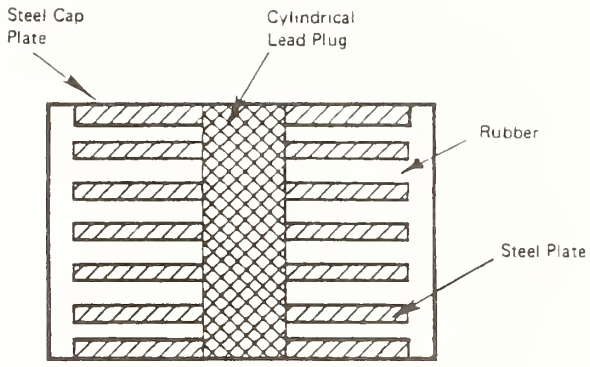

Figure 3. Idealized cross section of laminated rubber and steel/lead plug isolation bearing.

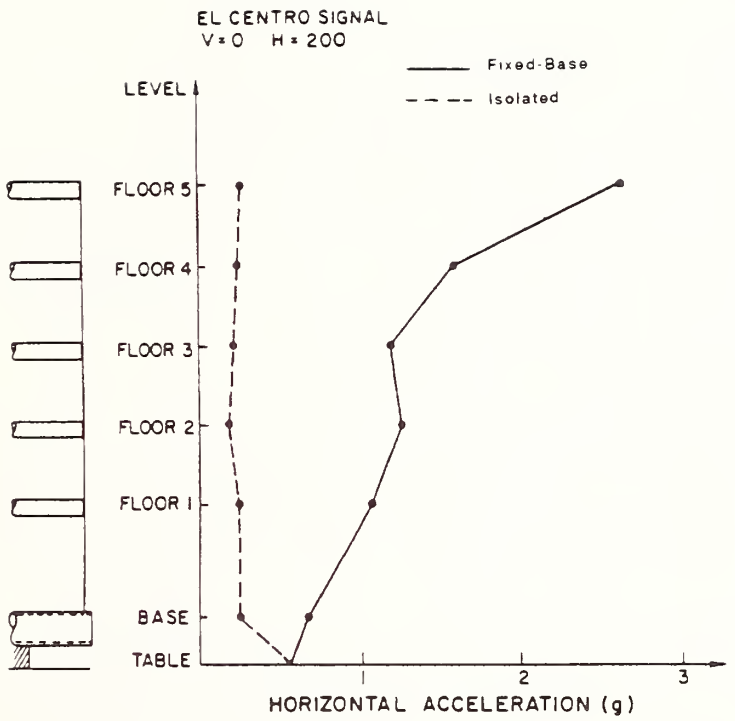

Figure 4. Floor accelerations for five-story, one-third scale model steel frame building loaded by 1940 El Centro earthquake time history with a scaled peak acceleration of 0.55g (after Ref 16).

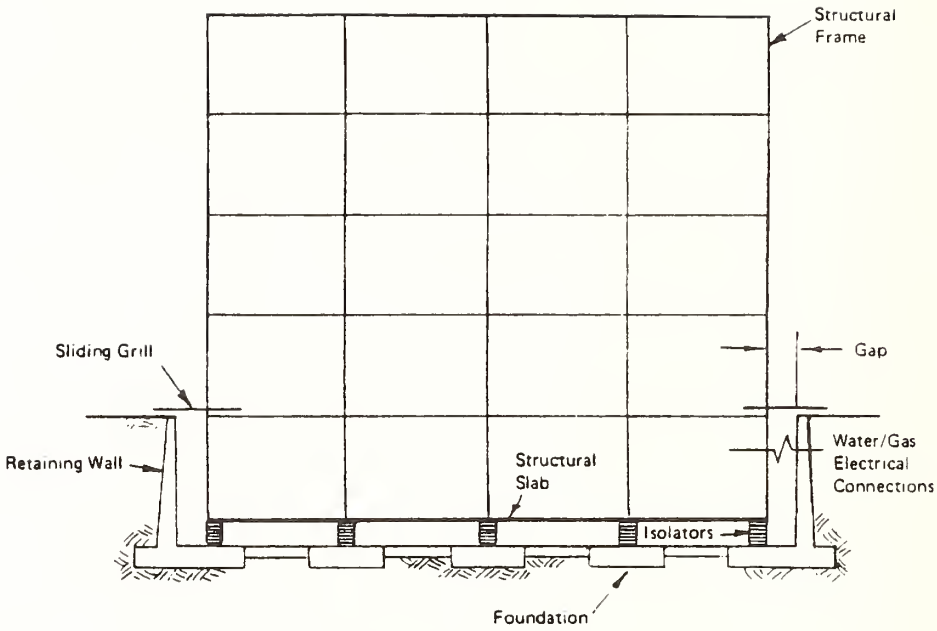

Figure 5. Typical layout for base isolated building.

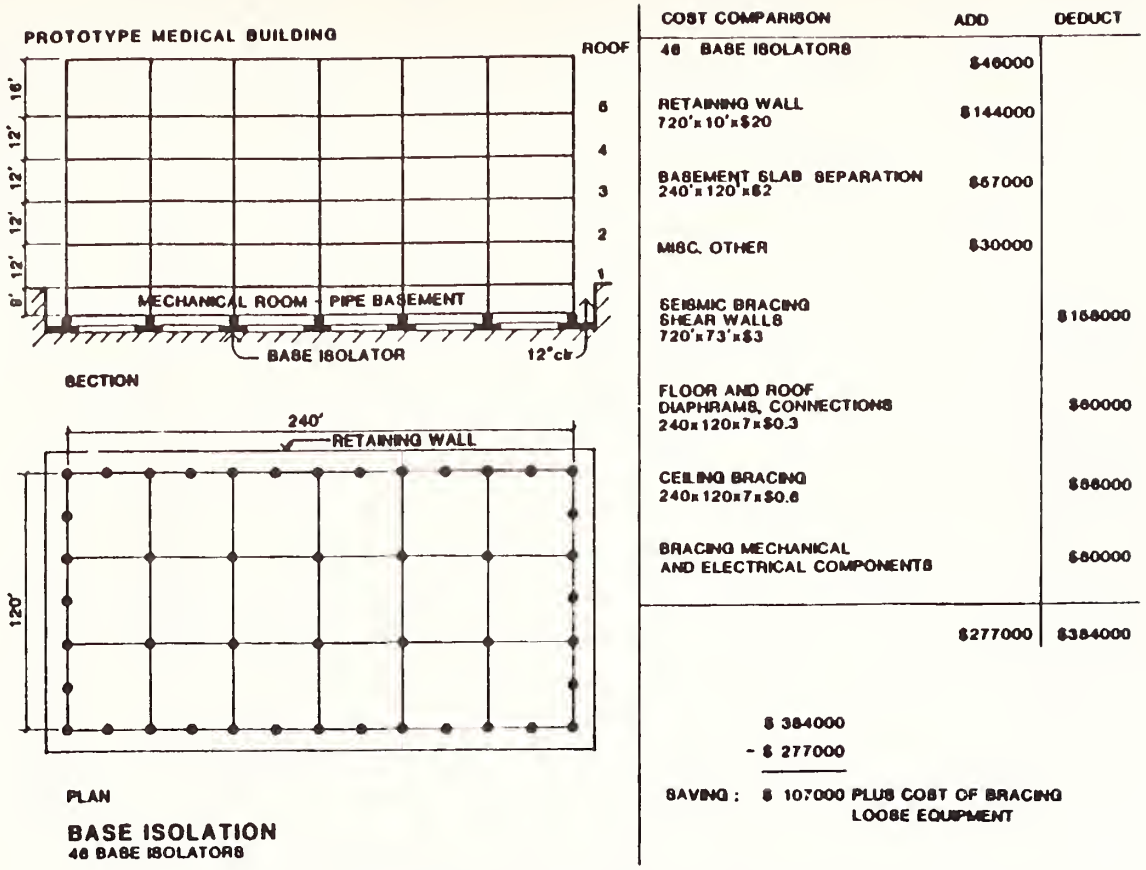

Figure 6. Cost comparison of medical building with conventional construction and when isolated (from Ref 16).

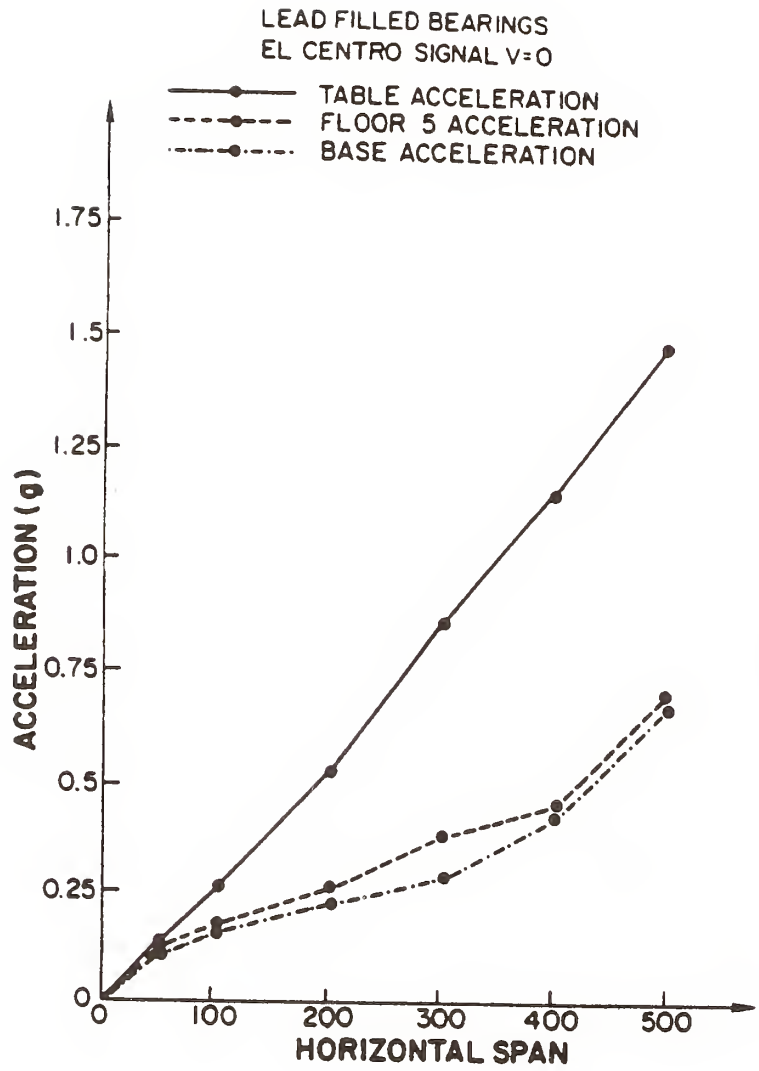

Figure 7. Nonlinear response with lead-filled bearings under increasing earthquake intensity (from Ref 16).

Damages Caused by Storm Surges in Maldives

by

Takaaki UDA*

SUMMARY

Maldives islands in Indian Ocean were inundated during April 10 and 14 in 1987 due to the storm surges. It is found by the analysis of the damage that land reclamation induces coastal disasters in storm surges. It is suggested that the coastal development should be planned under the deep consideration of the relation between land use and storm surges.

KEY WORDS : Maldives, Coral reef, Storm surges, Damages, Land reclamation.

1. INTRODUCTION

During April 10 through 14 in 1987 storm surges attacked the Maldives islands located in the Indian Ocean, and some islands including the capital island (Male island) were inundated. These islands are located in the tropical region, and consist of around 1200 islands. Usually wide coral reef develops around the islands and high incident waves break on the edge of the wide reef. For this reason it is considered that the coastal disasters related to storm waves are less frequent. Nevertheless large damages were caused by the storm waves in Maldives. One of the reasons of occurrence of this disaster is due to the unreasonable land reclamation along the shore on the coral island. It is pointed out that the sufficient assessment is required before the various coastal works.

2. COASTAL DISASTERS IN MALDIVES

2.1 Location of Maldives islands

Maldives islands consist of about 1200 small islands scattered between 0° 45'S and 7° N in about 73° E in the Indian Ocean as shown in Fig.1(a). The length of chain islands is 820km long in the north and south directions and 130km in the east and west directions. The shortest distance to India is 480km, and the distance between Male island and Colombo in Sri Lanka is 640km. Main part of Maldives with many population is shown in Fig.1(b). A group of atolls has a circular shape as a whole. North Male Atoll where Maldives capital is located is shown in Fig.1(c) in much larger scale. Male island is a small island located on the south end of North Male Atoll and Hulule island with international airport is next to this island. North Male Atoll itself consists of many small atolls. The number of islands appropriate for the habitation is around 200.

2.2 Land reclamation plan in Male island

Total area of Maldives is 298km^2, and the population is 181,453 as of March in 1985. The capital is located on Male island, and many people (46,334 as of March in 1985) live in a small island. Originally the area of this island before the land reclamation was as small as 108 ha, but in resent years land reclamation has been rapidly carried out.

Before 1979 land reclamation of 14.9 ha was carried out(Fig.2). Thick solid line in the figure shows the original shoreline, and dotted line is the revetment line existed in 1979. Since then population has continued to increase, and lack of the land proceeded. To this reason large scale land reclamation was started. Land reclamation was mainly conducted at the southern part of the island, and reclaimed area extended up to the vicinity of the reef edge (Fig.3). Reclaimed area attained 51.8 ha until November in 1985. This accounts for 87% of all the planned land reclamation area (59.7 ha). The sediment amount necessary for the planned land reclamation was about 85 10^4m^3, and almost all of sediment was the dredged sand in the port located in the northern part of Male island.

2.3 Damages due to storm surges

Storm surges began at 9 o'clock on April 10.

* Head, Coastal Eng. Div., Public Works Res. Inst. Ministry of Construction.

On April 12 sea water began to retreat, but the sea level was still high enough. Finally extraordinary high tide continued until the morning of April 14.

Meteorological observation at Hulule island where the international airport is located showed no strong wind during the disasters between April 9 through 13. The Meteorological Agency in Sri Lanka reported that overall tide condition did not change near Sri Lanka, and therefore storm surges in Maldives would be local phenomenon.

Inundated area in the southern part of Male island is shown in Fig. 4. The inundated area extends all around the island, while centering the southern part of the island. Total inundated area attains 48% of all the area of this island. Since this island is a coral island, the mean elevation is as low as about 1.5m above the mean sea level. Therefore wide area was inundated. It should be noted that the inland boundary of the inundated area agrees well with the original shoreline (Fig. 2) before the land reclamation. It clearly points out the weakness of the reclamation area against storm surges. By this storm surges about 20% of sand ($3.62\ 10^5 m^3$) used in the reclamation was carried away. The damage loss was about 1.3 million dollars. Since all islands in Maldives are composed of coral islands, it is very difficult to get sand for land reclamation, and therefore the loss of sand became a large social problem. Of all the five investigated islands, Emboodo and Finolu islands are in South Male Atoll, and Haru and Little Haru islands are located on the outer ridge of North Male Atoll. By the comparison of damages on each island, damages on two islands located in the North Male Atoll are smaller than those on the other islands. On the other hand, large damages were observed at the chain of islands extending northeastward from Male island and forming the outer boundary of the atoll as shown in Fig. 1(c). Furthermore, large damages concentrated on the southern and southeastern parts of the each island. Taking these conditions into consideration, it is concluded that the storm waves attacked the islands from southeast.

The causes of this storm surges are considered to be as follows. First, tidal range is 75cm in spring tide and 25cm in neap tide at Colombo in Sri Lanka due to the tidal record measured between 1956 and 1962, and usually spring tide appears in a period of March and April. Since the storm surge began from April 10, the tide in Maldives was at spring tide condition. Secondly, incident wave height was at least larger than 2m, judging the wave condition from the photographs or video record by inspection. Then it is considered that the mean sea level on coral reef rose by wave set-up and it accelerated the wave intrusion into the land. Although coral reef itself had a wave dissipation effect, coastal damages were accelerated because of the land reclamation up to the vicinity of the edge of coral reef.

3. CONCLUDING REMARKS

This paper describes the coastal disasters due to storm surges in Maldives. It was found through the analysis of the disasters that the artificial action (excess land reclamation) strongly relates to the natural disaster. Regarding the development of coastal zone, it is required to have sufficient reserve against storm surges. From this point it is concluded that not only the recovery of the damages but also the consideration of fundamental problems regarding coastal zone management is important for the prevention of the future coastal disasters.

REFERENCE

Uda, T. (1988) : Field investigation on damages caused by storm surge in Maldives, 35th Japanese Conf. on Coastal Eng., pp. 212-216 . (in Japanese)

(a) Location of Maldives

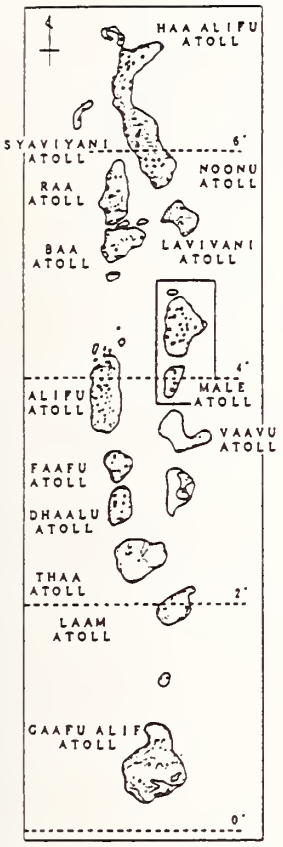

(b) Maldives Atolls

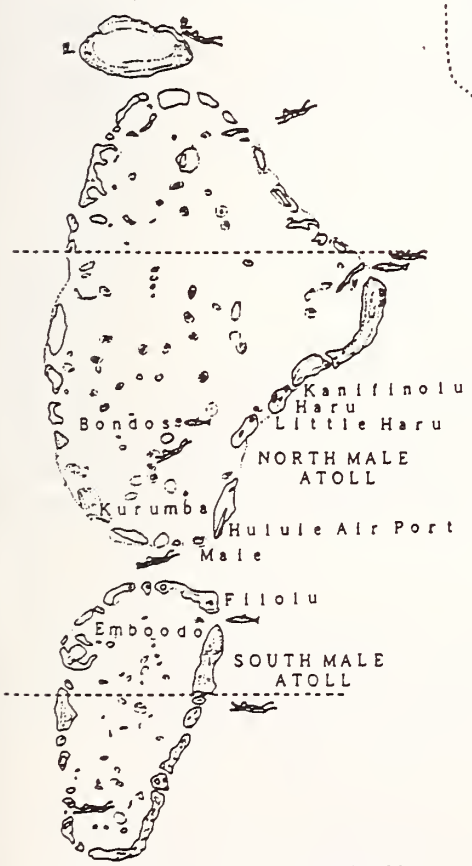

(c) North and South Male Atoll

Fig. 1 Maldives islands.

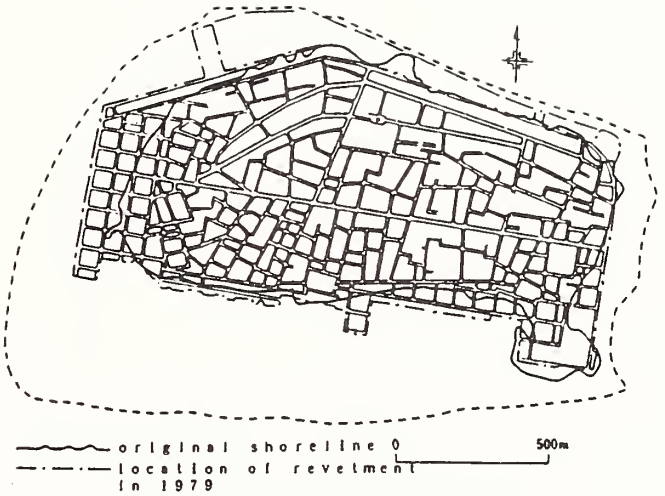

Fig. 2 Shoreline of Male island before land reclamation.

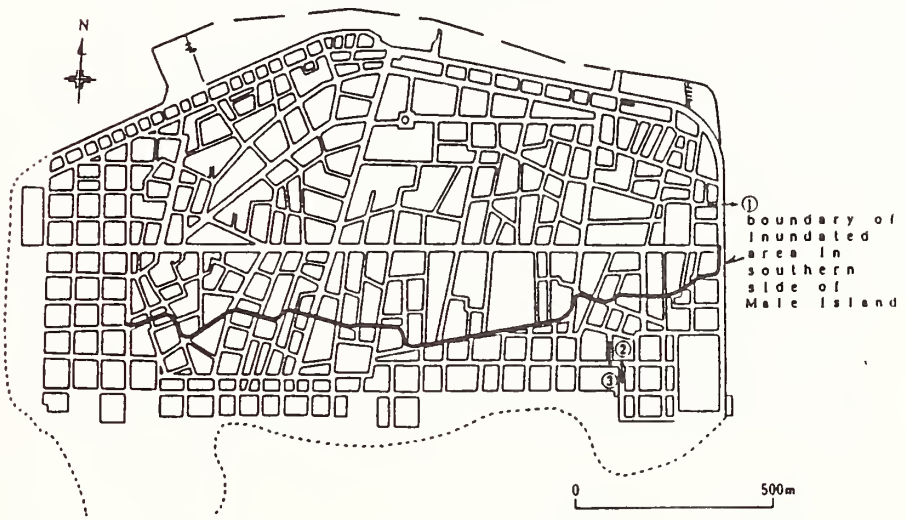

Fig. 3 Reclamation on Male island after 1979.

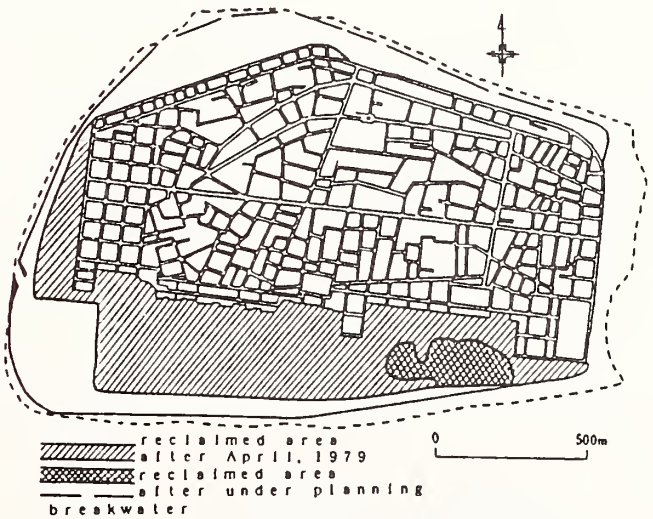

Fig. 4 Inundated area on southern side of Male island.

Performance of Structures in Hurricane Hugo

by

Richard D. Marshall*

ABSTRACT

Surface wind speeds and damage to structures during the passage of Hurricane Hugo through the Virgin Islands and Puerto Rico are described. Because of the scarcity of actual wind speed records and observations, it was necessary to resort to other indicators of surface wind speed such as reconnaissance aircraft data and intensity of damage. Maximum wind speeds on St. Croix corresponded to a mean recurrence interval of approximately 300 years, making Hugo one of the more intense hurricanes of the century. On St. Thomas and over northeastern Puerto Rico the wind speeds were equal to or less than the 50-year wind speed for this region of the Caribbean. Damage in the affected areas was extensive, in particular those areas exposed to the northeastern quadrant of the storm. The structural behavior of certain highrise and single-story buildings under overall wind loading was good. However, more attention needs to be given to the attachment of nonstructural elements such as doors, windows and cladding.

KEYWORDS: Buildings; building codes; damage; hurricane; tropical cyclone; wind; wind speed.

1. INTRODUCTION

Hurricane Hugo passed through the U.S. Virgin Islands and over northeastern Puerto Rico on September 18, 1989. The probable storm track is plotted in Figure 1 and the circles along the track represent a typical eye diameter of about 35 km. Other important meteorological characteristics of Hugo are presented at this meeting in a companion paper by Golden (1990). As usually happens following extreme events such as Hugo, there were numerous reports of extraordinarily high wind speeds in the affected areas. Problems encountered in tracking some of the more spectacular claims to their source and the methods used to establish probable maximum surface wind speeds from other than standard measurements have been described by Marshall (1990).

To assess the performance of buildings and other structures, it is important that representative surface wind speeds be ascertained. In the case of Hurricane Hugo, only two verifiable wind speed records were obtained on September 18, one at the Roosevelt Roads Naval Station directly southeast of Ceiba, Puerto Rico, and the other at San Juan International Airport. Other indirect sources of wind information used to estimate surface wind speeds were flight data from hurricane reconnaissance aircraft, observations of type and intensity of damage, the response of selected structures to wind effects, and eyewitness accounts of the storm.

This paper presents a summary of the estimated and measured surface wind speeds as well as the speeds corresponding to wind load design requirements contained in the relevant regional building codes and standards. These speeds provide the basis for assessments of structural performance described in the remainder of the paper.

2. SURFACE WIND SPEEDS

Surface wind speeds in Hurricane Hugo are summarized in Table 1. Note that these speeds represent SI conversions from the original units of knots, possibly giving the impression of a better resolution than is actually the case. These speeds have been adjusted for standard conditions of a 10-meter height in flat, open terrain (airport exposure) using techniques previously applied to wind records obtained in Hurricane Alicia on the Texas Gulf Coast (Marshall, 1984). It has been assumed here that the ratio of peak gust speed to

* National Institute of Standards & Technology
Gaithersburg, Maryland 20899

sustained speed is approximately 1.25. This ratio is consistent with wind speed records obtained in Hurricane Hugo and in other Atlantic and Gulf Coast hurricanes. For those areas where the local terrain promotes channeling or shielding, the actual speeds may differ significantly from those listed in Table 1. The code-specified design speeds for the areas affected by Hugo are listed in Table 2, along with the applicable code or standard and year of adoption. For ease of comparison, the specified design speeds have been converted to equivalent sustained speeds, i.e., wind speeds averaged over 1 minute.

Wind speed statistics for the Caribbean have been updated and refined by Davenport et al. (1985) and this source of information has been used to characterize the severity of Hugo's wind speeds in terms of their mean recurrence intervals as listed in Table 1. For St. Croix the probable maximum sustained speed of 57 m/s corresponds to a mean recurrence interval of about 300 years. For the island of Culebra this interval is approximately 200 years for the estimated speed of 54 m/s. On Vieques the probable maximum sustained speed of 49 m/s corresponds to an 85 year mean recurrence interval. For St. Thomas and northeastern Puerto Rico, the maximum sustained speeds were equal to or less than the 50 year speed of 45 m/s.

3. WIND DAMAGE

Observed damage in the affected areas is in general agreement with the surface wind speeds listed in Table 1. This damage ranged from superficial to total devastation. In general, the most damaging winds were located in the northeast quadrant of the storm. In the following paragraphs, the damage is described in sequential order, following the general path taken by Hugo.

3.1 St. Croix

The strongest winds came from the northeast and caused the heaviest damage along the north coast from the Salt River eastward to the end of the island. Damage in this area was intensified by the local terrain which slopes steeply upward to a central east-west ridge running the length of the island. This same ridge provided some shielding for structures located on its south slope.

In the southwest sector of the islands near Frederiksted the most damaging winds came from the southwest following passage of the eye. The airport and oil refinery are located in the south central portion of the island where the strongest winds were out of the northeast. However, the winds in this area were not as strong as those affecting the north coast near Christiansted where local terrain conditions increased the surface wind speeds.

Figure 2 shows typical damage to a condominium located on the north coast, approximately 6 km east of Christiansted. The building system consists of concrete floor slabs and concrete masonry walls with cast-in-place corner columns and perimeter beams. Balcony decks and roofs are of wood construction. The strongest winds from the northeast were approximately normal to the long axis of the building.

Figure 3 shows a series of newly constructed apartment buildings directly to the west of Christiansted. Although the hip roofs and their cladding suffered some damage along the edges and ridges, the main problem appears to be inadequate roof-to-wall connections. In fact, this mode of failure was common throughout St. Croix.

Figure 4 shows a failed metal building directly southwest of Christiansted and approximately one forth of the way up the north slope of the main east-west ridge. Again, the terrain undoubtedly caused an increase in wind speed and the strongest winds were approximately face-on to the failed wall. It appears that the roof sheets and purlins were carried away as a unit, leaving the end frame unsupported and allowing the windward wall to collapse inward.

Figure 5 shows damage to petroleum storage tanks at the oil refinery on the south coast of St. Croix, approximately 3 km east of the airport. Some reports put the wind speeds in excess of 95 m/s at this location, the highest of any surface speeds claimed for Hugo. However, a followup investigation concluded that no wind speed measurements were obtained here or at any other location on St. Croix.

Directly northwest of the airport is a public housing development with units of 2 or 3 stories in height. Panelized concrete construction is used throughout and the endwalls are fabricated of louvered metal panels mounted in a perimeter channel. This channel was attached to the concrete panels by means of explosive-driven studs. As can be seen in Figure 6, the concrete panels suffered no visible damage, but much of the louvered endwall was removed by the wind. Many of the housing units in this development appear to have been unoccupied at the time of Hurricane Hugo.

3.2 St. Thomas

Damage on St. Thomas was not as widespread as on St. Croix. However, the terrain is substantially rougher than on St. Croix and much of the structural damage appeared to be the result of accelerating flows due to hills and ridges. San Juan radar showed strong convection bands over the island and the possibility of locally intense winds due to microbursts (vertical momentum transport) cannot be ruled out. The radar images indicated that the strongest winds ranged from northeast to southeast. Intensity of damage was similar to that observed in northeastern Puerto Rico.

3.3 Culebra

In Puerto Rico, the island of Culebra experienced the most severe damage, being only slightly less intense than the damage observed on St. Croix. Figure 7 shows a housing area adjacent to the local airport which was totally destroyed. The quality of construction was poor and it is doubtful that there was any attempt to comply with the territorial building code. In addition, the terrain slopes steeply upward to the west and this very likely caused an acceleration of the intense easterly winds from Hugo. Directly to the south is the Ensenada Honda where many small watercraft were either sunk or were driven ashore by the strong easterly winds.

3.4 Vieques

This island is to the south and west of the storm track and, therefore, likely experienced less severe winds than did Culebra. Figure 8 shows a housing area where the individual units were cleanly removed from their concrete post-and-beam supporting systems. It was not possible to conduct a ground survey on Vieques, but it appears that the floor-to-frame connection details in this case need to be improved.

3.5 Puerto Rico

On Puerto Rico the sustained speeds ranged from 35 m/s at San Juan to 44 m/s at Roosevelt Roads. Neither station experienced a clear lull due to eye passage as did Cape San Juan at the extreme northeast tip of the island, although Roosevelt Roads came close.

Figure 9 shows two reinforced concrete buildings located on the east coast of Puerto Rico between Cape San Juan and Fajardo. The building on the right was oriented so that the strongest winds from the north were blowing directly onto its broad face. Subsequent inspection showed that many floors near the top of this building had suffered failure of the windward curtain walls and, subsequently, the interior partition walls and leeward curtain walls were completely blown out. Figure 10 shows an endwall of the building oriented so that the strongest winds came from left to right. Note the local damage to the perimeter beams under the floor slabs caused by transverse displacement of the building. The adjacent shearwalls showed no signs of distress. By reference to ANSI A58.1 (1982), the Puerto Rico Building Code has, until recently, specified a reference wind speed of 41 m/s. In 1988 the code was revised and the reference wind speed was increased to 50 m/s. However, seismic rather than wind requirements of the building code governed the structural design of the buildings shown in Figure 9.

The house shown in Figure 11 is typical of a class of structure in Puerto Rico that performed extremely well in Hugo. The walls are either cast-in-place concrete or are constructed of concrete masonry units with integral reinforced concrete columns and perimeter beams. The roof slab is 100 to 125 mm thick. As with the highrise concrete buildings just described, the seismic requirements of the building code governed the

design and the substantial dead loads make this type of structure highly resistant to wind forces. Observed damage was limited to inadequate attachment of doors and louvered window panels to the concrete walls and perimeter beams.

A type of failure commonly encountered in northeastern Puerto Rico is shown in Figure 12. The corrugated steel sheet is attached to the purlins by self-drilling/tapping screws. The high-strength sheet is susceptible to low cycle fatigue at the attachment points and develops fatigue cracks after only a few minutes of wind action. This problem has been investigated and reported by Morgan and Beck (1975). Use of a large washer, shaped to conform to the ridge contour of the corrugated steel sheet has been shown to be a simple, cost-effective solution to the problem.

4. CONCLUSIONS

For all of the regions affected by Hurricane Hugo on September 18, only two verifiable wind speed records were obtained. Because of the lack of data, it was necessary to rely on other sources of information and employ indirect methods to obtain estimates of surface wind speeds. Maximum speeds on St. Croix correspond to a mean recurrence interval of approximately 300 years. Estimated speeds on the islands of Culebra and Vieques are consistent with mean recurrence intervals of 200 and 85 years, respectively. Speeds on St. Thomas and over northeastern Puerto Rico were either equal to or less than the 50 year wind. Widespread loss of roof structures was observed on St. Croix which suggests that code requirements for wind uplift should be reviewed. In Puerto Rico, both highrise and single-story concrete buildings that were designed to meet seismic requirements performed well in Hugo. The attachment of nonstructural elements such as doors, windows and cladding needs to be improved. Loss of corrugated steel sheet roofing continues to be a widespread problem, even though cost-effective solutions have been available for several years.

5. ACKNOWLEDGMENTS

Photographs of damage were provided by Dr. Joseph H. Golden and Mr. John L. Vogel of the National Weather Service. Dr. Mark D. Powell, Atlantic Oceanographic and Meteorological Laboratory, made available his analyses of flight data in the Caribbean. The author collected information for this paper while a member of a post-disaster team organized by the Committee on Natural Disasters, National Research Council.

6. REFERENCES

1. ANSI A58.1 (1982). "Minimum Design Loads for Buildings and Other Structures," American National Standards Institute, New York, NY.

2. Caribbean Uniform Building Code (1989). "Part 2 - Structural Design Requirements." Caribbean Community Secretariat, Georgetown, Guyana.

3. Davenport, A.G., et al. (1985). "A Hurricane Wind Risk Study for the Eastern Caribbean, Jamaica and Belize With Special Consideration to the Influence of Topography." Report for the Pan-Caribbean Disaster Prevention Preparedness Project.

4. Golden, J.H. (1990). "Meteorological Data From Hurricane Hugo." Paper presented at 22nd Joint Meeting, UJNR, Panel on Wind and Seismic Effects, Gaithersburg, MD.

5. Marshall, R.D. (1990). "Hurricane Hugo in the Caribbean - Assessment of Surface Wind Speeds." Conference: Six Months After Hugo - Preliminary Findings, University of Puerto Rico, Mayaguez, PR.

6. Marshall, R.D. (1984). "Fastest-Mile Wind Speeds in Hurricane Alicia." NBS Technical Note, No. 1197, NBS, Gaithersburg, MD.

7. Morgan, J.W., and Beck, V.R. (1975). "Sheet Metal Roof Failures by Repeated Loading." Tech. Report No. 2, Housing Research Branch, Australian Department of Housing and Construction.

8. Puerto Rico Building Code (1968). Regulations and Permits Administration, San Juan, PR.

9. Virgin Islands Building Code (1972). Department of Planning and Natural Resources, St. Thomas, VI.

Table 1. Probable Maximum Wind Speeds in Hugo

LOCATION	SUSTAINED SPEED (m/s)	GUST SPEED (m/s)	MRI (yrs)
St. Croix, VI	57	70	300
St. Thomas	44	54	50
Vieques, PR	49	59	85
Culebra	54	67	200
Roosevelt Roads	44	54*	50
San Juan	35*	41*	<50

* Denotes actual measurement at Ht. = 7 m.

Table 2. Specified Design Wind Speeds

LOCATION	DESIGN SPEED Sustained (m/s)	CODE/STAND (year)
U.S. Virgin Islands	40	VI Bldg. Code (1972)
Puerto Rico	41	ANSI A58.1 (1982)
Puerto Rico	50	PR Bldg. Code (1988)
VI/PR (50-yr)	45	CUBC* (1989)
" (100-yr)	50	"

* Caribbean Uniform Building Code

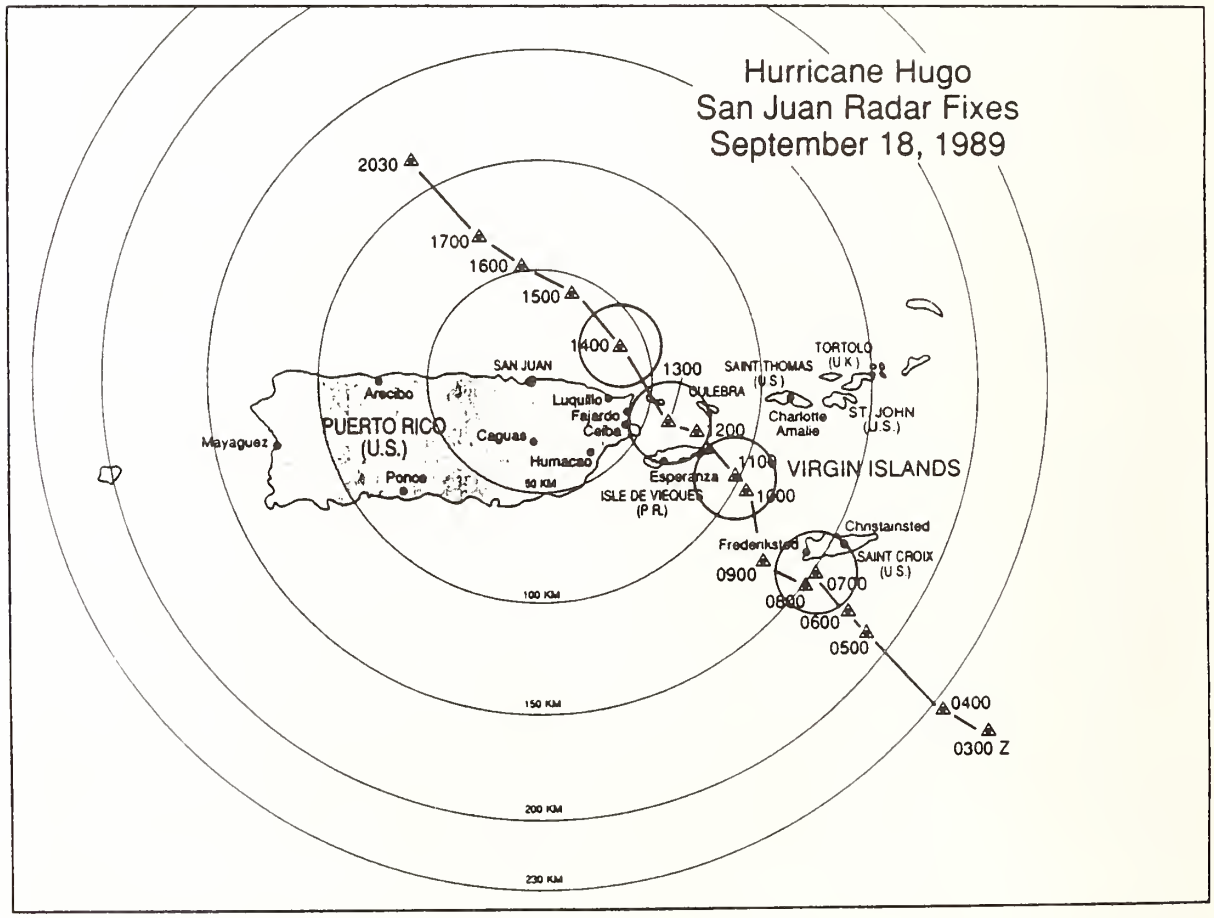

Figure 1. Hurricane Hugo Storm Track, September 18, 1990

Figure 2. Condominium on north coast of St. Croix

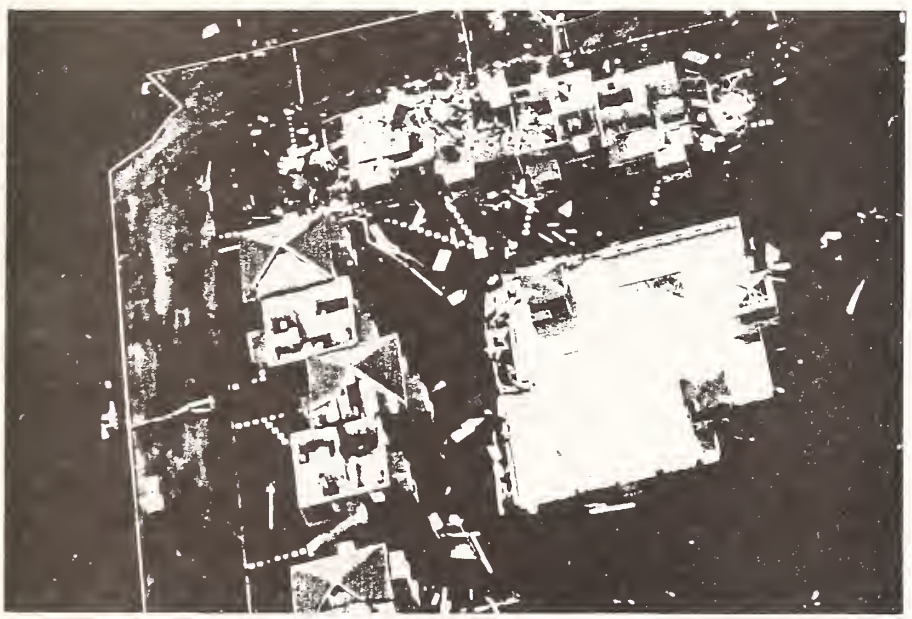

Figure 3. Apartment buildings on north coast of St. Croix

Figure 4. Metal building, Christiansted, St. Croix

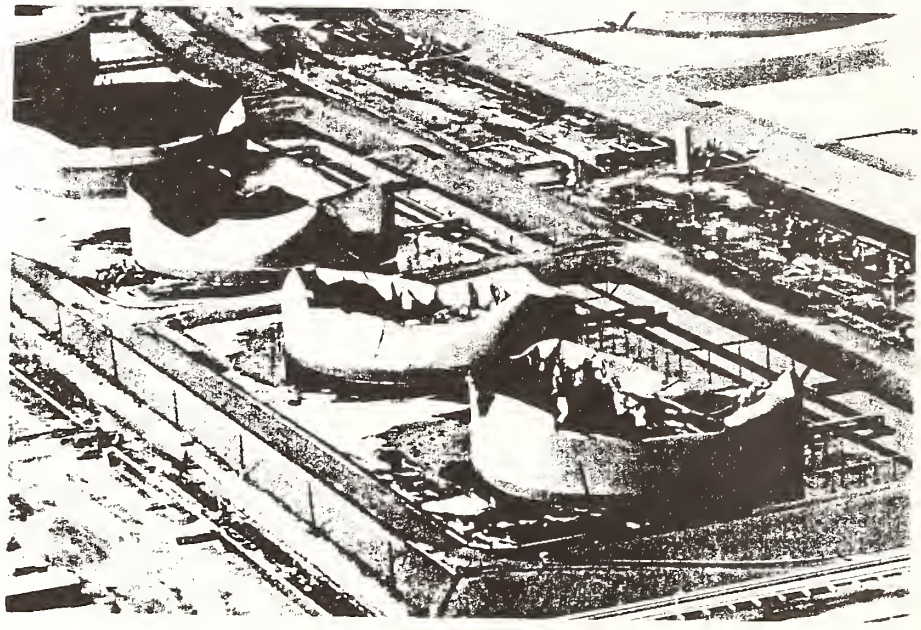

Figure 5. Petroleum storage tanks, St. Croix

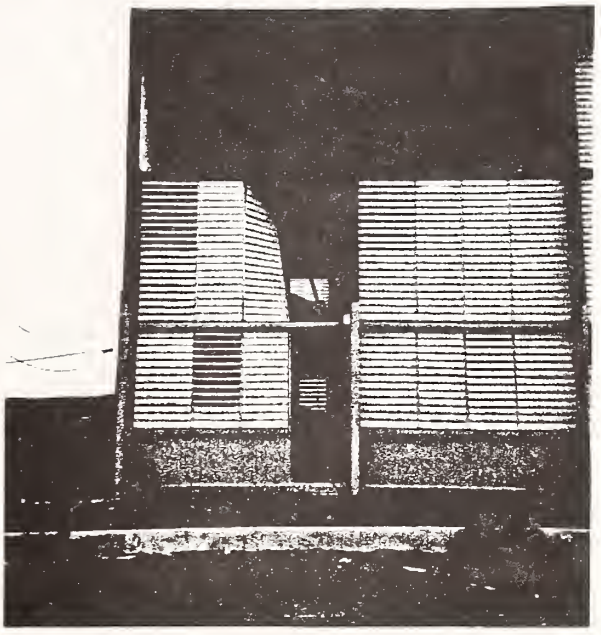

Figure 6. Concrete panel construction, St. Croix

Figure 7. Housing damage near Culebra airport

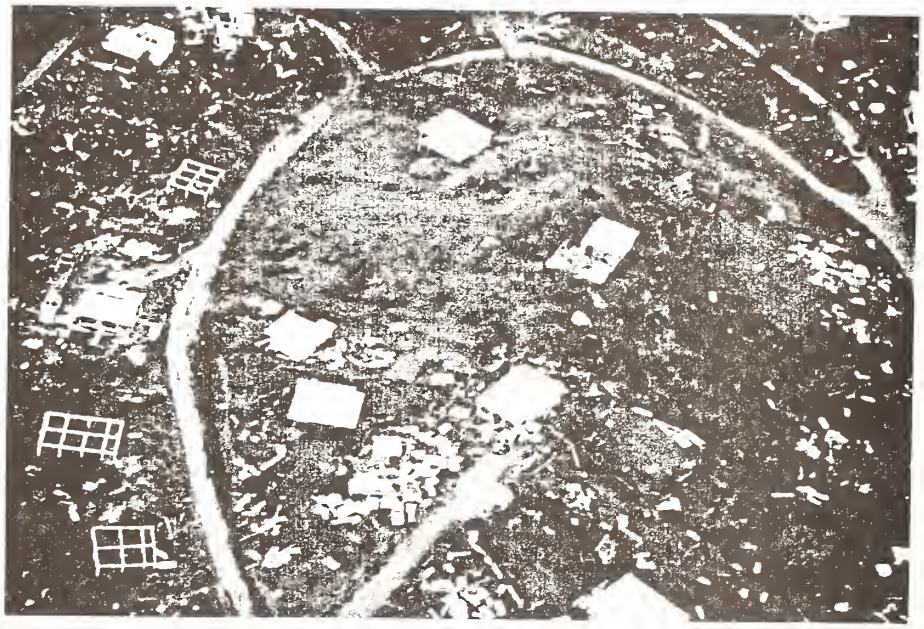

Figure 8. Housing damage on Vieques

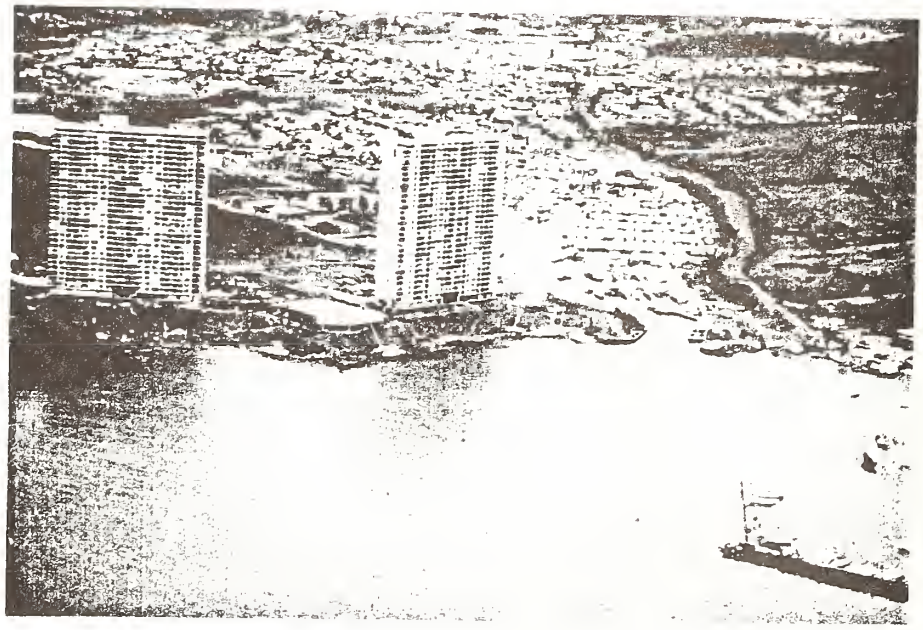

Figure 9. Concrete highrise buildings, Fajardo, Puerto Rico

Figure 10. Damaged edge beams, concrete highrise buildings Fajardo, Puerto Rico

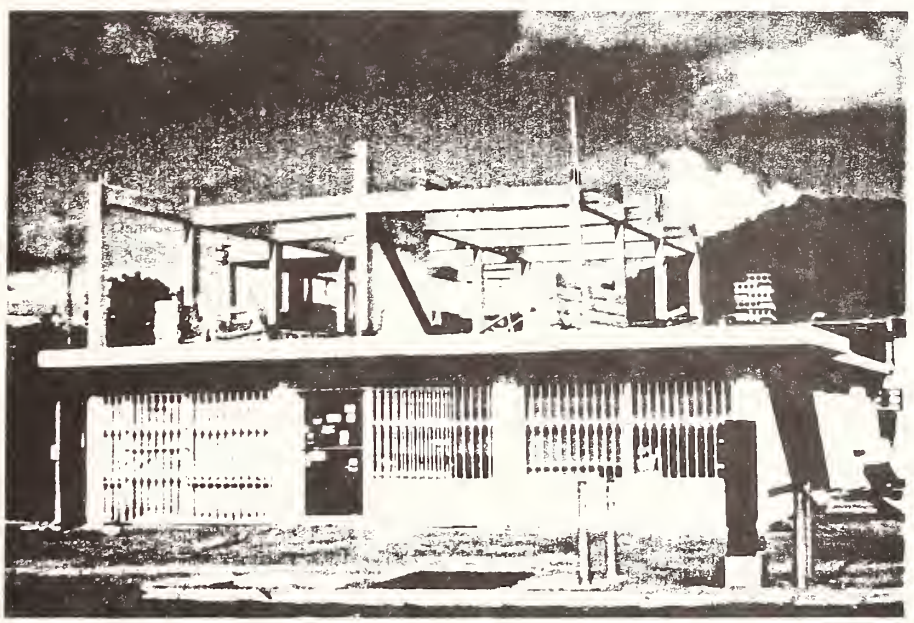

Figure 11. Concrete housing unit, Puerto Rico

Figure 12. Failed corrugated steel sheet roofing, Puerto Rico

The Performance of Structures in Hurricane Hugo 1989—The Carolinas

by

Peter R. Sparks[1]

ABSTRACT

A review is made of the performance of structures under the action of wind in Hurricane Hugo which crossed the Carolinas on September 21-22, 1989. It is shown that in most locations wind speeds in the storm were less than the design levels specified by local building codes; but failure to incorporate modern wind loading principles and to establish appropriate means of enforcing the codes left South Carolina, in particular, ill-prepared for a storm of the strength of Hugo. Extensive damage in such a storm was inevitable and had been predicted.

Most damage was in the form of roof and wall cladding failures which then led to extensive rain damage to the interior of the structure. Wood-frame construction performed well except in exposed locations in the highest wind areas where loss of roofs, shear failures and foundation failures were common. Unreinforced masonry buildings performed very poorly, even in sheltered locations. Older metal buildings experienced considerable damage but newer ones built to increased wind-load requirements performed better. The frames of steel and concrete multi-story buildings performed well but many suffered cladding damage even at relatively low wind speeds.

Recommendations are made to improve future construction with regard to wind resistance, including the establishment of a National Wind Hazards Reduction Program by the United States Government.

KEYWORDS: Wind; damage; structures; hurricanes; building codes; wind speeds.

INTRODUCTION

Hugo was a fast moving hurricane which made landfall on the mainland of the United States shortly after midnight on September 22, 1989. The center of the eye of the storm crossed the coast at Sullivans Island, South Carolina, and then moved across the state in a north-westerly direction. The storm weakened very slowly. It was still inflicting considerable damage when it entered North Carolina near the city of Charlotte at 6:00 a.m. and eventually caused tree damage as far north as the Appalachian Mountains of Virginia (Figure 1). Hugo had the dubious distinction of being the most expensive storm in U.S. history. Insured losses due to wind damage are estimated to be nearly $4 billion. To this must be added insured flood losses of $500 million and uninsured losses, including more than $1 billion in timber damage and over $300 million in damage to military establishments.

In most locations the wind speeds in Hugo were below the design levels specified in the locally adopted building codes. This paper examines the performance of structures under the action of wind in the hurricane and, where appropriate, seeks to explain their poor performance.

2. THE BUILDING CONTROL PROCESS

The United States does not have a national building code. Responsibility for building control lies with individual states and the quality and type of control varies considerably.

In South Carolina the state exercises very little control. Since 1972 local jurisdictions have been permitted, but not required, to adopt the Standard Building Code. Once adopted there is no requirement to update the code nor any state guidance on its enforcement. Any alterations to the code however have to be approved by the state. Some rural areas affected by Hugo had not adopted a building code.

The Standard Building Code (SBCCI 1974, 1982, 1988) is one of of three "model" building codes used in the United States. It is promulgated by the Southern Building Code Congress, a democratic, non-government body comprised mainly of building officials but few engineers.

Although an American National Standard, (ANSI, 1972,1982) prepared by experts, exists for wind loading, the Standard Building Code has chosen only to use it after extensive modification (Manning, 1985). This has led to a number of very serious shortcomings in the code, primarily the non-inclusion of gust effects, internal pressure, high suctions on the edges of roofs and near the corners of

[1] Department of Civil Engineering, Clemson University, Clemson, SC 29634-0911

buildings and increased wind velocities in areas adjacent to large bodies of water.

Some improvements have taken place in the specification of wind loads in recent years (SBCCI, 1988) but few buildings subjected to Hugo benefitted from these. Indeed many buildings continue to be constructed without reference to wind loads. Despite a long history of poor performance in severe storms, the code still permits certain forms of construction in wood and masonry which are inconsistent with its loading requirements. Such prescriptive requirements are particularly popular with architects who also often select wall cladding and roof systems without appropriate regard for wind loads.

A study of building practices in South Carolina conducted in the mid-1980s (Sparks, 1988) warned that a hurricane, even below the nominal design level, could create a multi-billion dollar loss in the state. Hurricane Hugo turned out to be that storm.

North Carolina has a tighter form of building control. There is a state building code (NCBCC, 1982), building inspectors and officials must be certified and all plans for major buildings are checked at the state level. However, in common with the Standard Building Code, the North Carolina State Building Code underestimates cladding loads near the edges of roofs and corners of buildings.

3. COMPARISON OF WIND CONDITIONS IN HUGO WITH DESIGN CONDITIONS

Building codes and standards in the United States use the fastest-mile wind-speed, measured at 33 ft. in open country, as their reference. These speeds are based on the time taken for a "mile" of wind to pass an observation point as recorded on a now obsolete instrument. In a hurricane such an instrument would average the wind speed over periods ranging from about 40 seconds to 1 minute.

None of the anemometers which recorded wind speeds in Hurricane Hugo measured a fastest-mile and only one made measurements close to 33 ft. The fastest-mile wind speeds reported in Table 1 are based on standard corrections for averaging time, height of anemometer and approach terrain, (Simiu and Scanlan, 1986, Cook, 1985) These corrections can introduce significant errors. Where several anemometers existed in one city, as in Charleston, greater weighting was given to airport locations with continuous anemometer traces. Measurements were made at or near each of the locations listed except as indicated in the table. The speeds given at locations where no measurements were made are based on correlations with aircraft measurements and comparisons with nearby ground stations.

The recurrence intervals listed are based on data assembled from a number of analyses of measured wind speeds and computer simulations carried out in the last 20 years. These values could be subject to considerable error. They should only be used to judge the relative severity of the storm.

The design wind speeds given in Table 1 are taken from the Standard Building Code (1973-1986). They are fastest-mile wind-speeds with a 100 year recurrence interval. However the code used these speeds as gust wind speeds and so, in effect, was using fastest-mile wind speeds approximately 25% lower or a mean recurrence interval of about 25 years. The code also made no allowance for the higher wind speeds experienced by areas adjacent to large bodies of water. With the rough seas of a hurricane these would be about 16% higher than those in open country. The design conditions for onshore winds therefore represented a recurrence interval of less than 15 years. The code also made no allowance for the reduced wind speeds in suburban areas. In those areas the design wind conditions probably did represent a recurrence interval approaching 100 years.

These recurrence intervals tend to represent upper bounds with regard to loads because the pressure coefficients for wall and roof cladding, used by the Standard Building Code to convert wind speeds to wind pressures, were often less than half those used by the American National Standard and many foreign standards.

It is apparent that while Hurricane Hugo was nominally less than the storm for which jurisdictions thought they were preparing through the use of the Standard Building Code, in actual fact the conditions, particularly in exposed areas, considerably exceeded the design level.

North Carolina uses a gust wind speed of 80 mph for all areas affected by Hugo. This was exceeded by about 20% in the Charlotte area and wind conditions equal to the design level may have been experienced as far north as the Virginia border.

4. SURVEY OF WIND DAMAGE

Wind damage to buildings and other structures was observed along the South Carolina coast from Edisto Beach to the North Carolina border and inland to beyond Charlotte. Damage to roof coverings, wall cladding and signs occurred

where the fastest-mile wind speed exceeded 60 mph. Major structural damage, including loss of roof structure, collapse of single story masonry buildings, complete destruction of mobile homes and extensive damage to wood-framed construction and older pre-engineered metal buildings, took place where the fastest-mile wind speed exceeded 85 mph. However, within these areas, damage was dependent on the upwind terrain. Damage occurred first in exposed locations adjacent to the sea and in open terrain inland. In sheltered locations even old wood-frame houses remained completely undamaged where the fastest-mile wind speed exceeded 100 mph.

North and South Carolina are heavily forested states. The trees provided significant protection from the wind and undoubtedly reduced the amount of damage to buildings. However pine trees apparently began to fall as the fastest-mile wind-speed approached 60 mph and many buildings, although protected from the wind by the trees, subsequently suffered damage from them.

In the Bull Bay area, where few trees were left standing, the exposure of buildings would have changed significantly during the course of the storm.

Two other factors greatly reduced the damage. Firstly, the densely populated islands of Folly Beach, Sullivans Island and Isle of Palms experienced the eye of the storm. This meant that the strongest winds would have come from the north-east and south-west i.e. along the shore. Many ocean-front buildings would therefore have received shelter from neighboring buildings. Secondly, the strongest winds in the storm affected the most lightly populated area of the coast, occupied primarily by a wildlife refuge. In this area all settlement is landward of the Intracoastal Waterway in forested areas. Had the storm hit 20 miles to the south, Charleston and the adjacent islands would have experienced onshore winds producing wind loads on ocean-front properties perhaps double those actually experienced. Had the storm hit 50 miles to the north, all of the buildings on the densely populated northern coast would have experienced wind loads more than twice those actually experienced.

4.1 One and Two Family Dwellings

In general these performed extremely well, probably more as a result of shelter than any other factor. Major structural damage, nearly always in exposed locations, resulted from loss of roofs with subsequent collapse of walls, shear failures and foundation failures.

Roof failures were far less common than in recent hurricanes, probably due to the use of steep-pitched roofs and hurricane anchors. However, in the highest wind areas, failures occurred even where hurricane anchors had been used, particularly after window damage (Figure 2) . The improved roof performance enabled the houses to survive long enough to show up other weaknesses.

Failure to provide proper bracing led to some shear failures in two story buildings (Figure 3). The traditional bracing techniques proved to be insufficient, especially in buildings with few interior cross-walls and large openings in exterior walls.

Foundation failures due to wind were much more common in this hurricane than in other recent ones. In most coastal flood-prone areas buildings are elevated on wood or reinforced concrete piles. On the South Carolina coast many buildings are constructed on concrete block piers. The Standard Building Code permits unreinforced masonry piers to have a height to width ratio of 10, if filled with concrete. Piers meeting this requirement failed, as did those that were lightly reinforced (Figure 4). In meeting the needs of flood insurance requirements, the very large forces applied to the piers by the wind acting on the building had apparently been overlooked.

Many one and two-family dwellings lost shingles. These apparently minor wind failures resulted in significant rain damage often magnifying the initial damage by a factor of 10. Repeated on an enormous scale, this contributed significantly to the total cost of the storm.

In a few areas wind and surge damage to single-family dwellings was difficult to differentiate, particularly in older buildings built on grade or newer elevated buildings subjected to surge in excess of the design level, as in the northern part of the Isle of Palms and in Bull Bay. In some instances wind debris was transported by the surge, making the nature of the wind failure difficult to determine.

Based on eye-witness reports and computer simulations, it appears that on Folly Beach, Sullivans Island and Isle of Palms, the strong winds from the north-easterly direction before the eye would have taken place while the islands were dry. The surge rose rapidly during the eye and would have been falling as winds rose from the south-westerly direction. Several types of failure were possible and observed.

1. Due entirely to north-easterly winds.
2. Initiated by north-easterly winds augmented by later surge action.
3. Initiated by surge action, augmented by later south-westerly winds.

In the Bull Bay area strong winds, initially from the north-east, would have veered to the south-east before the surge reached any elevated houses. Most surge action would have taken place as the winds veered to the south and began to diminish. Since the surge was several feet above the elevation level required to obtain flood insurance, some houses adjacent to the Intracoastal Waterway would have been subject to wave action while others farther inland would have been subjected to considerable upthrust. What

condition these houses were in as the result of wind action prior to surge action is difficult to determine.

From Pawleys Island north almost all major structural damage to single-family dwellings was due to surge action.

4.2 Multi-Family Wood-Framed Construction

Several of these professionally designed buildings in exposed locations suffered extensive roof failures, often precipitated by window damage, (Figures 5 and 6). In some of these buildings hurricane anchors had been used to secure the roof. Whether or not these had been selected after a structural analysis is not known, but consideration of internal pressure would not have been required by the building code and the uplift loads could have exceeded the design value after the failure of windward windows.

4.3 Masonry-Walled Buildings

Failure of masonry walls was observed inland as far as Charlotte and complete structural collapse was observed as far inland as Sumter, (Figures 7 and 8). All collapses took place in buildings using unreinforced concrete block or brick walls which would have met the height to thickness requirements of the Standard Building Code. In most cases the roof to wall anchors would also have met the requirements of that document. Failures of this type of structure have occurred in several recent hurricanes (Savage et al., 1984, Mitchell et al. 1986, Sparks et al., 1990). It was interesting to note that in this hurricane most of the failures were not in buildings of recent construction. Discussions with building officials in the Charleston area revealed that they no longer permit unreinforced masonry walls in their jurisdictions.

4.4 Pre-Engineered Metal Buildings

A number of these buildings located in exposed areas were seriously damaged, (Figure 9). These structures are very sensitive to the deficiencies of the older versions of the Standard Building Code. Buildings designed to the new wind-loading provisions appeared to have performed much better.

4.5 Steel and Concrete Framed Buildings

As observed in other hurricanes, the frames of buildings designed by structural engineers to meet the wind-load requirements in the building code performed well. The wall cladding, roof system and roof covering, often selected by architects without reference to the wind-load requirements, performed very poorly.

An exterior wall system employed extensively in the area uses gypsum board attached to metal studs. The gypsum board is covered with insulation and stucco. Based on published data on the ability of such systems to resist wind suction, these systems should not have been used on any building over 30 ft. on the South Carolina coast, even if designed in accordance with the older versions of the Standard Building Code. That code actually underestimated the loads on the corners of buildings by factors of 2 to 3. Nevertheless this system was used on hospitals, the Red Cross Headquarters, educational facilities, condominiums, office buildings and hotels in the Charleston area and almost all high-rise buildings in the Myrtle Beach area. Failures were found on the coast as far north as the North Carolina border where the actual wind speeds were less than half of the design value, (Figure 10). Several buildings in the Charleston area, including The Trident Medical Center and the Red Cross Headquarters, were seriously damaged. Window systems also failed due to both positive pressure and suction.
Failures of flat-roof coverings, both build-up-roofs and single-ply systems, sometimes coupled with the roof-deck failures, were also to be found along the South Carolina coast as far as the North Carolina border. They were found inland as far as Charlotte. These failures, which included schools used as emergency shelters, hospitals, and emergency operations centers, resulted in extensive rain damage to the interior structure and contents of buildings. Based on a limited survey of insurance data, the rain damage in high-rise buildings was often 20 to 30 times the actual wind damage to the structure and multi-million dollar claims occurred in areas where the storm had a recurrence interval of less than 10 years.

The Standard Building Code in use when most of these buildings were designed seriously underestimated the uplift loads on the edges of roofs. The design loads were almost certainly exceeded in many places in Hugo. In some cases the shortcomings in the building code may have led to the selection of an inadequate system, but in many cases the system was probably chosen on the basis of cost rather than wind-uplift resistance.

4.6 Mobile Homes

A significant proportion of the population of South Carolina lives in mobile homes. The failure rate of these homes was much greater than conventionally built homes and the number of deaths and injuries in the storm would probably have been much higher had the Governor not ordered the evacuation of all mobile-home dwellers in the coastal counties, (Figure 11).

Many mobile-home owners were either uninsured or underinsured and did not have the financial resources to face a storm like Hugo. It was this section of the community which was probably the most seriously affected by the storm.

As mobile-home communities rebuilt they were forced to conform to many new government regulations better suited to more permanent dwellings. For example,in order to obtain flood insurance mobile homes must be elevated above the base flood elevation. After Hugo this was being done by placing them on concrete block piers, in some cases more than

8 ft tall, making them very susceptible to wind damage, (Figure 12).

5. CONCLUSIONS AND RECOMMENDATIONS

Hugo did more damage than other hurricanes, not because of its severity as it crossed the coast, but because it affected a major metropolitan area and retained much of its strength as it moved inland. However, it should also be noted that the worst conditions were experienced by a very sparsely populated area and the damage could have been very much worse.

In most countries national governments accept the responsibility for developing and maintaining building codes. With regard to wind effects on buildings, these codes usually incorporate or refer to national loading standards prepared by experts but subject to public review.

In the United States, where hurricanes and tornadoes create one of the most hazardous wind climates in the world, the Federal Government has passed the responsibility for building codes to the states. Many of the states have passed that responsibility on to local jurisdictions. Many of these jurisdictions use model building codes which, until recently, have chosen to ignore or significantly modify the American National Standard A58.1, a standard prepared on the same lines as other national loading standards.

Although the model building codes are democratic non-government bodies, they have been encouraged by the Federal Government to set performance standards in the belief that the older prescriptive codes were too restrictive. Setting performance standards works well when a building is subjected to a structural analysis, but the vast majority of buildings damaged by wind have never been subjected to a complete structural analysis. In such cases performance-based codes are unenforceable, unless proper deemed-to-comply standards are available. Although such standards have been available in North Carolina and South Florida for many years, they are not yet available in areas such as South Carolina which are served by the Standard Building Code. The prescriptive construction requirements which do appear in that code are often inconsistent with the loading requirements. Their use has led to many buildings being very vulnerable to wind damage.

Much of the wind damage to buildings in Hurricane Hugo was avoidable. The state of knowledge of wind effects was such that no building constructed after the mid-1960s need have been damaged by the storm; but, for reasons more political than technical, South Carolina found itself with a large population of buildings vulnerable to wind damage. Owners, insurers and government agencies must expect this situation to develop in other states which have adopted similar building control practices. In the future extensive damage must be anticipated even in storms below the design level.

To reduce wind damage and loss of life in future storms the following recommendations are made.

1. The United States Government should take an active role in reducing the wind hazard through a National Wind Hazard Reduction Program. The Government has been very successful in reducing the risks associated with flood and earthquakes but has paid little attention to the wind hazard. Direct involvement in a national code would be desirable but may be politically unacceptable.

2. In the absence of a national building code, states should mandate the use of model building codes and set up properly financed code enforcement procedures.

3. Model building codes should adopt the American National Standard A58.1 and update their codes as new editions of the standard are issued.

4. Model building codes should introduce deemed-to-comply standards for non-engineered structures which are consistent with their wind loading requirements. Existing inconsistent prescriptive requirements for wood and masonry construction should be removed.

5. Insurers should recognize that in the past they have put unjustified faith in the building control process. As a result they are now insuring buildings which have a very high probability of wind damage and consequent rain damage. However, insurers should also note that not all structural systems are equally vulnerable to damage. Insurance premiums should reflect this. Premium rates should also be used to encourage good new construction .

6. Public officials should recognize that some buildings which must continue to function during severe storms, including hospitals, emergency operations centers, and public shelters are very vulnerable to wind damage. All such buildings should be checked to ensure that they are capable of carrying the wind loads specified in ANSI A58.1 and strengthened if necessary.

7. Public officials should draw up plans to evacuate people from certain classes of structure in hurricanes, even if there is no threat of flooding. In the past,

evacuation has been ordered from areas prone to flooding. In Hugo people were told to evacuate from mobile homes whether or not they were subject to flooding. This probably saved many lives. In future storms evacuation should be ordered from certain other classes of building which are very vulnerable to wind damage.

8. The Federal Flood Insurance Program should recognize that flooding and high winds are not independent events in coastal regions. Regulations to reduce one hazard should not increase the other. Raising mobile homes 8 to 10 ft on masonry piers transforms a relatively low flood risk into a very high and dangerous wind risk. To avoid this sort of problem, and difficulties in settling insurance claims where buildings are subjected to wind and flood damage, comprehensive storm insurance should be developed, backed, if necessary, by the Federal Government but contingent upon good construction standards.

9. Educational and advisory programs should be developed so that the construction industry can benefit from wind engineering knowledge. These programs should include owners, insurers, and mortgagors so that they can understand the risks associated with certain forms of construction and make informed financial decisions regarding those risks.

10. Wind engineering research is many years ahead of wind engineering practice in many areas, but research is urgently needed on sheltering effects and the risks associated with the selection of particular structural systems. The results of this research will enable the consequences of past construction practices to be determined.

Finally it is worth recalling that the purpose of building code enforcement is the protection of the health, safety and welfare of the population. Of the many thousands of buildings affected by Hurricane Hugo, probably less than 1% collapsed due to wind effects in a manner that posed any threat to the health and safety of the population. Most of these were residences in evacuated areas, commercial structures and mobile homes. Thus by good planning and some good design, Hugo posed a very small threat to the health and safety of the population. However, due to a lack of planning and poor design, it posed a large threat to the welfare of the population. Utilities were interrupted, in some places for several weeks, and many people were left unemployed because their places of work were unusable. Many homes which suffered relatively minor damage to their roofs and windows were uninhabitable for many months. Those responsible for building control should take note of this and enforce appropriate regulations so that the welfare of the population is protected and the community can recover rapidly after such a storm.

6. ACKNOWLEDGEMENTS

The author would like to thank Mark Powell, NOAA, and Richard Marshall, NIST, for their contributions to the establishment of the wind conditions in Hurricane Hugo.

7. REFERENCES

1. ANSI, 1972, 1982, "Minimum Design Loads for Buildings and Other Structures," ANSI-A58.1, American National Standards Institute, New York, New York.
2. Manning, B.R., 1985, "Hurricane Requirements of the Standard Building Code," in "Hurricane Alicia: One Year Later," American Society of Civil Engineers, New York, New York.
3. Cook, N.J., 1985, "The Designers Guide to Wind Loading of Building Structures," Butterworths, London, U.K.
4. Mitchell, J.K., Abdel-Gaffar, A.M., Gentry, R.C., Leatherman, S.P., Sparks, P.R., 1986, "Hurricane Diana, North Carolina, September 10-14," National Academy Press, Washington, D.C.
5. NCBCC, 1982, "The North Carolina State Building Code," North Carolina Building Code Council, Raleigh, North Carolina.
6. Savage, P.R., Baker, J., Golden, J.H., Kareem, A., Manning, B.R., 1984, "Hurricane Alicia, Galveston and Houston, Texas, August 17-18, 1983," National Academy Press, Washington, D.C.
7. SBCCI, 1974, 1982, 1988, "The Standard Building Code," Southern Building Code Congress International, Birmingham, Alabama.
8. Simiu, E. and Scanlan, R.H., 1986, "Wind Effects on Structures," Wiley, New York, New York.
9. Sparks, P.R., 1988, "The Risk of Hurricane Wind Damage on the South Carolina Coast," a white paper issued by the Coastal Hazards Advisory and Mitigation Project, Clemson University, Clemson, South Carolina.
10. Sparks, P.R., Baker, J., Bellville; J.D. and Perry, D.C., 1990, "Hurricane Elena, Gulf Coast, August 29 - September 2, 1985," National Academy Press, Washington, D.C.

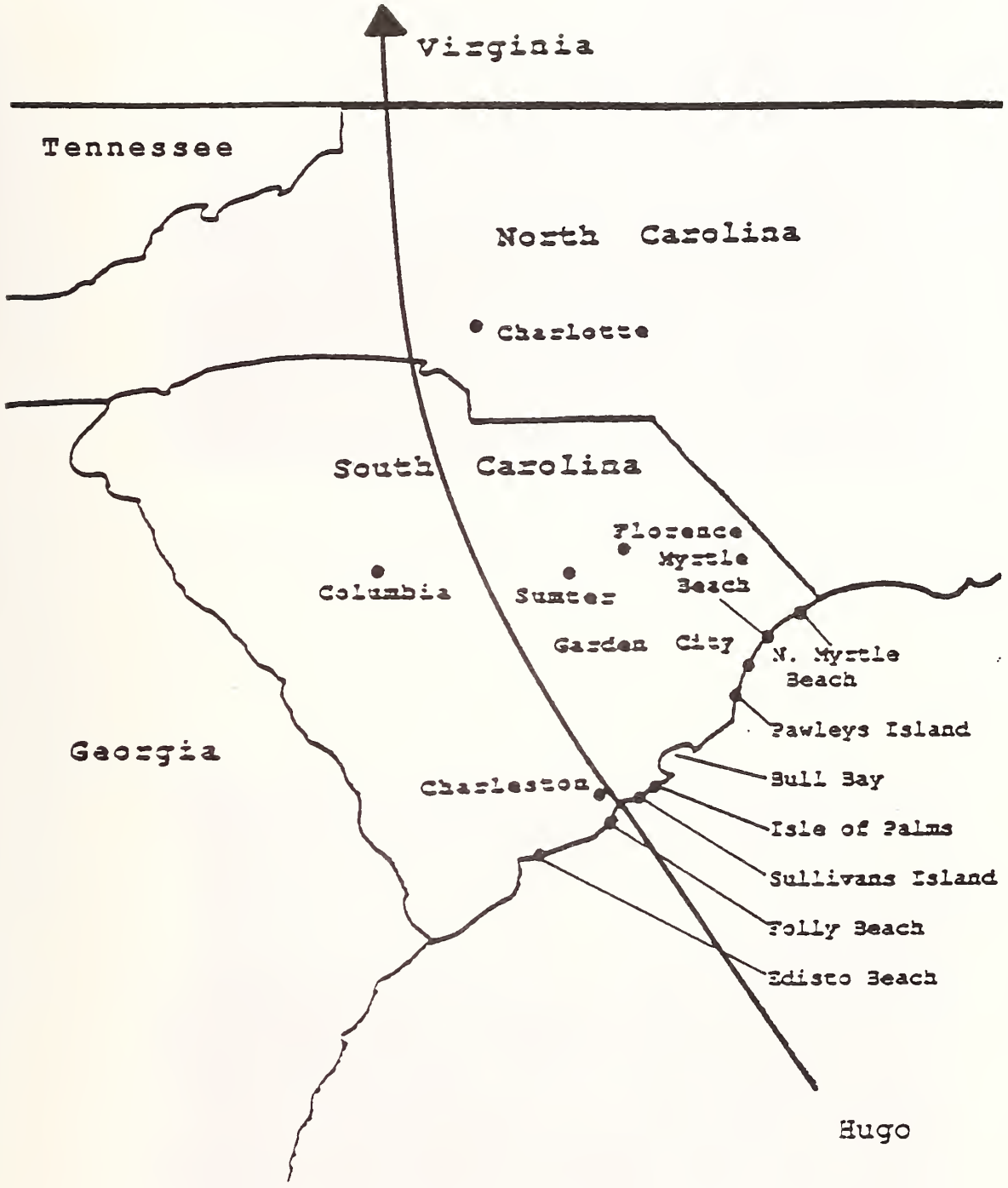

Figure 1. Track of Hurricane Hugo.

Figure 2. Heavily Damaged House, Bull Bay.

Figure 3. Shear Failure of House, Bull Bay.

Figure 4. Masonry Pier Failure, Isle of Palms.

Figure 5. Condominium Roof Failure, Isle of Palms.

Figure 6. Wind and Surge Damage to Condominium, Isle of Palms.

Figure 7. Collapse of Masonry Commercial Structure, North Charleston

Figure 8. Collapse of Masonry Commercial Structure, Sumter.

Figure 9. Damage to Metal Building, Charleston.

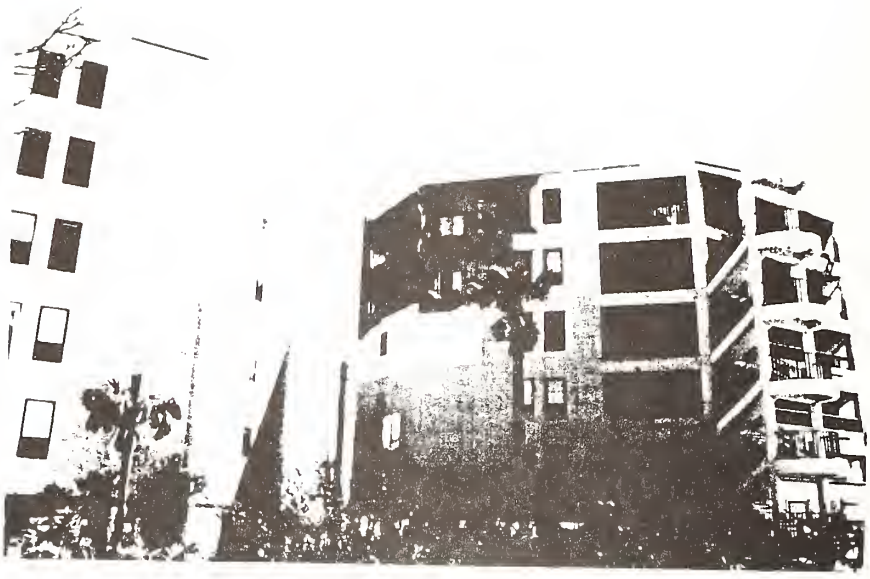

Figure 10. Typical Cladding Failure, Isle of Palms.

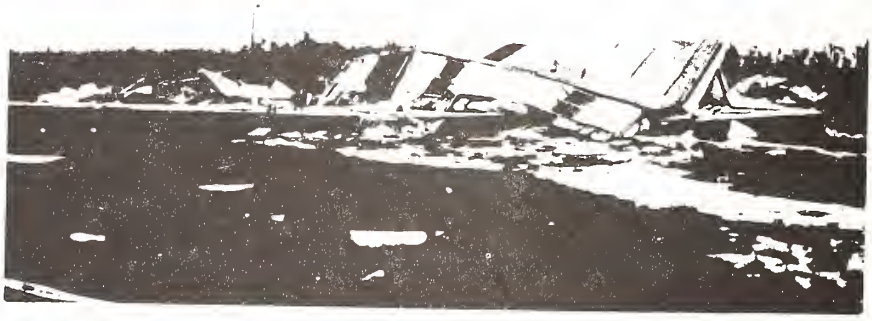

Figure 11. Damaged Mobile Homes near Sumter.

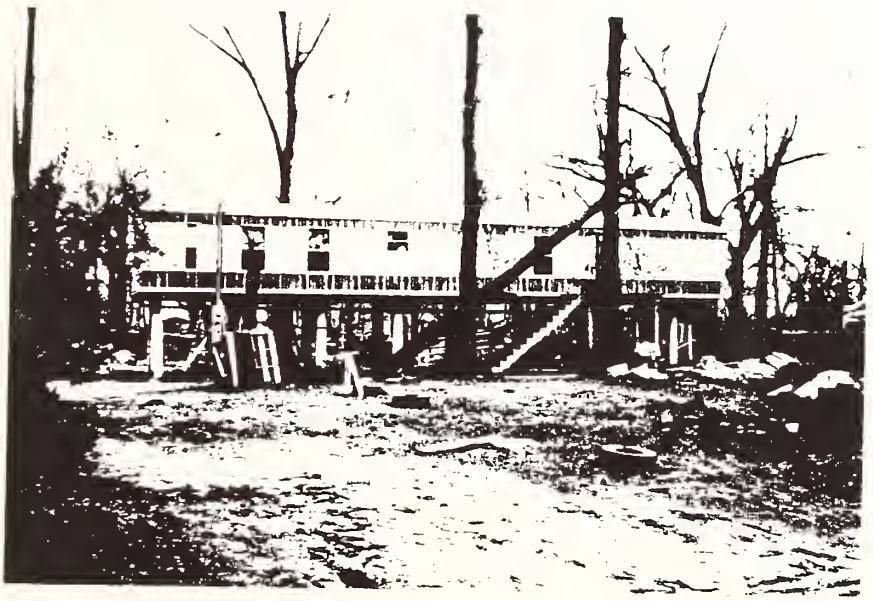

Figure 12. Elevated Mobile Home, Charleston County.

Summary of Task Committee Workshop Reports

REPORT OF U.S.-JAPAN WORKSHOP

REPAIR, RETROFIT, AND EVALUATION OF STRUCTURES

WIND AND EARTHQUAKE RESISTANCE

MAY 12 - 14, 1990

A. Activities of the Workshop:

1. Three sessions were held and 17 papers were presented on the following topics:

   Evaluation of Structures.

   1-1 Evaluation Procedures for Existing Buildings.
   1-2 Aseismic Countermeasures for Existing Buildings.
   1-3 Earthquake Hazard in Regions of Moderate Seismicity.
   1-4 Comparison of U.S. and Japan Aseismic Designs.

   Performance of Existing Structures.

   2-1 Performance of strengthened R/C Buildings.
   2-2 Performance of Buildings in Silicon Valley.
   2-3 Seismic Evaluation of Existing Buildings.
   2-4 Implications of Loma Prieta on Building Codes.
   2-5 Inspection, Evaluation, Restoration of Earthquake Damaged Buildings.

   Research on Techniques of Repair and Retrofit.

   3-1 Research on Repair & Strengthening of R/C Struct.
   3-2 Guide for Repair and Retrofit Design of R/C Bldgs.
   3-3 Research on Repair & Retrofit of Steel Structures.
   3-4 R/C Buildings Strengthened with Steel Members.
   3-5 Shear Strength of Anchor Bolts.
   3-6 Seismic Strengthening of R/C Office Buildings.
   3-7 Recent Research on Strengthening by Steel Bracing.
   3-8 Mortar Joints Between R/C Frame and Steel Bracing.

2. Another presentation was added on the topic of "NSF Research on Quantitative Non-Destructive Evaluation (QNDE) and Wind Engineering in the Year 2000.

3. Proceedings will be assembled and edited by J. Jirsa of the University of Texas, and will be submitted to the National Institute of Standards and Technology (NIST) for publishing. Included in the proceedings will be discussions, questions, and any modifications by the reporters or Task Committee Chairmen.

4. The following documents were exchanged during the workshop, or will be furnished to participants soon after the Joint U.S.- Japan Panel Meeting:

   a. Applied Technology Council (ATC) Reports No. 21 & 22 on "Evaluation Procedures for Existing Buildings."

   b. NIST Special Publication No. 778 (Jan 1990) on "Performance of Structures During the Loma Prieta Earthquake of October 17,1989."

   c. Japan TCCMAR "Design Guidelines for Medium-Rise Reinforced Masonry Buildings," which will be finalized after July 1990. The U.S. Side will attempt to have it translated into English.

   d. Mailing List of Japanese "International Institute of Seismology and Earthquake Engineering," so that copies of workshop proceedings can be furnished to each member.

5. It was recommended by workshop participants that future workshops be held in conjunction with U.S. - Japan Joint Panel Meetings on Wind and Seismic Effects. The Japanese Side recommended that the workshop proposed for 1991 in Tsukuba be more focused on a specific theme, to be determined by the Japanese members. Then a specific "Wind Engineering - Structural Performance Evaluation Workshop" will be planned to be held in the U.S. in 1992.

TASK COMMITTEE "J"

REPORT ON THE SIXTH U.S.-JAPAN BRIDGE ENGINEERING WORKSHOP
ANALYSIS, DESIGN, PERFORMANCE AND STRENGTHENING
LAKE TAHOE, NEVADA, U.S.A.
May 7 and 8, 1990

The following resolutions are hereby adopted:

1. The sixth U.S.-Japan Bridge Engineering Workshop provided valuable exchange of technical information which was beneficial to the bridge engineering communities of both countries. Forty seven participants representing government, academia, industry and private practice presented 41 papers in eight technical sessions. Main themes included: 1) "Wind Effects and Wind Resistant Design;" 2) "Retrofitting and Seismic Design;" 3) "Cable-Supported Bridges: Construction, Performance and Strengthening;" 4) "Seismic Performance and Analysis of Damaged Bridges;" 5) "Bridge Inspection, Repair, Testing, and Evaluation," 6) "Experimental Investigations and Computer Modelling;" 7) "Structural Monitoring, Diagnosis, System Identification and Non-Destructive Techniques;" and 8) "New Concepts, Dynamic Control, Seismic Isolation and Innovations in Construction." In view of the importance of cooperative programs on the subject of wind and seismic effects on bridges and on performance, strengthening, structural monitoring, safety, nondestructive evaluation and design innovation of these transportation structures, the continuation of technical cooperation and interaction is considered essential.

2. The Workshop recognizes the importance of continued exchange of personnel, technical information, research data and bridge response data from significant earthquakes and strong winds, and use of available unique research facilities in both countries.

3. The primary purpose of the Workshop is to exchange technical information on a timely basis that is usable by the bridge engineering profession. The specific objectives of this Workshop are:

   3.1 To ensure a first-hand exchange of information resulting from the unique problems each country is faced with; for example, the preliminary studies of the structural performance during the October 17, 1989, Loma Prieta earthquake and the recent full-scale vibration studies of the Yokohama Bay Cable-Stayed Bridge.

   3.2 To stimulate more collaborative research work in this important area of bridge engineering for better performance, rehabilitations and strengthening of bridge structures in both countries.

   3.3 To facilitate the exchange of technical information and ideas and to promote the broadening of viewpoints for those involved.

4. The Workshop identifies the following technical topics for continued cooperative research programs:

   4.1 Dynamic control and seismic isolation of bridge structures including: active and passive control, damping augmentation, experimental studies and application to long-span cable-supported bridges,

4.2 System identification techniques for wind and seismic engineering including: data interpretation studies, development of mathematical models, identification of non-linear systems, reduced-order models, computational algorithms and optimum sensor locations,

4.3 Non-destructive evaluation techniques including damage detection by sensor monitoring, expert systems, inspection techniques, structural monitoring, condition assessment for safety, performance evaluation and repair procedures,

4.4 Experimental and analytical studies on the effects of dynamic soil characteristics, including bridge-soil interactions, on the behavior of bridge structures.

5. The Workshop identifies the following technical topics for future cooperative technical programs:

5.1 Retrofitting and strengthening methodologies for bridge structures.

5.2 Development of design criteria based on limit-state concepts.

6. It is anticipated that the interaction among the delegates from the United States and Japan during the round-table discussions and the technical study tour will lead to an enhanced exchange of data and innovative ideas, and will also lead to the establishment of cooperative research efforts, both theoretical and experimental, on bridge engineering. Because of the importance, benefits and potential of these Workshops, it is recommended to conduct the 7th bridge engineering workshop, just prior to the 23rd UJNR joint meeting in Tsukuba, Japan, in May 1991. A study-tour will be planned to visit research laboratories and bridge-construction sites including the Honshu-Shikoku bridge site, and the base-isolated bridge.

Appendix:

Task Committees
A–J Reports

Report of Task Committee on

(A) STRONG-MOTION INSTRUMENT ARRAYS AND DATA

Date: May 15, 1990

Place: National Institute of Standards and Technology
Gaithersburg, Maryland 20899

Attendees:	Japan Side -	T. Uwabe (Acting Chairman)	(PHRI)
		K. Ohtani	(NRCDP)
		K. Tamura	(PWRI)
	U.S. Side -	A. G. Brady (Chairman)	(USGS)
		A. G. Franklin	(USAEWES)
		H. Meyers	(NOAA)

MISSION STATEMENT

1. Objective:

The objective of the Task Committee is to coordinate the provision of strong-motion earthquake data to researchers and to the practicing engineering community. The Task Committee focuses on instrumentation; recording, processing, and analyzing strong-motion data; research to ensure high-quality data dissemination; and analysis of ground motion and structural motion in dynamic response to earthquakes.

2. Scope of Work

The T/C coordinates strong-motion research, processing strong-motion data, and disseminating information on the recorded behavior of structures. In addition to regular exchange of data and publications, the T/C's technical approach includes:

* Planning and conducting T/C workshops and meetings, held generally in conjunction with UJNR Joint Meetings, often with IASPEI/IUGG conferences and with World Conferences on Earthquake Engineering.

* Conducting related technical sessions at professional society meetings.
* Creating procedures for the dissemination of significant strong-motion digital data with regard for the rights and expectations of (a) the owner, (b) the users of data, and (c) the earthquake engineering community.

* Creating an up-to-date information exchange on computer processing procedures and related research so all users of processed data are aware of valid ranges and practical limitations.

* Developing a research program for appropriate instrumentation and dynamic analysis of structures with base isolation or other response-reducing systems, under earthquake excitation.
* Developing a research program using temporary arrays and data derived to study site response.

3. Accomplishments

* Catalogs of strong-motion earthquake records observed both in the United States and Japan are being exchanged. U.S. data are published in the "Seismic Engineering Program Report", and the Japanese data are published in "Strong-Motion Earthquake Records in Japan". Many other publications were also exchanged.

* Mr. Keiichi Tamura of PWRI is a Visiting Scholar at Stanford University for one year from October 1989 working on strong-motion instrument arrays and data.

* Data tapes on the Loma Prieta earthquake of October 17, 1989, processed by USGS and CDMG, were delivered to Japanese side.

* Disks containing data on the Chiba-Toho-Oki earthquake of December 17, 1987, processed by the National Research Center for Disaster Prevention, were delivered to U.S. side.

* The Japanese Technical Study Team for the Loma Prieta Earthquake visited northern California, USA, between Nov. 16 & 29, 1989 to study the effects. The team and the U.S. hosts included many panel members.

* Dr. Sasaki visited the U.S. during March 20-29, 1990, visiting U.C Berkeley, USGS, Stanford, CALTRANS, CDMG; Loma Prieta Earthquake effects in San Francisco, Oakland, and epicentral area; and Washington (AID, NIST, NSF). Panel members hosted throughout; T/C A contacts included A. G. Brady and R. D. Borcherdt, of USGS, and A. G. Franklin of USAEWES.
(Other Panel members included J. Gates, R. Hanson, H.S. Lew and N. Raufaste).

4. Future Plans

* The T/C Chairmen will seek funding sources for a 3rd Workshop on Processing Strong Motion Records, concentrating on array data.

* Coordinate the analysis of records from arrays: downhole 3-D arrays (geophysics and earthquake engineering) and structural arrays (structural engineering).

* The T/C recognizes the efforts of the International Working Group on the Effects of Surface Geology and encourages wider participation by Panel members.

5. Information Exchange

* Will be performed within the domestic community through technical meetings, conferences, seminars, and workshops.

* Will be performed through participation in post-earthquake field investigations with concentration in areas where strong-motion stations have recorded data.

* Will be performed with the counterpart side through T/C workshops; visitor exchanges, seminars, lectures; and participation in annual Joint Panel meetings.

* The most crucial information exchange is rapid description of recovered strong motion (and subsequently, digital strong-motion data on tape or disk) from significant earthquakes, for example Loma Prieta Earthquake, CA of October 17, 1989.

6. Impact

* Most managers who process strong-motion recordings use techniques based, or closely associated with, the work of this T/C and its members. Foreign networks fitting this category include:

AUSTRALIA - Australian Seismological Center, Bureau of Mineral Resources, PO Box 378, Canberra ACT 2601.

CANADA - Pacific Geoscience Center, PO Box 6000, Sidney, BC. V8L 4B2.
ITALY - The Italian National Commission for Research and Development on Alternative Energy Sources (ENEA), Rome.

MEXICO - Japan-Mexico Earthquake and Disaster Prevention Center, Mexico City.

PERU - Japan-Peru Earthquake and Disaster Prevention Center, Lima.

TAIWAN - SMART Array

TURKEY - University of Bogazici, 80815 Bebek, Istanbul.

YUGOSLAVIA - Institute of Earthquake and Engineering Seismology, Skopje.

* Use of seismological and strong-motion data, in convenient form, is facilitated in countries other than where recorded.

* Dissemination of digital data from significant earthquakes increases the research data base; application of this data in design practice aids in reduction of earthquake hazards.

7. Barriers

* Lack of adequate funding for T/C joint endeavors.

* Establishing joint research efforts and maintaining close interaction between participants are difficult unless visiting research appointments are established. (Funding and staff availability are often barriers).

Report of Task Committee on

(B) LARGE-SCALE TESTING PROGRAM

Date: May 16, 1990

Place: National Institute of Standards and Technology
Gaithersburg, MD 20899

Attendees:	Japan Side -	K. Ohtani (Chairman)	(NRCDP)
		S. Okamoto	(BRI)
		T. Kaminosono	(BRI)
		S. Nakata	(BRI)
	U.S. Side -	H. S. Lew (Chairman)	(NIST)
		T. Lew	(NCEL)
		J. Tissell (Observer)	(American Plywood Assoc.)

MISSION STATEMENT

1. Objective

The objective of the Task Committee is to develop performance data of full-scale dynamic properties of structures to better resist wind and seismic loads through both laboratory testing of prototype structures and field testing of structures in situ. Improved full-scale test data will validate the results of small-scale model tests and substantiate the results of computer analyses of structural behavior.

2. Scope of Work

The Task Committee develops its research agenda in coordination with other appropriate T/Cs, such as T/C's "C" and "D", for full-scale evaluation of buildings, and other structures except bridges.

* Plans and conducts workshops and joint meetings to identify research topics and develops joint research programs.

* Coordinates research projects carried out by various laboratories in the U.S. and Japan. Facilitates publication of research results and implementation of findings in codes and standards.

* Facilitates exchange of research personnel, technical information and available testing facilities.

3. Accomplishments

* As part of the second phase, analytical and experimental research, including component and subassemblage tests, are being carried out at several U.S. universities. Funding for the third phase of the U.S.-Japan Coordinated Program for Masonry Building Research has been postponed by the National Science Foundation for U.S. researchers.

* The U. S. Technical Coordinating Committee on Masonry Research was held in July 1989.

* The 5th Joint Technical Coordinating Committee on Masonry Research (JTCCMAR) was held in October 1989 at Tsukuba, Japan. Progress on individual research projects were presented by principal investigators and future coordination of the Joint Program was discussed.

* A preliminary Joint U.S.-Japan Precast Seismic Structural Systems (PRESSS) Program Coordinating Meeting was held in October 1989 in Japan.
* The first phase of the U. S. Precast Seismic Structural Systems Program has been funded by NSF.

* The Government of Japan provided funding for the Japan PRESSS Committee research program beginning April 1989. The Japan Technical Coordinating Committee (TCC) Meeting was held in April 1990, and it approved the scope of research of the Japanese PRESSS project.

* Complement to the U.S. PRESSS program, NIST has carried out research on precast concrete beam-column connections.

4. Future Plans

* The 6th JTCCMAR will be held at Seattle, WA. in August 1990. Immediately following this meeting the U.S. TCCMAR will be held.

* The first Joint Technical Coordinating Committee (JTCC) on PRESSS will be held in San Diego in November, 1990. The U.S. TCC on PRESSS will meet prior to the first JTCC on PRESSS.

* A revised version of "Design Guidelines for Medium Rise Reinforced Masonry Buildings" will be published in Japan in August 1990.

* In support of IDNDR, findings of Joint research projects carried out under the auspices of T/C "B" should be disseminated widely to countries which has high seismic risks.

* Task Committee "B" recommends the establishment of a new Task

Committee on Passive and Active Energy Dissipation Systems.

* Continue exchange of information of the following topics between appropriate U.S. and Japan organizations.

  a. Seismic performance of composite and mixed construction,

  b. Application of high strength construction materials to structures in high seismic zones,

  c. Testings of large-scale structures other than buildings and bridges.

* Exchange of information on large-scale testing facilities and large-scale testing programs should be encouraged.

5. Information Exchange

* Technical reports and research documentation were exchanged with participating organizations in both countries.

6. Impact

* The results of the past joint research projects on reinforced concrete and steel structures have been published in both U.S. and Japanese technical journals. A number of key findings have been incorporated into U.S. and Japanese building codes and design guidelines.

* As a result of joint research projects, the state of practice and understanding in earthquake engineering has been improved in both countries. The results from the joint program have further stimulated research in both countries.

* Facilitate joint research projects utilizing available testing facilities in both countries.

7. Barriers

* There are no major technical barriers for the attainment of the Task Committee mission. However, different building practices and needs in the U.S. and Japan require careful planning for effective joint research projects.

* Securing funding to support exchange of research personnel is difficult in both countries. Funding agencies of both countries should be informed about the technical benefits resulting from the joint panel activities and encouraged to participate in researcher exchanges and joint programs.

Report of Task Committee on

(C) REPAIR AND RETROFIT OF EXISTING STRUCTURES

Date: May 16, 1990

Place: National Institute of Standards and Technology
Gaithersburg, MD 20899

Attendees:	Japan Side -	S. Nakata (Chairman)	(BRI)
		S. Okamoto	(BRI)
		T. Kaminosono	(BRI)
	U. S. Side -	K. P. Chong (Chairman)	(NSF)
		G. R. Fuller	(HUD)
		J. R. Hill	(DOE)
		G. E. Freeland	(LLNL)
		R. D. Marshall	(NIST)
		E. Sabadell	(NSF)

MISSION STATEMENT

1. Objective

The objective of the Task Committee is to encourage research and provide technology transfer activities in materials, components, and total buildings and structural systems related to evaluating the performance of existing buildings and structures subjected to environmental and earthquake forces. The research topics provide data and information for the repair and retrofit of existing buildings/structures.

2. Scope-of-Work

The T/C work includes information exchanges and planning and hosting workshops and seminars. Workshops are generally held in conjunction with the annual Panel's meeting. They provide T/C members with an opportunity to review related research and to direct plans for future research, share and implement results. The T/C conducts related technical sessions at professional society's meetings. The T/C studies new materials and methods to accomplish repair and retrofit operations on buildings e.g., fiberglass reinforced plastics, structural adhesives and exploits use of automation and robotics for repair and retrofit. Work focuses on coordinating research projects in Japan and the U.S. to minimize duplication and to maximize benefits

3. Accomplishments

* Held the 1-1/2 day NSF sponsored 5th Workshop on Evaluation, Repair and Retrofit of Existing Structures prior to the 22nd Joint Meeting, NIST, 1990 (24 delegates attended [12 from Japan and 12 from U.S.] 19 manuscripts were presented [13 from Japan and 6 from the US]).

* NSF issued a two-year initiative on Quantitative Nondestructive Evaluation for Large Structural Systems in April, 1990.

* NSF sponsored a workshop on non-destructive testing of civil engineering structures at University of Southern California (1988).

* NSF issued a five-year initiative on Repair and Rehabilitation Research for Seismic Resistance of Structures.

* A workshop was held at NIST in 1989 on International Workshop on Sensors and Measurement Techniques for Assessing Structural Performance.

* FEMA published cost data for various methods of repairing and retrofiting existing buildings.

* DOE has issued several design and evaluation guidelines for mitigating the effects of earthquakes, winds and tornados.

* In the U.S., FEMA published ATC 21, "A Handbook for Seismic Evaluation of Existing Buildings," and ATC 22, "Techniques for Seismically Rehabilitating Existing Buildings" (drafts).

4. Future Plans

* A separate or joint (with T/C "D") workshop is being planned on the Design Approaches and Construction Methods for Repair and Retrofit of Buildings and Structures in May 1991 in Japan. The workshop will focus on the use of newly developed methods for repair, retrofit and evaluation of buildings/structures.

* In Japan, the Guidelines for Evaluating and Strengthening Existing Buildings will be revised, and the Guidelines for Evaluation of Earthquake Damage and Repair Methods of Buildings will be published. Both guidelines will be available after August, 1990.

* In support of IDNDR activities, T/C "C" would like to participate in task committee activities related to repair and retrofit of damages due to various disasters.

* A possible session on wind damages will be planned in 1992 in U.S.

* NSF will sponsor a civil engineering non-destructive testing workshop in Fall, 1990, in Boulder, Colorado.

5. Information Exchange

* Publications of the 5th Joint T/C "C" of "D" Workshops were distributed, to all delegates and will be made available to design professionals through technical presentations at national meetings of professional societies.

* A U.S. Panel (Japanese Technology Evaluation Center Panel) will be going to Japan in July, 90, to study and exchange information on construction engineering.

* Published workshop reports and individual research papers; they were exchanged with the U. S. and JAPAN-side members.

6. Impact

* Contributed to development of US and Japan design criteria for repairing and strengthening reinforced concrete, steel, and other buildings.

* T/C recommendations were incorporated into building codes and professional practices, as illustrated by rehabilitation programs used by the City of Los Angeles to upgrade existing masonry buildings to resist earthquake forces.

* Influenced changes to U.S. and Japan design practices to upgrade existing structures.

7. Barriers

* Greater progress needs be made to implement available research results. Funding to sources need be identified to support this endeavor. Funding agencies of both countries should be encouraged to sponsor activities related to their mission, and to support participants attendance at Joint Panel Meetings and Workshops.

Report of Task Committee on

(D) EVALUATION OF STRUCTURAL PERFORMANCE

Date: May 15, 1990

Place: National Institute of Standards and Technology
Gaithersburg, MD 20899

Attendees:	Japan Side -	S. Okamoto (Chairman)	(BRI)
		S. Nakata	(BRI)
		T. Kaminosono	(BRI)
	U.S. Side -	G. R. Fuller (Chairman)	(HUD)
		K. P. Chong	(NSF)
		E. Sabadell	(NSF)
		J. R. Hill	(DOE)
		R. D. Marshall	(NIST)
		G. E. Freeland	(LLNL)
		J. Tissell (Observer)	(Am. Plywood Assoc.)

MISSION STATEMENT

1. Objective

The objectives of this Task Committee are to develop disaster mitigation policies and programs to improve the capacity of existing structures to resist wind and seismic forces. To provide adequate performance evaluation, each country will coordinate development of condition assessment, screening, and structural analysis methodologies. Structures will then be analyzed and instrumented, and evaluated after disasters.

2. Scope of Work

* Develop a complete inventory of "benchmark" structures that have been analyzed and instrumented for measurement of wind and seismic response.

* Coordinate development of a uniform system of screening and analyzing wind and seismic resistance and capacity of structures in each country.

* Develop sensor technology, instrumentation, and "expert" systems to provide condition assessment of existing structures.

* Evaluate masonry and precast concrete buildings, and seismic-isolation systems, and include these findings in each country's catalog of "benchmark" structures for post-disaster performance evaluation.

* Plan and conduct workshops at future UJNR Joint Panel Meetings, cooperatively with Task Committees "C" and "B".

3. Accomplishments

* A 1-1/2 day Joint Workshop with Task Committee "C" on "Repair, Retrofit and Performance of Structures", was held at NIST on May 12 and 14, 1990. Twenty-four delegates attended (12 from Japan and 12 from the U.S.). Nineteen manuscripts were presented (13 from Japan-side and 6 from the U.S. side).

* Exchanged several reports on Post-earthquake and Post-hurricane events: eg: Loma Prieta, and Hurricane Hugo, etc.

* Presented Applied Technology Council ATC-21 & ATC-22 draft reports on "Evaluation Procedures for Existing Buildings." C. Rojahn will supply copies to all workshop participants. (One copy was given to Japan Side).

* Received Japanese MOC first and second year reports on state-of-art and catalog of buildings with seismic base isolation or wind damping systems. The U.S. Side translated the documents into English; they will be published by NIST and distributed to Panel Members.

* A research workshop held in Washington, DC in August 1988 developed a U.S. research agenda for masonry. A working group was related to structural performance of masonry buildings. Evaluation techniques, nondestructive testing, and condition assessment research was identified in the Final Report (copies were provided to the Japanese Side).

* Copies of NIST SP 778 (ICSSC TR11) "Performance of Structures During the Loma Prieta Earthquake of October 17, 1989" were made available to all participants of the Workshop.

4. Future Plans

* Develop a reporting system and data collection form to catalog existing structures in the U.S. and Japan that have been evaluated for wind and seismic resistance or have been instrumented. Compile a computer data file for exchange between countries and report its progress at each UJNR Joint Panel Meeting.

* Encourage and enlist the participation of private industry, consulting engineering firms, universities, and other governmental agencies involved in the instrumentation, evaluation, and condition assessment of existing structures.

* Encourage each country to develop sensor technology and instrumentation of structures, for making condition

assessments and for determining the long term environmental and aging effects on building components and materials.

* Participate in development of a new Panel effort on the International Decade for Natural Disaster Reduction (IDNDR).

* Plan for Workshop prior to 23rd U.S.-Japan Panel Meeting in Tsukuba, Japan. Japan Side will determine specific topics for this Workshop. A Structural Performance Evaluation Workshop on Wind Engineering is proposed to be held in the U.S. in 1992.

5. Information Exchange

* Exchange methodologies for evaluation of structural performance and reports of post disaster evaluations of structures.

* Provide most current data of "benchmark" structures that have been evaluated and instrumented.

* Continue collection of related technical papers and other literature and encourage development of an annotated bibliography of information for periodic exchange.

* Prepare papers and reports for the 23rd UJNR Joint Panel Meeting and associated "Workshop on Structural Performance Evaluation".

* Japanese side will send to the U.S. T/C Chairman a copy of the Final Revision of "Design Guidelines for Medium Rise Reinforced Masonry Buildings" developed by TCCMAR-Japan (due end of July 1990). U.S. Side will explore feasibility of translating this manuscript into English. Summary report of the design guidelines was printed in the Pre-Proceedings of 22nd Joint Meeting (3-3 Okamoto).

* Other papers of interest to Task Committee "D" in the Pre-Proceeding of the 22nd Joint Panel Meeting are:

  3-1 PRESSS Precast Concrete Joint Research Project (Okamoto).

  3-2 U.S. Coordinated Program for Masonry Building Research (Noland).

  4-2 Major Seismic Building Upgrades at Lawrence Livermore National Laboratory (Freeland).

  4-9 Relation Between the Building Damage and Vibration Properties of Ground (Ohtani).

  5-4 Performance of Wood-Framed Structures in Loma Prieta

Earthquake (Tissell).

* Copies of NISTIR 89-4153, "Sensors and Measurement Techniques for Assessing Structural Performance," Proceedings of an International Workshop held at NIST in Sept. 1988, were distributed to all T/C members in Sept. of 1989.

6. Impact

* Developed revised standards and building code provisions to reduce destruction from high winds and earthquakes.

* Provided engineers with improved capability to conduct condition assessment of existing structures for developing cost effective repair, retrofit, strengthening or demolition programs.
* Increased the confidence level of the public, regulators, policy makers and engineers, to provide assurance that major structures will adequately resist high wind and earthquake forces.

7. Barriers

* Difficulty in identifying priorities and inadequate resources to document load carrying capacity of existing buildings subjected to highly probable extreme winds and earthquakes.

* Limited resources for instrumenting buildings, for conducting post-disaster evaluations, and for participating in foreign travel for coordination of activities.

Report of Task Committee on

(E) NATURAL HAZARD ASSESSMENT AND MITIGATION THROUGH LAND USE PROGRAMS

Date: May 15, 1990

Place: National Institute of Standards and Technology
Gaithersburg, MD 20899

Attendees:	Japan Side -	K. Kawashima (Chairman)	(PWRI)
		T. Iwasaki	(PWRI)
		K. Ohtani	(NRCDP)
		K. Tamura	(PWRI)
		T. Akagiri	(GSI)
	U.S. Side -	W. Hays (Acting Chairman)	(USGS)
		H. Meyers	(NOAA)
		G. Brady	(USGS)

MISSION STATEMENT

1. Objective

The objectives of this Task Committee are to exchange information and experiences on: 1) engineering characterization of ground motion 2) mapping techniques for displaying ground motion data, 3) microzonation, and 4) siting and design applications.

2. Scope of Work

New data acquired in Japan and the United States, and in other countries (e.g., Chile, Mexico, and Armenia, USSR) will be analyzed for future workshops in terms of the four above objectives.

3. Accomplishments

Ideas for future activities were exchanged through correspondence from T/C members of both sides.

4. Future Plan

* The Task Committee is exploring the feasibility of holding a one or two day planning meeting in conjunction with the anniversary meetings of the Loma Prieta earthquake which are being planned for October and November 1990. The T/C meeting could be held in California or in Tokyo in conjunction with IDNDR meetings being planned in October.

* A conference on the first T/C objective, Engineering Characterization of Ground Motion, planned for 1991, is

proposed to be held in conjunction with the 23rd Joint Panel Meeting.

* In view of the increased ground motion data resulting from the October 17, 1989, Loma Prieta earthquake and others throughout the world, it was agreed that the Task Committee should focus attention on increasing understanding of ground motion and seismic design forces within the framework of its current broad task. For such purpose, redefinition of the T/C name as, "Ground Motion and Seismic Design Forces", is proposed.

5. Information Exchange

Reprints of technical papers on ground motion, the Loma Prieta Earthquake, and the IDNDR were exchanged at the 22nd Joint Panel Meeting.

6. Impact

The work of the T/C will be of great value to each country and contribute to others throughout the world who have similar problems to solve.

7. Barriers

Lack of funding for travel to exchange information and to convene workshops has been the principal barrier in the past.

Report of Task Committee on

(F) DISASTER PREVENTION METHODS FOR LIFELINES SYSTEMS

Date: May 15, 1990

Place: National Institute of Standards and Technology

Attendees: Japan Side - K. Kawashima (Acting Chairman) (PWRI)
T. Iwasaki (PWRI)

U. S. Side - S. C. Liu (Chairman) (NSF)
C. J. Astill (NSF)
R. M. Chung (Observer) (NRC)
J. Cooper (FHWA)
T. Lew (NCEL)
H. S. Lew (NIST)
K. Sullivan (FEMA)

MISSION STATEMENT

1. Objective

The objectives of Task Committee "F" are to improve 1) the behavior of lifeline systems during earthquakes and 2) engineering and other seismic countermeasures such as damage estimation techniques and inspection procedures. These technologies provide users with improvements to existing standards of practice for safety and serviceability of lifeline systems. Lifeline systems such as gas, oil, water, and sewage pipelines; and power, communication, and transportation systems are crucial to the survival and health of a city or community. Earthquakes affecting such systems cause severe social and economic disruptions to communities and cause human suffering to the residents.

2. Scope of Work

* Plan and conduct T/C workshops and meetings; they generally are held in conjunction with the annual UJNR Joint Meeting. The purpose is to exchange the state-of-the-art knowledge and practice and to identify cooperatively key opportunities for exchange and studies which effectively implement research results.

* Conduct related technical sessions at professional society meetings.

* Create a research program on a selected lifeline system (similar in concept to the Large-Scale Testing Program). For example, through joint demonstration, produce criteria for emergency design and loss evaluation and on-line monitoring

systems for lifeline operation.

* Conduct special activities such as translating, printing, and distributing MOC PWRI's publication Manual for Repair Methods for Civil Engineering Structures Damaged by Earthquake.

* Develop performance standards and a manual on repair, restoration, and retrofit of lifelines.

3. Accomplishments

* A third UJNR Workshop on U.S.-Japan Lifeline Earthquake Engineering was held in May 1989 in Tsukuba. The Workshop proceedings were published and distributed to the research communities in both countries.

* Researchers from both sides have contributed several technical papers on lifeline systems at the 22nd joint panel meeting.

* Researchers from both sides have participated in the post-event field investigations on the collapse and damage of lifeline structures in the San Francisco Bay area following the Loma Prieta earthquake in October 1989. A number of in-depth studies on earthquake behavior, safety, repair and strengthening of the lifeline structures have been undertaken.

* Dr. Y. Sasaki, Japan Side T/C Chairman visited several organizations including NSF and NIST in March 1990 to discus active control research and to exchange information.

4. Future Plans

* Continue observation of instrumented buried pipes in Parkfield, California, and Chiba, Japan and exchange data.

* Conduct the 4th Joint Workshop on Disaster Prevention for Lifeline Systems tentatively scheduled in 1991 at an U.S. location.

* During the 3rd Lifeline workshop in May 1989, the importance of active control research was identified for mitigation of damage to lifeline structures during earthquakes. T/C "F" recommends establishment of a new task committee on Active/Passive control systems for exchanging technical information, undertaking joint research, and coordinating research programs carried out by panel member organizations.

* Initiate a new cooperative research project on seismic control systems for lifelines to mitigate damage. This work would complement the above activity.

5. Information Exchange

* Domestic community: through technical meetings, conference sessions, seminars, and workshops.

* Between U.S. and Japan: through T/C workshops and annual Joint Panel Meetings.

* Visits by researchers and participation in technical meetings sponsored by organizations such as NCEER and EERI.

* Short-term (3 to 12 months) researcher exchanges to participate in on-going lifeline research such as performed at the University of Michigan and PCA in the U.S. and at BRI in Japan.

6. Impact

* Contributed to increased field engineers' technical knowledge on repair methods, through seminars with lectures by T/C members using the MOC Manual in nine major cities in Japan, including Tokyo and Osaka; more than two thousand participants attended seminars.

* Contributed to the assessment of design, construction, and operating standards for lifeline systems through T/C member participation in the committee work e.g., the Technical Council on Lifeline Earthquake Engineering (TCLEE/ASCE) and the U. S. Building Seismic Safety Council.

7. Barriers

* Insufficient funds to conduct annual Task Committee Workshops and to publish proceedings and reports.

* Lack of participation by U.S. industrial organizations and utilities in research or in implementation of findings due to a reluctance to adopt new technologies and practices.

Report of Task Committee on

(H) SOIL BEHAVIOR AND STABILITY DURING EARTHQUAKES

Date: May 16, 1990

Place: National Institute of Standards and Technology
Gaithersburg, MD 20899

Attendees:

Japan Side -	T. Iwasaki (Acting Chairman)	(PWRI)
	T. Uwabe	(PHRI)
U.S. Side -	A. G. Franklin (Chairman)	(WES)
	R. L. Ledbetter	(WES)
	W. E. Roper	(COE)
	C. J. Astill	(NSF)

MISSION STATEMENT

1. Objective

The objectives of this Task Committee are to enhance technology for: predicting the dynamic behavior of soils, establishing procedures to analyze dynamic soil-structure interaction, and modifying the dynamic behavior of foundations and earth structures in order to assure their safe performance during earthquakes. Government agencies with responsibility for public works have a duty to provide for public safety and to make economical use of public funds. Consequently, government agencies have a need for more accurate methods of predicting soil behavior, and for improved, economical methods of controlling soil behavior, to assure the seismic safety of public works and to minimize the costs of construction by avoiding unnecessary over-design.

2. Scope of Work

* Present technical papers at annual joint panel meetings on technological developments and the state-of-the-art and practice related to soil behavior and stability during earthquakes.

* Exchange information and technical data relating to field performance, research and methods of practice.

* Plan and conduct T/C workshops in coordination with proposed or ongoing cooperative research programs.

* The Task Committee plans and conducts programs of cooperative research, exchange of researchers between U.S. and Japanese government laboratories, publication of research results and recommended practice. The benefits realized from available research funds can be amplified by bringing greater resources to bear on problems of mutual interest, and by coordinating

research tasks to make the best use of the respective strengths of the two sides' research capabilities.

* Exchange visiting researchers using mechanisms provided by formal and informal cooperative research programs. Such exchanges promote technical information exchanges, familiarization with methods of practice on the respective sides, and mutual understanding and cooperative relationships between researchers on the two sides.

3. Accomplishments

* U.S. researchers presented 5 papers, and Japanese researchers presented 11 papers, on soil behavior and stability during earthquakes, at the 21st and 22nd joint panel meetings 5/89,5/90

* Proceedings of the Workshop on the In-Situ Testing, held at San Francisco, California in 1985 was published and disseminated to the Panel members 4/89

* A planning meeting for cooperative research on preventive measures against soil liquefaction was held at Tsukuba prior to the 21st joint meeting.....5/89

* Mr. Keiichi Tamura of the PWRI is a one-year Guest Researcher at Stanford University, working on Seismic Response Characteristics of Ground 10/89

* Mr. Motoki Kazama of the PHRI is at the Scripps Institute of Oceanography as a one-year Guest Researcher, working on Effects of Offshore Environments on Seismic Response of Soil Deposits and Pile Foundations 10/89

* Mr. Nario Yasuda of the PWRI completed a one-year Guest Researcher assignment at the U.S. Bureau of Reclamation, doing research in Seismic Behavior of Soils 1/90

* Dr. Yasushi Sasaki of the PWRI visited sites of damage around the San Francisco Bay Area and the epicentral area of the Loma Prieta Earthquake. He was assisted by several U.S. Panel Members, including the T/C (H) U.S. Chairman.....3/90

* A set of 35mm slides showing the effects of the Loma Prieta Earthquake was provided to the Japanese side by the U.S. Side 3/90

* Dr. Ashok K. Chugh, of the U.S. Bureau of Reclamation, visited the PWRI in March and April 1990, to study the Dynamic Behavior of Rock-Fill Dams 4/90

4. Future Plans:

* Identification of research tasks on preventive measures against soil liquefaction that are of common interest, in accordance with the results of the planning meeting held at Tsukuba in May 1989.....9/90

* Hold the Second U.S.-Japan Workshop on Remedial Treatment of Potentially Liquefiable Soils, in Japan at a time to be determined between October 1990 and March 1991 ...2/91

* Develop plans for a cooperative research program to verify soil-pile interaction models for marine structures subject to earthquakes, measurement of sea floor earthquake motions, and the stability of gravity-based structures during seismic events 12/89

* T/C (H), at the 22nd Joint Panel Meeting, discussed the need for technological innovation and research to assist in saving lives following natural disasters caused by earthquakes. The principal areas of need were identified as improved technology for locating survivors, and the development of new equipment and systems for safe excavation of debris to remove survivors from collapsed structures. T/C (H) recognizes this subject is outside their area of responsibility but feels it is important and should be discussed by the full Joint Panel. The Task Committee suggests the following options for implementation: (a) Establish a new Task Committee which will address this topic area and provide the focal point to share experience and research in this area and (b) Incorporate this topic into another T/C e.g., T/C (D): on Evaluation of Structural Performance. T/C (H) will continue to explore methods whereby this topic will receive appropriate visibility.

5. Information Exchange:

* T/C workshops, exchange of visitors, and participation in annual joint panel meetings, and presenting technical papers.

* Exchange of researchers between U.S. and Japanese government laboratories.

* Visits by researchers and participation in technical activities such as post-earthquake field investigations.

* Professional community in the U.S. and Japan; publication of papers in journals; publication of research reports by the respective agencies; participation in professional society meetings and conferences; seminars; and workshops.

6. Impact

Through the exchange of researchers and the diffusion of earthquake-related technical data, experience, and information on methods of practice, the state of technology in geotechnical earthquake engineering has been raised on both sides. Through the cooperative research program on in-situ testing of soils which was carried out after the 1983 Nihonkai-Chubu Earthquake, improved and more accurate methods of using in-situ tests for evaluating the liquefaction potential of soils were achieved; these have been in general use in the United States since 1985. The Loma Prieta Earthquake stimulated renewed awareness of the need for further research in soil liquefaction and amplification effects of soft soils.

7. Barriers

* Insufficient U. S. and Japan Government funds allocated to adequately address earthquake engineering research.

* Administrative limitations on foreign travel.

Report of Task Committee on

(I) STORM SURGE AND TSUNAMI

Date: May 15, 1990

Place: National Institute of Standards and Technology
Gaithersburg, MD 20899

Attendees:	Japan Side -	K. Yokoyama (Temp. Chairman)	(PWRI)
		H. Ito	(MRI)
	U.S. Side -	H. Meyers (Chairman)	(NOAA)
		C. Barrientos	(NOAA)
		W. E. Roper	(COE)

MISSION STATEMENT

1. Objective

The objective of this T/C is to mitigate damages from storm surges and tsunamis through shared technologies, research, information sharing, and cooperative work. Storm surge and tsunami are hazards capable of inflecting damage of disastrous proportions. Storm surges are associated with hurricanes and typhoons where high winds and the mounding of water under the low barometric pressure of the storm's eye can cause extensive flooding and severe wave action. Tsunamis are predominately caused by underwater earthquakes and, to a lesser extent volcanic activity. Depending on the distance from the source tsunamis arrive within minutes to up to a day after generation.

2. Scope of Work

* Exchange results of research on storm surge and tsunami occurrence, generation, propagation, and costal effects. This includes observations on historical, current, and theoretical tsunamis. Of particular interest is the effort by US and JAPAN to acquire deep ocean tsunami measurements.

* Exchange results and status of anti-storm surge and tsunami; activities including analysis of the problem, planning, warning, and engineering approaches.

* Exchange information on planned and ongoing projects relating to storm surge and tsunamis.

* Exchange information on development of technologies such as computer programs to predict travel times, land-fall locations, run-up heights, and wave characteristics and analysis; improved instrumentation, and use of satellite communications for detection and warning.

* Facilitate dissemination through exchange of literature, technical reports at joint meetings, special workshops, joint projects, and direct interaction among participants.

3. Accomplishments

* Exchanged digital bathymetric data with the Japanese side; US side received a computer program to calculate tsunami travel time charts.

* Exchanged computer program forecasting storm surge run-up.

* Exchanged technical reports on related subjects.

* Expanded the number of active U.S. participants with representation from COE, University of Colorado, and NOAA, and NSF.

* The U.S. side has compiled detailed information on all tsunamis affecting the U.S. and its possessions. The publication, "United States Tsunamis 1690-1989" has been printed and given to the Japanese side.

4. Future Plans

* Develop exchanges of data and information on activities related to deep ocean tsunami measurements.

* A Second Tsunami Workshop is being arranged in Hawaii, November 5-7, 1990 to address advances since the first Workshop held in 1983 and to bring together computer modelers and potential users of modeling results. There will be approximately 8 participants from the Japanese side and 10 from the U.S. side. Site visits are also being planned.

* Explore and promote joint undertakings such as instrument testing, joint publications, scientist exchange, satellite communications, and assistance in contacts within the US and JAPAN.

* NOAA has adopted the travel time program developed by Mr. Okada (MRI/JMA) using NOAA gridded bathymetric data to run on NOAA computers. The first ever computed travel time charts have been prepared for the Caribbean Sea using this program developed by Mr. Okada. A copy of the published paper will be sent to the Japanese side.

* The U.S. and Japanese sides agree that there is a need to hold workshops at 2 or 3 year intervals to exchange the latest research and technology relating to various aspects of storm surge and tsunami hazards.

5. Information Exchange

* Continue exchange of publications, bibliographic data, technical reports, and personal contacts.

6. Impact

* Increased cooperation among scientists and engineers working in these fields.

* Hasten implementation of new modeling and design techniques developed by the US and Japan.

* Facilitated wider dissemination of information and technology to scientists and engineers in both countries.

7. Barriers

* Insufficient funding from government and private sector organizations to participate in T/C workshops and the Panel's annual joint meetings.

* The tsunami problem is less severe in the US than in JAPAN which leads to a smaller community of researchers. There are few US researchers focusing on tsunamis at any specific location; thus highlighting the importance of T/C periodic meetings and workshops.

* There are different approaches and degree of significance in dealing with problems in the U.S. and JAPAN e.g., in U.S. much of the hazard is from remote sources which leads the government to emphasizing developments of warning and evacuation schemes while in JAPAN the engineering approach is needed due to more locally generated tsunamis which often do not provide sufficient times for adequate warning and evacuation. This barrier is partially being addressed by inviting engineers and non-government specialists to participate as temporary or permanent members for the U.S. side at the annual meetings.

Report of Task Committee on

(J) WIND AND EARTHQUAKE ENGINEERING FOR TRANSPORTATION SYSTEMS

Date: May 15, 1990

Place: National Institute of Standards and Technology
Gaithersburg, MD 20899

Attendees: Japan Side - K. Yokoyama (Acting Chairman) (PWRI)
K. Hasegawa (PWRI)

U.S. Side - J. D. Cooper (Chairman) (FHWA)

MISSION STATEMENT

1. Objectives

The objectives of this Task Committee are to plan, promote, and foster research on the behavior of highway bridges when subjected to wind and seismic forces and to disseminate research results and provide specifications and guidelines based on the task committee's findings. Surface transportation systems for movement of goods and people play a vital part of commerce and intercourse between people. Highway bridges are especially influenced by the forces of wind and earthquakes because of their open exposure to those forces.

2. Scope-of-Work

* The scope of the work is applicable mostly to highway bridges without any limitation on their size and function: such as existing bridges and new bridge designs; whole system of bridges; and/or to single components of a bridge.

* The mission is performed through: conducting workshops, exchanging researchers, developing methods for design evaluations and test procedures, inspection techniques, rehabilitation and maintenance specifications and policies, and performing cooperative research programs and other relevant cooperative administrative activities.

3. Accomplishments

* United States and Japanese post earthquake investigative teams collaborated to investigate the damage to transportation systems with emphasis on highway bridges caused by the Loma Prieta Earthquake of October 17, 1989. Technical information was exchanged at the 22nd Joint Panel Meeting.

* Conducted coordinated research studies on the seismic performance of bridge piers and columns. Details of this work

involved determining the performance of reinforced concrete piers and columns subjected to dynamic cyclic loading, performing model tests on the failure of reinforced concrete piers, testing full-scale concrete columns and for the behavior of concrete filled steel tubes.

* Held the sixth bridge workshop in Lake Tahoe, Nevada U.S. in 1990 and the fifth bridge workshop in Tsukuba, Japan in 1989, dealing with the determination and evaluation of the performance and strengthening of bridge structures, structural monitoring, repairs, safety and non-destructive evaluation. Special attention was given to the seismic and wind loadings of modern cable-stayed bridges, vibration suppression, base isolation and dynamic control techniques.

* Both sides presented technical papers at the 21st and 22nd UJNR Joint Meeting and participated in technical study tours to buildings, bridges, factories, construction sites, and instrumented structures.

4. Future Plans

* Conduct the 7th bridge workshop just prior to the 23rd Joint Panel meeting in Japan.

* T/C (J) recognizes the importance of developing active and passive control systems to mitigate earthquake and wind induced damage to bridges. Because of the potential application and impact of these control systems to mitigate damage on other types of structures, T/C (J) recommends the establishment of a new Panel T/C to review the feasibility for and encourage and support the development of active and passive control systems to reduce earthquake and wind induced structural damage.
* Investigate and exchange technical information on improved seismic retrofit and strengthening procedures for highway bridges based on experimental, analytical, and field studies.

* Continue experimental research study on the seismic performance of bridge piers and columns, and continue emphasis on base isolation.

* Develop a coordinated research study on seismic, aeroelastic, and aerodynamic response of cable-supported bridges with emphasis on cable inspection, vibration and corrosion protection.

* Develop a coordinated research study to compare the seismic design criteria for bridges in Japan and the U.S., including application of limit state design.

* Encourage a coordinated research study on seismic response

control, system identification techniques, and non-destructive evaluation of bridge structures.

5. Information exchange

* Exchanged technical reports, research program documentation, construction logs, design plans, and assorted photographs and TV videos.

* Mr. Keiichi Tamura from PWRI studied at Stanford University and Mr. Kinji Hasegawa from PWRI studied at the University of California,
Berkeley. Mr. S. Unjoh returned to PWRI in March 1990 after working for one year at the University of Southern California.

6. Impact

* Greater uniformity was achieved in wind engineering test procedures and modeling resulting in more efficient solutions to the aerodynamic bridge problem.

* The workshops and study tours in the two countries have facilitated technology transfer, as an example, in the area of cable protection and vibration suppression of cable-stayed bridges.

* With respect to the earthquake protection of bridges, the free exchange of literature, instrumentation technology, and earthquake response data has led to the advancement in design technology, and development of preliminary retrofit guidelines, and to the calibration and verification of specifications.

* A set of priorities for needed research from a more international viewpoint has reduced the conduct of duplicative research efforts.

7. Barriers

There are no major technical barriers to achieve the Task Committee mission. However, financial barriers, especially funding needed to participate in workshops and panel meetings and for conducting actual bridge tests and large scale model tests, limit the effectiveness of the work in this Task Committee's work.

NIST-114A
(REV. 3-89)

U.S. DEPARTMENT OF COMMERCE
NATIONAL INSTITUTE OF STANDARDS AND TECHNOLOGY

BIBLIOGRAPHIC DATA SHEET

1. PUBLICATION OR REPORT NUMBER
NIST/SP-796

2. PERFORMING ORGANIZATION REPORT NUMBER

3. PUBLICATION DATE
September 1990

4. TITLE AND SUBTITLE

Wind and Seismic Effects--Proceedings of the 22nd Joint Meeting of the U.S.-Japan Cooperative Program in Natural Resources Panel on Wind and Seismic Effects

5. AUTHOR(S)

Noel J. Raufaste, Editor

6. PERFORMING ORGANIZATION (IF JOINT OR OTHER THAN NIST, SEE INSTRUCTIONS)

U.S. DEPARTMENT OF COMMERCE
NATIONAL INSTITUTE OF STANDARDS AND TECHNOLOGY
GAITHERSBURG, MD 20899

7. CONTRACT/GRANT NUMBER

8. TYPE OF REPORT AND PERIOD COVERED
Final

9. SPONSORING ORGANIZATION NAME AND COMPLETE ADDRESS (STREET, CITY, STATE, ZIP)

SAME AS ITEM # 6 ABOVE.

10. SUPPLEMENTARY NOTES

[ ] DOCUMENT DESCRIBES A COMPUTER PROGRAM; SF-185, FIPS SOFTWARE SUMMARY, IS ATTACHED.

11. ABSTRACT (A 200-WORD OR LESS FACTUAL SUMMARY OF MOST SIGNIFICANT INFORMATION. IF DOCUMENT INCLUDES A SIGNIFICANT BIBLIOGRAPHY OR LITERATURE SURVEY, MENTION IT HERE.)

The 22nd Joint Meeting of the U.S.-Japan Panel on Wind and Seismic Effects was held at the National Institute of Standards and Technology from May 15-18, 1990. This publication, the proceedings of the Joint Meeting, includes the program, list of members, panel resolutions, task committee reports, and 39 technical papers.

The papers were presented under six themes: (I) - Wind Engineering, (II) - Storm Surge and Tsunamis, (III) - Joint Cooperative Research Program, (IV) - Earthquake Engineering, (V) - Loma Prieta Earthquake, and (VI) - Summaries of Task Committee Workshop Reports.

12. KEY WORDS (6 TO 12 ENTRIES; ALPHABETICAL ORDER; CAPITALIZE ONLY PROPER NAMES; AND SEPARATE KEY WORDS BY SEMICOLONS)

accelerograph; bridges; codes; concrete; design criteria; disaster; earthquakes; geotechnical engineering; ground failures; inelastic ; lifelines; liquefaction; Loma Prieta; masonry; repair and retrofit; risk assessment; seismicity; soils; standards; storm surge; structural engineering; tsunami; and wind loads.

13. AVAILABILITY

[X] UNLIMITED

[ ] FOR OFFICIAL DISTRIBUTION. DO NOT RELEASE TO NATIONAL TECHNICAL INFORMATION SERVICE (NTIS).

[X] ORDER FROM SUPERINTENDENT OF DOCUMENTS, U.S. GOVERNMENT PRINTING OFFICE, WASHINGTON, DC 20402.

[ ] ORDER FROM NATIONAL TECHNICAL INFORMATION SERVICE (NTIS), SPRINGFIELD, VA 22161.

14. NUMBER OF PRINTED PAGES
524

15. PRICE

ELECTRONIC FORM

☆ U.S. GOVERNMENT PRINTING OFFICE: 1990 — 261-913/20707

NIST Technical Publications

Periodical

Journal of Research of the National Institute of Standards and Technology—Reports NIST research and development in those disciplines of the physical and engineering sciences in which the Institute is active. These include physics, chemistry, engineering, mathematics, and computer sciences. Papers cover a broad range of subjects, with major emphasis on measurement methodology and the basic technology underlying standardization. Also included from time to time are survey articles on topics closely related to the Institute's technical and scientific programs. Issued six times a year.

Nonperiodicals

Monographs—Major contributions to the technical literature on various subjects related to the Institute's scientific and technical activities.

Handbooks—Recommended codes of engineering and industrial practice (including safety codes) developed in cooperation with interested industries, professional organizations, and regulatory bodies.

Special Publications—Include proceedings of conferences sponsored by NIST, NIST annual reports, and other special publications appropriate to this grouping such as wall charts, pocket cards, and bibliographies.

Applied Mathematics Series—Mathematical tables, manuals, and studies of special interest to physicists, engineers, chemists, biologists, mathematicians, computer programmers, and others engaged in scientific and technical work.

National Standard Reference Data Series—Provides quantitative data on the physical and chemical properties of materials, compiled from the world's literature and critically evaluated. Developed under a worldwide program coordinated by NIST under the authority of the National Standard Data Act (Public Law 90-396). NOTE: The Journal of Physical and Chemical Reference Data (JPCRD) is published quarterly for NIST by the American Chemical Society (ACS) and the American Institute of Physics (AIP). Subscriptions, reprints, and supplements are available from ACS, 1155 Sixteenth St., NW., Washington, DC 20056.

Building Science Series—Disseminates technical information developed at the Institute on building materials, components, systems, and whole structures. The series presents research results, test methods, and performance criteria related to the structural and environmental functions and the durability and safety characteristics of building elements and systems.

Technical Notes—Studies or reports which are complete in themselves but restrictive in their treatment of a subject. Analogous to monographs but not so comprehensive in scope or definitive in treatment of the subject area. Often serve as a vehicle for final reports of work performed at NIST under the sponsorship of other government agencies.

Voluntary Product Standards—Developed under procedures published by the Department of Commerce in Part 10, Title 15, of the Code of Federal Regulations. The standards establish nationally recognized requirements for products, and provide all concerned interests with a basis for common understanding of the characteristics of the products. NIST administers this program as a supplement to the activities of the private sector standardizing organizations.

Consumer Information Series—Practical information, based on NIST research and experience, covering areas of interest to the consumer. Easily understandable language and illustrations provide useful background knowledge for shopping in today's technological marketplace.

Order the **above** *NIST publications from: Superintendent of Documents, Government Printing Office, Washington, DC 20402.*

Order the **following** *NIST publications—FIPS and NISTIRs—from the National Technical Information Service, Springfield, VA 22161.*

Federal Information Processing Standards Publications (FIPS PUB)—Publications in this series collectively constitute the Federal Information Processing Standards Register. The Register serves as the official source of information in the Federal Government regarding standards issued by NIST pursuant to the Federal Property and Administrative Services Act of 1949 as amended, Public Law 89-306 (79 Stat. 1127), and as implemented by Executive Order 11717 (38 FR 12315, dated May 11, 1973) and Part 6 of Title 15 CFR (Code of Federal Regulations).

NIST Interagency Reports (NISTIR)—A special series of interim or final reports on work performed by NIST for outside sponsors (both government and non-government). In general, initial distribution is handled by the sponsor; public distribution is by the National Technical Information Service, Springfield, VA 22161, in paper copy or microfiche form.

U.S. Department of Commerce
National Institute of Standards and Technology
(formerly National Bureau of Standards)
Gaithersburg, MD 20899